

IMPROVING OUR UNDERSTANDING OF  
SRC VARIABLE STARS

by

Kathleen Elizabeth Moncrieff

A thesis submitted to the faculty of  
Saint Mary's University

in partial fulfillment of the requirements for the degree of  
Doctor of Philosophy in Astronomy

April 2011, Halifax, Nova Scotia

Copyright © 2011 Kathleen Elizabeth Moncrieff

Approved: Dr. David G. Turner, Chair

Approved: Dr. C. Ian Short, Committee Member

Approved: Dr. Eric G. Hintz, External Examiner

Date: April 20, 2011



Library and Archives  
Canada

Published Heritage  
Branch

395 Wellington Street  
Ottawa ON K1A 0N4  
Canada

Bibliothèque et  
Archives Canada

Direction du  
Patrimoine de l'édition

395, rue Wellington  
Ottawa ON K1A 0N4  
Canada

*Your file Votre référence*  
ISBN: 978-0-494-79650-4  
*Our file Notre référence*  
ISBN: 978-0-494-79650-4

#### NOTICE:

The author has granted a non-exclusive license allowing Library and Archives Canada to reproduce, publish, archive, preserve, conserve, communicate to the public by telecommunication or on the Internet, loan, distribute and sell theses worldwide, for commercial or non-commercial purposes, in microform, paper, electronic and/or any other formats.

The author retains copyright ownership and moral rights in this thesis. Neither the thesis nor substantial extracts from it may be printed or otherwise reproduced without the author's permission.

---

In compliance with the Canadian Privacy Act some supporting forms may have been removed from this thesis.

While these forms may be included in the document page count, their removal does not represent any loss of content from the thesis.

#### AVIS:

L'auteur a accordé une licence non exclusive permettant à la Bibliothèque et Archives Canada de reproduire, publier, archiver, sauvegarder, conserver, transmettre au public par télécommunication ou par l'Internet, prêter, distribuer et vendre des thèses partout dans le monde, à des fins commerciales ou autres, sur support microforme, papier, électronique et/ou autres formats.

L'auteur conserve la propriété du droit d'auteur et des droits moraux qui protège cette thèse. Ni la thèse ni des extraits substantiels de celle-ci ne doivent être imprimés ou autrement reproduits sans son autorisation.

---

Conformément à la loi canadienne sur la protection de la vie privée, quelques formulaires secondaires ont été enlevés de cette thèse.

Bien que ces formulaires aient inclus dans la pagination, il n'y aura aucun contenu manquant.

\*\*  
Canada

## ABSTRACT

# IMPROVING OUR UNDERSTANDING OF SRC VARIABLE STARS

Kathleen Elizabeth Moncrieff

Department of Astronomy and Physics

Doctor of Philosophy in Astronomy

April 2011

SRC variables are evolved stars (mostly M supergiants) that vary in brightness with semi-regular periods ranging from several months to several years. Their light variation is caused by a combination of pulsation, convection, and other processes such as dust ejections. Much data exist for the stars, but they have been under-utilized. We studied 49 individual SRC variables using archival and newly-obtained data. We present new results including cyclic variation in radial velocity, spectral type, and luminosity class, period analysis, and changes in period and mean magnitude for individual stars. We have re-examined the period-luminosity and period-radius relations, and discovered a new relationship among spectral type, luminosity class, and light amplitude. To aid in future studies of the stars, we have subdivided them into three categories based on the quality of available data and the likelihood that they are periodic rather than simply varying irregularly.

## ACKNOWLEDGMENTS

I would like to thank my supervisor, David Turner, and the various people who have been on my committee throughout the process, Ian Short, Eric Hintz, Marcin Sawicki, and Phil Bennett, for their support and guidance. I am also grateful for the support of the other SMU students I have worked beside over the last four years, including (in no particular order) Andy Marquis, Liz Arcila, Jayme Derrah, Dan Majaess, Jon Ramsey, James Wurster, Mike Casey, Dave Williamson, Chris Geroux, Larkin Duelge, Catherine Lovekin, Bobby Sorba, Nick MacDonald, Jon Savoy, Anneya Golob, Michael Gruberbauer, Diego Castaneda, and Jason Sharpe. I would also like to thank Dave Lane, Elfrie Waters, Florence Woolaver, Jenna Hurry, David Guenther, and the other members of the Astronomy and Physics department for their support.

We would like to thank Bob Wing and Roger Griffin for providing us with their data. We thank the Dominion Astrophysical Observatory for the use of the 1.8-m telescope. We also thank Dave Balaam at the DAO for digitizing the photographic spectrum. We also acknowledge with thanks the variable star observations from the AAVSO International Database contributed by observers worldwide and used in this research. We thank the Harvard College Observatory and David Dunlap Observatory for the use of their photographic plate archives.

Finally, I would like to thank my family members and friends who are like family members for their continued support. Thank you to Marjorie Moncrieff, David Moncrieff, Kelly Moncrieff, James Moncrieff, Benjamin Moncrieff, Tabitha Buehler, David Buehler, Matt Lund, Liberty Evanko, and Marie Burgess. Without you, this would not have happened.

# Contents

<b>Acknowledgments</b>	<b>iii</b>
<b>1 Introduction</b>	<b>1</b>
1.1 Cool Luminous Variable Stars . . . . .	1
1.2 Motivation . . . . .	3
1.3 Previous Work . . . . .	4
1.3.1 The Work of Alfred Joy . . . . .	4
1.3.2 The Work of Stothers . . . . .	5
1.3.3 The Work of White and Wing . . . . .	5
1.3.4 The Work of Roberta Humphreys . . . . .	5
1.3.5 The Work of David Gray . . . . .	6
1.3.6 The Work of Levesque and Massey . . . . .	6
1.3.7 The Work of Turner and Rohanizadegan . . . . .	7
1.3.8 Questions Left Unanswered by Previous Work . . . . .	7
1.4 Photometry . . . . .	7
1.5 Spectroscopy . . . . .	9
1.6 Radial Velocities . . . . .	11
1.7 Causes of Variability . . . . .	12
<b>2 Observations and Data Reduction</b>	<b>14</b>
2.1 AAVSO Observations . . . . .	14
2.2 Data from the Harvard College Observatory Photographic Plate Collection . . . . .	15

2.3	Radial Velocity Measurements from Roger Griffin . . . . .	15
2.4	Radial Velocity and Spectral Type Measurements from Joy . . . . .	15
2.5	Spectrophotometric Measurements from Bob Wing . . . . .	15
2.6	Photographic Spectra from the David Dunlap Observatory . . . . .	16
2.7	Photographic Spectra from the Dominion Astrophysical Observatory .	16
2.8	CCD Spectra from the Dominion Astrophysical Observatory . . . . .	17
2.9	Data Reduction for CCD Spectra . . . . .	17
2.9.1	Continuum Calibration . . . . .	18
<b>3</b>	<b>Data Analysis</b>	<b>20</b>
3.1	Period Determination . . . . .	20
3.2	Spectral Classification . . . . .	27
3.3	The Effective Temperature Scale . . . . .	32
3.4	Radial Velocity Measurement . . . . .	32
<b>4</b>	<b>Results for Individual Stars</b>	<b>35</b>
4.1	Explanation of Table Columns for Individual Stars . . . . .	40
4.2	SS Andromedae . . . . .	42
4.3	V Arietis . . . . .	46
4.4	UX Aurigae . . . . .	47
4.5	V394 Aurigae . . . . .	50
4.6	RS Cancri . . . . .	52
4.7	UZ Canis Majoris . . . . .	56
4.8	BZ Carinae . . . . .	58
4.9	CK Carinae . . . . .	61
4.10	CL Carinae . . . . .	63
4.11	EV Carinae . . . . .	65
4.12	IX Carinae . . . . .	67
4.13	PZ Casseopeiae . . . . .	69
4.14	W Cephei . . . . .	73

4.15 SW Cephei . . . . .	77
4.16 VV Cephei . . . . .	80
4.17 MY Cephei . . . . .	85
4.18 $\mu$ Cephei . . . . .	86
4.19 T Ceti . . . . .	91
4.20 RW Cygni . . . . .	95
4.21 AZ Cygni . . . . .	99
4.22 BC Cygni . . . . .	103
4.23 V Eridani . . . . .	107
4.24 TV Geminorum . . . . .	109
4.25 IS Geminorum . . . . .	113
4.26 V959 Herculis . . . . .	115
4.27 $\alpha$ Herculis . . . . .	117
4.28 RV Hydrae . . . . .	121
4.29 W Indus . . . . .	123
4.30 U Lacertae . . . . .	125
4.31 Y Lyncis . . . . .	128
4.32 $\delta^2$ Lyrae . . . . .	132
4.33 $\alpha$ Orionis . . . . .	134
4.34 S Persei . . . . .	141
4.35 T Persei . . . . .	145
4.36 W Persei . . . . .	149
4.37 RS Persei . . . . .	153
4.38 SU Persei . . . . .	157
4.39 XX Persei . . . . .	161
4.40 AD Persei . . . . .	165
4.41 BU Persei . . . . .	169
4.42 FZ Persei . . . . .	173
4.43 V411 Persei . . . . .	177

4.44	VX Sagittarii . . . . .	180
4.45	KW Sagittarii . . . . .	182
4.46	AH Scorpii . . . . .	185
4.47	CE Tauri . . . . .	187
4.48	W Trianguli . . . . .	191
4.49	CM Velorum . . . . .	195
4.50	FG Vulpeculae . . . . .	197
4.51	Summary of Results . . . . .	199
<b>5</b>	<b>Group-Wide Trends</b>	<b>204</b>
5.1	Insights From the Radial Velocity Curves . . . . .	204
5.2	Spectral Type-Amplitude Relation . . . . .	206
5.3	Period-Luminosity and Period-Radius Relations . . . . .	210
5.3.1	Other Period-Luminosity Relations of Note . . . . .	214
5.4	Size Changes . . . . .	216
5.5	Remarks . . . . .	220
<b>6</b>	<b>Conclusions and Future Directions</b>	<b>221</b>
<b>References</b>		<b>223</b>
<b>A</b>	<b>Spectra</b>	<b>228</b>
<b>B</b>	<b>Light Curves</b>	<b>258</b>
<b>C</b>	<b>Periodograms</b>	<b>378</b>
<b>D</b>	<b>Observing Logs</b>	<b>403</b>
D.1	DAO CCD Spectra . . . . .	403
D.1.1	2005 . . . . .	403
D.1.2	2006 . . . . .	405
D.1.3	2007 . . . . .	406

D.1.4	2008	407
D.1.5	2009	408
D.1.6	2010	409
D.2	Scanned DAO Photographic Spectra	410

# List of Tables

2.1	White and Wing Filters . . . . .	16
3.1	Especially useful lines for classification. . . . .	29
3.2	Approximate luminosity classification ratios . . . . .	30
3.3	Keenan's classification criteria for M stars . . . . .	31
3.4	Effective temperature scale for M supergiants, taken from Levesque & Massey (2005) . . . . .	33
4.1	Summary of Information for Individual Stars . . . . .	37
4.2	Summary of Information for Individual Stars (continued) . . . . .	38
4.3	Summary of Information for Individual Stars (continued) . . . . .	39
4.4	AAVSO Observations of SS Andromedae . . . . .	43
4.5	Spectroscopic observations of SS Andromedae . . . . .	43
4.6	AAVSO Observations of <i>V</i> Arietis . . . . .	46
4.7	AAVSO Observations of UX Aurigae . . . . .	48
4.8	Spectroscopic observations of UX Aurigae . . . . .	48
4.9	Spectroscopic observations of V394 Aurigae . . . . .	50
4.10	AAVSO Observations of V394 Aurigae . . . . .	50
4.11	AAVSO Observations of RS Cancri . . . . .	52
4.12	Spectroscopic observations of RS Cancri . . . . .	53
4.13	AAVSO Observations of UZ Canis Majoris . . . . .	56
4.14	AAVSO Observations of BZ Carinae . . . . .	58
4.15	Spectroscopic observations of BZ Carinae . . . . .	59
4.16	AAVSO Observations of CK Carinae . . . . .	61
4.17	AAVSO Observations of CL Carinae . . . . .	63

4.18 AAVSO Observations of EV Carinae . . . . .	65
4.19 AAVSO Observations of IX Carinae . . . . .	67
4.20 AAVSO Observations of PZ Casseopeiae . . . . .	69
4.21 Spectroscopic observations of PZ Casseopeia . . . . .	70
4.22 AAVSO Observations of W Cephei . . . . .	73
4.23 Spectroscopic observations of W Cephei . . . . .	74
4.24 AAVSO Observations of SW Cephei . . . . .	77
4.25 Spectroscopic observations of SW Cephei . . . . .	78
4.26 AAVSO Observations of VV Cephei . . . . .	81
4.27 Spectroscopic observations of VV Cephei . . . . .	81
4.28 Spectroscopic observations of MY Cephei . . . . .	85
4.29 AAVSO Observations of $\mu$ Cephei . . . . .	87
4.30 Spectroscopic observations of $\mu$ Cephei . . . . .	88
4.31 AAVSO Observations of T Ceti . . . . .	91
4.32 Spectroscopic observations of T Ceti . . . . .	92
4.33 AAVSO Observations of RW Cygni . . . . .	95
4.34 Spectroscopic observations of RW Cygni . . . . .	96
4.35 AAVSO Observations of AZ Cygni . . . . .	99
4.36 Spectroscopic observations of AZ Cygni . . . . .	100
4.37 AAVSO Observations of BC Cygni . . . . .	103
4.38 Spectroscopic observations of BC Cygni . . . . .	104
4.39 AAVSO Observations of $V$ Eridani . . . . .	107
4.40 AAVSO Observations of TV Geminorum . . . . .	109
4.41 Spectroscopic observations of TV Geminorum . . . . .	110
4.42 AAVSO Observations of IS Geminorum . . . . .	113
4.43 AAVSO Observations of V959 Herculis . . . . .	115
4.44 Spectroscopic observations of V959 Herculis . . . . .	115
4.45 AAVSO Observations of $\alpha$ Herculis . . . . .	117
4.46 Spectroscopic observations of $\alpha$ Herculis . . . . .	118

4.47 AAVSO Observations of RV Hydrae . . . . .	121
4.48 AAVSO Observations of W Indus . . . . .	123
4.49 AAVSO Observations of U Lacertae . . . . .	126
4.50 Spectroscopic observations of U Lacertae . . . . .	126
4.51 AAVSO Observations of Y Lyncis . . . . .	128
4.52 Spectroscopic observations of Y Lyncis . . . . .	129
4.53 AAVSO Observations of $\delta^2$ Lyrae . . . . .	132
4.54 Spectroscopic observations of $\delta^2$ Lyrae . . . . .	132
4.55 Spectroscopic observations of $\alpha$ Orionis . . . . .	135
4.56 Spectroscopic observations of $\alpha$ Orionis (continued) . . . . .	136
4.57 AAVSO Observations of $\alpha$ Orionis . . . . .	136
4.58 Angular Diameter of $\alpha$ Orionis . . . . .	137
4.59 AAVSO Observations of S Persei . . . . .	142
4.60 Spectroscopic observations of S Persei . . . . .	142
4.61 AAVSO Observations of T Persei . . . . .	146
4.62 Spectroscopic observations of T Persei . . . . .	146
4.63 AAVSO Observations of W Persei . . . . .	149
4.64 Spectroscopic observations of W Persei . . . . .	150
4.65 AAVSO Observations of RS Persei . . . . .	154
4.66 Spectroscopic observations of RS Persei . . . . .	154
4.67 AAVSO Observations of SU Persei . . . . .	158
4.68 Spectroscopic observations of SU Persei . . . . .	158
4.69 AAVSO Observations of XX Persei . . . . .	162
4.70 Spectroscopic observations of XX Persei . . . . .	162
4.71 AAVSO Observations of AD Persei . . . . .	166
4.72 Spectroscopic observations of AD Persei . . . . .	166
4.73 AAVSO Observations of BU Persei . . . . .	170
4.74 Spectroscopic observations of BU Persei . . . . .	170
4.75 AAVSO Observations of FZ Persei . . . . .	174

4.76	Spectroscopic observations of FZ Persei . . . . .	174
4.77	AAVSO Observations of V411 Persei . . . . .	177
4.78	Spectroscopic observations of V411 Persei . . . . .	178
4.79	AAVSO Observations of VX Sagittarii . . . . .	180
4.80	AAVSO Observations of KW Sagittarii . . . . .	182
4.81	Spectroscopic observations of KW Sagitarii . . . . .	182
4.82	AAVSO Observations of AH Scorpii . . . . .	185
4.83	AAVSO Observations of CE Tauri . . . . .	187
4.84	Spectroscopic observations of CE Tauri . . . . .	188
4.85	Spectroscopic observations of W Trianguli . . . . .	191
4.86	AAVSO Observations of W Trianguli . . . . .	192
4.87	AAVSO Observations of CM Velorum . . . . .	195
4.88	AAVSO Observations of FG Vulpeculae . . . . .	197
4.89	Spectroscopic observations of FG Vulpeculae . . . . .	197
4.90	Summary of Results . . . . .	199
4.91	Summary of Results (continued) . . . . .	200
4.92	Summary of Results (continued) . . . . .	201
4.93	Summary of Results (continued) . . . . .	202
4.94	Summary of Results (continued) . . . . .	203
5.1	Stars that reach smallest dimensions near light maximum (Phase 0.75-0.99 and 0.00-0.25) . . . . .	205
5.2	Stars that reach smallest dimensions near light minimum (Phase 0.25-0.75) . . . . .	205
5.3	Stars used in spectral type-amplitude relation . . . . .	209
5.4	Stars used in period-luminosity and period-radius relations . . . . .	213
5.5	Bolometric corrections from Levesque & Massey (2005) . . . . .	213
5.6	Size Changes . . . . .	219
D.1	2005 Observing Log . . . . .	404
D.2	2006 Observing Log . . . . .	405

D.3	2007 Observing Log . . . . .	406
D.4	2008 Observing Log . . . . .	407
D.5	2009 Observing Log . . . . .	408
D.6	2010 Observing Log . . . . .	409
D.7	Scanned DAO Photographic Spectra . . . . .	410

# List of Figures

1.1	S Persei . . . . .	3
2.1	Continuum Calibration . . . . .	19
3.1	Peranso observations window . . . . .	21
3.2	Peranso period determination using CLEANest routine . . . . .	22
3.3	Peranso period determination using ANOVA routine . . . . .	23
3.4	Spectral Window for S Persei . . . . .	24
3.5	Peranso prominent periods window example . . . . .	25
3.6	Peranso CLEANest workbench example . . . . .	26
3.7	Peranso time of maximum light-finding example . . . . .	26
3.8	4953Å spectral type indicator . . . . .	28
3.9	4389Å luminosity class indicator . . . . .	29
3.10	Using RVIDLINES . . . . .	34
4.1	SS And spectra . . . . .	44
4.2	SS And period and magnitude changes . . . . .	45
4.3	UX Aur spectra . . . . .	49
4.4	V394 spectra . . . . .	51
4.5	RS Cnc spectra . . . . .	54
4.6	RS Cnc period and magnitude changes . . . . .	55
4.7	UZ CMa period and magnitude changes . . . . .	57
4.8	BZ Car spectra . . . . .	59
4.9	BZ Car period and magnitude changes . . . . .	60
4.10	CK Car period and magnitude changes . . . . .	62
4.11	CL Car period and magnitude changes . . . . .	64

4.12	EV Car period and magnitude changes . . . . .	66
4.13	IX Car period and magnitude changes . . . . .	68
4.14	PZ Cas spectra . . . . .	71
4.15	PZ Cas period and magnitude changes . . . . .	72
4.16	W Cep spectra . . . . .	75
4.17	W Cep period and magnitude changes . . . . .	76
4.18	SW Cep spectra . . . . .	79
4.19	VV Cep spectra . . . . .	82
4.20	VV Cep period and magnitude changes . . . . .	83
4.21	VV Cep $V_R$ residuals . . . . .	84
4.22	MY Cep spectrum . . . . .	85
4.23	$\mu$ spectra . . . . .	89
4.24	$\mu$ Cep period and magnitude changes . . . . .	90
4.25	$\mu$ spectra . . . . .	93
4.26	T Cet period and magnitude changes . . . . .	94
4.27	RW Cyg spectra . . . . .	97
4.28	RW Cyg period and magnitude changes . . . . .	98
4.29	AC Cyg spectra . . . . .	101
4.30	AZ Cyg period and magnitude changes . . . . .	102
4.31	BC Cyg spectra . . . . .	105
4.32	BC Cyg period and magnitude changes . . . . .	106
4.33	V Eri period and magnitude changes . . . . .	108
4.34	TV Gem spectra . . . . .	111
4.35	TV Gem period and magnitude changes . . . . .	112
4.36	IS Gem period and magnitude changes . . . . .	114
4.37	V959 Her spectra . . . . .	116
4.38	$\alpha$ Her spectra . . . . .	119
4.39	$\alpha$ Her period and magnitude changes . . . . .	120
4.40	RV Hya period and magnitude changes . . . . .	122

4.41	W Ind period and magnitude changes . . . . .	124
4.42	U Lac spectra . . . . .	127
4.43	Y Lyn spectra . . . . .	130
4.44	Y Lyn period and magnitude changes . . . . .	131
4.45	$\delta^2$ Lyr period and magnitude changes . . . . .	133
4.46	$\alpha$ Ori spectra . . . . .	138
4.47	$\alpha$ Ori angular diameter . . . . .	139
4.48	$\alpha$ Ori period and magnitude changes . . . . .	140
4.49	S Per spectra . . . . .	143
4.50	S Per period and magnitude changes . . . . .	144
4.51	T Per spectra . . . . .	147
4.52	T Per period and magnitude changes . . . . .	148
4.53	W Per spectra . . . . .	151
4.54	W Per period and magnitude changes . . . . .	152
4.55	RS Per spectra . . . . .	155
4.56	RS Per period and magnitude changes . . . . .	156
4.57	SU Per spectra . . . . .	159
4.58	SU Per period and magnitude changes . . . . .	160
4.59	XX Per spectra . . . . .	163
4.60	XX Per period and magnitude changes . . . . .	164
4.61	AD Per spectra . . . . .	167
4.62	AD Persei period and magnitude changes . . . . .	168
4.63	BU Per spectra . . . . .	171
4.64	BU Per period and magnitude changes . . . . .	172
4.65	FZ Per spectra . . . . .	175
4.66	FZ Per period and magnitude changes . . . . .	176
4.67	V411 Per spectra . . . . .	179
4.68	VX Sgr period and magnitude changes . . . . .	181
4.69	KW Sgr spectra . . . . .	183

4.70	KW Sgr period and magnitude changes . . . . .	184
4.71	AH Sco period and magnitude changes . . . . .	186
4.72	CE Tau spectra . . . . .	189
4.73	CE Tau period and magnitude changes . . . . .	190
4.74	W Tri spectra . . . . .	193
4.75	W Tri period and magnitude changes . . . . .	194
4.76	CM Vel period and magnitude changes . . . . .	196
4.77	FG Vul spectra . . . . .	198
5.1	Spectral type-amplitude relation . . . . .	208
5.2	$\Delta V$ vs T for varying $\Delta T$ values. . . . .	208
5.3	Period-luminosity relation . . . . .	212
5.4	Period-radius relation . . . . .	212
A.1	SS Andromedae Spectra . . . . .	228
A.2	UX Aurigae Spectra . . . . .	229
A.3	RS Cancri Spectra . . . . .	230
A.4	PZ Casseopeiae Spectra . . . . .	231
A.5	W Cephei Spectra . . . . .	232
A.6	SW Cephei Spectra . . . . .	233
A.7	VV Cephei Spectra . . . . .	234
A.8	MY Cephei Spectra . . . . .	235
A.9	$\mu$ Cephei Spectra . . . . .	236
A.10	RW Cygni Spectra . . . . .	237
A.11	AZ Cygni Spectra . . . . .	238
A.12	BC Cygni Spectra . . . . .	239
A.13	TV Geminorum Spectra . . . . .	240
A.14	$\alpha$ Herculis Spectra . . . . .	241
A.15	U Lacertae Spectra . . . . .	242
A.16	Y Lyncis Spectra . . . . .	243
A.17	$\alpha$ Orionis Spectra . . . . .	244

A.18	S Persei Spectra . . . . .	245
A.19	T Persei Spectra . . . . .	246
A.20	W Persei Spectra . . . . .	247
A.21	RS Persei Spectra . . . . .	248
A.22	SU Persei Spectra . . . . .	249
A.23	XX Persei Spectra . . . . .	250
A.24	AD Persei Spectra . . . . .	251
A.25	BU Persei Spectra . . . . .	252
A.26	FZ Persei Spectra . . . . .	253
A.27	V411 Persei Spectra . . . . .	254
A.28	CE Tauri Spectra . . . . .	255
A.29	W Triangulum Spectra . . . . .	256
A.30	FG Vulpeculae Spectra . . . . .	257
B.1	SS And light curve . . . . .	258
B.2	SS And light curve expanded view . . . . .	259
B.3	V Ari light curve . . . . .	260
B.4	V Ari light curve - expanded view . . . . .	261
B.5	UX Aur light curve . . . . .	262
B.6	UX Aur light curve - expanded view . . . . .	263
B.7	V394 Aur light curve . . . . .	264
B.8	RS Cnc light curve . . . . .	265
B.9	RS Cnc light curve - expanded view . . . . .	266
B.10	UZ CMa light curve . . . . .	267
B.11	UZ CMa light curve - expanded view . . . . .	268
B.12	BZ Car light curve . . . . .	269
B.13	BZ Car light curve - expanded view . . . . .	270
B.14	CK Car light curve . . . . .	271
B.15	CK Car light curve - expanded view . . . . .	272
B.16	CL Car light curve . . . . .	273

B.17	CL Car light curve - expanded view . . . . .	274
B.18	CL Car photographic light curve . . . . .	275
B.19	CL Car photographic light curve - expanded view . . . . .	276
B.20	EV Car light curve . . . . .	277
B.21	EV Car light curve - expanded view . . . . .	278
B.22	IX Car light curve . . . . .	279
B.23	IX Car light curve - expanded view . . . . .	280
B.24	IX Car photographic light curve . . . . .	281
B.25	IX Car photographic light curve - expanded view . . . . .	282
B.26	PZ Cas light curve . . . . .	283
B.27	PZ Cas light curve - expanded view . . . . .	284
B.28	W Cep light curve . . . . .	285
B.29	W Cep light curve - expanded view . . . . .	286
B.30	SW Cep light curve . . . . .	287
B.31	SW Cep light curve - expanded view . . . . .	288
B.32	VV Cep light curve . . . . .	289
B.33	VV Cep light curve - expanded view . . . . .	290
B.34	$\mu$ Cep light curve . . . . .	291
B.35	$\mu$ Cep light curve . . . . .	292
B.36	$\mu$ Cep light curve - expanded view, continued . . . . .	293
B.37	T Cet light curve . . . . .	294
B.38	T Cet light curve - expanded view . . . . .	295
B.39	RW Cyg light curve . . . . .	296
B.40	RW Cyg light curve - expanded view . . . . .	297
B.41	AZ Cyg light curve . . . . .	298
B.42	AZ Cyg light curve - expanded view . . . . .	299
B.43	BC Cyg light curve . . . . .	300
B.44	BC Cyg light curve - expanded view . . . . .	301
B.45	BC Cyg photographic light curve . . . . .	302

B.46	BC Cyg photographic light curve - expanded view . . . . .	303
B.47	V Eri light curve . . . . .	304
B.48	V Eri light curve - expanded view . . . . .	305
B.49	TV Gem light curve . . . . .	306
B.50	TV Gem light curve - expanded view . . . . .	307
B.51	IS Gem light curve . . . . .	308
B.52	IS Gem light curve - expanded view . . . . .	309
B.53	V959 Her light curve . . . . .	310
B.54	$\alpha$ Her light curve . . . . .	311
B.55	$\alpha$ Her light curve - expanded view . . . . .	312
B.56	RV Hya light curve . . . . .	313
B.57	RV Hya light curve - expanded view . . . . .	314
B.58	W Ind light curve . . . . .	315
B.59	W Ind light curve - expanded view . . . . .	316
B.60	U Lac light curve . . . . .	317
B.61	U Lac light curve - expanded view . . . . .	318
B.62	Y Lyn light curve . . . . .	319
B.63	Y Lyn light curve - expanded view . . . . .	320
B.64	$\delta^2$ Lyr light curve . . . . .	321
B.65	$\delta^2$ Lyr light curve - expanded view . . . . .	322
B.66	$\alpha$ Ori light curve . . . . .	323
B.67	$\alpha$ Ori light curve - expanded view . . . . .	324
B.68	S Per light curve . . . . .	325
B.69	S Per light curve - expanded . . . . .	326
B.70	S Per expanded light curve continued . . . . .	327
B.71	S Per photographic light curve . . . . .	328
B.72	S Per photographic light curve - expanded view . . . . .	329
B.73	T Per light curve . . . . .	330
B.74	T Per light curve - expanded view . . . . .	331

B.75	T Per photographic light curve . . . . .	332
B.76	T Per photographic light curve - expanded view . . . . .	333
B.77	W Per light curve . . . . .	334
B.78	W Per light curve . . . . .	335
B.79	W Per photographic light curve . . . . .	336
B.80	W Per photographic light curve - expanded view . . . . .	337
B.81	RS Per light curve . . . . .	338
B.82	RS Per light curve - expanded view . . . . .	339
B.83	RS Per photographic light curve . . . . .	340
B.84	RS Per photographic light curve - expanded view . . . . .	341
B.85	SU Per light curve . . . . .	342
B.86	SU Per light curve - expanded view . . . . .	343
B.87	SU Per photographic light curve . . . . .	344
B.88	SU Per photographic light curve - expanded view . . . . .	345
B.89	XX Per light curve . . . . .	346
B.90	XX Per light curve - expanded view . . . . .	347
B.91	XX Per photographic light curve . . . . .	348
B.92	XX Per photographic light curve - expanded view . . . . .	349
B.93	AD Persei light curve . . . . .	350
B.94	AD Persei light curve - expanded view . . . . .	351
B.95	AD Per photographic light curve . . . . .	352
B.96	AD Per photographic light curve - expanded view . . . . .	353
B.97	BU Per light curve . . . . .	354
B.98	BU Per light curve - expanded view . . . . .	355
B.99	BU Per photographic light curve . . . . .	356
B.100	BU Per photographic light curve - expanded view . . . . .	357
B.101	FZ Per light curve . . . . .	358
B.102	FZ Per light curve - expanded view . . . . .	359
B.103	FZ Per photographic light curve . . . . .	360

B.104	FZ Per photographic light curve - expanded view . . . . .	361
B.105	V411 Per light curve . . . . .	362
B.106	V411 Per photographic light curve . . . . .	363
B.107	V411 Per photographic light curve - expanded view . . . . .	364
B.108	VX Sgr light curve . . . . .	365
B.109	VX Sgr light curve - expanded view . . . . .	366
B.110	KW Sgr light curve . . . . .	367
B.111	KW Sgr light curve - expanded view . . . . .	368
B.112	AH Sco light curve . . . . .	369
B.113	AH Sco light curve - expanded view . . . . .	370
B.114	CE Tau light curve . . . . .	371
B.115	CE Tau light curve - expanded view . . . . .	372
B.116	W Tri light curve . . . . .	373
B.117	W Tri light curve - expanded view . . . . .	374
B.118	CM Vel light curve . . . . .	375
B.119	CM Vel light curve - expanded view . . . . .	376
B.120	FG Vul light curve . . . . .	377
C.1	SS And and Vari periodograms . . . . .	379
C.2	UX Aur and V394 Aur periodograms . . . . .	380
C.3	RS Cnc and UZ CMa periodograms . . . . .	381
C.4	BZ Car and CK Car periodograms . . . . .	382
C.5	CL Car and EV Car periodograms . . . . .	383
C.6	IX Car and PZ Cas periodograms . . . . .	384
C.7	W Cep and SW Cep periodograms . . . . .	385
C.8	VV Cep and $\mu$ Cep periodograms . . . . .	386
C.9	T Cet and RW Cyg periodograms . . . . .	387
C.10	AZ Cyg and BC Cyg periodograms . . . . .	388
C.11	V Eri and TV Gem periodograms . . . . .	389
C.12	IS Gem and V959 Her periodograms . . . . .	390

C.13	$\alpha$ Her and RV Hya periodograms . . . . .	391
C.14	W Ind and U Lac periodograms . . . . .	392
C.15	Y Lyn and $\delta^2$ Lyr periodograms . . . . .	393
C.16	$\alpha$ Ori and S Per periodograms . . . . .	394
C.17	T Per and W Per periodograms . . . . .	395
C.18	RS Per SU Per periodograms . . . . .	396
C.19	XX Per and AD Per periodograms . . . . .	397
C.20	BU Per and FZ Per periodograms . . . . .	398
C.21	V411 Per and VX Sgr periodograms . . . . .	399
C.22	KW Sgr and AH Sco periodograms . . . . .	400
C.23	CE Tau and W Tri periodograms . . . . .	401
C.24	CM Vel and FG Vul periodograms . . . . .	402

# Chapter 1

## Introduction

### 1.1 Cool Luminous Variable Stars

Most luminous stars on the cool side of the H-R diagram are light variable. Those of largest light amplitude are the Mira variables, all M giants with periods of variability of typically several hundred days. They are moderately regular, although all cool variables exhibit random fluctuations in period from cycle to cycle that are evidence for some chaotic influences affecting the mechanism, probably regular pulsation, that dominates the light variations.

Closely related to Miras are semi-regular variables types A and B (SRA's and SRB's). Both types are also late-type giants. SRAs exhibit persistent periodicity, but with smaller light amplitude than Miras ( $\Delta V$  less than  $2^m.5$ ), while SRBs exhibit either poorly-defined periodicity or alternating intervals of periodic and slow irregular changes. As a group, the stars represent a mixture of population types ranging from old disk stars of nearly solar metallicity to thick disk and near-halo stars of low metallicity. Their masses must lie close to that of the Sun, around  $1\text{-}2 M_\odot$ , with surface temperatures typical of M giants, 3000-4000 K.

Somewhat related are type D semi-regular variables (SRD), which comprise a mixed group of giant and supergiant variables of spectral types F, G, and K, rather than M. They are not well understood given that they comprise a mix of types in terms of their variability. A subgroup, the UU Herculis stars, display cepheid-like variability (Fernie 1986).

The type C semi-regulars (SRC) are uniquely different from Miras, SRAs, SRBs, and SRDs in comprising a group of  $15\text{-}20 M_\odot$  red supergiants of spectral type M, all of young disk, Population I metallicity with ages of less than 10 million years. They have masses on the order of  $15\text{-}25 M_\odot$  (Stothers & Leung 1971), effective

temperatures below 4,000 K (van Dyck et al. 1988; Levesque & Massey 2005), and radii of at least several hundred  $R_\odot$  (van Dyck et al. 1988). Many are surrounded by large circumstellar dust shells created mainly by their ongoing mass loss (Humphreys & Lockwood 1972; Stencel et al. 1988). They represent stars that were O-type main sequence objects during their hydrogen burning stage, but are now in the early or final stages of helium burning (or carbon burning, etc.), about to end their lives as core-collapse supernovae (Smartt 2009) on time scales that may be as short as a few decades to several hundred years, given the time steps evident in the last stages of evolution of  $20 M_\odot$  stars (Weaver et al. 1978). The nature of their variability may therefore provide clues to the time remaining prior to their eventual demise.

Like Miras, SRAs, and SRBs, the SRC variables also appear to display random fluctuations in period (Turner et al. 2006). Establishment of reliable long-term trends in the stars therefore requires observations over many decades, or even centuries. Their periods of variability are also somewhat larger than Miras, SRAs, and SRBs. Most have periods of one or two years or even longer, although a handful of the stars appear to display periods of only a few months.

Closely related to the semi-regular variables (class SR) are stars that display much less well-organized variability, typically at low light amplitudes  $1^m.0$ . Such objects are designated as class L, the slow irregular variables, and split into two subclasses: LB, M giants similar to the SRB variables, and LC, M supergiants similar to the SRC variables. Despite many years of observation of such stars by AAVSO observers, it has not yet been possible to establish reliable values for their likely periods of variability (Percy & Terziev 2011). While some may display a degree of repeatable light variability like that of the SR stars, precise estimates of  $V$  or  $B$  brightness are needed to demonstrate that.

Whether an M supergiant variable was assigned to the SRC class or the LC classes depended upon the nature of the original study. Therefore, some SRC variables of small amplitude may have been assigned to the class on the basis of an older study tied to a restricted interval of time where they displayed a rare degree of light curve

stability. Likewise, some LC variables may have been assigned to the class on the basis of simply a lack of sizable light variations or a lack of observational data. Some SRC variables may therefore be of the LC classification, while some LC variables may eventually prove to be low amplitude SRC's once more extensive series of observations become available.

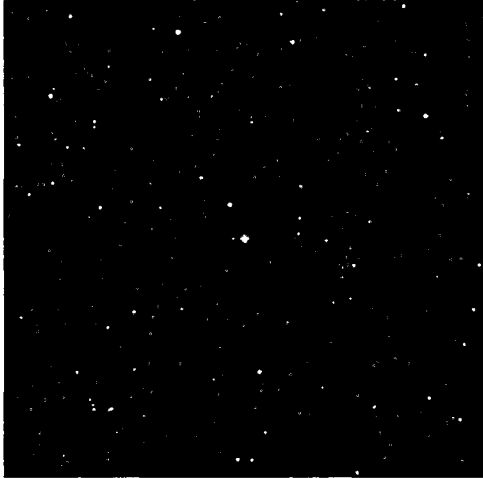


**Figure 1.1:** S Persei, an SRC Variable. Combined image created by the author using images from the Digitized Sky Survey.

## 1.2 Motivation

SRC variables, like other M supergiants, are thought to be the precursors to most core-collapse supernovae. Their periods and luminosities change with time. Like other pulsating variables, they appear to exhibit a period-luminosity relation, which means they have a potential use as distance indicators both within our own Galaxy and on the extragalactic scale. They have been identified in several nearby galaxies. As young Population I objects, they could also be used as tracers of spiral structure in our Galaxy (see, for example, Humphreys 1970).

One of the first, and one of very few, comprehensive studies of variation in M stars was made by Joy (1942). He compiled a collection of observations of spectral type and radial velocity of 118 irregular M-type variables. He found periods for some of the stars in his set, and for a subset of those he listed the phase at which the observations were made. He emphasized the importance of obtaining simultaneous light and radial velocity information in order to understand the relationship between the two variations. Although there have been many observations of Joy's M stars in the 68 years since his paper was published, there have been few attempts to study the group of SRC variables in depth. There is much we can learn about SRC variables and there are decades of underused observations of the stars. We have examined archival as well as newly-obtained observations to see what we can learn about how the stars behave as individual objects and as a group.

Understanding how SRC variables evolve leads to a better understanding of the processes that occur in the late stages of stellar evolution. Having an organized collection of temporal spectroscopic and photometric information available for SRC variables will help future efforts to model and understand the behavior of the stars. The purpose of this thesis is to collect available observational data for the stars and to use them to study the properties of the class in greater detail than has been done previously.

### 1.3 Previous Work

#### 1.3.1 The Work of Alfred Joy

As mentioned previously, Joy (1942) published a survey of spectroscopic and photometric observations of 118 "Less Regular M-Type Variable Stars". He observed that the general behavior of the stars resembles that of Mira, an M giant and one of the first known variable stars. He described their light curves as considerably irregular with periods that range from poorly-defined to fairly definite. He noted that the group is heterogeneous and likely contains several types of variable stars. One of

those types would later come to be known as the SRC variables. His survey includes a list of spectral types and brightness amplitudes with observation epochs that we use in a later chapter to examine how the stars have been changing temporally. We have made use of some of Joy's measurements in our study of the stars' cyclic variations in spectral type and radial velocity.

### 1.3.2 The Work of Stothers

Stothers (1969) showed that pulsation can account for the primary periods of variability in M supergiants. He calculated Q values for several M supergiants and showed that they agreed with those predicted by pulsation theory. He also noted that the cyclical variations in magnitude, spectral type, and radius, and the existence of a period-luminosity relation, suggest that the stars are pulsating.

### 1.3.3 The Work of White and Wing

White & Wing (1978) created a spectrophotometric classification system that used measurements in eight narrow-band filters to determine spectral types of M supergiants from photoelectric photometry. They recognized that it is difficult to classify M supergiants using conventional techniques as all M supergiants are variable and there are no reliable standard stars to use for comparison. Their system used eight narrow-band interference filters in the near-infrared that measure TiO and CN band strengths. They observed 128 M supergiants, determined spectroscopic information on temperatures and luminosities for all of the stars, and listed spectral type and luminosity class ranges for several of the more variable stars. We have obtained some of their spectrophotometric measurements and used them in our study of the changes in the stars' spectral types.

### 1.3.4 The Work of Roberta Humphreys

Humphreys (Humphreys 1970; Humphreys & Lockwood 1972; Humphreys et al. 1972; Humphreys 1983; Humphreys & Ney 1984; Elias et al. 1985) did extensive

work on supergiant stars in the Milky Way and nearby galaxies, including some SRC variables. She used M supergiants to calculate distances to some nearby galaxies. In addition to having observed the photometric and spectroscopic properties of individual stars in our own Galaxy, she compared the properties of Galactic M supergiants to the properties of M supergiants in other galaxies, finding that the average spectral types of the groups are earlier in galaxies with lower average metallicities. She compiled a catalog of bright stars in OB associations and clusters, and we have taken most of the distance moduli that we use to examine the SRC period-luminosity relation from her catalog.

### 1.3.5 The Work of David Gray

Gray (Gray 2000, 2001, 2005, 2008) studied one SRC variable,  $\alpha$  Orionis, in detail, using spectroscopic data. He found evidence that convection contributes to the star's brightness variations. The star's surface appears to be dominated by as few as 2-10 giant convection cells with lifetimes comparable to the star's primary period of approximately 400 days. By extension we can infer that convection contributes to the brightness variations of other SRC variables. It is important to remember that the stars also have long secondary periods on the order of 10 times their primary periods, and convection obviously does not explain all of the variation. Pulsation must also play a role. Gray's work highlights the complexity of the stars' atmospheres and shows us that their behavior is the result of several different processes occurring simultaneously and interacting.

### 1.3.6 The Work of Levesque and Massey

Levesque & Massey (2005) studied the physical properties and effective temperature scale of M supergiants in our Galaxy and in the Magellanic Clouds. They used MARCS models to determine spectral types and an effective temperature scale for the stars. They found that the stars were not as cool as had previously been

believed, and they refined the positions of the stars in the H-R diagram, bringing them closer to agreement with evolutionary tracks.

### 1.3.7 The Work of Turner and Rohanizadegan

Turner et al. (2006) present one of very few comprehensive studies of the brightness variations of a particular SRC variable, BC Cygni, over a long time scale. The study also illustrates the usefulness of archival data for learning about such stars. Our project performs some of the same analyses as that paper, but for more of the stars in the group.

### 1.3.8 Questions Left Unanswered by Previous Work

Much of the work done previously focuses on the spectroscopic and photometric properties of the stars, but very little of it addressed their variable nature. In the following chapters we examine the stars individually and as a group with the goal of improving our understanding of their variations. In chapter 4 we look at how the periods and average magnitudes have changed for individual stars and at cyclical changes in spectral type and radial velocity. In chapter 5 we examine properties of the group of stars using the chapter 4 results. We reinvestigate the period-luminosity relation and present a new relationship for the light amplitude as a function of spectral type and luminosity class.

## 1.4 Photometry

Ideally, the light variations of these stars would have been studied decades ago by means of precise photoelectric photometry. Unfortunately, dedicated observing runs of several years are needed for that purpose, something not possible at most observatories, and seasonal effects make color corrections for such cool, red stars unstable and difficult to establish reliably from one night to another.

Instead, all photometric studies of cool variable stars are made using photographic plates of specific star fields, or from collections of (mostly) visual, photographic, and photoelectric observations made by members of the American Association of Variable Star Observers (AAVSO). This study makes use of AAVSO observations available via the AAVSO online database at <http://www.aavso.org> as well as estimates made from survey plates in the Harvard College Observatory Photographic Plate Collection. The Harvard plates were scanned for the fields of several SRC variables in several sessions by the author, Dr. David Turner, and recent Saint Mary's B.Sc. graduate Michael Hiland. In each case the measurements were made by estimating the brightness of the variable through a small magnification eyepiece from the size and density of the star image relative to a sequence of confirmed non-variable stars lying in close proximity. Such measurements are generally accurate to within  $\pm 0.1$  to  $\pm 0.2$  magnitude, possibly slightly larger at the faint limits where the accuracy of the known magnitudes for the reference stars is less certain.

The natural sensitivity of the photographic plates in the Harvard collection corresponds roughly to that of the Jonson *B* filter, so the standard reference stars in each field were calibrated to *B* from available *BV* photometry for the stars in the literature or online surveys. The estimated accuracy of the individual photographic measures is therefore  $\pm 0.1$  to  $\pm 0.2$  in *B*.

The AAVSO measures are less reliable. While the visual acuity of good observers in the AAVSO frequently reaches a precision of  $\pm 0.1$  to  $\pm 0.2$  in their visual *V* magnitude estimates, a variety of factors often degrade the quality of the collected data. Poor observers often estimate star brightness systematically different from their true values, either through inexperience, the deleterious influence of the Purkinje effect, or, more likely, from estimating the star's brightness in inappropriate fashion. The precision of the human eye as a light detector reaches optimum values when working near the limits of vision, so eye estimates of variable stars made within a magnitude or two of the detector limit generate the best results. Some observers make the mistake of making eye estimates of bright variables using large telescopes

with much fainter visual limits, and in such cases the magnitude estimates may be off by  $0^m.5$  or more.  $\alpha$  Orionis is a particular problem since it is so bright, and all reference stars lie well away from the star, making it difficult to compare the brightness of the variable and the reference star using closely adjacent portions of the observer's retina, where the sensitivity should be about the same.

In the past, the AAVSO circumvented the problem of an intrinsic scatter of up to  $\pm 0.5$  in visual  $V$  estimates of brightness for cool variable stars by forming 10-day means, which display much smaller scatter. At present that practice has been discontinued, so the collections of eye estimates for variable stars often exhibit inordinate scatter, making it difficult to establish reliable times of light maximum or minimum. That must be kept in mind when deriving periods of variability for such stars.

## 1.5 Spectroscopy

Although most stars designated as Mira or semi-regular (SRA, SRB, SRC, and SRD) are believed to undergo radial pulsation, and such a possibility was demonstrated for SRC variables by Stothers (1969), the mechanism of such pulsation has not yet been demonstrated definitively. Spectroscopic observations were available for a few bright SRC variables from the old prism photographic spectra in the collection of the David Dunlap Observatory. The spectra, at a dispersion of mostly  $33 \text{ \AA/mm}$  (in a few cases  $66 \text{ \AA/mm}$ ) (at  $H\gamma$ ), were classified using a microscope by DGT by direct superposition of the spectra, adjacent to one another on a glass plate. Normally stellar spectra are classified in such fashion through inter-comparison of the unknown spectrum with spectra for MK standards. That was not possible here, given that some of the stars (e.g.  $\alpha$  Ori,  $\mu$  Cep) were themselves designated as standards (M2 Iab, etc.), and all such stars typically vary in temperature and luminosity during their cycles. The spectra were therefore inter-compared among themselves, and spectral

classifications were made on the basis of the criteria outlined by Keenan (see chapter 3 for more detail on classification criteria and chapter 2 for a description of the data reduction process for the CCD spectra).

As described by Keenan, the spectral subtypes for M supergiants (M0, M1, M2, M3, etc.) can be established in fairly precise fashion from the visibility of the various molecular band heads of TiO in M supergiant spectra. See table 3.3. The precision of such temperature classification can sometimes be made to  $\pm 0.5$  subtype (M3.5, M4.5, etc.) from good CCD spectra, which display the spectral flux variations extremely well. The precision of such temperature subtypes is lower with photographic spectra, but should be good to  $\pm 1$  subtype.

Luminosity ratios in stellar spectra are usually made from ratios of line strength for closely adjacent spectral lines affected in opposite fashion by differences in electron pressure,  $P_e$ , in stellar atmospheres, i.e. one line strengthens with decreasing  $P_e$  (lower gravity stars of higher luminosity) while the other weakens. Keenan provides a list of such possible pairs suitable for the identification of luminosity class in M supergiants, but some are more suitable than others for that purpose. We have used two specific features here for classification: the blend of Y II and Fe I at  $\lambda 4376$  relative to Fe I at  $\lambda 4383$ , and the blend of V I and Fe I at  $\lambda 4389$  relative to Fe I at 4383. See table 3.2. These line ratios appear to be valid over a range of effective temperatures, given that they apply in about the same fashion for both M2 and M4 stars (Keenan & McNeil 1976).

Classifications for the DDO plates were made using such techniques, and included are types for a few grating photographic spectra for southern hemisphere stars in the collection of R.F. Garrison. They are designated as "Garrison Collection" in this thesis. The same techniques were also used for grating spectra in the collection of the Dominion Astrophysical Observatory (DAO). A detailed observing log with technical specifications can be found in Appendix D. As noted, the temperature classifications provided here should be good to  $\pm 1$  subtype ( $\pm 0.5$  subtype for the CCD spectra) and to  $\pm 1$  subclass for the luminosity designations. Types such as

Ia-Iab designate an inherent uncertainty between luminosity classes Ia and Iab in the designations tied to the line ratios.

Spectral classifications from Wing are tied to spectrophotometry of the stars made using a system of narrow band filters centered at wavelengths corresponding to band heads of TiO in the near-IR, making them sensitive to spectral type (to  $\pm 0.1$  subtype) and to luminosity class (to  $\pm 1$  subclass).

## 1.6 Radial Velocities

Radial velocities were measured from all spectra by the same method, namely by measuring the wavelength shifts of individual line centers from their listed central wavelengths from the NIST database at

[http://physics.nist.gov/PhysRefData/ASD/lines\\_form.html](http://physics.nist.gov/PhysRefData/ASD/lines_form.html)

We found that while the precision of such estimates is reasonably small, the accuracy of the measurements displays an alarming tendency for systematic effects tied to continuum placement for the CCD spectra. Spectral lines superposed on deep TiO bands, for instance, tend to display systematic effects in the velocities that are difficult to explain. But although the velocities for a given star may be systematically too positive or too negative as a result of systematic errors, the trend seen in the velocities is assumed to be real. Poor continuum placement is the reason why the IRAF package *FXCOR* (which involves correlating the object spectrum with a template spectrum) generates erroneous radial velocities when it is used for cool M supergiants. As a result of such problems, we were alert to the possibility of systematic effects in the radial velocities for some stars (e.g. spectral types cooler than about M2 or M3). That is noticeable, for example, in our velocities for VV Cep and SU Persei.

Also available for two stars ( $\alpha$  Ori and VV Cep) were radial velocities obtained by Roger Griffin using his radial velocity spectrometer at Cambridge University. Such

measures are typically good to  $\pm 0.5$  km/s, but require a small offset ( $\sim 1$  km/s) to put them on the IAU system (see, for example, Griffin & Filiz Ak 2010).

## 1.7 Causes of Variability

There are three main mechanisms that are likely causes of the light variability seen in SRC variables: pulsation, convection, and dust ejections. Dust ejections are random short-term events that manifest themselves as brief, irregular decreases in mean brightness. They might look similar to eclipses in a light curve, but they do not occur at regular intervals and would not produce an obvious signal in a periodogram produced using Fourier analysis. The best way to find evidence of dust ejections is to simply examine the light curves and look for such events.

Convection can best be observed by studying the shapes of spectral line bisectors in unblended lines in high resolution spectra. Convective motion in stars' photospheres produces asymmetric bisector shapes because of the velocity gradient produced. The different parts of a spectral line are produced at different depths in the atmosphere, and if the velocity is changing because of convection, the line bisector will be asymmetric. Bisector shapes change as convective cells move across the star. Since dispersions on the order of mÅ/pixel are needed to study line bisectors, observations of convection in the stars is beyond the scope of this project. See Gray (2008) for an example of such a study in  $\alpha$  Orionis.

Stellar pulsation is caused by variable opacity in a layer of partially-ionized gas. In Cepheid-like stars, the instability occurs in a helium ionization zone, but in long-period stars, the instability is thought to occur in the hydrogen ionization zone (Christy 1962). When the star is at its smallest dimensions, the layer in question is at its highest ionization and opacity, and thus it is able to absorb energy and expand. This in turn lowers the opacity and ionization, and the star loses energy and contracts, and the pulsation continues. Cyclic variations in observable quantities such as brightness, temperature, and radial velocity are evidence of pulsation, and are the main focus of this study. We present evidence of cyclic changes in such quantities for

individual stars in chapter 4. Adherence to a period-luminosity relation by a group of stars is also evidence of pulsation, and we present a period-luminosity relation for SRC variables in chapter 5.

# Chapter 2

## Observations and Data Reduction

As this is an archival study, our observations come from a variety of sources, which we describe here, along with our data reduction procedures. Data analysis procedures are explained in the next chapter, and background information, including discussion of the uncertainties in various data sources, is given in the previous chapter.

### 2.1 AAVSO Observations

The American Association of Variable Star Observers (AAVSO) maintains an online database of visual and other magnitude measurements of variable stars made by amateur astronomers all over the world. We obtained visual magnitude estimates from the AAVSO for each star in the SRC list for which the AAVSO had data available. The data cover an interval of several decades. The reported data undergo a validation process described online at <http://www.aavso.org/data/validation.shtml> to insure quality control. The AAVSO collection is invaluable for an archival study of long-period variable stars, as it is the largest database of variable star observations and essentially the only source of data that covers a long enough baseline for a large enough number of the stars to undertake such a study. The Johnson  $V$  filter was designed to have the same peak wavelength as the human eye for normal (not dark-adapted) viewing, so visual magnitude estimates are analogous to Johnson  $V$  magnitudes (Turner & Forbes 1982). We obtained AAVSO magnitudes for 48 stars, the details of which are found in Chapter 4.

## 2.2 Data from the Harvard College Observatory Photographic Plate Collection

The Harvard College Observatory Photographic Plate Collection contains plates dating from the 1890s to the mid 1990s. We obtained magnitude estimates from the Harvard plates for the 10 SRC variables in Perseus. We have approximately 150-300 observations for each star. Observations from the photographic plates are approximately equivalent to Johnson *B* band observations, as the plates are sensitive to the blue part of the spectrum and the magnitudes for the standard stars used for comparison were Johnson *B* magnitudes. Details can be found in the stars' individual sections in chapter 4.

## 2.3 Radial Velocity Measurements from Roger Griffin

We acquired 30 radial velocity measurements for  $\alpha$  Orionis and approximately 280 radial velocity residuals (with the orbital solution removed) from Roger Griffin, obtained using his radial velocity spectrometer on the Cambridge 36-inch telescope. The measurements were taken between 2007 and 2010 and are included in our analysis of the star's radial velocity variation.

## 2.4 Radial Velocity and Spectral Type Measurements from Joy

Joy (1942) contains spectral type (not luminosity class) and radial velocity values for a number of M supergiant variables. We used Joy's observations as part of our analysis for the following stars: SS Andromedae, UX Aurigae, RS Cancri, T Ceti, BC Cygni, TV Geminorum, RS Persei, SU Persei, AD Persei, and W Triangulum.

## 2.5 Spectrophotometric Measurements from Bob Wing

We obtained spectrophotometric measurements from Bob Wing made for the paper discussed in section 1.3.3 for several stars for which White and Wing obtained multiple observations at different epochs. We include these in our analysis of the

cyclical changes in the stars' spectral types. White and Wing fit photometric observations made with eight reddening-free narrow-band filters (shown in table 2.1) to a blackbody curve to determine a spectral type. They obtained luminosity class values from a CN index calculated using filters 4 and 8. In Chapter 5, White and Wing's spectrophotometric measurements are plotted using a different color than the other spectral type values so that they can be easily identified.

**Table 2.1:** White and Wing Filters

Filter	$\lambda_c$	$\Delta\lambda$	Feature measured
1	7120	60	TiO band
2	7540	50	continuum
3	7810	40	TiO band
4	8120	50	CN band
5	10395	50	continuum
6	10540	60	VO
7	10810	60	continuum
8	10975	70	CN band

## 2.6 Photographic Spectra from the David Dunlap Observatory

David Turner traveled to the DDO in May 2008 and obtained spectral types for several of the stars in our list from photographic plates in the DDO collection. We include these measurements in our analysis of the changes in the stars' spectral types. Spectral classification was determined using the criteria described in section 3.2.

## 2.7 Photographic Spectra from the Dominion Astrophysical Observatory

We also obtained scans of high resolution photographic spectra from the DAO collection for a few of the brighter stars taken in the time period from the 1960s to the 1980s. Dave Balaam at the DAO scanned the plates and provided us with the

normalized, wavelength-calibrated 1-D spectra. Again, spectral classification was determined using the criteria described in section 3.2. Technical details and an observing log can be found in Appendix A.

## 2.8 CCD Spectra from the Dominion Astrophysical Observatory

We obtained CCD spectra for several of the stars each year from 2005-2010 at the Dominion Astrophysical observatory. These spectra cover the blue end of the visual wavelength range. The 2005 spectra have a dispersion of  $120 \text{ \AA mm}^{-1}$  and cover the wavelength range of 3500-6600  $\text{\AA}$ , while the 2006 and later spectra have a dispersion of  $60 \text{ \AA mm}^{-1}$  and cover the wavelength range of 3800-5200  $\text{\AA}$ . We obtained at least one spectrum for each star each year that the star was observed. The years for which a particular star was observed can be found in Chapter 4. A detailed observing log for each season can be found in Appendix A.

## 2.9 Data Reduction for CCD Spectra

The DAO CCD spectra were reduced using IRAF. All spectra were single-order. We first applied bias corrections, trimmed the spectra, and removed bad pixels using the *CCDPROC* package. We obtained 10-20 bias frames for each observing season and combined them using the *ZEROCOMBINE* package. Dark current corrections were not used, as the CCD was cooled to a sufficiently low temperature to make the dark current fluctuations over time negligible (in such cases, the bias correction also corrects for dark current). Iron-argon arc spectra were used for wavelength calibration. Flat fielding was done with the *APFLATTEN* package. We obtained 10-20 flat field frames for each observing season and combined them with the *FLATCOMBINE* package before using *APFLATTEN*. We used the *DOSLIT* package to extract 1-D spectra from the 2-D spectra, and to wavelength-calibrate and dispersion-correct the 1-D spectra. *DOSLIT* also removes cosmic ray hits and night sky line contamination. We then normalized the spectra using IRAF's *CONTINUUM* package, which fits a polynomial to the data to find the continuum and outputs the

ratio of the input spectra to the fitting function. The user is able to look at the fit to determine whether the program has identified proper continuum points. A very detailed description of the process of spectroscopic data reduction in IRAF can be found in Massey (1997) and Massey et al. (1992), and a guide to using *DOSLIT* can be found in Valdes (1993).

### 2.9.1 Continuum Calibration

Because normalization of M supergiant spectra is a non-trivial issue, we have included several screenshots of the process. The first image shows a wavelength-calibrated, dispersion-corrected, 1-D spectrum before continuum calibration. The second image shows IRAF's *CONTINUUM* package in use. The dashed line over-plotted on the spectrum is the fitting function. The open diamonds mark points that have been excluded by the program. The X's show points where the user has instructed the program to modify the function chosen. We found through trial and error that a 20th order Legendre polynomial seemed to provide the best balance between normalizing the spectra and not flattening out actual spectral features. As seen in the screenshot, the routine tends to miss some of the continuum points at the TiO band heads, but it is possible to manually force the fit to go through those points by manually rejecting points vertically below the tops of the band heads. Using a higher-order polynomial fits the band heads better, but it also flattens out the features within a band. Please note that the screenshots shown were created for illustration purposes only, and the polynomial fit shown is not necessarily one that would have been considered acceptable for research purposes.

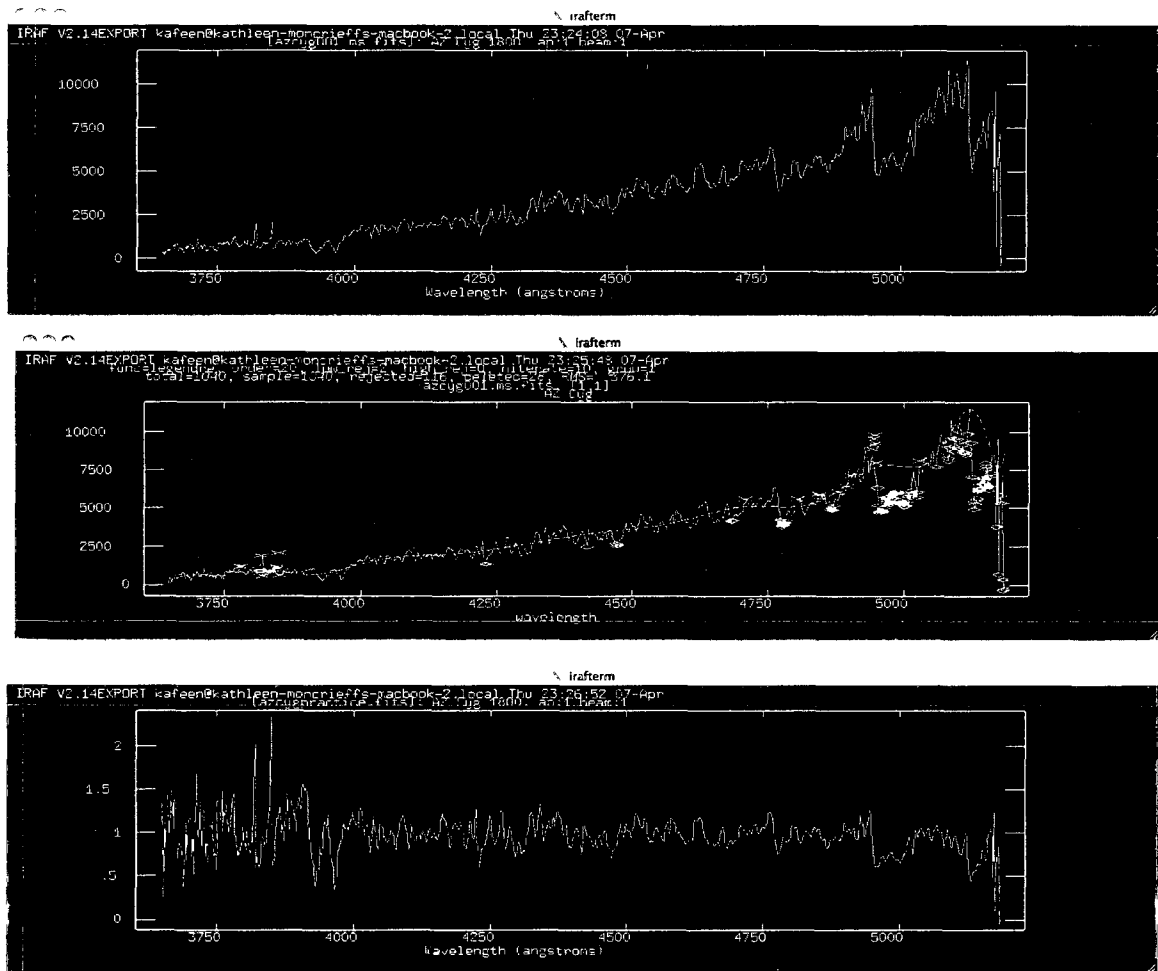


**Figure 2.1:** Top: A wavelength-calibrated, dispersion-corrected, 1-D spectrum before normalization. Middle: Running IRAF's *CONTINUUM* package. Bottom: The normalized 1-D spectrum.

## Chapter 3

### Data Analysis

#### 3.1 Period Determination

We used the software package Peranso to determine the periods of the stars. Peranso was written by Tonny Vanmunster and is available at <http://peranso.com>. Peranso contains several period finding routines. We chose the CLEANest routine, which is a Fourier decomposition routine that is appropriate for data series that vary irregularly and may have gaps in them. The CLEANest method is described by Foster (1995). We compared the results obtained with the CLEANest routine to results obtained with the ANOVA routine, which uses periodic orthogonal polynomials and the analysis of variance statistic, and the results were essentially identical. The ANOVA routine is described in Schwarzenberg-Czerny (1996). To determine uncertainties in the periods we found, we used the procedure described by Fernie (1989), which involves fitting a parabola to the Fourier peak. We used the program proFit to fit the parabolas. Uncertainties for the period values are indicated in chapter 4. Note that while this gives the uncertainty in the position of the power spectrum peak maximum, which corresponds to what could be described as an average period. In many cases the period of a star changes from cycle to cycle, and alternative method to determine an average period would be to simply take an average of the times between successive maxima. That is not possible at present because the datasets are not complete enough to determine precise times of maximum light for every cycle, but we note the alternative method here because it may be of use to future observers with better photometry.

We determined periods and examined changes in period and average magnitude by analyzing subsets of the data covering approximately 10-year intervals. 10-year intervals were chosen because they are long enough to contain several light

cycles, while still being relatively short compared to the overall data sets. It is very difficult and not always possible to study period changes in long-period semi-regular variables using O-C diagrams (see Turner et al. 2009). Figures 3.1 through 3.7 show screenshots that depict the process of using Peranso. In the figures, “Theta” is used by Peranso to represent the power in a given period value.

Average magnitudes for photometry datasets and subsets were obtained by simply taking the average of the magnitude values.  $\Delta V$  and  $\Delta B$  amplitudes were determined by subtracting the minimum magnitude from the maximum magnitude in a given dataset after eliminating any obvious outliers (i.e. if magnitude values ordered from largest to smallest showed something like 14.7, 11.0, 11.0, 11.0, 11.0, 10.9, 10.9, etc., we would have eliminated the 14.7 value from the amplitude determination).

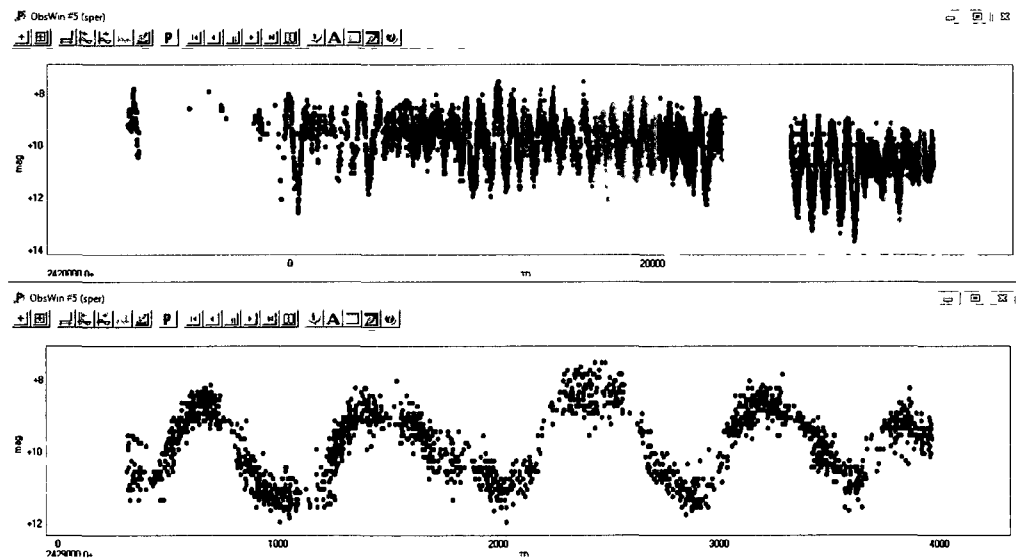


**Figure 3.1:** An example of the Peranso observations window for S Persei. The different colors in the top frame show different observation sets that can be analyzed separately or in groups. The bottom frame shows a close-up of one of the S Persei observation sets.

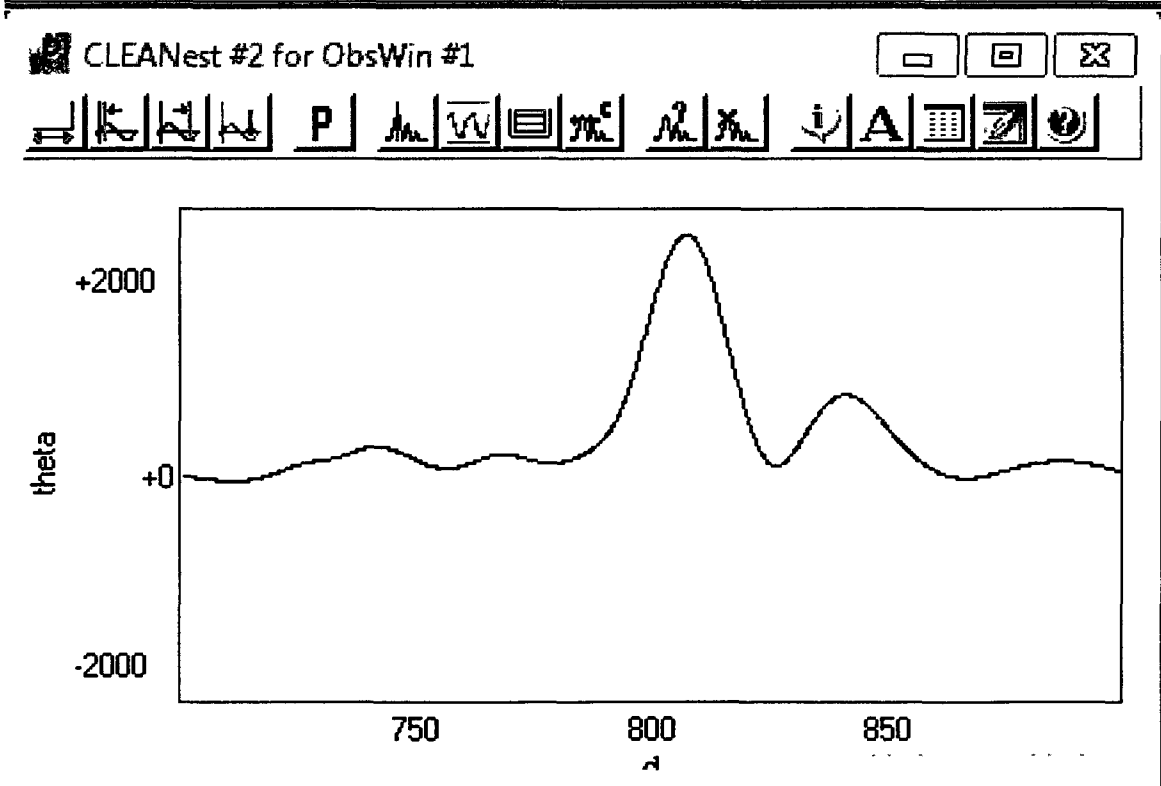
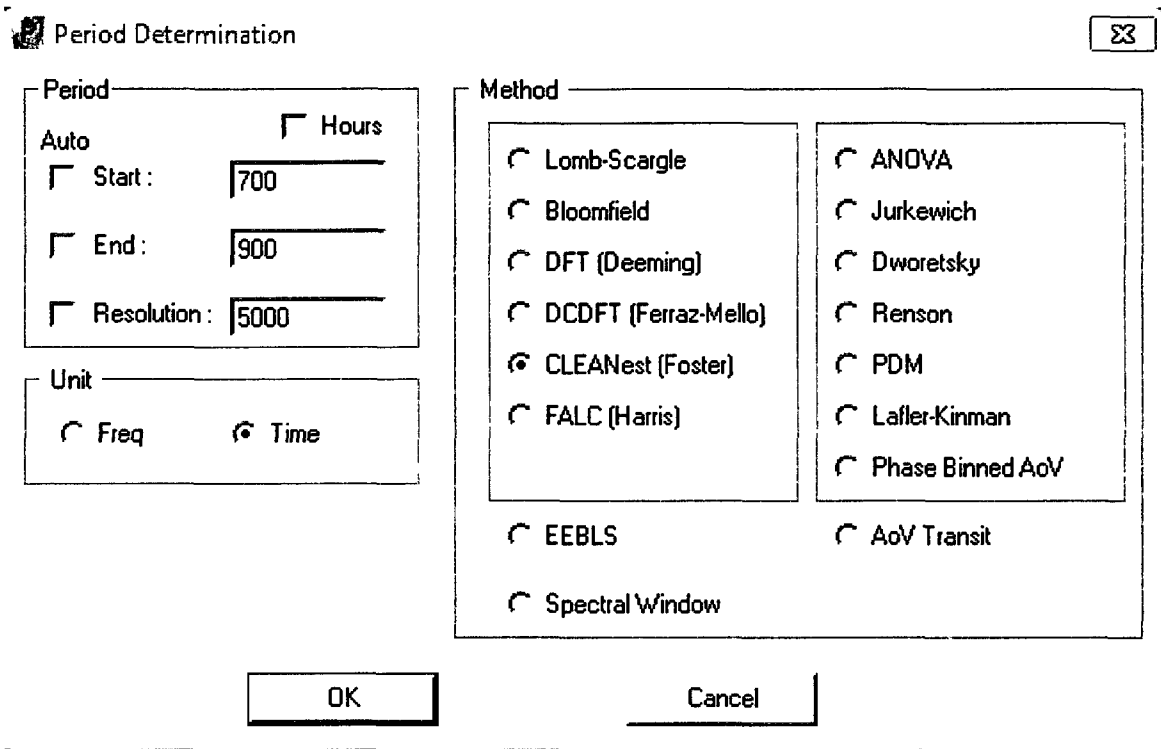


Figure 3.2: Period determination using Perano's CLEANest routine for S Persei. Top frame shows period determination window, bottom frame shows periodogram.

### Period Determination



Period		Method	
Auto	<input type="checkbox"/> Hours		
<input type="checkbox"/> Start:	<input type="text" value="700"/>	<input type="radio"/> Lomb-Scargle	<input checked="" type="radio"/> ANOVA
<input type="checkbox"/> End:	<input type="text" value="900"/>	<input type="radio"/> Bloomfield	<input type="radio"/> Jurkewich
<input type="checkbox"/> Resolution:	<input type="text" value="5000"/>	<input type="radio"/> DFT (Deeming)	<input type="radio"/> Dworetzky
Unit		<input type="radio"/> DCDFT (Ferraz-Mello)	<input type="radio"/> Renson
<input type="radio"/> Freq <input checked="" type="radio"/> Time		<input type="radio"/> CLEANest (Foster)	<input type="radio"/> PDM
Number harmonics: <input type="text" value="1"/>		<input type="radio"/> FALC (Harris)	<input type="radio"/> Lafler-Kinman
		<input type="radio"/> EEBLS	<input type="radio"/> Phase Binned AoV
		<input type="radio"/> Spectral Window	<input type="radio"/> AoV Transit

OK

Cancel

### ANOVA #1 for ObsWin #1

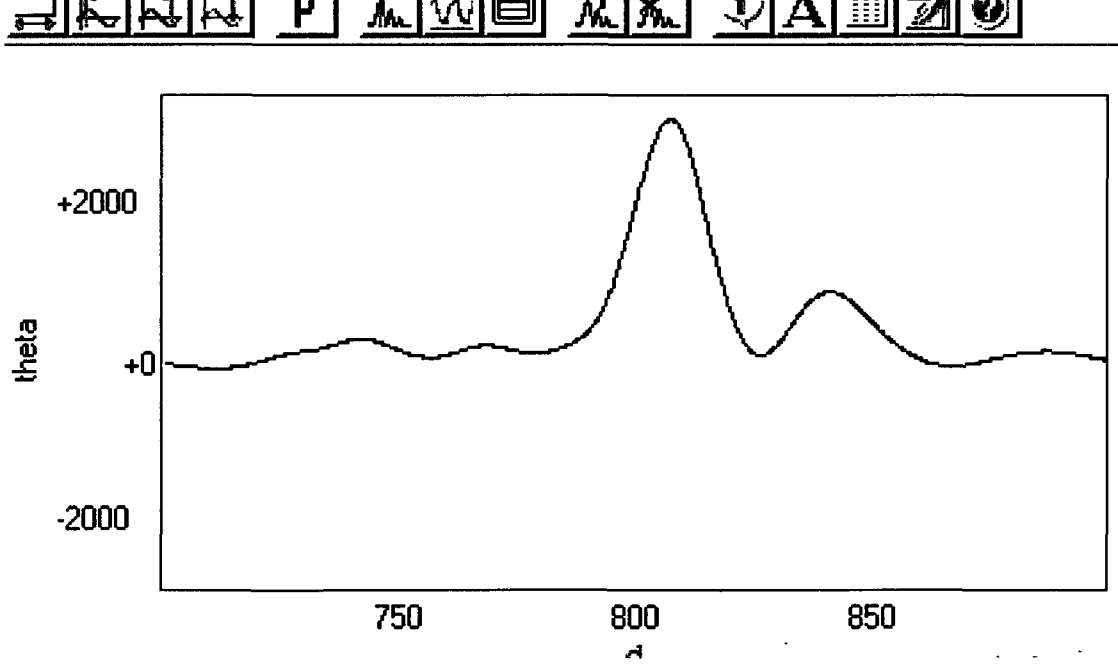


**Figure 3.3:** Period determination using Perano's ANOVA routine for S Persei. Top frame shows period determination window, bottom frame shows periodogram. Note that results match those for the CLEANest routine shown in the previous figure.

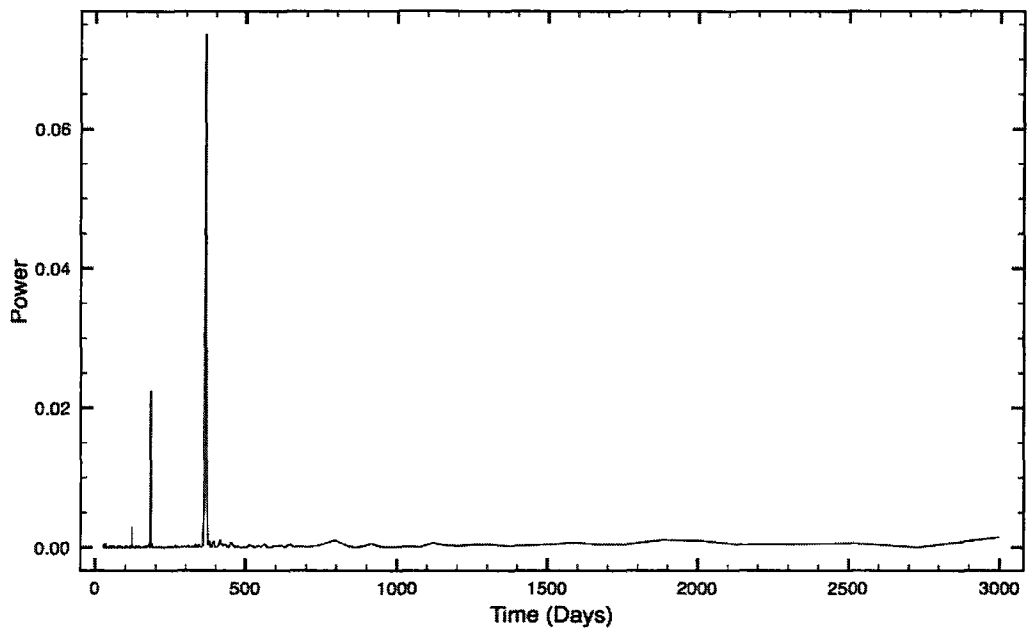


**Figure 3.4:** Spectral window for the Fourier analysis for S Persei shown in figure 3.2, used to check for aliasing by identifying patterns caused by the gaps in the data. Note that there are no peaks near the 806 day period value found for S Persei in the 2 preceding figures, but there are small peaks near values of 1 year, 1/2 year and 1/3 year.

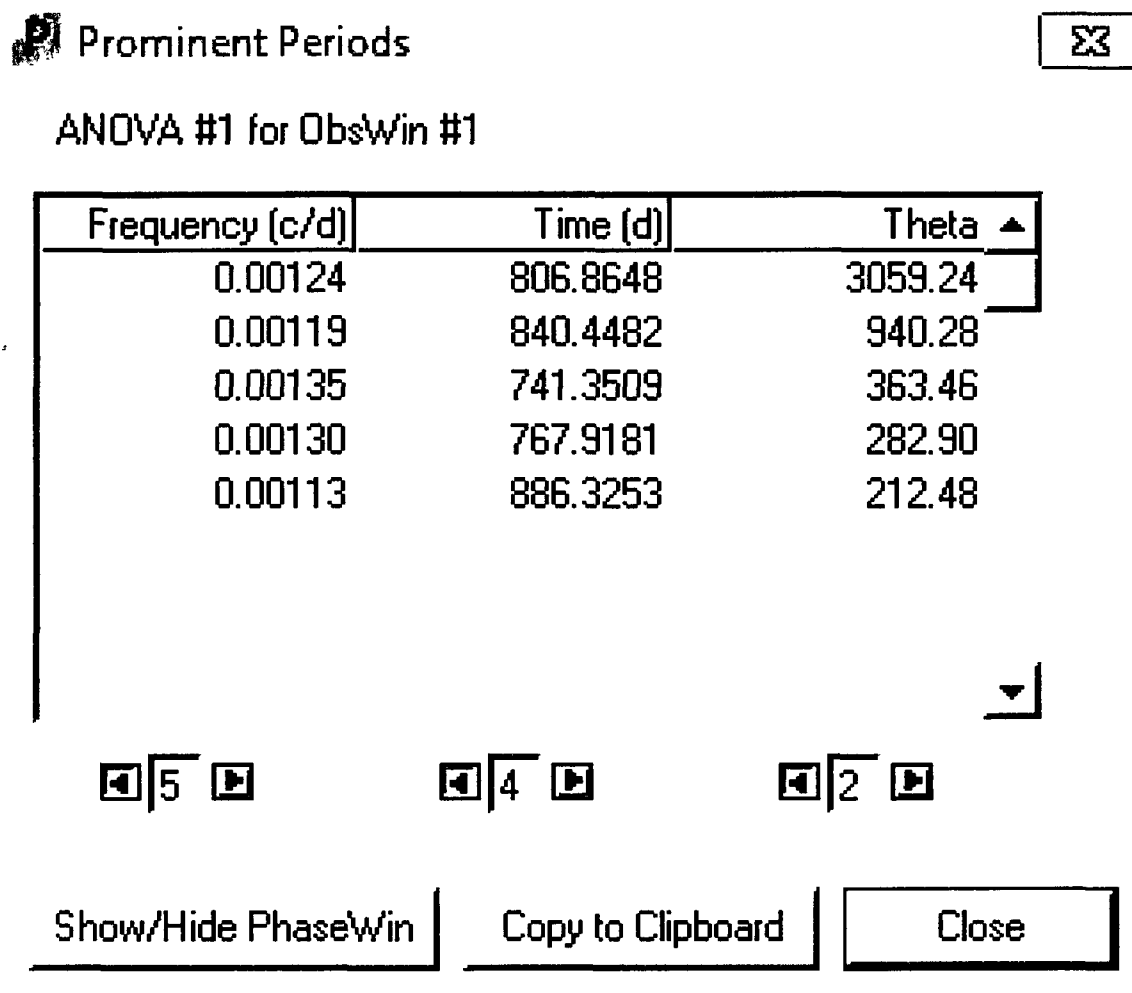


Figure 3.5: An example of Peranso's prominent periods window.

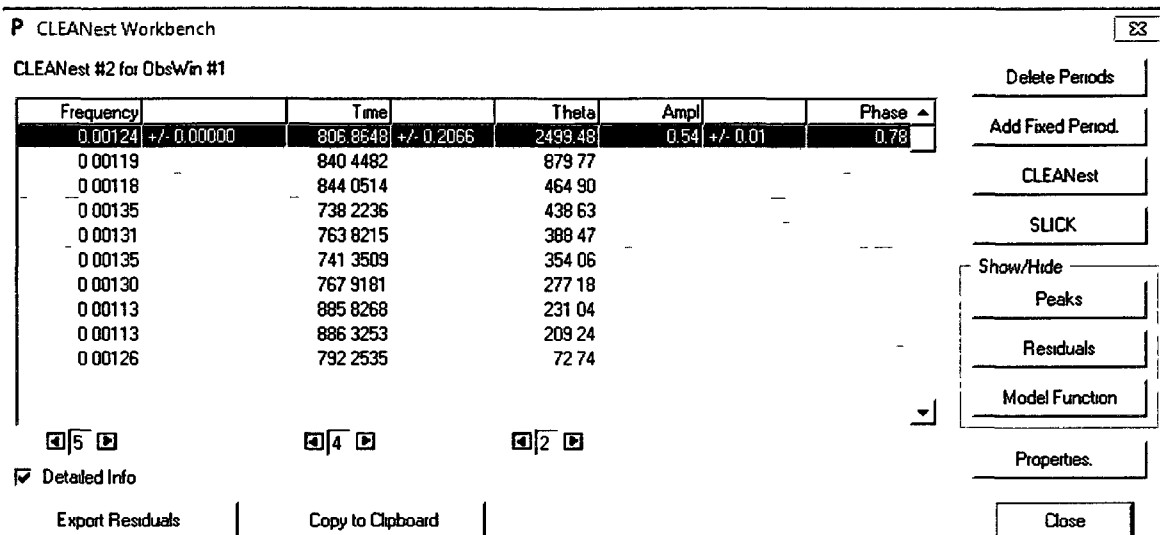


Figure 3.6: An example of Peranso's CLEANest workbench.

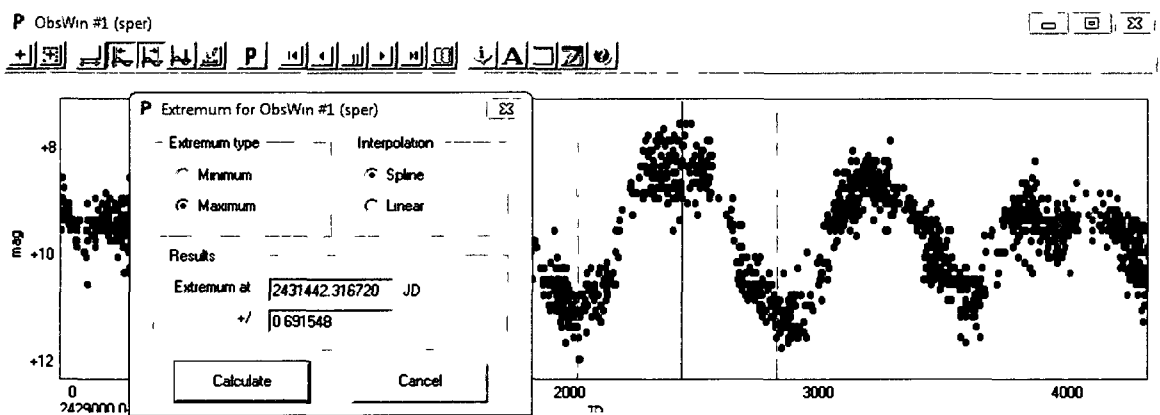
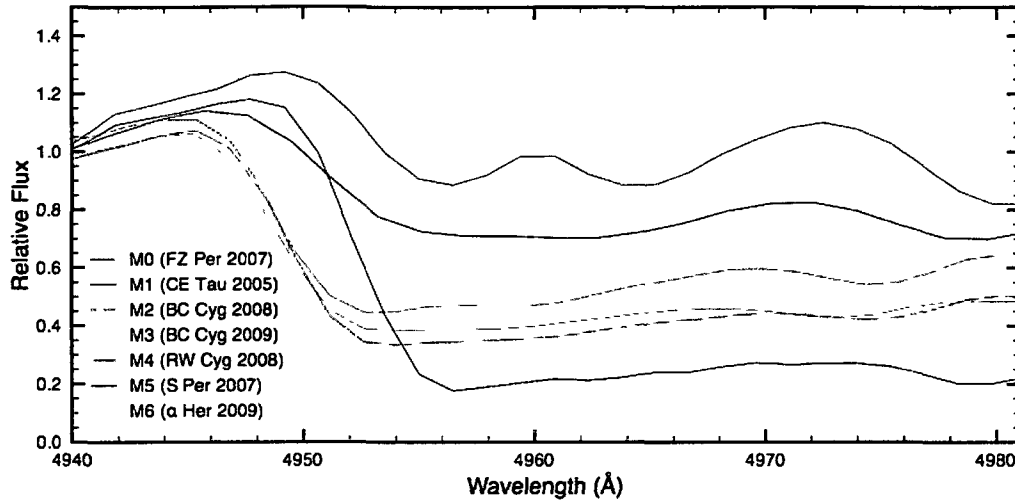


Figure 3.7: An example of Peranso's extremum-finding function, used to determine times of maximum light.

### 3.2 Spectral Classification

We used spectral atlases (Abt et al. 1968; Houk et al. 1974; Keenan & McNeil 1976; Houk & Newberry 1984) and Phillip Keenan's classification criteria for M stars published in Gray (2009) to identify lines that were temperature or luminosity indicators. We then examined the observed spectra to see which of the lines identified were best for classification. Some were easier to use than others because of their location and proximity (or lack thereof) to other lines. For example, all of the molecular band heads in the region are temperature indicators, but the effect is easiest to see in the TiO band head at 4954Å. Keenan's criteria are reproduced in table 3.3. Table 3.1 summarizes the lines that we found most useful for classification. Table 3.2 lists approximate line ratios for different luminosity classes. Figure 3.8 shows the behavior of the 4953Å TiO band head in different stars at different spectral types, and figure 3.9 shows the behavior of the 4389Å line compared to the 4383Å line in different luminosity classes. Shifts caused by differing radial velocities and problems with normalization are evident in the plots, but we were aware of and accounted for the shifts when determining spectral types. The newly-obtained CCD spectra and scanned photographic spectra were classified by overplotting spectra from the same star, as well as spectra from different stars with the same suspected spectral type, in order to see relative line depths. As a reality check, spectral type results were compared to published spectral types from the Simbad database. As program stars are not well-studied, it is not possible to find published values for what spectral type a star should have at a given phase, but we assumed published spectral types were roughly equivalent to average spectral types for the stars. Again we stress the fact that this study is the first of its kind, and our goal was to establish trends, not to produce precise measurements. The method of comparing the spectra of a given star to one another during classification should be sufficient to establish trends. Future studies involving long-baseline photometric observing campaigns could also make use of color index values obtained at the same epoch as spectroscopic measurements as



**Figure 3.8:** The behavior of the 4953 $\text{\AA}$  TiO band head as a function of spectral type.

a reality check for the spectral types. Unfortunately, such information does not currently exist. As stated in chapter 1, we estimate our uncertainties to be  $\pm 0.5$  subtype for the spectral types and  $\pm 1$  subclass for the luminosity classes.

**Table 3.1:** Especially useful lines for classification.

$\lambda$ (Å)	Species	Behavior
4861	$H\beta$	Appears to weaken with decreasing temperature when compared with nearby continuum, which is suppressed by the TiO band head.
4953	TiO band head	Strengthens with decreasing temperature. $\lambda 4953$ and other band heads are the primary determinants of spectral type for M stars. The $\lambda 4953$ band head is easiest to use.
4389	V I	Strengthens with increasing luminosity when compared with nearby Fe I line at $\lambda 4383$ Å. (See luminosity classification table for more information.)

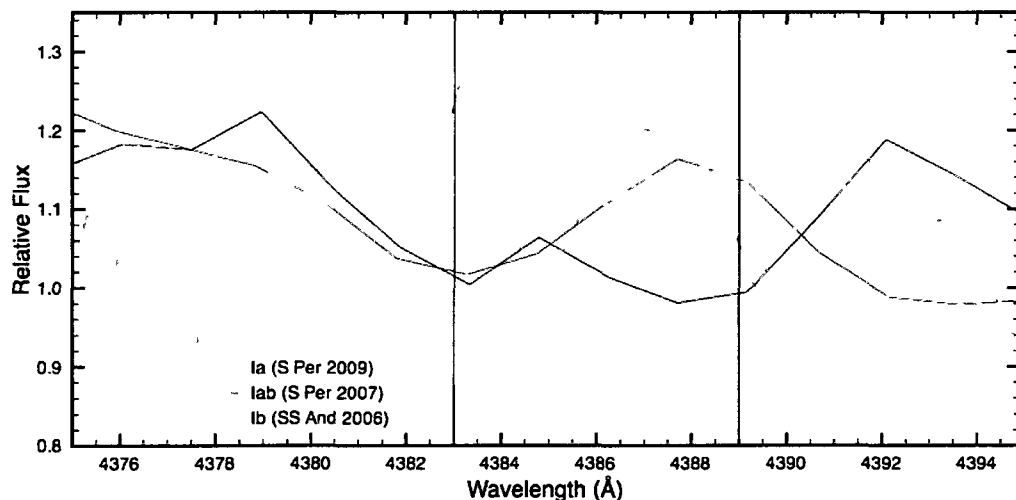


**Figure 3.9:** The behavior of the  $4389\text{\AA}$  line as a function of luminosity class.

**Table 3.2:** Approximate luminosity classification ratios

Luminosity Class	$\lambda 4376/\lambda 4383$	$\lambda 4389/\lambda 4383$
Ia	>1	$\sim 1$
Iab	$\sim 1$	$\sim 0.5$
Ib	<1	$\sim 0.25$
II	$\sim 0.5$	$\sim 0.1$
III	$\sim 0.25$	=0

**Table 3.3:** Keenan's classification criteria for M stars

Type	Blue Region	Visual Region
M0	$\lambda 4954$ clearly seen. The marginal appearance of this band at scales of $\sim 100 \text{ \AA mm}^{-1}$ helps define type K5.	$\lambda 6159$ clearly seen $\lambda 5448, \lambda 5167$ present
M1	$\lambda 4761$ present.	$\lambda 5448$ clearly seen. $\lambda 5167$ is now strong enough to form a distinct break in spite of the strong atomic lines nearby.
M2	$\lambda 4804$ present. Broadening of $\lambda 4667$ noticeable.	$\lambda\lambda 5448, 6159$ stronger.
M3	$\lambda 4584$ present; 4667, 4804 clearly seen.	$\lambda\lambda 5597, 5847$ present.
M4	$\lambda\lambda 4626, 4667$ distinct; $\lambda 4848$ present.	$\lambda\lambda 5759, 5810$ distinct.
M5	$\lambda\lambda 4352, 4462$ distinct.	VO 5736 present.
M6	$\lambda 4395$ present and becomes distinct at M6.5. $\lambda 4422$ distinct on plates of larger scale.	VO 5736 slightly weaker than $\lambda 5759$ .
M7	$\lambda\lambda 4082, 4310$ present.	VO 5736 = $\lambda 5759$ $\lambda\lambda 5591, 5615$ fairly strong.
M8	All of the spectrum longward from $\lambda 4100$ presents banded appearance. $\lambda\lambda 4082,$ 4310 fairly strong.	VO 5736 = $\lambda 5759$ $\lambda 5591$ comparable with $\lambda 5597$

### 3.3 The Effective Temperature Scale

The spectral type plots shown in later chapters use the effective temperatures given in table 3.4, from the effective temperature scale derived by Levesque & Massey (2005), which were calculated using MARCS model atmospheres. We show the corresponding  $T_{\text{eff}}$  values on our plots of spectral type versus phase. The other notable temperature scale for M supergiants is from Lee (1970). Lee's temperature scale is based on broadband colors and observed interferometric diameters rather than stellar atmosphere models, as models that accurately treated molecular opacities in M supergiant atmospheres were unavailable at the time. In addition to being based on model atmospheres, the Levesque and Massey scale provides better agreement with evolutionary models, and so we have chosen to assign temperatures based on this new scale, which is about 400K hotter than Lee's. We emphasize, however, that the current study is an attempt to understand the variability of the stars, and not necessarily an attempt to determine precise physical quantities. Our goal is simply to show that the temperatures of the stars change cyclically rather than to establish precise temperature values. As the effective temperatures were assigned solely based on our determined spectral types, uncertainties can be considered equivalent to  $\pm 0.5$  spectral subtype (i.e. if a star was assigned a spectral type of M2 and thus temperature 3660 K, the uncertainty in the temperature would be +50/-45 K).

### 3.4 Radial Velocity Measurement

We used the IRAF package *RVIDLINES* to calculate radial velocities for the spectra. *RVIDLINES* is a routine that uses the differences between observed wavelengths in a spectrum and rest wavelengths of the same lines to calculate a radial velocity. The user creates a list of rest wavelengths, then marks several lines in the spectrum and enters the rest wavelengths of the marked lines. We used the database at <http://physics.nist.gov> to create a list of approximately 250 strong lines of H I,

**Table 3.4:** Effective temperature scale for M supergiants, taken from Levesque & Massey (2005)

Spectral Type	Temperature (K)
M0	3790
M1	3745
M1.5	3710
M2	3660
M2.5	3615
M3	3605
M3.5	3550
M4-M4.5	3535
M5	3450

Fe I, Fe II, Ca I, Ca II, and Sr II in the wavelength region of our spectra. The software then uses the list to identify as many more lines in the spectrum as possible, and computes a velocity using the average wavelength shift, along with an uncertainty. When the software is run in heliocentric mode, it also uses the observatory location keyword in the header along with the date and time information to automatically apply a heliocentric correction to the computed velocity. The CCD spectra have much lower resolution than the photographic spectra, which means they have higher uncertainties, but the general pattern of variation can still be seen. For stars with sufficient radial velocity data points, we fit sine waves to the radial velocity versus phase curves using the program proFit. Figures 3.10 shows a screenshot of the *RVIDLINES* process (the screenshot shown was created for demonstration purposes only, and the lines marked are not necessarily centered properly and have not been checked for accuracy, as was done when actual measurements were being made).

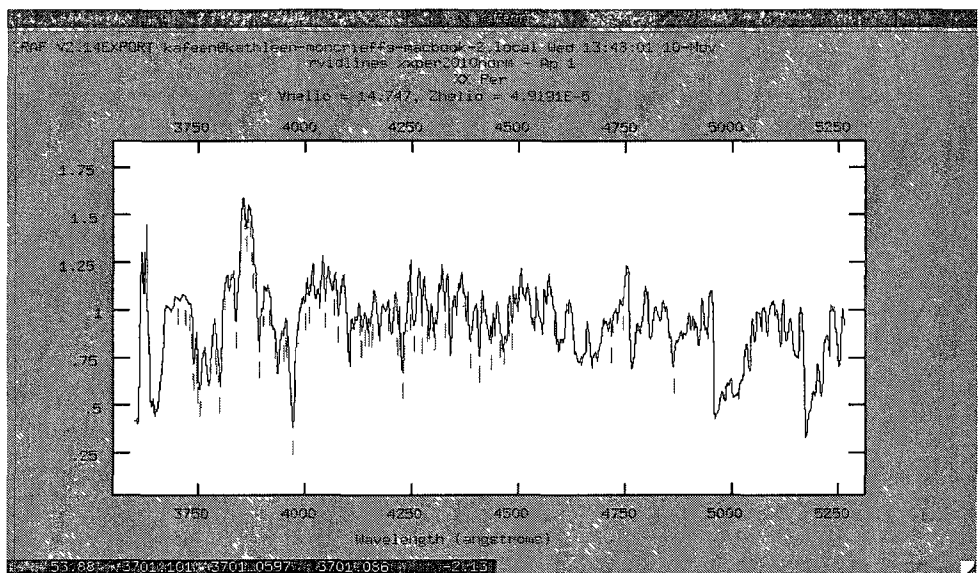


**Figure 3.10:** RVIDLINES in use. The red marks indicate spectral lines. The user is able to zoom in and mark individual lines, tell the program to find lines automatically, and examine the lines that the program has marked and delete erroneous lines that the program may have found.

## Chapter 4

### Results for Individual Stars

We present here the results of our analysis of the available data for each of 49 stars. All but one of the stars have AAVSO visual magnitude estimates, and 13 of the stars have photographic magnitude estimates from the Harvard plate collection. We present values of the average magnitude and period at approximately 10 year intervals for each star with a sufficient number of magnitude estimates, as well as overall periods and average magnitudes. We show light curves for the stars and plots of average magnitude and period as a function of time, as well as plots of average magnitude versus  $\log P$ , where  $P$  is the period. In plots of average magnitude and period versus time, horizontal lines indicate the average magnitude or period for the entire dataset.

For each star for which we have spectra, we determined spectral types and radial velocities,  $V_R$ , at various epochs. We present a montage of the CCD spectra for each star as well as plots showing changes in spectral type and  $V_R$  as functions of phase. Individual spectra are plotted in Appendix A. For stars with sufficient phase coverage, we fitted a sine wave to the radial velocity data. Sine waves were fitted using a Monte Carlo fit in all 4 parameters with the program proFit. From the sine wave, we determined the phase at which it goes through mean radial velocity after it reaches maximum radial velocity. Maximum radial velocity indicates the star's greatest photospheric recession, so the star should reach its smallest dimensions a quarter cycle later when it passes through the systemic velocity for the system. There are several stars for which we have only been able to obtain one spectrum. Although we cannot examine their variations in  $V_R$  and spectral type, we include our measurements of their radial velocities and spectral types, as they may be of use to future observers. Please note that throughout this chapter, dates listed in tables are

written as HJD – 2400000. A brief summary of the results and data available for each star can be found at the end of the chapter. Light curves for the stars can be found in Appendix B. Table 4.1 summarizes some basic information for the 49 stars discussed here (period, spectral types from SIMBAD, average  $V$  magnitude, available data, cluster/association membership, and binarity).

**Table 4.1:** Summary of Information for Individual Stars

Star	Coordinates (J2000)	(V) (AAVSO)	Spectral Type	Adopted Period	GCVS Period	AAVSO Observations	Harvard Observations	Spectral Type Measurements	Radial Velocities	Cluster Member or Binary?
SS And	23 11 30 0698 +52 53 12 479	9 79	M6-M7 Iab	178	152 5	475		6	6	no
V Ari	02 15 00 0767 +12 14 23 610	8 54	C5 II	58 7	58 7	124				no
UX Aur	05 15 57 8835 +49 32 47 266	8 71	M4-5 Ia-II	357/90	90	87		4	4	no
V394 Aur	06 06 22 4463 +29 30 44 689	6 21	M4 Ib II	32 5	32 9	8		4		no
RS Cnc	09 10 38 7990 +30 57 47 300	6 19	M6 M7 Iab Ib	240/120	120	9540		10	6	no
UZ CMa	06 18 47 35 17 02 27 0	11 68	M6 II	86 8	82 5	2613				no
BZ Car	10 54 06 2521 62 02 32 817	8 18	M2-4 Ia-Ib	130/97	97	881		4		no
CK Car	10 24 25 3580 60 11 29 039	8 05	M3 5 Iab	533	525	876				Car OB1-D (Levesque & Massey 2005)
CL Car	10 53 59 8814 61 05 31 339	8 83	M5 Iab	513	513	1111	769			
EV Car	10 20 21 608 60 27 15 55	8 20	M4 5 Ia	347	347	692				no
IX Car	10 50 26 2988 59 58 56 563	7 6	M2 Iab	350 400	400	1801	804			Car OB1 E (Levesque & Massey 2005)
PZ Cas	23 44 03 2819 +61 47 22 182	9 15	M2 4 Ia	253	925	1141		11	4	Cas OB5 (Levesque & Massey 2005)
W Cep	22 36 27 563 +58 25 33 97	7 67	K0 1 Ia Ib	2000/350		8005		7	5	Cep OB1 (?)
SW Cep	21 25 45 9174 +62 34 26 569	8 62	M3 5 Ia Iab	599/70	70	84		4	4	Cep OB2 B (Stencel et al 1988)
VV Cep	21 56 39 1437 +63 37 32 006	5 18	M4 Ia Iabe + B8 Ve	285	7430 (eclipse)	6970		6	4	B type companion (Wawrukiewicz & Lee 1974) Cep OB2 B (Humphreys 1978)
MY Cep	22 54 31 71 +60 49 38 9		M7 Ia					1	1	no

**Table 4.2:** Summary of Information for Individual Stars (continued)

Star	Coordinates (J2000)	$\langle V \rangle$ (AAVSO)	Spectral Type	Adopted Period	GCVS Period	AAVSO Observations	Harvard Observations	Spectral Type Measurements	Radial Velocities	Cluster Member or Binary?
$\mu$ Cep	21 43 30 4609 +58 46 48 166	4 15	M2 Iae	700-1000	730	47489		20	5	Trumpler 37 (Alksnis 1961)
T Cet	00 21 46 2737 -20 03 28 885	6 11	M5-6 IIe	160	158 9	6395		5	5	no
RW Cyg	20 28 50 590 +39 58 54 43	8 82	M2-4 Ia-Iab	520	550	1907		3	3	Cyg OB9 (Humphreys 1978)
AZ Cyg	20 57 59 4457 +46 28 00 618	8 63	M2-4 Ia-Ib	459	459	654		10	5	no
BC Cyg	20 21 38 5471 +37 31 58 932	9 72	M2 4 Ia Ib	693	700	937	866 (Harvard and Sternberg)	16	7	Berkeley 87 (Turner & Forbes 1982)
V Eri	04 04 18 802 -15 43 30 53	8 92	M6 II	290/97	97	3633				no
TV Gem	06 11 51 4140 +21 52 05 643	6 87	K5 5-M1 3 Iab	425/70		9501		13	3	Gem OB1 (Levesque & Massey 2005)
IS Gem	06 49 41 3110 +32 36 24 321	5 82	K3 II	359/47	47	3332				no
V959 Her	17 36 21 4199 +27 33 59 899	6 46	M4 Ib II	140		40		4		no
$\alpha$ Her	17 14 38 8584 +14 23 25 198	3 3	M5 Ib II	508 7		15632		8	5	Optical triple
RV Hya	08 39 43 758 -09 35 13 01	7 86	M5 II	243/116	116	410				no
W Ind	21 14 22 803 53 01 34 66	9 27	M4 5 IIe	198	198 8	722				no
U Lac	22 47 43 4271 +55 09 30 309	9 89	M4 Iabpe + B	395		345		9	5	B-type companion (Wawrukiewicz & Lee 1974) Cep OB1 (Humphreys 1978)
Y Lyn	07 28 11 6109 +45 59 26 207	7 39	M6 Ib II	283/110	110	8989		2	2	no
$\delta^2$ Lyr	18 54 30 2838 +36 53 55 007	4 46	M4 II	627		2141		1		B-type companion, Stephenson 1 (Stephenson 1969)

**Table 4.3:** Summary of Information for Individual Stars (continued)

Star	Coordinates (J2000)	(V) (AAVSO)	Spectral Type	Adopted Period	GCVS Period	AAVSO Observations	Harvard Observations	Spectral Type Measurements	Radial Velocities	Cluster Member or Binary?
$\alpha$ Ori	05 55 10 3053 +07 24 25 426	0 74	M1 2 Ia Ib	425/2335	2335	23349		21	35	no
S Per	02 22 51 7151 +58 35 11 423	9 99	M3 M7 Iae	807	822	27313	586	11	5	Per OB1-D (Levesque & Massey 2005)
T Per	02 19 21 8795 +58 57 40 327	8 89	M2 Iab	2457	2430	9212	567	5	5	Per OB1-A (Humphreys 1978)
W Per	02 50 37 8911 +56 59 00 251	9 79	M3 7 Ia-Iab	531/485	485	17051	415	4	4	Per OB1-D (Levesque & Massey 2005)
RS Per	02 22 24 297 +57 06 34 36	8 83	M4 Iab	244	244 5	2310	194	7	7	Per OB1-D (Levesque & Massey 2005)
SU Per	02 22 06 8939 +56 36 14 866	8 11	M3 5 Iab	468/533	533	3282	197	17	11	Per OB1-D (Levesque & Massey 2005)
XX Per	02 03 09 361 +55 13 56 60	8 47	M4 Ib + B	403	415	3412	263	4	4	B-type companion (Wawrukiewicz & Lee 1974) Per OB1-D (Humphreys 1978)
AD Per	02 20 29 0028 +56 59 35 226	8 3	M2 5 Iab	371	362 5	3338	196	8	8	Per OB1-D (Humphreys 1978)
BU Per	02 18 53 295 +57 25 16 81	9 4	M3 5 Ib	367/2960	367	1468	194	7	3	Per OB1-D (Levesque & Massey 2005)
FZ Per	02 20 59 676 +57 09 30 59	8 33	M0 5-2 Iab	371/184	184	2023	196	5	5	Per OB1-D (Humphreys 1978)
V411 Per	03 15 08 4471 +54 53 02 970	9 62	M3 4 Ia	467	467	29	160	4	4	no
VX Sgr	18 08 04 0485 -22 13 26 614	9 77	M4-10 Iae	756 65	732	6970				ASCC 093 (Kharchenko et al 2005)
KW Sgr	17 52 00 7257 28 01 20 562	9 67	M0 4 Ia	352/670	670	529		5		Sgr OB5 (Levesque & Massey 2005)
AH Sco	17 11 17 0201 32 19 30 728	7 94	M4 5 Ia Iab	766	713 6	1644				no
CE Tau	05 32 12 7511 +18 35 39 243	4 81	M2 Iab Ib	174	165	3280		21	3	no
W Tri	02 41 30 5714 +34 30 57 967	8 20	M5 II	593	108	5719		5	5	no
CM Vel	10 07 32 8240 53 15 36 534	8 16	M0-5 II	762	780	238				no
FG Vul	20 34 33 0365 +28 16 51 355	9 61	M5 II	352/86	86	29		2	2	NGC 6940 (Mermilliod et al 2008)

#### 4.1 Explanation of Table Columns for Individual Stars

The section for each star contains up to two tables, depending on what data are available for the star. The first table contains information about visual observations from the AAVSO database and period estimates. The columns are:

- Subset: The first row contains information about the entire data set. The second and subsequent rows contain information about subsets of the data in chronological order and divided into approximately 10-year intervals
- Dates: The beginning and ending HJD of the observations, written as HJD – 2400000
- V: The average visual magnitude for the observations
- % Diff.: The % difference in average visual magnitude compared to the preceding subset (not available for subset 1 or for the entire data set)
- $\Delta V$ : The difference between the maximum and minimum visual magnitude for the subset
- $P$  (days): The period found through Fourier analysis, with associated uncertainty, following the methods described in Chapter 4
- $N$ : Number of data points in the data set or subset
- % Diff.: The % difference in period compared to the preceding subset (again, not available for subset 1 or for the entire data set)

The second table contains information about any archival or newly obtained spectra for the star. The columns are:

- Year: The calendar year in which the observation was made
- HJD: The heliocentric Julian date of the observation

- Phase: The phase of the observation, where 0.0 is light maximum, calculated using the period and time of maximum light stated for the star
- $V_R$ : The radial velocity in km/s with associated uncertainty where available. Where the data source is “DAO CCD” or “DAO Photographic”, radial velocities were determined using the technique described in Chapter 4. Where the source is another author, details about the radial velocity determination can be found in the associated reference.
- Spectral type: Spectral type and luminosity class (where available) for the observation. Where the data source is “DAO CCD”, “DAO Photographic”, “DDO”, or “Garrison collection”, the value was determined using the classification procedure described in Chapter 3. For other sources, classification information can be found in the associated reference.
- Source: One of the following options (more information on sources can be found in chapter 2):
  - DAO CCD: Our own newly-obtained observations from the DAO
  - DAO Pg: Digitized archival photographic spectra from the DAO collection
  - DDO: Photographic spectra from the David Dunlap Observatory examined by David Turner
  - Garrison: A photographic spectrum from Bob Garrison’s collection examined by David Turner
  - R. Griffin: Radial velocity measurements obtained from Roger Griffin
  - Joy: Measurements reported in Joy (1942)
  - Wing: Spectrophotometric measurements obtained from Bob Wing

## 4.2 SS Andromedae

Figure 4.1 shows SS And's variations in spectral type and radial velocity, as well as a montage of CCD spectra taken at different epochs. The observations were phased using a period of 178.35 days and a time of maximum light of JD2440519, determined from the AAVSO observations. There are not enough observations to determine at what phase SS And reaches its highest temperature. Its luminosity class did not vary according to our limited observations. Figure 4.2 shows SS And's changes in period and average visual magnitude taken at approximately 10-year intervals. The AAVSO observations do not indicate a regular pattern of variability in SS And, although some peaks in brightness are evident. Also, any evidence for period changes in the star is limited by the small number of observations, seasonal effects in the data, and the different eye sensitivities of AAVSO observers, so any evidence for temporal changes in period from Fourier analysis must be considered in that light. The light amplitude is small,  $\Delta V \simeq 1^m.2$ . Consequently, tracing potential pulsation in the star is nearly impossible with the limited observations. Additional photometric data with a long baseline are needed to establish that the star is a true SRC variable and not an LC variable. The few spectroscopic observations would be more useful if they could be properly phased to the star's light variations.

**Table 4.4:** AAVSO Observations of SS Andromedae

Subset	Dates	$\langle V \rangle$	% Diff.	$\Delta V$	$N$	$P$ (days)	% Diff.
All	29544-55159	9.70	...	3.0	475	$178.35 \pm 0.04$	...
1	29544-32920	9.34	-3.71	1.6	25	$180.93 \pm 1.25$	1.45
2	33237-36842	9.76	0.62	1.7	87	$174.69 \pm 0.46$	-2.05
3	36901-40486	9.89	1.96	2.8	124	$177.59 \pm 0.33$	-0.43
4	40514-44103	9.87	1.75	2.1	70	$171.73 \pm 1.00$	-3.71
5	44428-47793	9.55	-1.55	1.6	13	$175.18 \pm 1.14$	-1.78
6	47822-51107	9.52	-1.86	1.3	22	$176.36 \pm 1.21$	-1.11
7	52322-55159	9.51	-1.96	1.3	134	$175.60 \pm 0.52$	-1.54

**Table 4.5:** Spectroscopic observations of SS Andromedae

Year	HJD	Phase	$V_R$ (km/s)	Spectral Type	Source
1939	2428852	0.8212	-23	M6	Joy
1939	2429562	0.7877	-32	M6	Joy
1940	2429854	0.4190	-25	M6	Joy
1940	2429894	0.6425	-22	M5	Joy
2006	2454027	0.4623	$-0.8 \pm 7.8$	M6 Ib	DAO CCD
2010	2455489	0.6303	$-4.0 \pm 17.6$	M7 Ib	DAO CCD

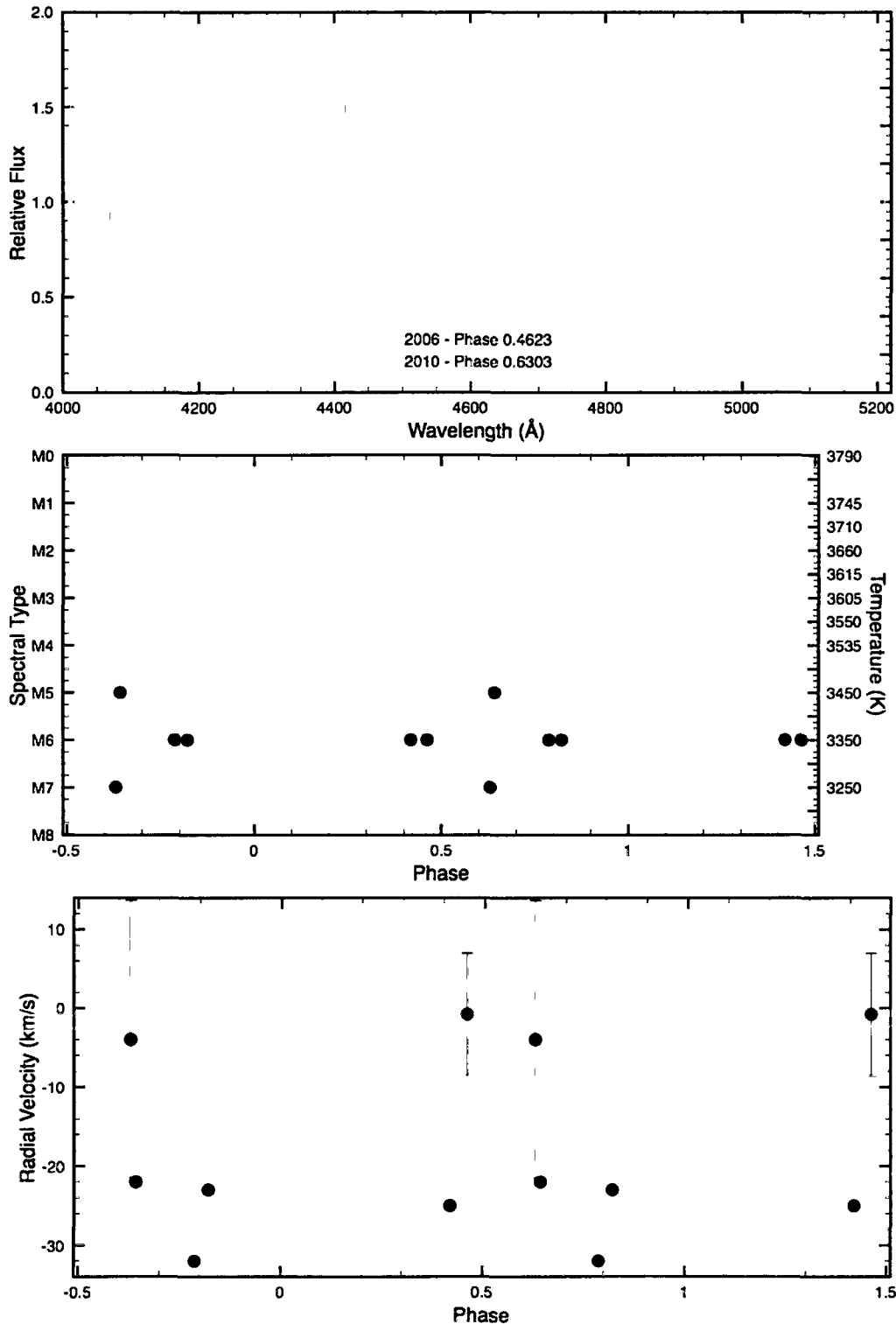


**Figure 4.1:** Spectral variation in SS Andromedae. Top: Spectra from different epochs. Middle: Spectral type as a function of phase. Bottom: Radial velocity as a function of phase. Data phased with 178.35 day period.

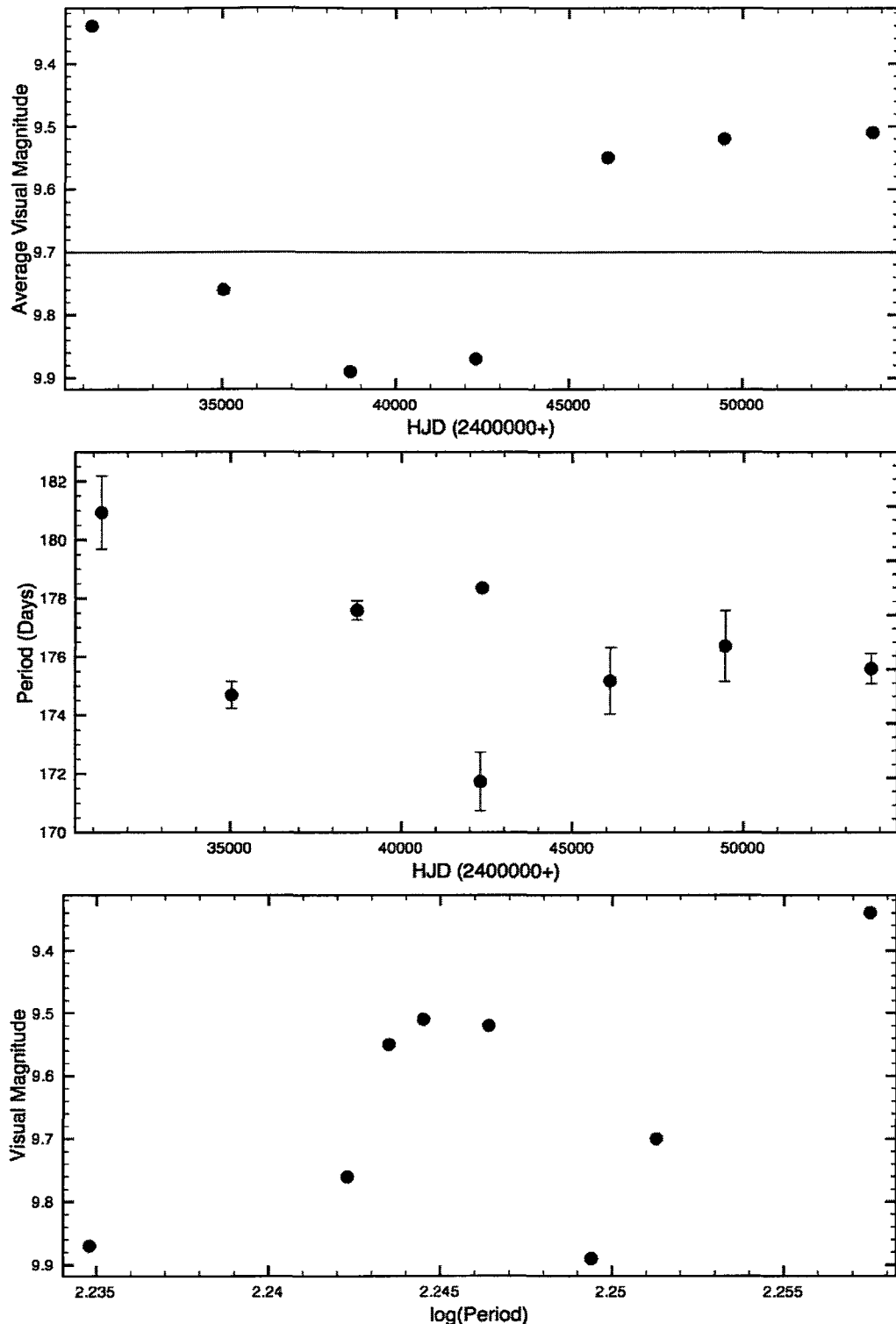


**Figure 4.2:** Period and average magnitude changes in SS Andromedae from AAVSO observations.

### 4.3 V Arietis

V Ari is a small-amplitude variable,  $\Delta V \simeq 0^m.9$ , for which the available AAVSO observations are not particularly useful for finding a reliable period. The star may be an LC variable rather than an SRC variable. It is also the only carbon star in the sample. The “SRC” designation originated recently from Pojmanski (2005). Spectroscopic observations for the star would be useful for learning more about it.

**Table 4.6:** AAVSO Observations of *V* Arietis

Subset	Dates	$\langle V \rangle$	% Diff.	$\Delta V$	$N$	$P$ (days)	% Diff.
All	35065-54502	8.54	...	1.7	124	$56.81 \pm 0.03$	...
1	35065-38681	8.46	-0.94	1.7	38	...	...
2	38766-41632	8.60	0.70	0.8	22	...	...
3	44226-45758	8.72	2.11	0.5	6	...	...
4	46026-46877	8.53	-0.12	0.9	9	...	...
5	46970-54502	8.56	0.23	1.1	49	...	...

#### 4.4 UX Aurigae

Figure 4.3 shows UX Aur’s variations in spectral type and radial velocity (phased using a period of 357 days and a time of maximum light of JD2454756.56 determined from the AAVSO observations), and a montage of CCD spectra taken at different epochs. We do not have enough observations to determine at what phase UX Aur reaches its highest temperature, although its greatest luminosity class (Ia) occurs for its hottest temperature class (M4). UX Aur exhibits changes in mean brightness, upon which there may be regular shorter period variability, although the dominant 357 day period found by Fourier analysis may be an alias caused by seasonal variations. The General Catalog of Variable Stars, hereafter referred to as GCVS (Samus et al. 2009) lists a period of 90.9 days for the star, but we found that the data actually phase better with the 357 day period. It is unclear what the original source of the 90.9 day period is, as the handful of papers that make reference to it simply refer to the GCVS as the source of the period (for example, Feast et al. 1972, the earliest mention of the star in the literature). Not much can be said about the star until we have a better idea of its true periodicity. Our spectroscopic observations indicate that both spectral and radial velocity changes occur, but accurately phasing the data is not yet possible, and more photometric observations with a longer baseline are needed.

**Table 4.7:** AAVSO Observations of UX Aurigae

Subset	Dates	$\langle V \rangle$	% Diff.	$\Delta V$	$N$	$P$ (days)	% Diff.
All	21632-54915	8.71	...	1.6	87	$356.57 \pm 0.37$	...
1	21632-21685	8.60	-1.26	0.9	4	...	...
2	33741-37048	8.46	-2.87	1.2	18	...	...
3	45024-47178	8.90	2.18	0.8	34	...	...
4	47199-50831	8.93	2.53	0.9	6	...	...
5	50837-50902	8.60	-1.26	0.4	4	...	...
6	54550-54915	8.58	-1.49	1.1	21	...	...

**Table 4.8:** Spectroscopic observations of UX Aurigae

Year	HJD	Phase	$V_R$ (km/s)	Spectral Type	Source
1939	2425159	0.1217	34	M5	Joy
1939	2428910	0.6287	33	M5	Joy
2007	2454382	0.9797	$38.5 \pm 16.5$	M5 Ib	DAO CCD
2010	2455484	0.0655	$29.5 \pm 17.3$	M4 Ia	DAO CCD

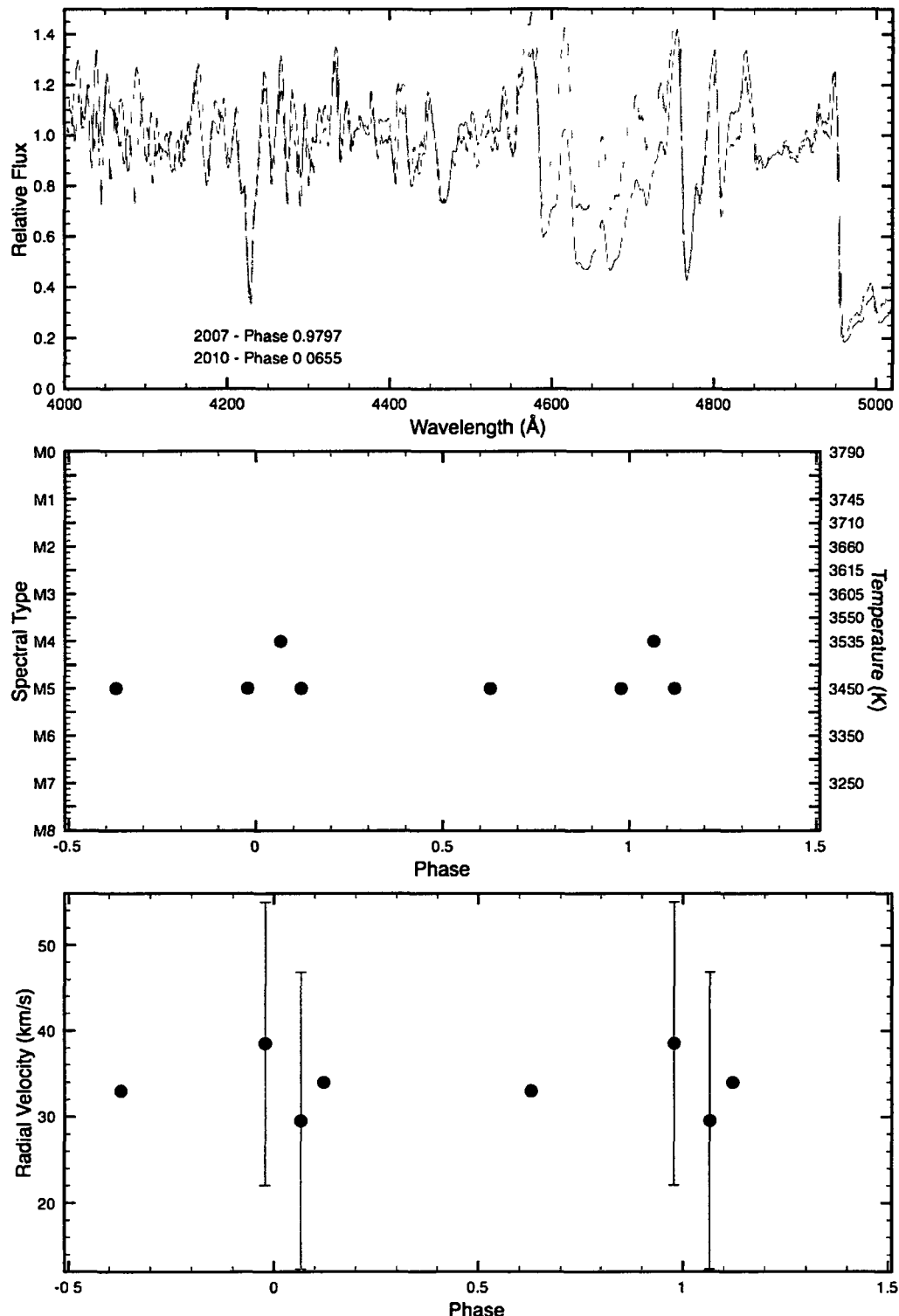


**Figure 4.3:** Spectral variation in UX Aurigae. Top: Spectra from different epochs. Middle: Spectral type as a function of phase. Bottom: Radial velocity as a function of phase. Data phased with 357 day period.

## 4.5 V394 Aurigae

Figure 4.4 shows V394 Aur's variations in spectral type, phased using a period of 32.5 days and a time of maximum light of JD2448285, which we obtained from Snyder (1991), as there were not enough AAVSO observations to determine a period. The temperature is varying, but it is not clear at what phase it reaches maximum. Its luminosity class stayed fairly constant, but one observation may indicate that it reaches greatest luminosity class at latest spectral type. The spectral type variations are somewhat large for a cool M4 Ib-II SRC variable, and the period derived by Snyder is also atypically small, so this object is strongly in need of additional observations, both photometric and spectroscopic. Snyder's study of the star is based on only 27 data points obtained over 102 days, and many more observations over a longer baseline are needed to confirm that the star is actually an SRC variable.

**Table 4.9:** Spectroscopic observations of V394 Aurigae

Year	HJD	Phase	$V_R$ (km/s)	Spectral Type	Source
1942	2430628	0.1347	...	M4 II	DDO
1944	2431093	0.8628	...	M3.5 II	DDO
1944	2431397	0.5972	...	M2.5 II	DDO
1945	2431459	0.2986	...	M4 Ib	DDO

**Table 4.10:** AAVSO Observations of V394 Aurigae

Subset	Dates	$\langle V \rangle$	% Diff.	$\Delta V$	$N$	$P$ (days)	% Diff.
All	54751-54862	6.21	...	0.3	8	...	...

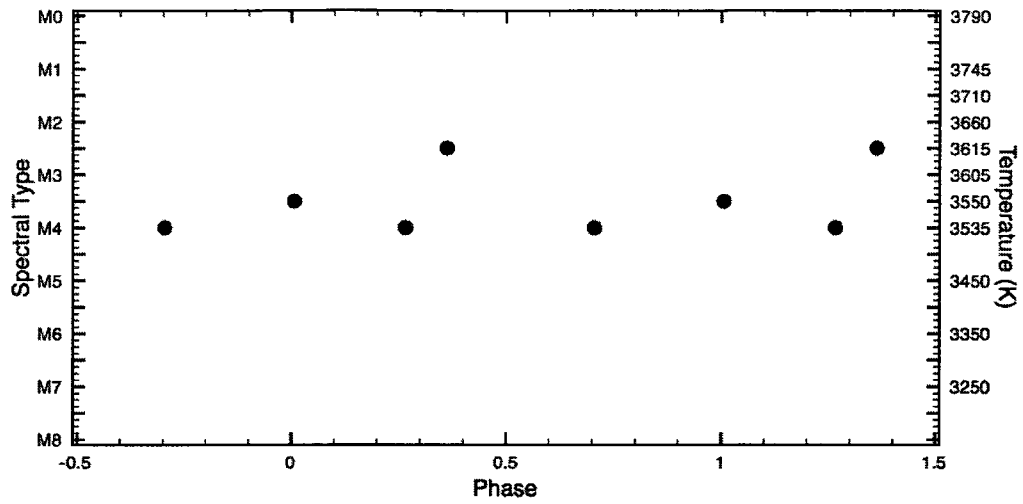


**Figure 4.4:** Spectral variation in V394 Aur, phased with 32.5 day period.

## 4.6 RS Cancri

Figure 4.5 shows RS Cnc's variations in spectral type and radial velocity, and a montage of photographic spectra taken at different epochs. We found a period of 240.32 days and a time of maximum light of JD2443255.71 from the AAVSO observations. The GCVS lists a period of 120 days for the star. We found both a 240 day and 120 day period with our Fourier analysis. Although there was more power in the longer period, the shorter period produced better phasing and was used to produce the plots of spectral type and  $V_R$  variation. We fitted the radial velocity variations with a sine wave and found that the star's phase of smallest dimensions is approximately 0.93. The temperature is varying, but it is not clear at what phase the temperature reaches maximum. Its luminosity class stayed fairly constant but the observations suggest that it may reach greatest luminosity class at latest spectral type. Figure 4.6 shows RS Cnc's changes in period and average visual magnitude taken at approximately 10-year intervals. Additional photometric observations would help to better constrain the period. The light amplitude is about  $\Delta V \simeq 2^m.5$ . More spectroscopic observations are needed to determine how the radial velocity and spectral type change during the star's cycle.

**Table 4.11:** AAVSO Observations of RS Cancri

Subset	Dates	$\langle V \rangle$	% Diff.	$\Delta V$	$N$	$P$ (days)	% Diff.
All	22721-55380	6.19	...	2.5	9540	$240.32 \pm 0.05$	...
1	22721-25324	6.32	2.10	0.9	51	$258.35 \pm 1.38$	7.50
2	28668-29891	6.28	1.45	1.1	81	$269.65 \pm 2.74$	12.20
3	32266-33664	6.16	-0.48	1.3	220	$227.20 \pm 1.47$	-5.46
4	33673-37321	6.19	0.00	1.7	726	$225.80 \pm 0.36$	-6.04
5	37337-40948	6.07	-1.94	1.6	75	$239.37 \pm 0.41$	-0.40
6	40969-44619	5.99	-3.23	2.0	864	$217.52 \pm 1.07$	-9.49
7	44623-48272	6.17	-0.32	2.5	1931	$233.26 \pm 0.18$	-2.94
8	48272-51921	6.22	0.48	1.9	795	$238.88 \pm 0.16$	-0.60
9	51923-55380	6.25	0.97	2.1	397	$242.62 \pm 0.26$	0.96

**Table 4.12:** Spectroscopic observations of RS Cancri

Year	HJD	Phase	$V_R$ (km/s)	Spectral Type	Source
1939	2427137	0.6774	13	M6	Joy
1939	2429413	0.6441	15	M6	Joy
1939	2429440	0.8691	2	M5	Joy
1940	2429647	0.5941	12	M6	Joy
1943	2430786	0.0835	...	M6 Iab	DDO
1943	2430831	0.4573	...	M6 Iab	DDO
1944	2431192	0.4656	...	M6.5 Iab	DDO
1944	2431200	0.5323	...	M6 Iab	DDO
1978	2443640	0.2001	$-27.4 \pm 0.7$	M6 Ib	DAO Pg
1979	2439495	0.1584	$-29.0 \pm 0.2$	M7 Ib	DAO Pg

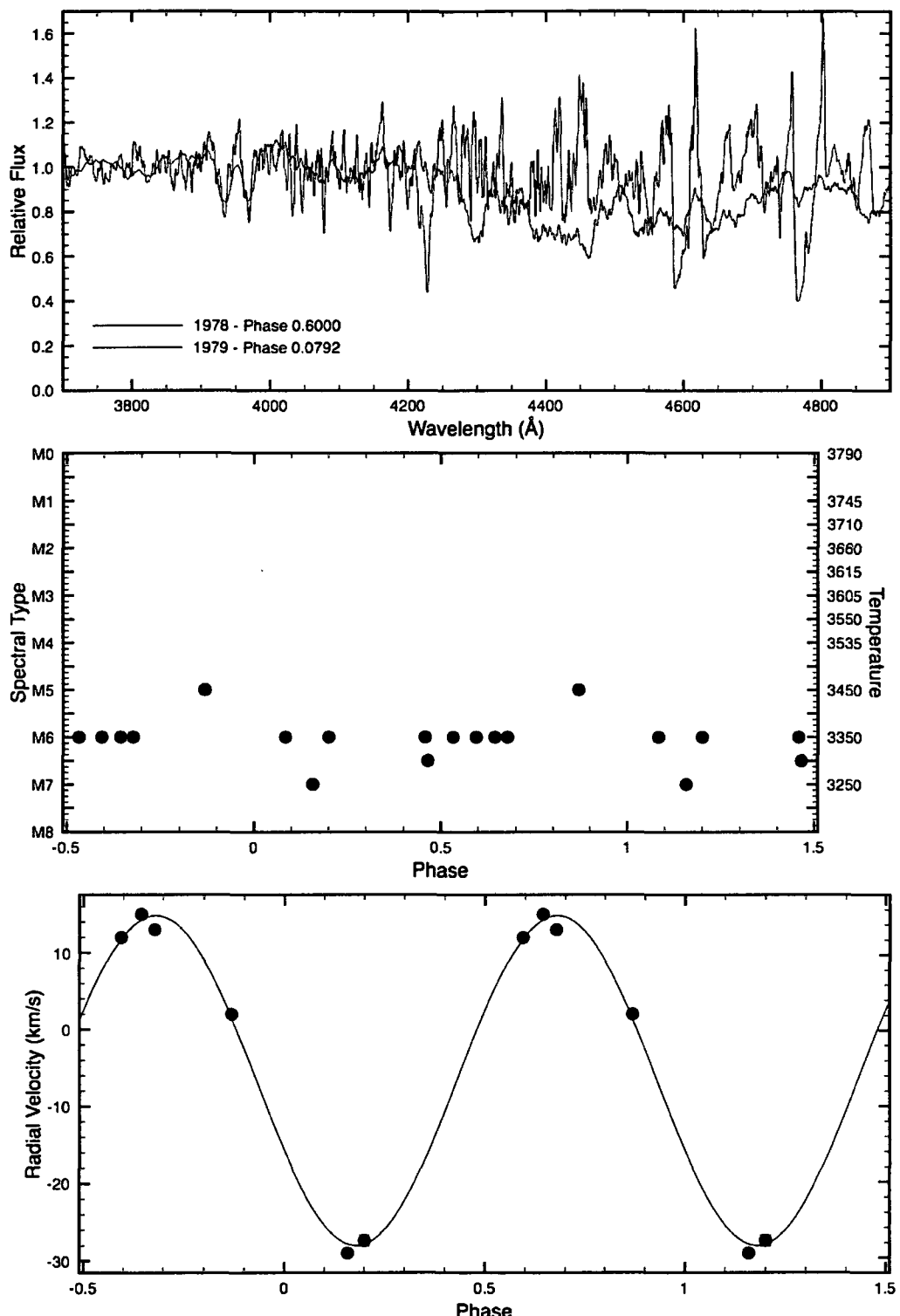


**Figure 4.5:** Spectral variation in RS Cancri. Top: Spectra from different epochs. Middle: Spectral type as a function of phase. Bottom: Radial velocity as a function of phase. Data phased with 120 day period.

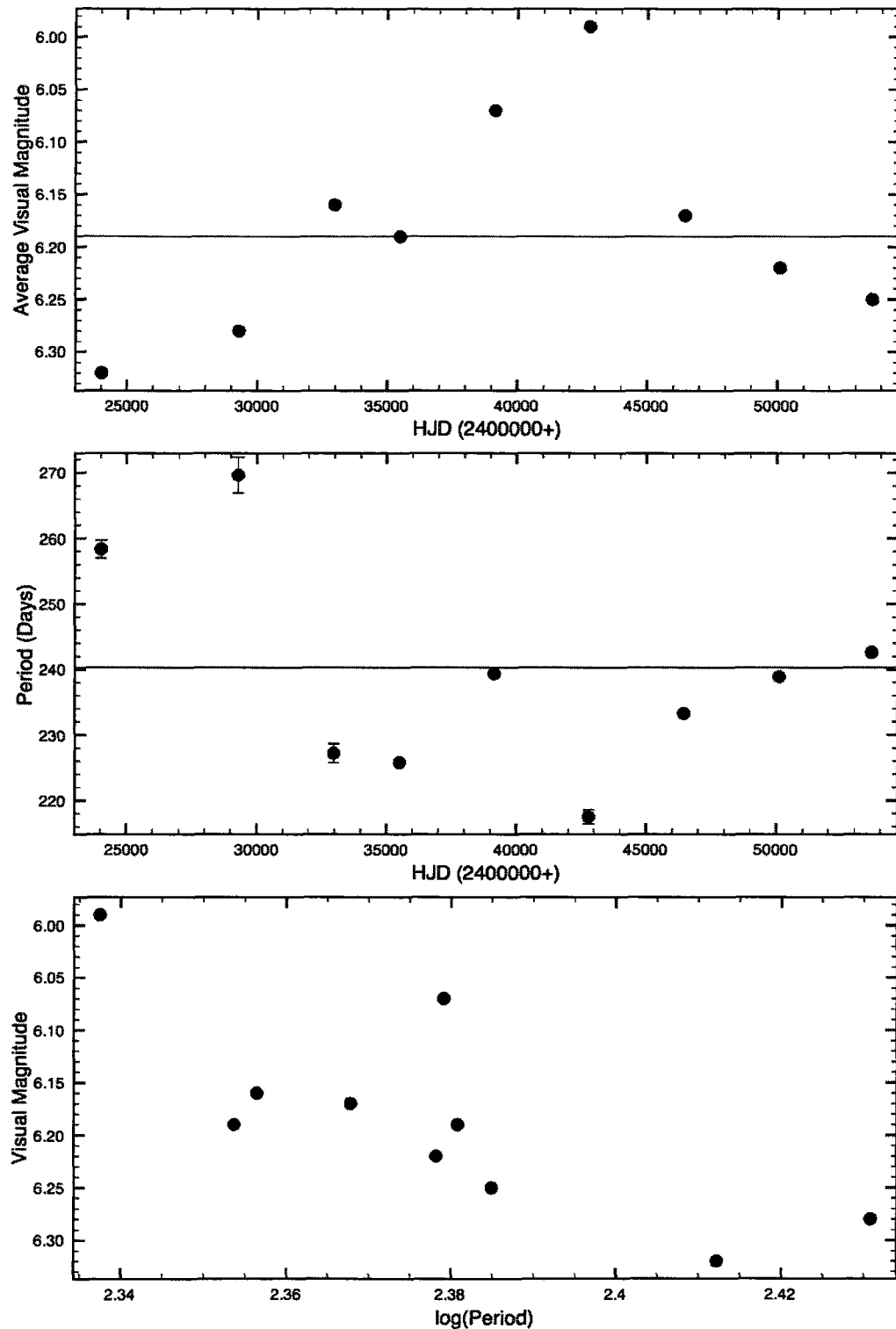


Figure 4.6: Period and average magnitude changes in RS Cancri from AAVSO observations.

## 4.7 UZ Canis Majoris

Figure 4.7 shows UZ CMa's changes in period and average visual magnitude taken at approximately 10-year intervals. Changes in both quantities are evident. The star displays regular periodicity, but simply lacks spectroscopic observations. Its brightness increases as its period decreases, which suggests that its effective temperature increases as its size decreases. Not much more can be learned without further observations, both spectroscopic and photometric.

**Table 4.13:** AAVSO Observations of UZ Canis Majoris

Subset	Dates	$\langle V \rangle$	% Diff.	$\Delta V$	$N$	$P$ (days)	% Diff.
All	36317-55299	11.68	...	3.4	2613	$86.25 \pm 0.01$	...
1	36317-39962	11.82	1.20	3.0	409	$85.95 \pm 0.06$	-0.35
2	39967-43615	11.70	0.17	2.2	430	$86.51 \pm 0.05$	0.30
3	43629-47265	11.67	-0.09	2.9	767	$84.75 \pm 0.05$	-1.74
4	47270-50909	11.68	0.00	1.9	726	$84.65 \pm 0.04$	-1.86
5	50917-55299	11.50	-1.54	2.9	281	$83.85 \pm 0.05$	-2.78

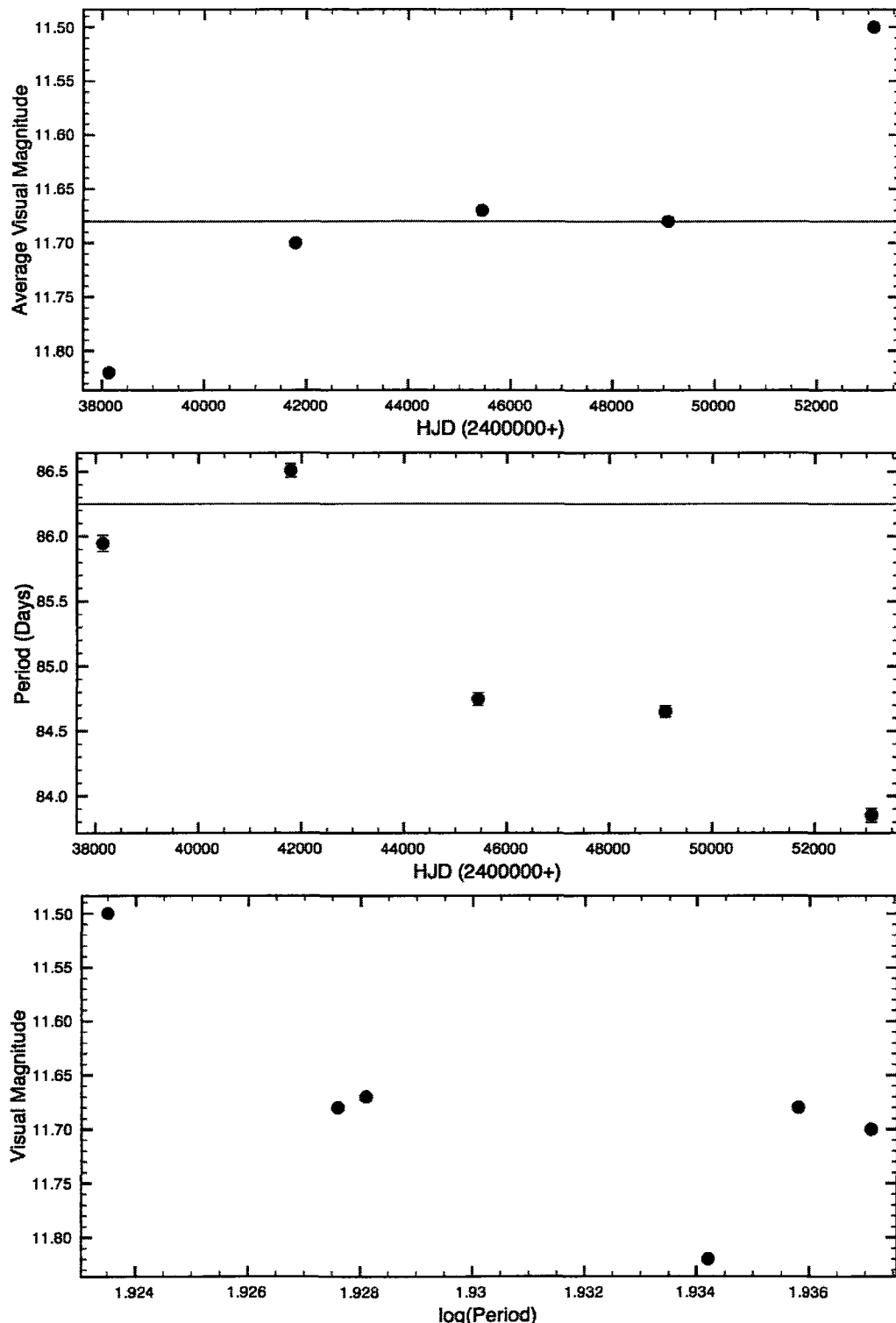


**Figure 4.7:** Period and average magnitude changes in UZ Canis Majoris from AAVSO observations.

## 4.8 BZ Carinae

Figure 4.8 shows BZ Car's variations in spectral type. The observations were phased using a period of 129.71 days and a time of maximum light of JD2447619.7, determined from the AAVSO observations. Note that this differs from the 97 day period listed in the GCVS, but our period had the strongest Fourier signal and produced better phasing. The star appears to reach highest temperature perhaps a quarter cycle before light maximum, but better photometry to determine the period is needed to confirm that conclusively. It reaches greatest luminosity class at highest temperature. Figure 4.9 shows BZ Car's changes in period and average visual magnitude. BZ Car's light amplitude is  $\Delta V \simeq 2^m.0$ . It appeared to undergo a sudden drop in brightness around JD2410000, which could have been caused by a dust extinction event. Early observations show clear brightness variations, but more recent observations appear to be more irregular. Its period determined by Fourier analysis also appears to have increased suddenly by approximately 10 days in recent observations. BZ Car needs additional spectroscopic and  $V_R$  data (only possible from a southern hemisphere site) to make more definitive conclusions about the nature of its variability.

**Table 4.14:** AAVSO Observations of BZ Carinae

Subset	Dates	$\langle V \rangle$	% Diff.	$\Delta V$	$N$	$P$ (days)	% Diff.
All	31669-55316	8.18	...	4.2	881	$129.71 \pm 0.02$	...
1	31669-32006	8.47	3.55	1.0	51	$129.02 \pm 2.91$	-0.53
2	39154-41539	9.08	11.00	2.3	208	$129.04 \pm 0.22$	-0.51
3	43604-46247	7.58	-7.33	2.3	72	$123.36 \pm 5.17$	-4.90
4	46271-49906	7.93	-3.06	2.8	239	$128.26 \pm 0.14$	-1.12
5	49930-53123	7.57	-7.46	1.4	147	$136.31 \pm 0.36$	5.09
6	53953-55316	8.12	-0.73	1.6	164	$139.80 \pm 0.50$	7.78

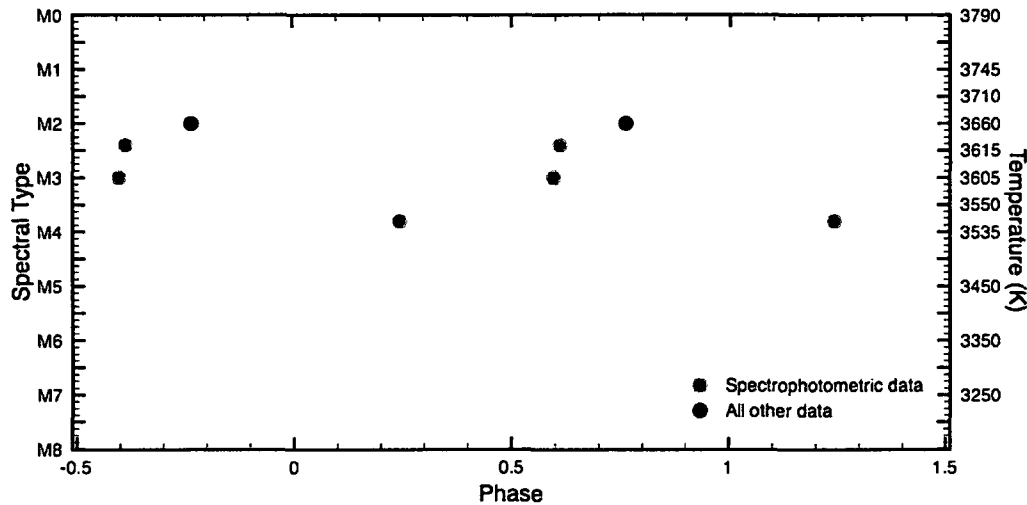


**Figure 4.8:** Spectral variation in BZ Carinae, phased with 129.71 day period.

**Table 4.15:** Spectroscopic observations of BZ Carinae

Year	HJD	Phase	$V_R$ (km/s)	Spectral Type	Source
1970	2440787	0.2438	...	M3.8 Iab	Wing
1971	2441111	0.6116	...	M2.4 Iab	Wing
1976	2442861	0.5980	...	M3.0 Ib	Wing
1986	2446580	0.7628	...	M2 Ia-Iab	Garrison collection

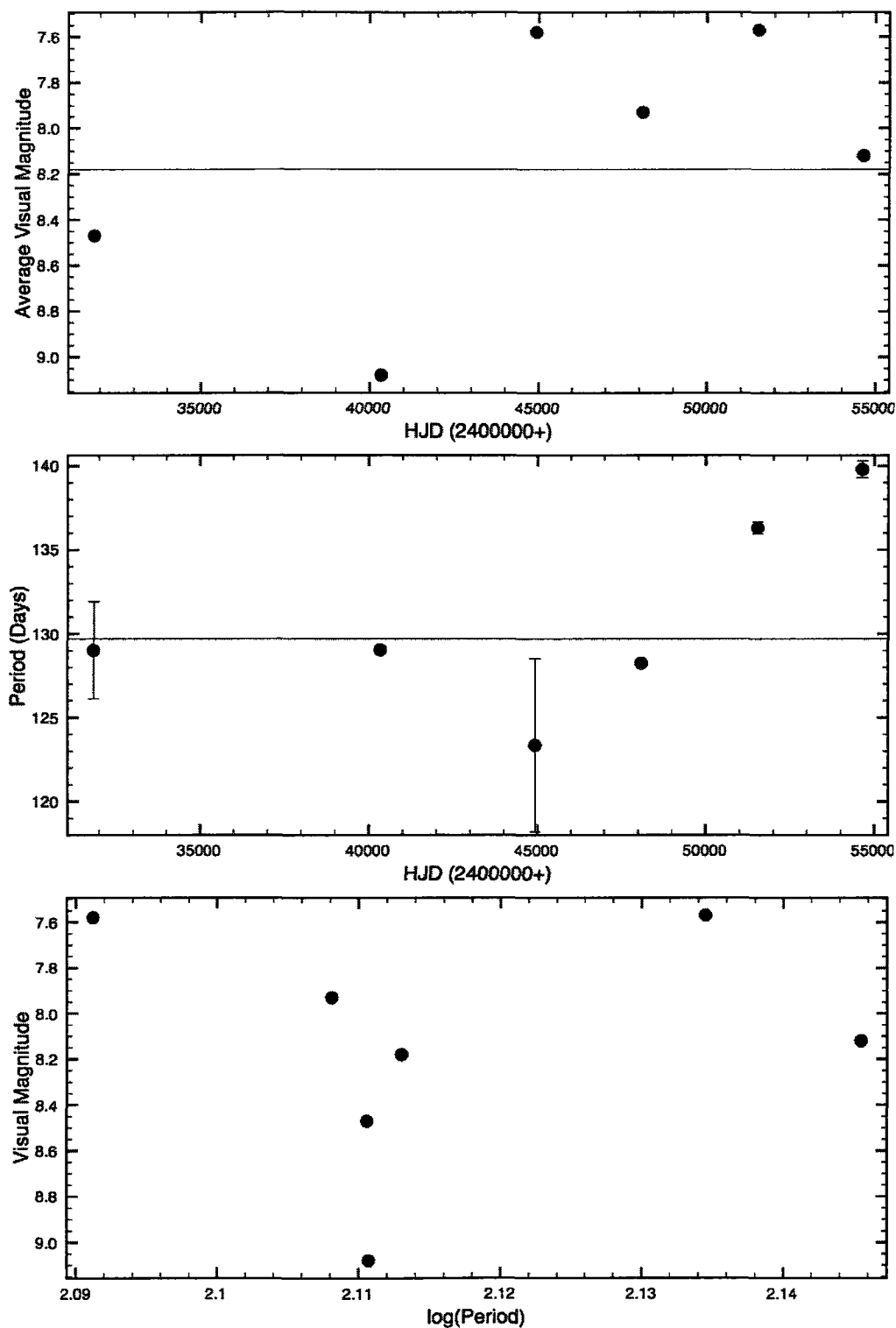


Figure 4.9: Period and average magnitude changes in BZ Carinae from AAVSO observations.

## 4.9 CK Carinae

The GCVS lists CK Car's period as 525 days, similar to the 533.61 day period we found through Fourier analysis. Figure 4.10 shows CK Car's changes in period and average visual magnitude taken at approximately 10-year intervals. There is obvious irregularity in its brightness variations for no obvious reason. It is possible that the star may actually be an LC variable. More photometry as well as spectroscopic and  $V_R$  observations are necessary to say more about the nature of CK Car.

**Table 4.16:** AAVSO Observations of CK Carinae

Subset	Dates	$\langle V \rangle$	% Diff.	$\Delta V$	$N$	$P$ (days)	% Diff.
All	39157-55330	8.05	...	3.4	876	$533.61 \pm 0.33$	...
1	39157-41683	8.15	1.24	2.8	567	$522.23 \pm 1.80$	-2.13
2	43258-46442	7.79	-3.23	1.5	30	$488.22 \pm 5.93$	-8.51
3	46507-50082	8.00	-0.62	1.9	199	$528.83 \pm 7.27$	-0.90
4	50112-55330	7.55	-6.21	1.8	80	$529.19 \pm 3.52$	-0.83

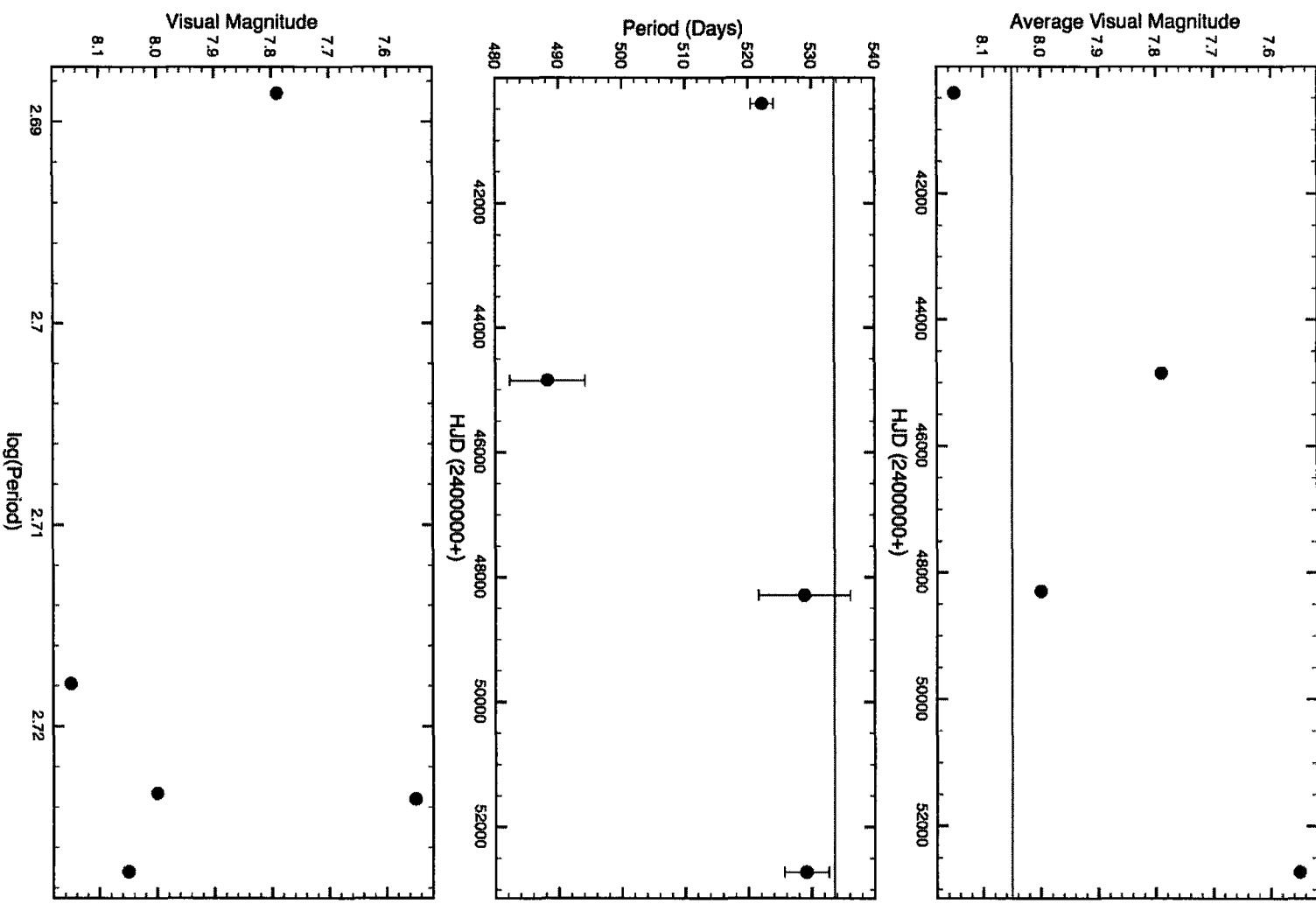


Figure 4.10: Period and average magnitude changes in CK Carinae from AAVSO observations.

## 4.10 CL Carinae

The GCVS notes a 513 day period for CL Car, identical to that found with our Fourier analysis. Details of the AAVSO observations are found in the table. We also have blue light observations from the Harvard collection for the star, covering the dates JD2414979.80-2434507.27, with an average  $B$  magnitude of 10.63 and  $\Delta B \simeq 2^m.1$ . We found a period of  $692.21 \pm 0.25$  days for these observations. Figure 4.11 shows CL Car's changes in period and average visual magnitude. The period is well-established from the AAVSO observations and GCVS, but the star displays intriguing changes in mean brightness that could be dust episodes. Spectroscopic observations are needed to confirm the nature of its variability, although the regularity of its brightness variations suggests pulsation.

**Table 4.17:** AAVSO Observations of CL Carinae

Subset	Dates	$\langle V \rangle$	% Diff.	$\Delta V$	$N$	$P$ (days)	% Diff.
All	34747-55328	8.83	...	2.6	1111	$512.86 \pm 0.26$	...
1	34747-38358	8.85	0.23	1.5	227	$505.22 \pm 2.06$	-1.49
2	38405-41907	8.61	-2.49	2.4	437	$555.79 \pm 3.49$	8.37
3	42174-45690	8.80	-0.34	1.7	66	$499.12 \pm 5.05$	-2.68
4	45742-49206	9.08	2.83	1.6	63	$515.58 \pm 5.30$	0.53
5	49433-52988	9.17	3.85	1.4	122	$492.80 \pm 4.57$	-3.91
6	52999-55328	9.02	2.15	2.5	196	$495.65 \pm 3.73$	-3.36

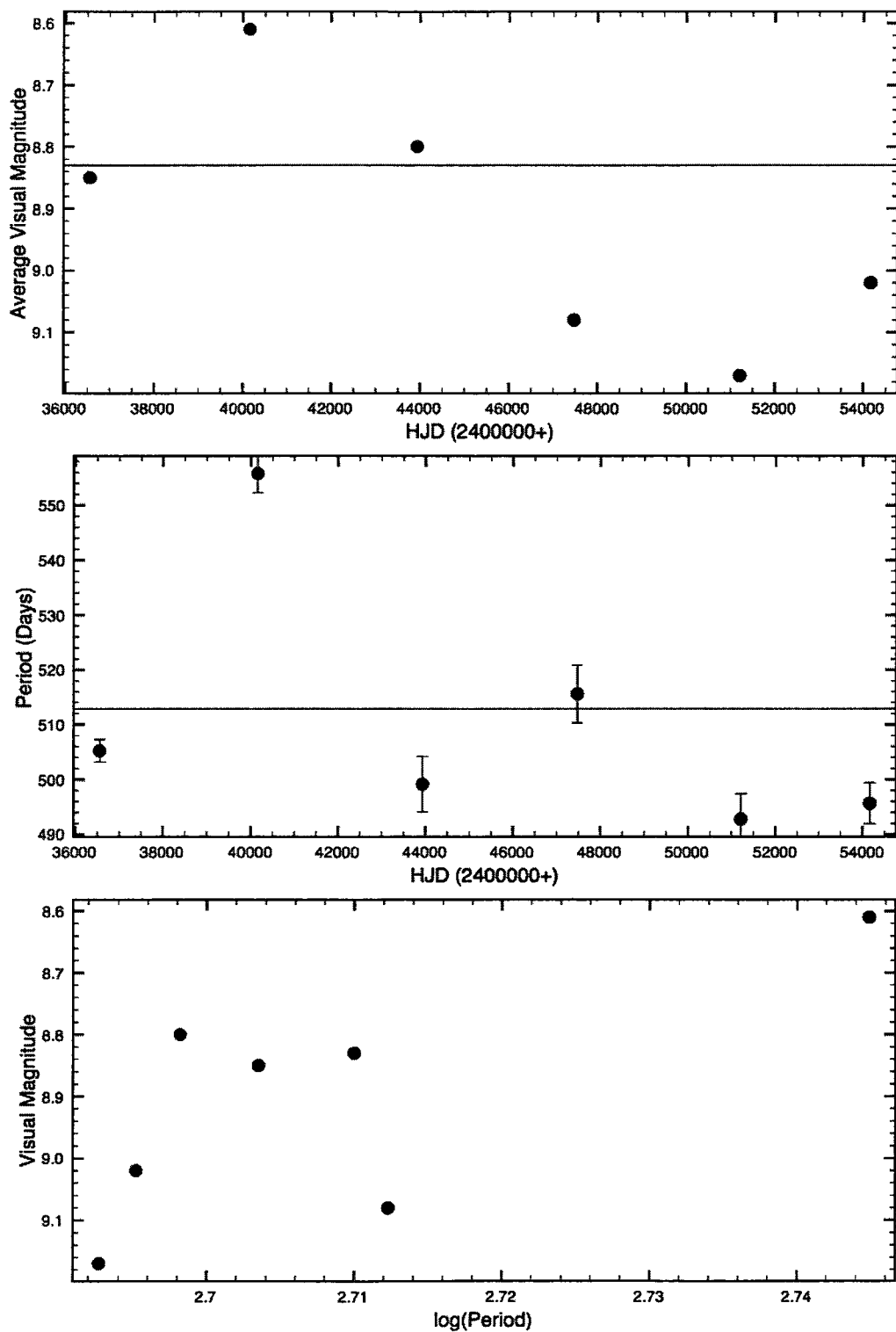


Figure 4.11: Period and average magnitude changes in CL Carinae from AAVSO observations.

#### 4.11 EV Carinae

The GCVS lists a period for EV Car of 347 days, similar to the 374.97 day period found from our Fourier analysis. Figure 4.12 shows EV Car's changes in period and average visual magnitude. It exhibits non-variability at times along with changes in mean brightness. There is no evidence of regularity in its light curve. The derived period is too close to one year to be definitive, as seasonal effects are strong in the AAVSO observations. Future observations may show it to actually be an LC variable.

**Table 4.18:** AAVSO Observations of EV Carinae

Subset	Dates	$\langle V \rangle$	% Diff.	$\Delta V$	$N$	$P$ (days)	% Diff.
All	39155-55240	8.20	...	4.5	692	$374.97 \pm 0.20$	...
1	39155-41683	8.22	0.24	1.6	569	$384.35 \pm 1.22$	2.50
2	43143-46442	8.17	-0.37	3.7	32	$368.72 \pm 2.87$	-1.67
3	46508-50082	8.43	2.80	2.5	39	$362.52 \pm 2.11$	-3.32
4	50112-54240	7.90	-3.66	2.7	52	$383.10 \pm 2.11$	2.17

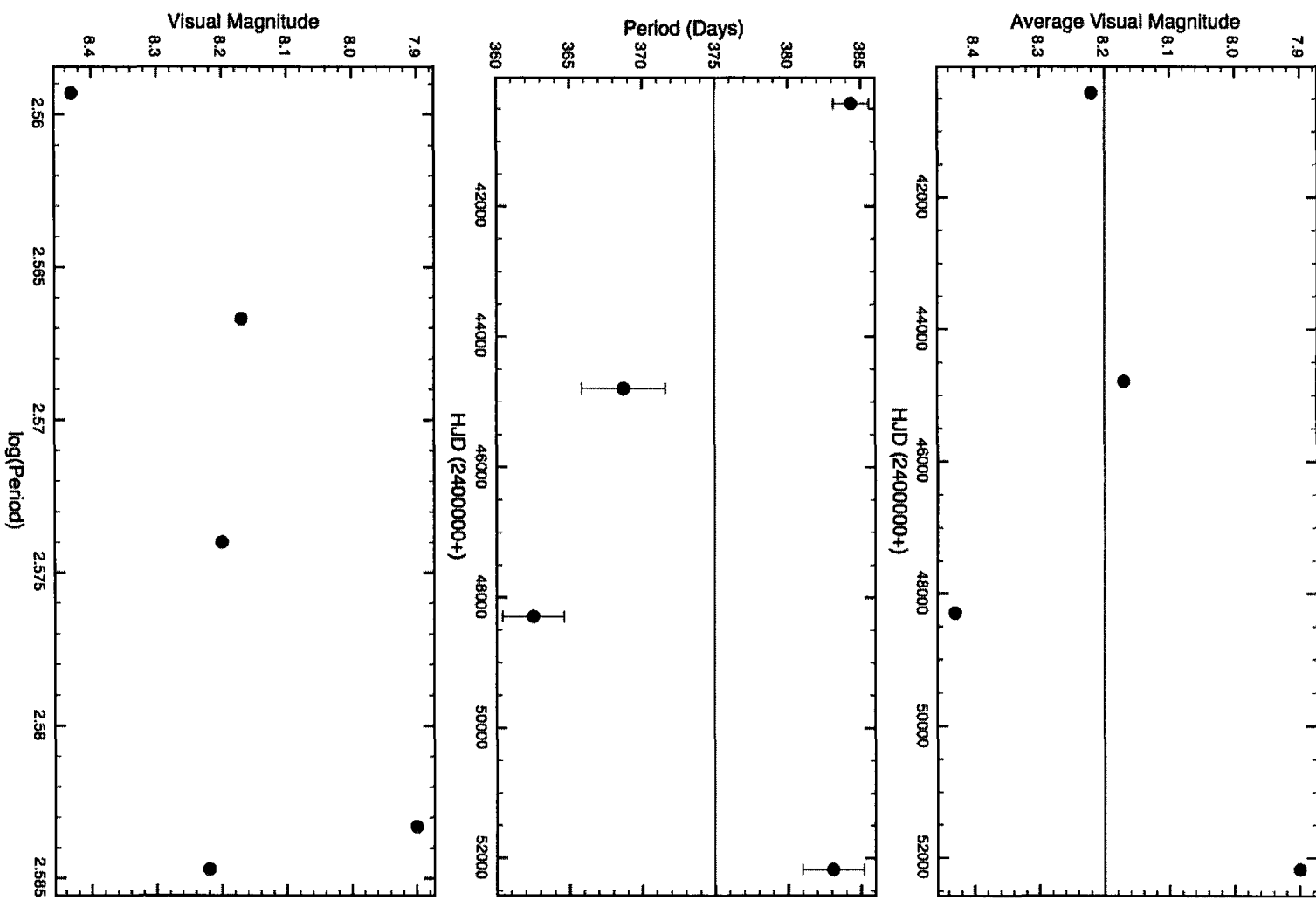


Figure 4.12: Period and average magnitude changes in EV Carinae from AAVSO observations.

## 4.12 IX Carinae

The GCVS lists a 400 day period for IX Car. Our Fourier analysis found a dominant 369.10 day period. Turner et al. (2009) found a 357 day period for the star from 804 blue light observations from the Harvard collection. The blue light observations cover the dates JD2414979.80-2434507.27, with an average  $B$  magnitude of 9.71 and  $\Delta B \simeq 1^m.6$ . Figure 4.12 shows IX Car’s changes in period and average visual magnitude. IX Car appears in some ways to be a clone of  $\alpha$  Ori, one of the most well-studied SRC variables. It has a small amplitude which varies temporally in a curious manner — it increases as the star’s brightness increases. Spectroscopic and  $V_R$  data are essential for understanding its nature. Its brightness changes, unlike those in CL Car, do not appear to be caused by dust episodes.

**Table 4.19:** AAVSO Observations of IX Carinae

Subset	Dates	$\langle V \rangle$	% Diff.	$\Delta V$	$N$	$P$ (days)	% Diff.
All	39116-55316	7.60	...	2.4	1801	$369.10 \pm 1.16$	...
1	39166-41683	7.38	-2.89	1.3	316	$411.02 \pm 1.74$	11.36
2	43612-46434	7.07	-6.97	1.9	107	$418.12 \pm 3.29$	13.28
3	46471-50106	7.64	0.53	2.3	698	$382.98 \pm 1.16$	3.76
4	50116-53442	7.72	1.58	2.1	509	$417.78 \pm 1.91$	13.19
5	53953-55316	7.83	3.03	1.6	171	$338.90 \pm 3.24$	-8.18

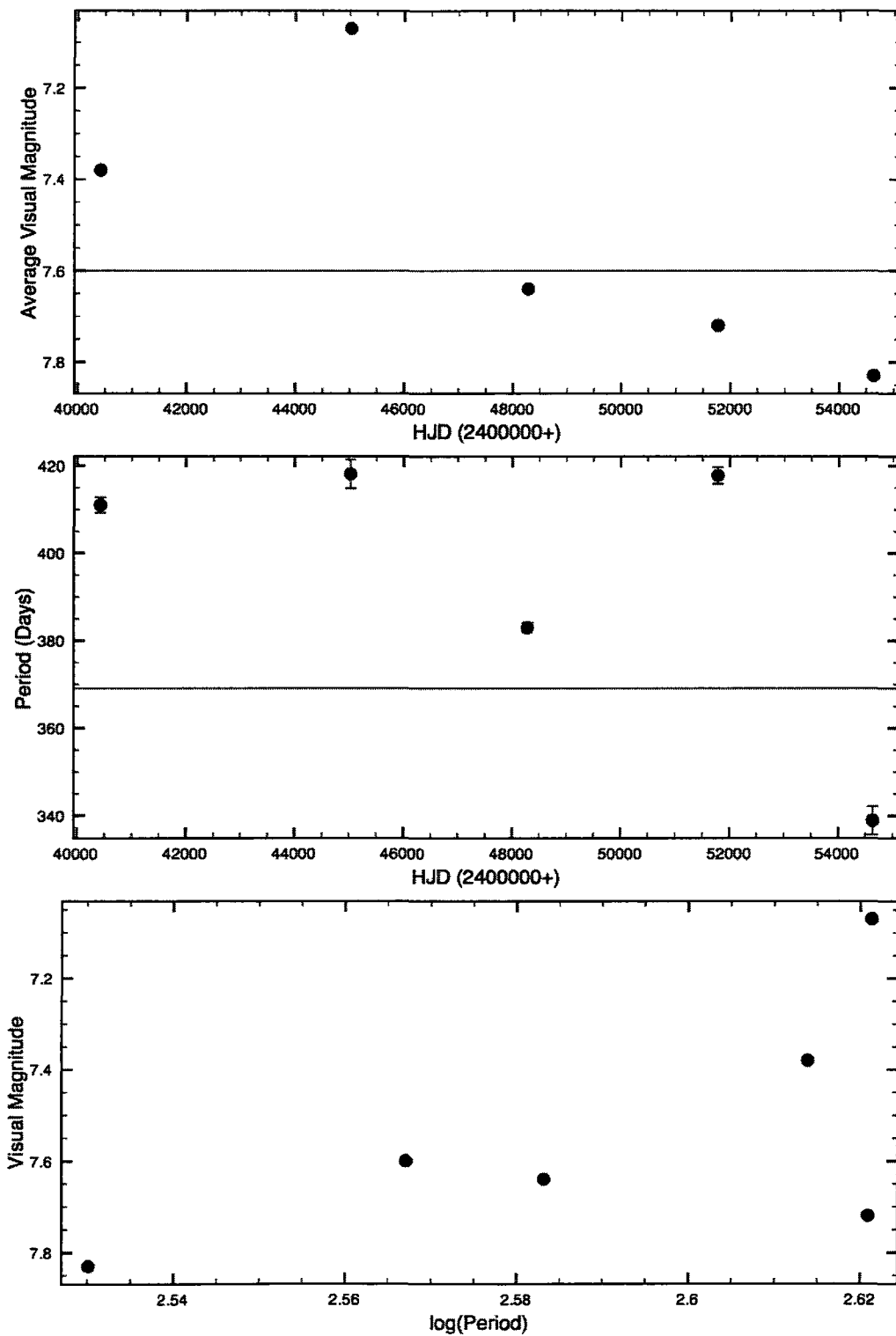


Figure 4.13: Period and average magnitude changes in IX Carinae from AAVSO observations.

### 4.13 PZ Casseopeiae

Figure 4.14 shows PZ Cas's variations in spectral type and radial velocity, and a montage of CCD spectra taken at different epochs. The observations were phased using a period of 925 days and a time of maximum light of JD2440483.95, determined from the AAVSO observations. The GCVS lists its spectral type as M2-4 Ia and lists a period of 925 days. We also found a prominent period of 253.97 days in the AAVSO observations (referred to in the table, as it is prominent in the 10-year subsets of the photometry), but the 925 day period is much more prominent in the overall dataset and produced better phasing. Using the two different periods did not change the plots of spectral type and  $V_R$  variation significantly, so we used the period found from our Fourier analysis. We fitted the radial velocity variations with a sine wave and found that the star appears to reach mean radial velocity after passing through velocity maximum near a phase of 0.34, indicating the phase of smallest dimensions. The sine wave fit is restricted by the limited phase coverage, and needs additional observations for confirmation. The star appears to reach highest temperature near light minimum, and reaches greatest luminosity class at its highest temperature. Figure 4.15 shows PZ Cas's changes in period and average visual magnitude taken at approximately 10-year intervals. The star's light curve appears to be seasonably regular, and the observed marked decreases in brightness could indicate regular dust extinction episodes.

**Table 4.20:** AAVSO Observations of PZ Casseopeiae

Subset	Dates	$\langle V \rangle$	% Diff.	$\Delta V$	$N$	$P$ (days)	% Diff.
All	34253-55397	9.15	...	3.6	1141	$253.97 \pm 0.07$	...
1	34253-43791	9.35	2.19	3.4	266	$256.64 \pm 0.77$	1.06
2	43832-47449	9.17	0.22	2.5	120	$277.73 \pm 0.98$	9.36
3	47479-51085	9.03	-1.31	3.2	301	$261.83 \pm 0.95$	3.10
4	51105-54752	9.11	-0.44	2.8	357	$247.93 \pm 2.53$	-2.38
5	54758-55397	9.08	-0.77	1.1	67	$252.39 \pm 1.10$	-0.62

**Table 4.21:** Spectroscopic observations of PZ Casseopeia

Year	HJD	Phase	$V_R$ (km/s)	Spectral Type	Source
1970	2440850	0.3952	...	M2.0 Ia	Wing
1970	2440871	0.4179	...	M2.2 Ia	Wing
1970	2440905	0.4546	...	M2.3 Ia	Wing
1970	2441906	0.4557	...	M2.3 Ia	Wing
1973	2441931	0.5638	...	M3.7 Iab	Wing
1973	2441962	0.5974	...	M3.5 Iab	Wing
1973	2442015	0.6546	...	M3.7 Iab	Wing
2005	2453652	0.2356	$2.6 \pm 20.6$	M3 Ia	DAO CCD
2007	2454379	0.0214	$25.65 \pm 17.0$	M3.5 Iab	DAO CCD
2007	2454382	0.0247	$26.5 \pm 15.9$	M3.5 Iab	DAO CCD
2010	2455489	0.2215	$8.4 \pm 19.6$	M3.5 Iab	DAO CCD

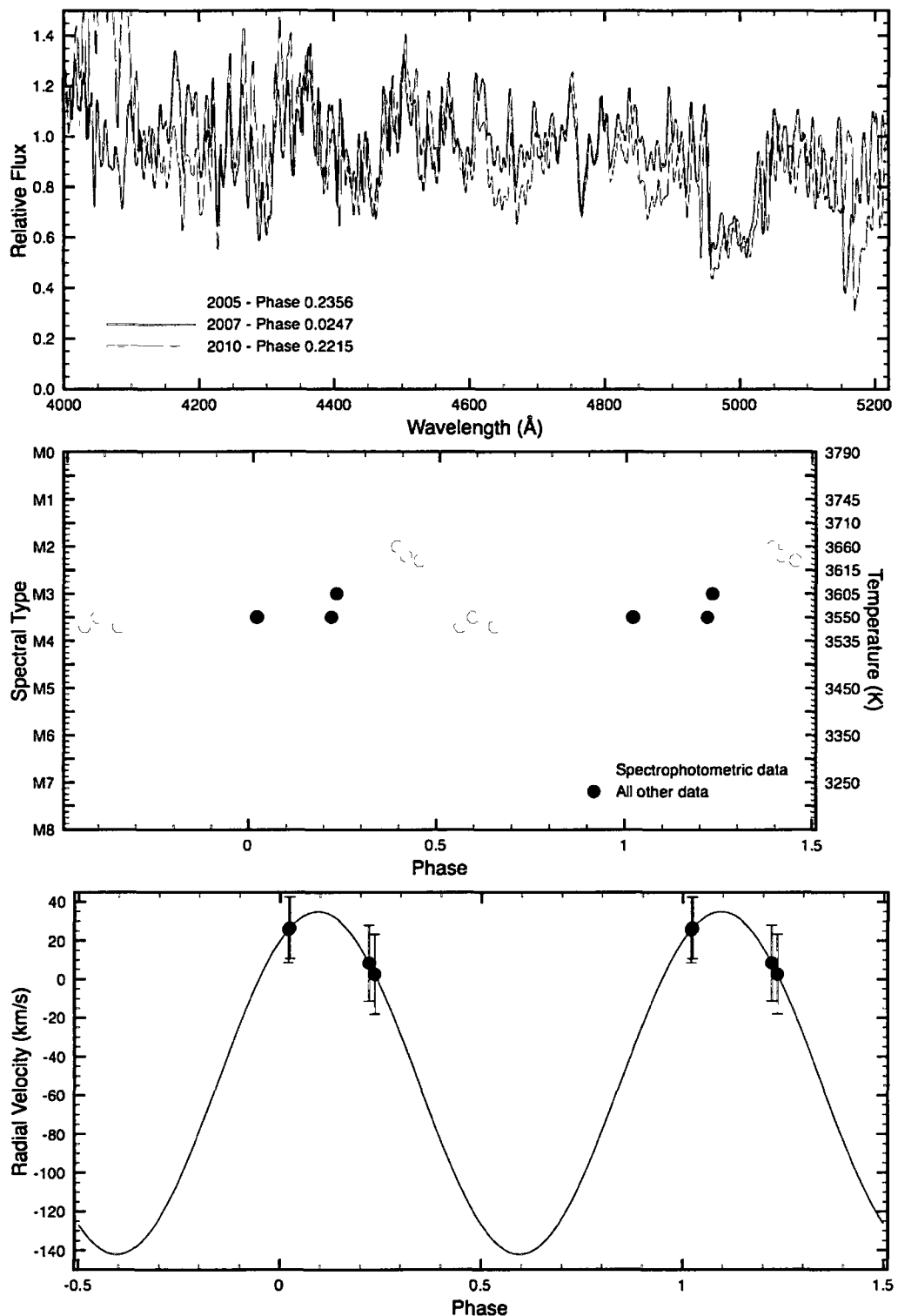


**Figure 4.14:** Spectral variation in PZ Casseopeiae. Top: Spectra from different epochs. Middle: Spectral type as a function of phase. Bottom: Radial velocity as a function of phase. Data phased with 253.97 day period.

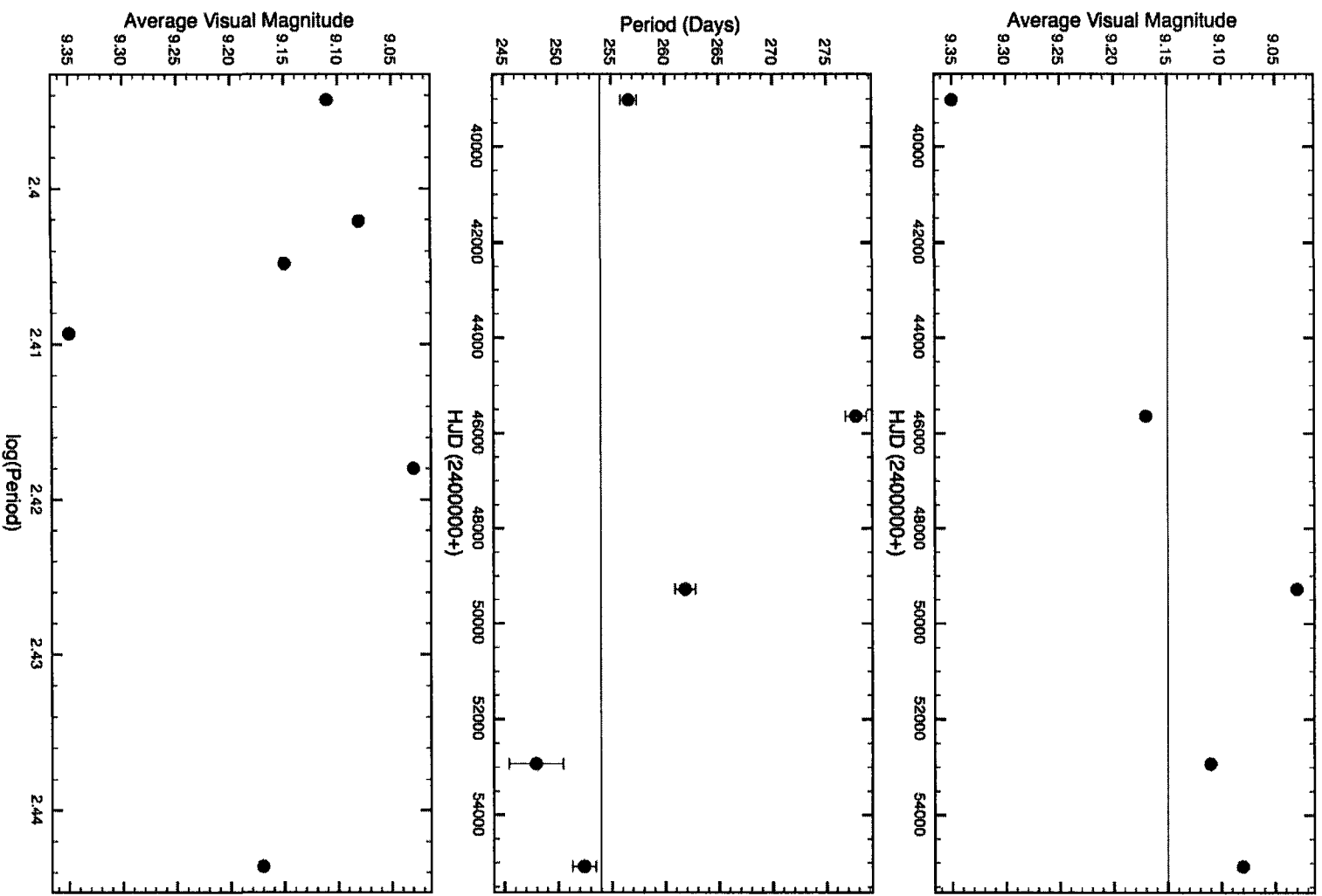


Figure 4.15: Period and average magnitude changes in PZ Cassiopeiae from AAVSO observations.

## 4.14 W Cephei

Figure 4.17 shows W Cep's changes in period and average visual magnitude taken at approximately 10-year intervals. W Cep is the hottest star in the sample, and yet it does not appear to be a regular light variable. The spectral type and radial velocity variations appear counterintuitive relative to results for other, cooler stars in the sample. The GCVS lists a period of 350 days for the star as well as a long secondary period of 2000 days. The near-one-year periods are likely to be seasonal effects. It appears to be mislabeled in the GCVS as an SRC variable. Perhaps it is actually an LC variable? The most recent AAVSO observations show it to be almost light and spectral type constant, and it may not be exhibiting detectable variability, despite the large value of  $\Delta V \simeq 2^m$  listed in the GCVS.

**Table 4.22:** AAVSO Observations of W Cephei

Subset	Dates	$\langle V \rangle$	% Diff.	$\Delta V$	N	P (days)	% Diff.
All	25529-55416	7.67	...	2.7	8005	$346.26 \pm 0.03$	...
1	25529-29144	7.92	3.26	1.1	70	...	...
2	29188-32817	7.58	-1.17	0.9	20	...	...
3	33435-36471	8.00	4.30	1.9	715	$333.61 \pm 1.01$	-3.65
4	36483-40123	7.91	3.13	1.6	320	$371.14 \pm 0.93$	7.19
5	40130-43777	7.68	0.13	1.7	703	$388.09 \pm 0.86$	12.08
6	43782-47425	7.70	0.39	2.4	1255	$348.93 \pm 0.55$	0.77
7	47430-51077	7.85	2.35	2.4	1615	$356.89 \pm 0.41$	3.07
8	51079-54729	7.46	-2.74	1.9	2977	$334.46 \pm 0.28$	-3.41
9	54735-55406	7.63	-0.52	2.3	330	$334.05 \pm 0.97$	-3.53

**Table 4.23:** Spectroscopic observations of W Cephei

Year	HJD	Phase	$V_R$ (km/s)	Spectral Type	Source
1947	2432491	0.0984	...	K1 Ia	DDO
1947	2432533	0.2195	...	K1 Ia	DDO
2005	2453652	0.2581	$28.1 \pm 21.2$	K1 Ib	DAO CCD
2007	2454377	0.3534	$9.7 \pm 17.7$	K0 Ib	DAO CCD
2008	2454754	0.4429	$23.6 \pm 17.4$	K1 Ib	DAO CCD
2009	2455086	0.4030	$8.5 \pm 21.4$	K0 Ib	DAO CCD
2010	2455489	0.5673	$10.7 \pm 21.7$	K1 Ib	DAO CCD

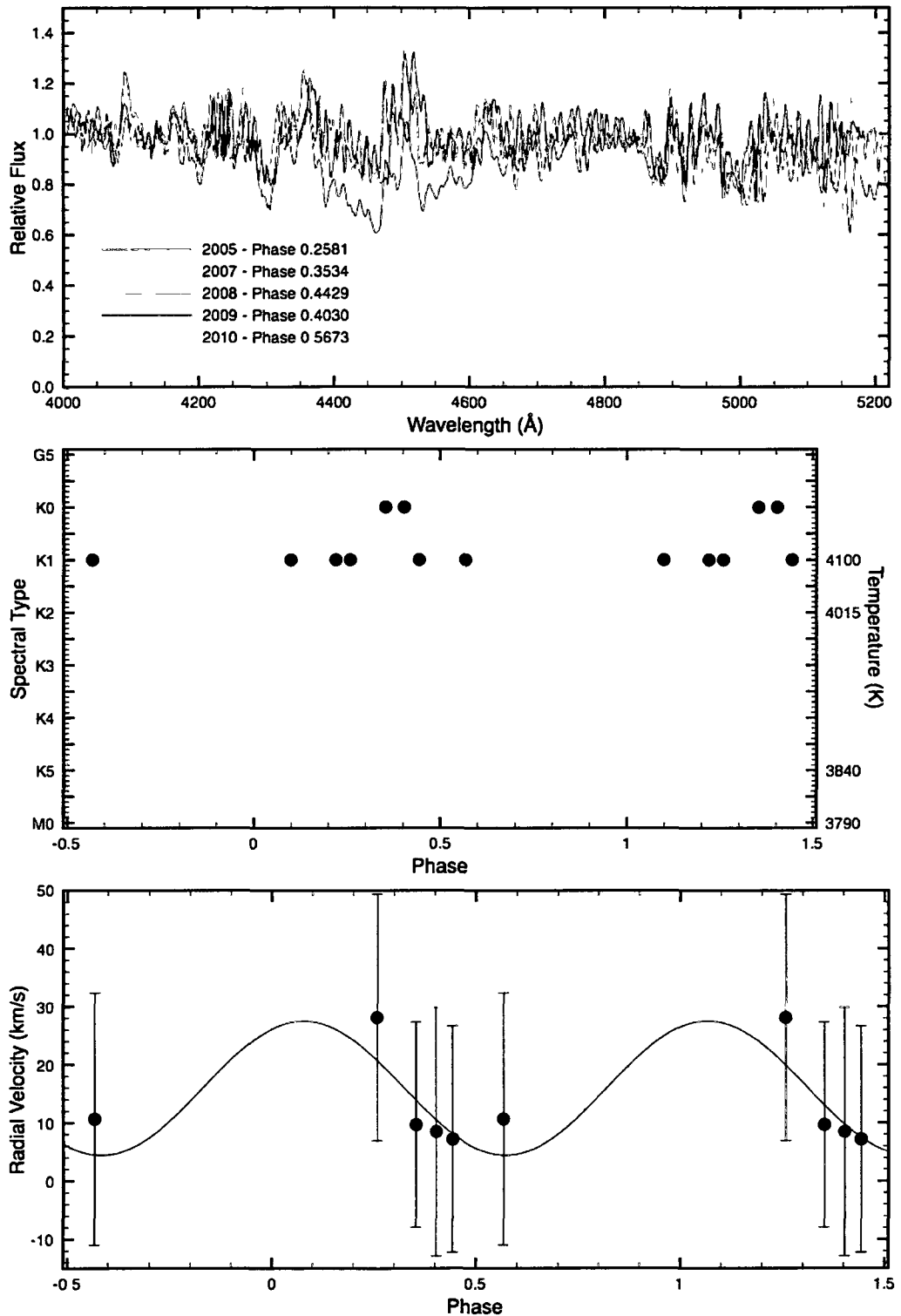


**Figure 4.16:** Spectral variation in W Cephei. Top: Spectra from different epochs. Middle: Spectral type as a function of phase. Bottom: Radial velocity as a function of phase. Data phased with 346.26 day period.

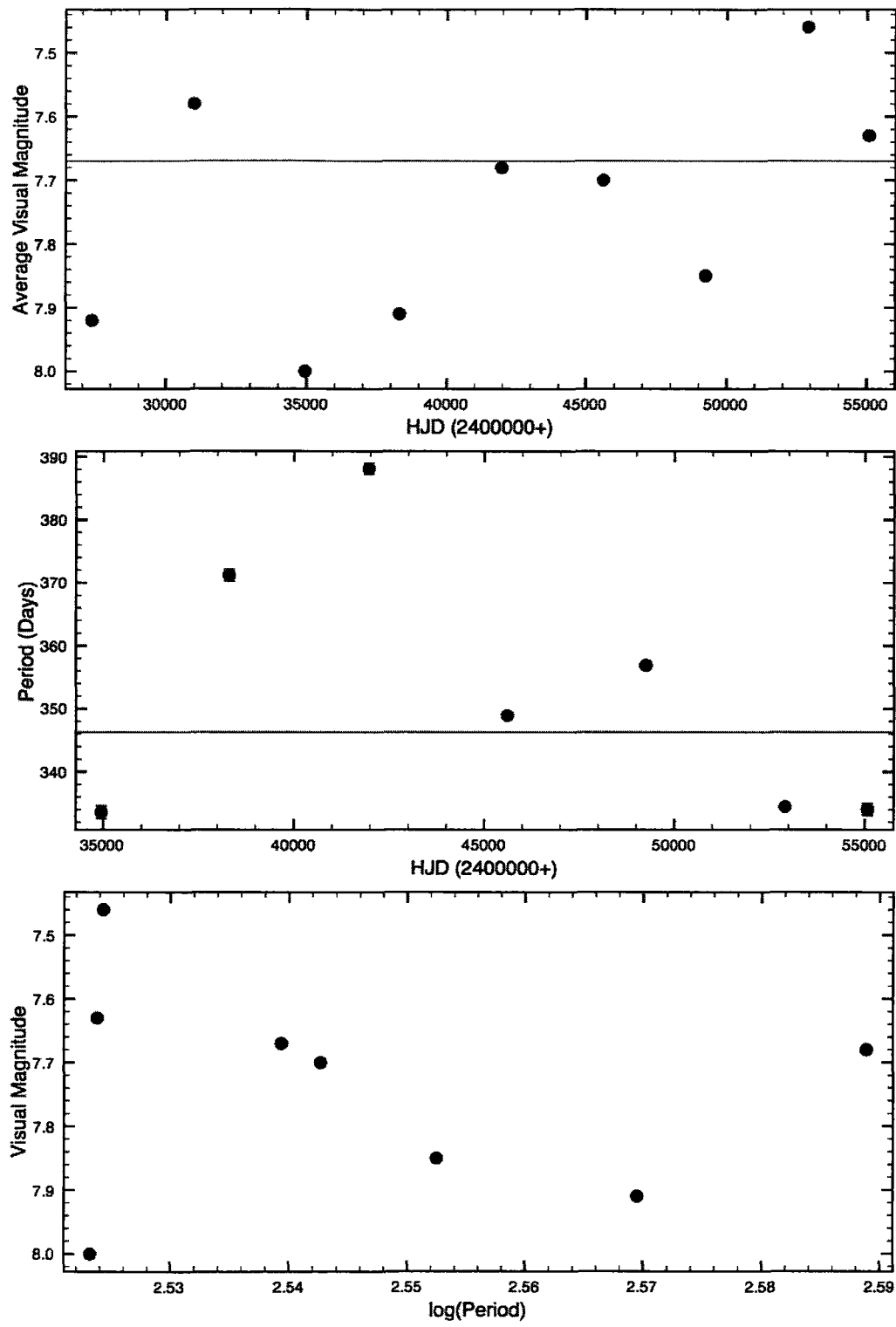


Figure 4.17: Period and average magnitude changes in W Cephei from AAVSO observations.

## 4.15 SW Cephei

Figure 4.18 shows SW Cep's variations in spectral type and radial velocity, phased using a period of 599.10 days and a time of maximum light of JD2455086.57 from the AAVSO observations, and a montage of CCD spectra taken at different epochs. It appears to reach smallest dimensions near phase 0.98, along with highest temperature and greatest luminosity class. The lack of photometric observations for the star limits drawing any conclusions about the nature of its variability, despite the availability of spectroscopic data. The GCVS lists a period for the star of 70 days and a spectral type of M3.5 Ia-Iab. We found that the data phased better with the 599 period, but it is possible that the star is multiperiodic, or perhaps the 70-day period was found using a short baseline of observations. SW Cep is an excellent candidate for obtaining archival data from the Harvard plate stacks, since photometry is the star's greatest need.

**Table 4.24:** AAVSO Observations of SW Cephei

Subset	Dates	$\langle V \rangle$	% Diff.	$\Delta V$	$N$	$P$ (days)	% Diff.
All	27925-54845	8.62	...	2.1	84	$599.10 \pm 7.13$	...
1	27925-29628	8.19	-4.99	0.4	9	...	...
2	42240-49216	8.30	-3.71	1.4	4	...	...
3	50657-51832	8.70	0.93	0.9	17	...	...
4	53938-54845	8.69	0.81	1.4	52	$599.10 \pm 8.91$	...

**Table 4.25:** Spectroscopic observations of SW Cephei

Year	HJD	Phase	$V_R$ (km/s)	Spectral Type	Source
2007	2454377	0.5614	$2.3 \pm 14.7$	M3 Iab	DAO CCD
2008	2454749	0.1857	$-11.0 \pm 21.3$	M2 Ia	DAO CCD
2009	2455086	0.7485	$6.7 \pm 22.0$	M4 Iab	DAO CCD
2010	2455489	0.4211	$-0.1 \pm 18.1$	M4 Iab	DAO CCD

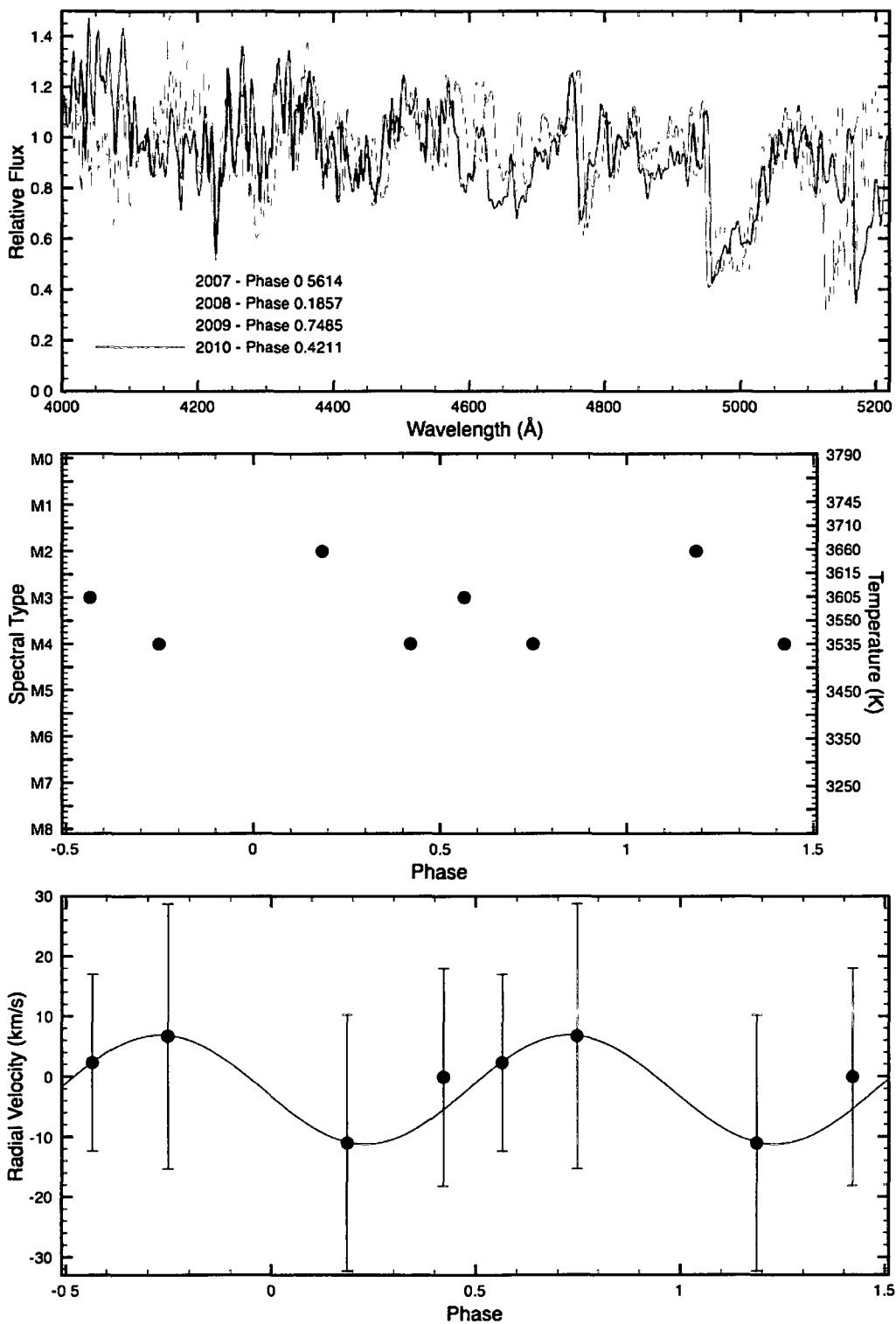


**Figure 4.18:** Spectral variation in SW Cephei. Top: Spectra from different epochs. Middle: Spectral type as a function of phase. Bottom: Radial velocity as a function of phase. Data phased with 599.10 day period.

#### 4.16 VV Cephei

The period of variability for VV Cep outside of eclipses is essentially unknown and cannot be estimated reliably from AAVSO observations. Figure 4.21 shows a plot of  $V_R$  O-C residuals from a new orbital solution obtained by Roger Griffin phased with the 285-day period determined from Fourier analysis of the measurements. Figure 4.19 shows VV Cep's variations in spectral type and radial velocity, phased using a period of 285 days determined from Roger Griffin's radial velocity residuals and a time of maximum light of JD2453392.76 from the AAVSO observations, as well as a montage of CCD spectra taken at different epochs. VV Cep shows strong emission in the cores of its hydrogen lines, presumably arising from material in the associated accretion disk in the system. From the Griffin radial velocity residuals, the star appears to reach smallest dimensions near phase 0.76, although we note that is not a conclusive result, as the AAVSO observations do not provide a reliable period and there is a lot of scatter in the Griffin radial velocity residuals. It is not clear at what phase the temperature reaches maximum. Its luminosity class has remained fairly constant, but the observations suggest that it may reach greatest luminosity class at earliest spectral type.

Figure 4.20 shows VV Cep's period and average visual magnitude taken at approximately 10-year intervals from the AAVSO data. The 364-day period found is most likely an alias. Lack of proper phasing for the spectroscopic data means that they cannot be used at present to study pulsation in the star. The lack of any obvious periodicity in its light curve indicates that it may actually be an LC variable or some other type of variable. VV Cephei's eclipse period is 7430 days, which is approximately 20 years. Its most recent eclipse in 1997-1998 occurred approximately 68 days late (Leedjärv et al. 1999). Pulsation of the M supergiant component could explain the eclipse delay.

**Table 4.26:** AAVSO Observations of VV Cephei

Subset	Dates	$\langle V \rangle$	% Diff.	$\Delta V$	$N$	$P$ (days)	% Diff.
All	24371-55396	5.18	...	1.4	6970	$364.21 \pm 0.16$	...
1	24371-27804	5.33	2.90	0.3	113	...	...
2	27828-27960	5.48	5.79	0.2	10	...	...
3	33052-33068	5.39	4.05	0.8	20	...	...
4	41172-42195	5.35	3.28	0.6	10	...	...
5	43301-49907	5.25	1.35	0.7	560	$361.00 \pm 0.84$	-0.88
6	49922-53565	5.17	-0.19	1.4	1970	$365.60 \pm 0.46$	0.38
7	53571-55396	5.11	-1.35	1.3	950	$356.79 \pm 1.47$	-2.04

**Table 4.27:** Spectroscopic observations of VV Cephei

Year	HJD	Phase	$V_R$ (km/s)	Spectral Type	Source
1936	2428470	0.7936	...	M1.5 Ia-Ib	DDO
1936	2438484	0.7955	...	M3 Ib	DDO
2005	2453655	0.1833	$-15.0 \pm 25.1$	M2 Ib	DAO CCD
2007	2454382	0.2812	$14.3 \pm 14.8$	M2 Ib	DAO CCD
2008	2454749	0.3306	$4.1 \pm 17.9$	M2 Ib	DAO CCD
2010	2455489	0.4302	$25.2 \pm 16.5$	M2 Ib	DAO CCD

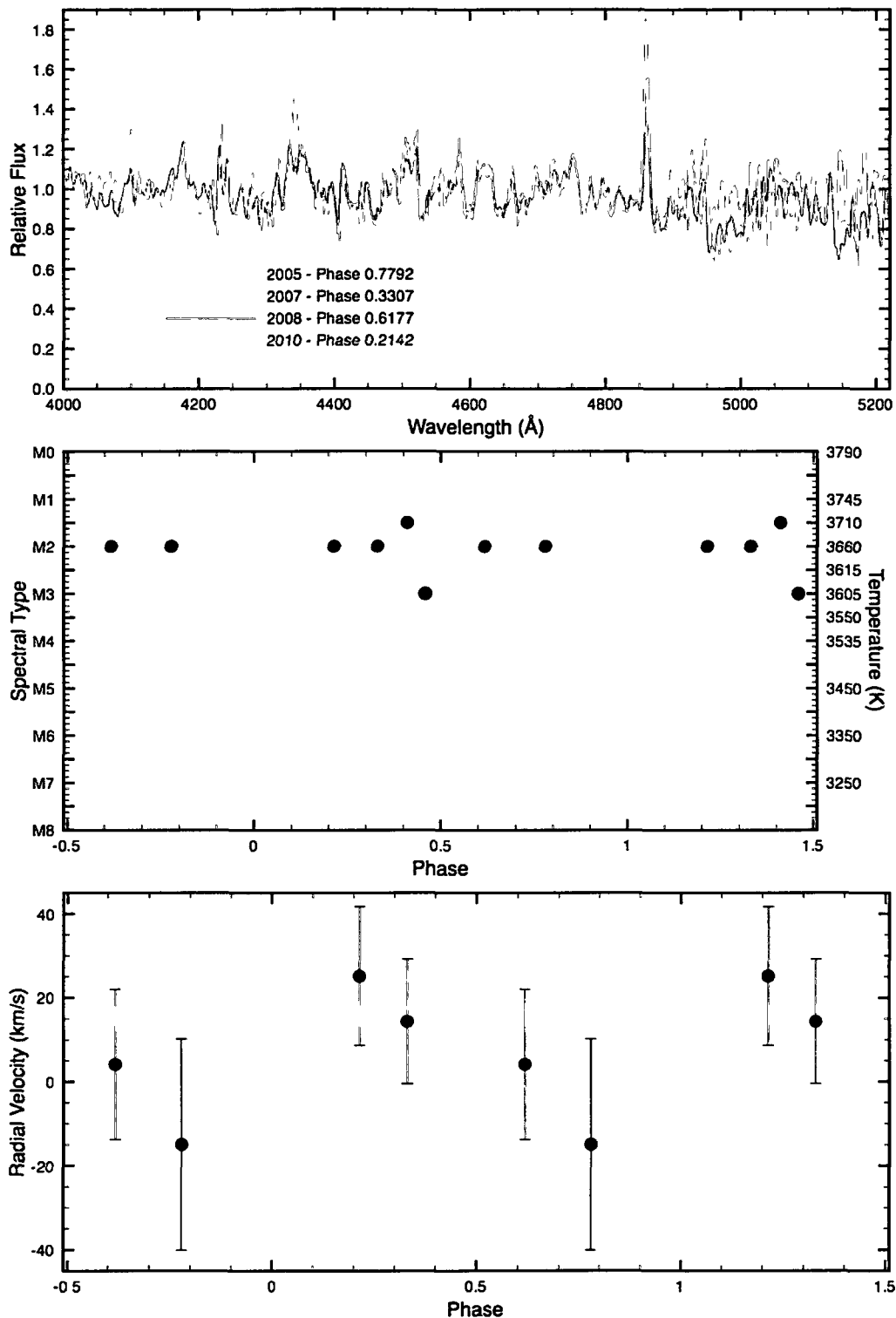


**Figure 4.19:** Spectral variation in VV Cephei. Top: Spectra from different epochs. Middle: Spectral type as a function of phase. Bottom: Radial velocity as a function of phase. Data phased with 364.21 day period.

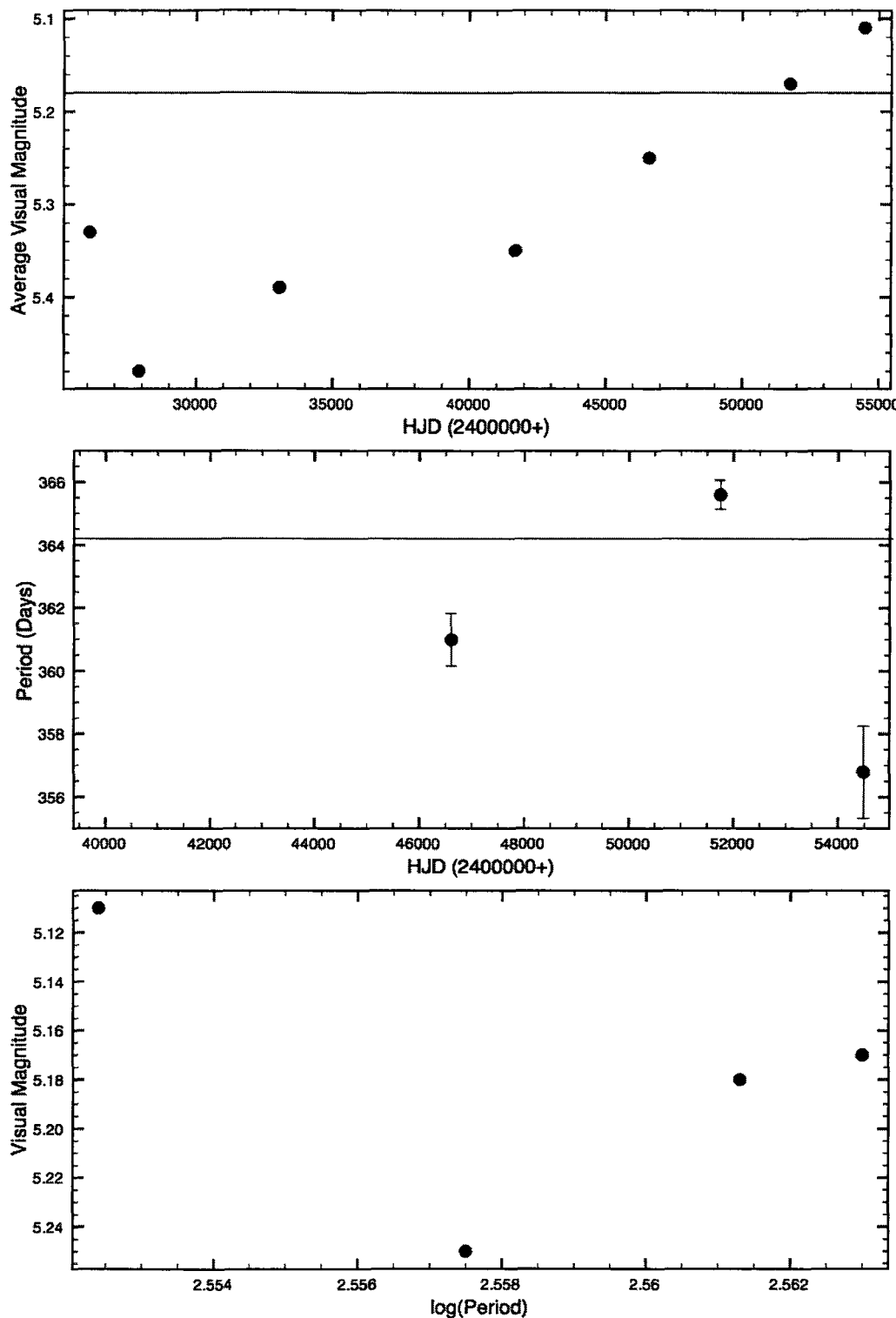
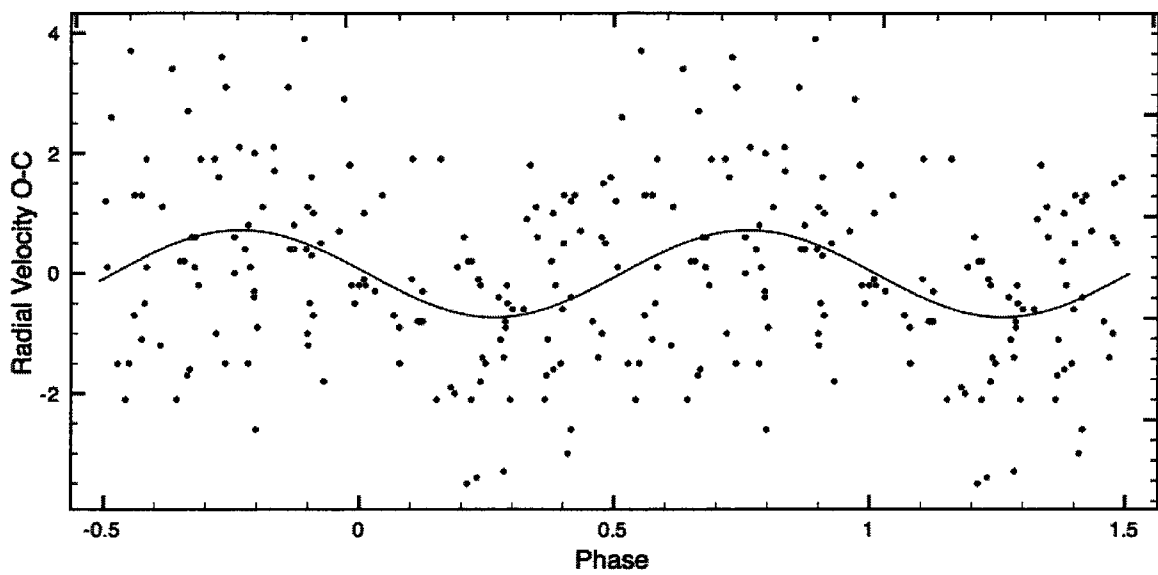


Figure 4.20: Period and average magnitude changes in VV Cephei from AAVSO observations.



**Figure 4.21:** Phased  $V_R$  O-C values for VV Cephei

## 4.17 MY Cephei

Figure 4.22 shows our spectrum of MY Cep, obtained in 2005. We could not determine the phase, as there are not enough photometric observations in the literature to find a solid period. Table 4.28 lists the details of our single observation. With a spectral type of M7, MY Cep is one of the coolest SRC variables in our sample. Because there are no published photometric observations of the star, it is not possible to infer a periodicity, although its M7 Ia spectral type is typical of long-period SRC variables. Thus, our single spectroscopic observation of the star cannot be used to infer anything about its variability, which has a small amplitude ( $\Delta V \simeq 0^m.9$ ) according to the GCVS.

**Table 4.28:** Spectroscopic observations of MY Cephei

Year	HJD	Phase	$V_R$ (km/s)	Spectral Type	Source
2005	2453655	...	$-26.9 \pm 14.6$	M7 Ia	DAO CCD

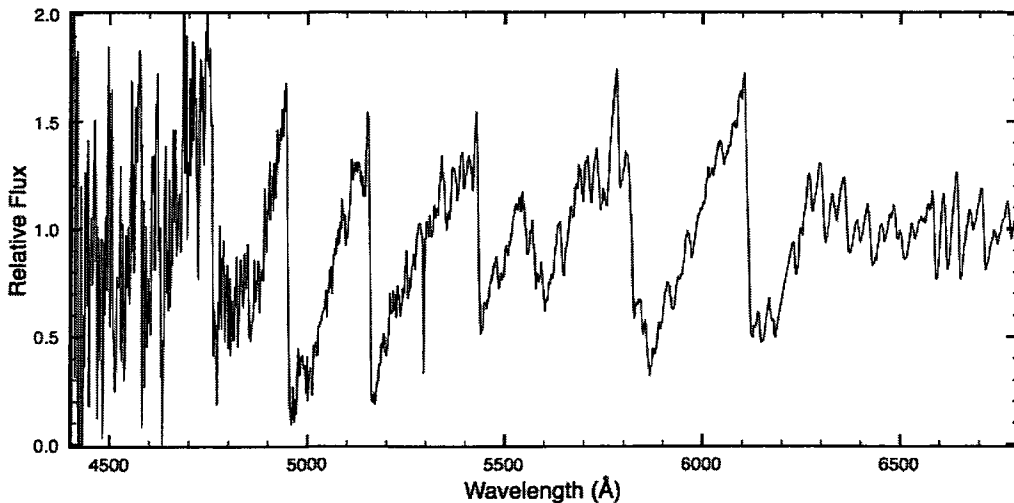


**Figure 4.22:** Spectrum of MY Cephei

#### 4.18 $\mu$ Cephei

Figure 4.23 shows  $\mu$  Cep's variations in spectral type and radial velocity, phased using a period of 843.65 days and a time of maximum light of JD2451656.51 from the AAVSO observations, and a montage of CCD spectra taken at different epochs. The star appears to reach smallest dimensions near phase 0.54. The temperature is varying, but it is not clear at what phase it reaches maximum. Its luminosity class did not vary much over the period of spectroscopic observation examined. Figure 4.24 shows  $\mu$  Cep's changes in period and average visual magnitude taken at approximately 10-year intervals. The period and average magnitude undergo changes, some in consistent fashion. Its period is shorter when its average magnitude is brighter. The GCVS lists its period as 730 days. The light amplitude of  $\mu$  Cep is small and variable, possibly masked by long-time-scale variations in mean brightness. Periodicity is not obvious. The spectroscopic observations are compromised by the lack of a firm phasing for the star. Is it indeed stable? Or is  $\mu$  Cep actually an LC variable? Ongoing monitoring of the star is needed to determine its true nature.

**Table 4.29:** AAVSO Observations of  $\mu$  Cephei

Subset	Dates	$\langle V \rangle$	% Diff.	$\Delta V$	$N$	$P$ (days)	% Diff.
All	-4771-55442	4.15	...	2.5	47489	$843.65 \pm 0.12$	...
1	-4771- -1150	4.17	0.48	1.0	45	$899.96 \pm 14.45$	6.67
2	-959-1989	4.04	-2.65	1.4	113	$749.10 \pm 7.95$	-11.21
3	2924-6157	4.33	4.34	2.0	173	$747.23 \pm 8.01$	-11.43
4	6187 -9820	4.28	3.13	1.1	139	$837.03 \pm 7.50$	-0.78
5	9855 -13466	4.16	0.24	0.9	132	$810.98 \pm 7.06$	-3.87
6	13487-17127	4.10	-1.20	1.1	327	$853.37 \pm 4.98$	1.15
7	17133-20774	4.16	0.24	1.8	509	$999.62 \pm 16.45$	18.49
8	20786-24428	4.18	0.72	1.3	336	$697.69 \pm 4.95$	-17.30
9	24445-20876	4.01	-3.37	1.0	472	$797.72 \pm 4.51$	-5.44
10	28086-31730	3.98	-4.10	0.8	388	$753.24 \pm 3.30$	-10.72
11	31730-35380	4.23	1.93	1.8	2405	$886.56 \pm 2.16$	5.09
12	35381-39029	4.25	2.41	2.2	1830	$1116.24 \pm 4.33$	32.31
13	39029-42680	4.28	3.13	2.4	5809	$977.21 \pm 2.78$	15.83
14	42680-46229	4.23	1.93	2.3	6215	$863.31 \pm 1.92$	2.33
15	46231-49980	4.19	0.96	2.1	9634	$859.99 \pm 1.29$	1.94
16	49980-53629	4.05	-2.41	2.3	13290	$870.46 \pm 0.94$	3.18
17	53630-55442	4.00	-3.61	1.8	5672	$853.57 \pm 2.66$	1.18

**Table 4.30:** Spectroscopic observations of  $\mu$  Cephei

Year	HJD	Phase	$V_R$ (km/s)	Spectral Type	Source
1920	2422633	0.4845	...	M1 Ia	DAO Pg
1921	2423015	0.9372	...	M1.5 Ia+	DAO Pg
1922	2423295	0.2689	...	M2 Ia	DAO Pg
1945	2431688	0.2129	...	M1 Ia-Iab	DDO
1949	2433192	0.9952	...	M1 Ia-Iab	DAO Pg
1951	2433960	0.9057	...	M0.5-1 Ia	DDO
1967	2394794	0.8170	...	M2 Ia	DDO
1968	2394864	0.9010	...	M2 Ia	DDO
1970	2440848	0.0657	...	M2.8 Ia	Wing
1970	2440875	0.0977	...	M2.7 Ia	Wing
1970	2440900	0.1273	...	M2.5 Ia	Wing
1970	2440904	0.1321	...	M2.4 Ia	Wing
1973	2441962	0.3856	...	M0.6 Ia	Wing
1974	2442291	0.7754	...	M1.3 Ia	Wing
1975	2442591	0.1309	...	M2.5 Ia	Wing
2005	2453655	0.2403	$30.4 \pm 19.9$	M2 Ia	DAO CCD
2007	2454375	0.0934	$24.2 \pm 16.9$	M1 Ia	DAO CCD
2008	2454749	0.5364	$16.8 \pm 16.5$	M1 Ia	DAO CCD
2009	2455086	0.9359	$-3.0 \pm 19.6$	M1 Ia	DAO CCD
2010	2455489	0.4132	$21.8 \pm 19.2$	M1 Ia	DAO CCD

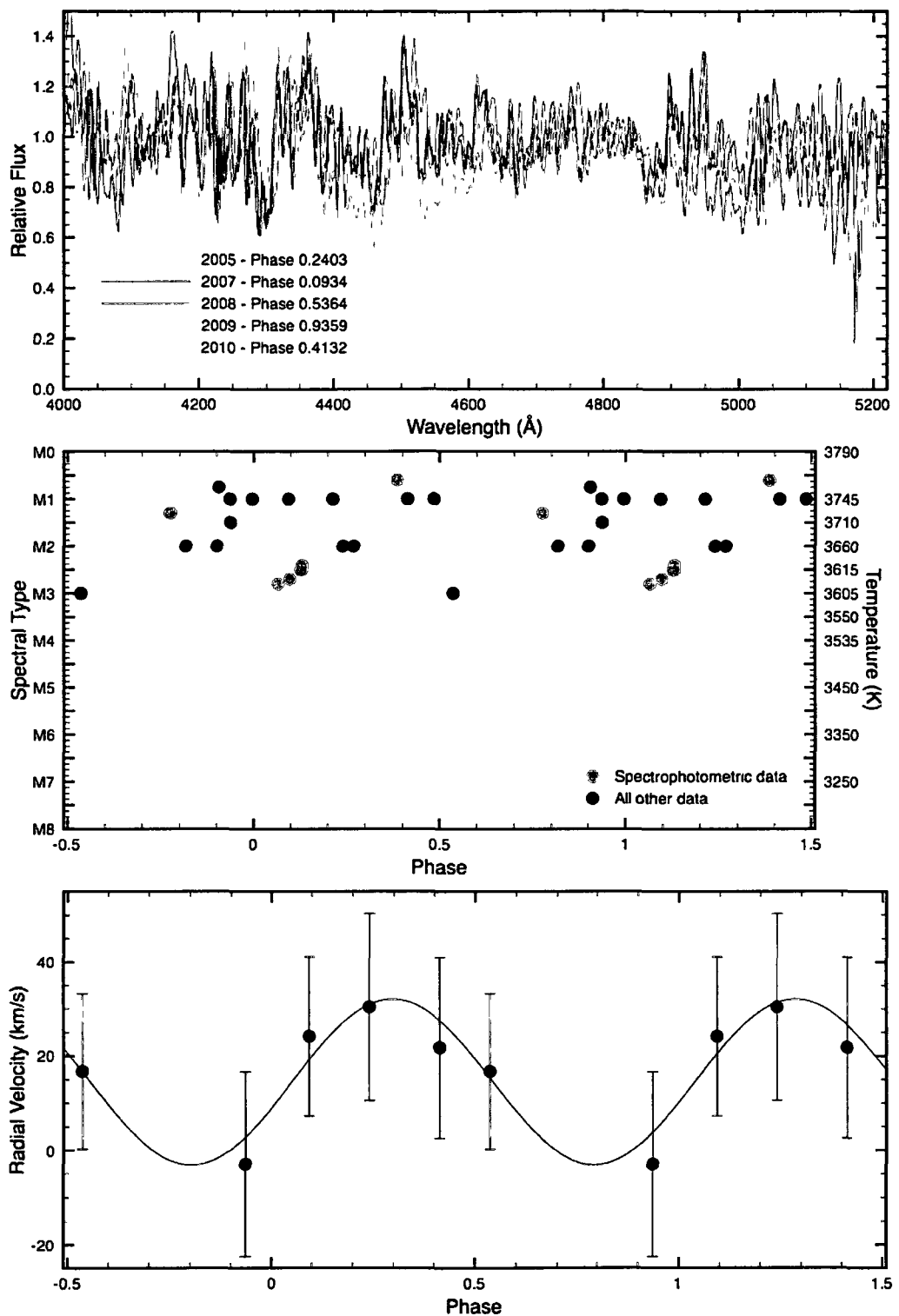


**Figure 4.23:** Spectral variation in  $\mu$  Cephei. Top: Spectra from different epochs. Middle: Spectral type as a function of phase. Bottom: Radial velocity as a function of phase. Data phased with 843.65 day period.

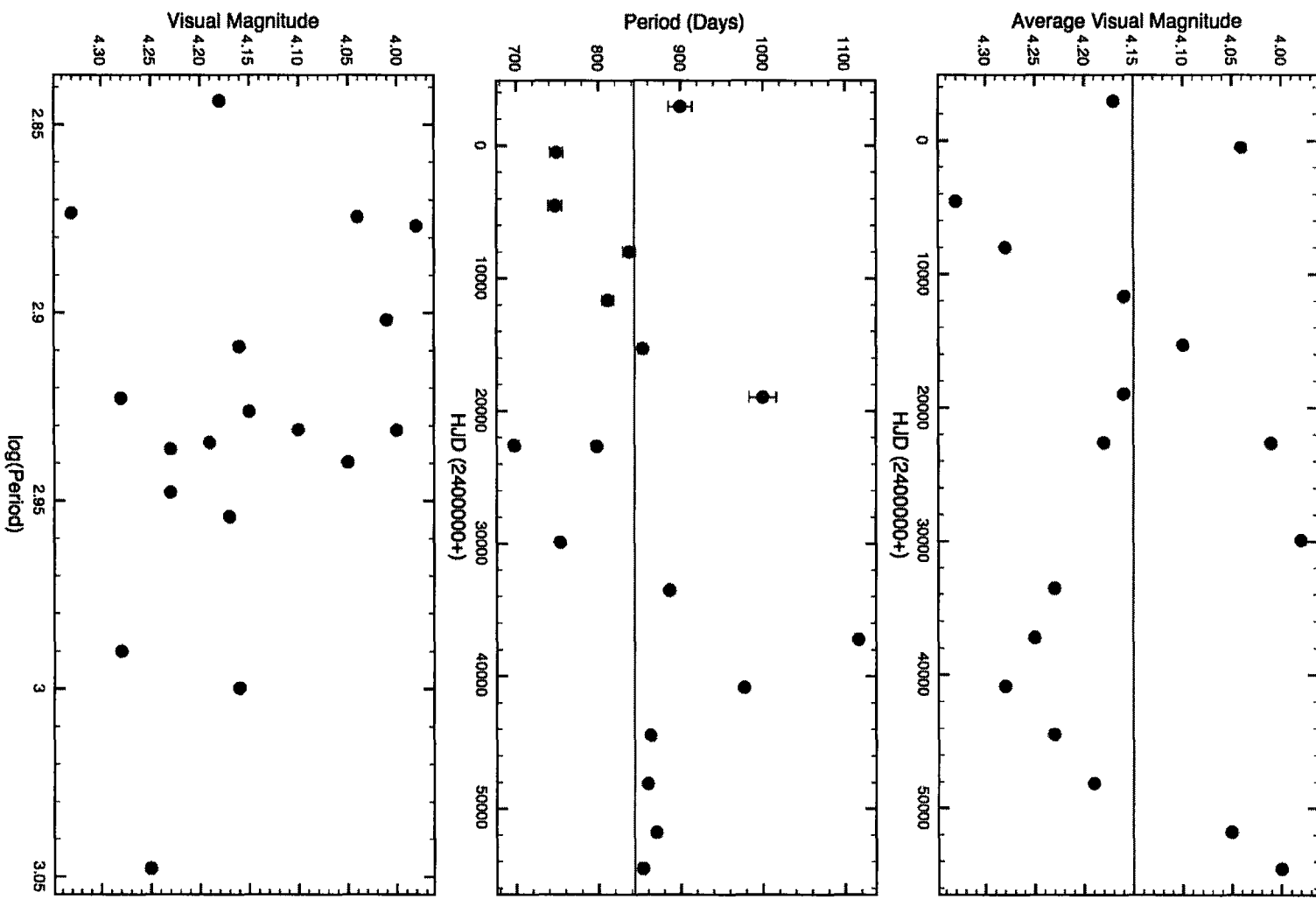


Figure 4.24: Period and average magnitude changes in  $\mu$  Cephei from AAVSO observations.

## 4.19 T Ceti

Figure 4.25 show's T Cet's changes in spectral type and radial velocity, phased with a period of of 160.84 days and a time of maximum light of JD2422499.4 from the AAVSO observations. Although Joy found the spectral type to be constant, the radial velocity variation hints at pulsation. The radial velocity plot indicates that T Cet reaches smallest dimensions near phase 0.46. Figure 4.26 shows T Cet's changes in period and average visual magnitude taken at approximately 10-year intervals. The GCVS lists a period of 158.9 days, nearly identical to that found through our Fourier analysis. The periodicity is well-established, but lack of spectroscopic data impedes progress in learning more about the nature of its variability. Variations in mean magnitude may imply dust extinction episodes. It is odd that Joy's spectra of the star show no variation, but it is possible that they were underexposed or taken at a high airmass (T Cet would have been low on the horizon when Joy was observing it at Mount Wilson, as it has a declination of  $-20^\circ$ ), making them difficult to classify.

**Table 4.31:** AAVSO Observations of T Ceti

Subset	Dates	$\langle V \rangle$	% Diff.	$\Delta V$	$N$	$P$ (days)	% Diff.
All	20178-55237	6.11	...	3.0	6395	$160.84 \pm 0.01$	...
1	20178-23824	5.99	-1.96	1.8	194	$158.13 \pm 0.28$	-1.69
2	23987-27475	6.24	2.13	1.5	397	$160.23 \pm 0.19$	-0.38
3	27632-29883	6.18	1.15	1.9	231	$161.93 \pm 0.39$	0.68
4	31388-34775	5.99	-1.96	2.7	389	$162.26 \pm 0.20$	0.88
5	34781-38427	6.20	1.47	2.2	786	$159.69 \pm 0.17$	-0.72
6	38428-42072	6.19	1.31	2.2	825	$164.85 \pm 0.16$	2.49
7	42078-45722	6.07	-0.65	2.3	1049	$161.59 \pm 0.11$	0.46
8	45728-49374	5.99	-1.96	2.3	916	$164.92 \pm 0.79$	2.53
9	49381-53026	6.03	-1.31	2.1	1177	$157.65 \pm 0.17$	-1.99
10	53030-55237	6.29	2.95	2.8	431	$163.14 \pm 0.31$	1.43

**Table 4.32:** Spectroscopic observations of T Ceti

Year	HJD	Phase	$V_R$ (km/s)	Spectral Type	Source
1939	2424012	0.4044	29	M5	Joy
1939	2424037	0.5598	28	M5	Joy
1939	2424073	0.7836	17	M5	Joy
1939	2424333	0.4001	37	M5	Joy
1939	2424365	0.5991	26	M5	Joy
1939	2424393	0.7732	26	M5	Joy
1939	2424404	0.8416	28	M5	Joy
1939	2424432	0.0157	35	M5	Joy
1939	2424450	0.1276	40	M5	Joy

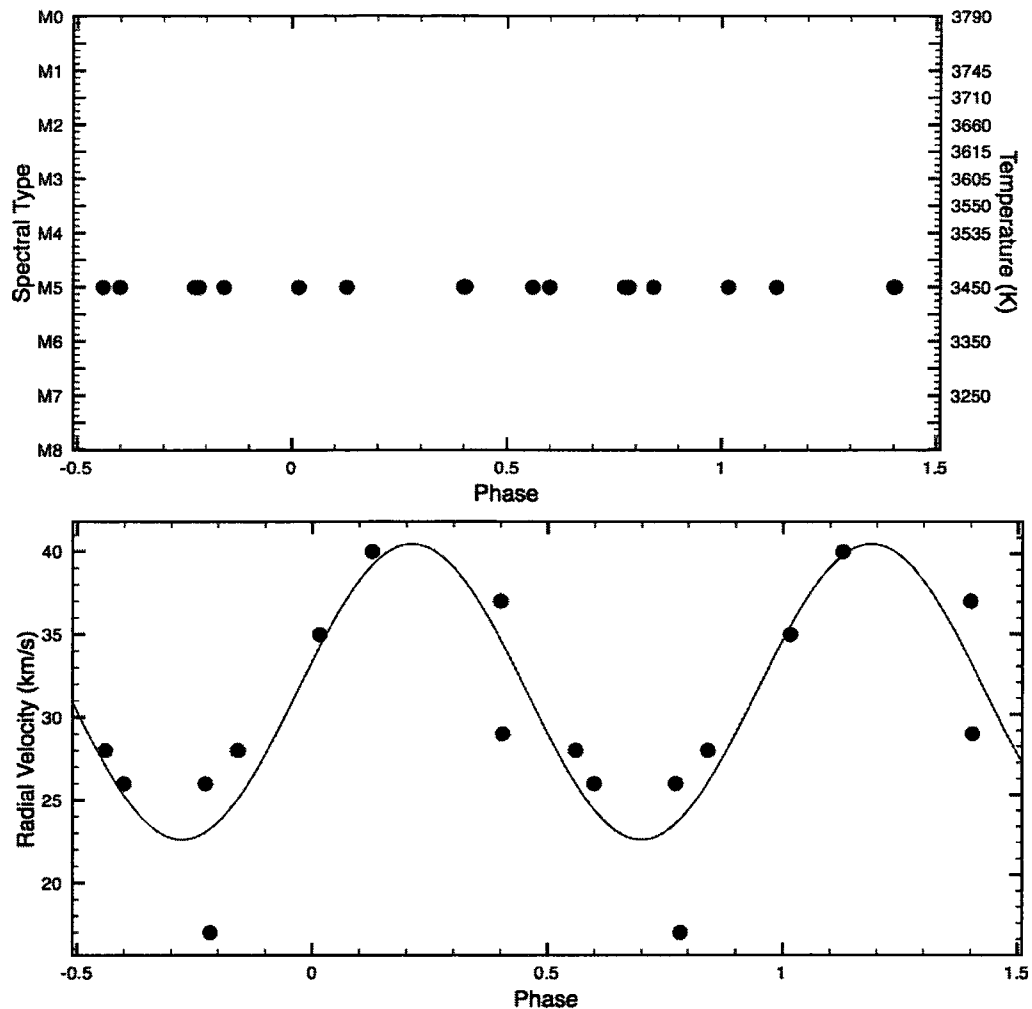


**Figure 4.25:** Spectral variation in T Ceti. Top: Spectral type as a function of phase. Bottom: Radial velocity as a function of phase. Data phased with 160.84 day period.

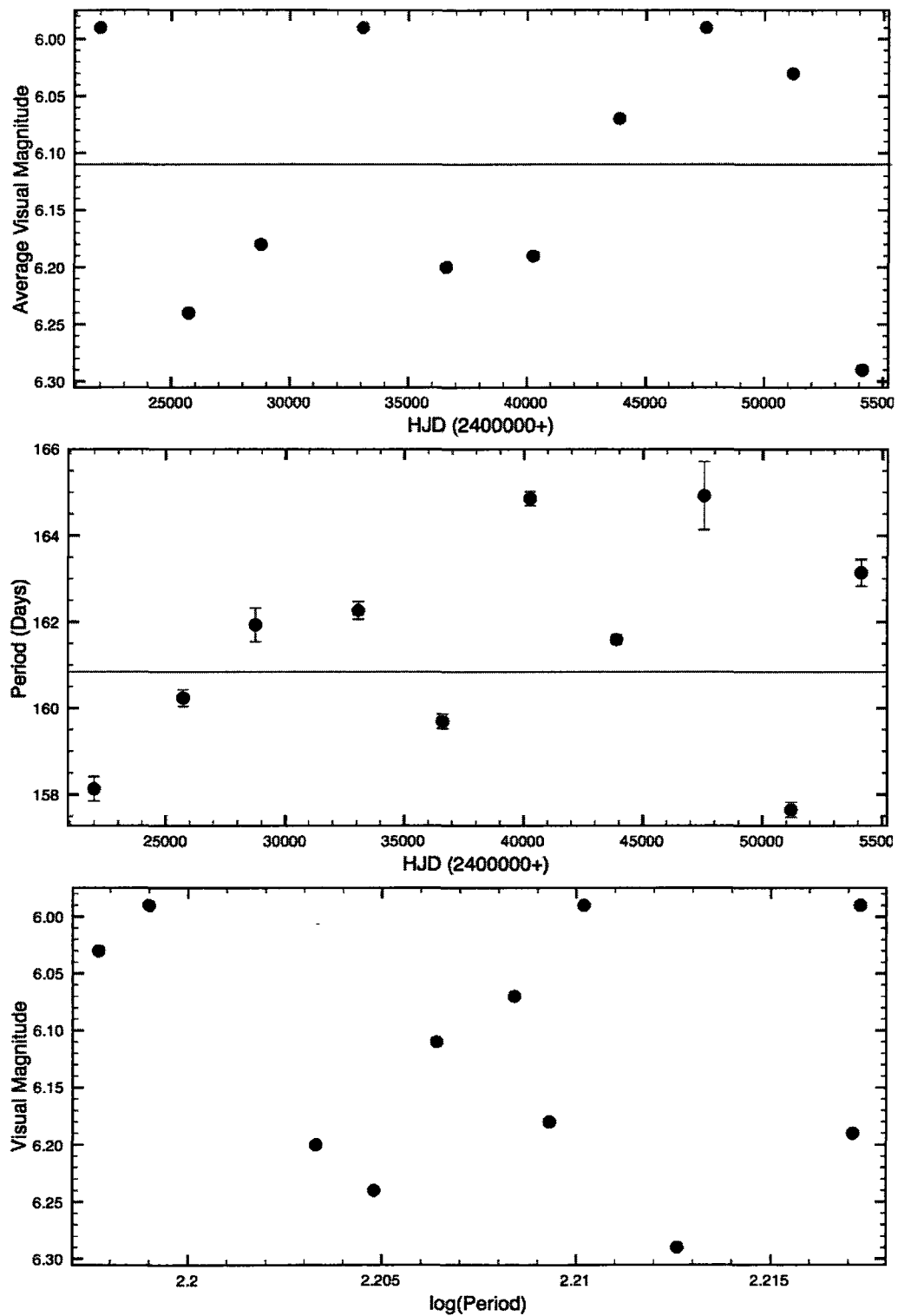


Figure 4.26: Period and average magnitude changes in T Ceti from AAVSO observations.

## 4.20 RW Cygni

Figure 4.27 shows RW Cyg's variations in spectral type and radial velocity phased with a period of 520.52 days and a time of maximum light of JD2444834.79 from the AAVSO observations, as well as a montage of CCD spectra taken at different epochs. The star appears to reach smallest dimensions near phase 0.63. It also appears to reach highest temperature near light minimum. Its luminosity class did not vary over the course of the observations we obtained. Figure 4.28 shows RW Cyg's changes in period and average visual magnitude taken at approximately 10-year intervals. The star's mean brightness appears to change, but its periodicity needs to be better established with more reliable photometry. The GSVS lists a period of 550 days, 30 days longer than our 520 day period. Once better photometry is available, the spectroscopic data will be more useful for interpreting the nature of the star's variability. The star appears to have undergone a dramatic change in light amplitude recently, as it was larger in the past ( $\Delta V \simeq 3^m$ ) compared with at present ( $\Delta V \simeq 1^m.5$ ).

**Table 4.33:** AAVSO Observations of RW Cygni

Subset	Dates	$\langle V \rangle$	% Diff.	$\Delta V$	$N$	$P$ (days)	% Diff.
All	16429-55244	8.82	...	3.4	1907	$520.52 \pm 0.06$	...
1	16429-20077	8.29	-6.01	2.0	90	$516.86 \pm 3.44$	-0.70
2	20079-23624	8.74	-0.91	3.4	534	$550.39 \pm 3.96$	5.74
3	23892-26660	9.02	2.27	2.1	66	$571.95 \pm 14.59$	9.88
4	28503-29264	8.83	0.11	2.4	7	...	...
5	33485-33578	8.47	-3.97	1.2	3	...	...
6	34954-38323	8.95	1.47	2.4	91	$653.70 \pm 8.81$	25.59
7	38331-41974	9.03	2.38	1.0	194	$634.31 \pm 5.90$	21.86
8	41983-45624	9.02	2.27	1.5	226	$554.16 \pm 9.65$	6.46
9	45638-49275	8.84	0.23	1.9	234	$524.22 \pm 4.05$	0.71
10	49303-52686	8.67	-1.70	1.6	315	$525.51 \pm 2.28$	0.96
11	52997-55244	9.06	2.72	1.6	102	$478.36 \pm 6.43$	-8.10

**Table 4.34:** Spectroscopic observations of RW Cygni

Year	HJD	Phase	$V_R$ (km/s)	Spectral Type	Source
2007	2454382	0.3240	$-0.1 \pm 16.6$	M3.5 Iab	DAO CCD
2008	2454749	0.0286	$-25.5 \pm 22.2$	M4 Iab	DAO CCD
2009	2455086	0.6758	$-27.8 \pm 19.6$	M3 Ib	DAO CCD

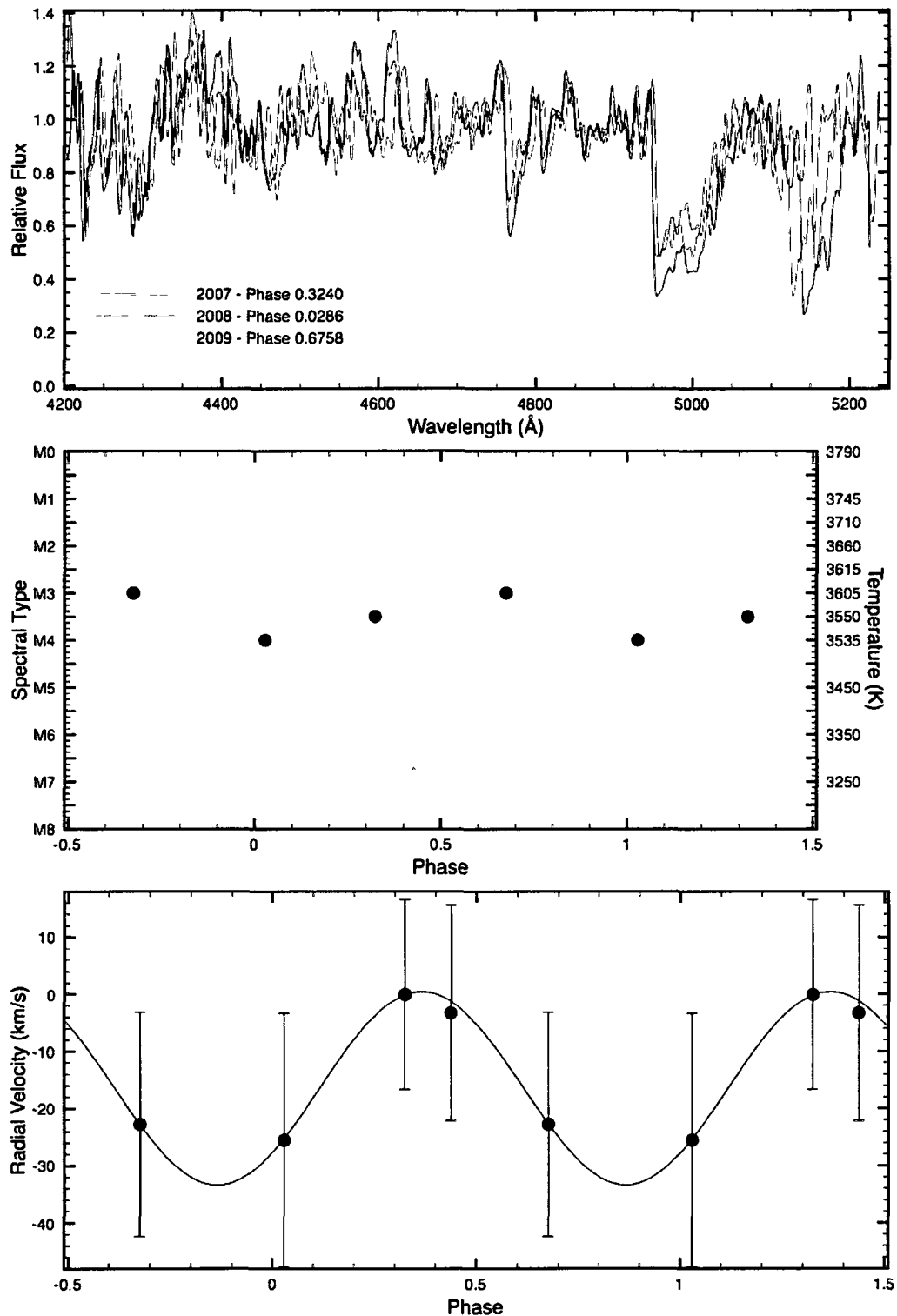


**Figure 4.27:** Spectral variation in RW Cygni. Top: Spectra from different epochs. Middle: Spectral type as a function of phase. Bottom: Radial velocity as a function of phase. Data phased with 520.52 day period.

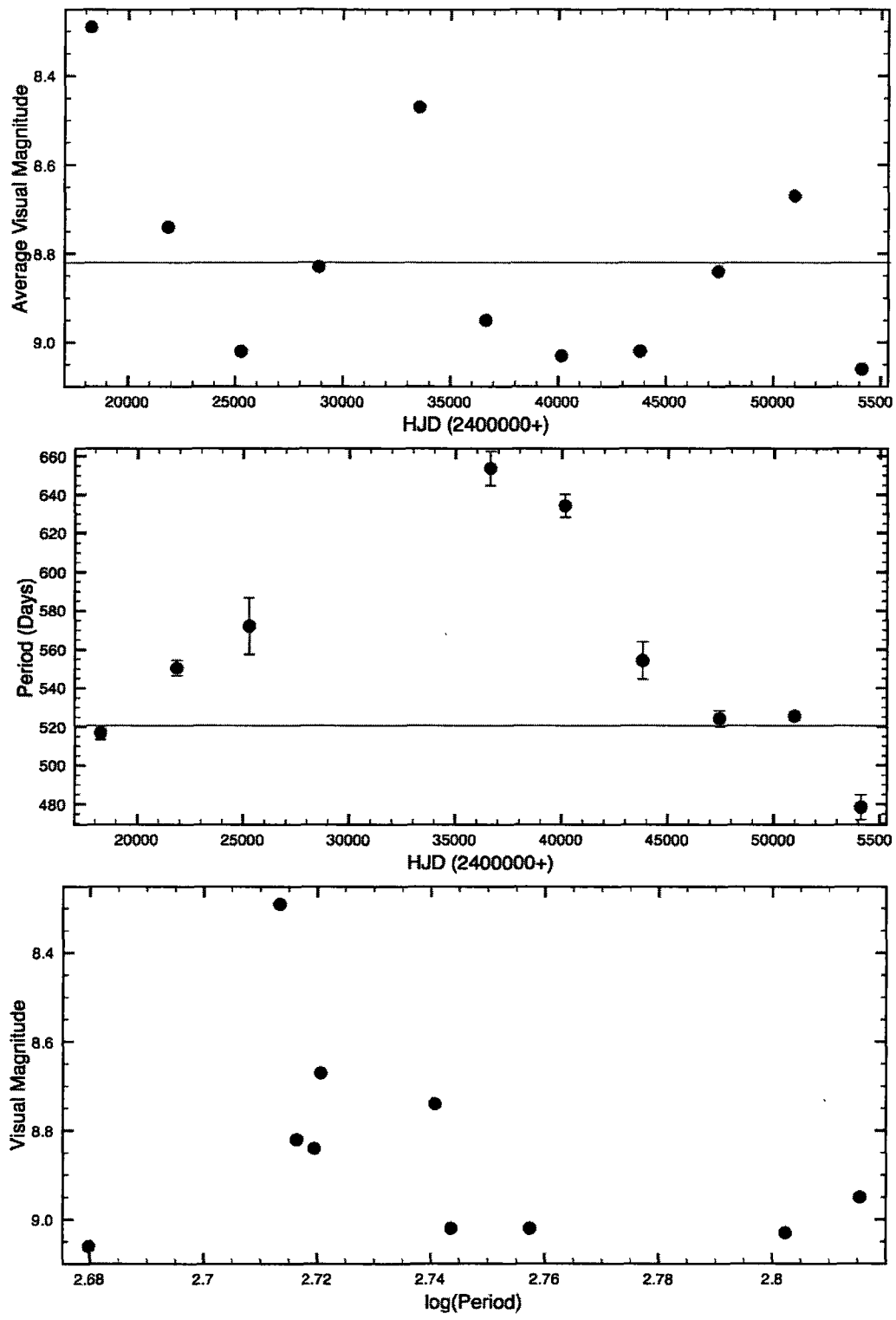


Figure 4.28: Period and average magnitude changes in RW Cygni from AAVSO observations.

## 4.21 AZ Cygni

Figure 4.29 shows AZ Cyg's variations in spectral type and radial velocity and a montage of CCD spectra taken at different epochs. The spectroscopic observations were phased using a period of 459.17 days, determined from the AAVSO observations. We used a time of maximum light of JD2440074.4 for the older spectrophotometric observations and JD2451418.62 for the recent CCD observations. The GCVS lists an identical period of 459 days and a light amplitude of  $\Delta B \simeq 1^m.8$ . From the data we have at present, we fitted the radial velocity variations with a sine wave and found that the star appears to reach mean radial velocity after passing through velocity maximum near phase 0.75, indicating its phase of smallest dimensions. AZ Cyg appears to reach smallest dimensions near phase 0.75. It appears to reach highest temperature and greatest luminosity near light maximum. Figure 4.30 shows AZ Cyg's changes in period and average visual magnitude taken at approximately 10-year intervals. The star has a small amplitude and exhibits possible extinction dips, but phasing of recent spectroscopic data is difficult because of the lack of recent photometric data. Further study awaits additional photometry to support the results described here.

**Table 4.35:** AAVSO Observations of AZ Cygni

Subset	Dates	$\langle V \rangle$	% Diff.	$\Delta V$	$N$	$P$ (days)	% Diff.
All	29451-55156	8.63	...	3.1	654	$459.17 \pm 0.11$	...
1	29541-40426	8.56	-0.81	2.4	126	$449.58 \pm 5.56$	-2.09
2	40426-44048	8.57	-0.70	1.9	169	$417.99 \pm 3.31$	-8.97
3	44137-47737	8.29	-3.94	2.3	112	$489.36 \pm 4.07$	6.57
4	47745-51282	8.63	0.00	2.5	78	$474.18 \pm 3.66$	3.27
5	51385-55156	8.96	3.82	3.0	170	$417.16 \pm 2.13$	-9.15

**Table 4.36:** Spectroscopic observations of AZ Cygni

Year	HJD	Phase	$V_R$ (km/s)	Spectral Type	Source
1970	2440869	0.7301	...	M3.3 Iab	Wing
1970	2440872	0.7366	...	M3.2 Iab	Wing
1970	2440875	0.7431	...	M3.4 Iab	Wing
1970	2440904	0.8063	...	M2.9 Iab	Wing
1973	2441962	0.1113	...	M2.8 Ia	Wing
2005	2453652	0.8654	$-11.6 \pm 21.8$	M3 Iab	DAO CCD
2007	2454377	0.4449	$2.01 \pm 16.9$	M2 Ia	DAO CCD
2008	2454749	0.2552	$-7.4 \pm 20.3$	M2 Ia	DAO CCD
2009	2455090	0.0006	$-12.4 \pm 20.1$	M3 Ib	DAO CCD
2010	2455489	0.8674	$-12.2 \pm 15.7$	M3 Iab	DAO CCD

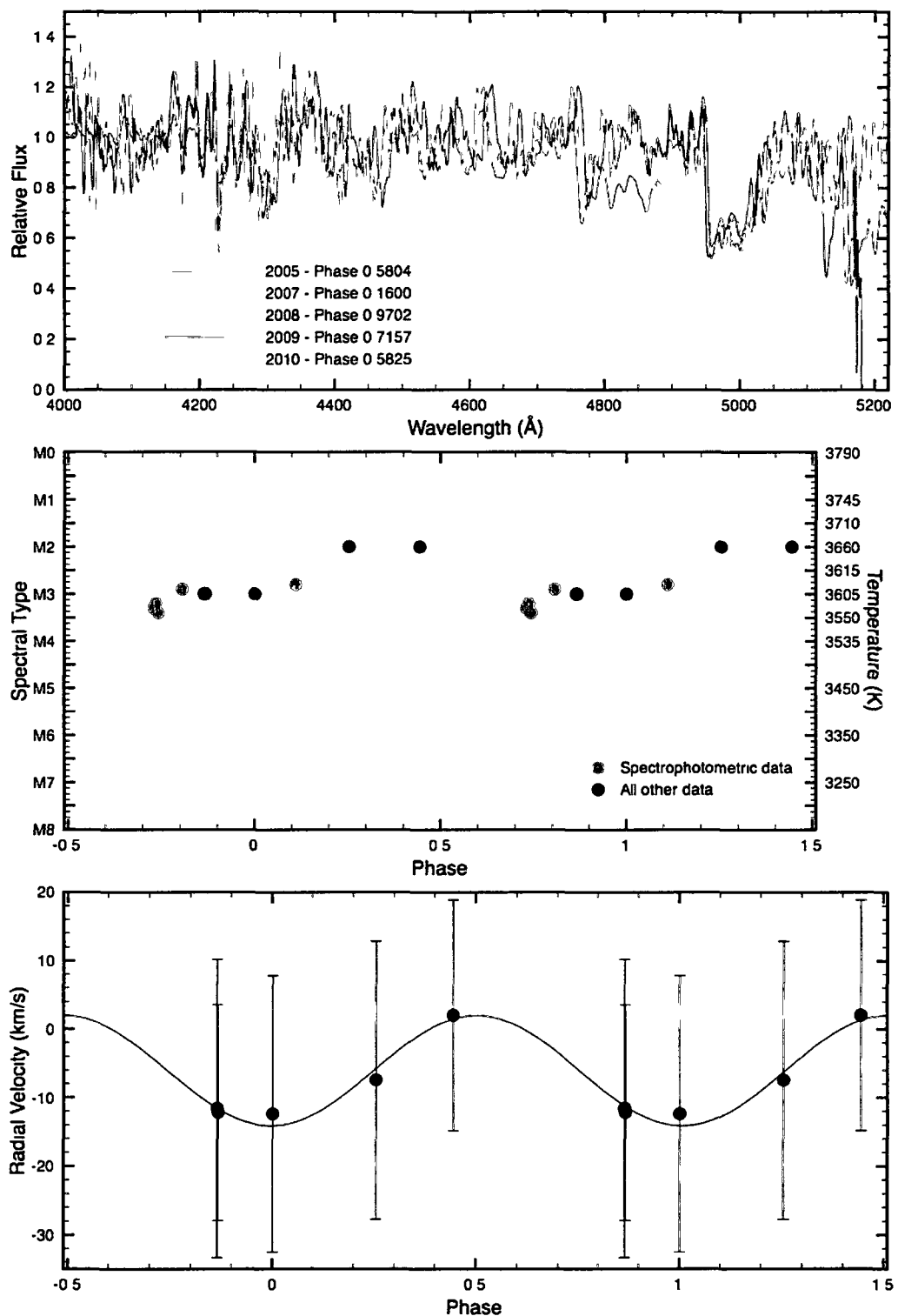


**Figure 4.29:** Spectral variation in AZ Cygni. Top: Spectra from different epochs. Middle: Spectral type as a function of phase. Bottom: Radial velocity as a function of phase. Data phased with 459.17 day period.

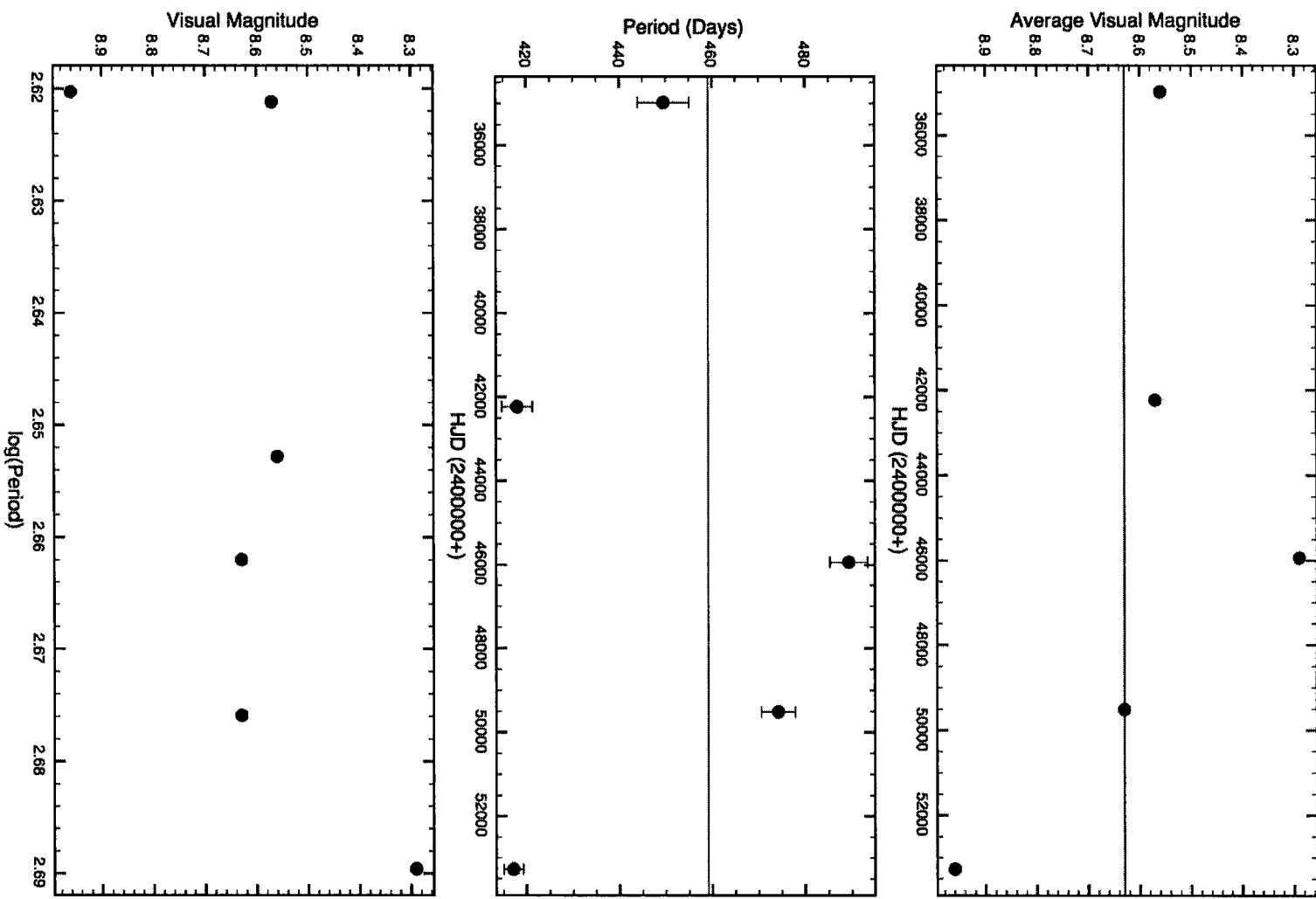


Figure 4.30: Period and average magnitude changes in AZ Cygni from AAVSO observations.

## 4.22 BC Cygni

Figure 4.31 shows BC Cyg's variations in spectral type and radial velocity, as well as a montage of CCD spectra taken at different epochs. The spectroscopic observations were phased using a period of 692.7863 days, found by plotting successive times of maximum light versus cycle number and performing a linear regression. That period gave better results than the period found through Fourier analysis. We fitted the radial velocity variations with a sine wave and found that the star appears to reach mean radial velocity after passing through velocity maximum near phase 0.44, indicating the phase of smallest dimensions. BC Cyg appear to reach smallest dimensions near phase 0.44. It appears to reach highest temperature near light maximum. It reaches greatest luminosity class at highest temperature, but is apparently near largest size then. Figure 4.32 shows BC Cyg's changes in period and average visual magnitude taken at approximately 10-year intervals. We also have 866 blue light observations from the Harvard and Sternberg collections. They cover the dates JD2411584.7-2540284.44, with an average  $B$  magnitude of 12.76 and  $\Delta B \simeq 1^m.8$ . We found a period of  $692.21 \pm 0.25$  days for the photographic observations. The period is well-established from both sets of photometry and appears to be increasing, and the light amplitude from the AAVSO observations is  $\Delta V \simeq 2^m.0$ . There is good spectroscopic coverage for the star. Occasional decreases in mean magnitude may indicate episodes of dust extinction.

**Table 4.37:** AAVSO Observations of BC Cygni

Subset	Dates	$\langle V \rangle$	% Diff.	$\Delta V$	$N$	$P$ (days)	% Diff.
All	33207-53422	9.72	..	2.8	937	$699.35 \pm 0.52$	...
1	33207-44155	10.17	4.63	2.8	177	$746.37 \pm 1.97$	6.72
2	44164-47803	9.82	1.03	1.7	129	$693.83 \pm 7.99$	-0.79
3	47810-51442	9.56	-1.65	1.8	210	$690.43 \pm 4.79$	-1.28
4	51460-55422	9.58	-1.44	2.0	421	$745.05 \pm 3.83$	6.53

**Table 4.38:** Spectroscopic observations of BC Cygni

Year	HJD	Phase	$V_R$ (km/s)	Spectral Type	Source
1940	2429855	0.9498	-6	M4	Joy
1940	2429893	0.0046	1	M3	Joy
1970	2440768	0.7021	...	M3.1 Ia	Wing
1970	2440799	0.7469	...	M2.9 Ia	Wing
1970	2440848	0.8176	...	M2.9 Ia	Wing
1970	2440868	0.8464	...	M2.7 Iab	Wing
1970	2440869	0.8479	...	M2.7 Iab	Wing
1970	2440894	0.8840	...	M3.0 Iab	Wing
1973	2441930	0.3794	...	M4.8 Ib	Wing
1973	2441931	0.3808	...	M4.7 Iab	Wing
1973	2441962	0.4256	...	M4.7 Ib	Wing
2005	2454652	0.2992	$1.34 \pm 15.8$	M4 Iab	DAO CCD
2007	2454378	0.3469	$-2.3 \pm 13.7$	M3 Iab	DAO CCD
2008	2454749	0.8825	$-21.9 \pm 19.8$	M3 Ia	DAO CCD
2009	2455086	0.3690	$2.2 \pm 20.7$	M3 Ib	DAO CCD
2010	2455487	0.9478	$-25.8 \pm 16.5$	M3 Ia	DAO CCD

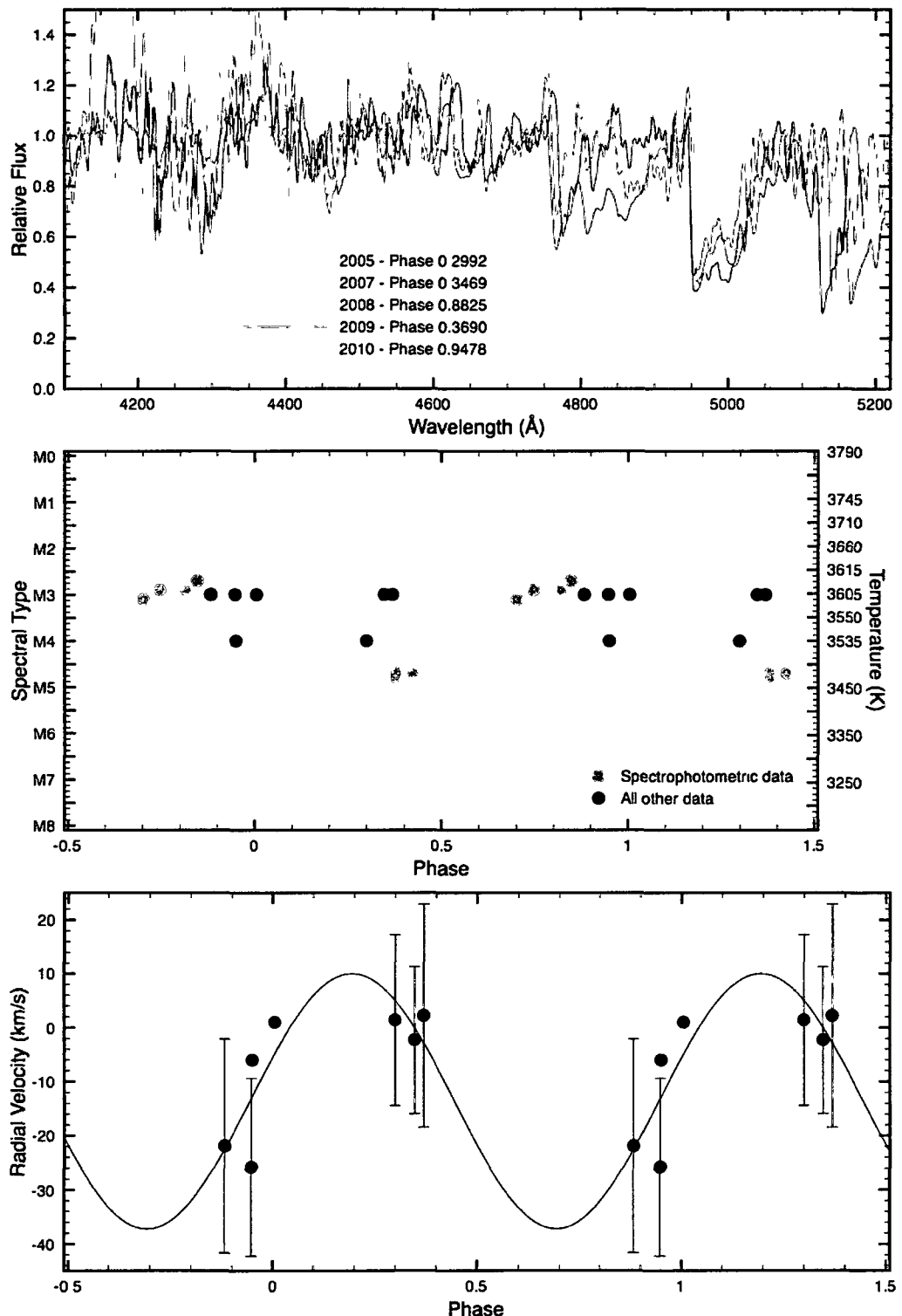


**Figure 4.31:** Spectral variation in BC Cygni. Top: Spectra from different epochs. Middle: Spectral type as a function of phase. Bottom: Radial velocity as a function of phase. Observations phased using 692.7863 day period.

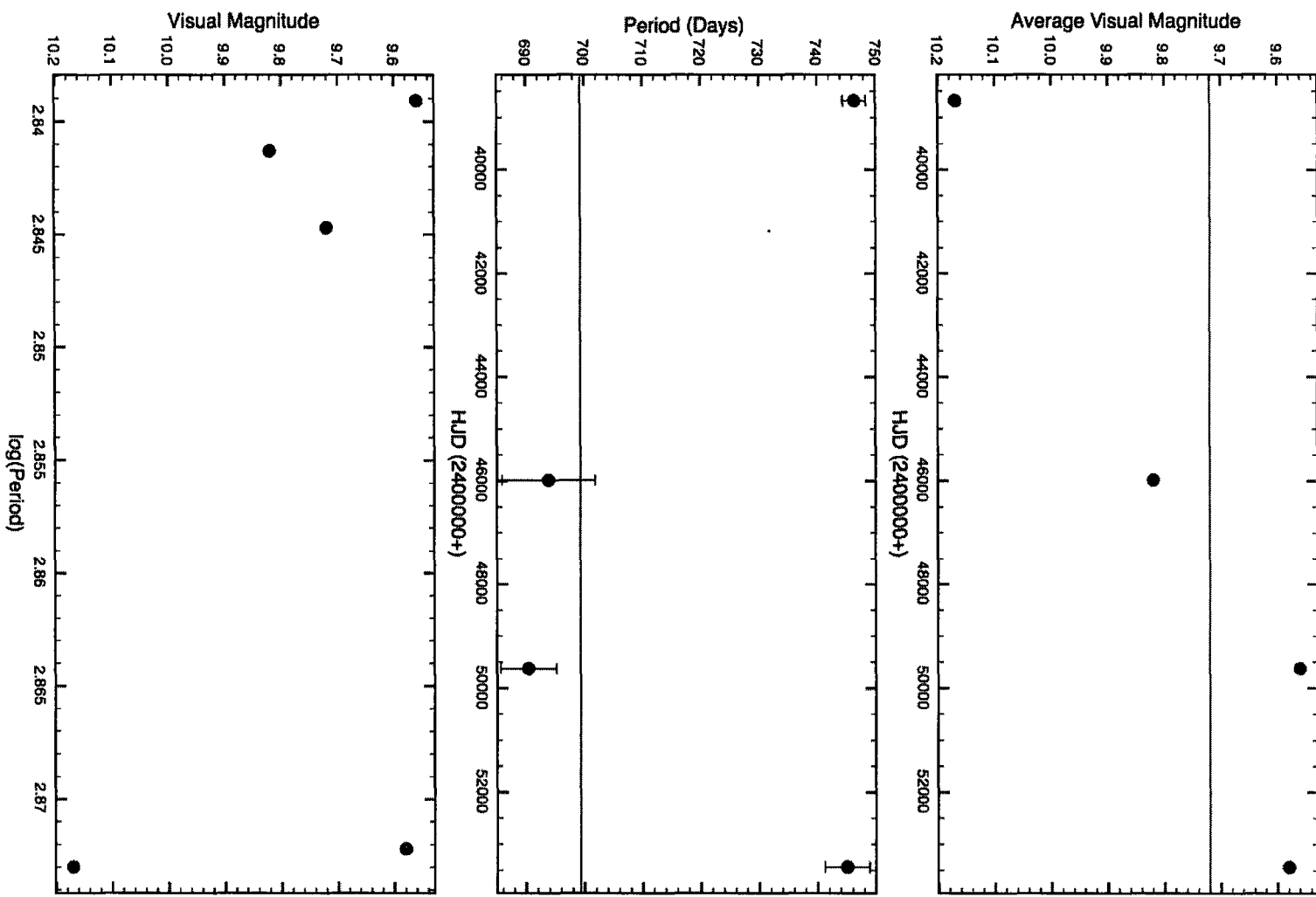


Figure 4.32: Period and average magnitude changes in BC Cygni from AAVSO observations.

## 4.23 V Eridani

Figure 4.33 shows *V* Eri's changes in period and average visual magnitude taken at approximately 10-year intervals. The GCVS lists a period for the star of 97 days, quite different from the 290 day period we found through Fourier analysis, and a spectral type of M6 II. The period is not well established, and the star undergoes variations in mean brightness, possibly from dust extinction episodes. Its small amplitude is in agreement with an expected low pulsation amplitude for a luminosity class II M supergiant, where convection and larger gravity are more efficient at damping radial pulsation.

**Table 4.39:** AAVSO Observations of *V* Eridani

Subset	Dates	$\langle V \rangle$	% Diff.	$\Delta V$	$N$	$P$ (days)	% Diff.
All	19484-55266	8.92	...	4.6	3633	$289.77 \pm 0.21$	...
1	19484-22967	8.85	-0.78	2.6	93	$278.39 \pm 2.44$	-3.93
2	25253-25328	8.96	0.45	0.5	5	...	...
3	32626-37703	9.06	1.57	2.1	28	$292.05 \pm 1.74$	0.79
4	37973-41384	9.03	1.23	1.9	78	$278.18 \pm 1.66$	-4.00
5	41654-44465	8.74	-2.02	1.7	25	$276.51 \pm 1.89$	-4.57
6	45048-48683	8.78	-1.57	3.4	29	$286.45 \pm 2.39$	-1.14
7	49038-52314	8.64	-3.14	1.9	74	$288.05 \pm 2.31$	-0.59
8	52340-55266	9.52	6.73	1.3	27	$296.46 \pm 3.40$	2.31

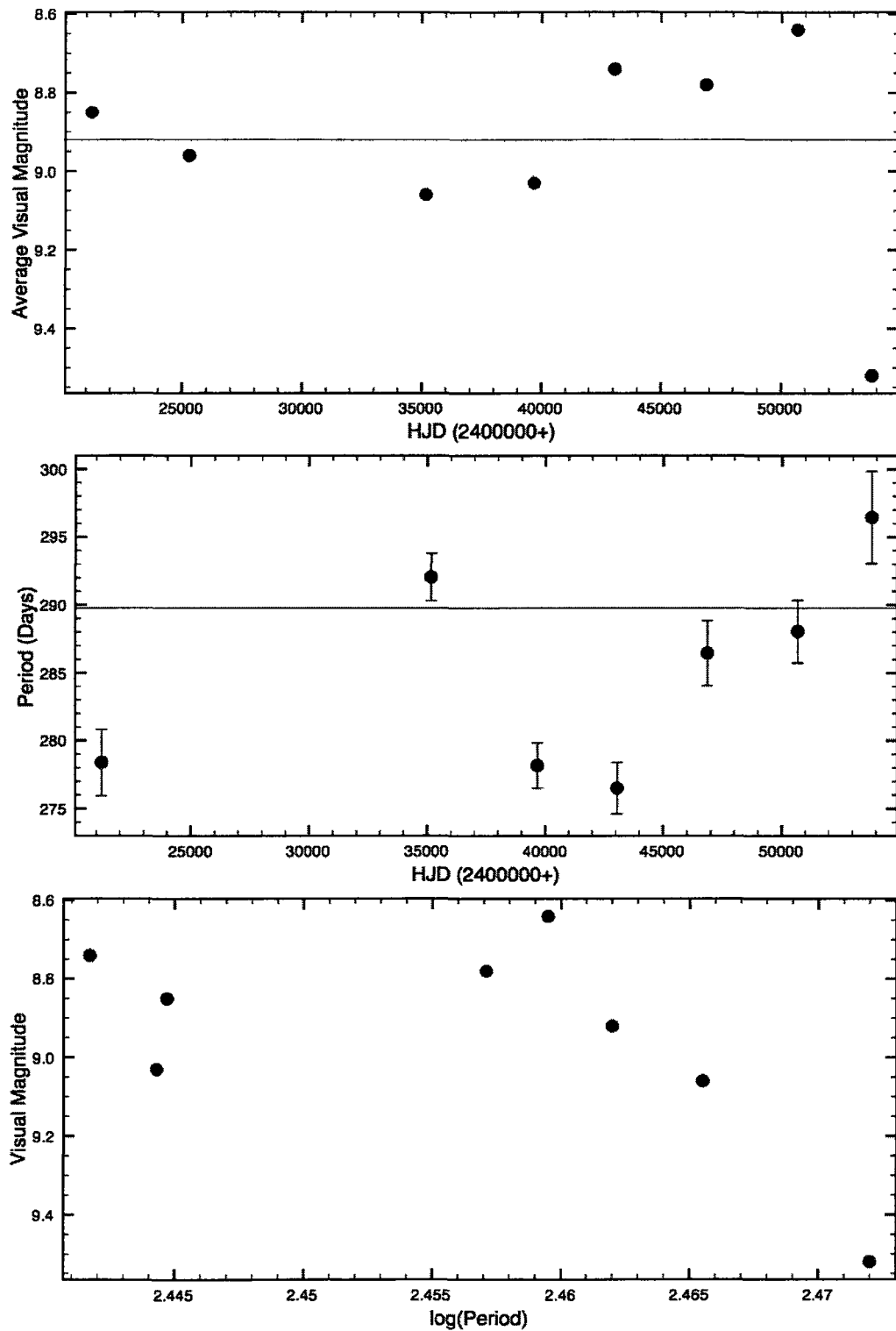


Figure 4.33: Period and average magnitude changes in *V* Eridanus from AAVSO observations.

## 4.24 TV Geminorum

Figure 4.34 shows TV Gem's variations in spectral type and radial velocity, phased using a period of 425.14 days and a time of maximum light of JD2437219.03 from the AAVSO observations, and the one CCD spectrum we obtained. The star appears to reach its lowest temperature near light maximum. Its luminosity class does not vary much over the course of observation. The radial velocity results are inconclusive, being separated by 68 years temporally. Figure 4.35 shows TV Gem's changes in period and average visual magnitude taken at approximately 10-year intervals. The period is well established in older archival observations, but not from the most recent AAVSO data. The light curve also suggests a possible 2000-day long cycle from starspot activity. TV Gem has a roughly constant mean brightness, but the pulsation is less marked with recent data. The star needs more radial velocities and precise photometry to establish a reliable period, which would likely reduce the scatter in figure 4.34 through improved phasing.

**Table 4.40:** AAVSO Observations of TV Geminorum

Subset	Dates	$\langle V \rangle$	% Diff.	$\Delta V$	$N$	$P$ (days)	% Diff.
All	27750-55329	6.87	...	2.6	9501	$425.14 \pm 0.07$	...
1	27750-29881	6.78	-1.31	0.7	22	$425.78 \pm 10.12$	0.15
2	32176-35049	7.13	3.78	1.2	262	$432.06 \pm 2.59$	1.63
3	35053-38670	6.85	-0.29	2.3	767	$457.32 \pm 1.61$	7.57
4	38701-42348	6.88	0.15	1.8	1512	$507.74 \pm 1.11$	19.43
5	42357-45984	6.89	0.29	2.3	1841	$431.92 \pm 0.87$	1.60
6	46001-49640	6.86	-0.15	2.3	2154	$443.55 \pm 0.59$	4.33
7	49654-53132	6.81	-0.87	2.5	2434	$419.86 \pm 0.72$	-1.24
8	53963-55329	6.90	0.44	1.7	838	$485.66 \pm 2.78$	14.24

**Table 4.41:** Spectroscopic observations of TV Geminorum

Year	HJD	Phase	$V_R$ (km/s)	Spectral Type	Source
1940	2430416	0.9981	16	M2	Joy
1940	2430423	0.0146	18	M2	Joy
1969	2440562	0.8620	...	M0.6 Iab	Wing
1970	2440592	0.9326	...	M1.0 Iab	Wing
1970	2440630	0.0220	...	M1.2 Iab	Wing
1970	2440633	0.0290	...	M1.1 Iab	Wing
1970	2440869	0.5842	...	M0.3 Iab	Wing
1970	2440899	0.6547	...	M0.3 Iab	Wing
1970	2440903	0.6641	...	M0.0 Ia	Wing
1970	2440951	0.7770	...	M0.6 Iab	Wing
1971	2441015	0.9276	...	M1.3 Iab	Wing
1973	2442015	0.2797	...	K5.5 Iab	Wing
2010	2455490	0.9762	$24.4 \pm 21.0$	M1 Iab	DAO CCD

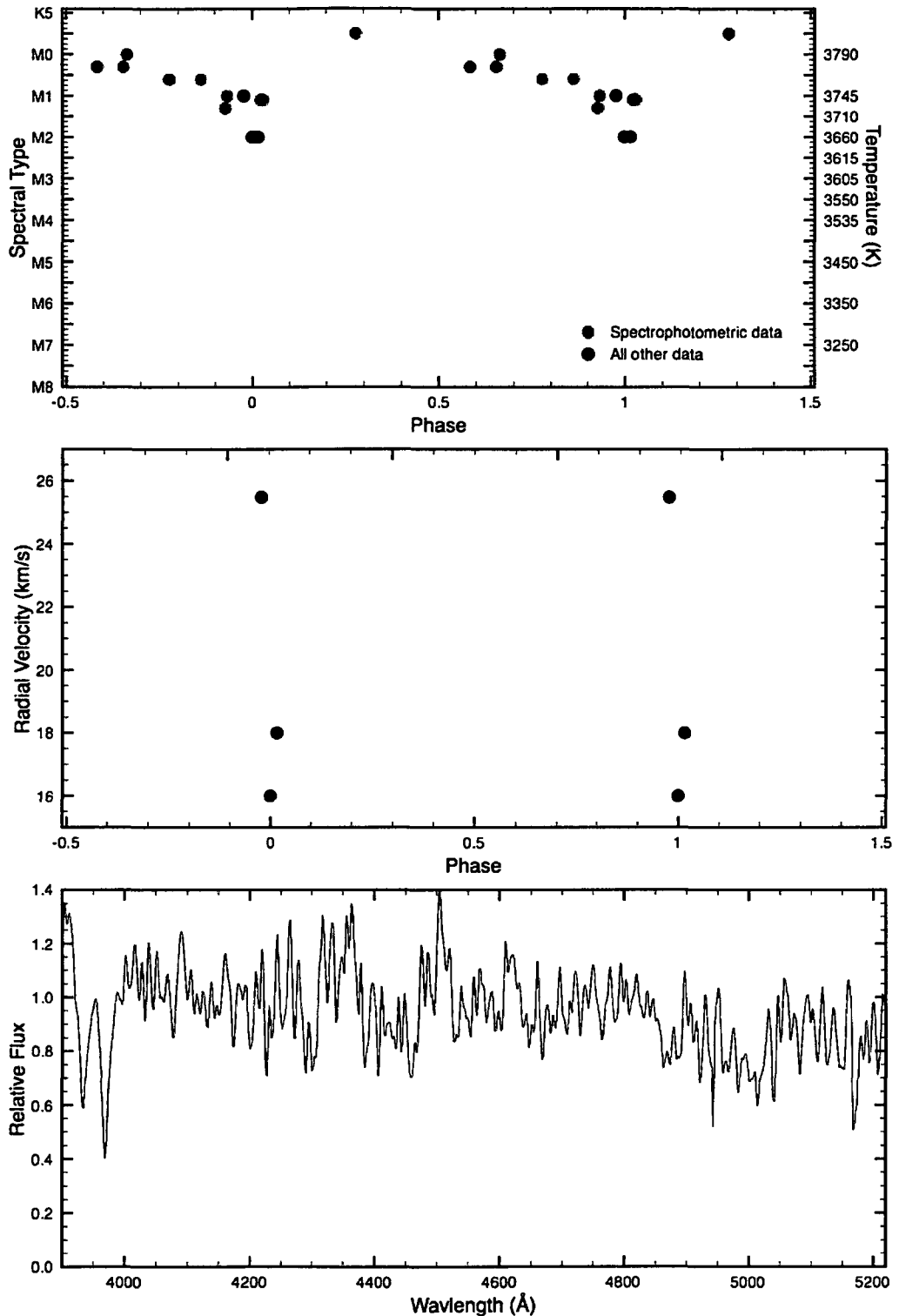


**Figure 4.34:** Top: Spectral variation in TV Geminorum. Middle: Radial velocity variation. Bottom: CCD spectrum of TV Geminorum. Data phased with 425.14 day period.

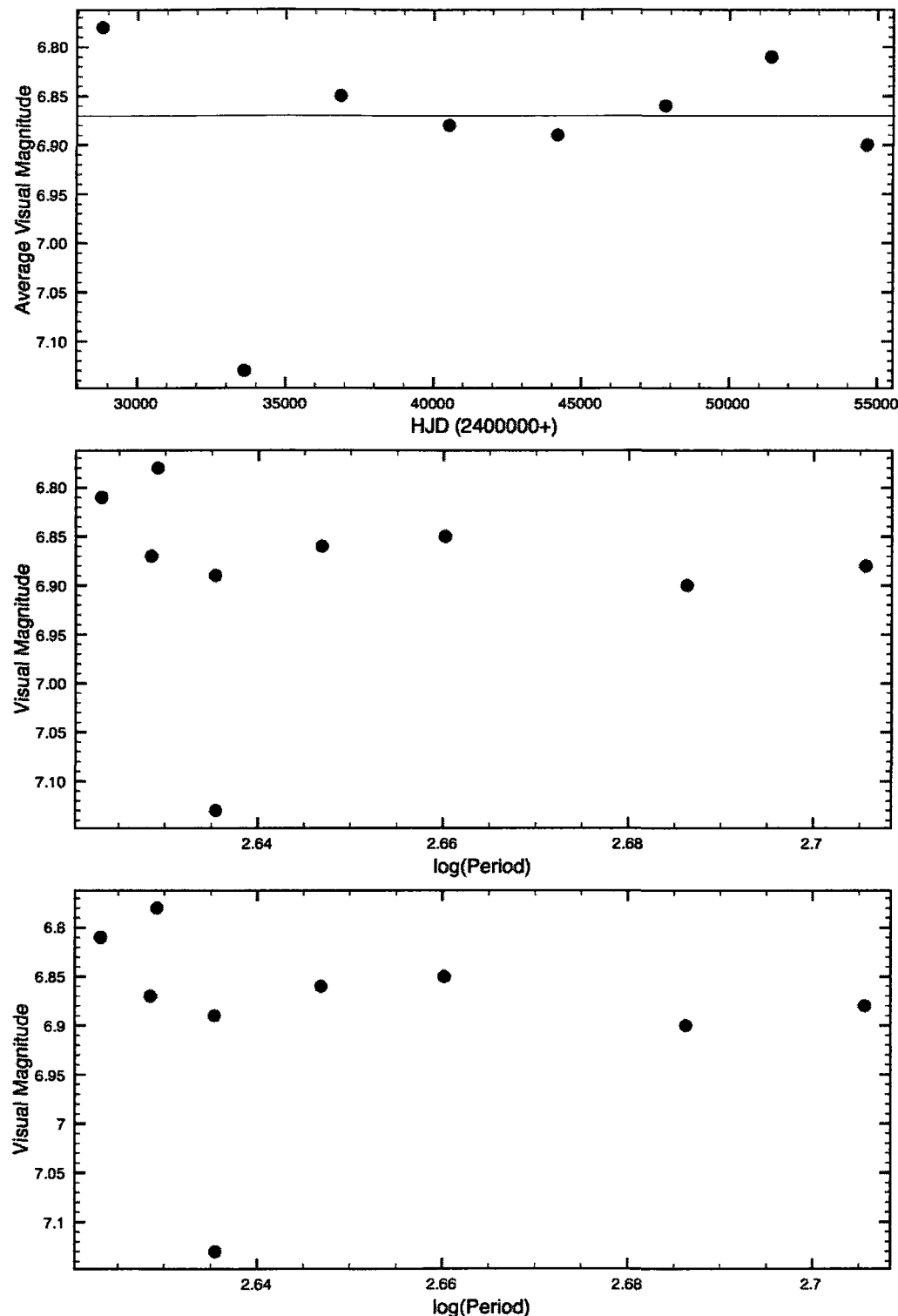


**Figure 4.35:** Period and average magnitude changes in TV Geminorum from AAVSO observations.

## 4.25 IS Geminorum

Figure 4.36 shows IS Gem's changes in period and average visual magnitude taken at approximately 10-year intervals. The 359-day period found by Fourier analysis is likely a result of the seasonal gaps in the observations. Wroblewski (1961) obtained  $P = 47$  days from unpublished observations. In any event, the star's early spectral type of K3 II (from the GCVS) implies it is not a true SRC variable. The light amplitude listed in the GCVS of  $\Delta B = 1^m.7$  is confirmed by the AAVSO visual observations, but it is difficult to say anything more.

**Table 4.42:** AAVSO Observations of IS Geminorum

Subset	Dates	$\langle V \rangle$	% Diff.	$\Delta V$	$N$	$P$ (days)	% Diff.
All	40313-55348	5.82	...	3.0	3332	$359.25 \pm 0.33$	...
1	40313-39460	5.89	1.20	1.7	711	$351.82 \pm 0.50$	-2.07
2	39467-47610	5.88	1.03	1.2	562	$366.85 \pm 0.46$	2.12
3	47613-51261	5.85	0.52	1.3	632	$364.85 \pm 0.71$	1.56
4	51265-54913	5.75	-1.20	1.7	1315	$376.56 \pm 0.30$	4.82
5	54915-55348	5.79	-0.52	2.3	112	$319.44 \pm 9.09$	-11.08

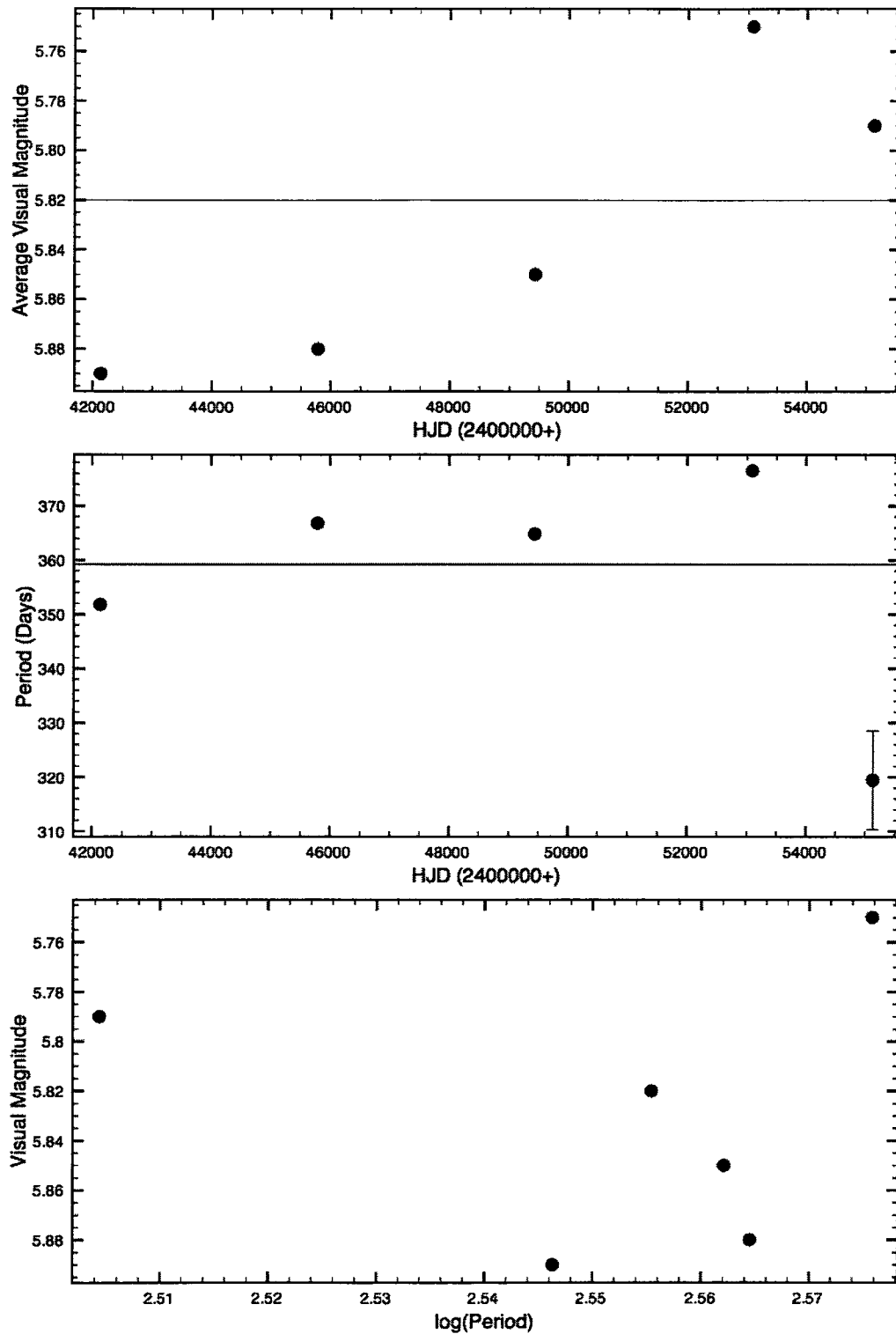


**Figure 4.36:** Period and average magnitude changes in IS Geminorum from AAVSO observations.

## 4.26 V959 Herculis

Figure 4.37 shows V959 Her's spectral type, phased with a period of 140.37 days and a time of maximum light of JD2454838, determined from the very few AAVSO observations (the only available photometry). The spectral type did not change over the course of the observations that we obtained. Figure B.53 shows V959 Her's light curve. Very little can be concluded about the star given the lack of photometric data and the non-variability in spectral type. Is it an SRC variable or an LC variable?

**Table 4.43:** AAVSO Observations of V959 Herculis

Subset	Dates	$\langle V \rangle$	% Diff.	$\Delta V$	$N$	$P$ (days)	% Diff.
All	51274-55059	6.46	...	0.4	40	$140.37 \pm 0.73$	...

**Table 4.44:** Spectroscopic observations of V959 Herculis

Year	HJD	Phase	$V_R$ (km/s)	Spectral Type	Source
1947	2432317	0.1347	...	M4 Ib	DDO
1948	2432699	0.8628	...	M4 II	DDO
1950	2432317	0.5972	...	M4 Ib	DDO
1952	2432317	0.2986	...	M4 II	DDO

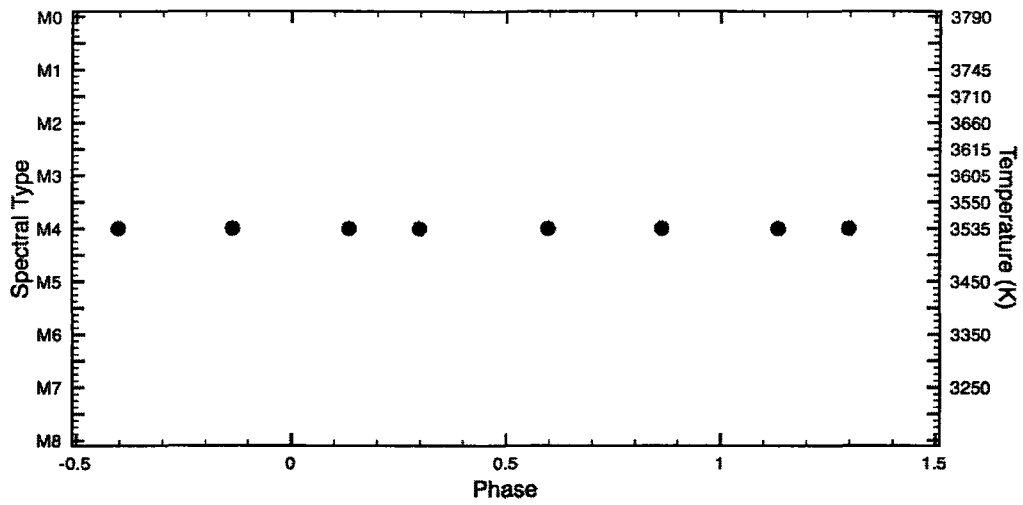


**Figure 4.37:** Spectral type versus phase for V959 Herculis, phased with 140.37 day period.

## 4.27 $\alpha$ Herculis

Figure 4.38 shows  $\alpha$  Her's variations in spectral type and radial velocity, phased with a period of 508.07 days and a time of maximum light of 2451153.34 from the AAVSO observations, and a montage of CCD spectra taken at different epochs. It appears to reach smallest dimensions near phase 0.12. The temperature is varying, but it is not clear at what phase it reaches maximum. Greatest luminosity class appears to occur at highest temperature. Figure 4.39 shows  $\alpha$  Her's changes in period and average visual magnitude taken at approximately 10-year intervals. The light variations do not appear strikingly marked in the AAVSO data and are more irregular. Even the light amplitude is difficult to define. The brightness is roughly constant but not particularly periodic. The phasing with  $P = 508$  days appears to give reasonable results, however.

**Table 4.45:** AAVSO Observations of  $\alpha$  Herculis

Subset	Dates	$\langle V \rangle$	% Diff.	$\Delta V$	$N$	$P$ (days)	% Diff.
All	28182-55423	3.30	...	2.2	15632	$508.07 \pm 3.90$	...
1	28182-30316	3.31	0.30	1.0	211	$499.78 \pm 1.14$	-1.63
2	31585-35139	3.31	0.30	1.5	1345	$539.60 \pm 1.06$	6.21
3	35142-38774	3.36	1.82	2.1	964	$560.59 \pm 17.14$	10.34
4	38855-42429	3.26	-1.21	1.6	2393	$542.35 \pm 1.00$	6.75
5	42452-46083	3.33	0.91	1.9	2206	$553.43 \pm 1.22$	8.93
6	46097-49689	3.31	0.30	1.4	2661	$526.62 \pm 1.00$	3.65
7	49746-53388	3.30	0.00	1.8	3856	$487.41 \pm 3.08$	-4.07
8	53391-55424	3.25	-1.52	1.8	1996	$477.09 \pm 2.03$	-6.10

**Table 4.46:** Spectroscopic observations of  $\alpha$  Herculis

Year	HJD	Phase	$V_R$ (km/s)	Spectral Type	Source
1935	2427978	0.3787	...	M5 Ia-Ib	DDO
1935	2437984	0.3905	...	M5 Ia-Ib	DDO
1966	2394293	0.3476	$-65.9 \pm 0.7$	M4 Ia	DAO Pg
1968	2440033	0.1089	...	M5 Ib	DDO
1971	2441047	0.8806	$-58.7 \pm 0.4$	M4 Ia	DAO Pg
1975	2442513	0.0087	$-20.5 \pm 0.3$	M4 Ia	DAO Pg
2006	2454027	0.6562	$-37.1 \pm 8.1$	M5 Iab	DAO CCD
2009	2455086	0.7407	$-55.2 \pm 19.8$	M6 Ib	DAO CCD

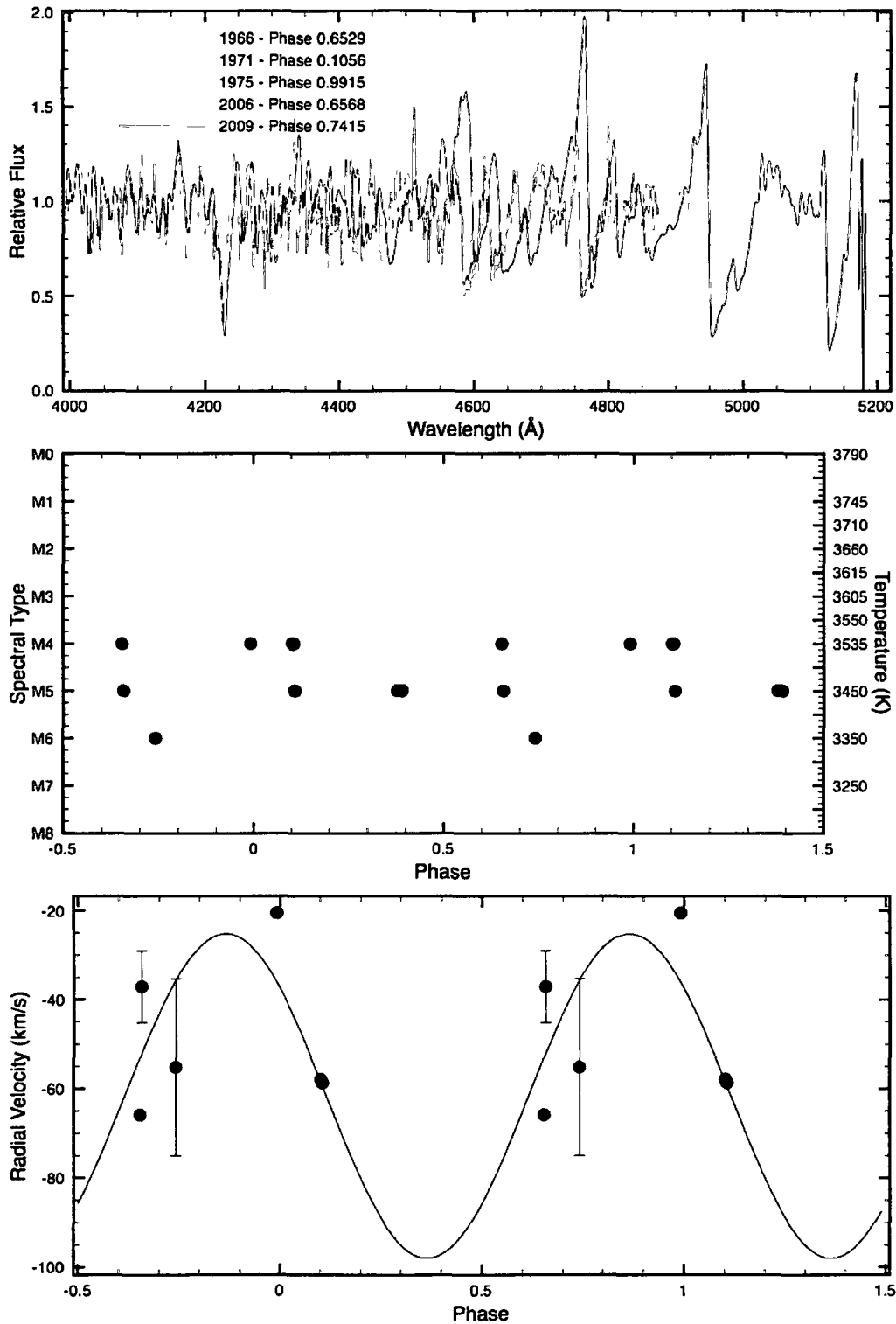


**Figure 4.38:** Spectral variation in  $\alpha$  Herculis. Top: Spectra from different epochs. Middle: Spectral type as a function of phase. Bottom: Radial velocity as a function of phase. Data phased with 508.07 day period.

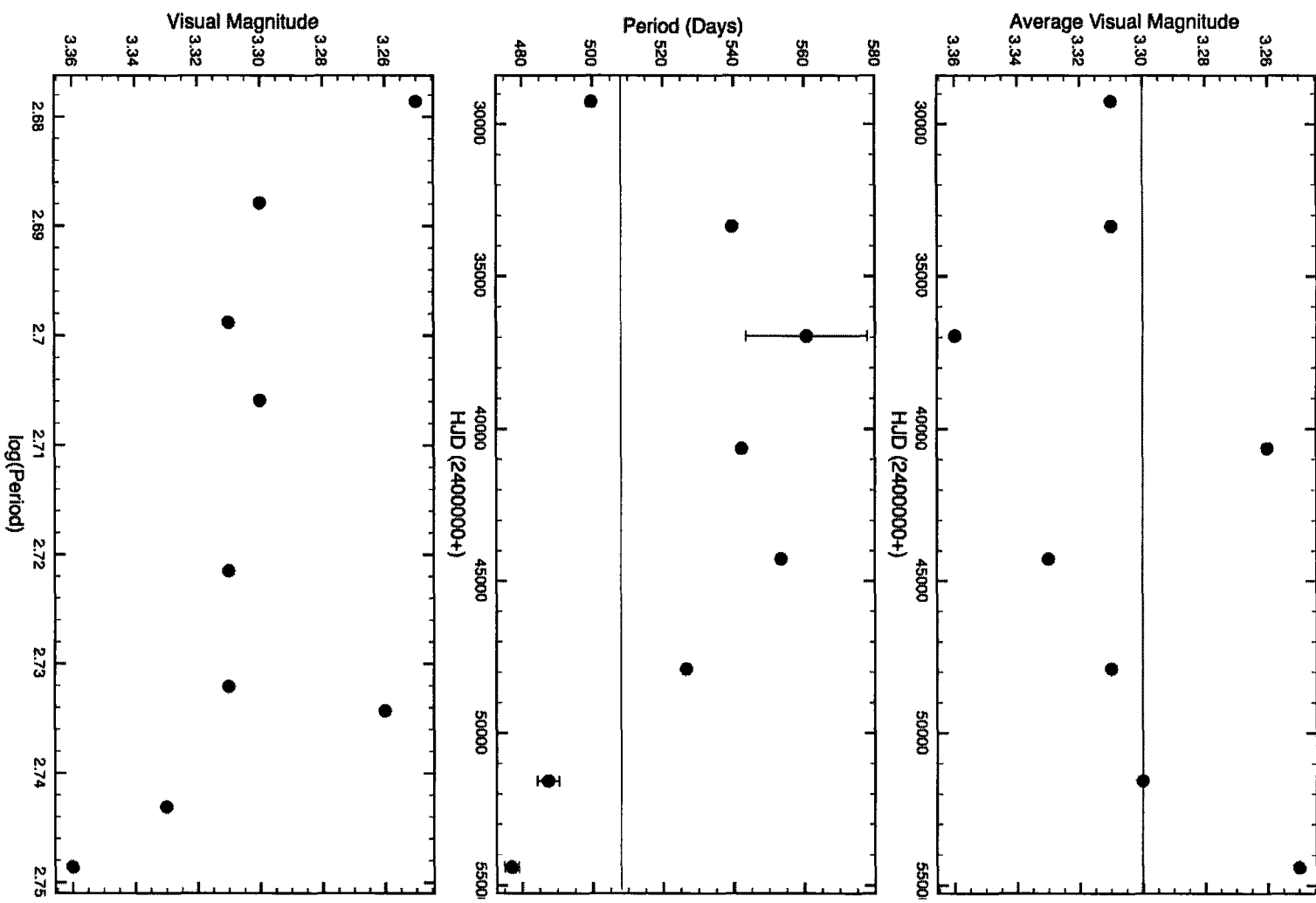


Figure 4.39: Period and average magnitude changes in  $\alpha$  Herculis from AAVSO observations.

## 4.28 RV Hydrae

Figure 4.40 shows RV Hya's changes in period and average visual magnitude taken at approximately 10-year intervals. A poor distribution in the AAVSO observations makes a reliable period determination difficult. A lack of spectroscopic data makes understanding the nature of the star's variability an insurmountable challenge. More observations of both types are needed. The GCVS lists a period of 116 days for the star, but we found that the 243 day period had a stronger signal in the Fourier analysis. Its spectral type is listed as M5 II in the GCVS. Note the discrepancy between the period listed in the GCVS and that derived here, the later of which is more consistent with a small amplitude cool SRC variable, if indeed it is a member of the class.

**Table 4.47:** AAVSO Observations of RV Hydrae

Subset	Dates	$\langle V \rangle$	% Diff.	$\Delta V$	$N$	$P$ (days)	% Diff.
All	21663-55245	7.86	...	1.7	410	$243.27 \pm 0.10$	...
1	21663-26851	8.09	2.93	1.4	28	$247.83 \pm 1.10$	1.88
2	34744-36255	7.81	-0.64	1.2	86	$252.04 \pm 2.27$	3.61
3	36271-39911	7.83	-0.38	1.6	195	$241.54 \pm 1.52$	-0.71
4	39940-43513	7.87	0.13	0.5	44	$238.07 \pm 1.15$	-2.14
5	43599-47098	7.89	0.38	1.3	38	$247.54 \pm 1.67$	1.76
6	47214-55245	8.01	1.91	1.0	19	$233.53 \pm 0.89$	-4.00

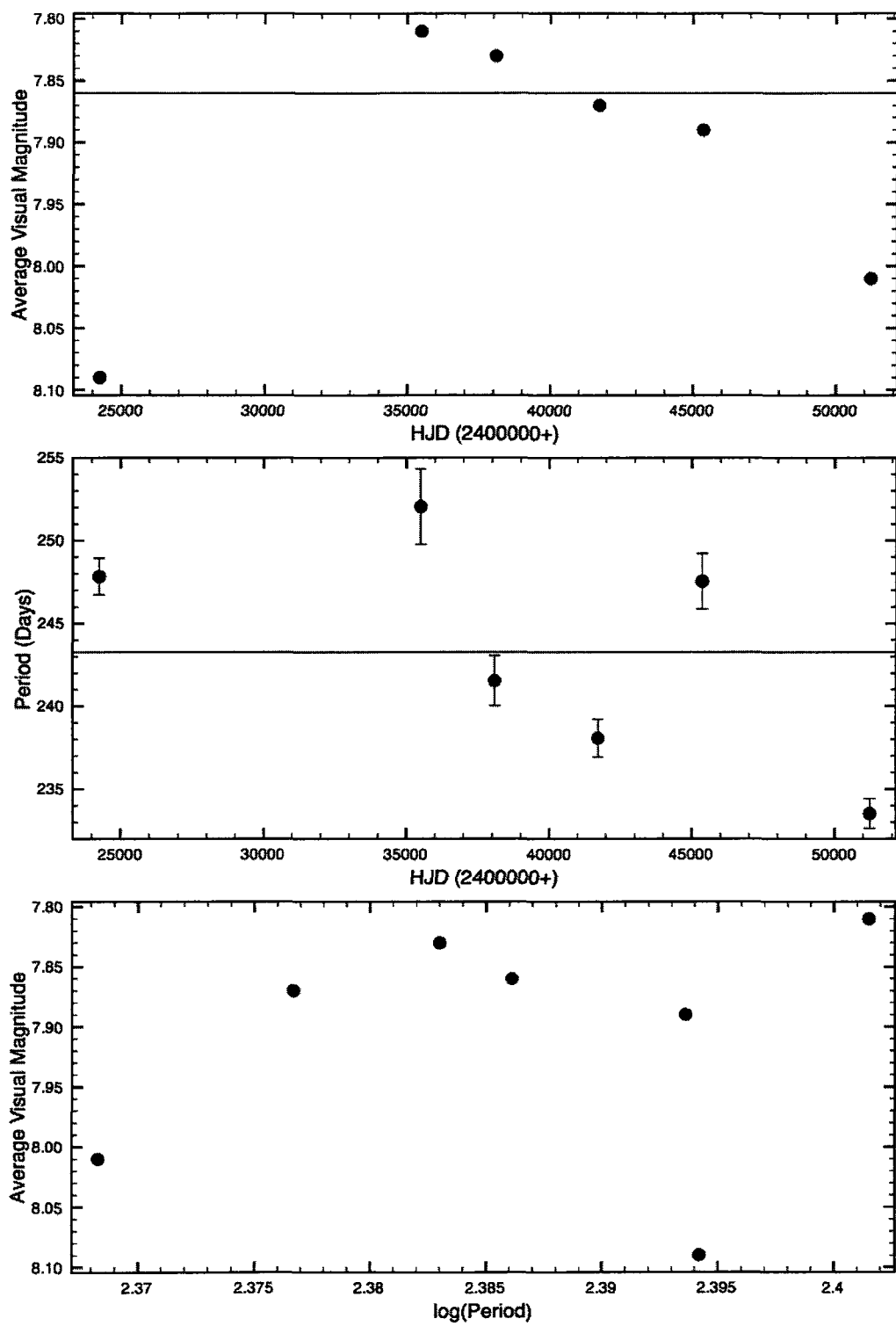


Figure 4.40: Period and average magnitude changes in RV Hydrae from AAVS) observations.

## 4.29 W Indus

We found a period for W Ind of 198.57 days through Fourier analysis of the AAVSO observations. The GCVS confirms a period of 198 days for the star. Figure 4.41 shows W Ind's changes in period and average visual magnitude taken at approximately 10-year intervals. Variations are well-marked in the light curve despite the small light amplitude. The mean magnitude is relatively unchanging. The star is in need of spectroscopic observations to study the nature of its variability.

**Table 4.48:** AAVSO Observations of W Indus

Subset	Dates	$\langle V \rangle$	% Diff.	$\Delta V$	$N$	$P$ (days)	% Diff.
All	26454-55392	9.27	...	3.3	722	$198.57 \pm 0.09$	...
1	40507-44157	9.35	0.86	2.4	162	$200.59 \pm 0.41$	1.02
2	44170-47767	9.37	1.08	3.1	183	$199.88 \pm 0.46$	0.66
3	47808-55392	9.20	-0.76	2.8	376	$197.55 \pm 0.46$	-0.52

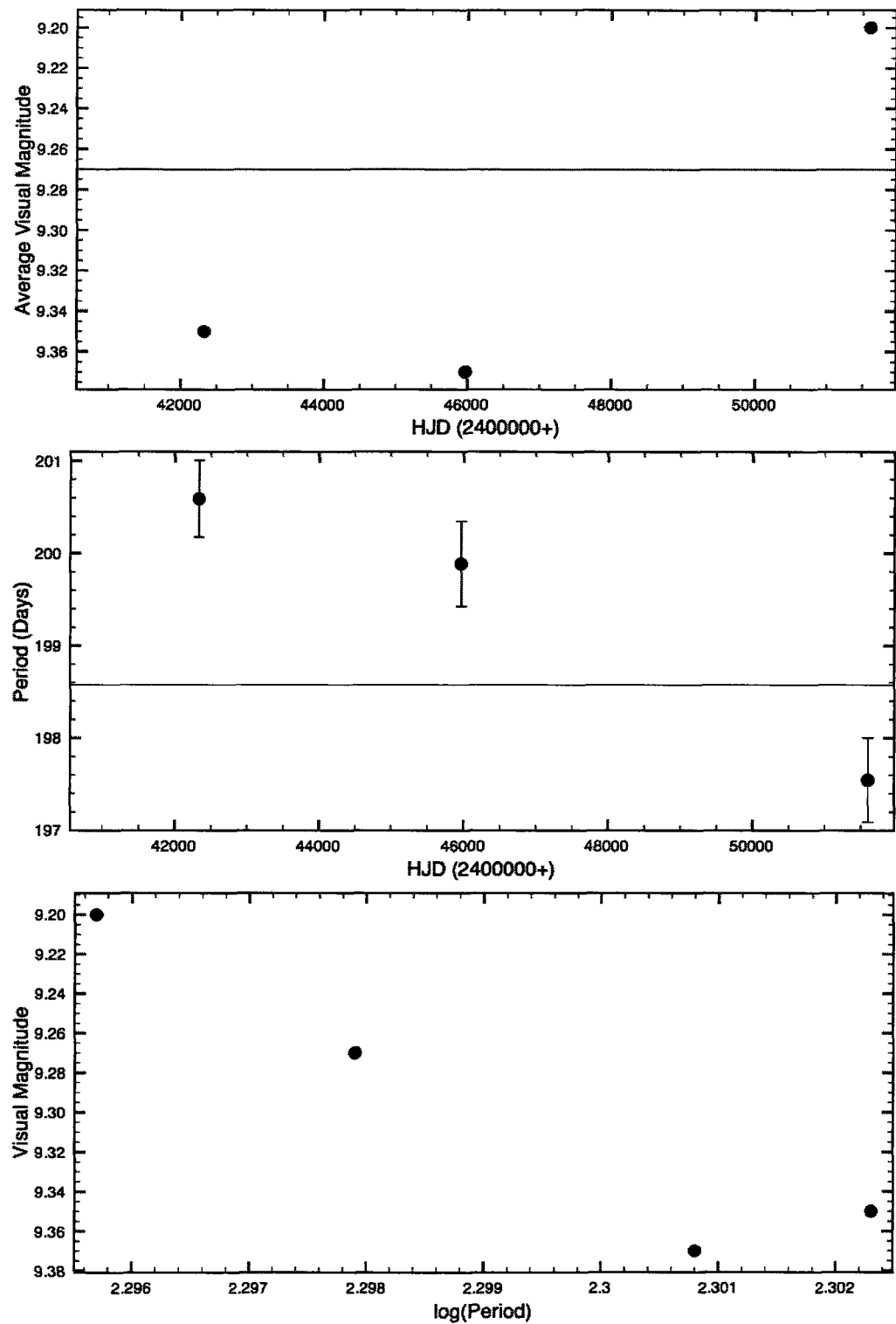


Figure 4.41: Period and average magnitude changes in W Indus from AAVSO observations.

#### 4.30 U Lacertae

Figure 4.42 shows U Lac's variations in spectral type and radial velocity, phased with a period of 395.00 days and a time of maximum light of JD2452387.37 from the AAVSO observations, as well as a montage of CCD spectra taken at different epochs. The star appears to reach smallest dimensions near phase 0.56. The temperature is varying, but it is not clear at what phase it reaches maximum. The luminosity class was fairly constant, so we are unable to determine at what spectral type it reaches its greatest value. Changes in mean brightness suggest extinction events from dust production. The period is consistent with obvious maxima in the light curve.

**Table 4.49:** AAVSO Observations of U Lacertae

Subset	Dates	$\langle V \rangle$	% Diff.	$\Delta V$	N	P (days)	% Diff.
All	25215-55420	9.89	...	3.4	345	$395.00 \pm 0.67$	...
1	25215-25298	8.43	-14.76	0.7	6	...	...
2	34639-43130	10.30	4.15	2.2	2	...	...
3	48605-52253	9.49	-4.04	2.1	40	...	...
4	52264-55420	9.97	0.81	1.7	297	...	...

**Table 4.50:** Spectroscopic observations of U Lacertae

Year	HJD	Phase	$V_R$ (km/s)	Spectral Type	Source
1970	2440850	0.7902	...	M2.8 Ia	Wing
1970	2440875	0.8535	...	M2.6 Iab	Wing
1970	2440906	0.9320	...	M2.3 Ia	Wing
1970	2440909	0.9396	...	M2.2 Ia	Wing
2005	2453648	0.1912	$11.6 \pm 16.4$	M3 Ia+	DAO CCD
2007	2454373	0.0263	$-13.1 \pm 14.1$	M4 Iab	DAO CCD
2008	2454755	0.9933	$-36.5 \pm 19.8$	M4 Ia	DAO CCD
2009	2455092	0.8468	$-42.0 \pm 22.0$	M4 Ia	DAO CCD
2010	2455489	0.8518	$-48.8 \pm 19.5$	M4 Ia	DAO CCD

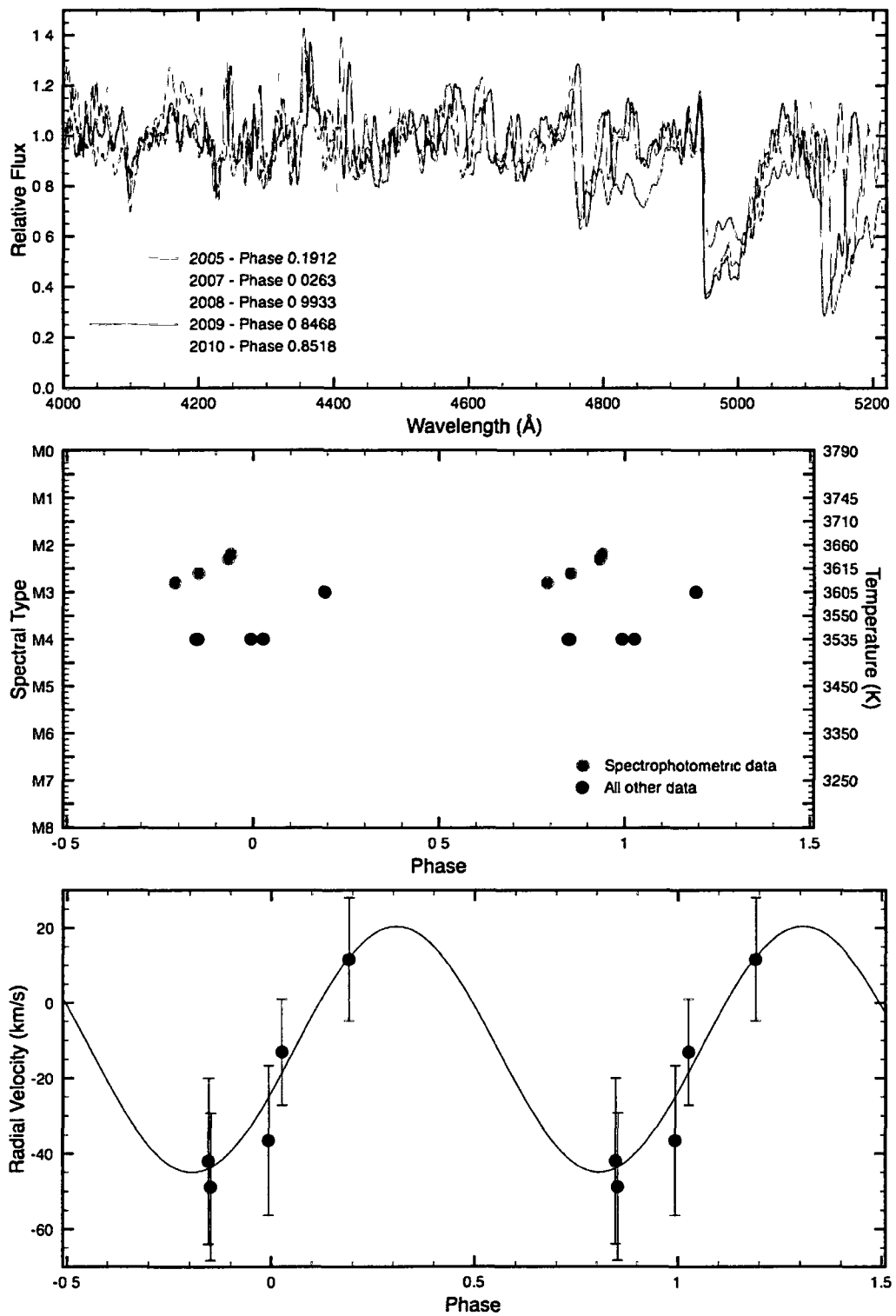


**Figure 4.42:** Spectral variation in U Lacertae. Top: Spectra from different epochs. Middle: Spectral type as a function of phase. Bottom: Radial velocity as a function of phase. Data phased with 395.00 day period.

### 4.31 Y Lyncis

Figure 4.43 shows Y Lyn's variations in spectral type and radial velocity, phased with a period of 282.56 days and a time of maximum light of JD2437973.93 from the AAVSO observations, along with a montage of CCD spectra taken at different epochs. The star's spectral type and luminosity class were the same for the two observations, and the observations were also obtained at similar phases. Figure 4.44 shows Y Lyn's changes in period and average visual magnitude taken at approximately 10-year intervals. Over the course of the observations, the period has decreased along with the brightness, but only by small amounts. Because of the small light amplitude and the lack of spectral data, it is difficult to categorize the pulsation in Y Lyn. Additional photometry and spectroscopy would help. The small light amplitude of  $\Delta V \simeq 2^m$  is consistent with the spectral type of M6 II, but also makes it a challenging object for AAVSO observers.

**Table 4.51:** AAVSO Observations of Y Lyncis

Subset	Dates	$\langle V \rangle$	% Diff.	$\Delta V$	$N$	$P$ (days)	% Diff.
All	34784-55387	7.39	...	2.9	8989	$282.56 \pm 0.04$	...
1	34784-38432	7.29	-1.35	2.0	515	$282.02 \pm 0.75$	-0.19
2	38394-42081	7.29	-1.35	1.7	1737	$300.64 \pm 0.38$	6.40
3	42084-45732	7.41	0.27	2.3	1527	$274.82 \pm 0.29$	-2.74
4	45734-49382	7.44	0.68	2.3	2342	$278.64 \pm 0.29$	-1.39
5	49384-53030	7.46	0.95	2.8	1762	$278.08 \pm 0.29$	-1.59
6	53034-53387	7.36	-0.41	2.2	1106	$282.49 \pm 0.51$	-0.03

**Table 4.52:** Spectroscopic observations of Y Lyncis

Year	HJD	Phase	$V_R$ (km/s)	Spectral Type	Source
2006	2454029	0.7317	$19.5 \pm 8.6$	M6 II	DAO CCD
2010	2455484	0.8730	$14.4 \pm 22.3$	M6 II	DAO CCD

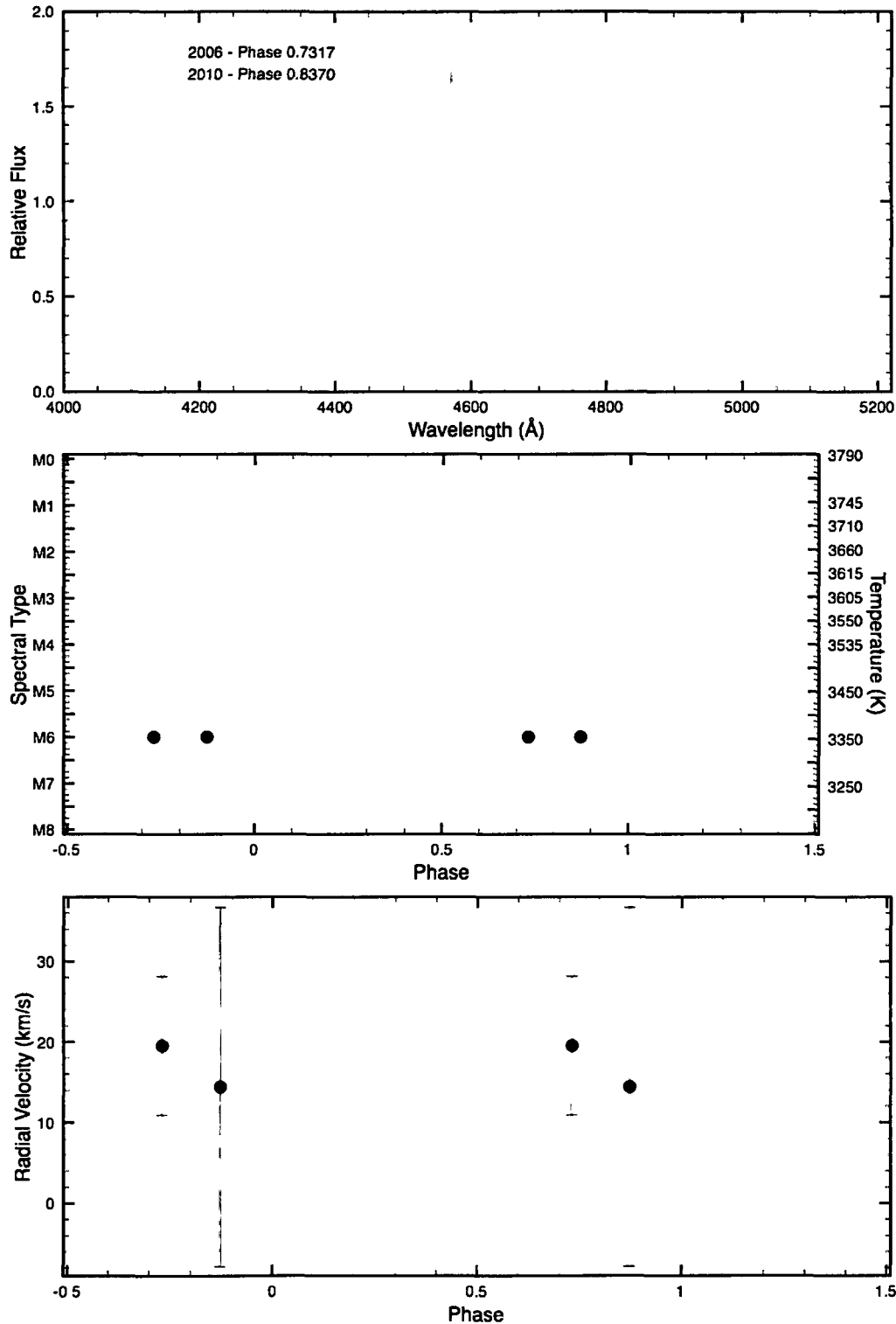


**Figure 4.43:** Spectral variation in Y Lyncis. Top: Spectra from different epochs. Middle: Spectral type as a function of phase. Bottom: Radial velocity as a function of phase. Note that the apparent differences in the two spectra (although classified as the same type) are caused by problems with normalization at the red end. Data phased with 282.56 day period.

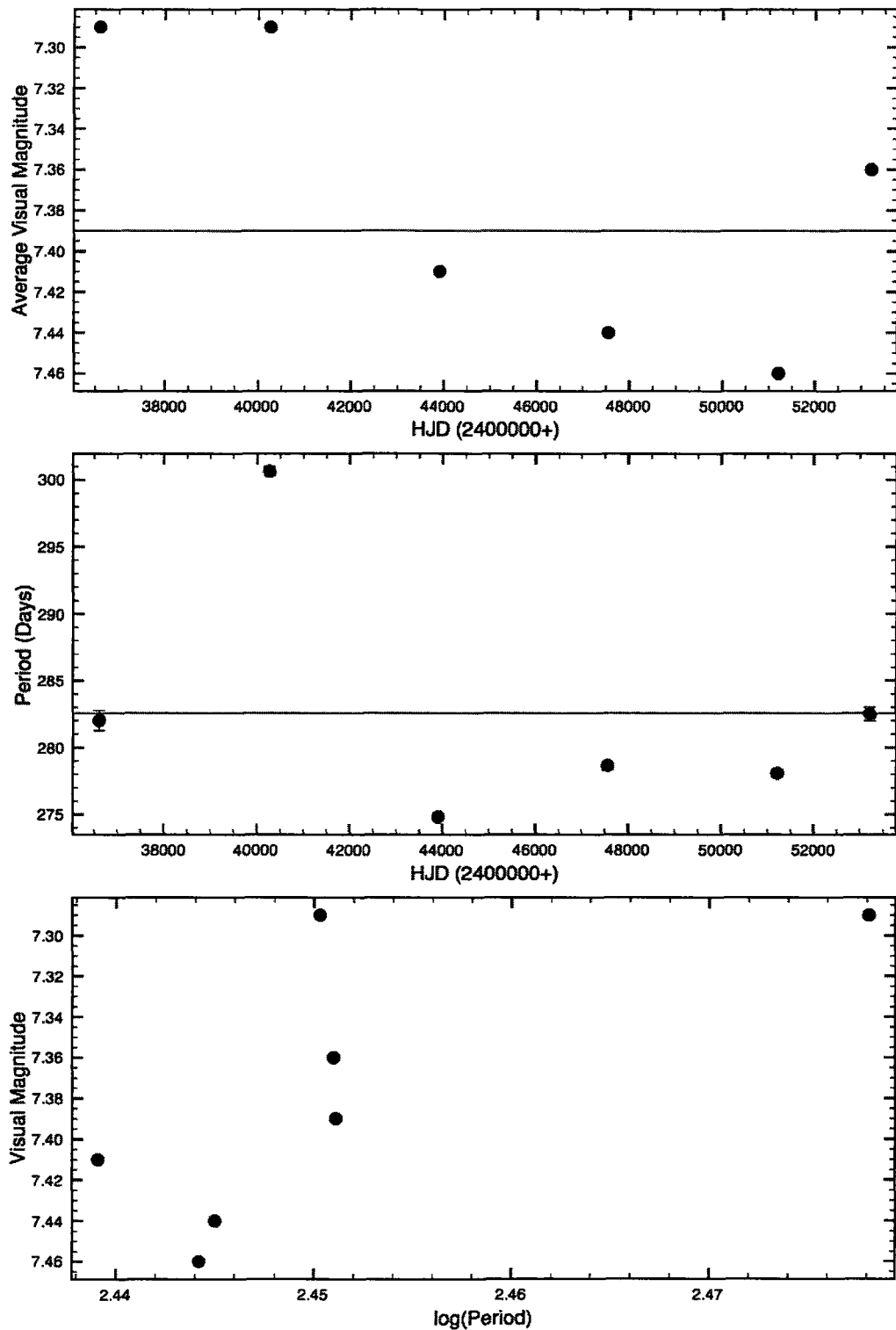


Figure 4.44: Period and average magnitude changes in Y Lyncis from AAVSO observations.

### 4.32 $\delta^2$ Lyrae

Figure 4.45 shows  $\delta^2$  Lyr's changes in period and average visual magnitude taken at approximately 10-year intervals, and figures B.64 and B.65 show  $\delta^2$  Lyr's light curve. Light variability is not obvious from the AAVSO measurements, and the implied amplitude of  $\Delta V \simeq 1^m.1 - 2^m.0$  is significantly larger than the value listed in the GCVS ( $\Delta V \simeq 0^m.11$ ), which may be based on photovisual photographic data. The derived period of  $P = 627$  days may not be properly representative of what is happening in the star. The implied  $M_V$  from cluster membership is  $M_V \simeq -2.5$ , consistent with an M3 Ib star, but only low-amplitude variability is expected. More precise photometry is needed to determine the nature of the star's light variations.

**Table 4.53:** AAVSO Observations of  $\delta^2$  Lyrae

Subset	Dates	$\langle V \rangle$	% Diff.	$\Delta V$	$N$	$P$ (days)	% Diff.
All	35036-55424	4.46	...	2.0	2141	$627.10 \pm 0.37$	...
1	35036-38661	4.58	2.69	1.1	429	$628.43 \pm 2.42$	0.21
2	38671-42339	4.43	-0.67	2.0	586	$662.68 \pm 2.93$	5.67
3	42342-45973	4.39	-1.57	1.3	455	$626.33 \pm 2.83$	-0.12
4	45993-49634	4.55	2.02	1.3	343	$687.23 \pm 4.68$	9.59
5	50667-53006	4.45	-0.22	1.1	210	$609.19 \pm 10.77$	-2.86
6	53922-55424	4.26	-4.48	1.4	118	$620.12 \pm 15.17$	-1.11

**Table 4.54:** Spectroscopic observations of  $\delta^2$  Lyrae

Year	HJD	Phase	$V_R$ (km/s)	Spectral Type	Source
1944	2431369	0.3262	...	M3 Ib	DDO

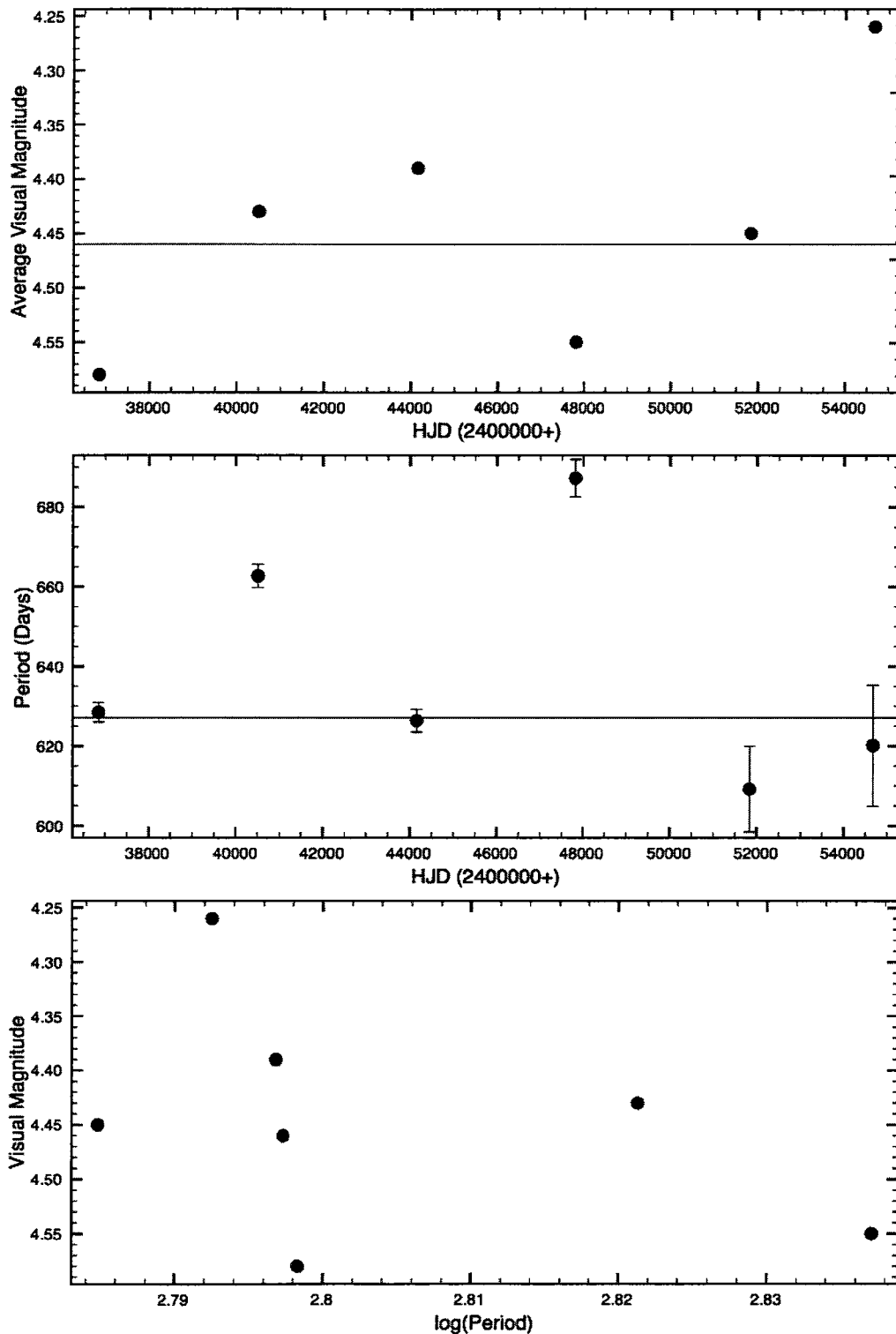


**Figure 4.45:** Period and average magnitude changes in  $\delta^2$  Lyrae from AAVSO observations.

### 4.33 $\alpha$ Orionis

Figure 4.46 shows  $\alpha$  Ori's variations in spectral type and radial velocity and a montage of CCD spectra taken at different epochs. The observations were phased using a period of 425.59 days and a time of maximum light of JD2454816.9, determined from the AAVSO observations. The GCVS lists a period of 2335 days, and although we found a similar long period in our Fourier analysis, the data phased better using the shorter period. We fitted primarily the Griffin radial velocity variations with a sine wave and found that the star appears to reach smallest dimensions near phase 0.27. The star appears to reach highest temperature and greatest luminosity class near light maximum, although there is some scatter in the observations for the latter. As  $\alpha$  Orionis is a large and relatively nearby star, some interferometric measurements of its angular diameter have been made. Townes et al. (2009) used angular diameter measurements from a variety of sources to show that the angular size of  $\alpha$  Ori decreased between 1993 and 2009. We took the measurements compiled in that paper and elsewhere (table 4.58) and phased them with both a short period of 425.59 days and a long period of 2335 days. Results are shown in 4.47. The trend is actually clearer when the data are phased with the long period, but it is apparent that  $\alpha$  Ori reaches smallest dimensions shortly after light maximum, consistent with the result of the radial velocity measurements.

Figure 4.48 shows  $\alpha$  Ori's changes in period and average visual magnitude taken at approximately 10-year intervals. The AAVSO observations for  $\alpha$  Ori provide no clear picture of its variability. No obvious series of maxima stand out in the general noise, although the radius of the star is measured to change (Townes et al. 2009). Preliminary results with our derived period are reasonably consistent, and suggest that the star reaches maximum radial velocity around phase 0.0 and is smallest near phase 0.25 (largest near phase 0.75). It also appears to be hottest when it is largest, although that result requires verification.

**Table 4.55:** Spectroscopic observations of  $\alpha$  Orionis

Year	HJD	Phase	$V_R$ (km/s)	Spectral Type	Source
1951	2433937	0.8704	...	M1.5-2 Iab	DDO
1962	2437957	0.3295	...	M2 Iab	DDO
1968	2394921	0.9498	...	M1.5-2 Iab	DDO
1969	2440577	0.4932	...	M1.2 Ib	Wing
1970	2440593	0.5308	...	M1.2 Iab	Wing
1970	2440635	0.6296	...	M1.4 Ib	Wing
1970	2440882	0.2155	...	M1.5 Ia	Wing
1971	2441006	0.5026	...	M2.7 Ib	Wing
1971	2441009	0.5086	...	M2.7 Ib	Wing
1971	2441020	0.5355	...	M2.6 Ib	Wing
1971	2441043	0.5908	$19.9 \pm 0.4$	M1 Ia	DAO Pg
1971	2441132	0.8002	$-12.7 \pm 0.1$	M1 Ia	DAO Pg
1971	2441233	0.0379	$10.3 \pm 0.2$	M2 Iab	DAO Pg
1972	2441360	0.3355	...	M1.9 Iab	Wing
1972	2441362	0.3402	...	M2.0 Iab	Wing
1972	2441364	0.3449	...	M1.9 Iab	Wing
1972	2441683	0.0955	...	M2.5 Ib	Wing
1973	2442015	0.8767	...	M2.4 Iab	Wing
1974	2442087	0.0461	...	M2.7 Ib	Wing
1975	2442458	0.9202	$-21.9 \pm 0.8$	M3 Ib	DAO Pg
1976	2442819	0.7696	$-22.6 \pm 0.1$	M3 Ib	DAO Pg
2006	2450401	0.1736	23.5	...	R. Griffin
2006	2454057	0.2112	23.8	...	R. Griffin
2006	2454079	0.2629	23.3	...	R. Griffin
2007	2454124	0.3685	22.6	...	R. Griffin
2007	2454186	0.5164	18.5	...	R. Griffin
2007	2454360	0.9242	18.7	...	R. Griffin
2007	2453941	0.9984	22.3	...	R. Griffin
2007	2454414	0.0511	24.7	...	R. Griffin
2007	2454421	0.0676	24.9	...	R. Griffin
2007	2454429	0.0884	24.7	...	R. Griffin
2007	2454443	0.1193	24.7	...	R. Griffin

continued on next page

**Table 4.56:** Spectroscopic observations of  $\alpha$  Orionis (continued)

Year	HJD	Phase	$V_R$ (km/s)	Spectral Type	Source
continued from previous page					
2008	2454472	0.1874	22.2	...	R. Griffin
2008	2454490	0.2319	21.8	...	R. Griffin
2008	2454508	0.2742	21.4	...	R. Griffin
2008	2454523	0.3094	21.0	...	R. Griffin
2008	2454757	0.8585	22.8	...	R. Griffin
2008	2454779	0.9100	25.1	...	R. Griffin
2008	2454804	0.9686	25.5	...	R. Griffin
2009	2454845	0.0672	26.6	...	R. Griffin
2009	2454876	0.1402	26.9	...	R. Griffin
2009	2454897	0.1893	26.3	...	R. Griffin
2009	2454929	0.2645	25.4	...	R. Griffin
2009	2455114	0.6984	25.1	...	R. Griffin
2009	2455128	0.7313	25.2	...	R. Griffin
2009	2455167	0.8228	23.9	...	R. Griffin
2009	2455187	0.8697	23.4	...	R. Griffin
2010	2455214	0.9354	23.2	...	R. Griffin
2010	2455227	0.9638	23.3	...	R. Griffin
2010	2455258	0.0388	25.2	...	R. Griffin
2010	2455295	0.1257	24.6	...	R. Griffin

**Table 4.57:** AAVSO Observations of  $\alpha$  Orionis

Subset	Dates	$\langle V \rangle$	% Diff.	$\Delta V$	$N$	$P$ (days)	% Diff.
All	19790-55417	0.74	...	2.9	23349	$425.29 \pm 0.03$	...
1	19790-23394	0.87	17.57	1.2	79	$350.25 \pm 2.31$	-17.64
2	23446-27081	0.62	-16.22	1.4	262	$392.73 \pm 1.81$	-7.65
3	27092-30738	0.79	6.76	1.6	507	$392.85 \pm 1.44$	-7.63
4	30759-34389	0.73	-1.35	2.1	2139	$414.30 \pm 0.88$	-2.58
5	33940-38038	0.85	14.86	1.6	2054	$451.47 \pm 0.61$	6.16
6	38040-41689	0.71	-4.05	1.8	3346	$397.19 \pm 0.50$	-6.61
7	41690-45339	0.76	2.70	1.8	3827	$448.71 \pm 0.58$	5.51
8	45340-48989	0.80	8.11	2.1	2996	$402.04 \pm 0.46$	-5.47
9	48989-52640	0.71	-4.05	1.6	4164	$385.62 \pm 0.45$	-9.33
10	52640-55417	0.68	-8.11	1.7	3981	$436.22 \pm 1.47$	2.57

**Table 4.58:** Angular Diameter of  $\alpha$  Orionis

Date	HJD	Phase (P=425 d)	Phase (P=2335 d)	Diameter (mas)	Source
Nov 1978	2443821.5	0.1643	0.2910	55.0	Balega et al. (1982)
Feb 1979	2443926.5	0.4111	0.3360	59.0	Balega et al. (1982)
Feb 1989	2447572.5	0.9780	0.8975	54.0	Balega et al. (1982)
Oct 1993	2449290.5	0.0147	0.6332	56.0	Bester et al. (1996)
Aug 1994	2449572.5	0.6773	0.7540	56.0	Bester et al. (1996)
Oct 1995	2450016.6	0.7206	0.9442	50.5	Bester et al. (1996)
Nov 1999	2451497.5	0.2005	0.5784	54.9	Weiner et al. (2003)
Nov 2000	2451853.5	0.3070	0.7309	53.4	Weiner et al. (2003)
Nov 2000	2451876.5	0.0910	0.7407	55.8	Weiner et al. (2003)
Dec 2000	2451899.5	0.1450	0.7506	54.8	Weiner et al. (2003)
Aug 2001	2452141.5	0.7137	0.8542	53.4	Weiner et al. (2003)
Sep 2001	2452182.5	0.8100	0.8718	52.9	Weiner et al. (2003)
Oct 2001	2452211.5	0.8781	0.8842	53.5	Weiner et al. (2003)
Dec 2001	2452262.5	0.9980	0.9060	52.7	Weiner et al. (2003)
Nov 2006	2454068.5	0.2415	0.6795	48.4	Tatebe et al. (2007)
Dec 2007	2454440.5	0.1156	0.8388	50.0	Townes et al. (2009)
Feb 2008	2454499.5	0.2542	0.8641	49.0	Townes et al. (2009)
Oct 2008	2454768.5	0.8863	0.9793	47.0	Townes et al. (2009)
Dec 2008	2454805.5	0.9732	0.9951	47.0	Townes et al. (2009)
Jan 2009	2454848.5	0.0742	0.0135	48.0	Townes et al. (2009)
Feb 2009	2454864.5	0.1118	0.0204	48.0	Townes et al. (2009)

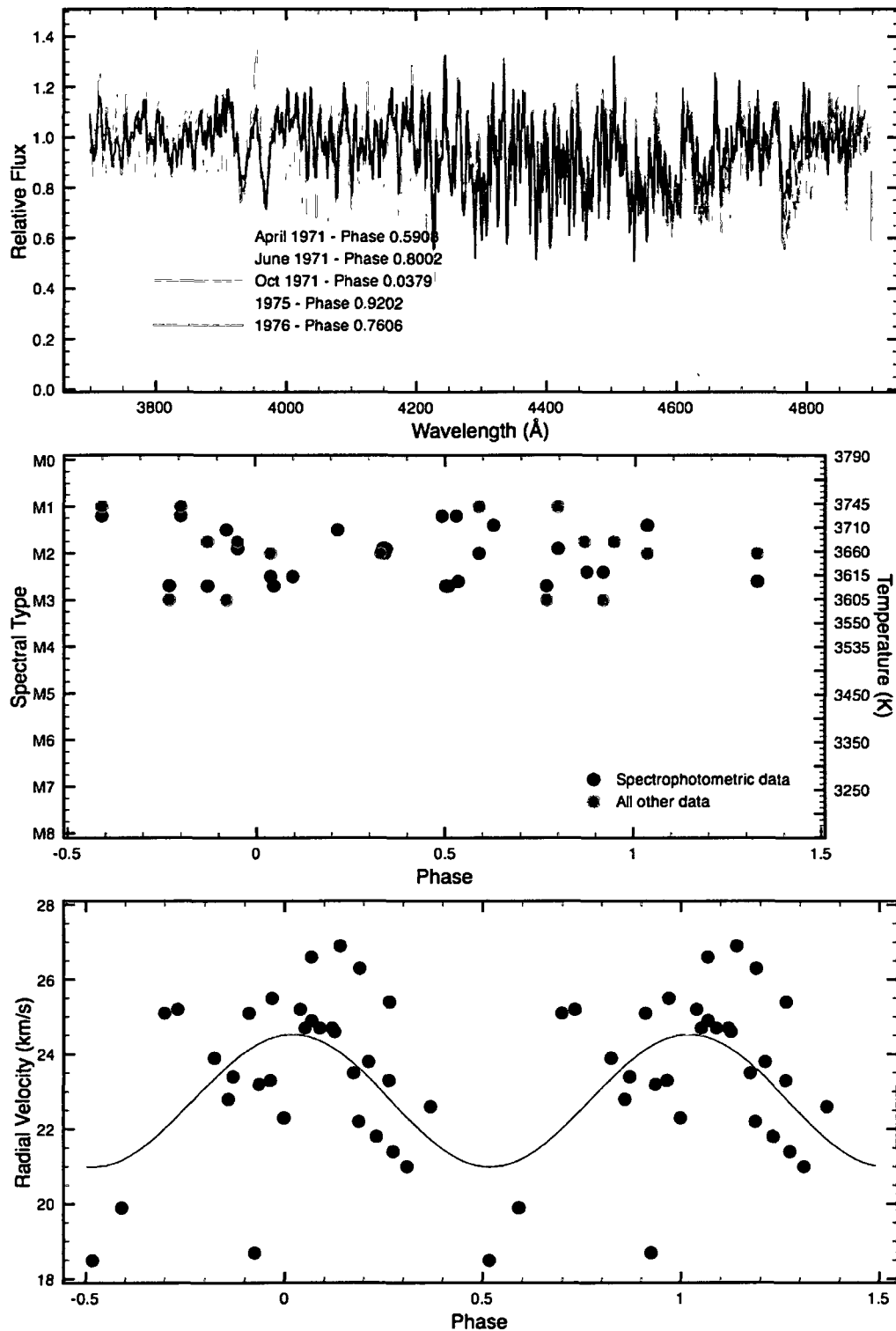


**Figure 4.46:** Spectral variation in  $\alpha$  Orionis. Top: Spectra from different epochs. Middle: Spectral type as a function of phase. Bottom: Radial velocity as a function of phase. Data phased with 425.59 day period.

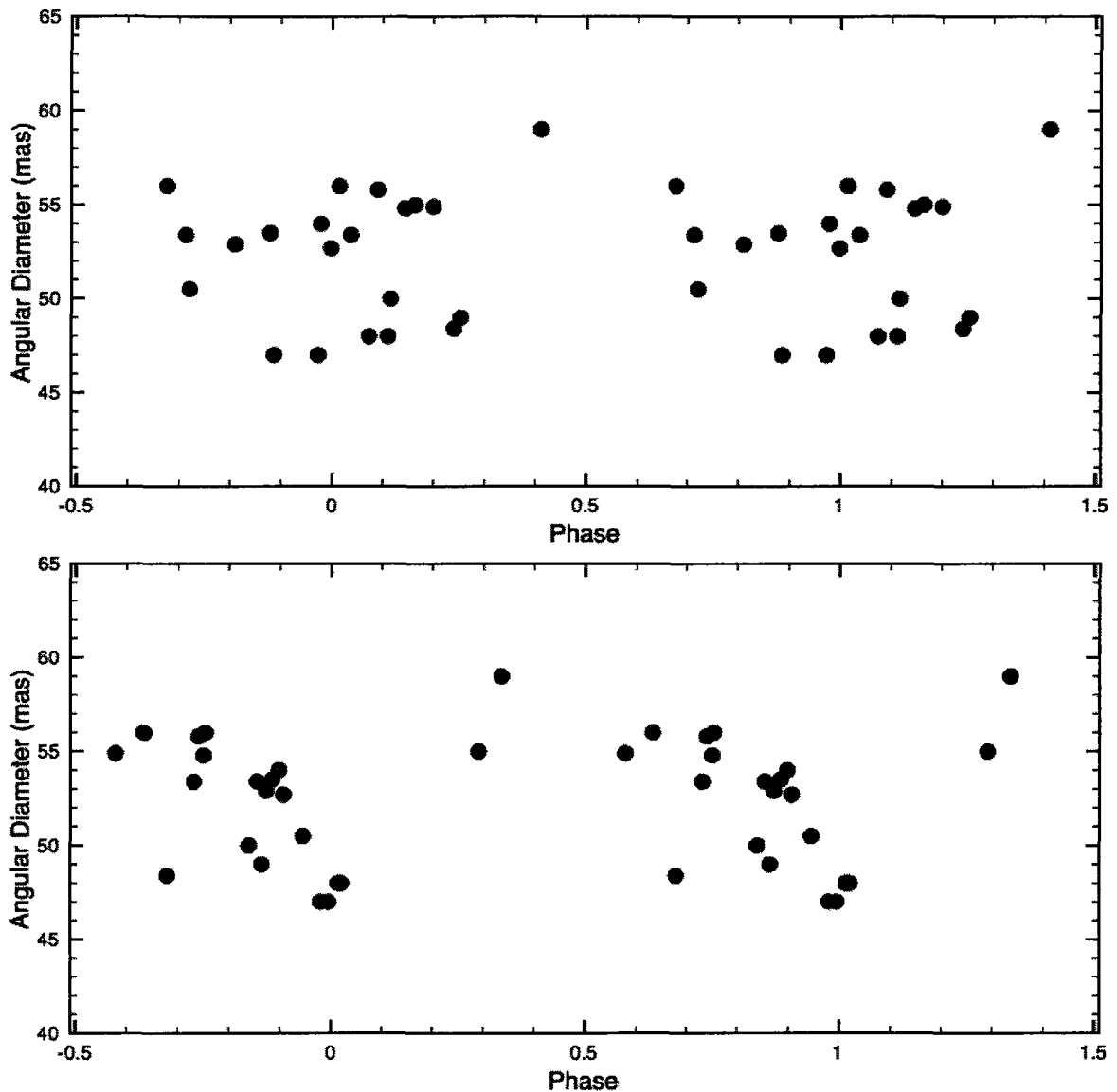


**Figure 4.47:** Angular diameter of  $\alpha$  Orionis as a function of phase. Top plot is phased with 425.59 day period, bottom with 2335 day period

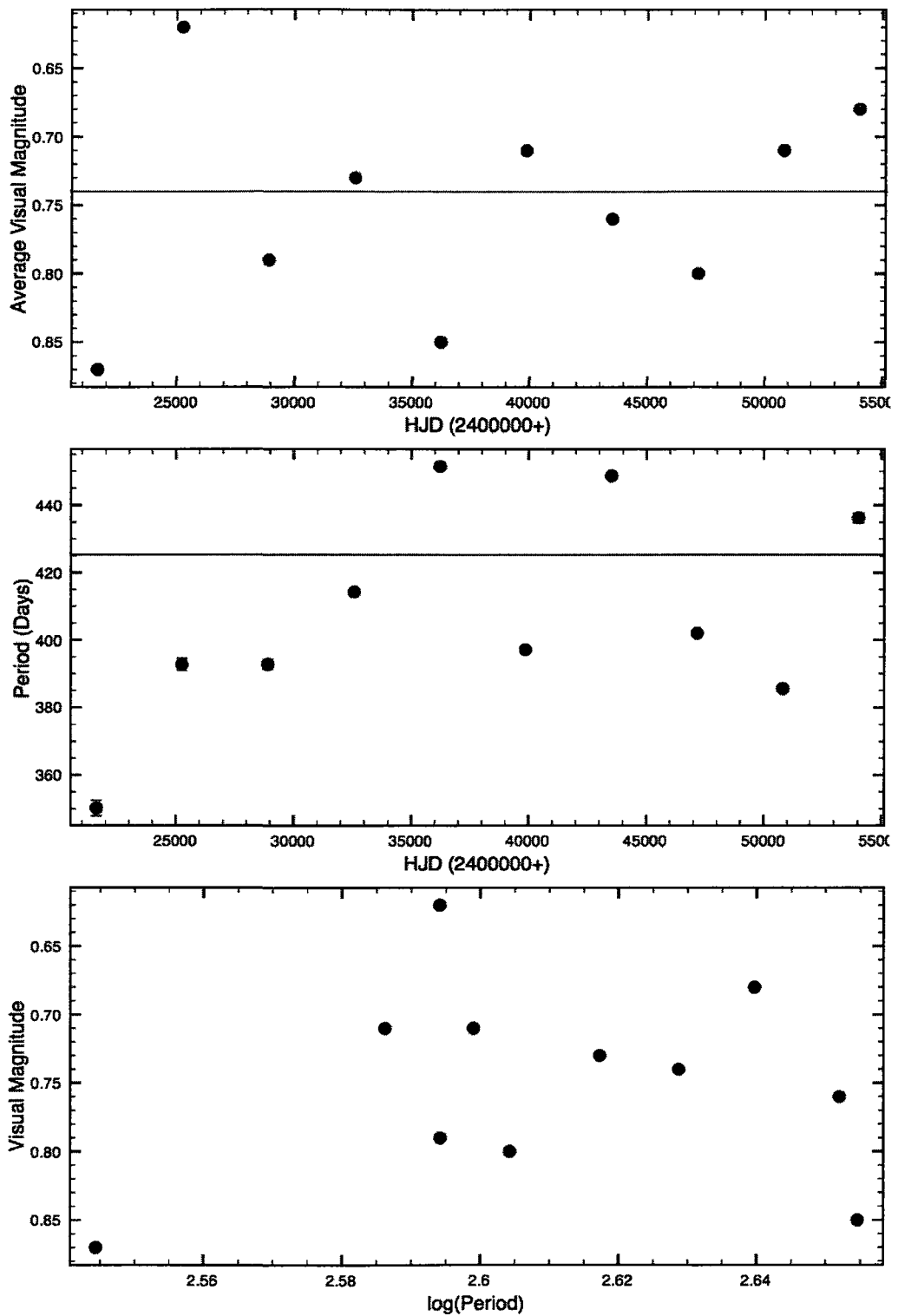


Figure 4.48: Period and average magnitude changes in  $\alpha$  Orionis from AAVSO observations.

#### 4.34 S Persei

Figure 4.49 shows S Per's variations in spectral type and radial velocity and a montage of CCD spectra taken at different epochs. The observations were phased using a period of 806.64 days, determined from the AAVSO observations. We used a time of maximum light of JD2454707.17 for the recent CCD observations and JD247363.8 for the older spectrophotometric observations. The radial velocity variations indicate that the star reaches minimum dimensions near phase 0.17. It appears to reach highest temperature and greatest luminosity class near light maximum. We also obtained 586 photographic (blue light) observations of S Per from the Harvard plate collection. The observations covered the dates JD2412463-2434283. We found a period of  $828.55 \pm 2.94$  days for the star from the Harvard observations, a difference of 2.72% from the period found using the AAVSO observations. The star's average magnitude during the observations was 11.83 with a magnitude range of  $3^m.1$ .

Figure 4.50 shows S Per's changes in period and average visual magnitude taken at approximately 10-year intervals. The star's average brightness is increasing, while the period is increasing slightly. The periodicity is well-expressed in the light curve for S Per, and the spectroscopic observations are consistent with pulsation. Chipps & Stencel (2004) completed a Fourier analysis of the AAVSO data and found that the light curve is likely a combination of sinusoids with different periods. They found prominent periods of 745, 797 (closest to the period of 806 days found in this study), 952, and 2857 days. The star undergoes changes in mean brightness that may reflect episodes of dust ejection. The amplitude is large,  $\Delta V \simeq 4^m - 5^m$ .

**Table 4.59:** AAVSO Observations of S Persei

Subset	Dates	$\langle V \rangle$	% Diff.	$\Delta V$	$N$	$P$ (days)	% Diff.
All	11063-55423	9.99	...	6.1	27313	$806.64 \pm 0.07$	...
1	11063-14415	8.96	-10.31	2.6	55	$808.99 \pm 14.58$	0.29
2	15472-18352	8.86	-11.31	1.8	31	$797.53 \pm 15.56$	-1.13
3	18368-21986	9.65	-3.40	4.5	415	1051.0315.33	30.30
4	22167-25562	9.59	-4.00	3.9	441	$859.25 \pm 8.27$	6.52
5	25563-29311	9.40	-5.91	3.0	2448	$864.71 \pm 3.06$	7.20
6	29313-32958	9.66	-3.30	4.4	2161	$856.38 \pm 2.37$	6.17
7	32966-36612	9.61	-3.80	4.0	1563	$793.02 \pm 2.27$	-1.69
8	36613-40262	9.70	-2.90	3.9	3036	$848.94 \pm 2.69$	5.24
9	40263-39411	9.83	-1.60	4.1	3892	$883.26 \pm 2.83$	9.50
10	39415-47560	9.60	-3.90	3.8	4613	$777.93 \pm 1.89$	-3.56
11	47563-51209	10.81	8.21	4.8	4487	$795.41 \pm 1.50$	-1.39
12	51214-54862	10.64	6.51	3.7	3801	$881.45 \pm 1.89$	9.27
13	54862-55423	10.66	6.71	1.9	370	$470.45 \pm 18.33$	-41.68

**Table 4.60:** Spectroscopic observations of S Persei

Year	HJD	Phase	$V_R$ (km/s)	Spectral Type	Source
1970	2440899	0.9885	...	M4.3 Ia	Wing
1970	2440902	0.9922	...	M4.4 Ia	Wing
1970	2440903	0.9934	...	M4.4 Ia	Wing
1970	2440906	0.9971	...	M4.4 Iab	Wing
1973	2441962	0.3057	...	M5.8 Iab	Wing
1973	2442015	0.3714	...	M5.7 Iab	Wing
2005	2453648	0.6875	$33.5 \pm 14.8$	M4 Ia	DAO CCD
2007	2454379	0.5933	$23.7 \pm 13.5$	M5 Iab	DAO CCD
2008	2454749	0.0518	$12.4 \pm 15.9$	M3 Ia+	DAO CCD
2009	2455087	0.4707	$20.7 \pm 19.7$	M4.5 Ia	DAO CCD
2010	2455484	0.9625	$24.6 \pm 11.4$	M4 Ia	DAO CCD

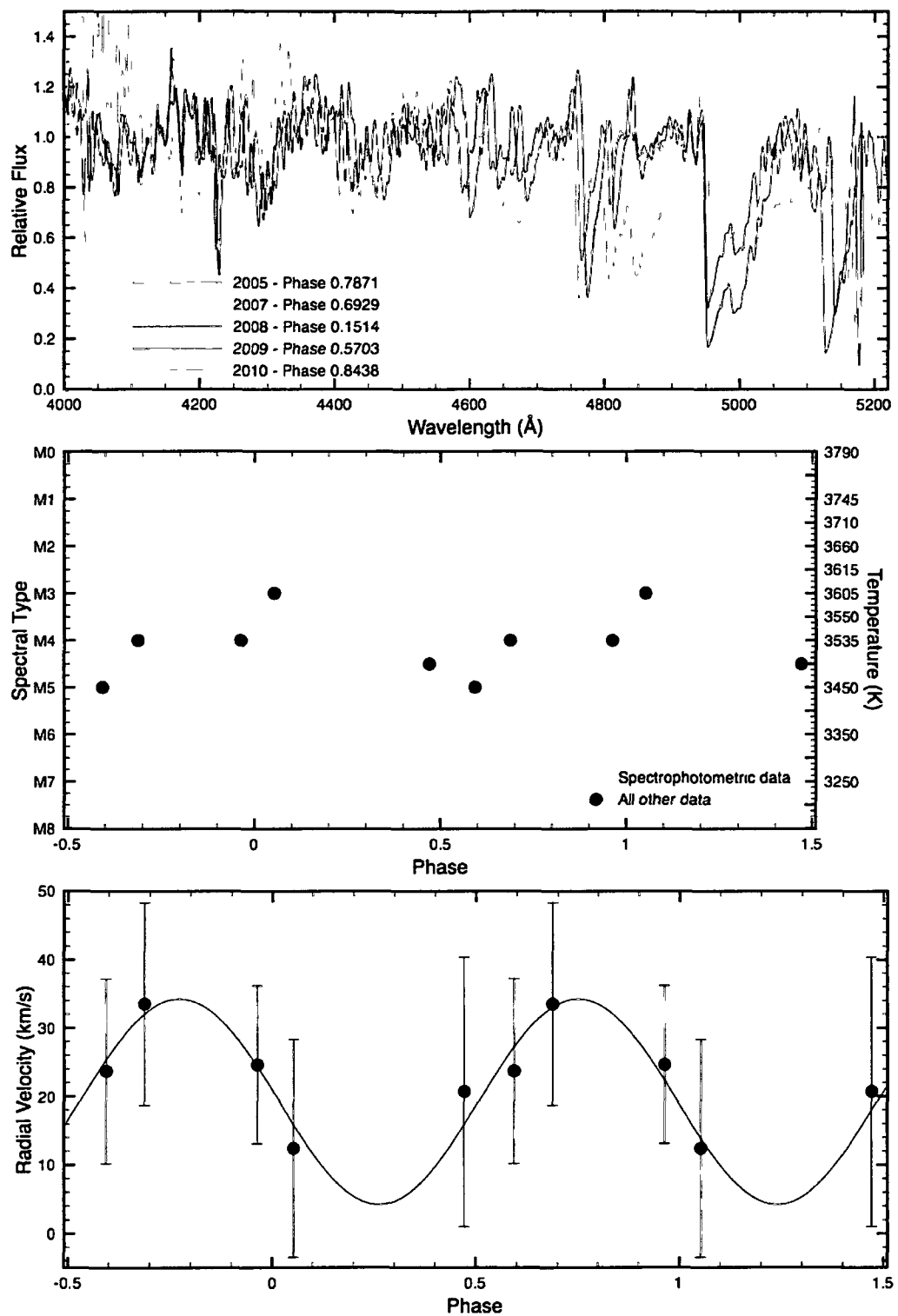


**Figure 4.49:** Spectral variation in S Persei. Top: Spectra from different epochs. Middle: Spectral type as a function of phase. Bottom: Radial velocity as a function of phase. Data phased with 806.64 day period.

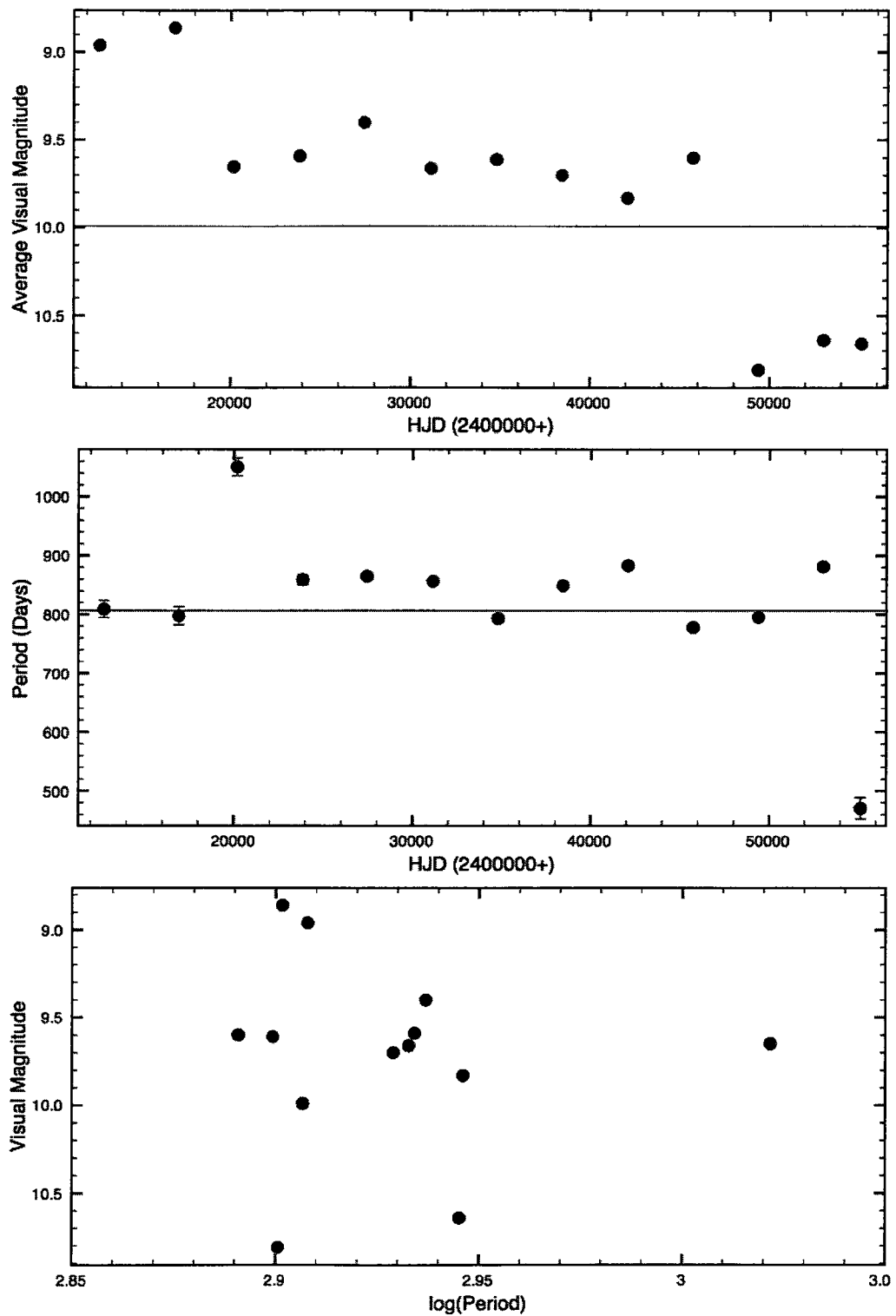


Figure 4.50: Period and average magnitude changes in S Persei from AAVSO observations.

### 4.35 T Persei

Figure 4.51 shows T Per's variations in spectral type and radial velocity and a montage of CCD spectra taken at different epochs. The observations were phased using a period of 2457 days and a time of maximum light of JD2441127.04, determined from the AAVSO observations. Note that while the 2457 day period first appears to be a long secondary period, compared to the shorter 300-400 day period, the spectroscopic data phase much better with the longer period than with a shorter period. The GCVS lists a period of 2430 days and a spectral type of M2 Iab. The radial velocity variations indicate that the star reaches minimum dimensions near phase 0.45. T Per appears to reach highest temperature and greatest luminosity class following light maximum. We also obtained 567 blue light observations of T Per from the Harvard plate collection. The observations covered the dates JD2412462-2433999. We found a period of  $358.86 \pm 46.98$  days for the star from the Harvard observations, noting that a period so close to one year may be heavily biased by seasonal effects. The star's average *B* magnitude with the photographic observations was 11.33, with a range of 1<sup>m</sup>.3.

Figure 4.52 shows T Per's changes in period and average visual magnitude taken at approximately 10-year intervals. The period and average magnitude both undergo changes. Surprisingly enough, given the scatter in the photometry, the long period of 2457 days appears to be more closely linked to the spectral changes, and it generates results consistent with pulsation. There are problems with such a long period, however, given that pulsation would imply an extremely large size. This star needs more data, both spectroscopic and photometric.

**Table 4.61:** AAVSO Observations of T Persei

Subset	Dates	$\langle V \rangle$	% Diff.	$\Delta V$	$N$	$P$ (days)	% Diff.
All	16161-55423	8.89	...	2.5	9212	$2457.00 \pm 1.19$	...
1	16161-19808	9.00	1.24	1.1	71	$377.33 \pm 3.35$	...
2	19824-23400	9.00	1.24	1.9	57	$352.40 \pm 2.36$	...
3	23485-27109	8.69	-2.25	1.5	610	$353.30 \pm 0.64$	...
4	27117-30735	8.88	-0.11	1.7	1479	$394.88 \pm 6.69$	...
5	30765-34401	8.90	0.11	1.7	270	$373.43 \pm 0.88$	...
6	34412-38057	8.92	0.34	1.3	481	$377.73 \pm 1.02$	...
7	38079-40115	8.94	0.56	1.8	632	$309.34 \pm 1.04$	...
8	40121-45336	8.95	0.67	2.0	1394	$353.01 \pm 0.28$	...
9	45357-49009	8.88	-0.11	1.8	1522	$360.23 \pm 0.48$	...
10	49010-52659	8.87	-0.22	1.7	1826	$346.07 \pm 0.47$	...
11	52664-55423	8.90	0.11	2.1	870	$344.55 \pm 1.03$	...

**Table 4.62:** Spectroscopic observations of T Persei

Year	HJD	Phase	$V_R$ (km/s)	Spectral Type	Source
2005	2453648	0.0960	$2.3 \pm 14.7$	M1 Ia+	DAO CCD
2007	2454379	0.3935	$24.8 \pm 15.6$	M2 Iab	DAO CCD
2008	2454749	0.5441	$-3.4 \pm 14.2$	M2 Iab	DAO CCD
2009	2455087	0.6817	$-9.3 \pm 22.9$	M2 Ia	DAO CCD
2010	2455483	0.8428	$-7.1 \pm 23.2$	M2 Ia	DAO CCD

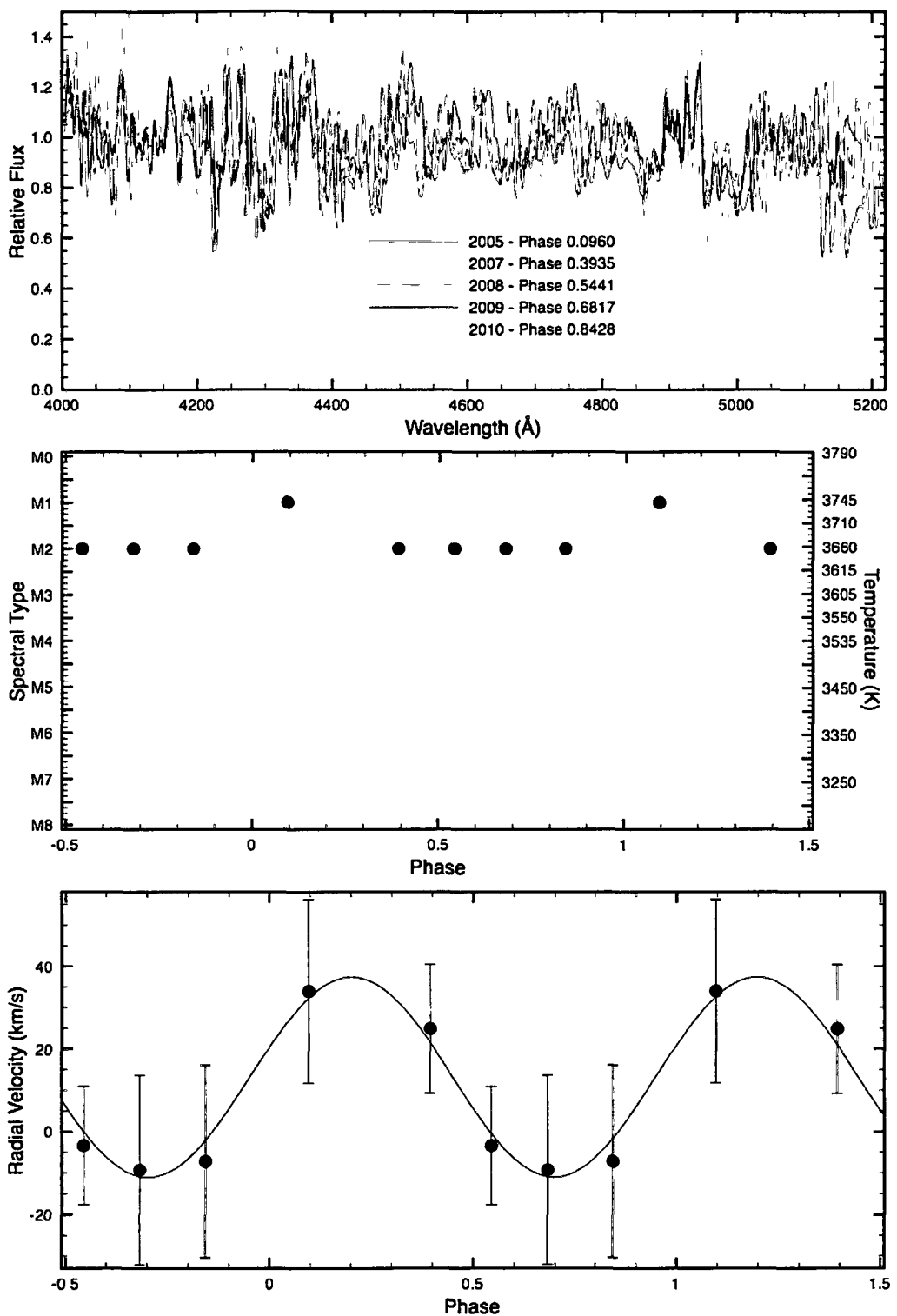


**Figure 4.51:** Spectral variation in T Persei. Top: Spectra from different epochs. Middle: Spectral type as a function of phase. Bottom: Radial velocity as a function of phase. Data phased with 2457 day period.

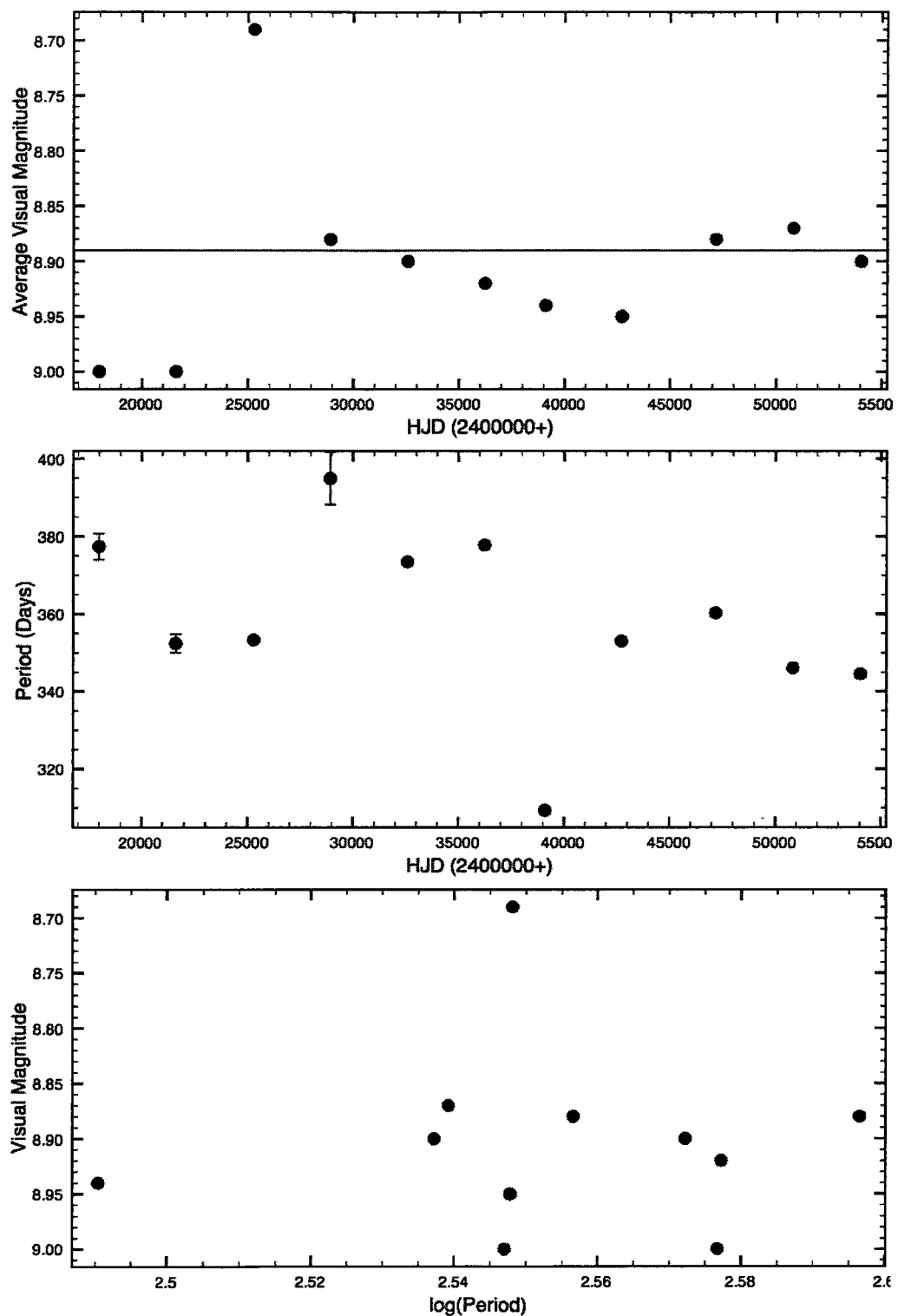


Figure 4.52: Period and average magnitude changes in T Persei from AAVSO observations.

### 4.36 W Persei

Figure 4.53 shows W Per's variations in spectral type and radial velocity, phased using a period of 531.47 days and a time of maximum light of JD2421890.61 from the AAVSO observations, along with a montage of CCD spectra taken at different epochs. The GCVS lists a period for the star of 485 days and a spectral type of M3-7 Ia-Iab. The star appears to reach minimum dimensions near phase 0.88. The star appears to reach its highest temperature and greatest luminosity class near light minimum. We also obtained 415 blue light observations of W Per from the Harvard plate collection. The observations covered the dates JD2413252-2433999. We found a period of  $541.93 \pm 0.53$  days for the star from the Harvard observations, a difference of 1.97% from the period found using the AAVSO observations. The star's average *B* magnitude for the photographic observations was 12.14 with a range of  $2^m.3$ . Figure 4.54 shows W Per's changes in period and average visual magnitude taken at approximately 10-year intervals. The mean brightness of the star is reasonably constant, and the variability is well-expressed. The phased spectroscopic data are consistent with pulsation, although the period of variability needs confirmation.

**Table 4.63:** AAVSO Observations of W Persei

Subset	Dates	$\langle V \rangle$	% Diff.	$\Delta V$	$N$	$P$ (days)	% Diff.
All	19070-55423	9.79	...	3.6	17051	$531.47 \pm 4.05$	...
1	19070-22717	9.63	-1.63	3.5	873	$475.58 \pm 1.55$	-10.52
2	22728-26369	9.57	-2.25	3.1	939	$542.12 \pm 1.10$	2.00
3	26378-30019	9.62	-1.74	3.2	3206	$523.80 \pm 0.77$	-1.44
4	30022-33668	9.67	-1.23	3.1	1653	$567.73 \pm 1.14$	6.82
5	33672-37319	10.04	2.55	3.0	1182	$527.21 \pm 1.18$	-0.80
6	37320-40970	9.94	1.53	3.2	1637	$460.11 \pm 1.17$	-13.43
7	40970-44618	9.98	1.94	3.3	2278	$466.43 \pm 0.98$	-12.24
8	44621-48269	9.91	1.23	3.1	2180	$534.92 \pm 0.90$	0.65
9	48275-51915	9.87	0.82	3.4	1897	$486.61 \pm 1.09$	-8.44
10	51920-55423	9.59	-2.04	3.0	1206	$477.47 \pm 1.61$	-10.16

**Table 4.64:** Spectroscopic observations of W Persei

Year	HJD	Phase	$V_R$ (km/s)	Spectral Type	Source
2005	2453654	0.8068	$44.1 \pm 20.3$	M3.5 Ia	DAO CCD
2008	2454749	0.8801	$23.5 \pm 11.1$	M5 Ib	DAO CCD
2009	2455092	0.5223	$18.7 \pm 21.4$	M4 Ia	DAO CCD
2010	2455484	0.2643	$20.1 \pm 19.5$	M5 Iab	DAO CCD

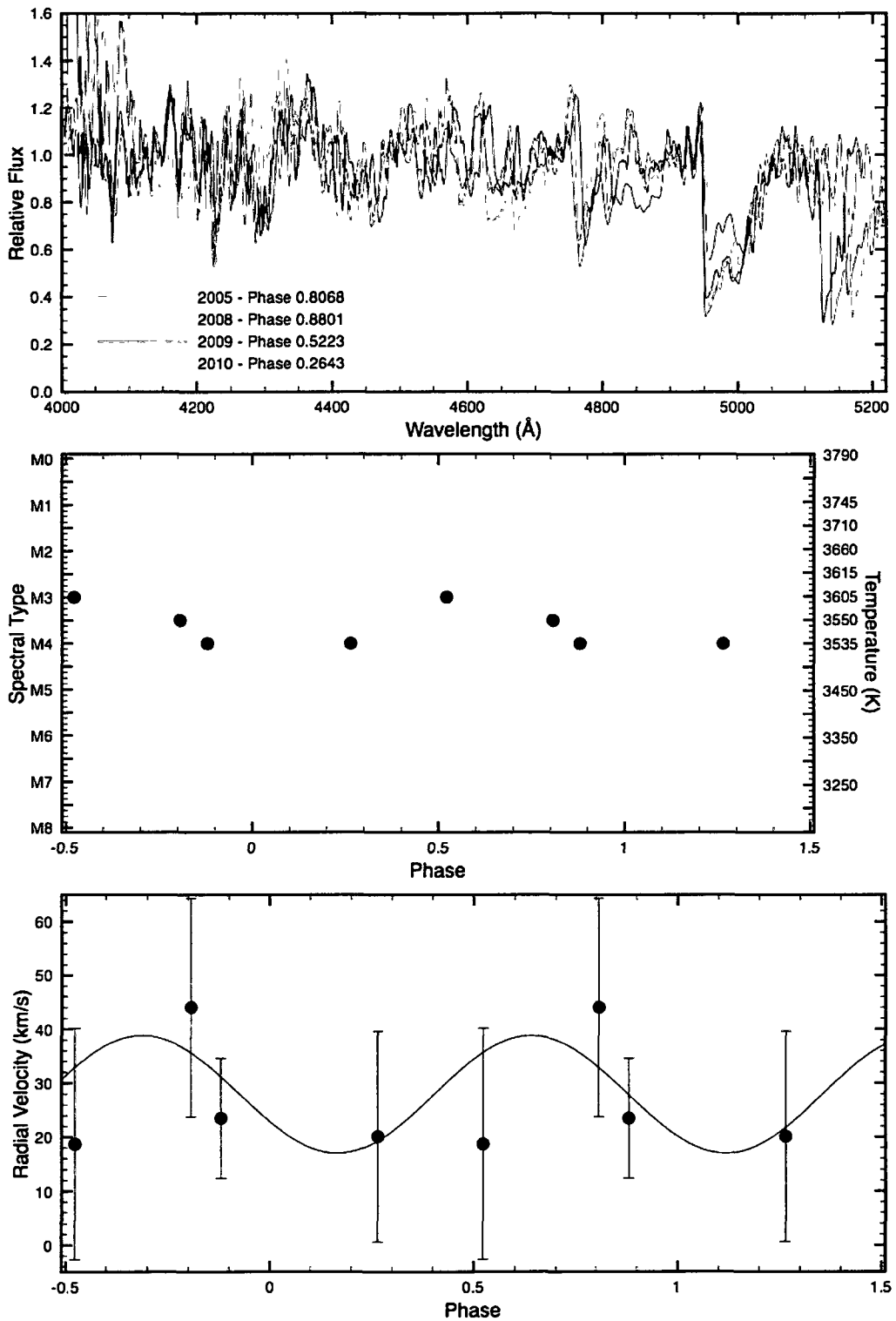


**Figure 4.53:** Spectral variation in W Persei. Top: Spectra from different epochs. Middle: Spectral type as a function of phase. Bottom: Radial velocity as a function of phase. Data phased with 531.47 day period.

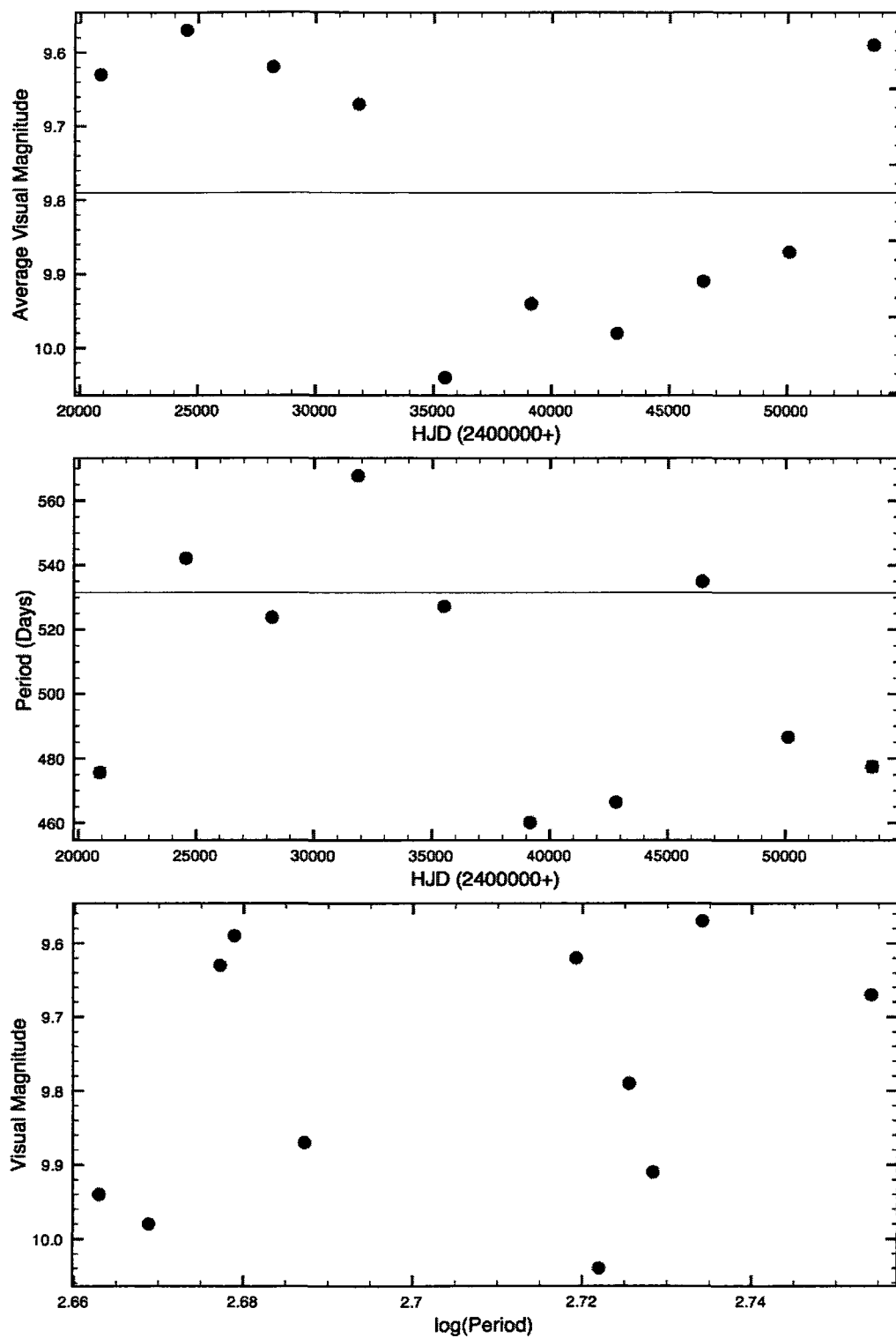


Figure 4.54: Period and average magnitude changes in W Persei from AAVSO observations.

#### 4.37 RS Persei

Figure 4.55 shows RS Per's variations in spectral type and radial velocity, phased with a period of 244.21 days and a time of maximum light of JD2442087.12 from the AAVSO observations, as well as a montage of CCD spectra taken at different epochs. The GCVS confirms a period of 244.5 days for the star and lists a spectral type of M4 Iab. We also obtained 194 blue light observations of RS Per from the Harvard plate collection. The observations covered the dates JD2415405-2433999. We found a period of  $245.13 \pm 20.05$  days for the star from the Harvard observations, a difference of 0.38% from the period found using the AAVSO observations. The star's average photographic magnitude during the observations was 11.08 with a magnitude range of  $1^m.8$ . The radial velocity variations (except the values from Joy's work) indicate that the star reaches smallest dimensions near phase 0.64. The two sets of radial velocities do not fit together nicely, and we have not been able to resolve the discrepancy, although we do note that there is a large temporal separation between the two sets of measurements. There are problems with the red end calibration for the spectra of this star that could bias our velocities. RS Per appears to reach highest temperature and greatest luminosity class near light minimum. Figure 4.56 shows RS Per's changes in period and average visual magnitude taken at approximately 10-year intervals. The periodicity is not well expressed in the star's light curve, and there appears to be a long-term brightness fluctuation that may be caused by dust extinction episodes. Our inferred period of 244 days is consistent with GCVS results, and the phased spectroscopic observations hint at pulsation. The definition of light maximum needs to be confirmed with better photometry.

**Table 4.65:** AAVSO Observations of RS Persei

Subset	Dates	$\langle V \rangle$	% Diff.	$\Delta V$	$N$	$P$ (days)	% Diff.
All	33490-55394	8.83	...	2.9	2310	$244.21 \pm 0.02$	...
1	33490-36896	9.02	2.15	2.4	56	$248.73 \pm 1.61$	1.85
2	37208-40785	9.06	2.60	2.5	253	$260.35 \pm 0.59$	6.61
3	40802-44436	8.83	0.00	2.1	237	$265.31 \pm 0.68$	8.64
4	44445-48087	8.65	-2.04	2.5	541	$250.11 \pm 0.28$	2.42
5	48094-51737	8.76	-0.79	2.2	565	$247.25 \pm 0.29$	1.25
6	51748-55394	8.93	1.13	2.5	658	$266.04 \pm 0.37$	8.94

**Table 4.66:** Spectroscopic observations of RS Persei

Year	HJD	Phase	$V_R$ (km/s)	Spectral Type	Source
1939	2423742	0.1220	-36	M4	Joy
1939	2423803	0.3709	-39	M4	Joy
1939	2423829	0.4771	-41	M4	Joy
2005	2453648	0.1873	$45.6 \pm 19.3$	M4 Ia	DAO CCD
2008	2454754	0.7011	$16.7 \pm 20.6$	M3 Iab	DAO CCD
2009	2455091	0.0770	$0.7 \pm 20.1$	M5 Ia+	DAO CCD
2010	2455484	0.6808	$19.9 \pm 13.1$	M3.5 Ia	DAO CCD

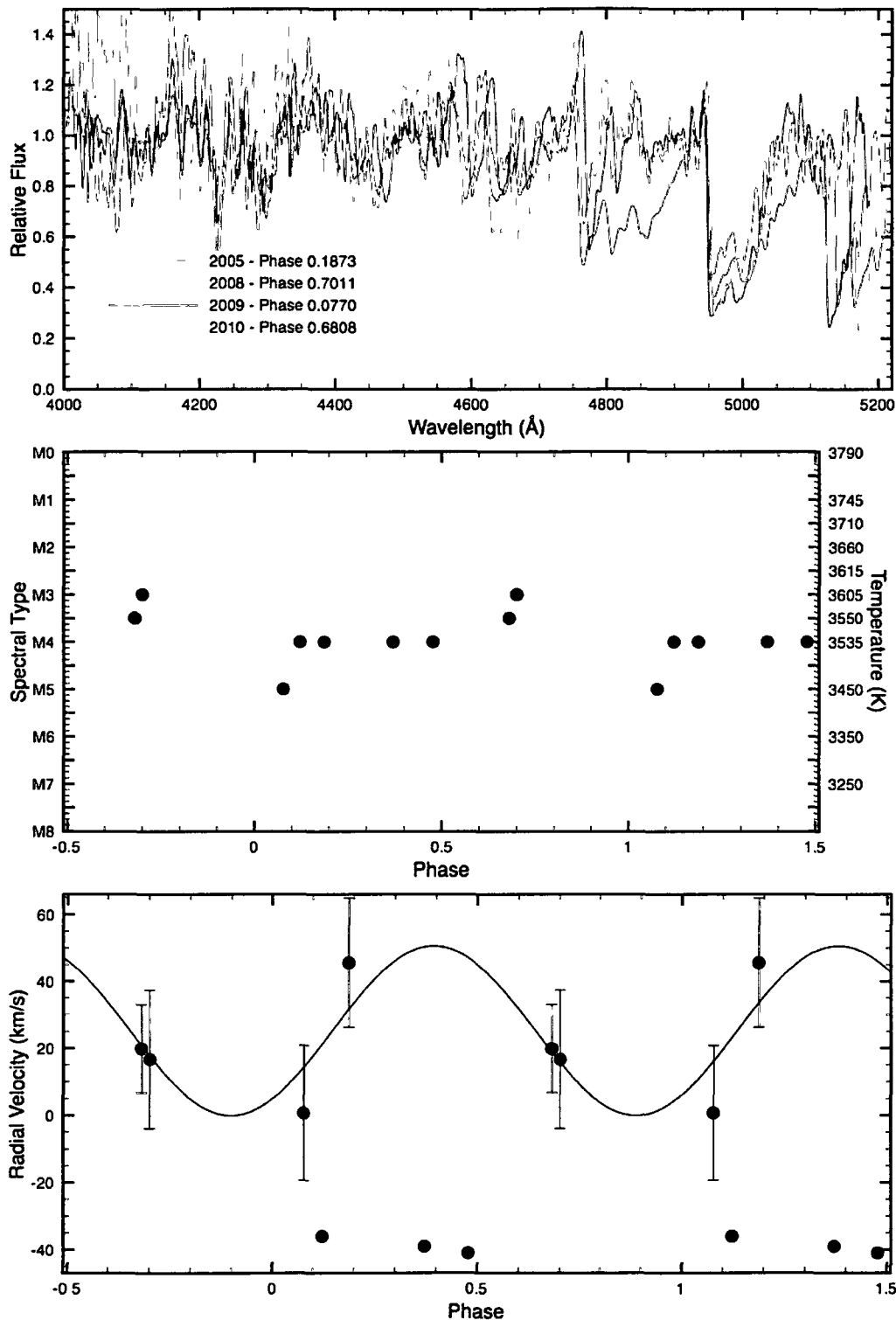


**Figure 4.55:** Spectral variation in RS Persei. Top: Spectra from different epochs. Middle: Spectral type as a function of phase. Bottom: Radial velocity as a function of phase. Data phased with 244.21 day period.

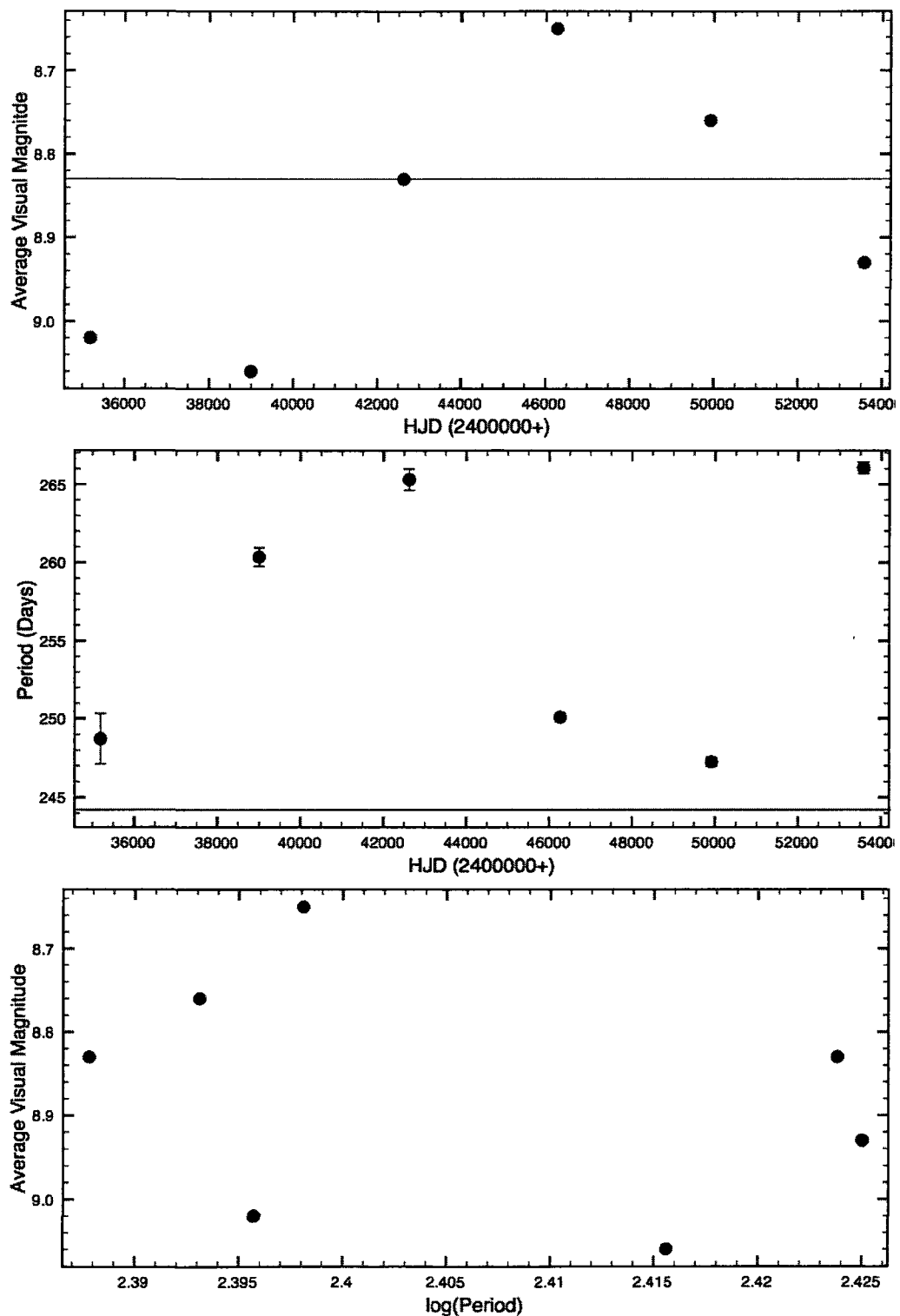


**Figure 4.56:** Period and average magnitude changes in RS Persei from AAVSO observations.

### 4.38 SU Persei

Figure 4.57 shows SU Per's variations in spectral type and radial velocity, phased with a period of 468.91 days and a time of maximum light of JD2434920.21 from the AAVSO observations, along with a montage of CCD spectra taken at different epochs. The GCVS lists a period of 533 days and a spectral type of M3.5 Iab. We also obtained 197 blue light observations of SU Per from the Harvard plate collection. The observations covered the dates JD2415405-2433999. We found a period of  $461.56 \pm 7.45$  days for the star from the Harvard observations, a difference of -1.57% from the period found using the AAVSO observations. The star's average magnitude during the observations was 9.89 with a range of  $1^m.4$ . We fitted the radial velocity variations (except for Joy's values) with a sine wave and found that the star appears to reach smallest dimensions near phase 0.12. Again, as in the case of RS Persei, the two sets of radial velocities (with a large temporal separation) do not fit together well and we have not been able to resolve the discrepancy. The star appears to reach its lowest temperature at light minimum, although there is a lot of scatter in the observations. There is too much scatter in the luminosity class measurements to determine at which phase it reaches greatest luminosity class. Figure 4.58 shows SU Per's changes in period and average visual magnitude taken at approximately 10-year intervals. The period has decreased, and the average magnitude undergoes changes. The light variations in this star are not well-expressed, but the periodicity appears to be centered around  $469 \pm 60$  days, so phasing is difficult. There are also superposed long-term trends that may represent dust ejection episodes. The results are otherwise consistent with pulsation. Additional photometry would help to establish a firm period of variability.

**Table 4.67:** AAVSO Observations of SU Persei

Subset	Dates	$\langle V \rangle$	% Diff.	$\Delta V$	$N$	$P$ (days)	% Diff.
All	21396-55423	8.11	...	2.8	3282	$468.91 \pm 0.13$	...
1	21396-21597	8.10	-0.12	0.2	14	...	...
2	27724-27924	8.05	-0.74	0.3	11	...	...
3	29546-29880	7.95	-1.97	0.2	12	...	...
4	33572-35959	8.18	0.86	1.8	198	$525.11 \pm 5.01$	11.99
5	36020-39593	8.24	1.60	2.0	200	$496.88 \pm 2.66$	5.96
6	39680-43287	8.14	0.37	2.5	340	$472.25 \pm 1.63$	0.71
7	43335-46937	8.13	0.25	2.4	508	$460.95 \pm 1.24$	-1.70
8	46947-50555	8.04	-0.86	2.3	964	$468.86 \pm 1.09$	-0.01
9	50627-54231	8.12	0.12	2.6	784	$447.38 \pm 2.07$	-4.59
10	54252-55423	8.19	0.99	1.9	251	$410.25 \pm 5.61$	-12.51

**Table 4.68:** Spectroscopic observations of SU Persei

Year	HJD	Phase	$V_R$ (km/s)	Spectral Type	Source
1938	2423742	0.1659	-39	M4	Wing
1938	2423803	0.2949	-39	M4	Wing
1939	2423829	0.3514	-39	M4	Wing
1939	2426621	0.4516	-36	M4	Wing
1939	2426373	0.7757	-43	M4	Wing
1939	2426646	0.3578	-34	M4	Wing
1969	2440562	0.0283	...	M3.2 Ib	Wing
1970	2440868	0.6808	...	M3.2 Iab	Wing
1970	2440905	0.7597	...	M3.1 Ib	Wing
1971	2441018	0.0006	...	M3.0 Iab	Wing
1971	2441019	0.0028	...	M3.1 Iab	Wing
1973	2442015	0.1264	...	M4.2 Ib	Wing
2005	2453648	0.9314	$23.1 \pm 22.1$	M4 Ia	DAO CCD
2007	2454379	0.4900	$19.4 \pm 16.8$	M4 Iab	DAO CCD
2008	2454754	0.2894	$13.6 \pm 20.0$	M3 Iab	DAO CCD
2009	2455091	0.0080	$26.7 \pm 22.8$	M3 Iab	DAO CCD
2010	2455483	0.8438	$29.1 \pm 18.7$	M4 Ia	DAO CCD

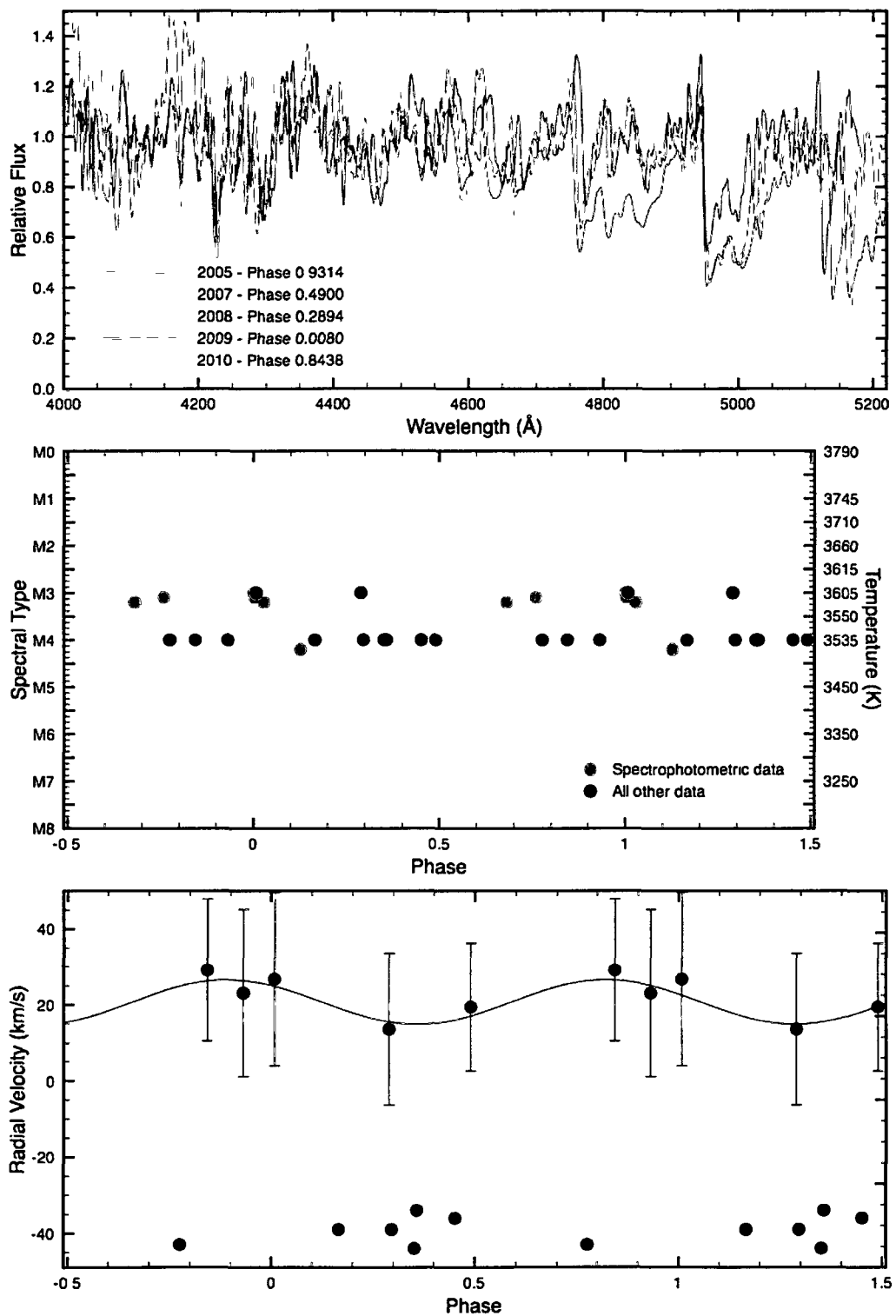


**Figure 4.57:** Spectral variation in SU Persei. Top: Spectra from different epochs. Middle: Spectral type as a function of phase. Bottom: Radial velocity as a function of phase. Data phased with 468.91 day period.

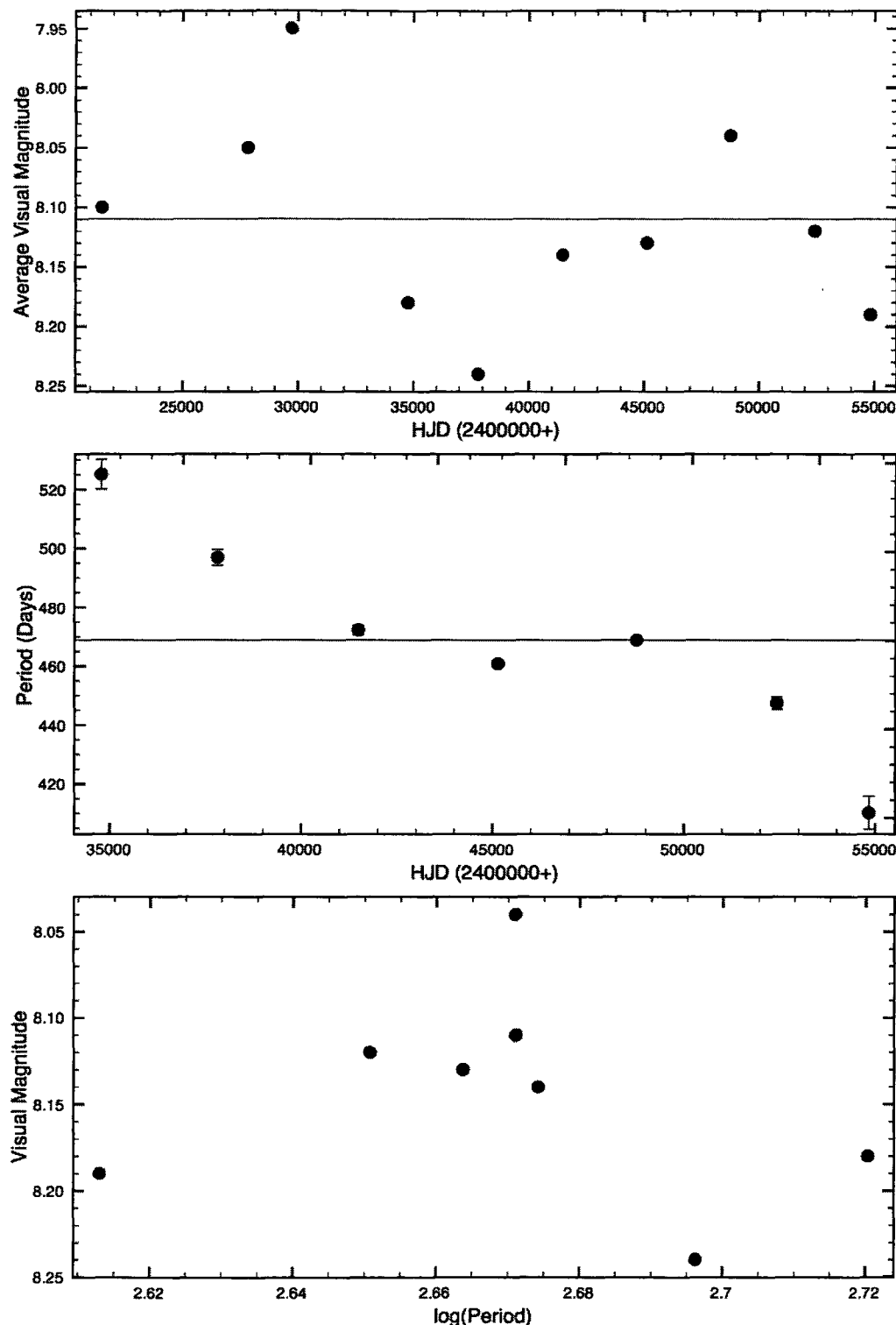


Figure 4.58: Period and average magnitude changes in SU Persei from AAVSO observations.

#### 4.39 XX Persei

Figure 4.59 shows XX Per's variations in spectral type and radial velocity and a montage of CCD spectra taken at different epochs. The observations were phased with a period of 403.00 days and a time of maximum light of JD2446063.19, determined from the AAVSO observations. We used that period rather than the period of 421 days found using the most recent data, as it has a longer baseline and the phasing is about the same with both values. The GCVS lists a period of 415 days and a spectral type of M4 Ib + B. The star appears to reach smallest dimensions near phase 0.17. The star appears to reach highest temperature and greatest luminosity class near light maximum. We also obtained 263 blue light observations of XX Per from the Harvard plate collection. The observations covered the dates JD2415405-33999. We found a period of  $399.68 \pm 3.91$  days for the star from the Harvard observations, a difference of -0.82% from the period found using the AAVSO observations. The star's average *B* magnitude for the photographic observations was 10.24 with a range of 1<sup>m</sup>.6. Figure 4.60 shows XX Per's changes in period and average visual magnitude taken at approximately 10-year intervals. The period is reasonably well-expressed, although there are superposed variations in mean brightness. The phased spectroscopic data are consistent with pulsation, despite a low amplitude of  $\Delta V \simeq 1^m.6$ .

**Table 4.69:** AAVSO Observations of XX Persei

Subset	Dates	$\langle V \rangle$	% Diff.	$\Delta V$	$N$	$P$ (days)	% Diff.
All	23469-55406	8.47	...	2.5	3412	$403.00 \pm 0.15$	...
1	23469-27095	8.15	-3.78	1.2	95	$386.78 \pm 2.39$	-4.03
2	27125-30669	8.36	-1.30	1.0	160	$400.38 \pm 1.75$	-0.65
3	30779-34414	8.37	-1.18	1.4	94	$406.26 \pm 2.19$	0.81
4	34420-38028	8.43	-0.47	1.4	207	$402.92 \pm 1.77$	-0.02
5	38104-41720	8.56	1.06	1.4	283	$393.54 \pm 1.54$	-2.35
6	41738-45358	8.42	-0.59	1.6	288	$395.41 \pm 1.17$	-1.88
7	45375-49016	8.31	-1.89	1.6	726	$356.79 \pm 2.41$	-11.47
8	49028-52668	8.47	0.00	1.6	862	$402.61 \pm 0.83$	-0.10
9	52670-55406	8.71	2.83	2.1	697	$421.85 \pm 0.57$	4.68

**Table 4.70:** Spectroscopic observations of XX Persei

Year	HJD	Phase	$V_R$ (km/s)	Spectral Type	Source
2005	2453654	0.8355	$49.5 \pm 18.1$	M4 Ia	DAO CCD
2007	2454382	0.6445	$22.2 \pm 18.1$	M5 Iab	DAO CCD
2009	2455092	0.4039	$-1.0 \pm 23.2$	M4 Ia	DAO CCD
2010	2455483	0.3739	$14.8 \pm 12.1$	M4 Ia	DAO CCD

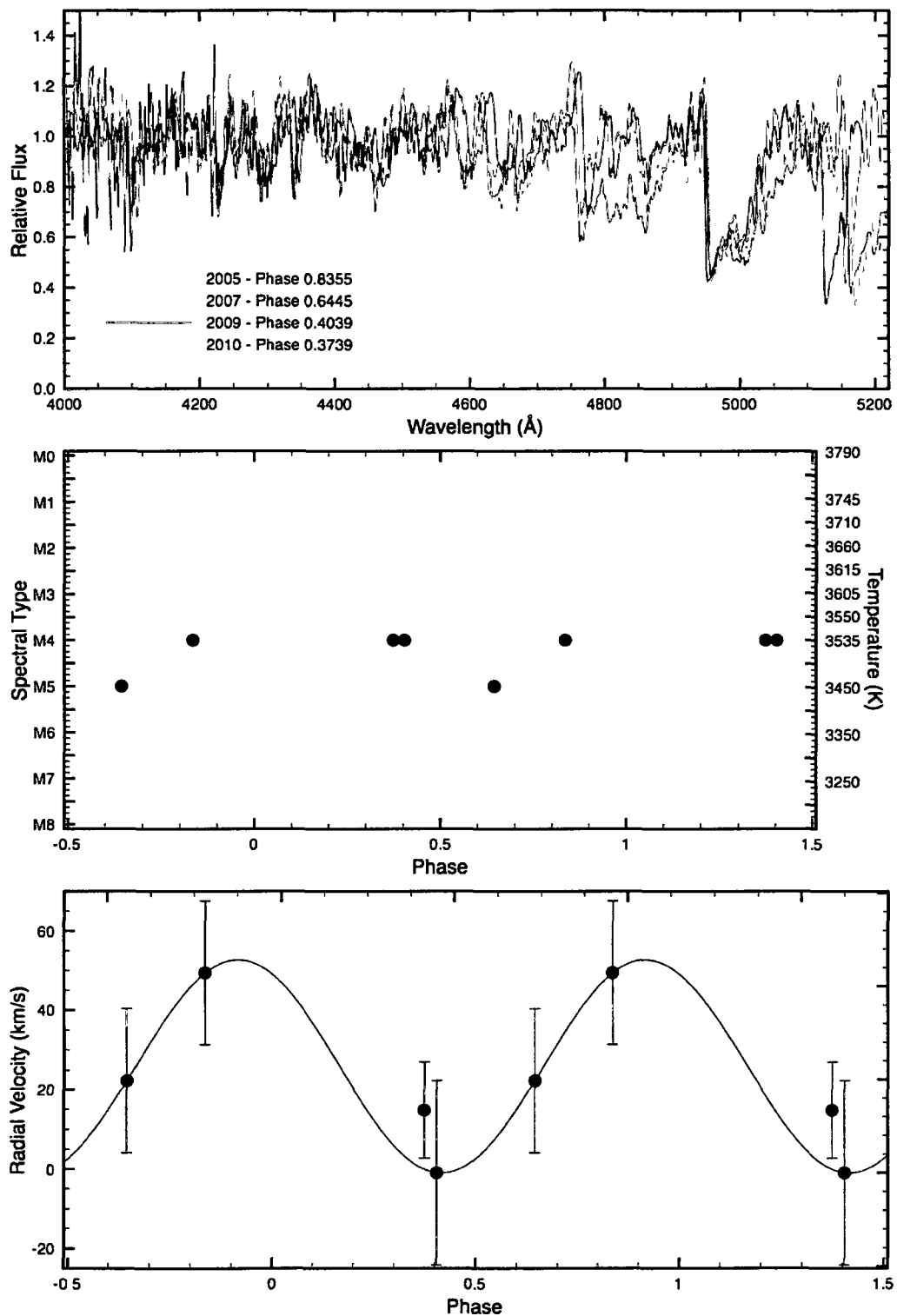


**Figure 4.59:** Spectral variation in XX Persei. Top: Spectra from different epochs. Middle: Spectral type as a function of phase. Bottom: Radial velocity as a function of phase. Data phased with 403.00 day period.

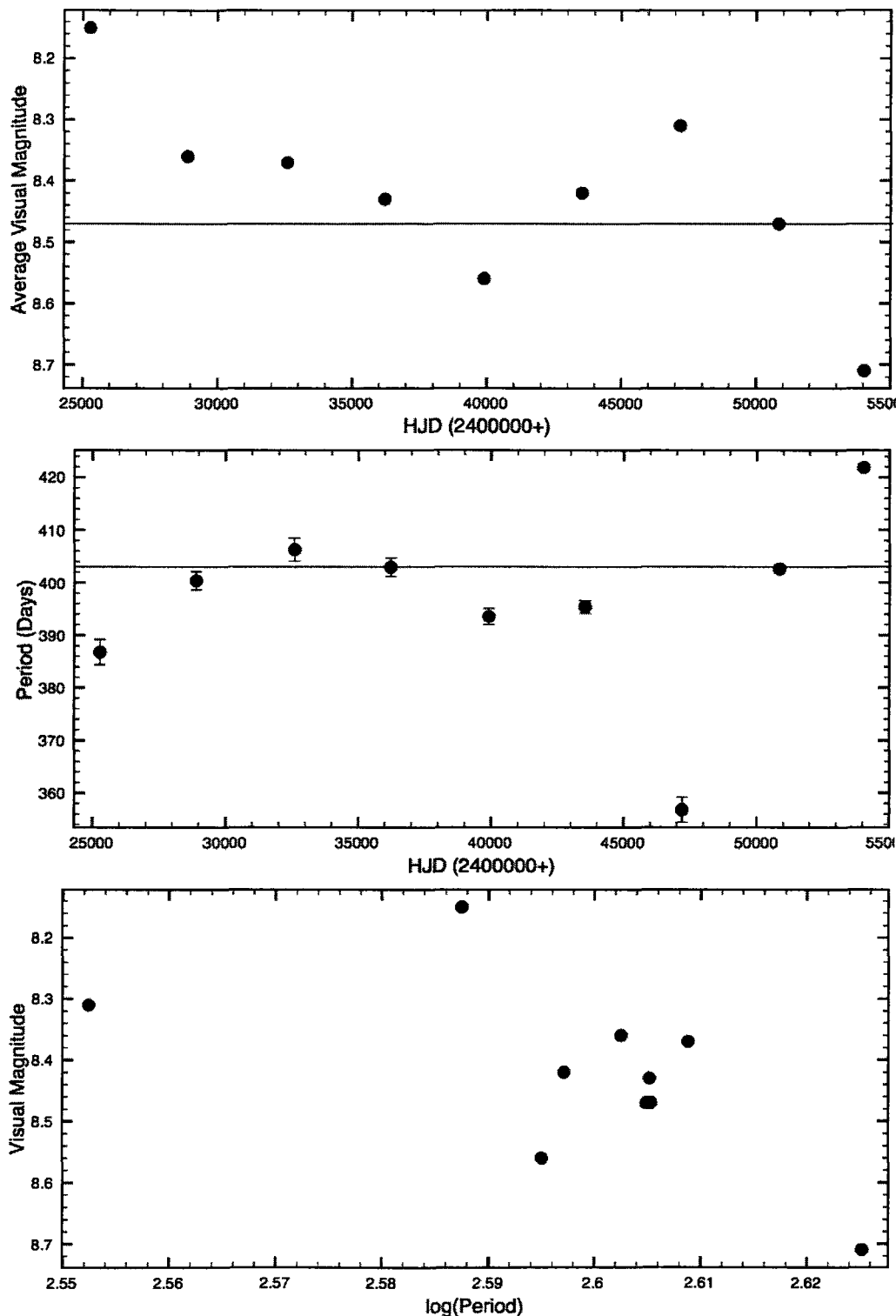


**Figure 4.60:** Period and average magnitude changes in XX Persei from AAVSO observations.

#### 4.40 AD Persei

Figure 4.61 shows AD Per's variations in spectral type and radial velocity, phased with a period of 371.34 days and a time of maximum light of JD2433597.42 from the AAVSO observations, as well as a montage of CCD spectra taken at different epochs. We fitted the radial velocity variations (except for Joy's measurements) with a sine wave and found that the star appears to reach smallest dimensions near phase 0.49, although the data are too close together in phase to state that as a definitive conclusion. Again, as in the cases of RS Per and SU Per, the two data sets do not show much agreement. We do note that, in this case, the two sets of measurements appear to follow the same general trend despite their offset. AD Per appears to reach highest temperature and greatest luminosity class at light maximum. We also obtained 196 observations of AD Per from the Harvard plate collection. The observations in blue light covered the dates JD2415405-2433999. We found a period of  $369.58 \pm 19.30$  days for the star from the Harvard observations, a difference of -0.47% from the period found using the AAVSO observations. The star's average blue magnitude for the observations was 10.56, with a magnitude range of  $1^m.5$ . Figure 4.62 shows AD Per's changes in period and average visual magnitude taken at approximately 10-year intervals. The evidence for repeatable variability for the star is weak, although the phased spectroscopic observations are reasonably consistent with pulsation. Better photometric data would help to confirm the periodicity found here, which is too close to a year to rule out seasonal bias. AD Per is a promising case that needs more data. Irregular brightness variations may indicate possible dust extinction episodes.

**Table 4.71:** AAVSO Observations of AD Persei

Subset	Dates	$\langle V \rangle$	% Diff.	$\Delta V$	$N$	$P$ (days)	% Diff.
All	28182-55423	8.30	...	2.3	3338	$371.24 \pm 0.08$	...
1	28182-29545	8.38	0.96	0.8	12	$353.38 \pm 9.74$	-4.81
2	33491-35480	8.36	0.72	1.5	188	$414.15 \pm 4.53$	11.56
3	35490-39131	8.51	2.53	1.2	215	$372.98 \pm 1.66$	0.47
4	39134-42769	8.42	1.45	2.2	302	$350.36 \pm 7.20$	-5.62
5	42783-46418	8.15	-1.81	2.0	480	$407.07 \pm 1.90$	9.65
6	46433-50081	8.23	-0.84	2.0	933	$370.91 \pm 0.68$	-0.87
7	50089-53775	8.34	0.48	1.8	824	$365.41 \pm 1.11$	-1.57
8	53785-55423	8.37	0.84	1.9	384	$381.80 \pm 3.31$	2.85

**Table 4.72:** Spectroscopic observations of AD Persei

Year	HJD	Phase	$V_R$ (km/s)	Spectral Type	Source
1938	2423358	0.4005	-34	M2	Joy
1938	2423475	0.7158	-45	M3	Joy
1939	2426373	0.5272	-51	M3	Joy
2005	2453648	0.0447	$27.7 \pm 20.2$	M2 Ia	DAO CCD
2007	2454384	0.0286	$15.4 \pm 16.8$	M3 Iab	DAO CCD
2008	2454755	0.0281	$15.4 \pm 20.3$	M3 Iab	DAO CCD
2009	2455091	0.9368	$-4.4 \pm 23.4$	M4 Ib	DAO CCD
2010	2455483	0.9906	$2.3 \pm 15.7$	M4 Ib	DAO CCD

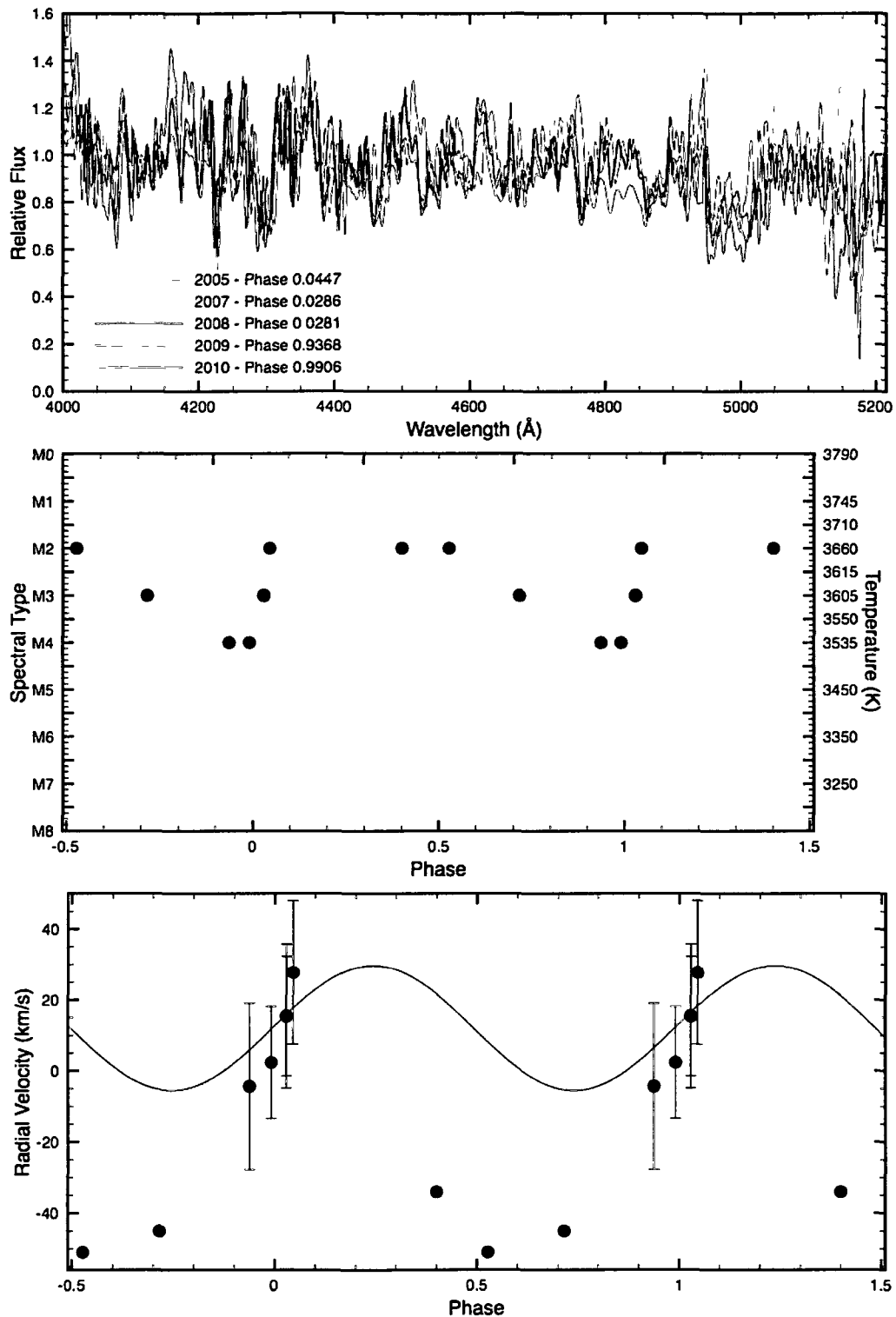


**Figure 4.61:** Spectral variation in AD Persei. Top: Spectra from different epochs. Middle: Spectral type as a function of phase. Bottom: Radial velocity as a function of phase. Data phased with 371.34 day period.

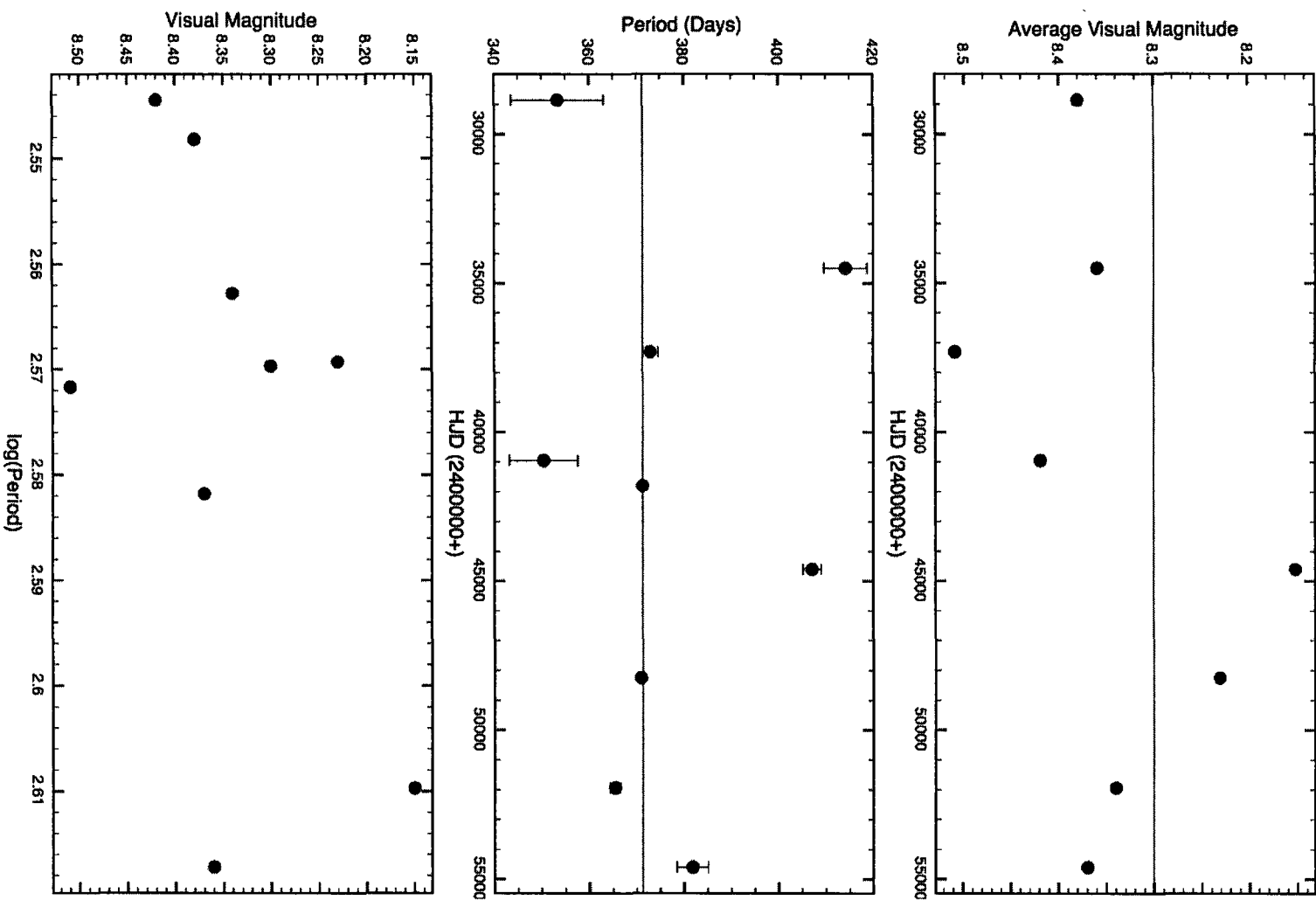


Figure 4.62: Period and average magnitude changes in AD Persei from AAVSO observations.

#### 4.41 BU Persei

Figure 4.63 shows BU Per's variations in spectral type and radial velocity, phased with a period of 363.00 days and a time of maximum light of JD2445741.77 from the AAVSO observations, as well as a montage of CCD spectra taken at different epochs. The GCVS lists a period for the star of 367 days, and a long secondary period of 2960 days. Its spectral type is listed as M3.5 Ib. The observations were all obtained at similar phases because of seasonal restrictions, so we cannot comment on when the star reaches maximum temperature. The luminosity class did not appear to vary over the course of our observations. We also obtained 194 photographic (blue) observations of BU Per from the Harvard plate collection. The observations covered the dates JD2415405-2433999. We found a period of  $353.73 \pm 44.63$  days for the star from the Harvard observations, a difference of -2.55% from the period found using the AAVSO observations. The star's average photographic magnitude for the observations was 11.62 with a range of 1<sup>m</sup>.2. Figure 4.64 shows BU Per's changes in period and average visual magnitude taken at approximately 10-year intervals. The periodicity in the star is poorly expressed and is compounded by irregular changes in mean brightness. Is the period of variability actually a year, or is that a seasonal bias? Because the spectroscopic observations were made yearly around the same time, there is no phase spread to test the pulsation hypothesis. A more concerted observational program is needed to clarify the nature of the star's variability and to confirm the pulsation hypothesis.

**Table 4.73:** AAVSO Observations of BU Persei

Subset	Dates	$\langle V \rangle$	% Diff.	$\Delta V$	$N$	$P$ (days)	% Diff.
All	33572-55394	9.40	...	3.3	1468	$363.00 \pm 10.32$	...
1	33572-40688	9.46	0.64	2.3	58	$353.59 \pm 24.11$	-2.86
2	41658-44515	9.73	3.51	2.8	80	$322.21 \pm 2.74$	-11.48
3	44522-48169	9.46	0.64	2.2	367	$355.16 \pm 1.17$	-2.43
4	48175-51815	9.32	-0.85	3.1	482	$321.16 \pm 0.73$	-11.77
5	51822-55394	9.42	0.21	2.2	481	$364.67 \pm 1.09$	-.19

**Table 4.74:** Spectroscopic observations of BU Persei

Year	HJD	Phase	$V_R$ (km/s)	Spectral Type	Source
1969	2440562	0.7293	...	M3.7 Ib	Wing
1970	2440903	0.6687	...	M4.0 Ib	Wing
1970	2440951	0.8009	...	M3.9 Ib	Wing
1973	2442015	0.7320	...	M3.2 Ib	Wing
2006	2454027	0.8240	$29.1 \pm 8.1$	M4 Ib	DAO CCD
2008	2454755	0.8290	$14.7 \pm 19.3$	M4 Ib	DAO CCD
2010	2455483	0.8350	$32.5 \pm 14.9$	M4 Ib	DAO CCD

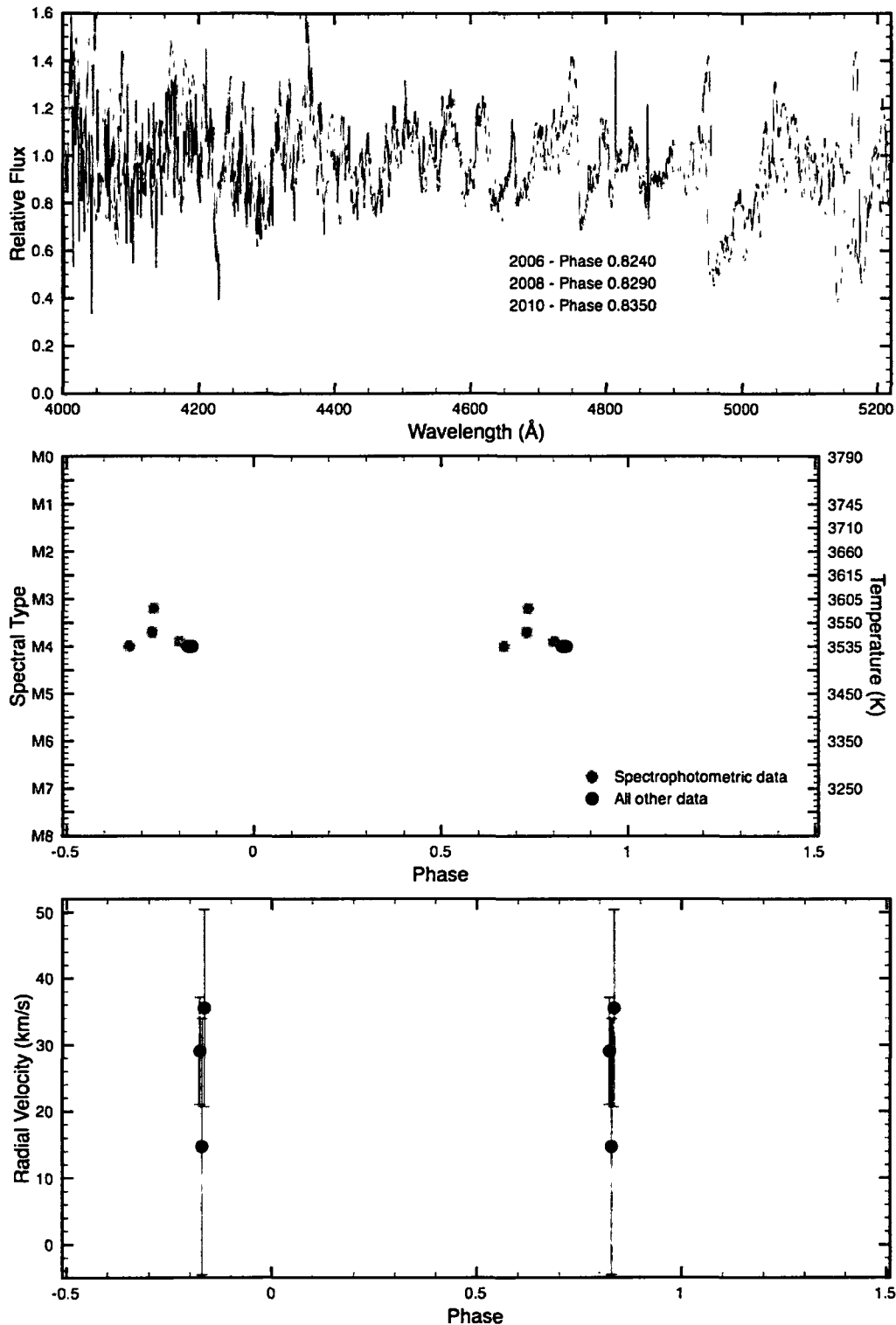


**Figure 4.63:** Spectral variation in BU Persei. Top: Spectra from different epochs. Middle: Spectral type as a function of phase. Bottom: Radial velocity as a function of phase. Data phased with 363.00 day period.

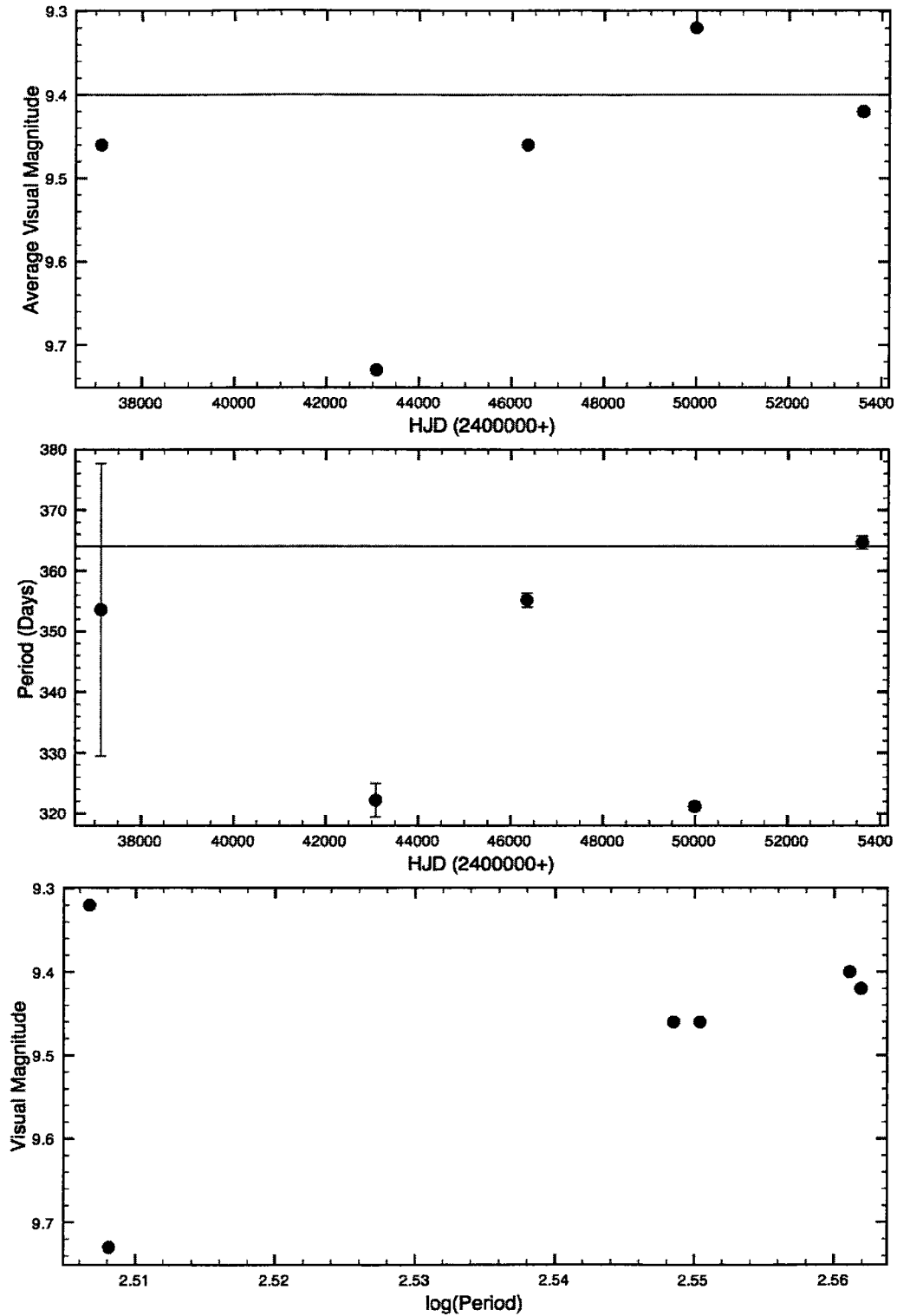


Figure 4.64: Period and average magnitude changes in BU Persei from AAVSO observations.

#### 4.42 FZ Persei

Figure 4.65 shows FZ Per's variations in spectral type and radial velocity, phased with a period of 371.00 days and a time of maximum light of JD2443173.28 from the AAVSO observations, along with a montage of CCD spectra taken at different epochs. The GCVS lists a period for the star of 184 days and a spectral type of M0.5-2.0 Iab. Using either period gives approximately the same results in the plots of spectral type and  $V_R$ . The radial velocity variations indicate that the star reaches minimum dimensions near phase 0.89, although the period and phasing are poorly established, so that is not a conclusive result. The temperature is varying, but it is not clear at what phase it reaches maximum. We also obtained 196 blue light observations of FZ Per from the Harvard plate collection. The observations covered the dates JD2415405-2433999. We found a period of  $371.91 \pm 9.57$  days for the star from the Harvard observations, a difference of 0.25% from the period found using the AAVSO observations, with a large uncertainty. The star's average photographic magnitude during the observations was 10.33, with a magnitude range of 1<sup>m</sup>.5. Figure 4.66 shows FZ Per's changes in period and average visual magnitude taken at approximately 10-year intervals. The period and average magnitude undergo changes, but we cannot establish an unambiguous period. The variability is poorly expressed by the observations, but a period near 1/2 year seems to be indicated, as given in the GCVS. The mean brightness of the star varies by only a small amount.

**Table 4.75:** AAVSO Observations of FZ Persei

Subset	Dates	$\langle V \rangle$	% Diff.	$\Delta V$	$N$	$P$ (days)	% Diff.
All	33898-55423	8.33	...	2.3	2023	$371.00 \pm 0.11$	...
1	33898-37526	8.49	1.92	1.4	1773	$360.42 \pm 0.30$	-2.85
2	37631-41186	8.30	-0.36	0.9	32	$352.21 \pm 3.01$	-5.06
3	41214-44819	8.34	0.12	1.3	127	$378.10 \pm 2.31$	1.91
4	44853-48495	8.16	-2.04	1.7	465	$369.20 \pm 1.03$	-0.49
5	48500-52140	8.31	-0.24	1.8	699	$367.10 \pm 0.81$	-1.05
6	52151-55423	8.44	1.32	2.1	527	$368.13 \pm 1.51$	-0.77

**Table 4.76:** Spectroscopic observations of FZ Persei

Year	HJD	Phase	$V_R$ (km/s)	Spectral Type	Source
2005	2453648	0.2338	$45.8 \pm 17.8$	M0 Ia+	DAO CCD
2007	2454382	0.2122	$26.4 \pm 15.3$	M0 Ia+	DAO CCD
2008	2454755	0.2172	$-1.2 \pm 20.0$	M1 Ia	DAO CCD
2009	2455092	0.1259	$-6.0 \pm 23.2$	M1 Ia	DAO CCD
2010	2455483	0.1796	$45.6 \pm 18.0$	M1 Ia	DAO CCD

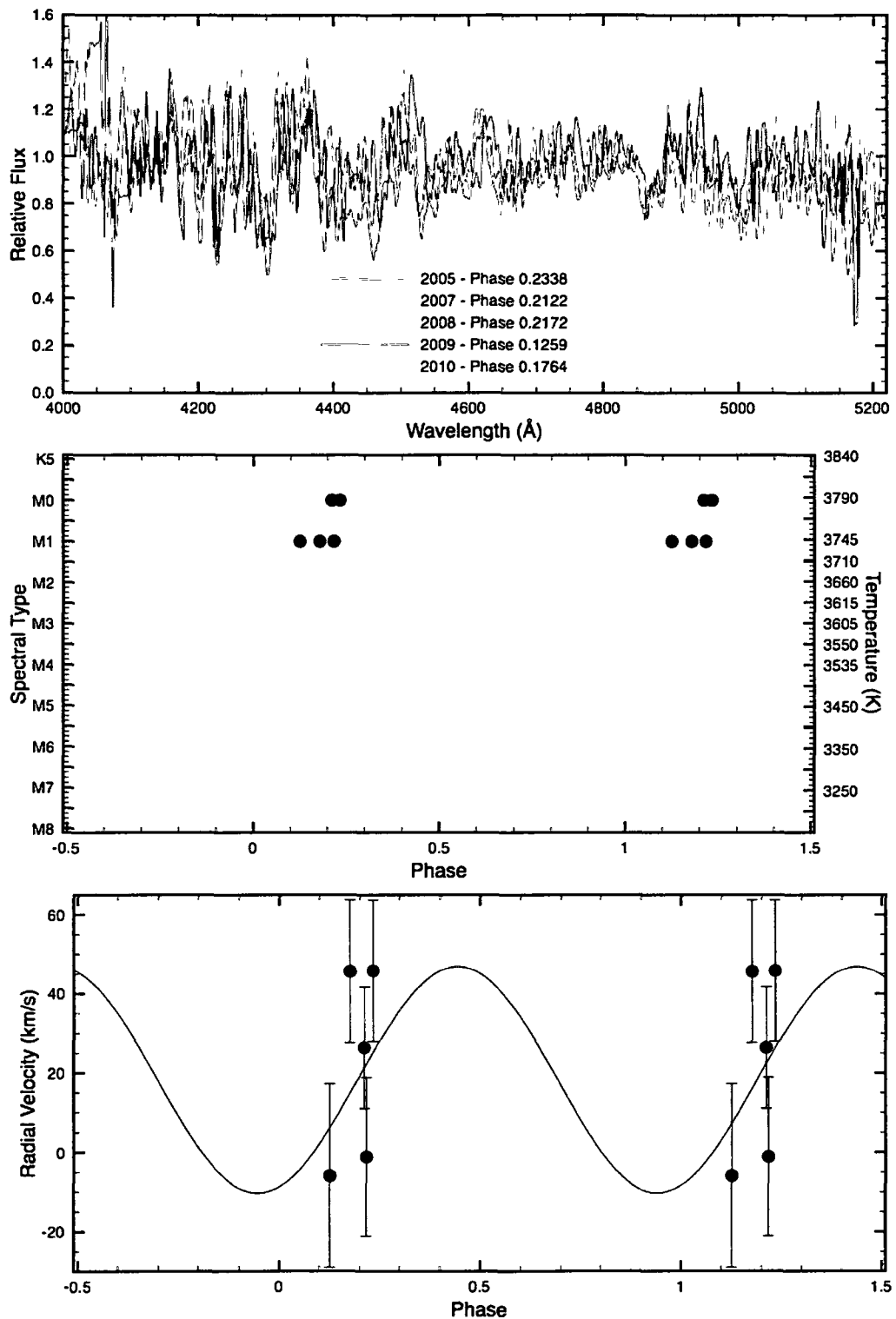


**Figure 4.65:** Spectral variation in FZ Persei. Top: Spectra from different epochs. Middle: Spectral type as a function of phase. Bottom: Radial velocity as a function of phase. Data phased with 371.00 day period.

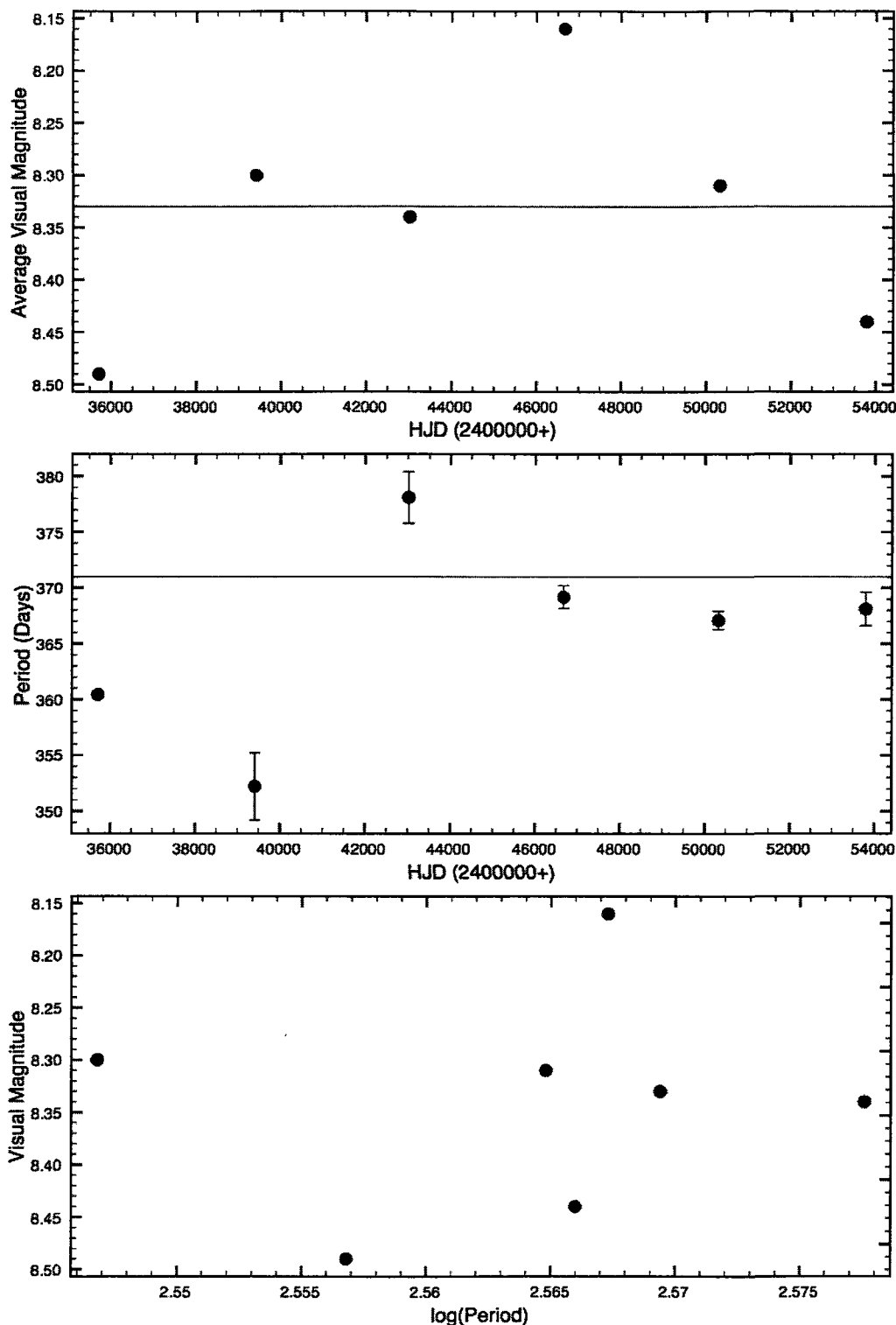


Figure 4.66: Period and average magnitude changes in FZ Persei from AAVSO observations.

#### 4.43 V411 Persei

Figure 4.67 shows V411 Per's variations in spectral type and radial velocity and a montage of CCD spectra taken at different epochs. The observations were phased using a period of 394.55 days and a time of maximum light of JD2453520.19, determined from the few AAVSO observations. The GCVS lists a period of 467 days and a spectral type of M3.4 Ia. The radial velocity variations appear to indicate that the star reaches minimum dimensions near phase 0.72. The star appears to reach highest temperature near light maximum. We do note, however, that these results are not conclusive because of the lack of photometry and firm phasing. Its luminosity class did not appear to vary over the course of the observations we obtained. We also obtained 160 blue light observations of V411 Per from the Harvard plate collection. The observations covered the dates JD2415405-2433999. We found a period of  $391.99 \pm 1.03$  days for the star from the Harvard observations, a difference of -0.65% from the period found using the AAVSO observations. The star's average photographic magnitude during the observations was 12.68, with a range of 2<sup>m</sup>.0. There are insufficient photometric observations available for this star to obtain a reliable period or to study its light variations. Although the spectroscopic results are consistent with pulsation for  $P = 395$  days, the results need confirmation. The star also exhibits changes in mean brightness, consistent with dust ejection episodes.

**Table 4.77:** AAVSO Observations of V411 Persei

Subset	Dates	$\langle V \rangle$	% Diff.	$\Delta V$	$N$	$P$ (days)	% Diff.
All	52623-54906	9.62	...	1.1	29	$394.55 \pm 6.05$	...

**Table 4.78:** Spectroscopic observations of V411 Persei

Year	HJD	Phase	$V_R$ (km/s)	Spectral Type	Source
2005	2453648	0.3237	$27.9 \pm 17.4$	M2 Iab	DAO CCD
2007	2454382	0.1818	$14.3 \pm 14.8$	M2 Iab	DAO CCD
2008	2454755	0.1258	$4.4 \pm 19.6$	M1 Iab	DAO CCD
2010	2455484	0.9714	$4.4 \pm 16.3$	M2 Iab	DAO CCD

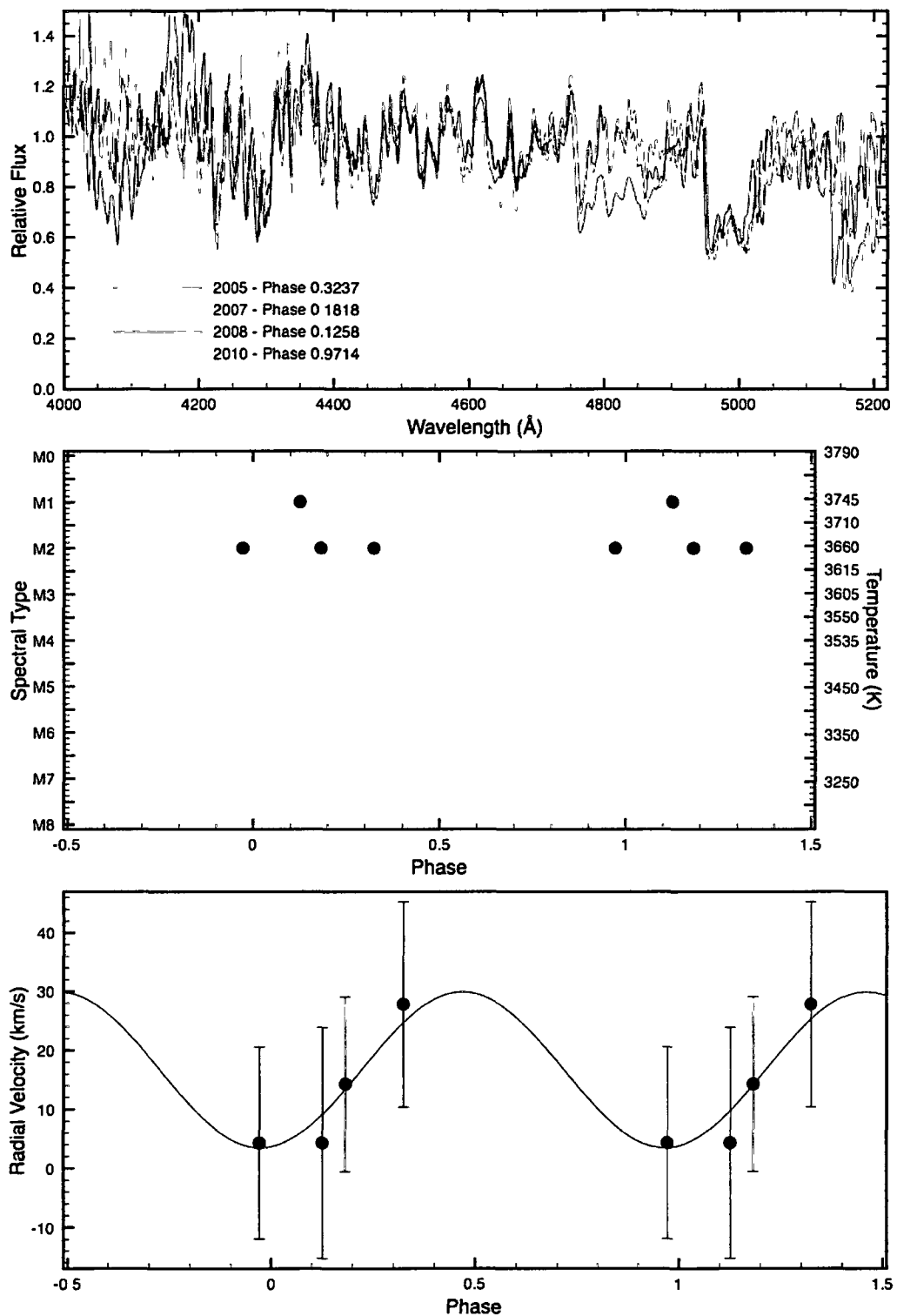


**Figure 4.67:** Spectral variation in V411 Persei. Top: Spectra from different epochs. Middle: Spectral type as a function of phase. Bottom: Radial velocity as a function of phase. Data phased with 394.55 day period.

#### 4.44 VX Sagittarii

The GCVS lists a period of 732 days for VX Sgr and an incredible spectral type range of M4-10 Iae. Our Fourier analysis found a similar period of 756.65 days. Figure 4.68 shows VX Sgr's changes in period and average visual magnitude taken at approximately 10-year intervals. The average brightness has decreased, and the period is undergoing changes. The variability is well-established, despite changes in mean brightness that likely reflect dust ejection events. Unfortunately, there are few spectroscopic observations available and none that we found with associated observation dates to study the pulsation. Spectroscopic data are essential to study the pulsation in this fascinating star, but would need to be obtained from a site further south than the DAO. The star's periodicity is obvious in the light curve, as is the extremely large amplitude of at least  $5^m - 6^m$ .

**Table 4.79:** AAVSO Observations of VX Sagittarii

Subset	Dates	$\langle V \rangle$	% Diff.	$\Delta V$	$N$	$P$ (days)	% Diff.
All	27949-55416	9.77	...	7.6	6970	$756.65 \pm 0.16$	...
1	27549-31591	9.55	-2.25	5.0	834	$777.58 \pm 2.59$	2.77
2	31603-35248	9.25	-5.32	6.2	1137	$823.65 \pm 3.29$	8.86
3	35251-38899	9.11	-6.76	4.5	1270	$751.08 \pm 5.39$	-0.74
4	38901-42544	9.56	-2.15	7.2	753	$754.49 \pm 2.45$	-0.29
5	42568-46194	10.03	2.66	5.7	730	$797.25 \pm 3.54$	5.36
6	46201-49848	10.26	5.02	5.2	1103	$745.27 \pm 2.57$	-1.51
7	49861-53479	10.24	4.81	4.9	871	$769.79 \pm 2.12$	1.74
8	53522-55416	10.18	4.20	4.0	272	$769.30 \pm 18.08$	1.67

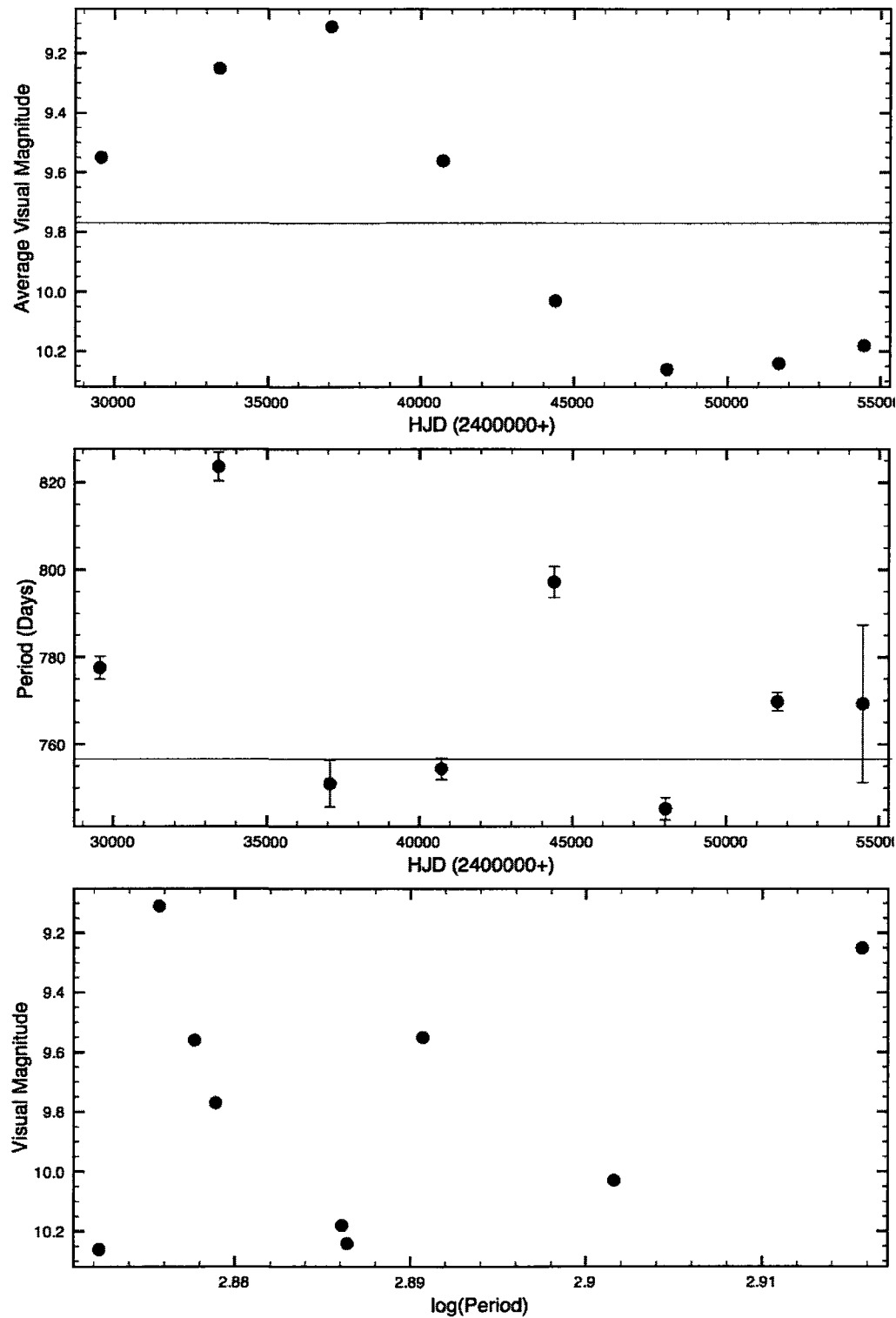


**Figure 4.68:** Period and average magnitude changes in VX Sagittarii from AAVSO observations.

#### 4.45 KW Sagittarii

Figure 4.69 shows KW Sgr's variations in spectral type. We found a period of 352.47 days and a time of maximum light of JD2449437.57 from the AAVSO observations. The GCVS lists a period of 670 days, and we used the longer period to phase the spectral type plot as it gave a better result. The star appears to reach highest temperature near light maximum. Its luminosity class did not change over the course of the observations. Figure 4.70 shows KW Sgr's changes in period and average visual magnitude taken at approximately 10-year intervals. The slight variations are poorly expressed, although a period of 670 days is evident in Swope's early photographic estimates (Swope 1940). The AAVSO observations are less useful. Radial velocity measurements are also needed.

**Table 4.80:** AAVSO Observations of KW Sagittarii

Subset	Dates	$\langle V \rangle$	% Diff.	$\Delta V$	N	P (days)	% Diff.
All	47088-55304	9.67	...	2.5	529	$352.47 \pm 0.50$	...
1	47088-50733	9.46	-2.17	1.6	249	$334.67 \pm 1.30$	-5.05
2	50739-55304	9.86	1.96	2.1	280	$341.33 \pm 1.44$	-3.16

**Table 4.81:** Spectroscopic observations of KW Sagitarii

Year	HJD	Phase	$V_R$ (km/s)	Spectral Type	Source
1970	2440766	0.0566	...	M1.6 Ia	Wing
1970	2440768	0.0596	...	M1.7 Ia	Wing
1970	2440769	0.0611	...	M1.5 Ia	Wing
1970	2440790	0.0924	...	M1.7 Ia	Wing
1971	2441118	0.5820	...	M3.3 Ia	Wing

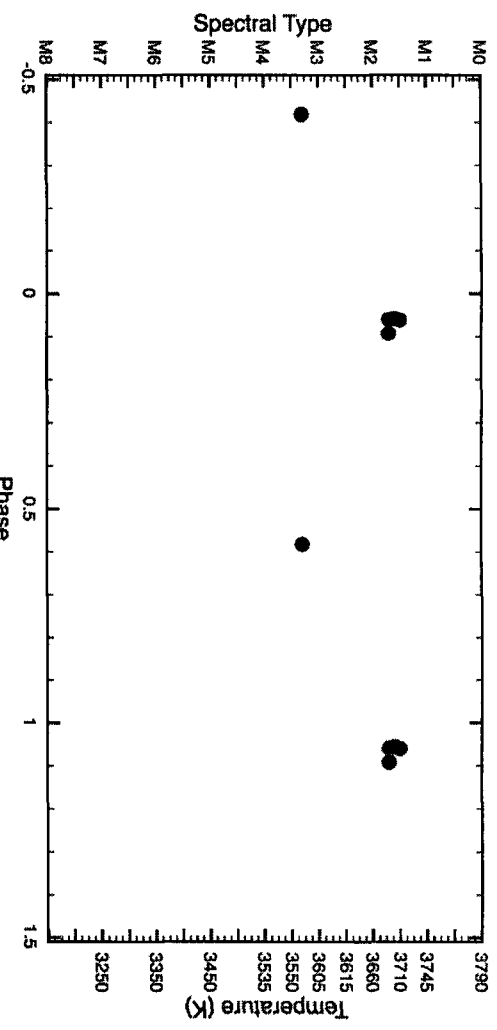
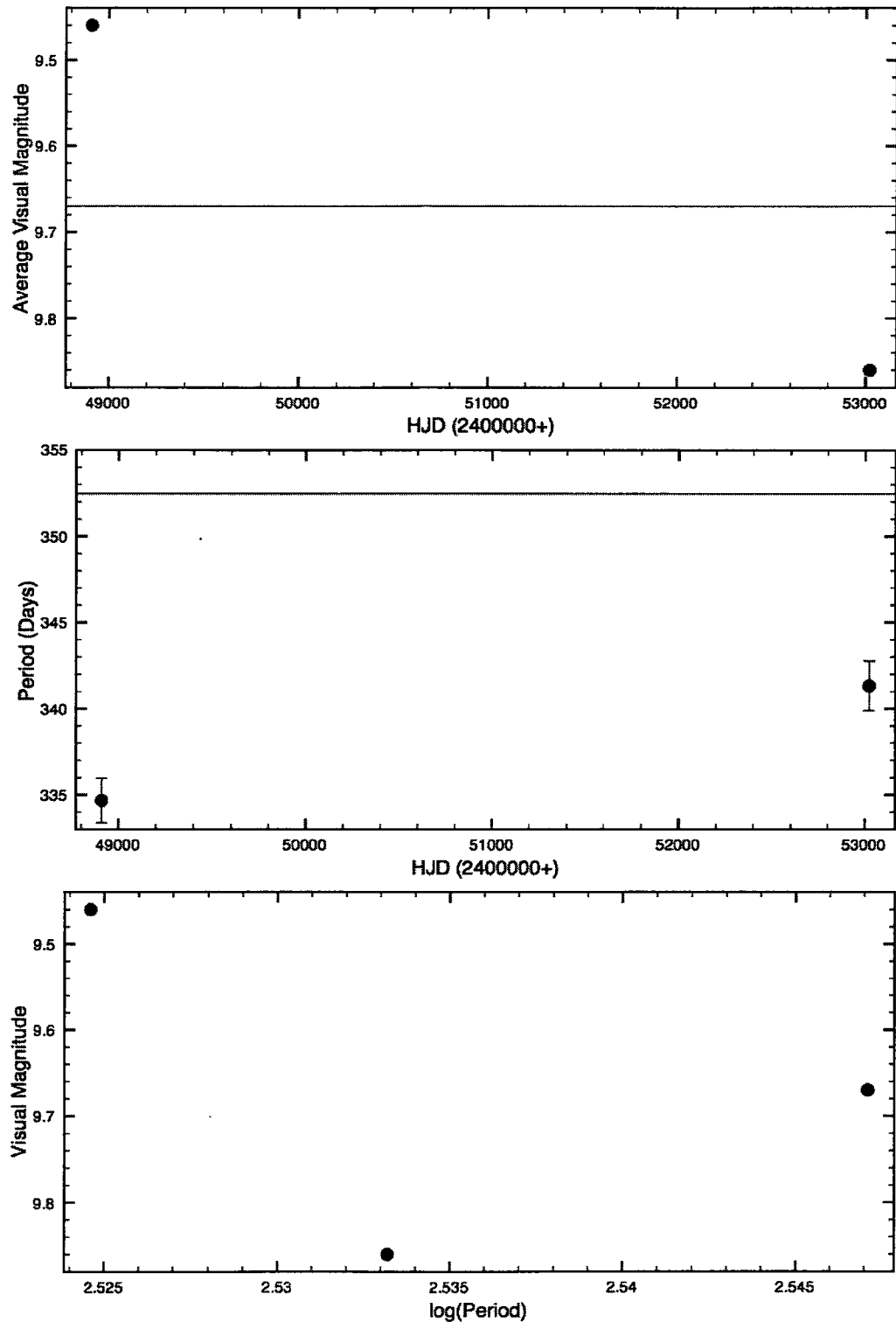


Figure 4.69: Spectroscopic variation in KW Sagittarii. Data phased with 670 day period.



**Figure 4.70:** Period and average magnitude changes in KW Sagittarii from AAVSO observations.

#### 4.46 AH Scorpii

The GCVS lists a spectral type of M4.5 Ia-Iab for AH Sco, and a period of 713.6 days for AH Sco, similar to the 766 day period found from our Fourier analysis, and a spectral type of M4-5 Ia-Iab. Figure 4.71 shows AH Sco's changes in period and average visual magnitude taken at approximately 10-year intervals. The brightness has decreased and the period is undergoing changes. The periodicity is well-established from photometry and the period is well-determined. However, spectroscopic data are needed to study the pulsation in the star.

**Table 4.82:** AAVSO Observations of AH Scorpii

Subset	Dates	$\langle V \rangle$	% Diff.	$\Delta V$	$N$	$P$ (days)	% Diff.
All	38995-55423	7.94	...	4.3	1644	$766.12 \pm 1.16$	...
1	38995-42601	7.79	-1.89	2.2	57	$826.98 \pm 9.96$	7.94
2	42628-46293	7.91	-0.38	3.6	163	$783.80 \pm 8.73$	2.31
3	46296-49943	7.75	-2.39	3.4	926	$873.01 \pm 6.09$	13.95
4	49945-53593	8.31	4.66	3.3	406	$709.74 \pm 3.55$	-7.36
5	53607-55247	8.48	6.80	2.0	90	$706.41 \pm 26.41$	-7.79

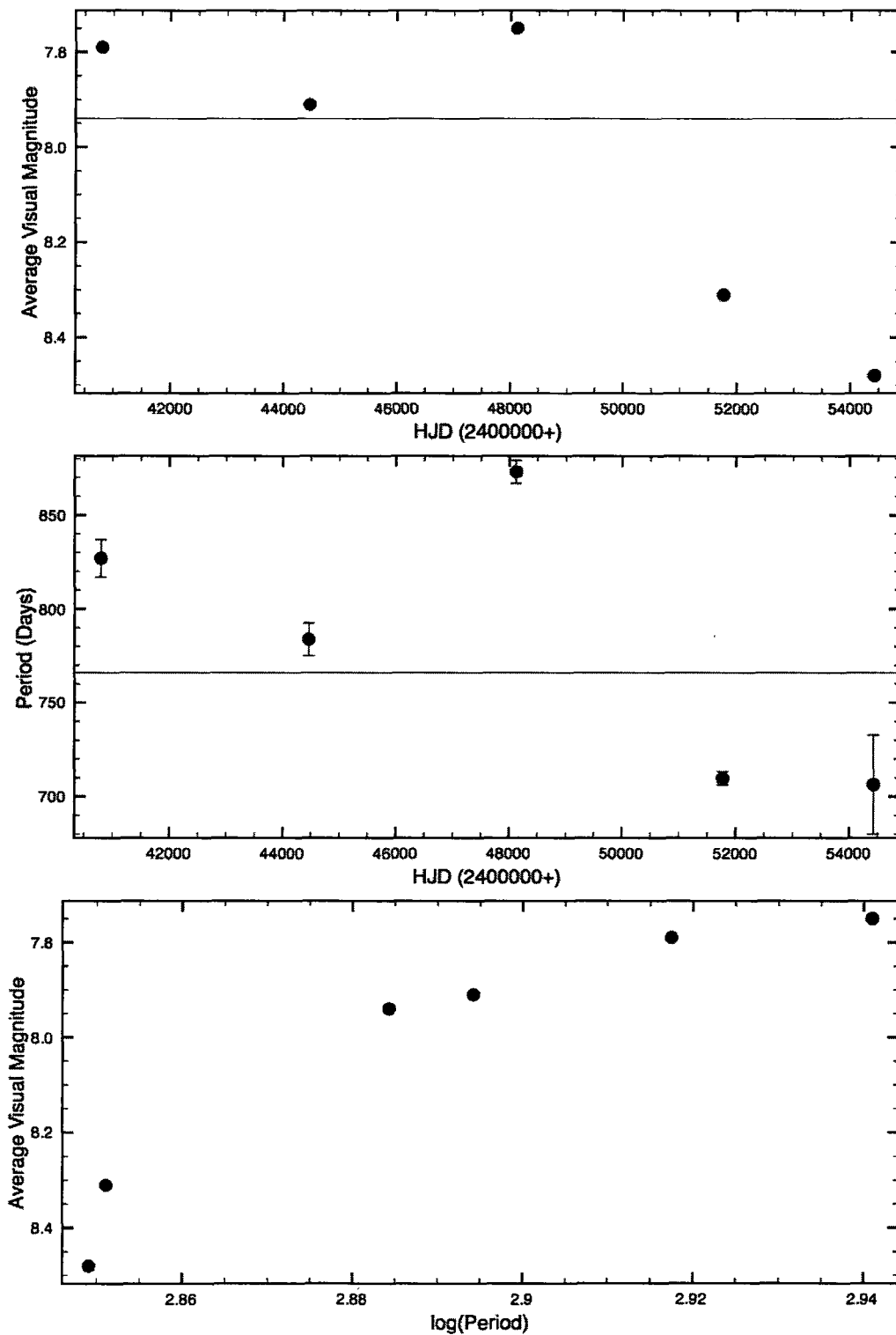


Figure 4.71: Period and average magnitude changes in AH Scorpii from AAVSO observations.

#### 4.47 CE Tauri

Figure 4.72 shows CE Tau's variations in spectral type and radial velocity and a montage of CCD spectra taken at different epochs. The observations were phased using a period of 174.39 days and a time of maximum light of JD2447099.77, determined from the AAVSO observations. The GCVS lists a period of 165 days and a spectral type of M2 Iab-Ib. The radial velocity variations appear to indicate that the star reaches minimum dimensions near phase 0.26. The temperature is varying, but it is not clear at what phase it reaches maximum. It reaches greatest luminosity class at highest temperature. Figure 4.73 shows CE Tau's changes in period and average visual magnitude taken at approximately 10-year intervals. The period of variability appears to be reasonably well-established from previous observations (GCVS) and the AAVSO data, despite a small amplitude:  $\Delta V \simeq 0^m.31$  (GCVS),  $\Delta V \simeq 1^m - 2^m$  (our analysis). Additional photometry is needed to confirm the pulsation period.

**Table 4.83:** AAVSO Observations of CE Tauri

Subset	Dates	$\langle V \rangle$	% Diff.	$\Delta V$	$N$	$P$ (days)	% Diff.
All	35054-55323	4.81	...	4.3	3280	$174.39 \pm 0.14$	...
1	35054-38701	4.94	2.70	1.6	299	$175.45 \pm 0.23$	-0.61
2	38768-42345	4.88	1.46	1.0	227	$173.63 \pm 0.38$	-0.44
3	42354-45995	4.87	1.25	1.9	804	$178.94 \pm 0.24$	2.61
4	46008-49653	4.86	1.04	2.0	627	$178.12 \pm 0.17$	2.14
5	49654-53293	4.67	-2.91	1.9	892	$171.23 \pm 0.23$	-1.81
6	53306-55323	4.84	0.62	1.8	429	$175.17 \pm 0.44$	0.45

**Table 4.84:** Spectroscopic observations of CE Tauri

Year	HJD	Phase	$V_R$ (km/s)	Spectral Type	Source
1951	2433937	0.3508	...	M1.5-2 Iab	DDO
1956	2435576	0.7688	...	M2 Ib	DDO
1957	2435898	0.6202	...	M2 Ib	DDO
1967	2394766	0.8515	...	M2 Ib	DDO
1968	2394924	0.7575	...	M2 Ib	DDO
1968	2394935	0.8208	...	M1.5 Iab	DDO
1970	2440621	0.7628	...	M1.8 Iab	Wing
1970	2440633	0.8318	...	M2.0 Iab	Wing
1970	2440635	0.8433	...	M1.8 Iab	Wing
1970	2440635	0.8433	...	M2.0 Iab	Wing
1970	2440899	0.3605	...	M2.0 Iab	Wing
1970	2440903	0.3835	...	M2.0 Iab	Wing
1970	2440951	0.6594	...	M2.6 Iab	Wing
1971	2441009	0.9927	...	M2.3 Iab	Wing
1971	2441015	0.0272	...	M2.5 Iab	Wing
1972	2441363	0.0329	...	M2.1 Iab	Wing
1973	2442015	0.7743	...	M2.4 Ib	Wing
1975	2442763	0.0743	...	M2 Ib	DDO
2005	2454655	0.6742	$28.3 \pm 19.8$	M1 Iab	DAO CCD
2007	2454382	0.8517	$52.1 \pm 16.5$	M2 Ib	DAO CCD
2010	2455484	0.1851	$50.7 \pm 13.7$	M2 Ib	DAO CCD

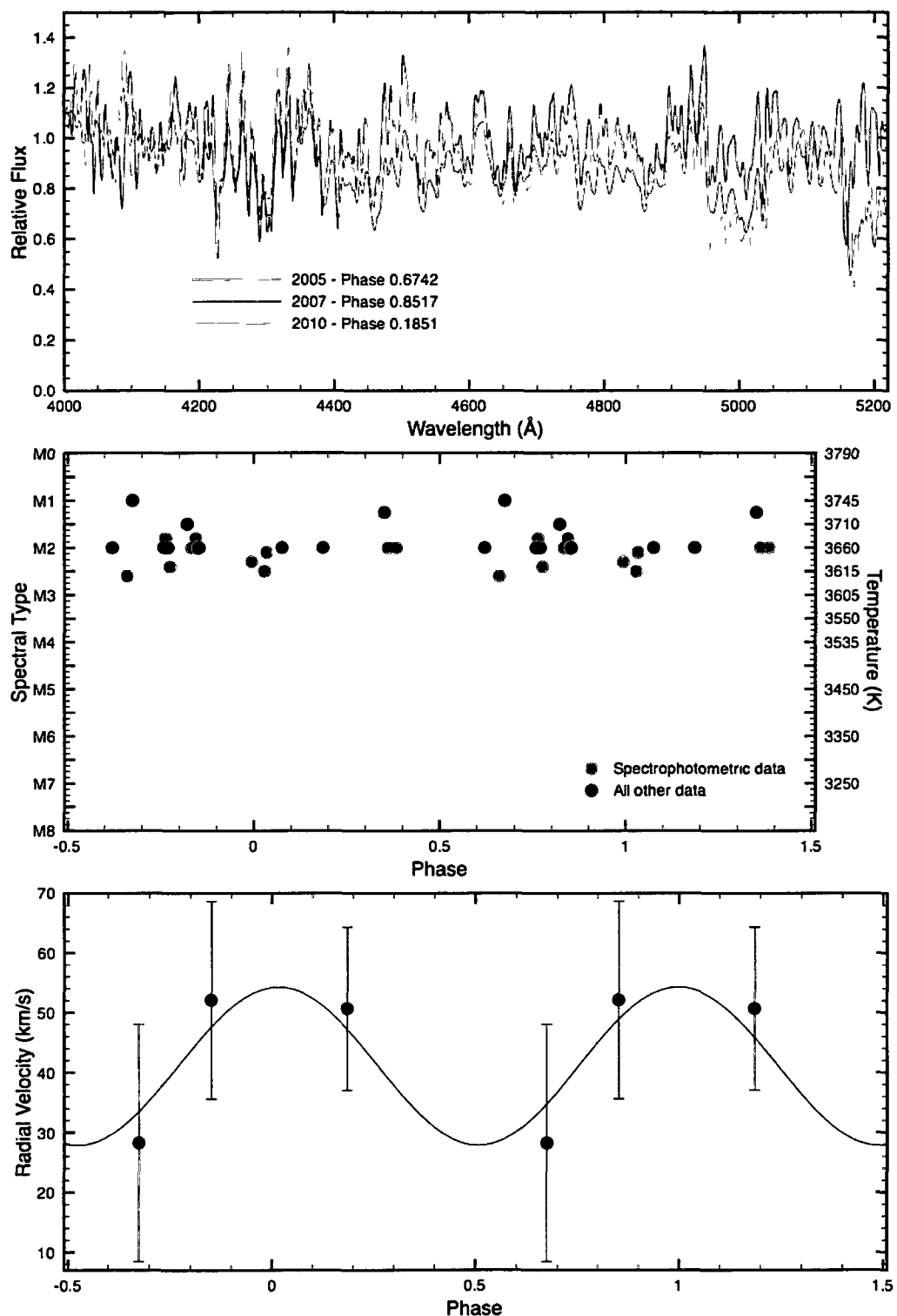


**Figure 4.72:** Spectral variation in CE Tauri. Top: Spectra from different epochs. Middle: Spectral type as a function of phase. Bottom: Radial velocity as a function of phase. Data phased with 174.39 day period.

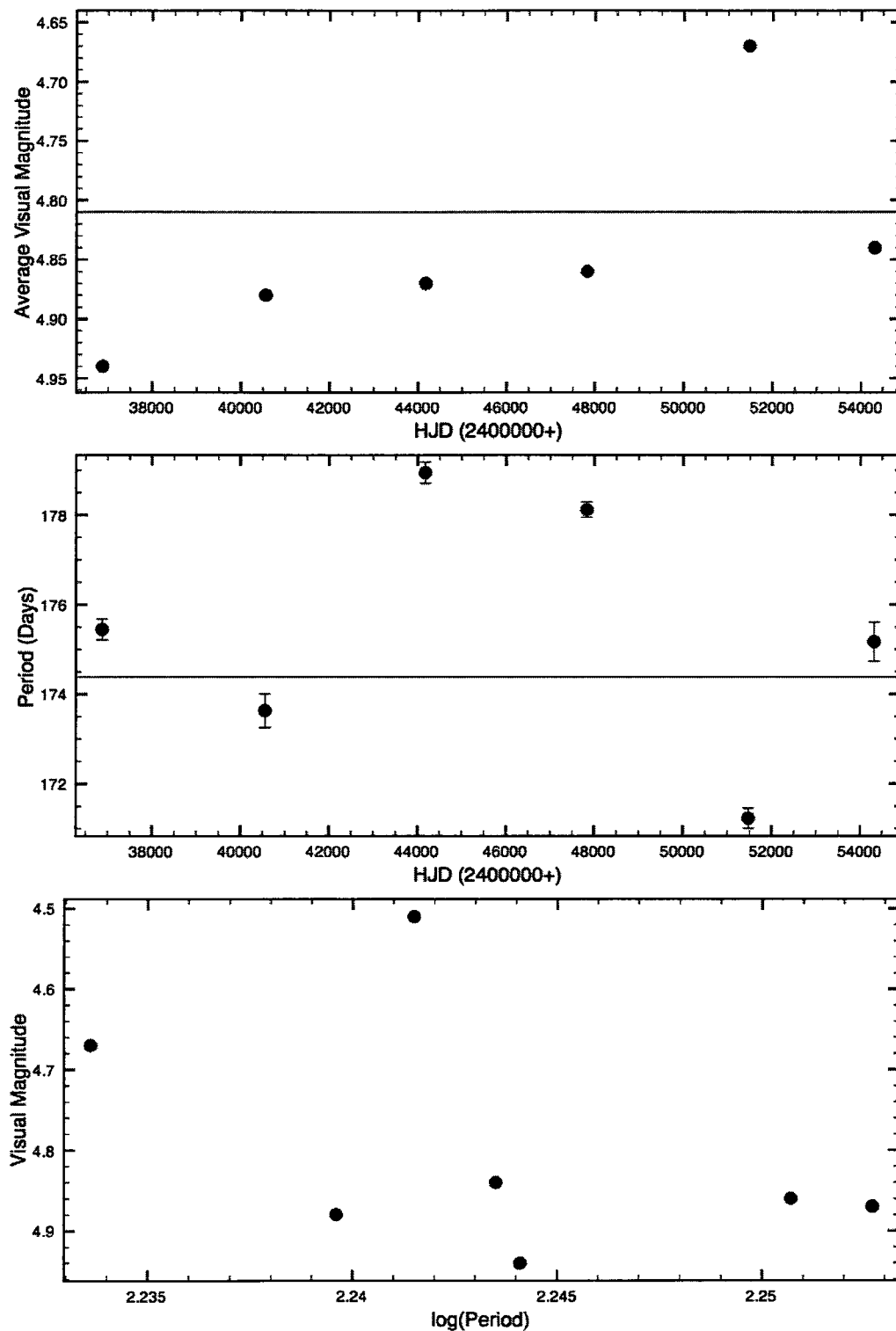


Figure 4.73: Period and average magnitude changes in CE Tauri from AAVSO observations.

#### 4.48 W Trianguli

Figure 4.74 shows W Tri's variations in spectral type and radial velocity and a montage of CCD spectra taken at different epochs. The spectroscopic observations were phased using a period of 592.86 days and a time of maximum light of JD2438933.62, determined from the AAVSO observations. The GCVS lists a period of 108 days and a spectral type of M5 II. The spectral type and luminosity class did not appear to change over the course of our observations. Figure 4.75 shows W Tri's changes in period and average visual magnitude taken at approximately 10-year intervals. The AAVSO data indicate a period closer to 600 days than the value of 108 days cited in the GCVS. The variability is reasonably well-defined and appears to be the result of regular pulsation. However, spectroscopic data are lacking so the nature of the pulsation cannot be studied. Additional spectroscopic observations would be welcomed.

**Table 4.85:** Spectroscopic observations of W Trianguli

Year	HJD	Phase	$V_R$ (km/s)	Spectral Type	Source
1939	2429505	0.1001	12	M5	Joy
1940	2429932	0.9202	2	M5	Joy
1940	2429957	0.8624	6	M5	Joy
2005	2453648	0.8135	$37.9 \pm 20.4$	M5 II	DAO CCD
2010	2455484	0.9094	$8.1 \pm 21.1$	M5 II	DAO CCD

**Table 4.86:** AAVSO Observations of W Trianguli

Subset	Dates	$\langle V \rangle$	% Diff.	$\Delta V$	$N$	$P$ (days)	% Diff.
All	31018-55407	8.20	...	2.7	5719	$592.86 \pm 0.13$	...
1	31018-34665	8.29	1.10	0.9	122	$561.28 \pm 5.19$	-5.33
2	34683-38319	8.29	1.10	2.4	508	$598.61 \pm 1.90$	0.97
3	38321-41962	8.38	2.20	1.9	482	$701.24 \pm 7.33$	18.28
4	41973-45615	8.12	-0.98	2.0	678	$691.30 \pm 2.56$	16.60
5	45624-49268	8.14	-0.73	2.4	1136	$628.01 \pm 2.55$	5.93
6	49269-52918	8.20	0.00	1.9	1662	$593.12 \pm 1.94$	0.04
7	52919-55407	8.21	0.12	1.8	1131	$615.14 \pm 1.55$	3.76

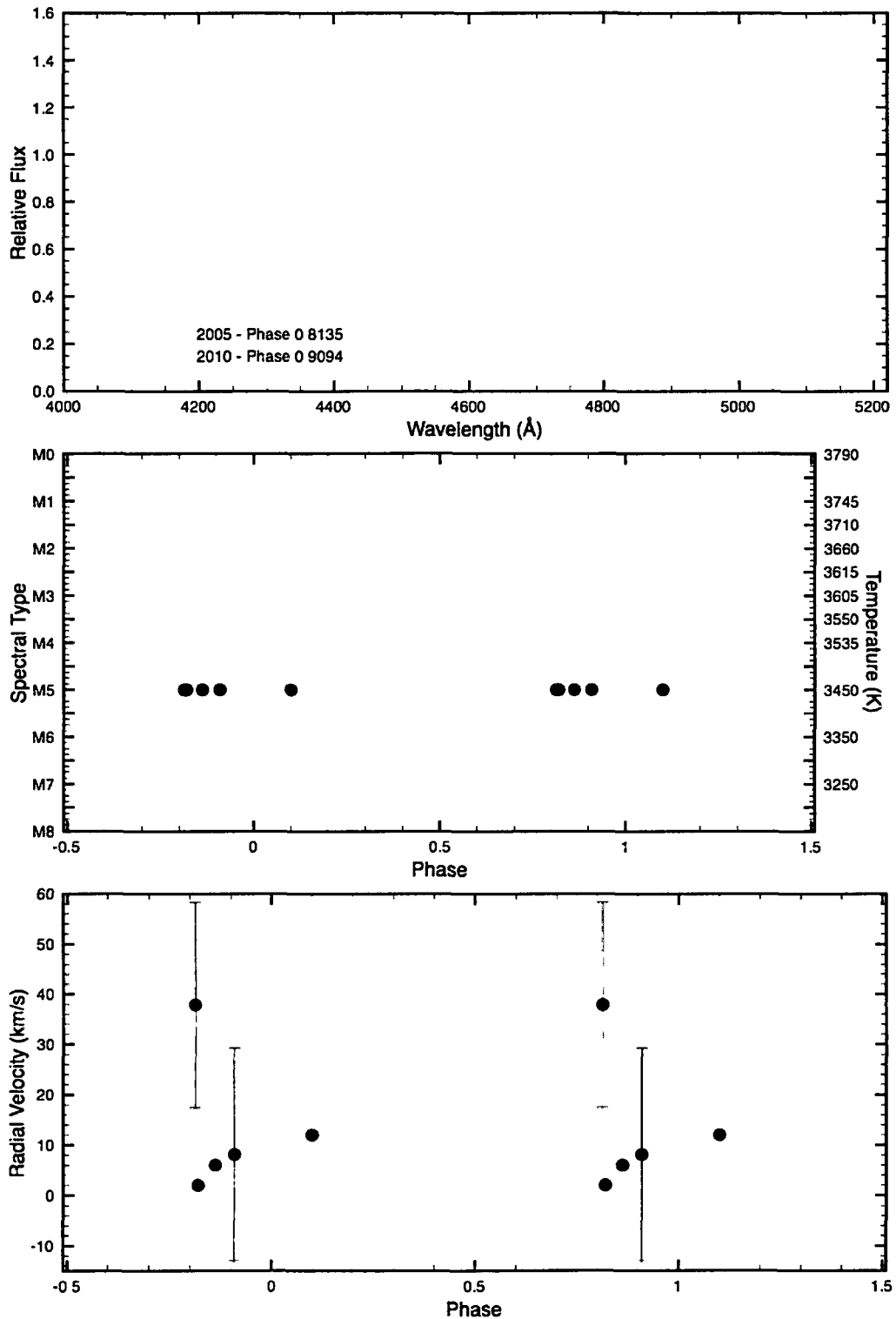


**Figure 4.74:** Spectroscopic variation in W Triangulum. Top: Spectra from different epochs. Middle: Spectral type as a function of phase. Bottom: Radial velocity as a function of phase. Data phased with 592.86 day period.

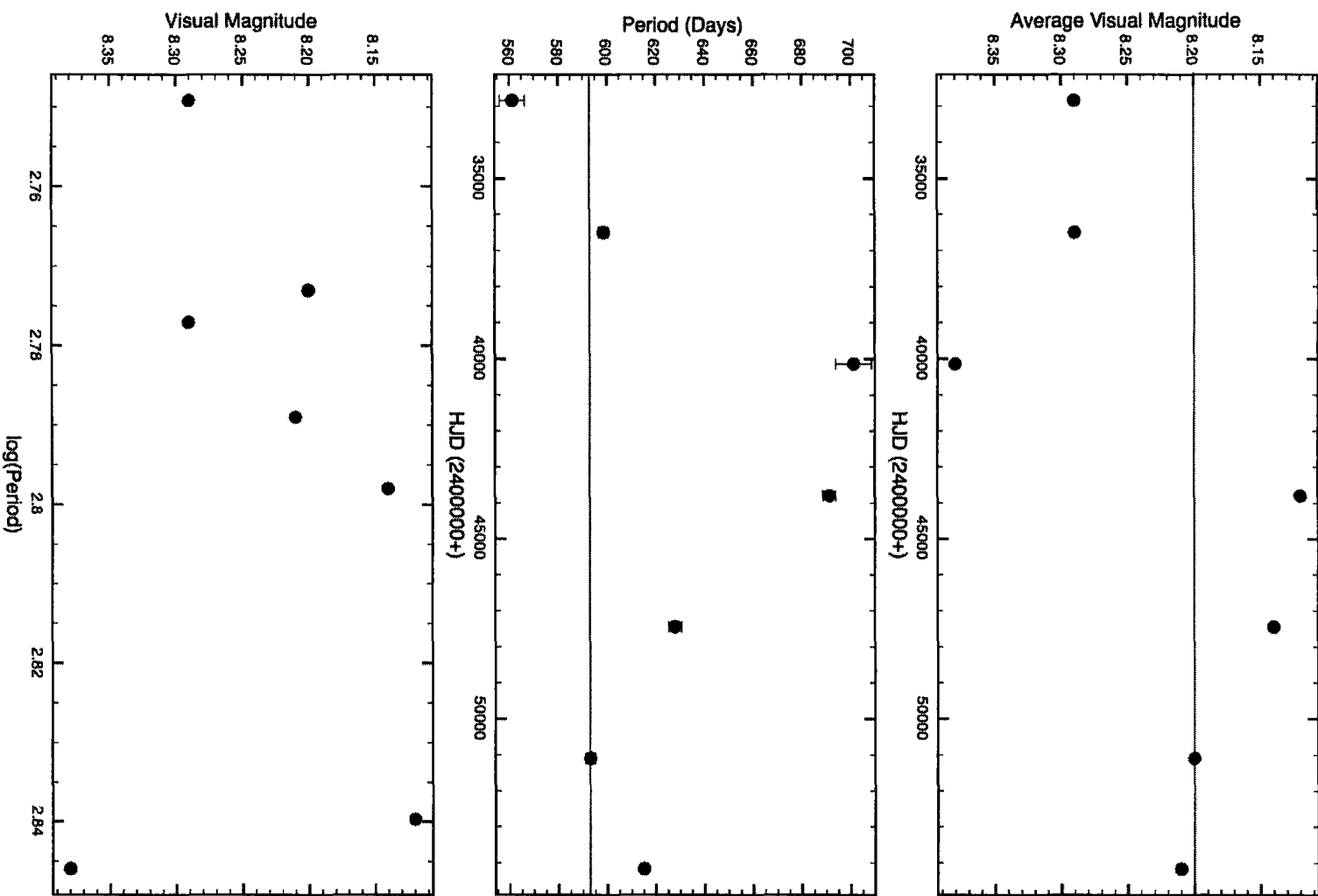


Figure 4.75: Period and average magnitude changes in W Triangulum from AAVSO observations.

#### 4.49 CM Velorum

We determined a period of 762.00 days for CM Vel from the AAVSO observations. The GCVS lists a period of 780 days and a spectral type of M0-5 II. Figure 4.76 shows CM Vel's changes in period and average visual magnitude taken at approximately 10-year intervals. The average brightness has increased and the period is undergoing changes. The variability is reasonably well-established in the AAVSO observations, and presumably can be explained by pulsation. However, spectroscopic observations are lacking for this southern hemisphere star, so the nature of the pulsation cannot be studied with the data at hand.

**Table 4.87:** AAVSO Observations of CM Velorum

Subset	Dates	$\langle V \rangle$	% Diff.	$\Delta V$	$N$	$P$ (days)	% Diff.
All	39164-54613	8.16	...	2.1	238	$762.00 \pm 2.19$	...
1	39164-46240	8.00	-1.96	1.5	55	$761.27 \pm 2.98$	-0.10
2	46440-50068	8.19	0.37	2.0	142	$768.89 \pm 3.37$	0.90
3	50489-54613	8.24	0.98	1.7	41	$696.01 \pm 10.21$	-8.66

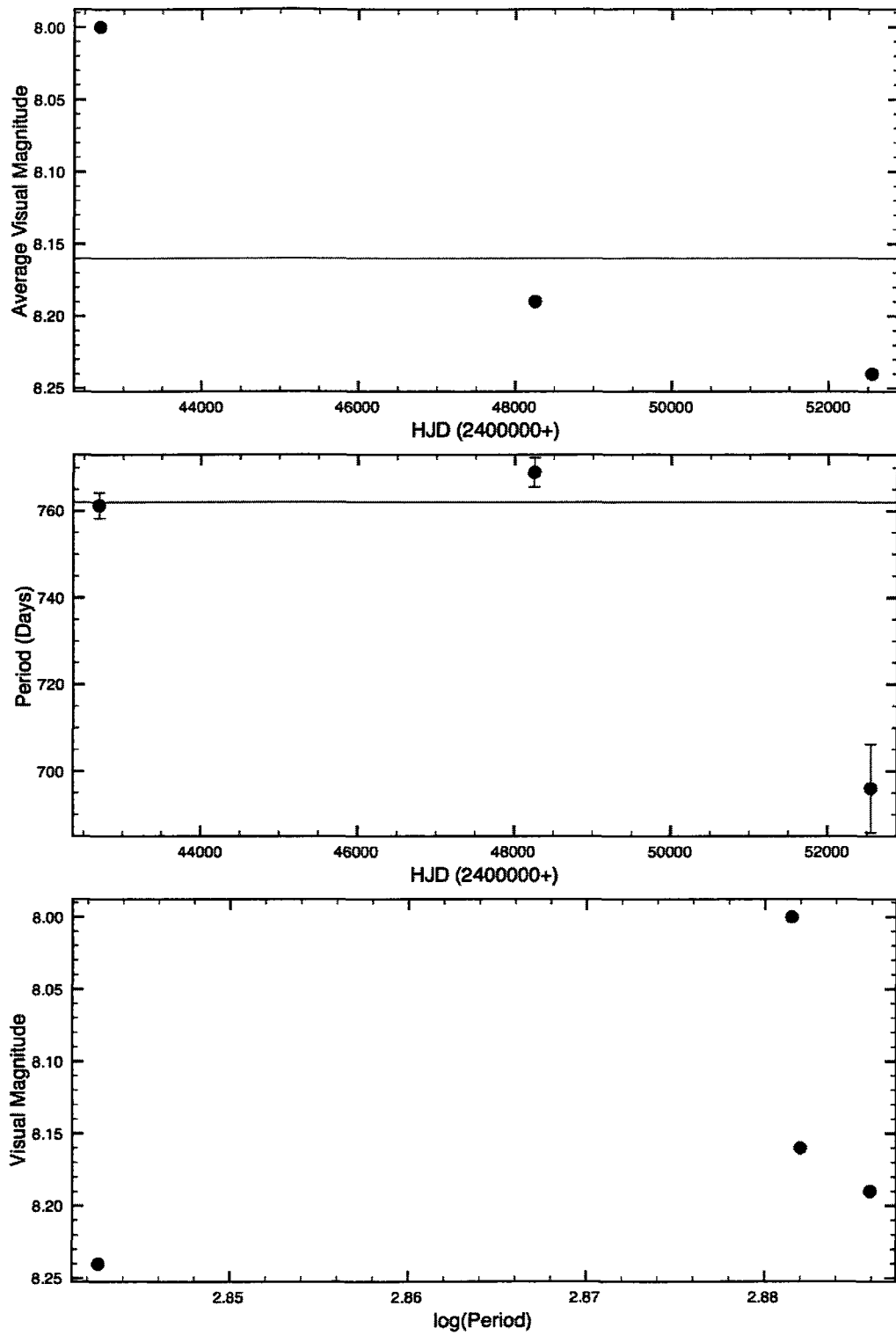


**Figure 4.76:** Period and average magnitude changes in CM Velorum from AAVSO observations.

## 4.50 FG Vulpeculae

Figure 4.77 shows FG Vul's variations in spectral type and radial velocity, along with a montage of CCD spectra taken at different epochs. The spectroscopic observations were phased using a period of 351.77 days and a time of maximum light of JD2453951.13, determined from the AAVSO observations. The GCVS lists a period of 86 days and a spectral type of M5 II. Both periods result in approximately the same phasing for the two spectroscopic observations. We do not have enough observations to determine at what phase FG Vul reaches highest temperature and luminosity class. There are insufficient AAVSO measurements to use for a period study of the star, but a previous photographic study by Götz (1984), tied to published photographic data, gave a period of 86 days. The 351-day period may be a result of seasonal bias. The two spectroscopic observations hint at consistency with pulsation, but additional observations are needed to fully study pulsation in the star.

**Table 4.88:** AAVSO Observations of FG Vulpeculae

Subset	Dates	$\langle V \rangle$	% Diff.	$\Delta V$	$N$	$P$ (days)	% Diff.
All	50949-54807	9.61	...	1.0	29	$351.77 \pm 3.71$	...

**Table 4.89:** Spectroscopic observations of FG Vulpeculae

Year	HJD	Phase	$V_R$ (km/s)	Spectral Type	Source
2009	2455092	0.2495	$-40.5 \pm 19.2$	M5 Ib	DAO CCD
2010	2455489	0.3807	$-31.6 \pm 20.9$	M5 Iab	DAO CCD

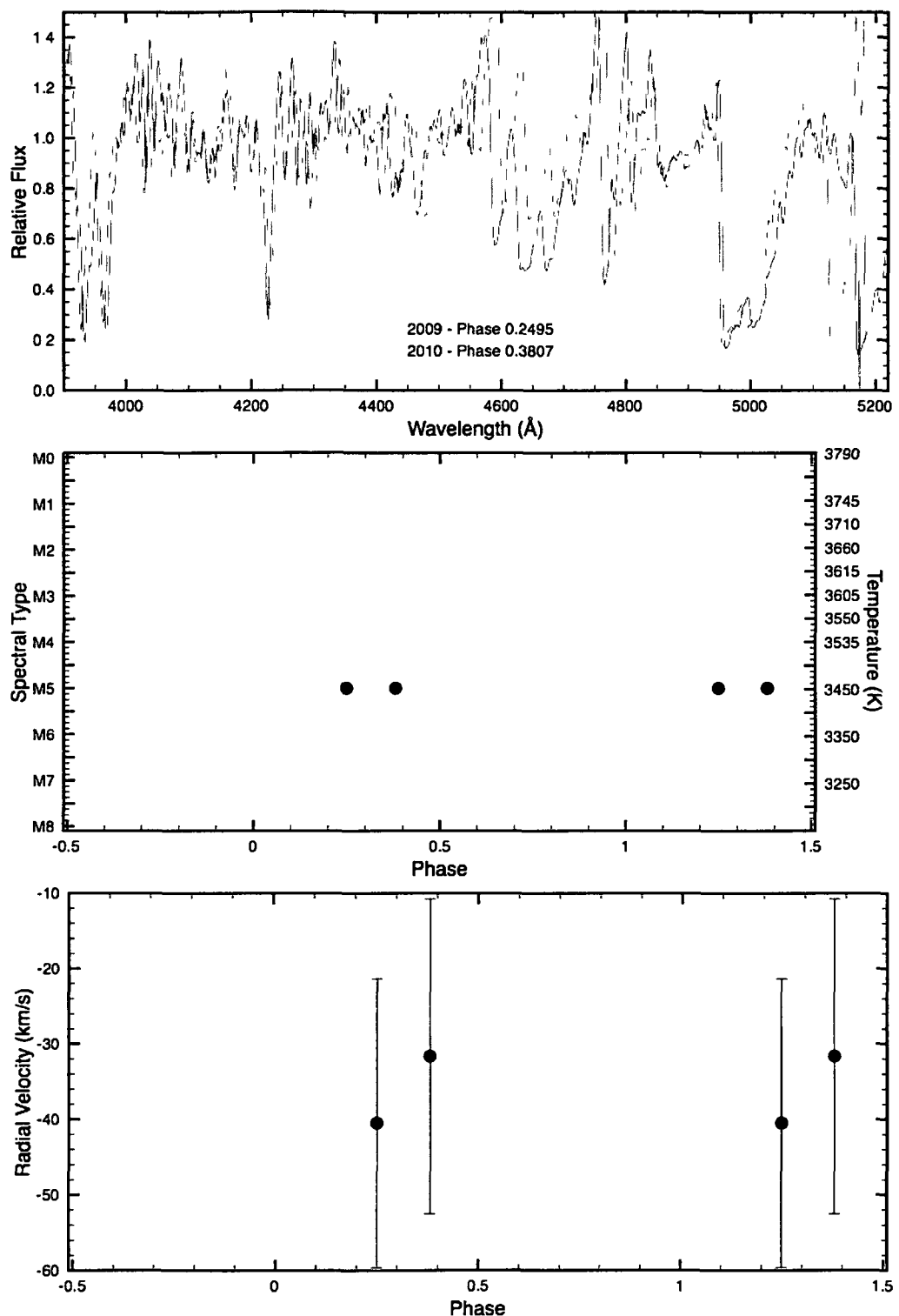


**Figure 4.77:** Spectroscopic variation in FG Vulpeculae. Top: Spectra from different epochs. Middle: Spectral type as a function of phase. Bottom: Radial velocity as a function of phase. Data phased with 351.77 day period.

## 4.51 Summary of Results

Table 4.90 presents a concise summary of the results found. We have divided the stars into three new classifications that have arisen as a result of our work. Class A includes stars that may be LC variables rather than SRC variables, or that have very little available data. Class *B* includes stars that are most likely SRC variables, but need more data. Class C includes stars that are most certainly SRC variables and have enough data available that we have been able to make some conclusions about the nature of their variability. 13 stars are in class A, 22 stars are in class B, 8 stars are borderline cases between classes *B* and C, and 6 stars are in class C.

**Table 4.90:** Summary of Results

Star	Class	Spectral Type	Period (d)	Comments
SS And	A	M6-M7 Iab	178	Irregular light curve, possible LC
V Ari	A	C5 II	58.7	Very poor, irregular light curve, period not well-established, possible LC
UX Aur	<i>B</i>	M4-5 Ia-II	357/90	Periodicity uncertain, needs better photometry
V349 Aur	<i>B</i>	M4 Ib-II	32.5	No photometry for finding period, but spectral type changes observed
RS Cnc	<i>B</i>	M6-M7 Iab-Ib	240/120	Period well-established, only 2 spectra with $V_R$ , needs more spectroscopic data
UZ CMa	<i>B</i>	M6 II	86.8	Period well-established, needs spectroscopic data
BZ Car	A	M2-4 Ia-Ib	130/97	Periodicity reasonable, strange brightness drop, recent irregularity
CK Car	A	M3.5 Iab	533	Period well-established, irregular brightness variability, possible LC

continued...

**Table 4.91:** Summary of Results (continued)

Star	Class	Spectral Type	Period (d)	Comments
CL Car	B	M5 Iab	513	Period well-established, brightness drops possibly from dust, needs spectroscopy
EV Car	A	M4.5 Ia	347	Period not well-established brightness variability, needs spectroscopy, possible LC
IX Car	B	M2 Iab	350-400	Variability well-established, small amplitude, mean brightness changes
PZ Cas	C	M2-4 Ia	253	Solid period, some changes in mean brightness
W Cep	B	K0-I Ia-Ib	2000/350	Variable but not consistently, is it in fact pulsating? Periodicity reasonable, but starspot activity likely
SW Cep	B/C	M3.5 Ia-Iab	599/70	Good spectra, but lacks photometry. Period needs confirmation.
VV Cep	A	M4 Ia-Iabe + B8 Ve	364	AAVSO data too scattered, eclipses and orbit well-studied, but pulsation not. Is it an LC?
MY Cep	A	M7 Ia	...	No photometry, small amplitude, 1 spectrum
$\mu$ Cep	B	M2 Iae	700-1000	Lots of data, period unstable, could be LC?
T Cet	B/C	M5-6 IIe	160	Good photometry, good period, needs more spectra
RW Cyg	B	M2-4 Ia-Iab	520	Amplitude changes, needs better phasing
AZ Cyg	B/C	M2-4 Ia-Ib	459	Period well-defined, amplitude small, needs improved phasing
BC Cyg	C	M2-4 Ia-Ib	693	Good data, well-established period, good spectra, dust extinction episodes

continued...

**Table 4.92:** Summary of Results (continued)

Star	Class	Spectral Type	Period (d)	Comments
V Eri	A	M6 II	290/97	Periodicity not well-marked, no spectra, borderline SRC at best
TV Gem	B	K5.5-M1.3 Iab	425/70	Needs better period, but spectral type changes consistent with pulsation
IS Gem	A	K3 II	359/47	K star with short P, small amplitude, no good data
V959 Her	A	M4 Ib-II	140	Not in old GCVS, no spectral type changes, lack of photometry. Don't know why it was classified SRC.
$\alpha$ Her	B/C	M5 Ib-II	508.7	Highly irregular light curve, period uncertain, but spectral data good
RV Hya	A	M5 II	243/116	Poor photometry, no spectra, don't know if period is accurate
W Ind	B	M4-5 IIe	198	Period well-established, but needs spectra
U Lac	B/C	M4 Iabpe + B	395	Good light curve and reasonable period
Y Lyn	B	M6 Ib-II	283/110	Period needs to be better constrained, need more spectral data, pulsation is small amplitude
$\delta^2$ Lyr	A	M4 II	627	Needs spectral data, light variation is not obvious in AAVSO data
$\alpha$ Ori	B	M1-2 Ia-Ib	425/2335	Lots of observations, but difficult to phase, period not well-defined, good $V_R$ and spectral types

continued...

**Table 4.93:** Summary of Results (continued)

Star	Class	Spectral Type	Period (d)	Comments
S Per	C	M3-M7 Iae	807	Good results
T Per	C	M2 Iab	2457	Good results, but amplitude small, and 2457 day period is unusual for M2 star
W Per	B/C	M3-7 Ia-Iab	531/485	Good spectral results, but period needs confirmation
RS Per	B	M4 Iab	244	Promising case, but needs better photometry.
SU Per	C	M3.5 Iab	468/533	Good results, period needs to be better-constrained
XX Per	C	M4 Ib + B	403	Good spectral results, but period needs confirmation
AD Per	B	M2.5 Iab	371	Spectral results okay, but photometry is poor. Is the 1 year period real?
BU Per	A	M3.5 Ib	367/2960	Period to close to 1 year to be certain. Brightness is varying, but better photometry is needed.
FZ Per	B/C	M0.5-2 Iab	371/184	Promising case, but period needs to be confirmed. Spectral results are good.
V411 Per	B	M3.4 Ia	467	Period is poorly established. Needs more photometry.
VX Sgr	B	M4-10 Iae	756.65	Good photometry and period, but needs spectra.
KW Sgr	B	M0-4 Ia	352/670	Promising, but period not well-established. Needs $V_R$ and more photometry.

continued...

**Table 4.94:** Summary of Results (continued)

Star	Class	Spectral Type	Period (d)	Comments
AH Sco	<i>B</i>	M4-5 Ia-Iab	766	Great photometry, good period, no spectra
CE Tau	B/C	M2 Iab-Ib	174	Reasonably good photometry, period needs to be a bit better constrained
W Tri	<i>B</i>	M5 II	593	Good period, but spectra don't show variation
CM Vel	<i>B</i>	M0-5 II	762	Good period, no spectra
FG Vul	<i>B</i>	M5 II	352/86	Period okay, but needs more spectra

# Chapter 5

## Group-Wide Trends

In this chapter we examine the properties of the stars as a group using the results presented in the preceding chapter. We look at insights gained from studying the period changes and spectroscopic variability, as well as a relationship among spectral type, luminosity class, and amplitude, and the period-luminosity relation.

### 5.1 Insights From the Radial Velocity Curves

It is apparent from our analysis of the radial velocity curves that some of the stars seem to reach their smallest dimensions near light minimum while others seem to reach their smallest dimensions near light maximum. Tables 5.1 and 5.2 list the stars in each group. Since maximum luminosity invariably corresponds to hottest temperature, and most stars are hottest when smallest, it would seem that all of the program stars should reach their smallest dimensions near light maximum, which is why it seems essential to examine their radial velocity variations more closely. Otherwise, there is no obvious common characteristic for the two groups that could provide an explanation for such a dichotomy.

Maximum temperature and greatest luminosity class occur near light maximum in essentially all cases, making the two groups appear to behave similarly despite the radial velocity results. Uncertainties in the radial velocity measurements and difficulties in determining accurate periods and phasing for some of the stars could be complicating the issue. It is likely that better photometry would lead to improved phasing that would resolve the discrepancy.

**Table 5.1:** Stars that reach smallest dimensions near light maximum (Phase 0.75-0.99 and 0.00-0.25)

Star	Phase of Smallest Size	Spectral Type	Period	$\Delta V$	Phase of Max T	Max L
RS Cnc	0.93	M6-M7 Iab-Ib	120	2.5	...	at min T <sup>1</sup>
SW Cep	0.98	M2-M4 Ia-Iab	599.10	2.1	near 0.0	at max T
VV Cep	0.76	M1.5-M3 Ia-Ib	364.21	1.4	...	at max T
$\alpha$ Her	0.11	M4-M6 Ia-Ib	508.07	2.2	...	at max T
S Per	0.017	M4-M5 Ia+ - Iab	806.64	6.1	near 0.0	at max T
SU Per	0.12	M3-M4 Ia-Ib	468.91	2.8	...	...
W Per	0.87	M3.5-M5 Ia-Ib	531.47	3.6	near 0.5	at max T

<sup>1</sup>Sole anomalous object

**Table 5.2:** Stars that reach smallest dimensions near light minimum (Phase 0.25-0.75)

Star	Phase of Smallest Size	Spectral Type	Period	$\Delta V$	Phase of Max T	Max L
PZ Cas	0.34	M2-M4 Ia-Iab	253.97	3.6	near 0.5	at max T
$\mu$ Cep	0.54	M0.5-M3 Ia+ - Iab	843.65	2.5	...	...
W Cep	0.33	K0-K1 Ia-Ib	346.2	2.7	near 0.5	...
T Cet	0.46	M5	160.84	...	...	
AZ Cyg	0.75	M2-M3.5 Ia-Ib	459.17	3.1	near 0.0	at max T
BC Cyg	0.44	M2-M5 Ia-Ib	699.35	2.8	near 0.0	at max T
RW Cyg	0.63	M3-M4 Iab	520.52	3.4	near 0.5	...
U Lac	0.56	M2-M4 Ia+ - Iab	395.00	3.4	...	...
$\alpha$ Ori	0.27	M1-M3 Ia-Ib	425.59	2.9	near 0.0	at max T
AD Per	0.49	M2-M4 Ia-Ib	371.24	2.3	near 0.0	at max T
FZ Per	0.69	M0-M1 Ia+ - Ia	371.00	2.3	...	at max T
RS Per	0.64	M3-M5 Ia+ - Iab	244.21	2.9	near 0.5	at min T
T Per	0.45	M1-M2 Ia+ - Iab	358.86	2.5	near 0.0	at max T
V411 Per	0.72	M1-M2 Iab	394.55	1.1	near 0.0	...
XX Per	0.67	M4-M5 Ia-Iab	403.00	2.5	near 0.0	at max T
CE Tau	0.26	M1-M2.5 Iab-Ib	174.39	4.3	...	at max T

## 5.2 Spectral Type-Amplitude Relation

It became apparent as we studied the stars that some of the coolest stars had some of the largest amplitudes, while some of the hottest stars had some of the smallest amplitudes. Figure 5.1 shows median spectral type plotted versus light amplitude. There is some scatter in the plot, but a trend towards larger amplitudes in cooler stars and smaller amplitudes in hotter stars is apparent. Some of the scatter can be explained by the difficulties in actually defining the pulsation amplitude and median spectral type in stars that are undergoing so many changes, but when we used luminosity class to sub-divide the plot, tighter correlations within luminosity classes became apparent. Stars with greater luminosities and later spectral types generally have higher amplitudes.

Table 5.3 lists the stars used in the spectral-type amplitude relation, and figure 5.1 shows the relation categorized according to luminosity class. This is a new observational result, although a theoretical investigation of the pulsation properties of red supergiants by Bono & Panagia (2000) found that model stars of lower effective temperature have greater pulsation amplitudes. As a further theoretical basis for the result, we integrated a simple Planck function over the wavelength range of the Johnson  $V$  filter for temperatures of 3200-3800 K, and plotted the trend in  $\Delta V$  as a function of temperature for three values of  $\Delta T$ . Results are shown in figure 5.2, and they confirm the trends seen in the observational data. Note that greater  $\Delta T$  values produce larger slopes and zeropoints. Comparison with our observational results seems to indicate that Ia stars undergo the greatest temperature changes while Ib-II stars undergo the smallest temperature changes.

We performed linear regressions to determine lines of best fit for each of the three luminosity subgroups (excluding points in each group that crossed into the region of a neighboring group). We obtained the following results:

For the Ia stars:

$$\Delta V = 0.6242 \pm 0.1596(\text{Spectral Type}) + 1.6752 \pm 0.3684 \quad (5.1)$$

For the Iab stars:

$$\Delta V = 0.5385 \pm 0.1258(\text{Spectral Type}) + 0.5288 \pm 0.3945 \quad (5.2)$$

For the Ib-II stars:

$$\Delta V = 0.8248 \pm 0.1855(\text{Spectral Type}) - 2.3482 \pm 0.9627 \quad (5.3)$$

The equations have correlation coefficients of 0.8475, 0.8680, and 0.5893, respectively. One source of uncertainty in the result that could be reduced with future dedicated SRC observing campaigns is a lack of spectral type measurements over the entire pulsation cycles of the stars. We have used the median spectral types found from the measurements that we have, but filling in the spectral type vs. phase plots with more data points in order to determine median spectral types more confidently would remove some of the uncertainty. More spectroscopic data would also allow us to determine the full range of the spectral type variation for each star and conclusively state whether or not stars of greater luminosity class undergo greater temperature changes.

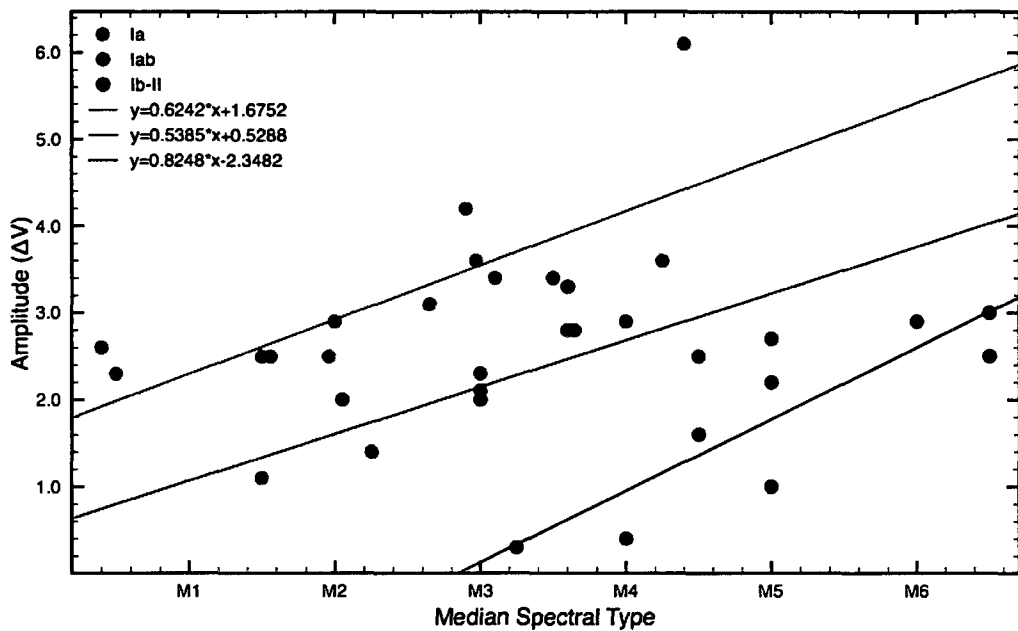


Figure 5.1: Relationships among spectral type, luminosity class, and amplitude.

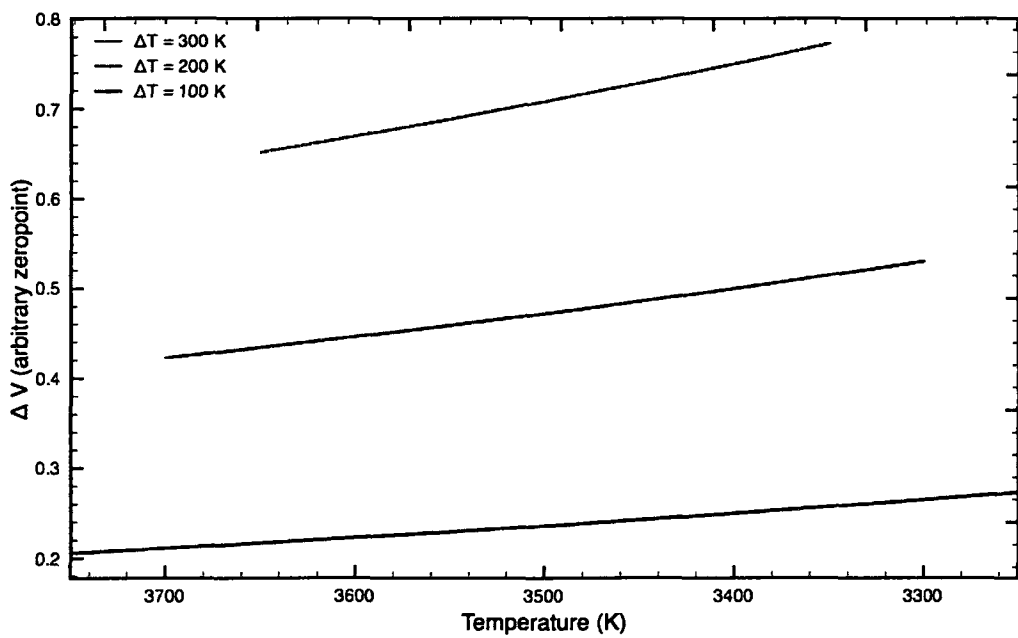


Figure 5.2:  $\Delta V$  as a function of  $T$  for various values of temperature amplitude,  $\Delta T$ .

**Table 5.3:** Stars used in spectral type-amplitude relation

Star	Spectral Type	$\Delta V$
SS Andromedae	M6.50 Ib	3.0
UX Aurigae	M4.50 Ib	1.6
V394 Aurigae	M3.25 Ib	2.5
RS Cancri	M6.50 Ib	2.5
BZ Carinae	M2.90 Ia	4.2
PZ Cassseopeiae	M2.97 Ia	3.6
$\mu$ Cephei	M1.56 Ia	2.5
SW Cephei	M3.00 Iab	2.1
VV Cephei	M2.25 Iab	1.4
AZ Cygni	M2.65 Ia	3.1
BC Cygni	M3.65 Ia	2.8
RW Cygni	M3.50 Iab	3.4
TV Geminorum	M0.40 Iab	2.6
$\alpha$ Herculis	M5.00 Ib	2.2
V959 Herculis	M4.00 Ib	0.4
U Lacertae	M3.10 Ia	3.4
Y Lyncis	M6.00 II	2.9
$\delta^2$ Lyrae	M3.00 Ib	2.0
$\alpha$ Orionis	M2.00 Iab	2.9
AD Persei	M3.00 Iab	2.3
BU Persei	M3.60 Ib	3.3
FZ Persei	M0.50 Ia	2.3
RS Persei	M4.00 Iab	2.9
S Persei	M4.40 Ia	6.1
SU Persei	M3.60 Iab	2.8
T Persei	M1.50 Ia	2.5
V411 Persei	M1.50 Iab	1.1
W Persei	M4.25 Ia	3.6
XX Persei	M4.50 Iab	2.5
KW Sagittarii	M1.96 Ia	2.5
CE Tauri	M2.05 Iab	2.0
W Triangulii	M5.00 II	2.7
FG Vulpeculae	M5.00 Ib	1.0

### 5.3 Period-Luminosity and Period-Radius Relations

We used stars with known distances that are cluster or association members to examine the SRC period-luminosity relation. Table 5.4 lists the stars used in the analysis, figure 5.3 shows the period-luminosity relation, and figure 5.4 shows the period-radius relation. The anomalous star in both cases is RS Per, which seems to have an unusually short period of variability for its spectral type (M3-M5) and luminosity class (Ia-Iab). We chose to include only stars with distances established from cluster/association membership rather than using HIPPARCOS parallaxes because the systematic errors in the HIPPARCOS values are unacceptably large at the distances involved.

Initially we used all stars that were known cluster members and calculated bolometric magnitudes using the bolometric corrections from Levesque & Massey (2005), distances and reddening values from a variety of sources, average apparent visual magnitudes from the AAVSO data, and periods determined in chapter 4. That produced relations with a lot of scatter and insignificant correlations. We investigated whether subsets of the data showed significant relations (including plotting different luminosity classes separately and plotting cluster and association members separately) and saw no obvious patterns. Finally, we plotted only the stars listed in Levesque & Massey (2005) using the bolometric magnitudes calculated in that paper and the periods we determined in chapter 4. That produced period-luminosity and period-radius relations with significant correlations, and we believe that the problem was with the AAVSO average magnitudes. Perhaps they are simply too uncertain, either because of differences in observers for stars with fewer data points or an uneven distribution of data across different epochs of observations. We have chosen, therefore, to include only stars with either bolometric magnitudes determined by Levesque & Massey (2005) or with absolute visual magnitudes determined by Humphreys (1978) in conjunction with the Levesque & Massey (2005) bolometric corrections. Data sources are indicated in the table.

Our results show that stars with greater luminosities have longer periods, similar to period-luminosity relations for other types of pulsating variables. The equation of the line of best fit through the data is

$$M_{bol} = (-4.18 \pm 0.90) \log(P) + (3.49 \pm 2.42), \quad (5.4)$$

with a correlation coefficient of -0.78. Our period-radius relation has a positive slope, also similar to what is expected for pulsating variables. The line of best fit is given by

$$\log(R/R_\odot) = (1.06 \pm 0.46) \log(P) + (0.066 \pm 0.17), \quad (5.5)$$

with a correlation coefficient of 0.86. RS Persei was not included when determining the lines of best fit, as it appears to be an outlier. T Persei was included with its shorter period of 377 days, as the short period produced a better fit with the rest of the stars than its longer period of 2457 days. We have not excluded stars that were assigned to class A in chapter 4, as they have not yet been conclusively eliminated from the SRC class.

Both relations contain some scatter, which likely has several causes. First, the periods of the stars are not constant and in some cases are not established reliably. We have already shown that the periods change when examined over 10-year intervals, and it is apparent from the light curves that even the duration from one maximum to the next is not always the same. The second issue is that factors other than pulsation contribute to the brightness variations. Although cyclic changes in the radial velocities give supporting evidence to the theory that the stars do pulsate, the scatter in some of the spectral type plots indicates that pulsation does not tell us the entire story. We know from the work of Gray (2008) that  $\alpha$  Orionis is covered by a few giant convection cells, which has a significant impact on its light variations, and it seems reasonable to conclude that the other SRC variables experience a similar type of convection. The dust production and mass ejections that occur in the atmospheres of such variables further complicate the issue.

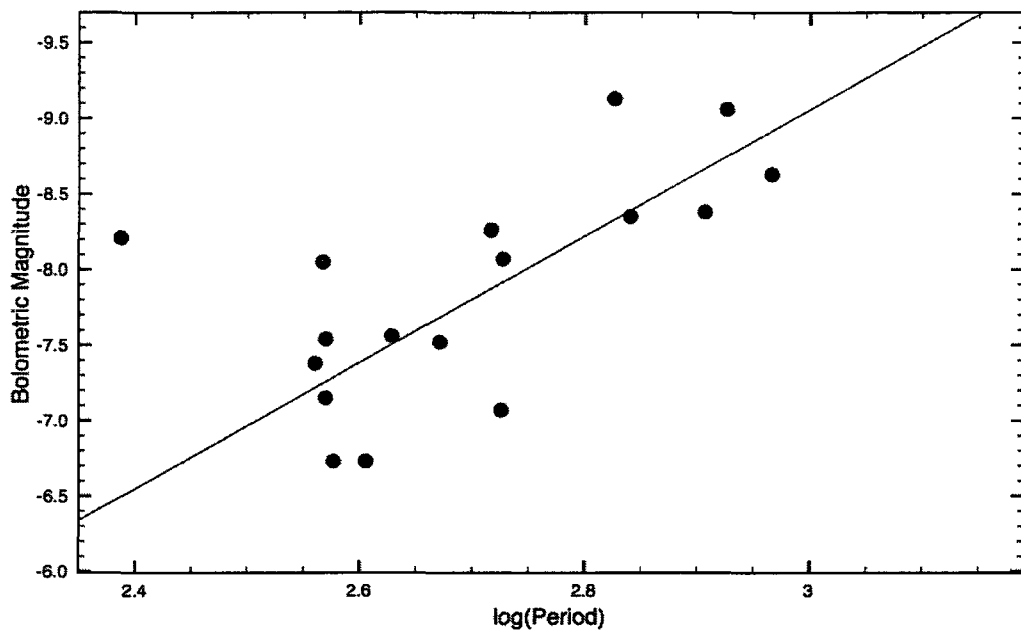


Figure 5.3: Period-luminosity relation.

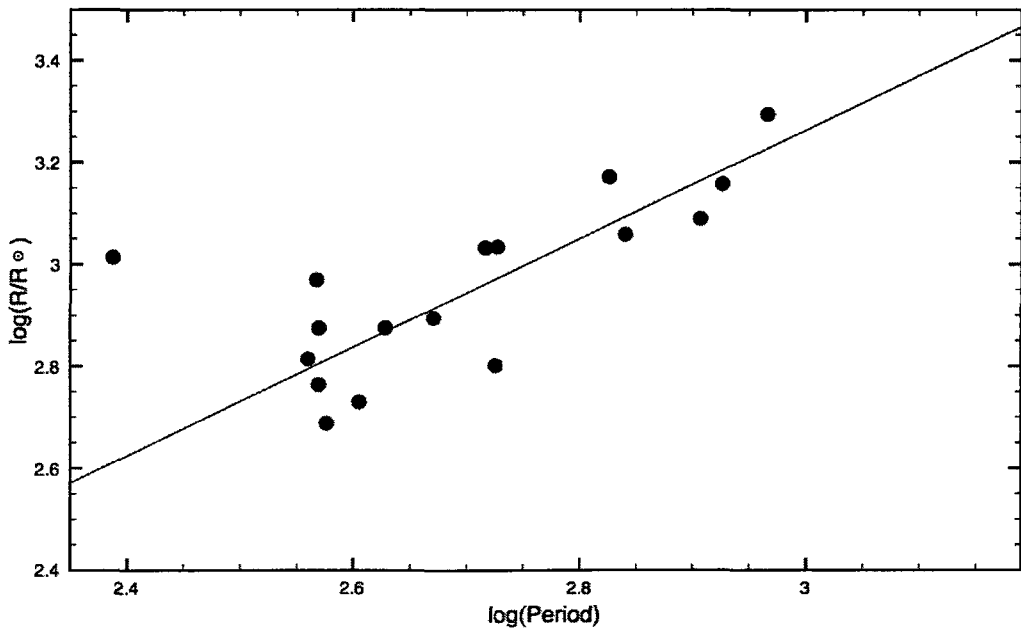


Figure 5.4: Period-mean radius relation.

**Table 5.4:** Stars used in period-luminosity and period-radius relations

Star	Cluster/ Association	Period (days)	V	V-M <sub>v</sub>	A <sub>v</sub>	M <sub>v</sub>	BC	M <sub>bol</sub>	T <sub>eff</sub> (K)	log(L/L <sub>○</sub> )	R/R <sub>○</sub>
CK Car <sup>1</sup>	Car OB1-D	533 61	7 45	11 70	1 86	-6 11	-1 96	-8 27	3550	5 2	1082
IX Car <sup>1</sup>	Car OB1-E	369 1	7 38	12 00	1 86	-6 48	-1 57	-8 08	3660	5 1	933
PZ Cas <sup>1</sup>	Cas OB5	925	9 50	11 90	4 49	-6 89	-1 74	-9 64	3605	5 8	1972
$\mu$ Cep <sup>1</sup>	Trumpler 37	843 65	4 08	9 70	2 01	-7 63	-1 43	-9 08	3710	5 5	1438
RW Cyg <sup>2</sup>	Cyg OB9	520 52	8 13	10 36	4 07	-6 3	-1 96	-8 26	3550	5 2	1077
BC Cyg <sup>1</sup>	Berkeley 87	692	9 97	11 00	5 58	-6 61	-1 74	-8 46	3605	5 3	1145
TV Gem <sup>1</sup>	Gem OB1	425 14	6 56	10 70	2 17	-6 31	-1 25	-7 76	3790	5 02	751
S Per <sup>1</sup>	Per OB1-D	806 64	9 23	11 40	4 18	-6 35	-2 03	-8 53	3535	5 3	1230
T Per <sup>2</sup>	Per OB1	377	8 64	12 15	2 09	-5 3	-1 43	-6 73	3710	4 6	487
W Per <sup>1</sup>	Per OB1-D	531 47	10 39	11 40	4 03	-5 04	-2 03	-7 09	3535	4 8	634
RS Per <sup>1</sup>	Per OB1-D/ NGC 884	244	8 35	11 90	2 63	-6 18	-2 03	-8 15	3535	5 2	1032
SU Per <sup>1</sup>	Per OB1-D	468 91	7 63	11 40	2 01	-5 78	-1 74	-7 64	3605	5 0	785
XX Per <sup>2</sup>	Per OB1	403	8 26	11 94	1 12	-4 7	-2 03	-6 73	3535	4 6	537
AD Per <sup>2</sup>	Per OB1	371 24	7 9	11 59	1 91	-5 8	-1 74	-7 54	3605	4 9	750
BU Per <sup>1</sup>	Per OB1-D	363	9 23	11 40	3 25	-5 42	-1 96	-7 17	3550	4 8	652
FZ Per <sup>2</sup>	Per OB1	371	7 96	11 62	1 94	-5 8	-1 35	-7 15	3745	4 8	580
KW Sgr <sup>1</sup>	Sgr OB5	670	9 35	12 40	4 65	-7 70	-1 43	-9 15	3710	5 6	1486

<sup>1</sup> V, V-M<sub>v</sub>, A<sub>v</sub>, BC, M<sub>bol</sub> from Levesque & Massey (2005), T<sub>eff</sub> determined from Levesque & Massey (2005) based on author's spectral types, log(L/L<sub>○</sub>) & R/R<sub>○</sub> calculated by author

<sup>2</sup> V, V-M<sub>v</sub>, A<sub>v</sub> from Humphreys (1978), BC & T<sub>eff</sub> determined from Levesque & Massey (2005) based on author's spectral types, M<sub>bol</sub>, log(L/L<sub>○</sub>) & R/R<sub>○</sub> calculated by author

**Table 5.5:** Bolometric corrections from Levesque & Massey (2005)

Spectral Type	B.C.
K1-K1.5	-0.79
K2-K3	-0.90
K5-M0	-1.16
M0	-1.25
M1	-1.35
M1.5	-1.43
M2	-1.57
M2.5	-1.70
M3	-1.74
M3.5	-1.96
M4-M4.5	-2.03
M5	-2.49

### 5.3.1 Other Period-Luminosity Relations of Note

We are including here a brief summary of period-luminosity relations for similar stars (M giants and supergiants, Miras, SR variables, etc.) and a few comments on the Cepheid period-luminosity relations for context.

The Cepheid period-luminosity relation can be described by

$$\log(L/L_{\odot}) = (2.415 \pm 0.035) + (1.148 \pm 0.044) \log(P) \quad (5.6)$$

(see Turner 2010), which has a similar trend to what we found for SRC variables, albeit with less scatter as Cepheids have well-defined periods and mean magnitudes. Period increases with luminosity in both cases. It is well-established theoretically that the Cepheid period-luminosity relation is a result of pulsation in the stars.

As mentioned in the introduction, Stothers (1969) demonstrated theoretically that pulsation could cause the brightness variations seen in M supergiants. His study was not limited to SRC variables specifically. He did not plot a period-luminosity relation or give an equation describing it, but his “revised periods” for the stars (calculated from temperatures and luminosities using a  $Q$  value consistent with pulsation) increase as the stars’ brightness increases (decreasing bolometric magnitude), consistent with what we found here.

Feast et al. (1980) derived bolometric magnitudes for 24 red supergiant variables (again, not limited to SRC variables) in the Large Magellanic Cloud using infrared photometry. They found a period-luminosity relation for the stars of

$$M_{\text{bol}} = -8.6 \log(P) + 16.4. \quad (5.7)$$

Although there is a large amount of scatter in their plotted relation, it again shows the same general trend we found, although with a slope twice as large as what we find. Catchpole & Feast (1981) did the same for 22 red supergiant variables in the

Small Magellanic Cloud, and found the same trend, this time described by

$$M_{\text{bol}} = -7.2 \log(P) + 12.8. \quad (5.8)$$

Pierce et al. (2000) observed period-luminosity relations in the R band and several near-infrared bands for red supergiant variables in the Per OB1 association, the LMC, and M33. Jurcevic et al. (2000) did the same for red supergiant variables in M101. In all cases, the same trends were seen (periods increasing with decreasing absolute magnitudes). Slopes in the two papers range from  $-1.78$  to  $-3.29$ , slightly smaller than the slope we found.

Similar results can also be found in the following papers. All show period increasing with luminosity, although there is a lot of scatter in some of the results and the slope values vary. The only paper in the list that is limited to SRC variables specifically is Turner et al. (2006).

- Guo & Li (2002), for model M supergiants. Varying slopes are seen depending on the model choice.
- Knapp et al. (2003), for Miras, SRA variables, and SRB variables using Hipparcos parallaxes and K band absolute magnitudes. The authors finds slopes of  $-3.39 \pm 0.47$  for the Miras and  $-1.34 \pm 0.06$  for the SRA and SRB variables.
- Yeşilyaprak & Aslan (2004), for SR stars (mainly giants) using Hipparcos parallaxes and absolute magnitudes in the *R* band a variety of near-IR bands (although the opposite slope is seen with absolute magnitudes in the *U*, *B*, and *V* bands, which is curious and likely has something to with the fact that most of the light output is not in those wavelength ranges). Slopes range from  $2.89 \pm 0.49$  in the *V* band to  $-4.09 \pm 0.71$  in the [25] band.
- Kiss et al. (2006), for both short and long periods (determined using Fourier analysis of the AAVSO observations) in the same red supergiants and *K* band

absolute magnitudes. The stars showed the same trend we found, with the long periods forming a parallel relation with a smaller zeropoint. We note that in our own relation, a point formed using T Persei’s long period lies to the right of our main relation, but falls in the same region as the long period relation of Kiss et al. (2006) relation. The short-period relation in the paper has a slope of  $-3.44 \pm 0.6$ .

- Turner et al. (2006), for BC Cyg and four SRC variables in the Per OB1 association. This is the only previously published period-luminosity relation that is limited to SRC variables specifically. The slope found here is approximately -3 in  $M_{bol}$  vs.  $P$ .
- Glass & van Leeuwen (2007), for SR variables (mainly giants) in the solar neighborhood using  $K$ -band magnitudes and Hipparcos parallaxes. There is a lot of scatter in the results, but slopes are near -2.
- Tabur et al. (2010), for RGB and AGB stars in the Magellanic clouds and solar neighborhood using Hipparcos parallaxes. There is a lot of scatter in the results, but the authors found a slope of -3.72 for a chosen reference sequence of stars.
- Yang & Jiang (2011), for groups of red supergiants in the LMC in the  $V$  band and various near- and mid-infrared bands. Slopes range from  $-1.97 \pm 1.03$  in the  $V$  band to  $-7.83 \pm 0.75$  in the [24] band.

#### 5.4 Size Changes

For stars with radial velocity data, we estimated  $\Delta R$ , the change in radius, using the Baade-Wesselink method. Given that  $V_R = \frac{dR}{dt}$ , we can integrate over half a pulsation cycle as follows to obtain an estimate of the size change (provided that the radial velocity variation is caused by pulsation and can be approximated with a sine wave):

$$dR = p v_R dt \quad (5.9)$$

where  $p$  is the projection factor

$$\int_{R_{min}}^{R_{max}} dR = p \int_{R_{min}}^{R_{max}} V_R dt \quad (5.10)$$

$$\int_{R_{min}}^{R_{max}} dR = R_{max} - R_{min} = 2\Delta R \quad (5.11)$$

where  $\Delta R$  is the variation about the mean radius

$$2\Delta R = p \int_{R_{min}}^{R_{max}} v_R dt = p \Delta V_R \frac{P}{2} \int_0^\pi \frac{\sin(\theta)}{\pi} d\theta \quad (5.12)$$

where  $P$  is the period

$$2\Delta R = p \Delta V_R \frac{P}{2} \frac{1}{\pi} [\cos(\theta)]_0^\pi \quad (5.13)$$

$$2\Delta R = p \Delta V_R \frac{P}{2} \frac{2}{\pi} \quad (5.14)$$

$$\Delta R = p \Delta V_R \frac{P}{2\pi} \quad (5.15)$$

The projection factor,  $p$ , for M supergiants has not been well-studied, but for Cepheids the projection factor is near 1.3 (see, for example Mérand et al. 2005). Based on the fact that M supergiants display greater limb darkening than Cepheids, we would assume that they have a smaller projection factor. In the absence of an established value in the literature, we have simply taken  $p$  to be equal to 1 for the purpose of our estimates. That gives us the following to approximate  $\Delta R$ :

$$\Delta R = \Delta V_R \frac{P}{2\pi} \quad (5.16)$$

Table 5.6 shows the stars' radius change estimates in Solar radii and as fractions of the stars' individual radii for stars that are cluster members with available distance estimates. Note that some of the stars do not have radial velocity measurements that cover the entire phase, so some of the estimates are likely small. But in most cases, the size changes implied by the radial velocity variation are small enough that they are consistent with pulsation. However, in several of the longer period stars, the size changes implied are on the order of the size of the star. T Persei is an extreme example, with an implied size change of over 2 stellar radii when its long period is taken to be the pulsation period. That hints at another process, such as convection, being at least partly responsible for the observed radial velocity changes in such stars.

**Table 5.6:** Size Changes

Star	$P$ (days)	$\Delta R$ ( $R_{\odot}$ )	$\Delta R/R$
SS And	178.35	55.0	...
UX Aur	357	31.8	...
RS Cnc	120	50.8	...
PZ Cas	253.97	66.3	0.034
W Cep	346.26	78.7	...
SW Cep	599.10	107.2	...
VV Cep	364.21	110.9	...
$\mu$ Cep	843.65	293.5	0.20
T Cet	160.84	28.3	...
RW Cyg	520.52	163.6	0.15
AZ Cyg	459.17	72.6	...
BC Cyg	692.78	323.2	0.28
TV Gem	425.14	35.3	0.047
$\alpha$ Her	508.07	376.6	...
U Lac	395	254.5	...
Y Lyn	282.56	14.2	...
$\alpha$ Ori (long period)	2335	92.3	...
$\alpha$ Ori (short period)	425.59	16.8	...
S Per	806.64	239.2	0.19
T Per (long period)	2457	1175.4	2.41
T Per (short period)	377	180.3491	0.37
W Per	531.47	114.5	0.18
RS Per	244.21	122.1	0.12
SU Per	468.91	54.7	0.070
XX Per	403	214.3	0.40
AD Per	371.34	129.2	0.17
BU Per	363	66.4	0.10
FZ Per	371	209.7	0.36
V411 Per	394.55	103.0	...
CE Tau	174.39	5.5	...
W Tri	592.86	151.8	...
FG Vul	351.77	30.94	...

## 5.5 Remarks

As previous theoretical and observational work has shown, at least three mechanisms work together to cause the brightness variations seen in SRC variables: pulsation, convection, and intermittent dust ejections. We have certainly found new evidence of pulsation. The cyclic changes in temperature and radial velocity that we have found in many of the stars are caused by pulsation. The period-luminosity and period-radius relations that we have shown are the result of pulsation. The new spectral type-light amplitude relation is driven by temperature changes, and thus it can also be considered as evidence of pulsation. The size of the radius changes implied by the radial velocities (found using the shorter periods for the stars rather than periods over 2000 days) are small enough to be consistent with pulsation, since implied size changes on the order of the radius of the star or greater would indicate that the radial changes are the result of something other than pulsation.

We have also found some evidence of dust ejections in the stars. Dust ejections are the best explanation for the irregular temporary decreases in mean brightness observed in some of the stars in chapter 4. We would expect continued ongoing monitoring of all of the stars to produce more evidence of intermittent dust ejections.

Convection is a bit more difficult to observe and we cannot make any conclusions about it based on our study (with the exception of the large size changes found using the long periods of  $\alpha$  Ori and T Per, which are inconsistent with pulsation). Work like that done by Gray (2000, 2001, 2005, 2008) for  $\alpha$  Orionis would be needed to study convection in the other stars. Gray's study of convection involves the shape of the bisectors of unblended spectral lines, which requires higher-resolution spectra than those obtained here. The lines that Gray uses are also further to the red than our spectra. We recommend that future surveys of SRC variables include high resolution spectra in the red and near-IR in order to facilitate the study of convection in the stars.

## Chapter 6

### Conclusions and Future Directions

Our survey of 49 SRC variables has shown that they form a diverse group of stars that are undergoing changes. Each star exhibits changes in period and average magnitude. The stars' temperatures and luminosities change over the course of their pulsation cycles, but the stars do not all exhibit the same types of changes in temperature or luminosity. Some of the stars appear to reach their minimum dimensions near light minimum while others appear to reach their minimum dimensions near light maximum. There is also a great deal of variation in the amplitude of the magnitude changes that the stars undergo. Some of the stars have fairly regular light curves, while others appear to change dramatically from cycle to cycle. Despite their individual differences, the stars appear to follow a period-luminosity relation, a period-mean radius relation, and a relationship involving spectral type, luminosity class, and amplitude, albeit with scatter. The existence of such relations indicates that similar processes are occurring in the stars.

We have observed cyclic changes in radial velocity and temperature in many of the stars, which provide further evidence that pulsation is one of the processes occurring in SRC variables. In several of the stars, we have been able to determine that maximum temperature occurs near smallest dimensions, consistent with the behavior of other pulsating variables. Strangely, some of the stars also appear to reach maximum luminosity near the same time that they reach smallest dimensions and maximum temperature, which is the opposite of what would be expected in a pulsating star. We do note that the stars have very low surface gravities to begin with, and the actual changes in luminosity class are usually small and sometimes not even detected. In some cases the stars also appear to undergo irregular decreases in mean brightness that could be explained by dust ejection.

This study is the most comprehensive survey of the behavior of SRC variables yet made. We have presented many new results for individual stars, as well as a new spectral type-luminosity class-amplitude relation. We have constructed period-luminosity and period-mean radius relations for the stars with more data points than have been used previously, and the relations show trends that would be expected for pulsating variables. We have used both newly obtained data and data from existing sources. The study of long-period variable stars is difficult because of the time scales involved, and perhaps one of the reasons that not many have attempted it is that there was no certainty that the results obtained would be worth the effort and time required. We have shown here that the study of SRC variables does yield intriguing results. There are more questions to be answered, and more data to be obtained. Our study provides justification and a foundation for continued and ongoing monitoring of SRC variables.

## References

- Abt, H. A., Meinel, A. B., & Morgan, W. W. 1968, "An Atlas of Low-Dispersion Grating Stellar Spectra"
- Alksnis,A. 1961, Trudy Astrophysics Lab Riga, 7, 33
- Balega, Y. et al. 1982, A&A, 115, 253
- Bester, M. et al. 1996, ApJ, 463, 336
- Brelstaff, T. et al. 1997, JBAA, 107, 135
- Bono, G. & Panagia, N. 2000, ASP Conf. Series, 203, 105
- Catchpole, R. M. & Feast, M. W. 1980, MNRAS, 197, 385
- Chipps, K. A. & Stencel, R. E. 2004, JAVSO, 32, 1C
- Christy, R. F. 1962 ApJ, 136, 887
- Elias, J. H. et al. 1985, ApJS, 57, 91
- Feast, M. W., Wolley, R., & Ylimaz, N. 1972, MNRAS, 158, 23
- Feast, M. W. et al 1980, MNRAS, 193, 377
- Fernie, J. D. 1986, AJ, 306, 642
- Fernie, J. D. 1989, PASP, 101, 225
- Foster, G. 1995, AJ, 109, 1889
- Gahm, G. F. 1970, A&A, 4, 268
- Glass, I. S. & van Leeuwen, F. 2007, MNRAS, 378, 1543
- Götz, W. 1984, IBVS, 2461, 1

- Gray, D. F. 2000, ApJ, 532, 487
- Gray, D. F. 2001, PASP, 113, 789
- Gray, D. F. 2005, PASP, 117, 711
- Gray, D. F. 2008, AJ, 135, 1450
- Gray, R. O. & Corbally, C. J. 2009, “Stellar Spectral Classification”
- Griffin, R. F. & Filiz Ak, N. 2010, Ap&SS, 330, 47
- Guo, J. H. & Li, Y. 2002, ApJ, 565, 559
- Houk, N., Irvine, N. J., & Rosenbush, D. 1974, “An Atlas of Objective-Prism Spectra”
- Houk, N. & Newberry, M. V. 1984, “A Second Atlas of Objective-Prism Spectra”
- Humphreys, R. W. 1970, ApJ, 160, 1149
- Humphreys, R. M. & Lockwood, G. W. 1972, ApJ, 172, L59
- Humphreys, R. M., Strecker, D. W., & Ney, E. P. 1972, ApJ, 172, 75
- Humphreys, R. M. 1978, ApJS, 38, 309
- Humphreys, R. M. 1983, ApJ, 269, 335
- Humphreys, R. M. & Ney, E. P. 1974, ApJ, 194, 623
- Jurcevic, J. S., Pierce, M. J., & Jacoby, G. H. 2000, MNRAS, 313, 868
- Joy, A. H. 1942, ApJ, 96, 344
- Keenan, P. C. & Hynek, J. A. 1945, ApJ, 101, 265
- Keenan, P. C., & McNeil, R. C., 1976, *An Atlas of Spectra of the Cooler Stars: Types G, K, M, S and C*, (Columbus: Ohio State University)

- Keenan, P. C. & McNeil, R. C. 1989, ApJS, 71, 245
- Kiss, L. L. et al. 2006, MNRAS, 372, 1721
- Kharchenko, N. et al. 2005, A&A, 440, 403
- Knapp, G. R. et al. 2003, A&A, 403, 993
- Lee, T. A. 1970 ApJ, 162, 217
- Leedjärv, L. et al. 1999, A&A, 349, 511L
- Levesque, E. M. & Massey, P. 2005, ApJ, 628, 973
- Lim, J. et al. 1998, Nature, 392, 575
- Massey, P., Valdes, F., & Barnes, J. 1992, “A User’s Guide to Reducing Slit Spectra with IRAF” (available at <http://iraf.net/irafdocs/spect.pdf>)
- Massey, P. 1997, “A User’s Guide to CCD Reductions with IRAF” (available at <http://iraf.net/irafdocs/ccduser3.pdf>)
- Mérand, A. et al. 2005, A&A, 438, 9
- Mermilliod, Mayor, & Udry 2008, A&A, 485, 303
- Palacios, A. et al. 2010, A&A, 516, 13
- Percy, J. R. et al. 1996, PASP, 108, 139
- Percy, J. R. & Terziev, E. 2011, JAVSO, accepted for publication
- Pierece, M. J., Jurcevic, J. S., & Crabtree, D. 2000, MNRAS, 313, 271
- Pojmanski, G. 2005, The ASAS-3 Variable Star Catalog
- Samus, N. N. et al., General Catalog of Variable Stars
- Shcwarzenberg-Czerny, A. 1996, ApJ, 460, L107  
225

- Sharpless, S. & Wawrukiewicz, A. S. 1973, AJ, 78, 477
- Smartt, S. J. 2009, Annual Review of Astronomy & Astrophysics, 47, 63
- Snyder, L.F. 1991, IBVS, 3632, 1
- Solf, J. 1978, A&AS, 34, 409
- Stencel, R. E. et al. 1988, AJ, 95, 141
- Stephenson, C. B. 1959, PASP, 71, 145
- Stothers, R. 1969, ApJ, 156, 541
- Stothers, R. & Leung, K. C. 1971, A&A, 10, 290
- Swope, H. H. 1940, HA, 109, 1
- Tabur, V. et al. 2010, MNRAS, 409, 777
- Tatebe, K. et al. 2007, ApJ, 670, L21
- Townes, C. H. et al. 2009, ApJ, 697L, 127T
- Turner, D. G. & Forbes 1982, PASP, 94, 789
- Turner, D. G. 2003, JAVSO, 31, 160
- Turner, D. G. et al. 2006, PASP, 118, 1533
- Turner, D. G. et al. 2009, MNRAS, 397, 1046
- Turner, D. G. 2010, Ap&SS, 326, 219
- Valdes, F. 1993, “Guide to the Slit Spectra Reduction Task DOSLIT” (available at <http://iraf.net/irafdocs/doslit.pdf>)
- Van den Bergh, S. 1984, Astrophysics and Space Science, 102, 295

- van Dyck, H. M. et al. 1998, AJ, 116, 981
- Wawrukiewicz, A. S. & Lee, T. A. 1974, PASP, 86, 51
- Weaver, T.A., Zimmerman, G. B., & Woosley, S. E. 1978 ApJ, 225, 1021
- Weiner, J. et al. 2003, ApJ, 589, 976
- White, N. M. & Wing, R. F. 1978, ApJ, 222, 209
- Wilson, R. W. et al. 1992, MNRAS, 257, 369
- Wroblewski, A. 1961, Uranke, 32, 1
- Yang, S. L. S. et al. 1999, ASP Conf. Series, 185, 228
- Yang, M. & Jiang, B. W. 2011, ApJ, 727, 53
- Yeşilyaprak, C. & Aslan, Z. 2004, MNRAS, 355, 601

## Appendix A

### Spectra

The following figures show individual spectra for each star (DAO CCD and scanned DAO photographic). Each spectrum is labelled with the observation year and a close-up of the wavelength region used for luminosity classification is shown to the right of the entire spectrum. Observation years of 2005-2010 correspond to CCD spectra; years earlier than 2005 correspond to scanned photographic spectra.

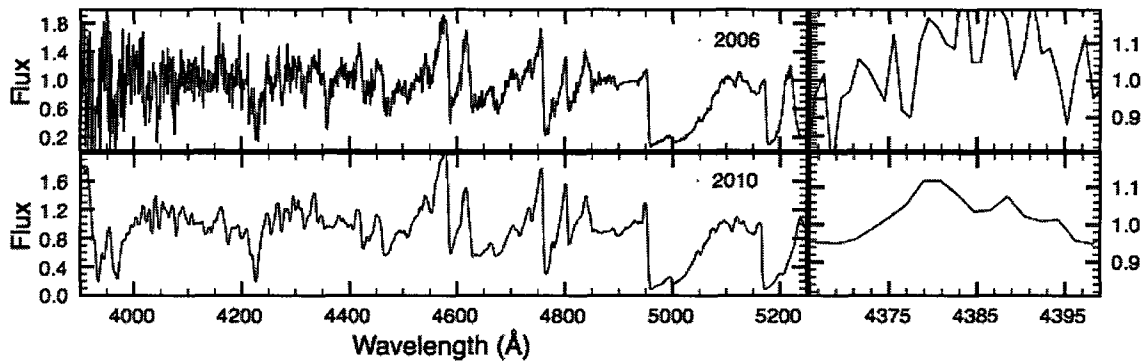


**Figure A.1:** SS Andromedae

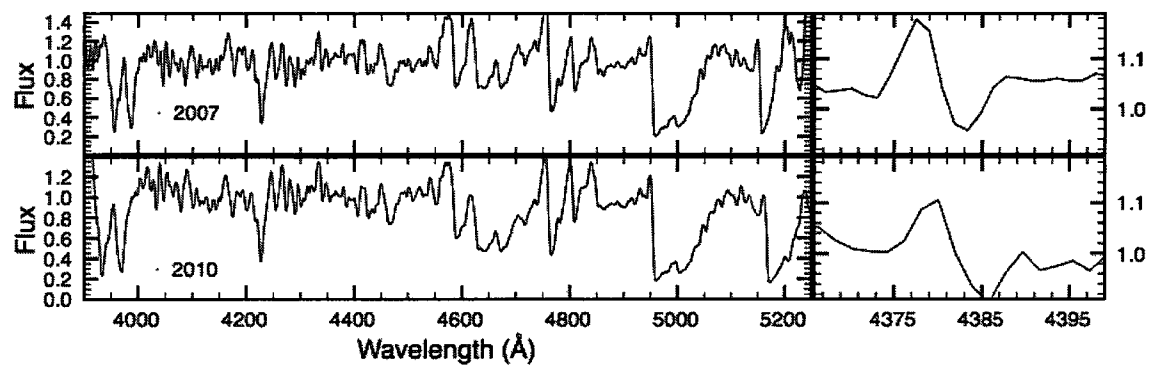


Figure A.2: UX Aurigae

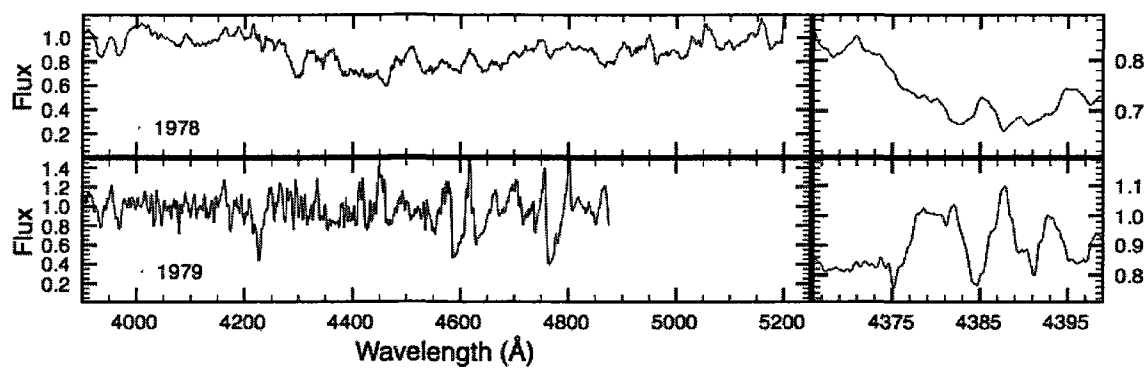
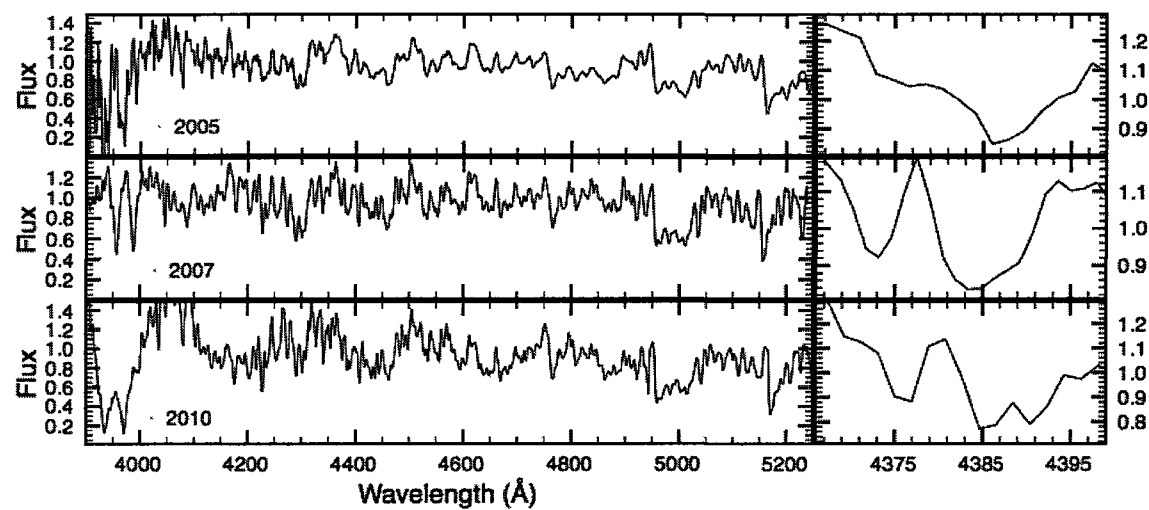


Figure A.3: RS Cancri



**Figure A.4:** PZ Casseopeiae

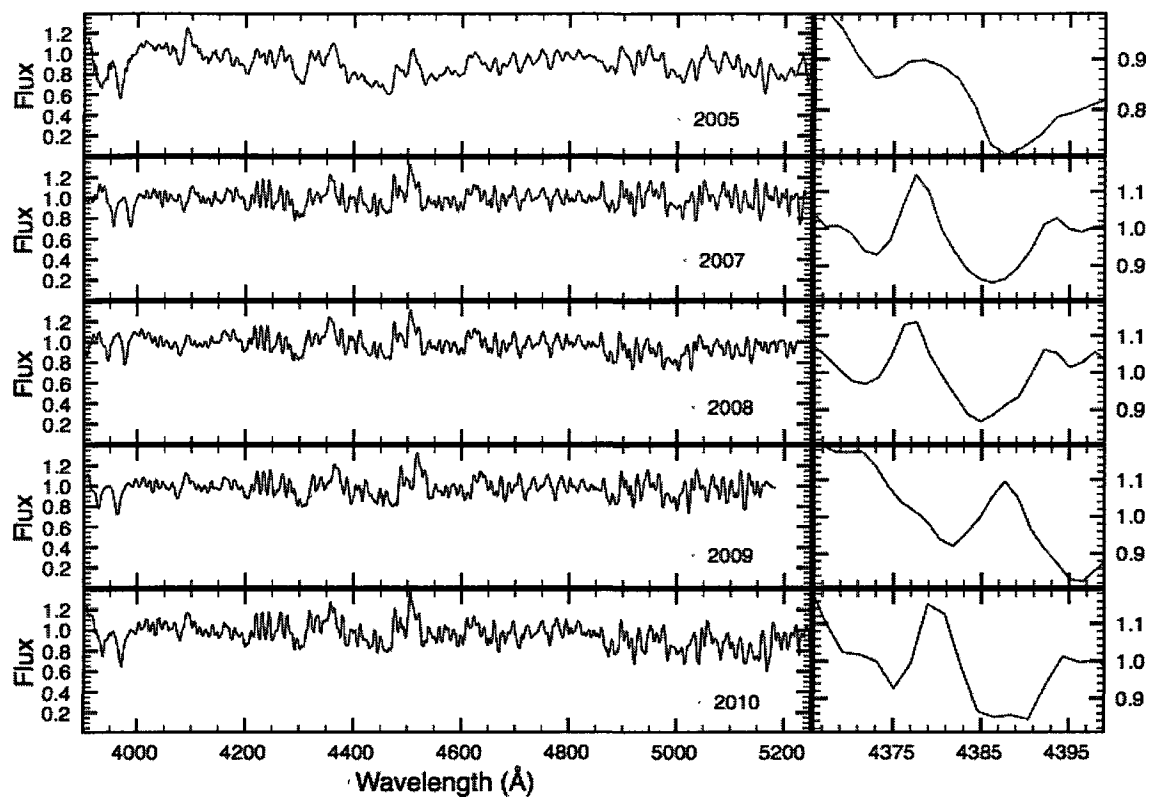


Figure A.5: W Cephei

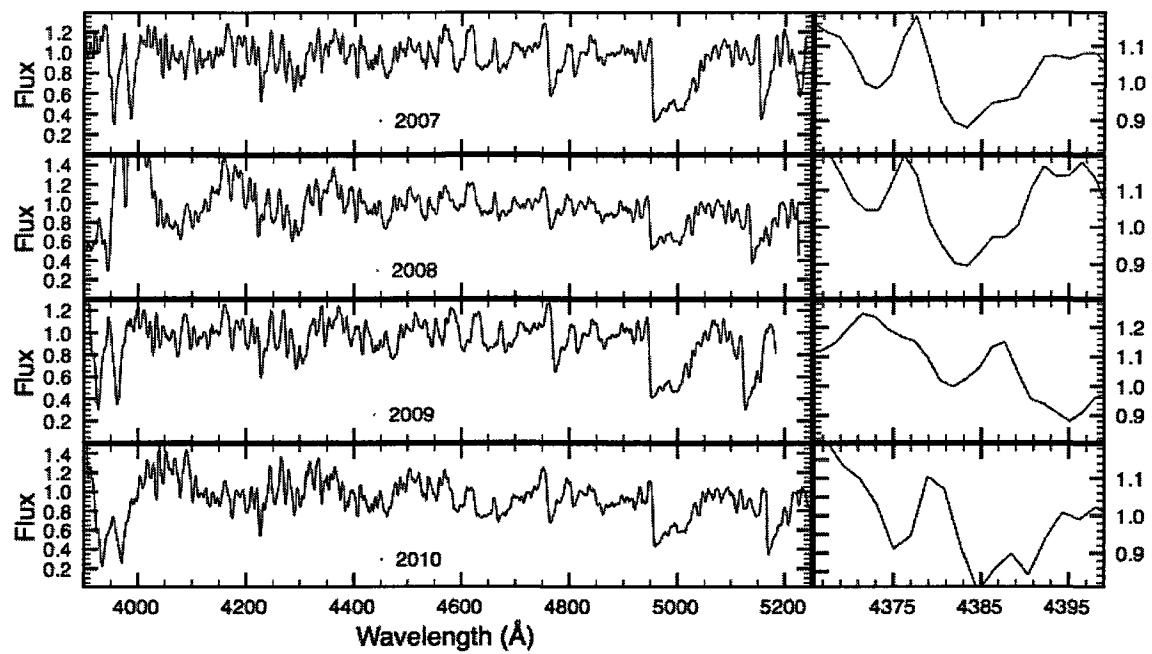


Figure A.6: SW Cephei

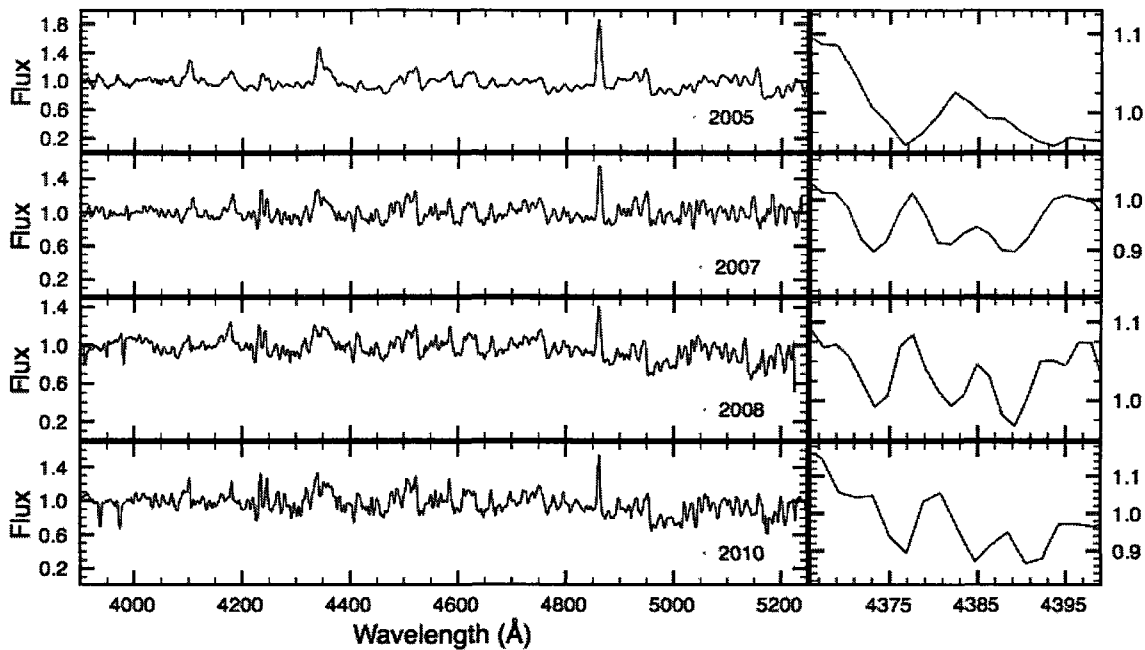


Figure A.7: VV Cephei

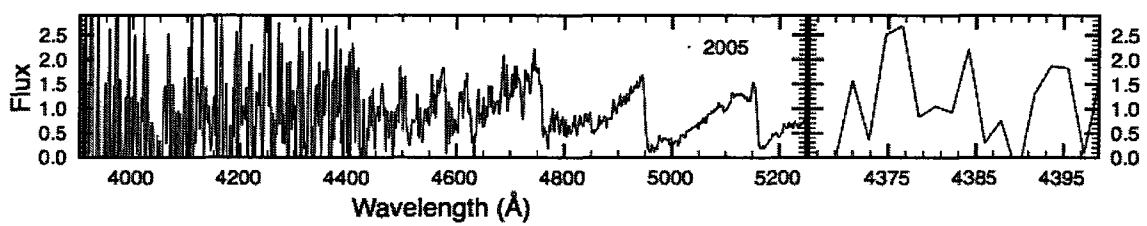


Figure A.8: MY Cephei

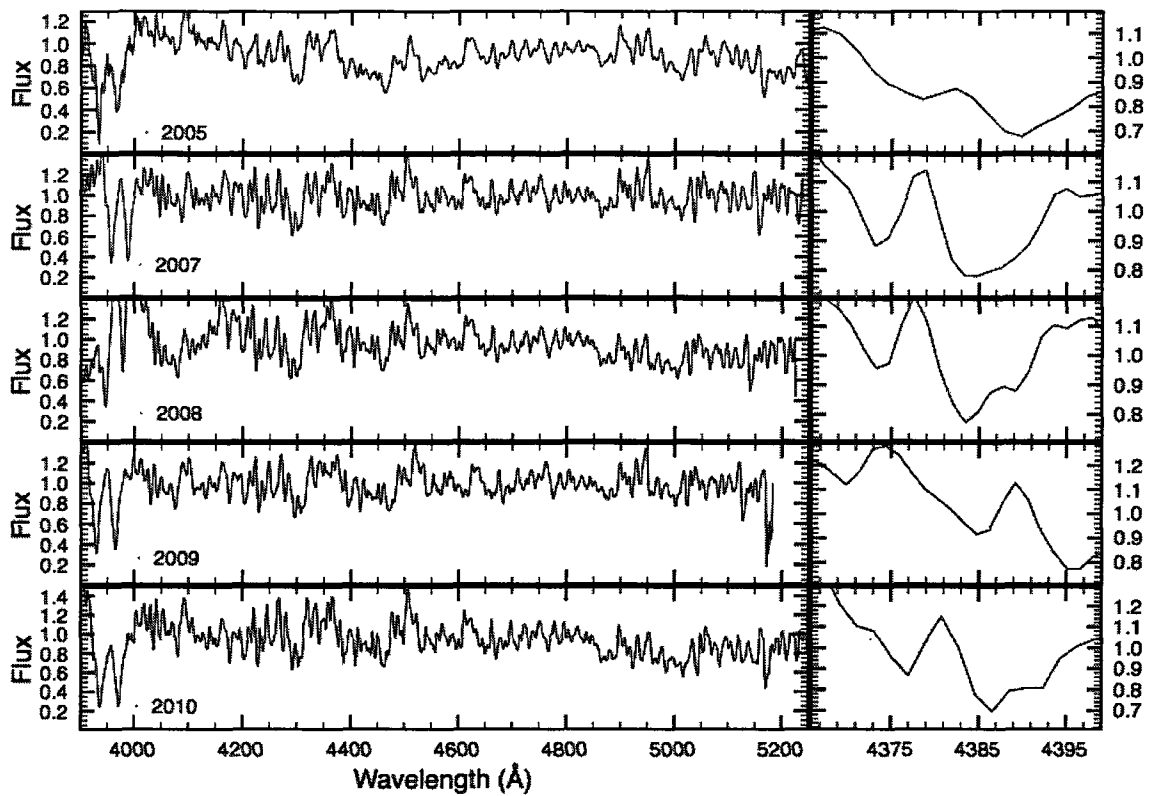


Figure A.9:  $\mu$  Cephei

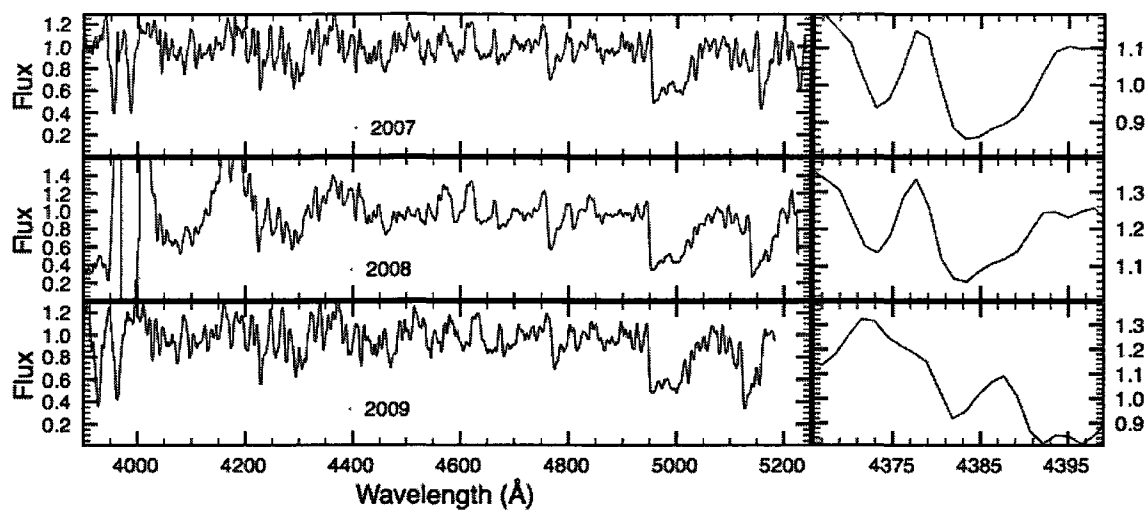


Figure A.10: RW Cygni

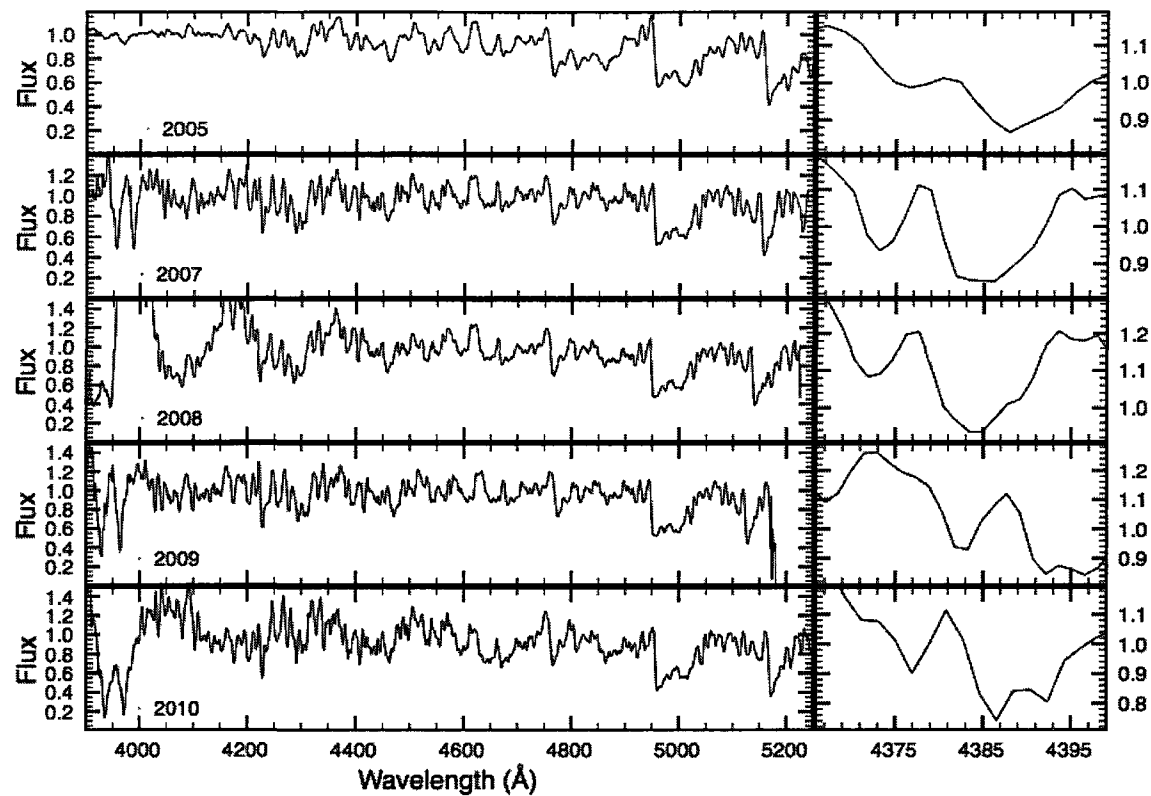


Figure A.11: AZ Cygni

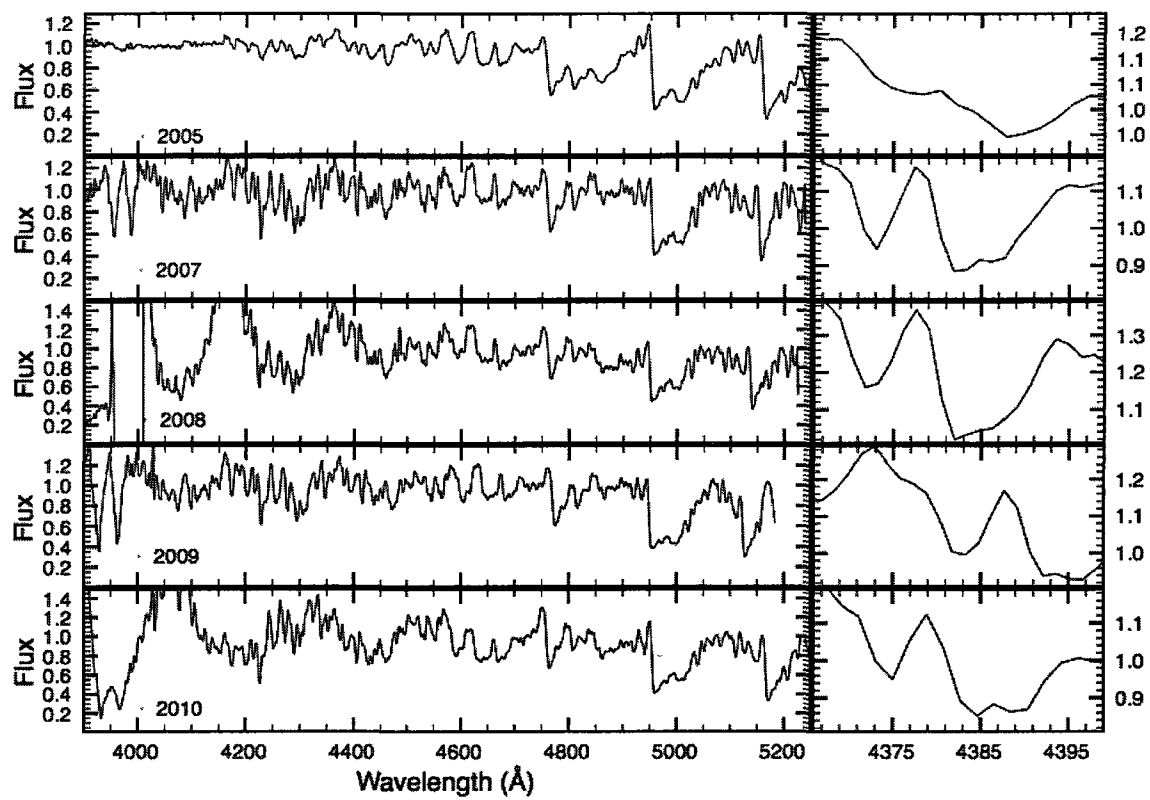


Figure A.12: BC Cygni

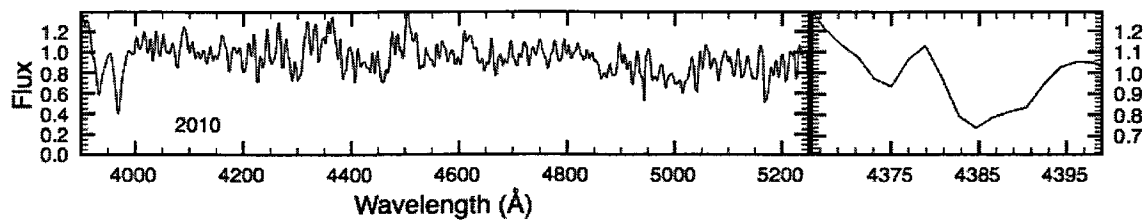


Figure A.13: TV Geminorum

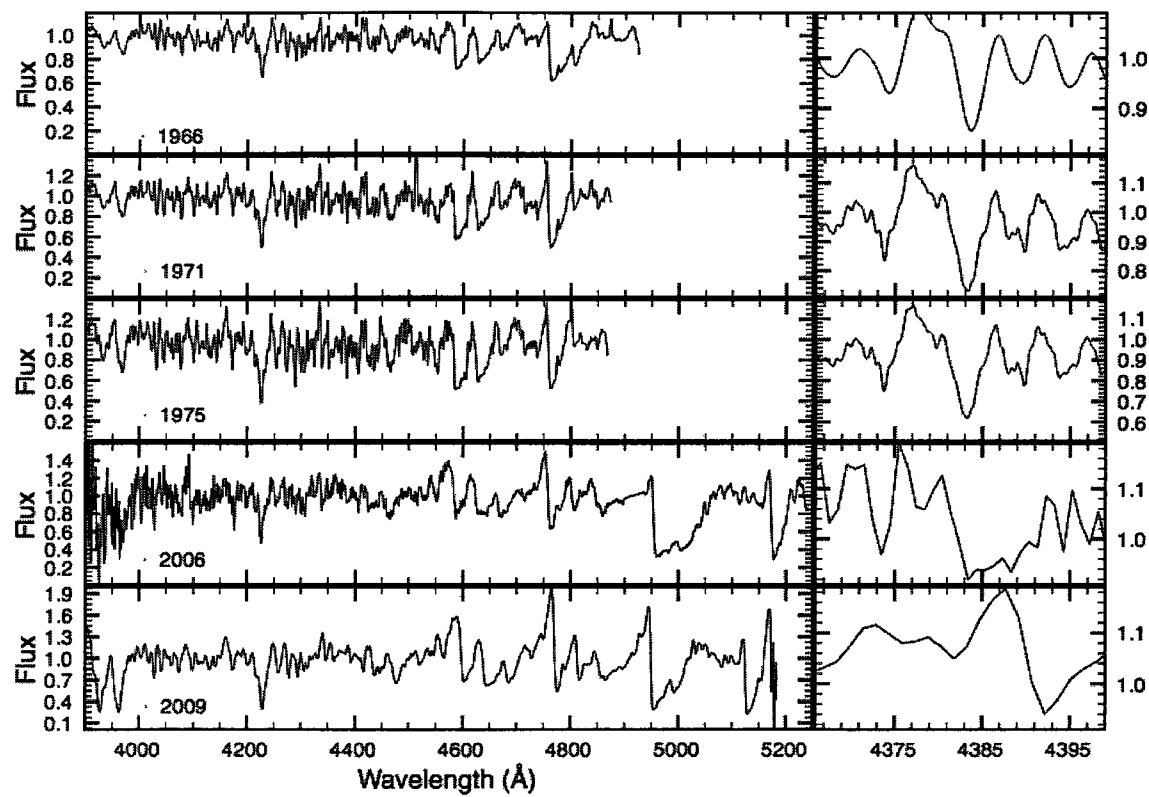


Figure A.14:  $\alpha$  Herculis

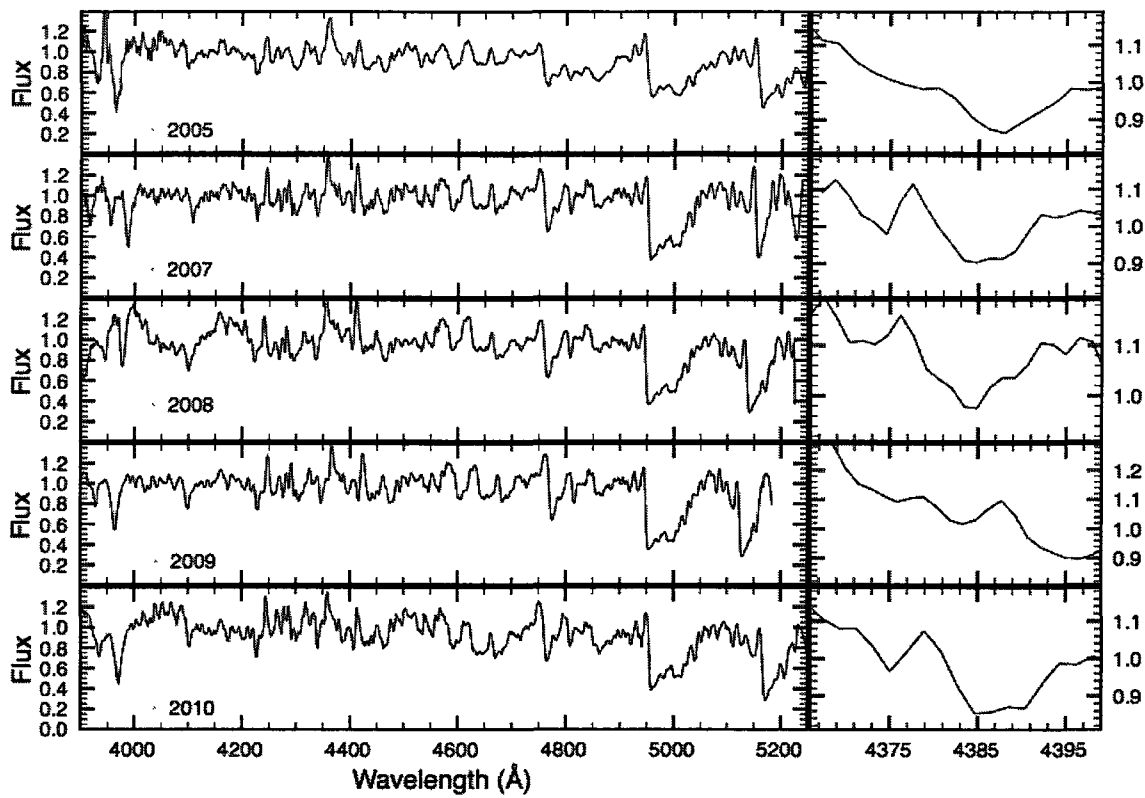


Figure A.15: U Lacertae

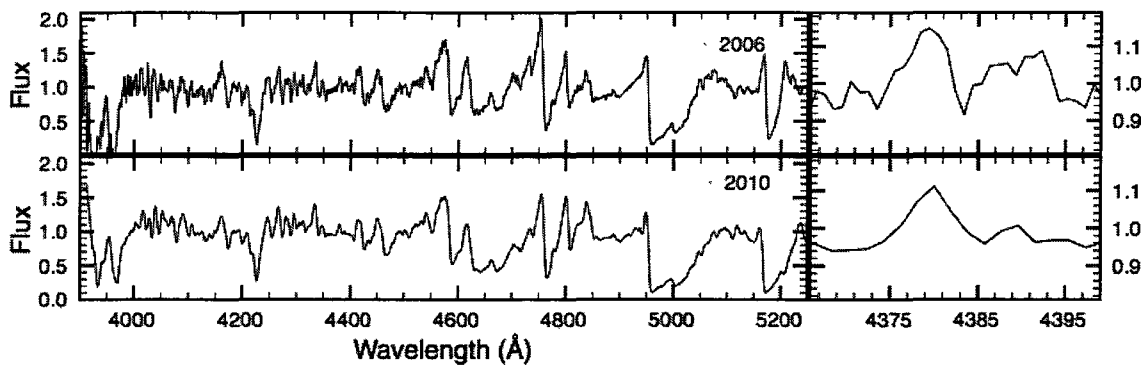


Figure A.16: Y Lyncis

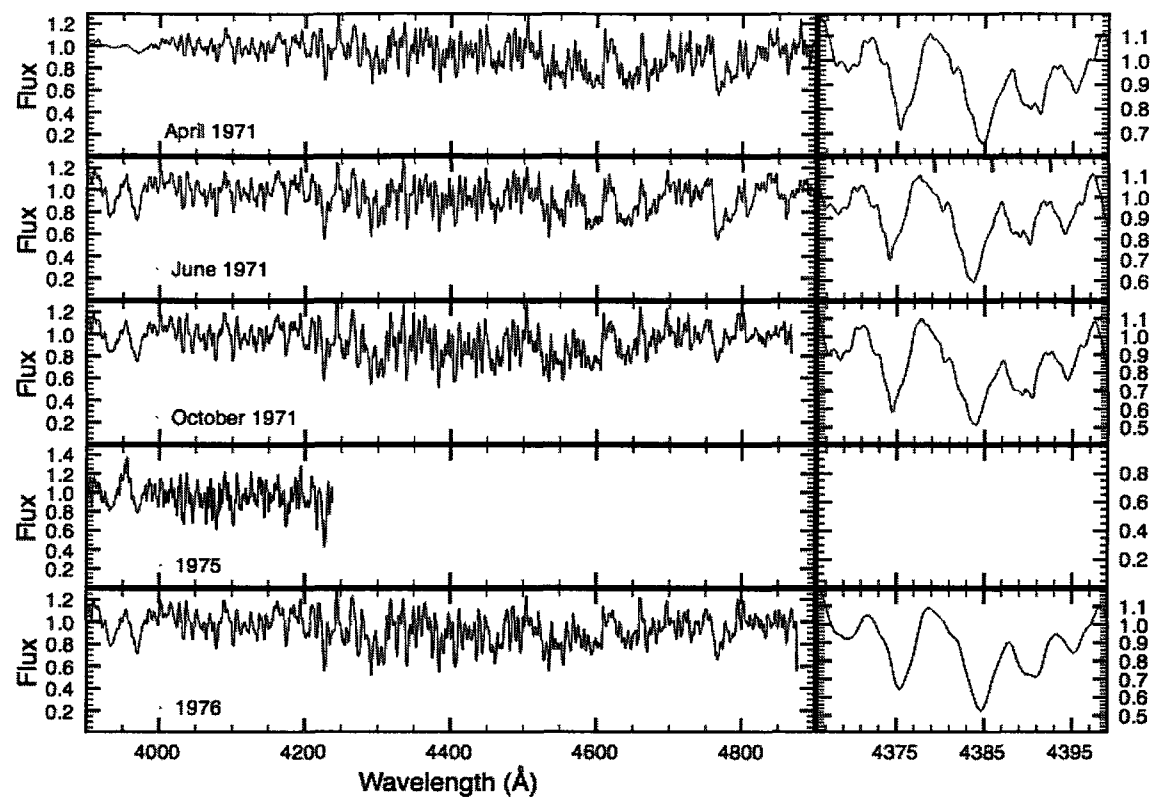


Figure A.17:  $\alpha$  Orionis

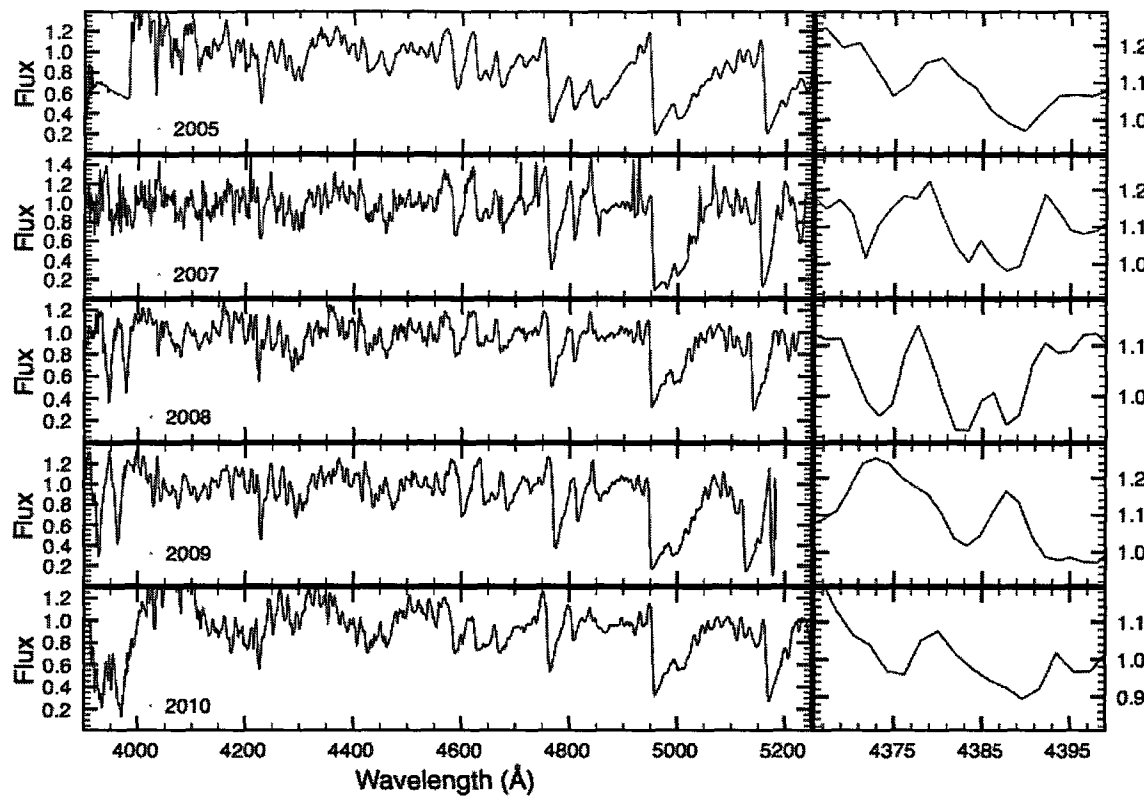


Figure A.18: S Persei

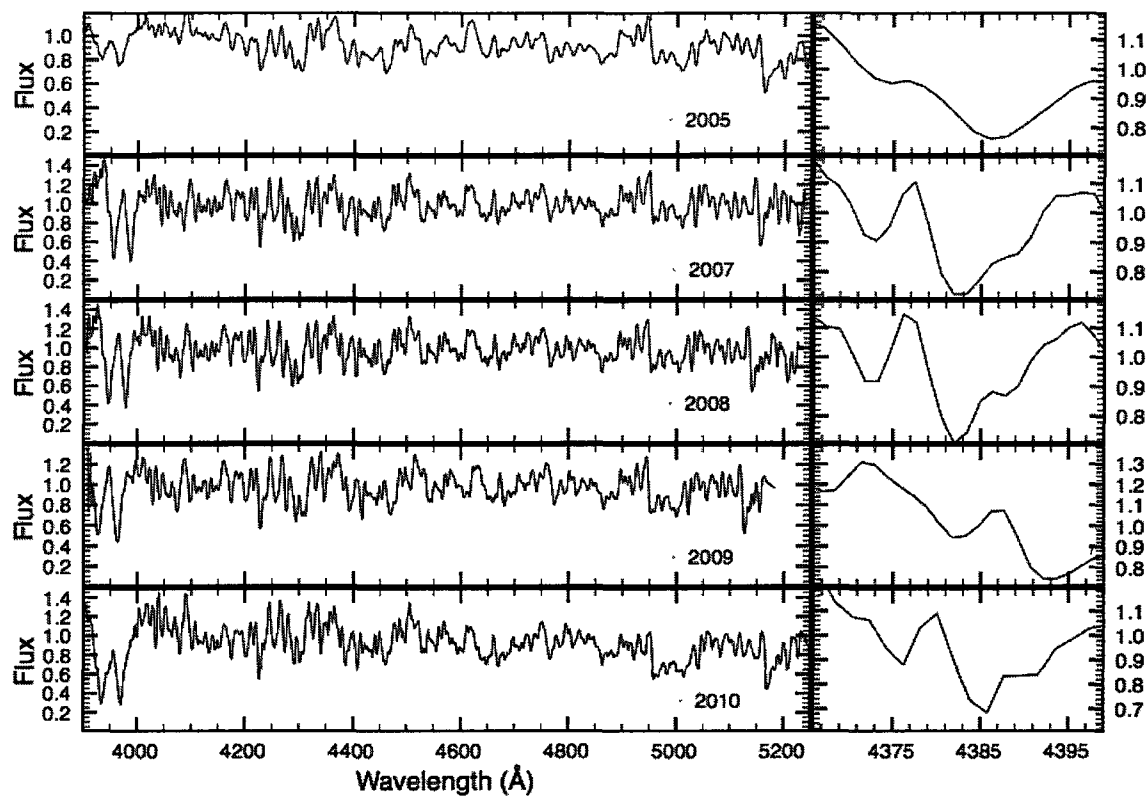


Figure A.19: T Persei

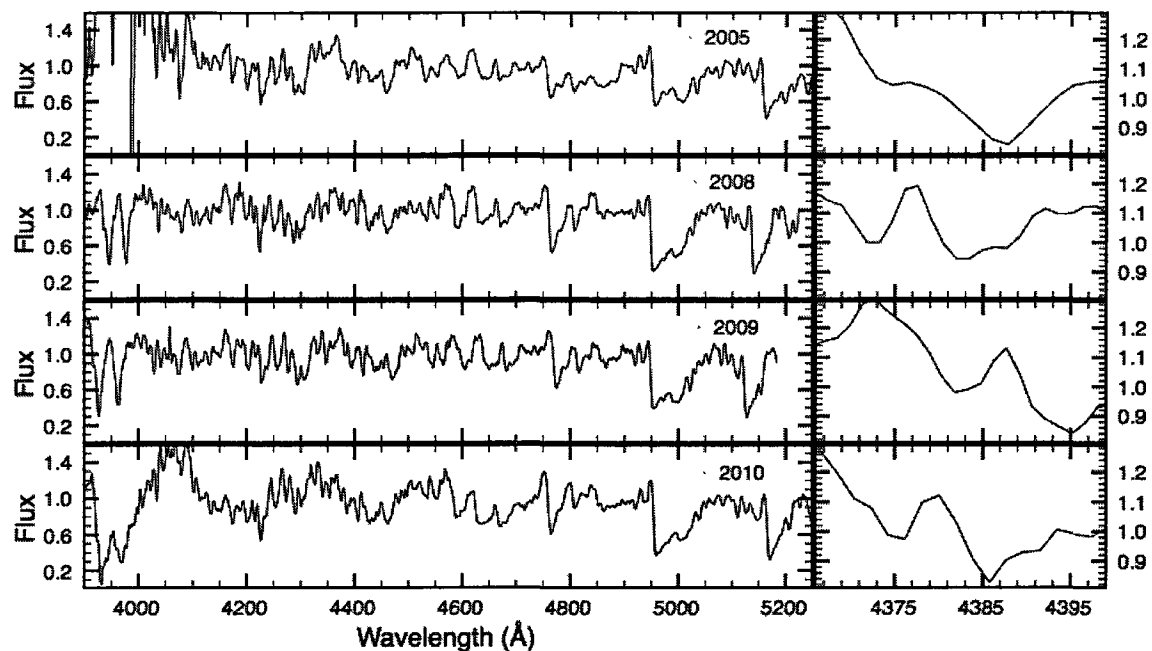


Figure A.20: W Persei

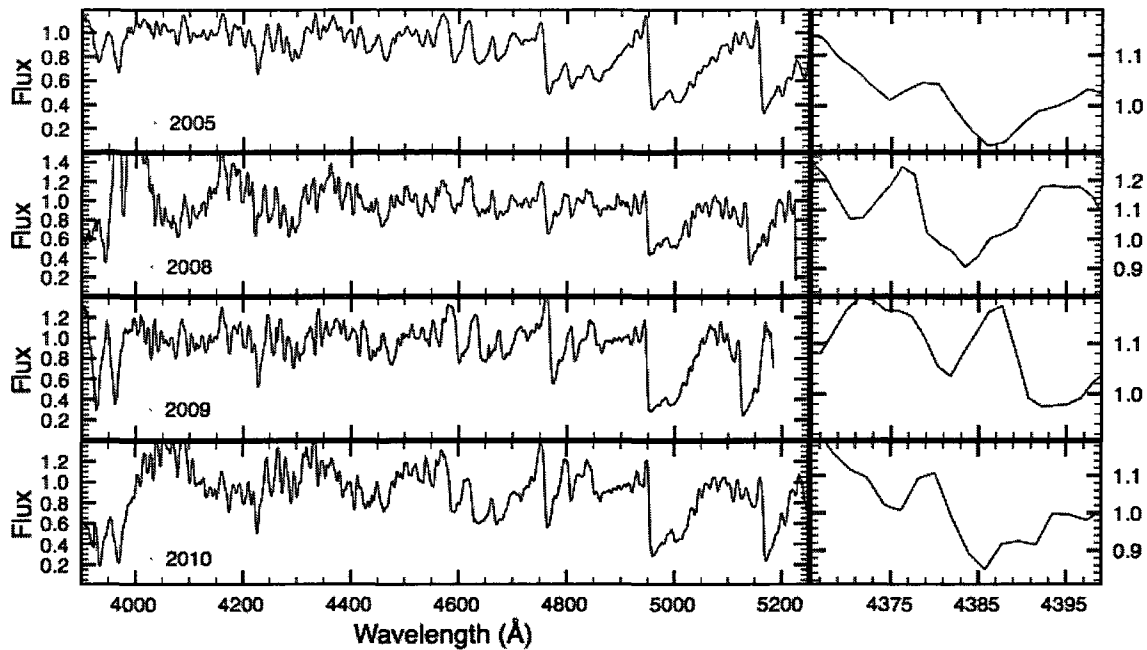


Figure A.21: RS Persei

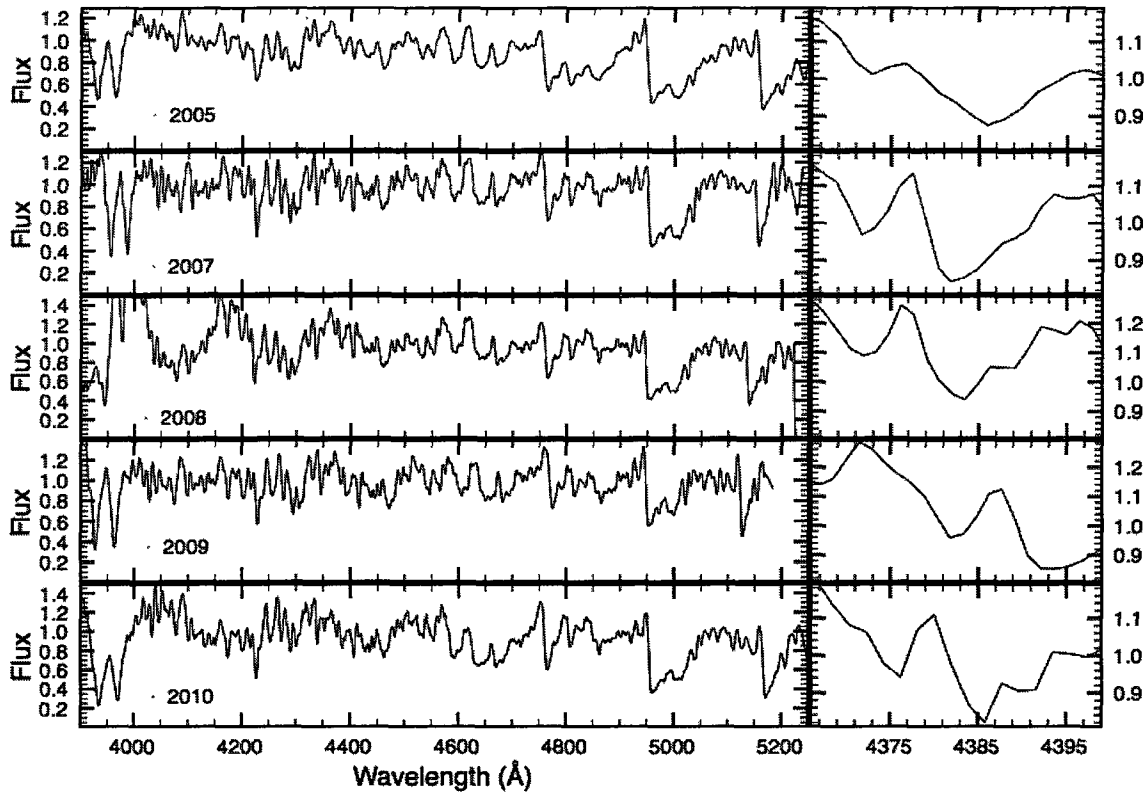


Figure A.22: SU Persei

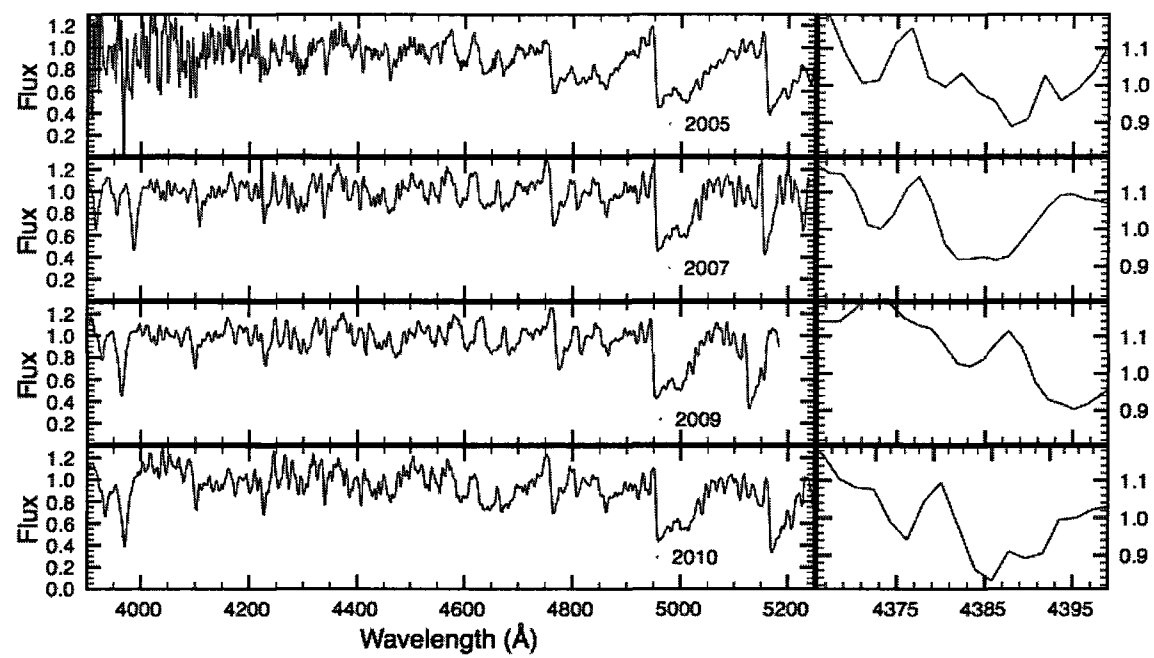


Figure A.23: XX Persei

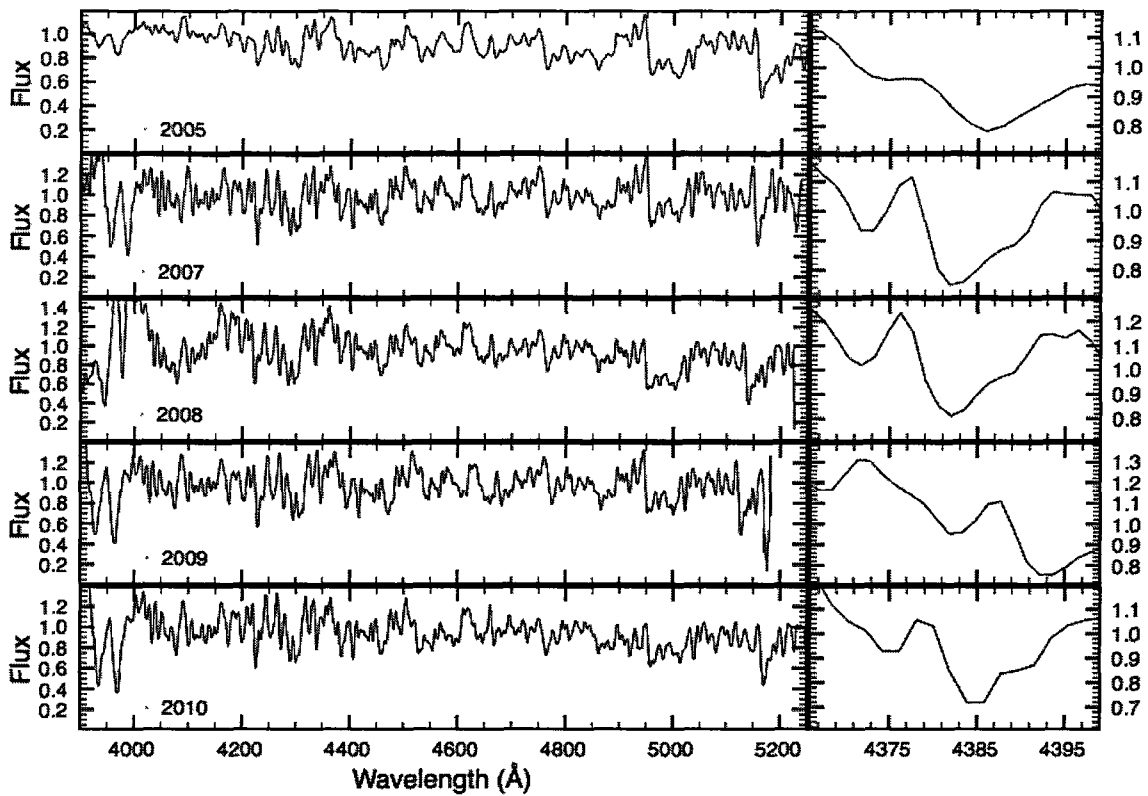


Figure A.24: AD Persei

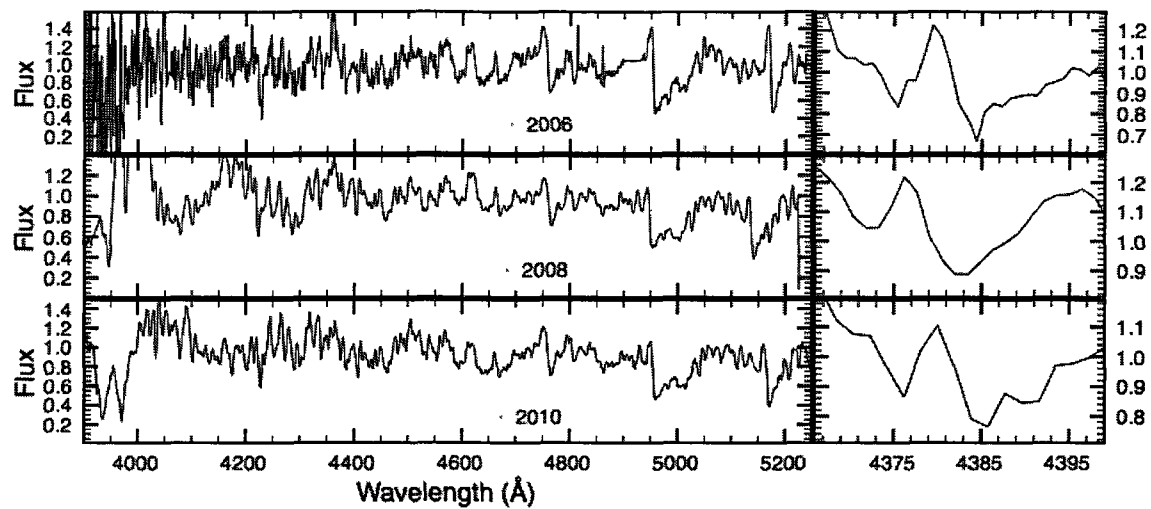


Figure A.25: BU Persei

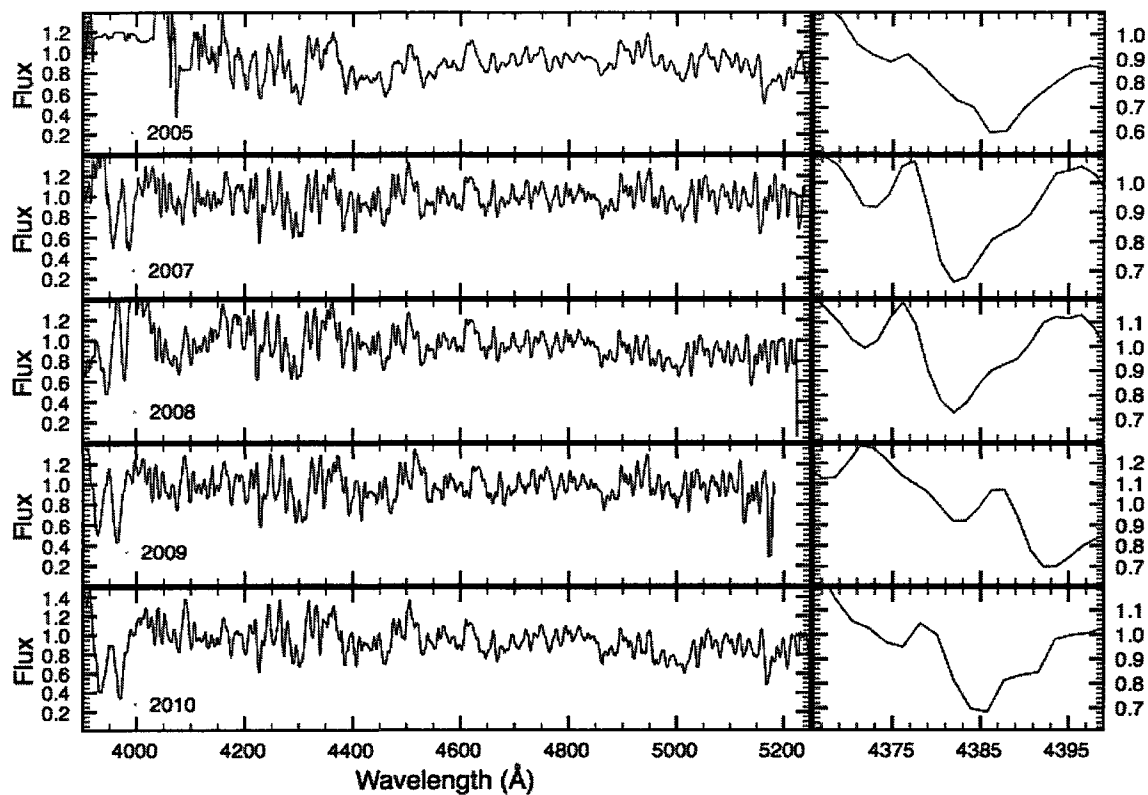


Figure A.26: FZ Persei

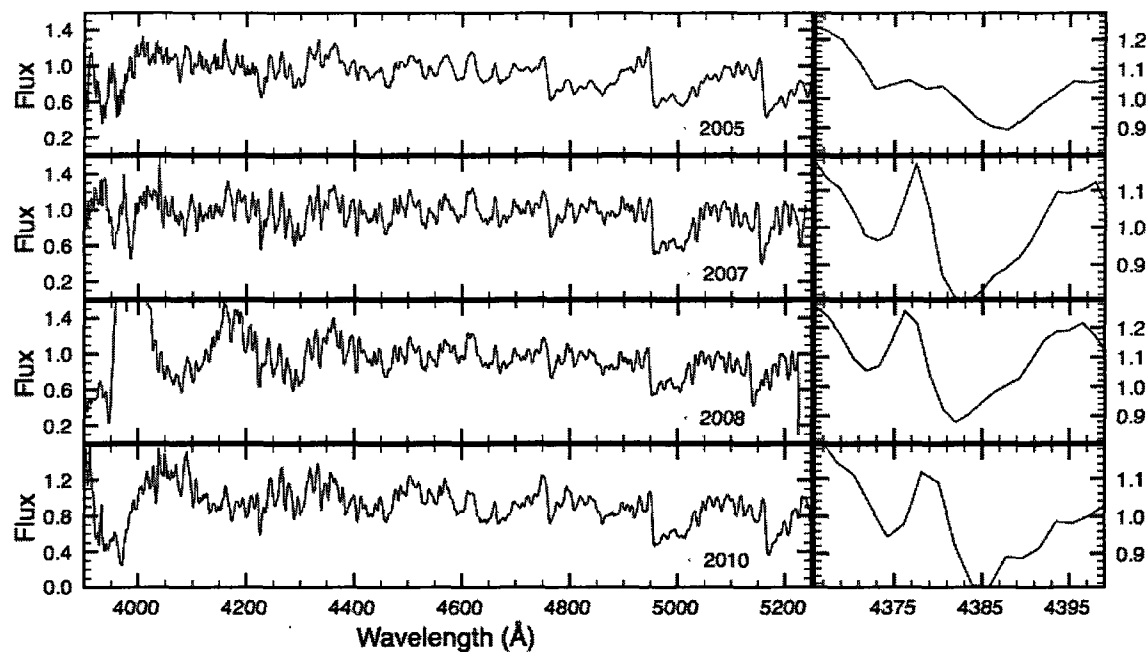


Figure A.27: V411 Persei

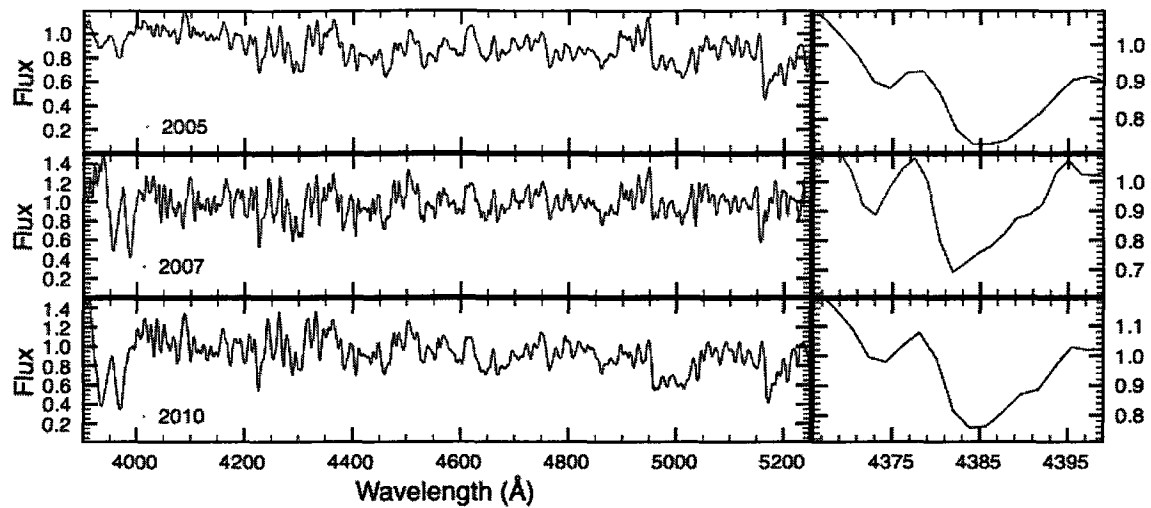
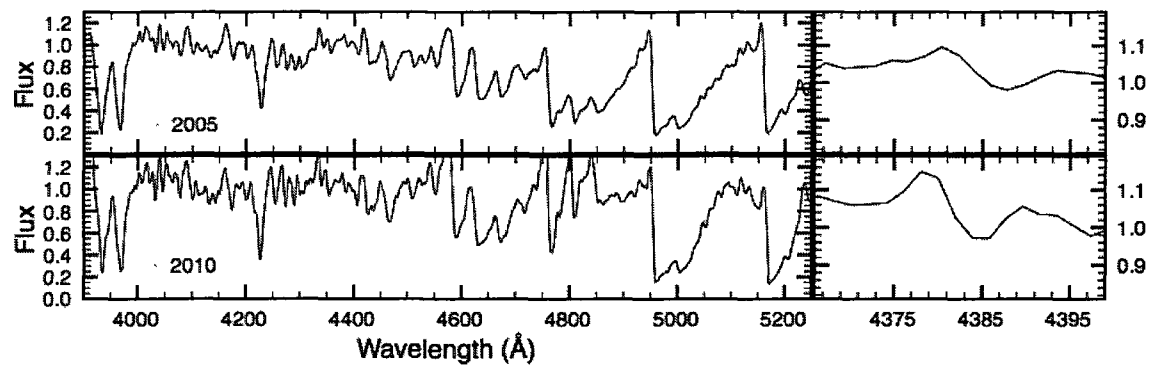


Figure A.28: CE Tauri



**Figure A.29:** W Triangulum

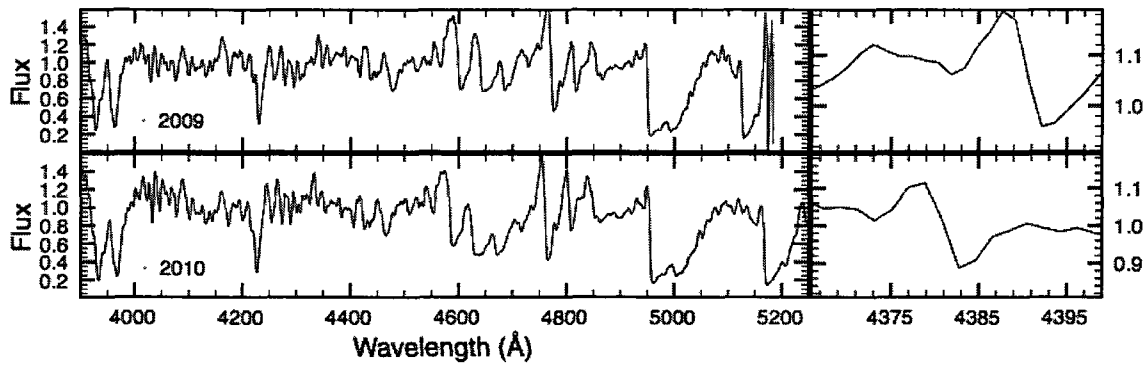
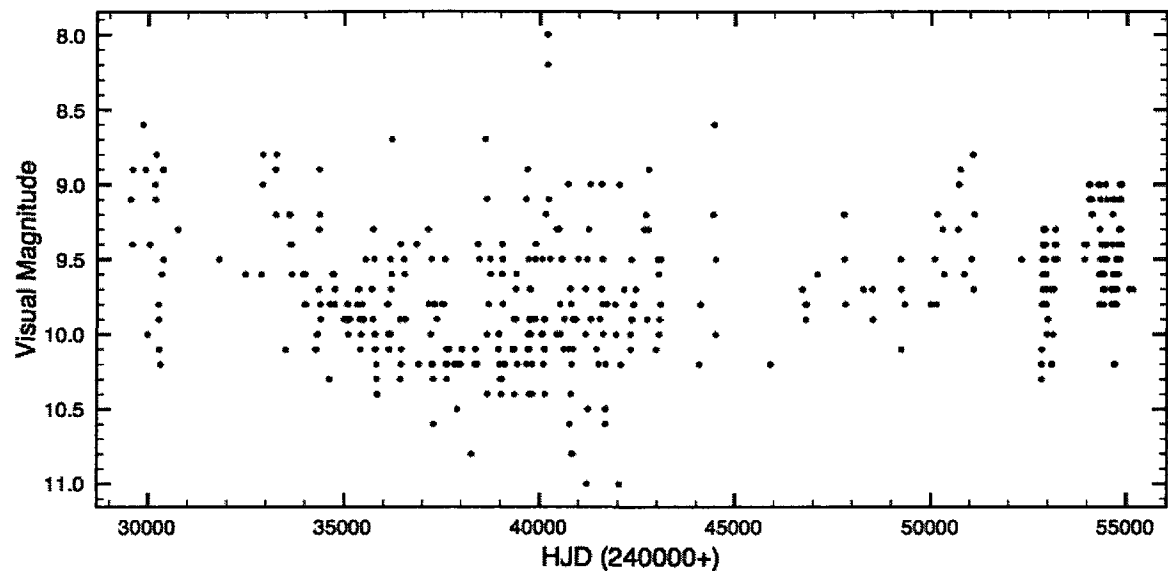


Figure A.30: FG Vulpeculae

## Appendix B

### Light Curves



**Figure B.1:** SS Andromedae visual (AAVSO) light curve.

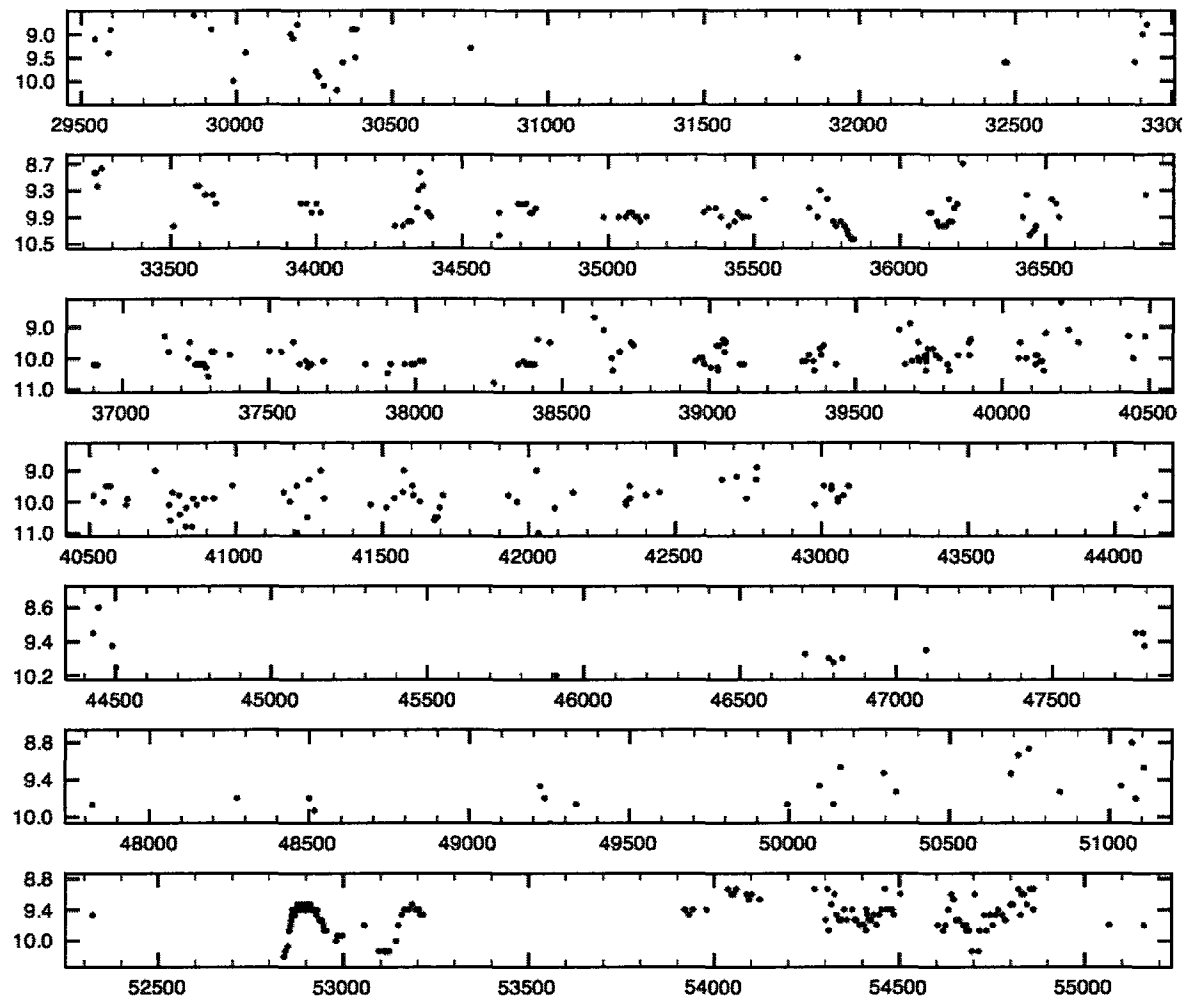


**Figure B.2:** SS Andromedae visual (AAVSO) light curve - expanded view of figure B.1.

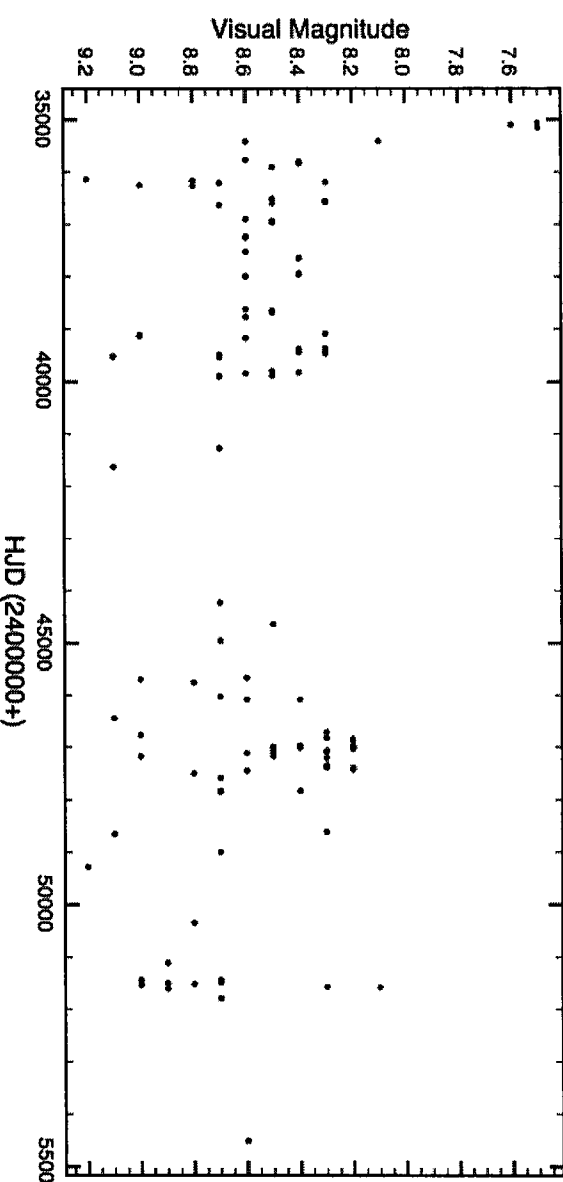
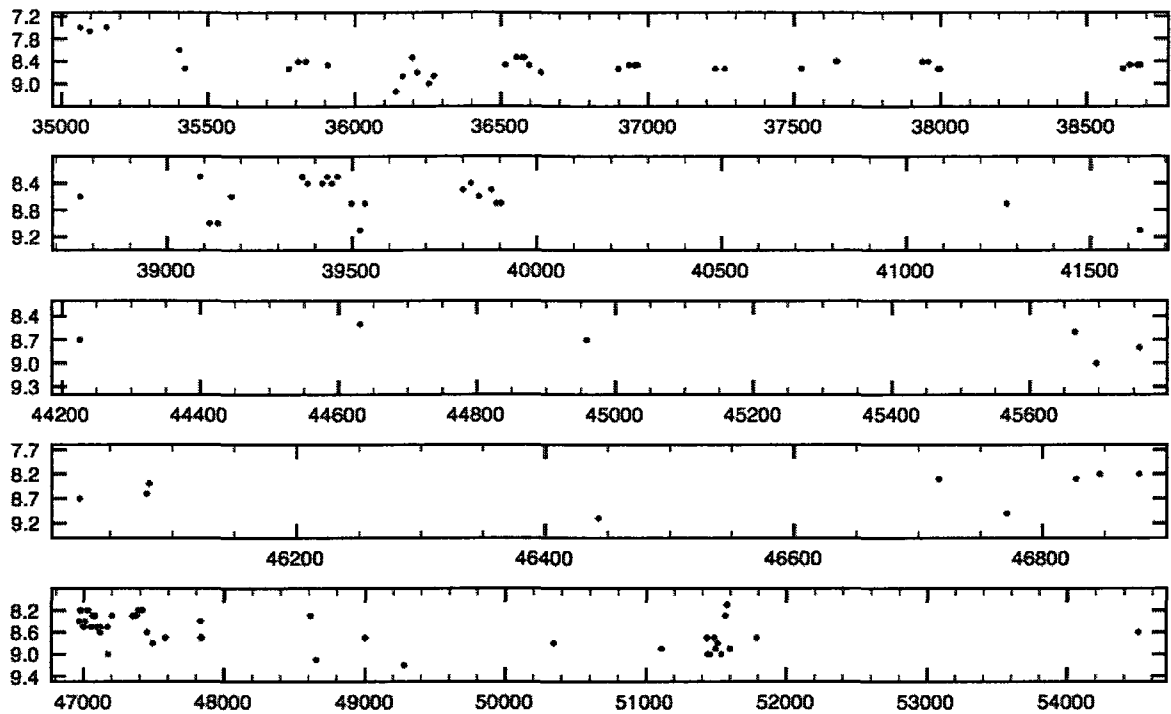


Figure B.3: V Arietis visual (AAVSO) light curve.



**Figure B.4:** V Arietis visual (AAVSO) light curve - expanded view of figure B.3.

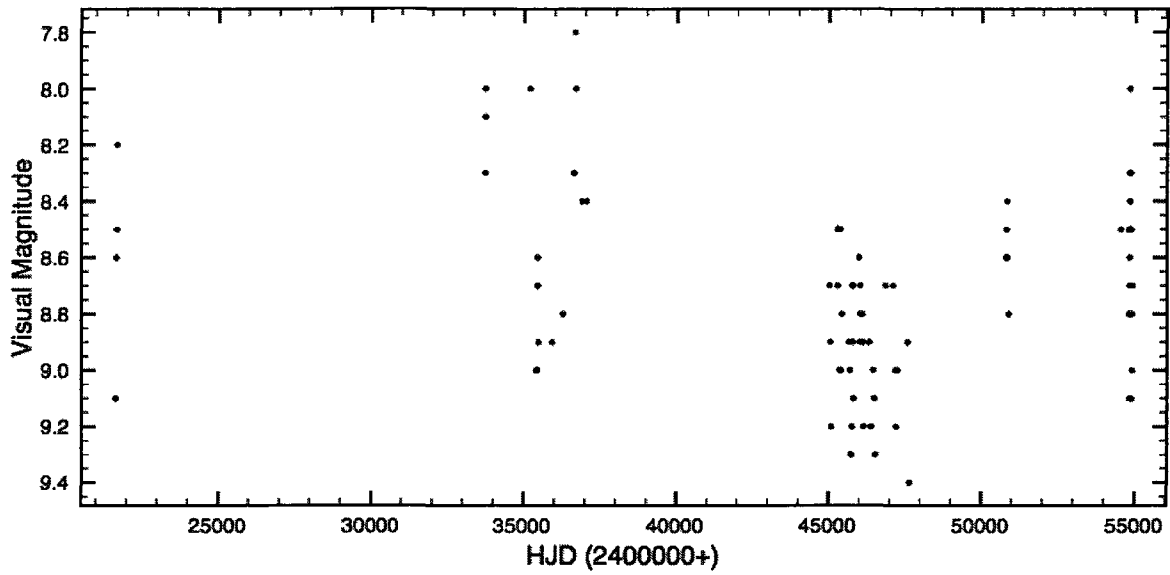
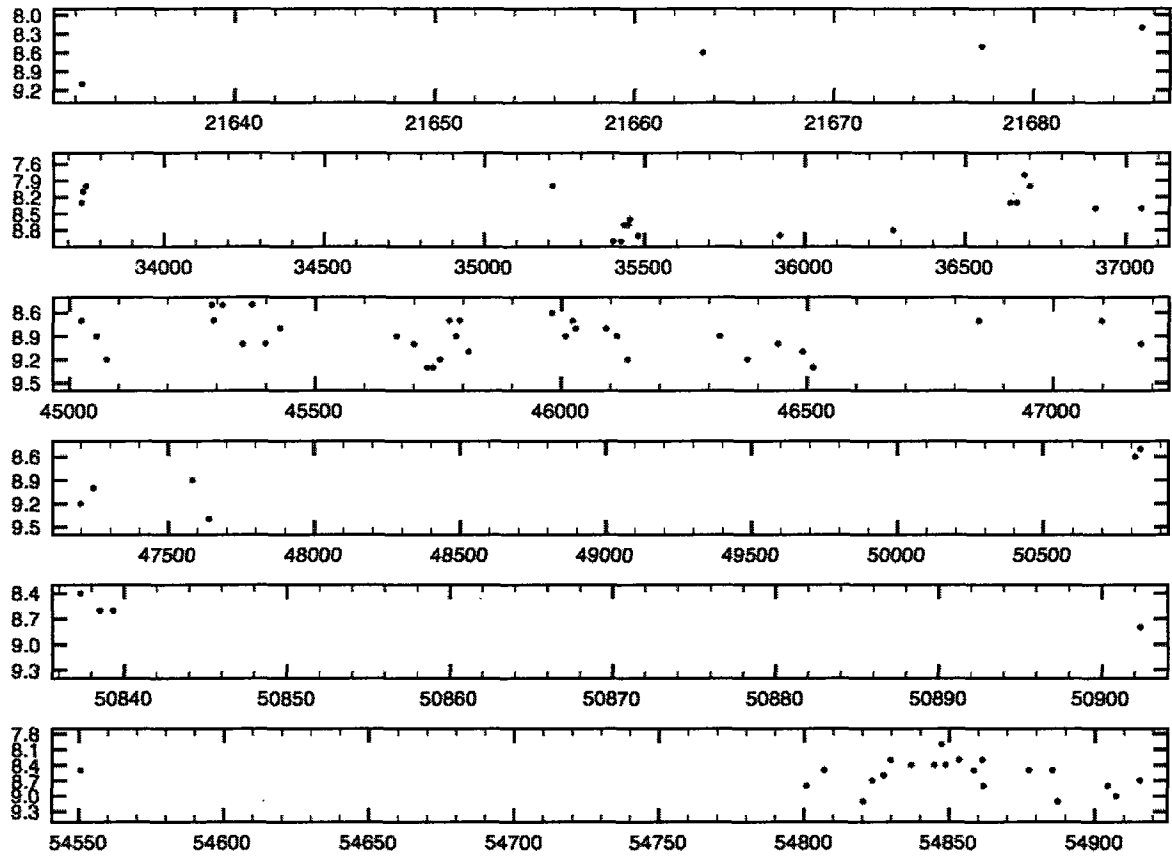
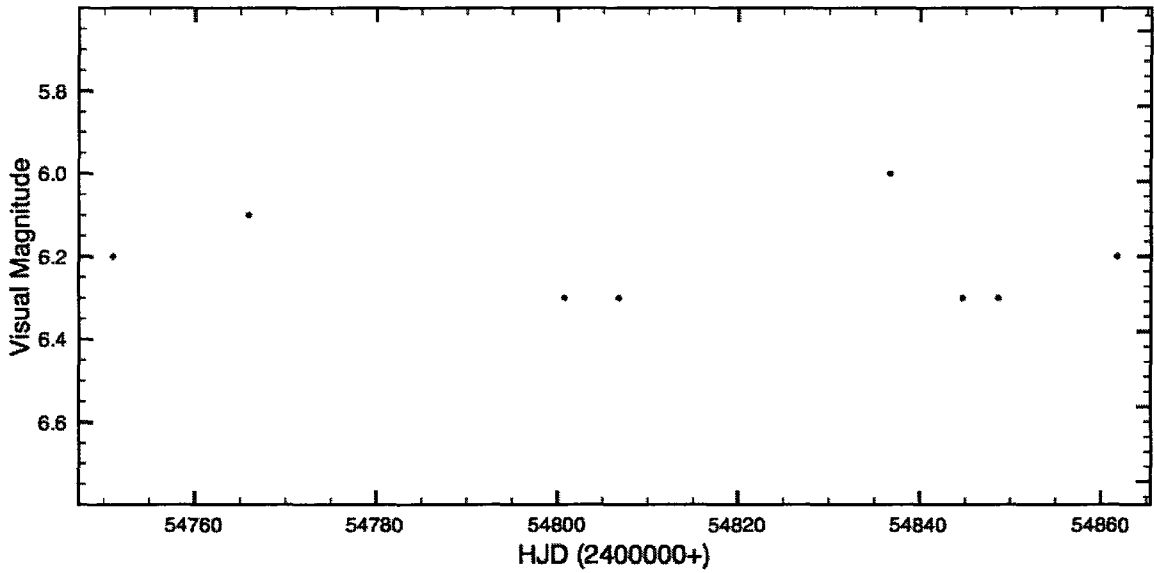


Figure B.5: UX Aurigae visual (AAVSO) light curve.



**Figure B.6:** UX Aurigae visual (AAVSO) light curve - expanded view of figure B.5.



**Figure B.7:** V394 Aurigae visual (AAVSO) light curve.

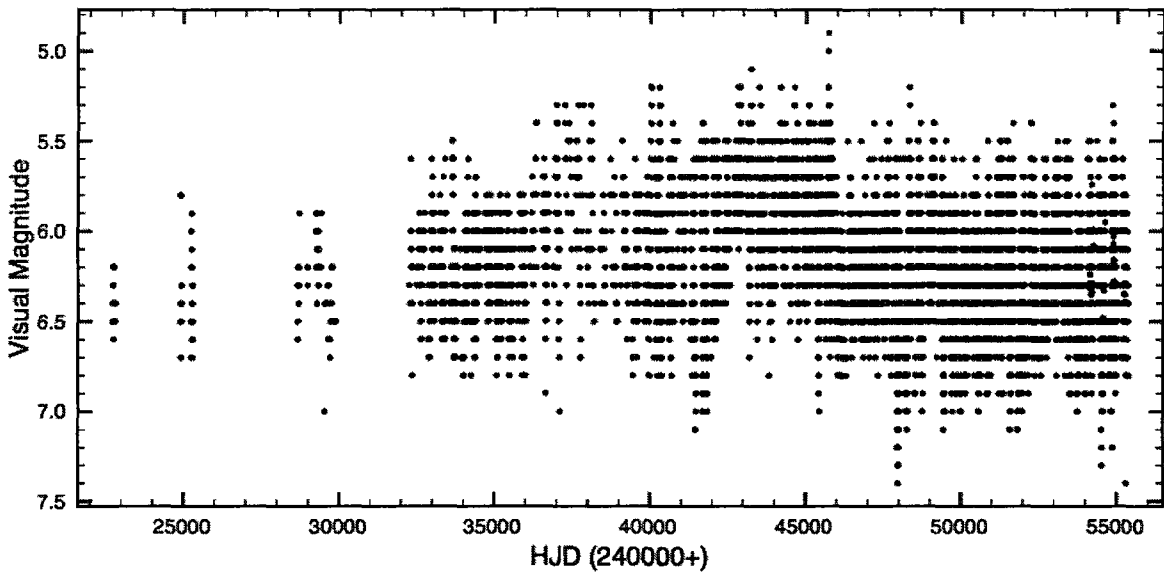
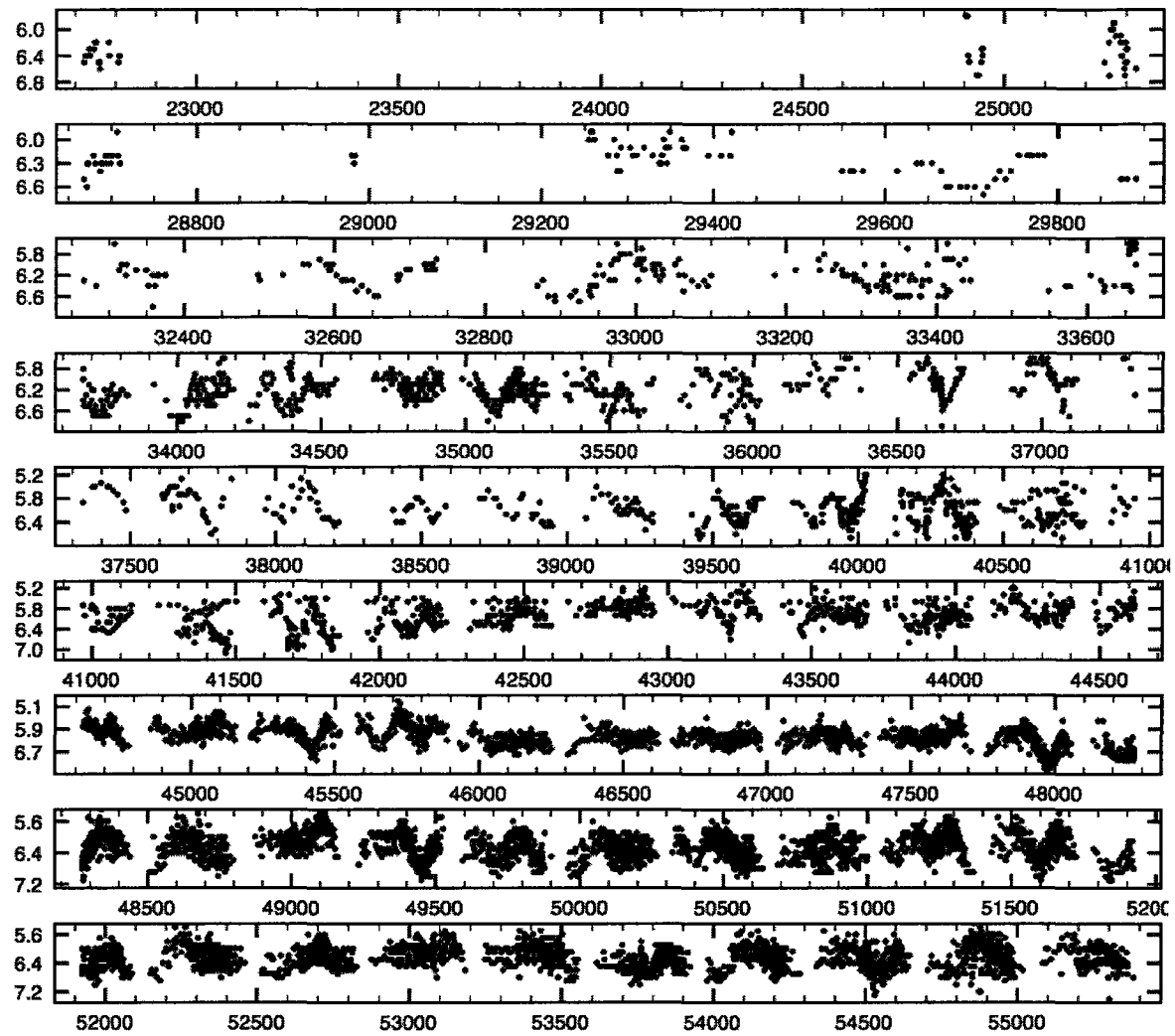


Figure B.8: RS Cancri visual (AAVSO) light curve.



**Figure B.9:** RS Cancri visual (AAVSO) light curve - expanded view of figure B.8.

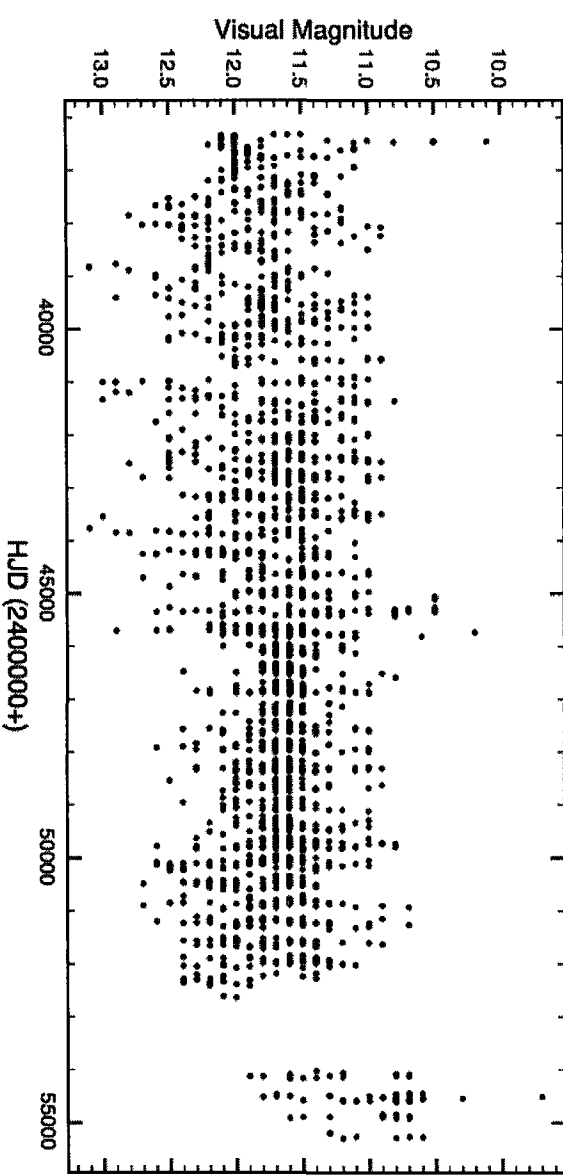


Figure B.10: UZ Canis Majoris visual (AAVSO) light curve.

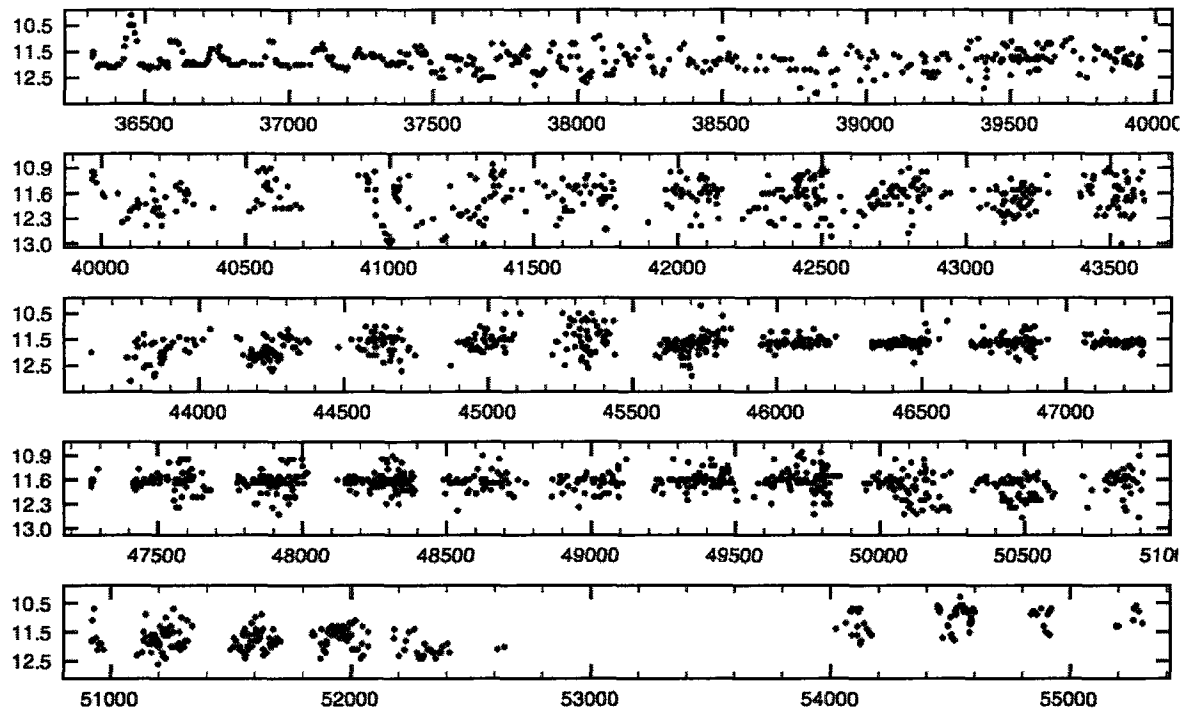
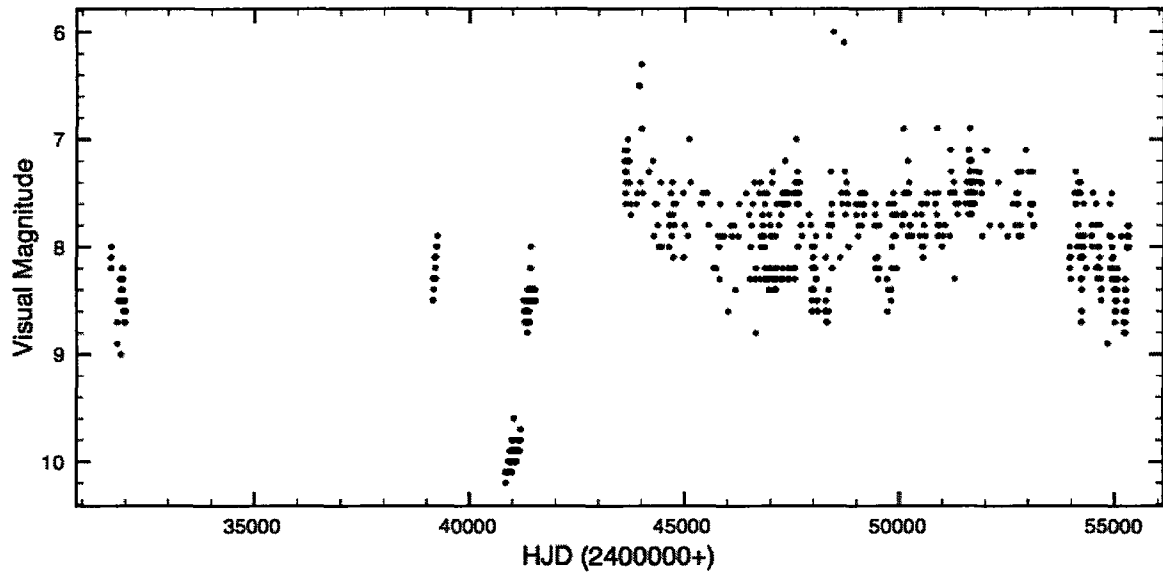
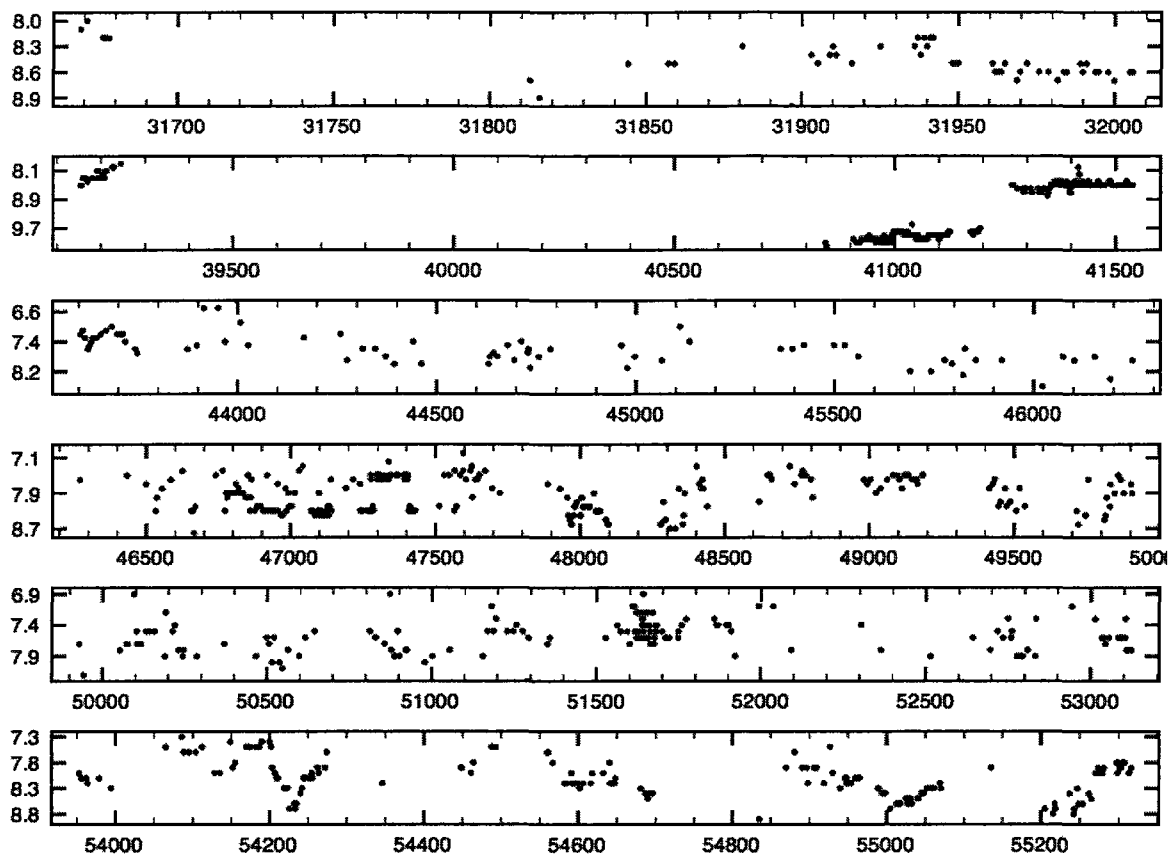


Figure B.11: UZ Canis Majoris visual (AAVSO) light curve - expanded view of figure B.10.



**Figure B.12:** BZ Carinae visual (AAVSO) light curve.



**Figure B.13:** BZ Carinae visual (AAVSO) light curve - expanded view of figure B.12.

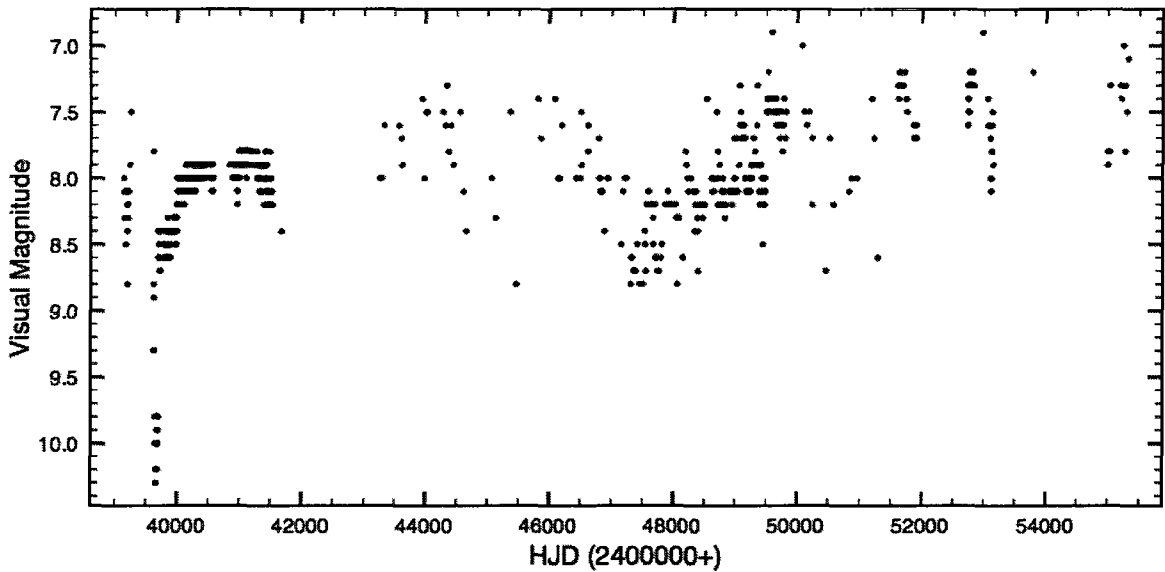


**Figure B.14:** CK Carinae visual (AAVSO) light curve.

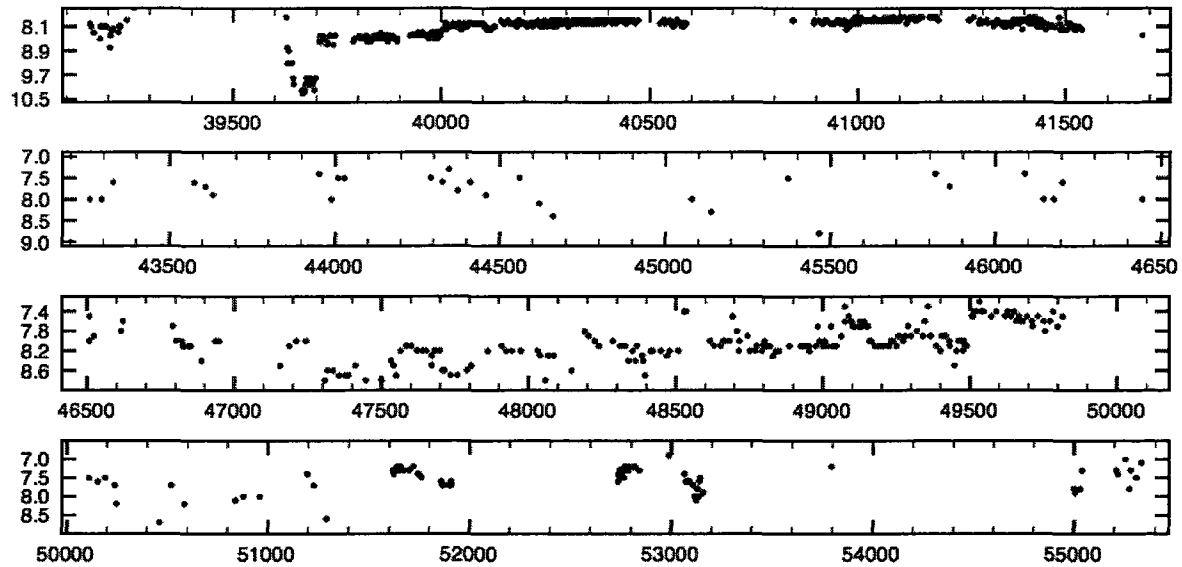


**Figure B.15:** CK Carinae visual (AAVSO) light curve - expanded view of figure B.14.

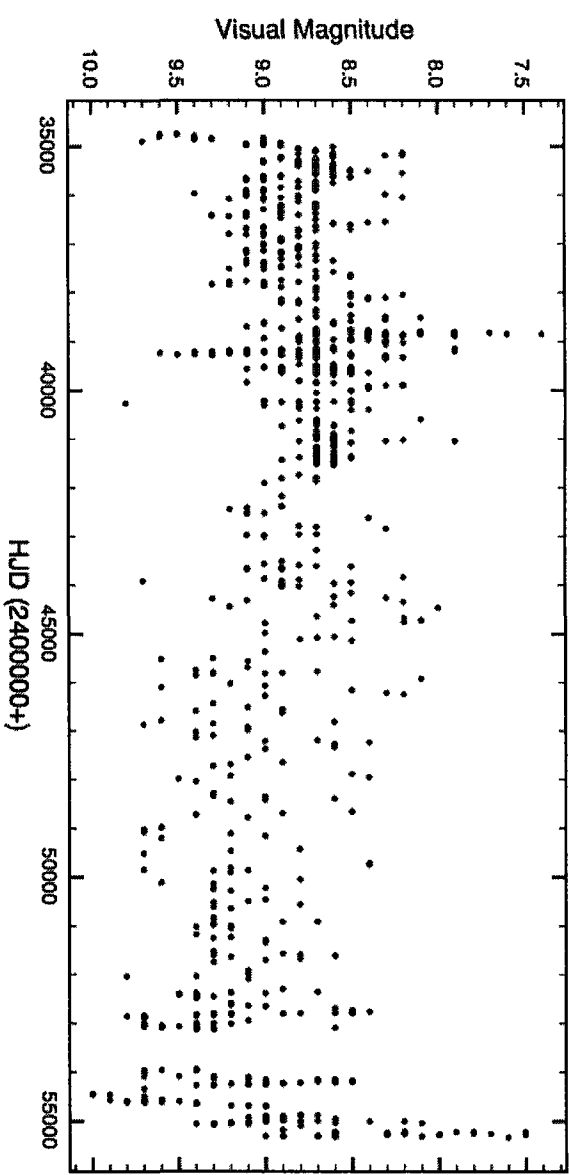
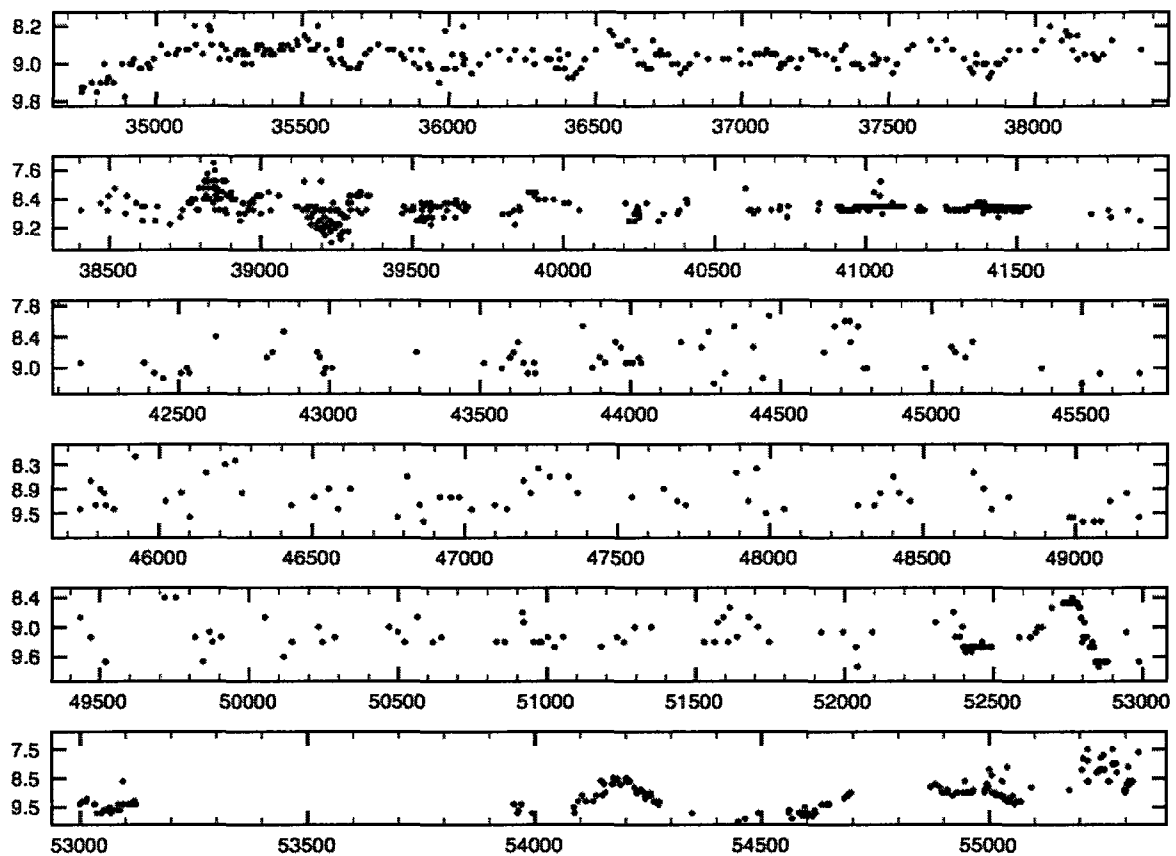
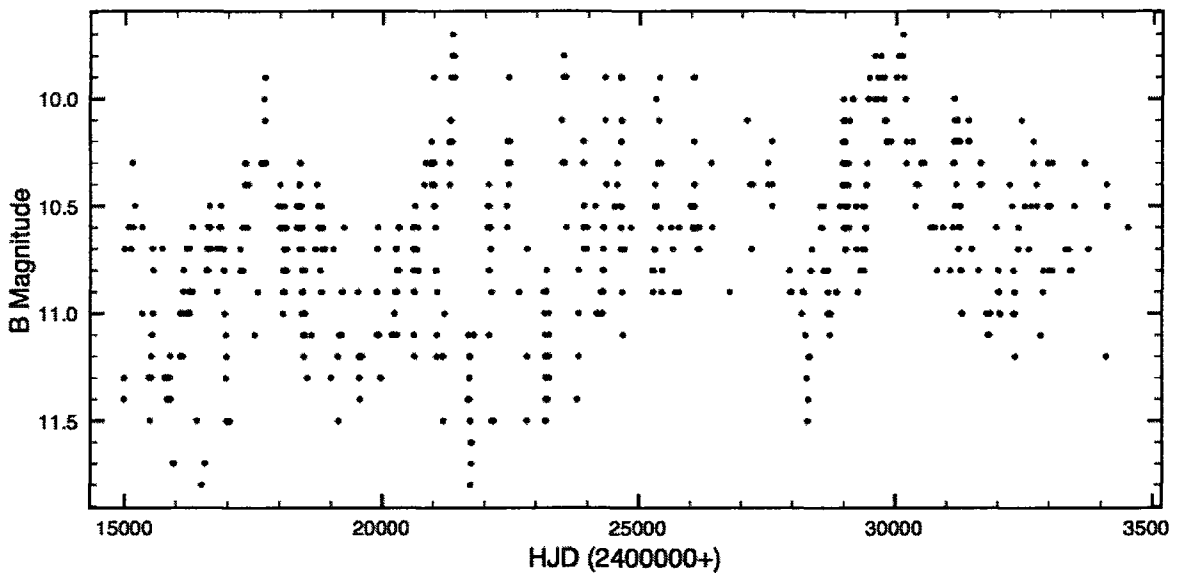


Figure B.16: CL Carinae visual (AAVSO) light curve.



**Figure B.17:** CL Carinae visual (AAVSO) light curve - expanded view of figure B.16.



**Figure B.18:** CL Carinae photographic light curve.

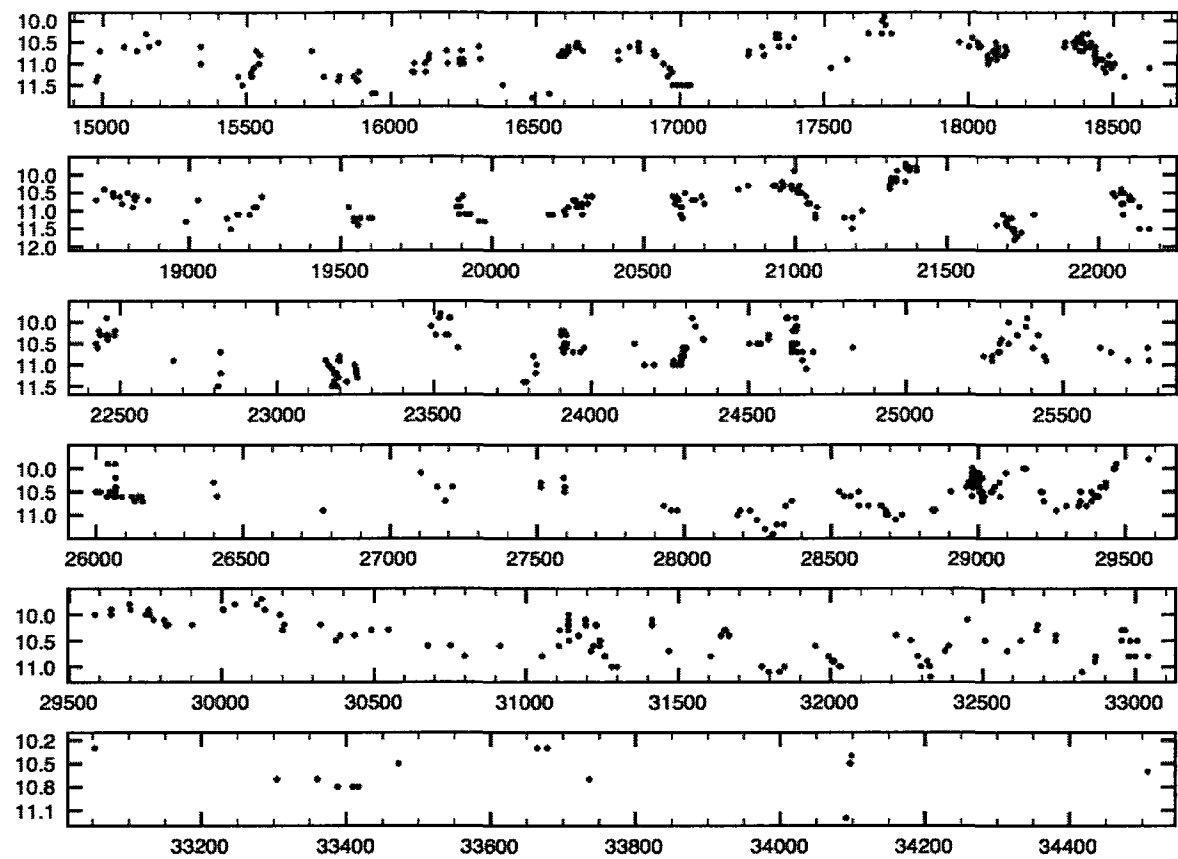


**Figure B.19:** CL Carinae photographic light curve - expanded view of figure B.18.

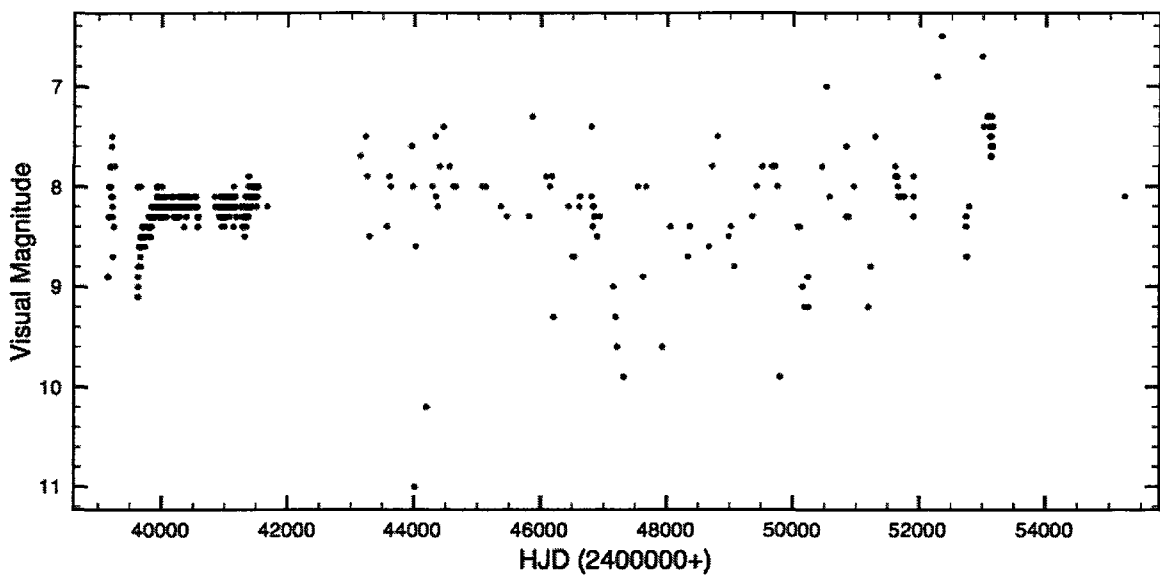


**Figure B.20:** EV Carinae visual (AAVSO) light curve.

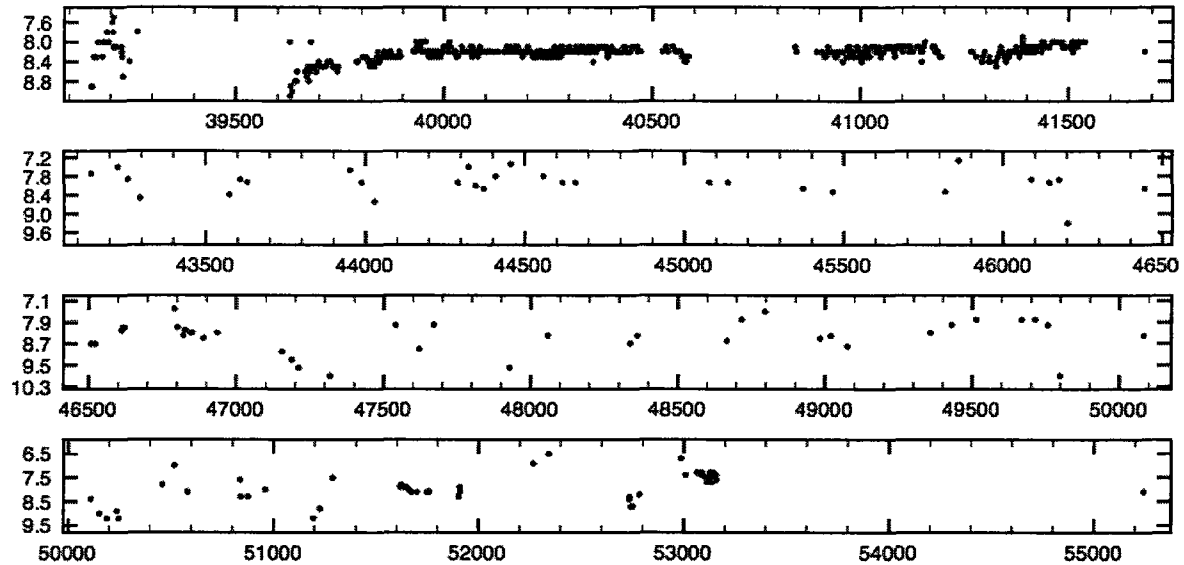


**Figure B.21:** EV Carinae visual (AAVSO) light curve - expanded view of figure B.20.

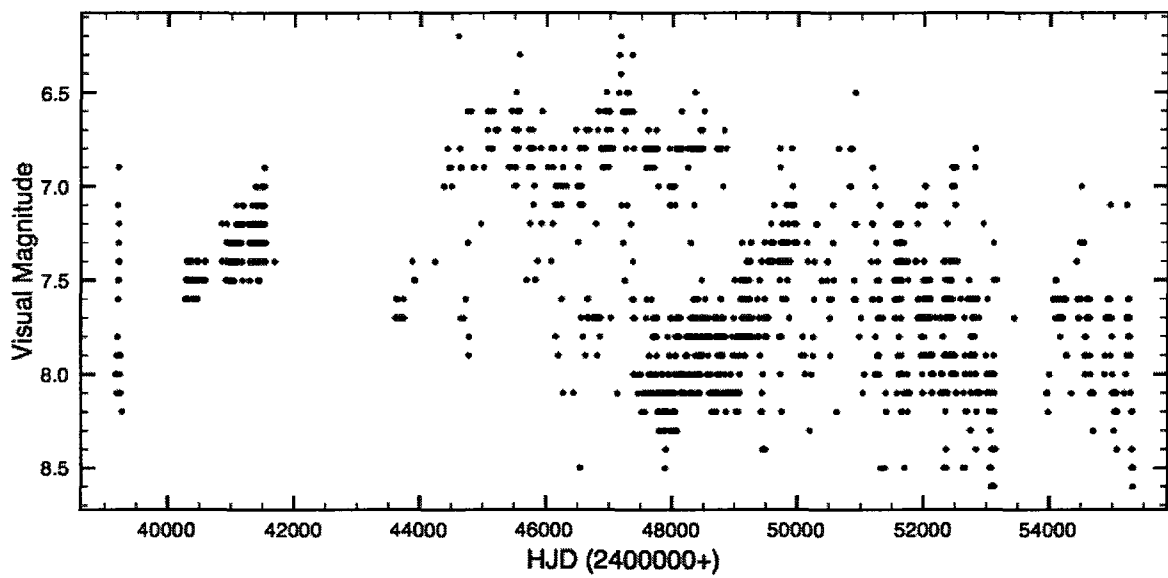


**Figure B.22:** IX Carinae visual (AAVSO) light curve.

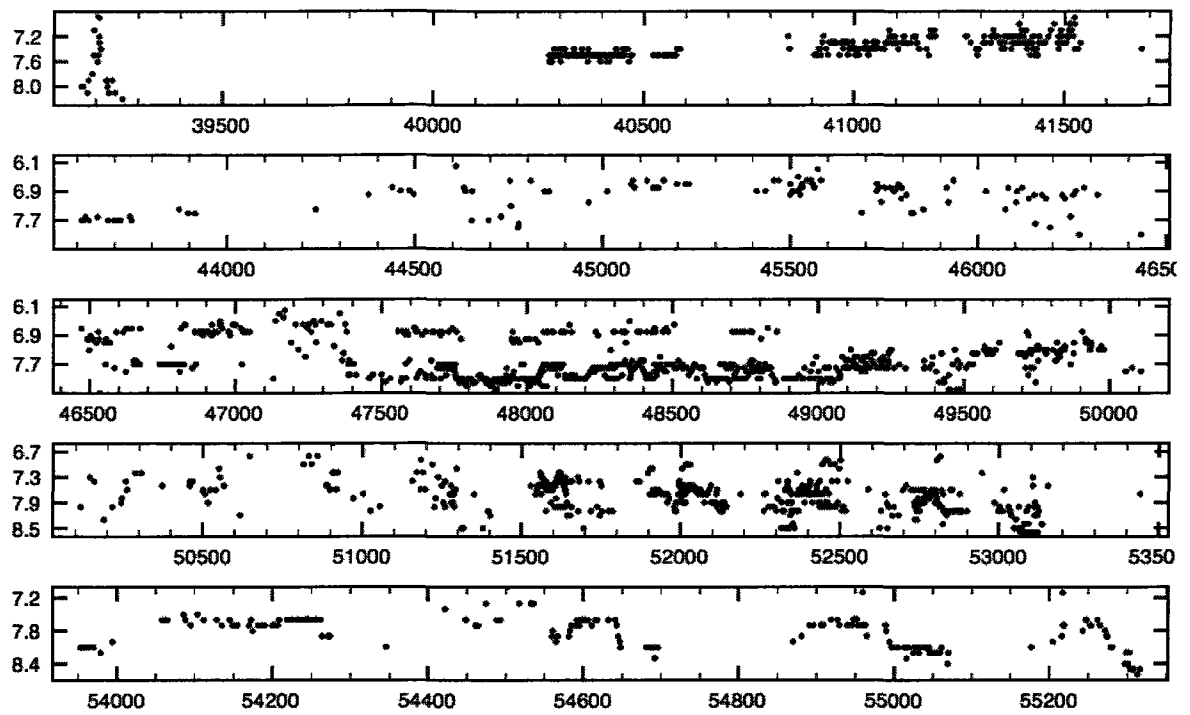


**Figure B.23:** IX Carinae visual (AAVSO) light curve - expanded view of figure B.22.

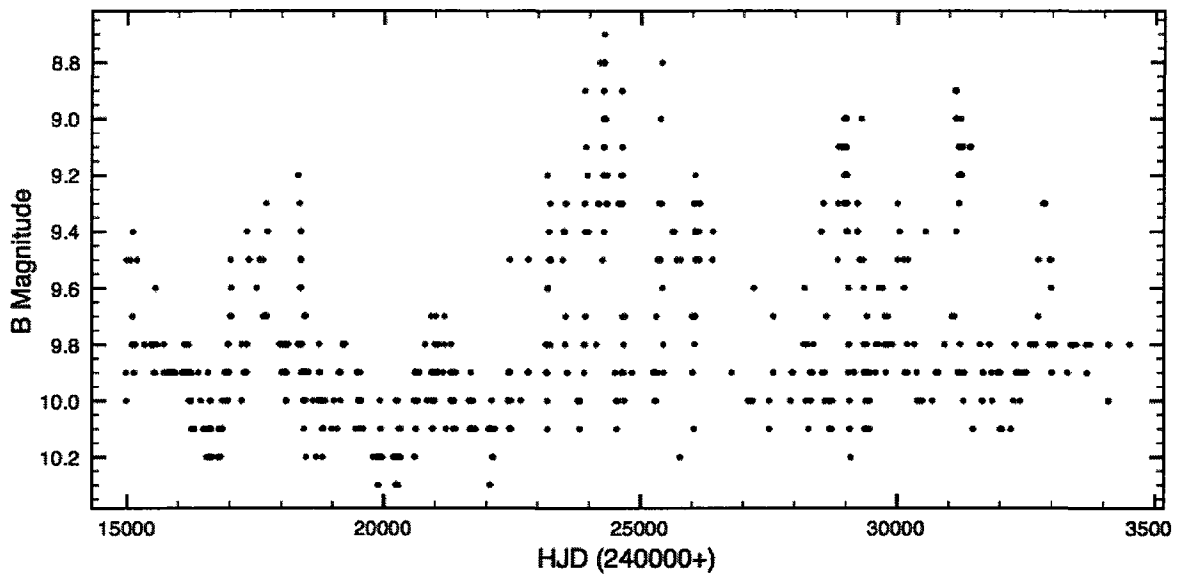


**Figure B.24:** IX Carinae photographic light curve.

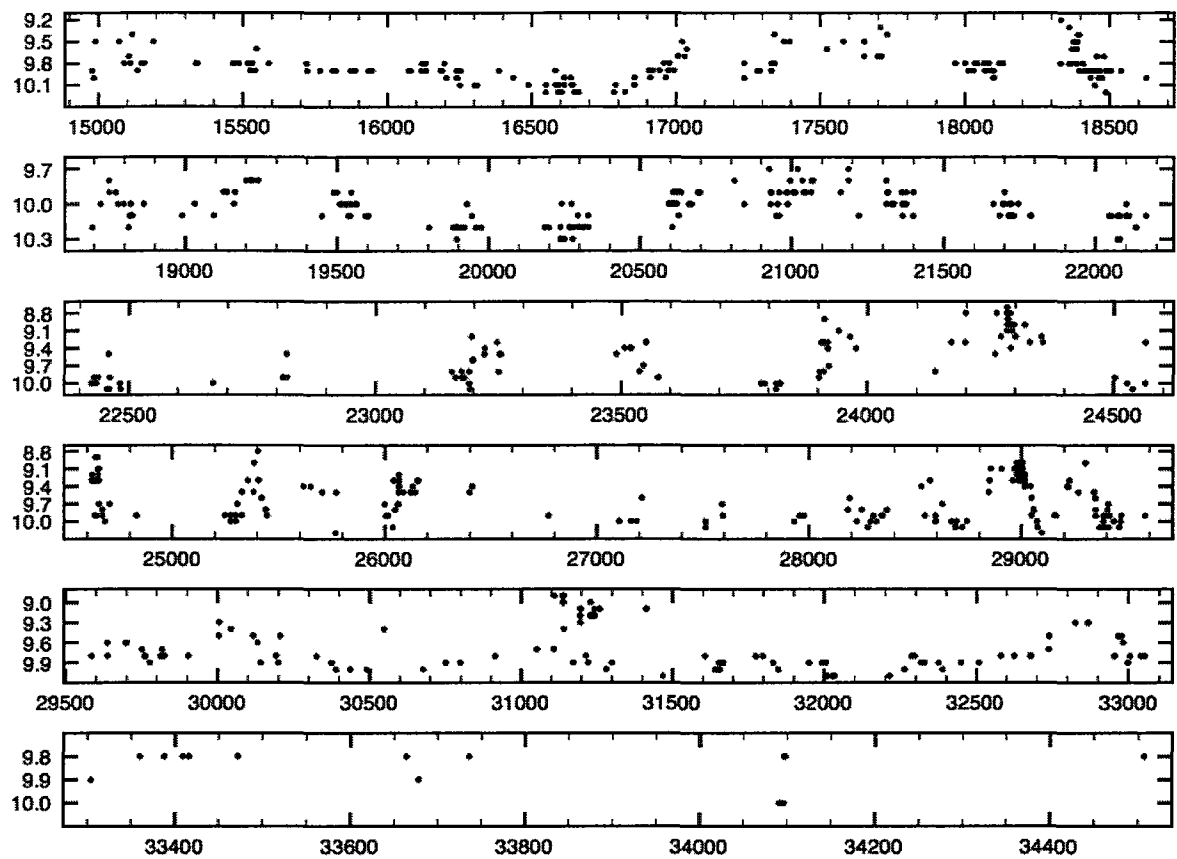


**Figure B.25:** IX Carinae photographic light curve - expanded view of figure ??.

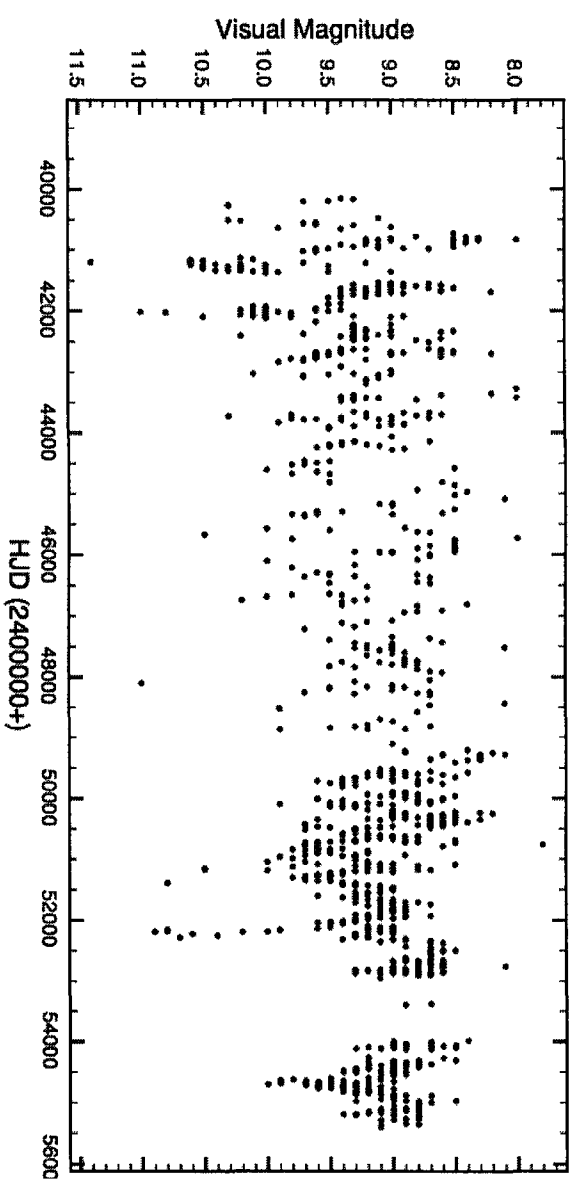


Figure B.26: PZ Casseopaeiae visual (AAVSO) light curve.

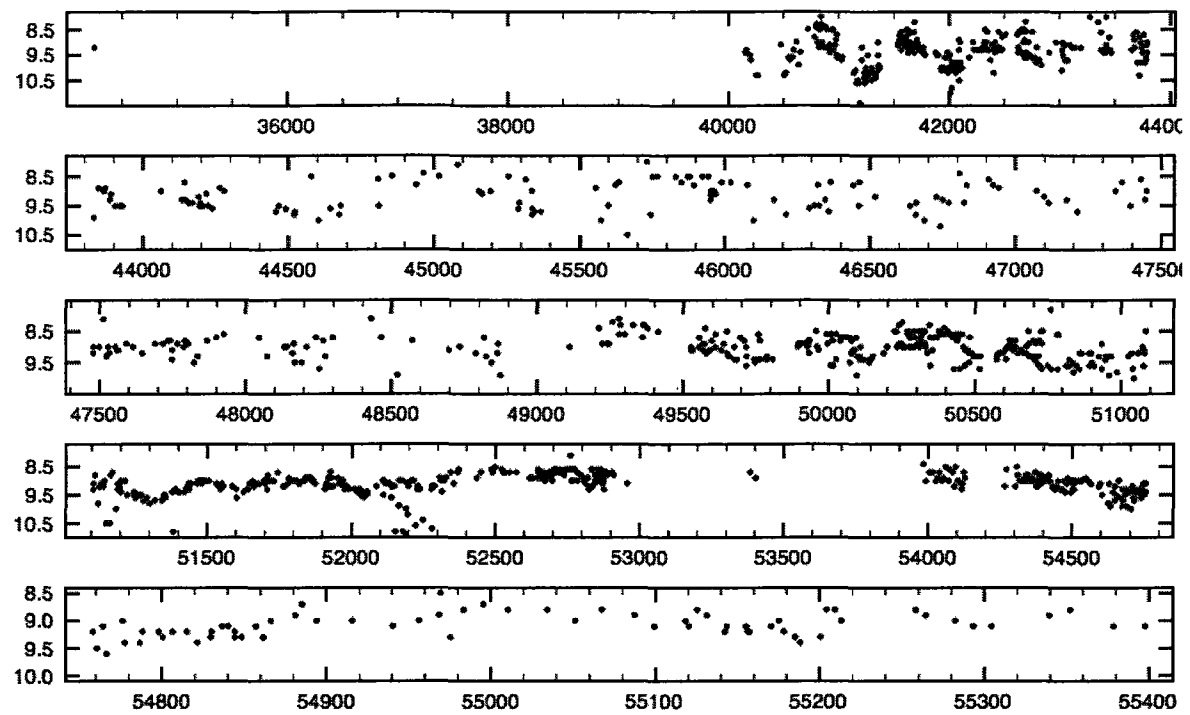
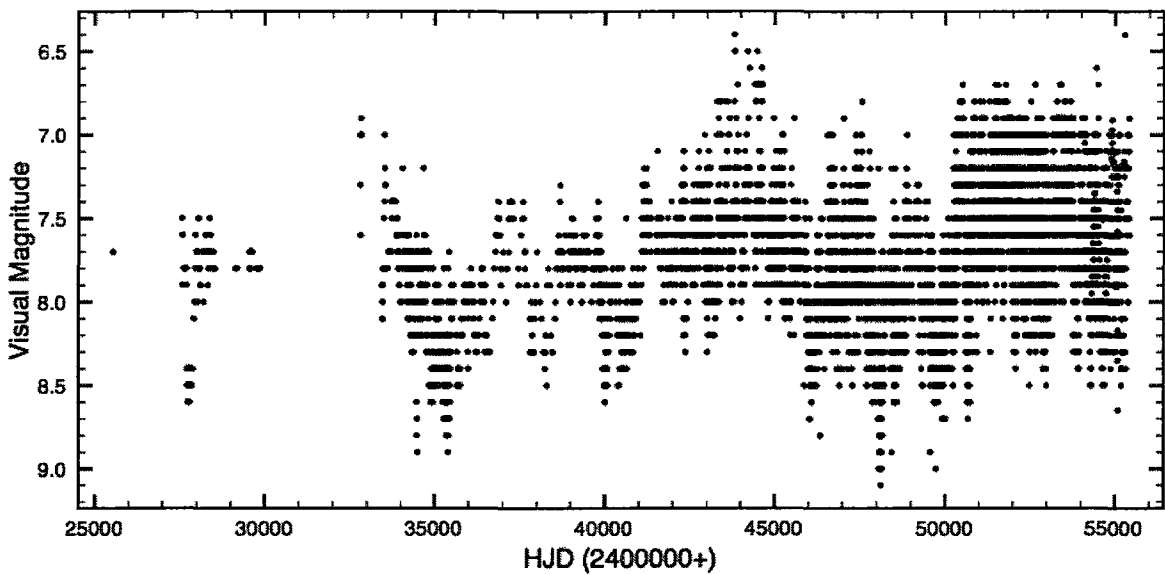
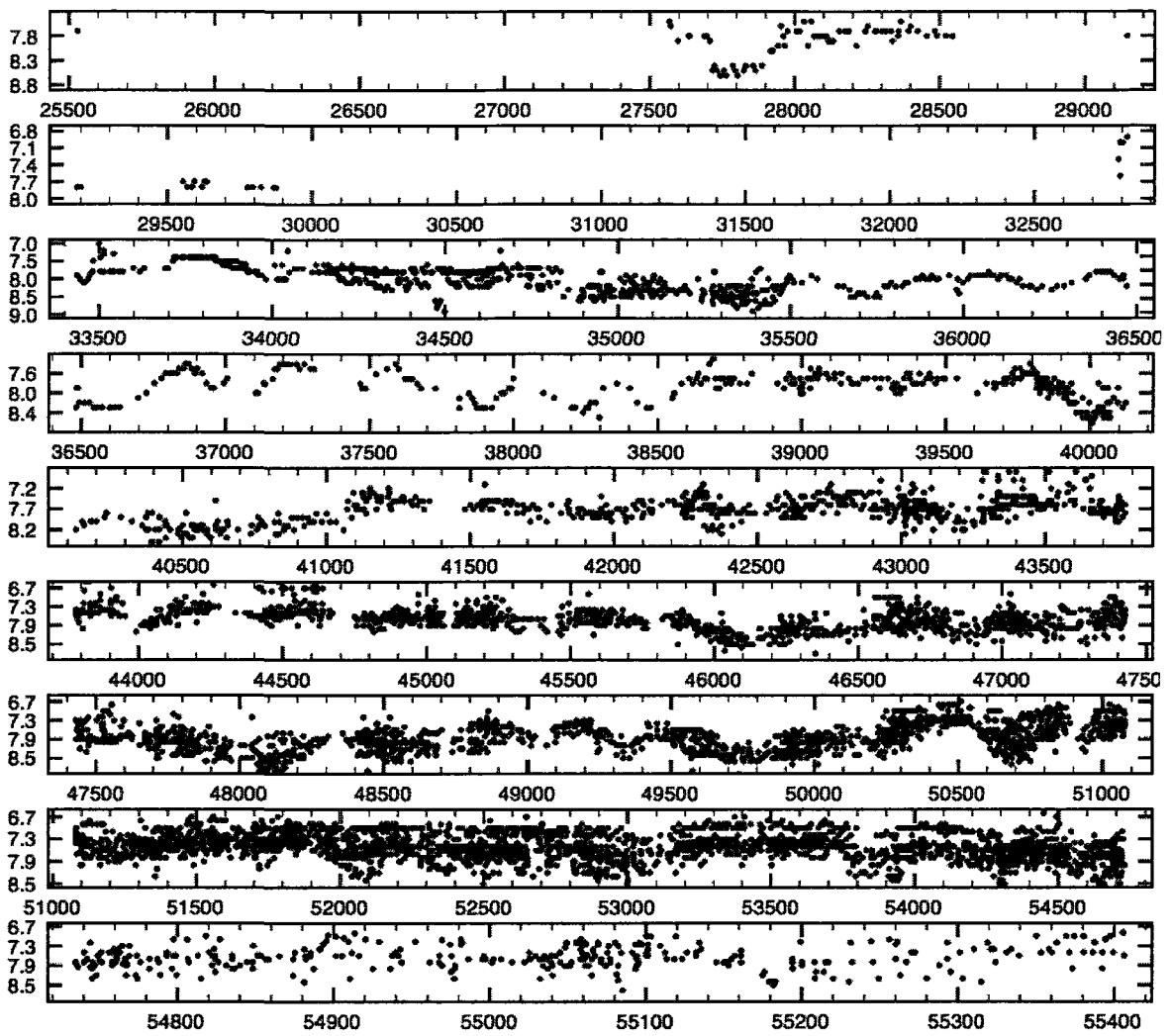


Figure B.27: PZ Casseopeiae visual (AAVSO) light curve - expanded view of figure B.26.



**Figure B.28:** W Cephei visual (AAVSO) light curve.



**Figure B.29:** W Cephei visual (AAVSO) light curve - expanded view of figure B.28.

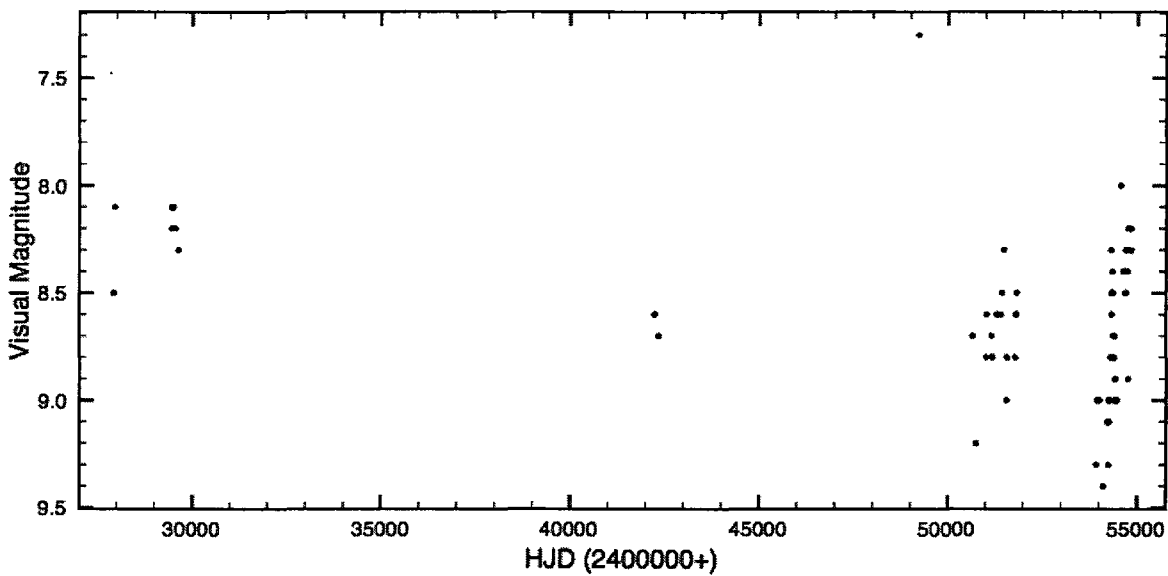


**Figure B.30:** SW Cephei visual (AAVSO) light curve.

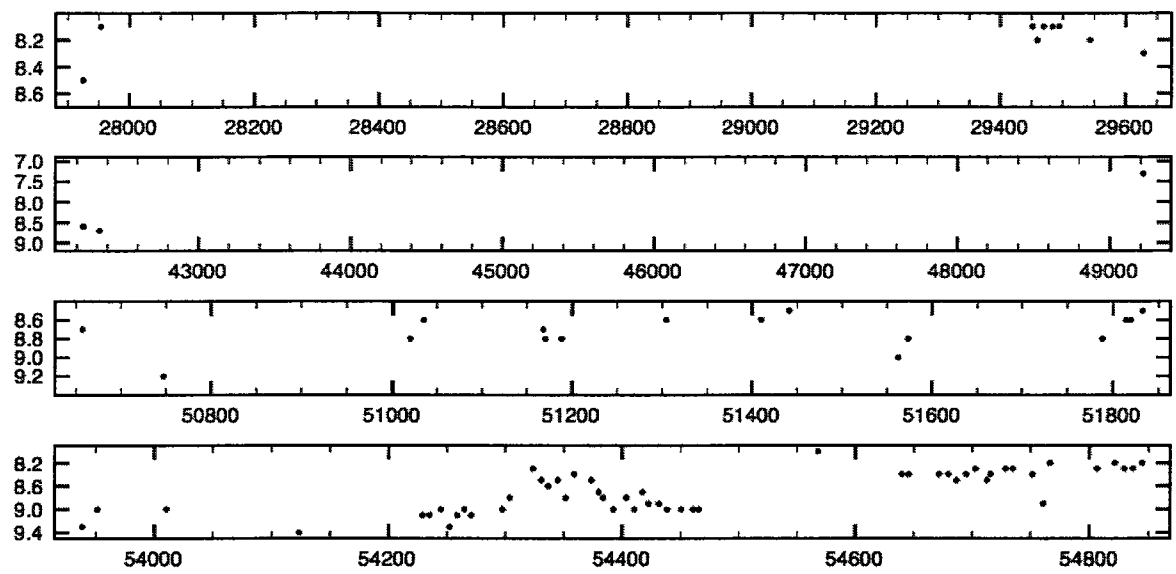


**Figure B.31:** SW Cephei visual light curve - expanded view of figure B.30.

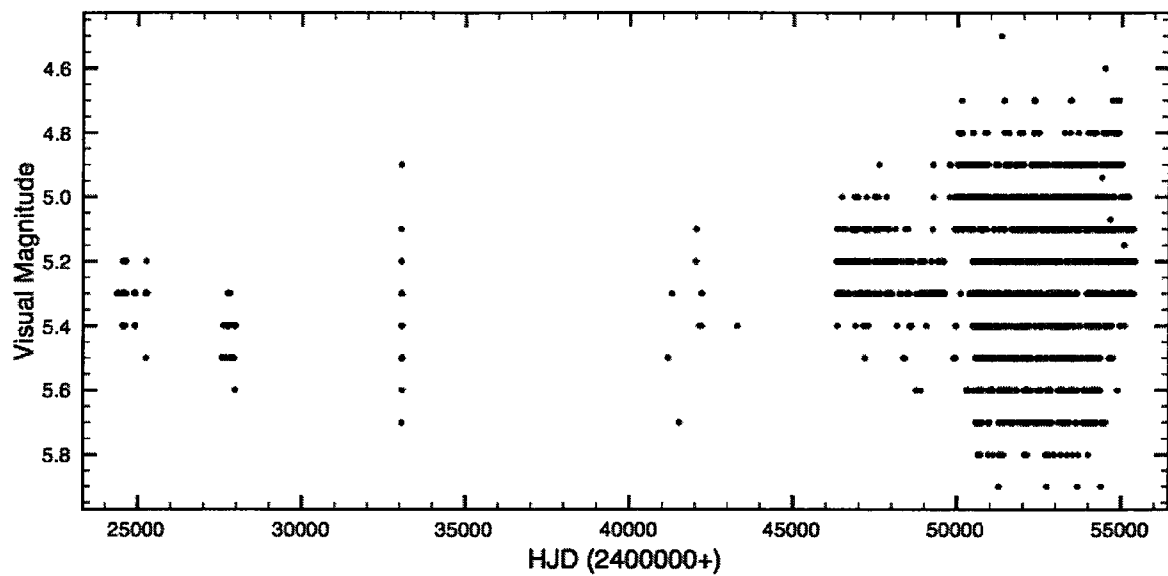


**Figure B.32:** VV Cephei visual (AAVSO) light curve.

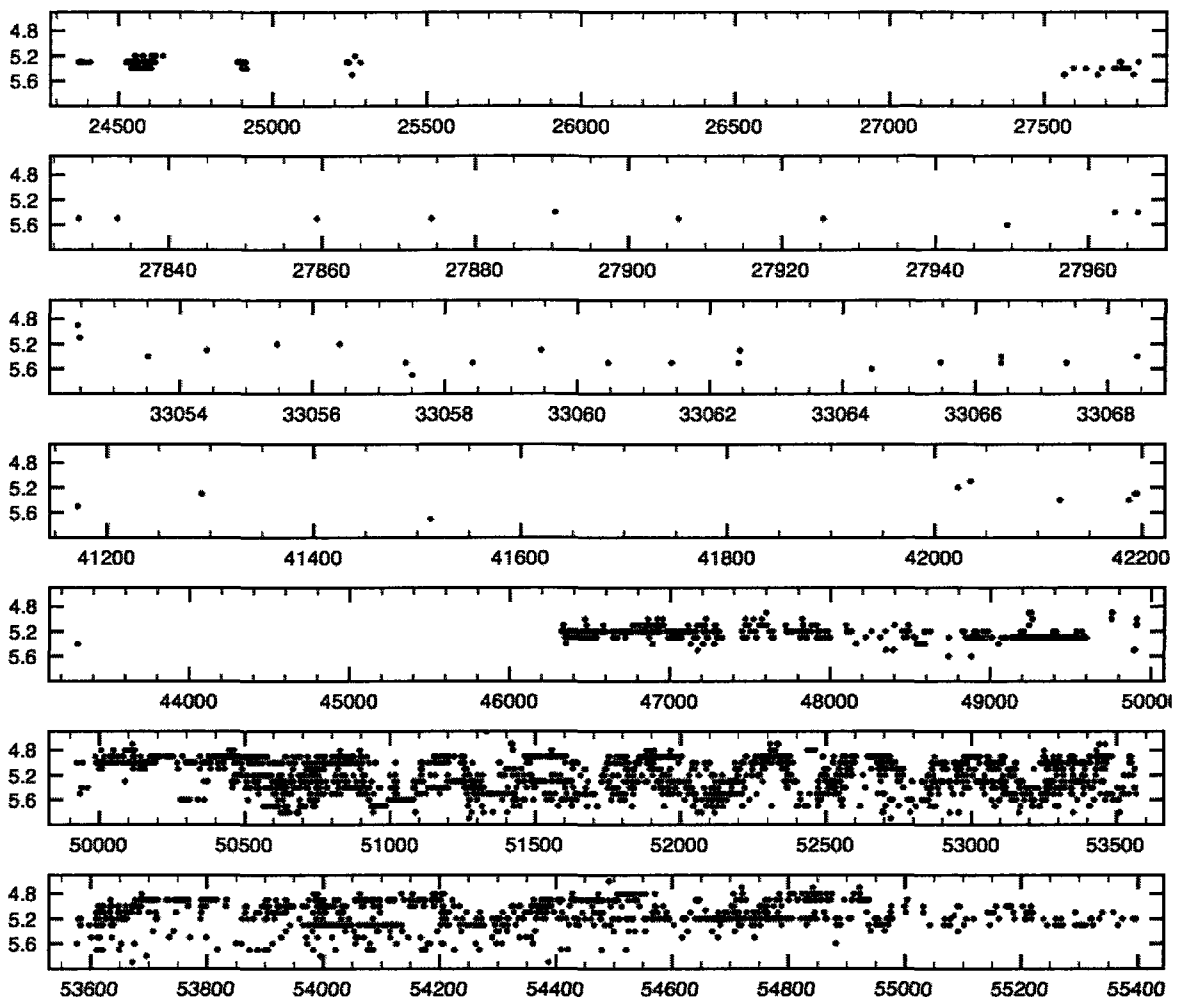


**Figure B.33:** VV Cephei visual (AAVSO) light curve - expanded view of figure B.32.

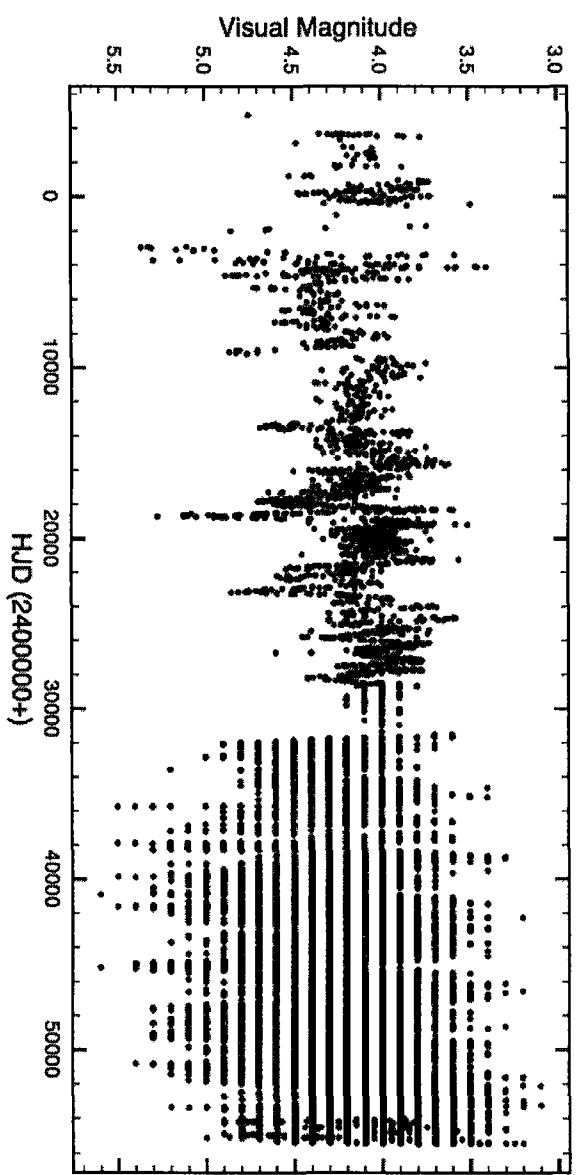


Figure B.34:  $\mu$  Cephei visual (AAVSO) light curve.

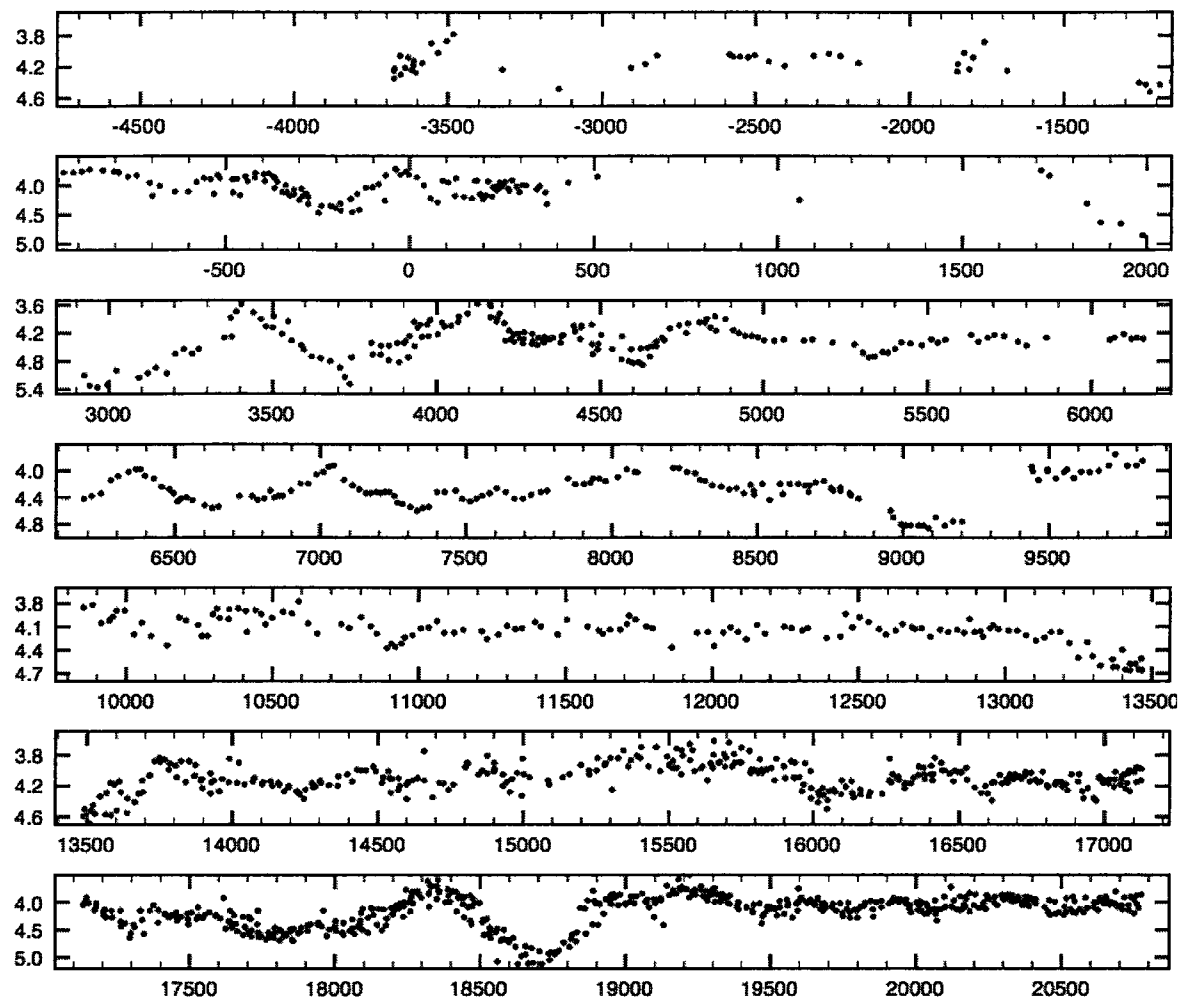
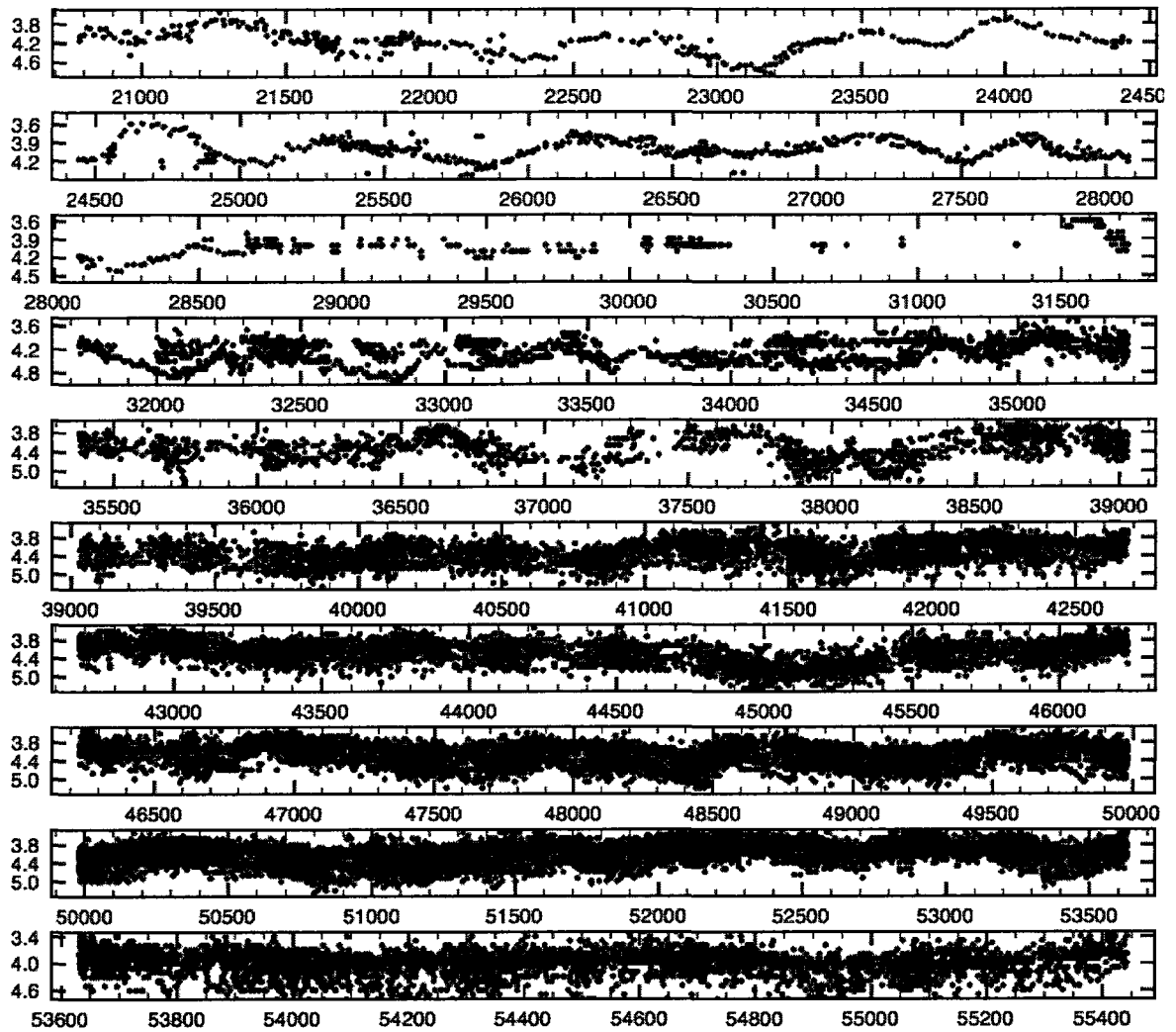
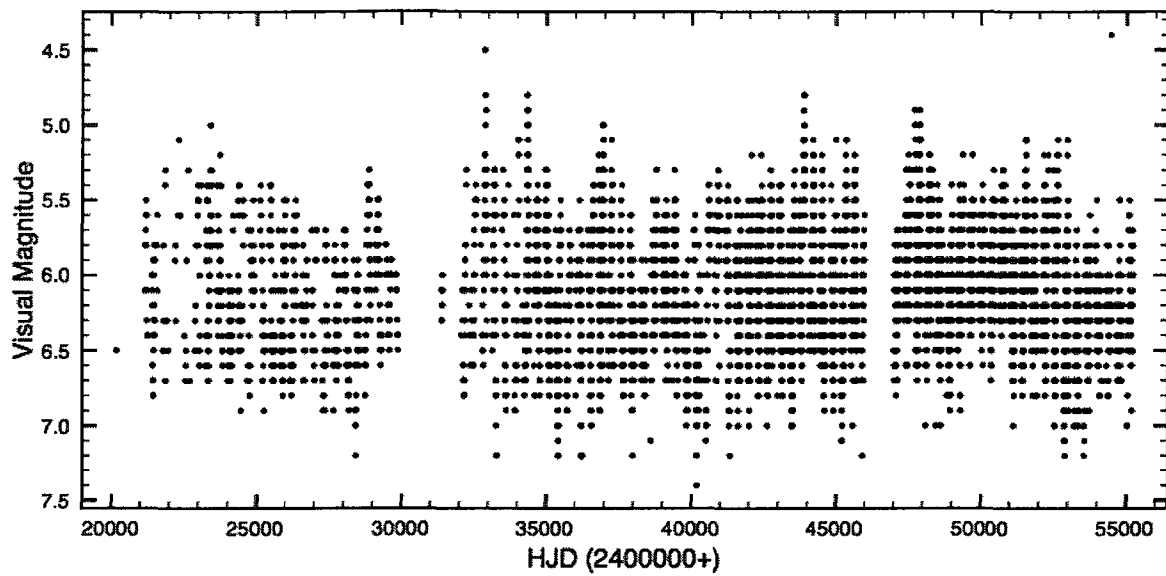


Figure B.35:  $\mu$  Cephei light curve - expanded view of figure B.34 (continued in next figure).



**Figure B.36:**  $\mu$  Cephei expanded light curve (continued).



**Figure B.37:** T Cet visual (AAVSO) light curve.

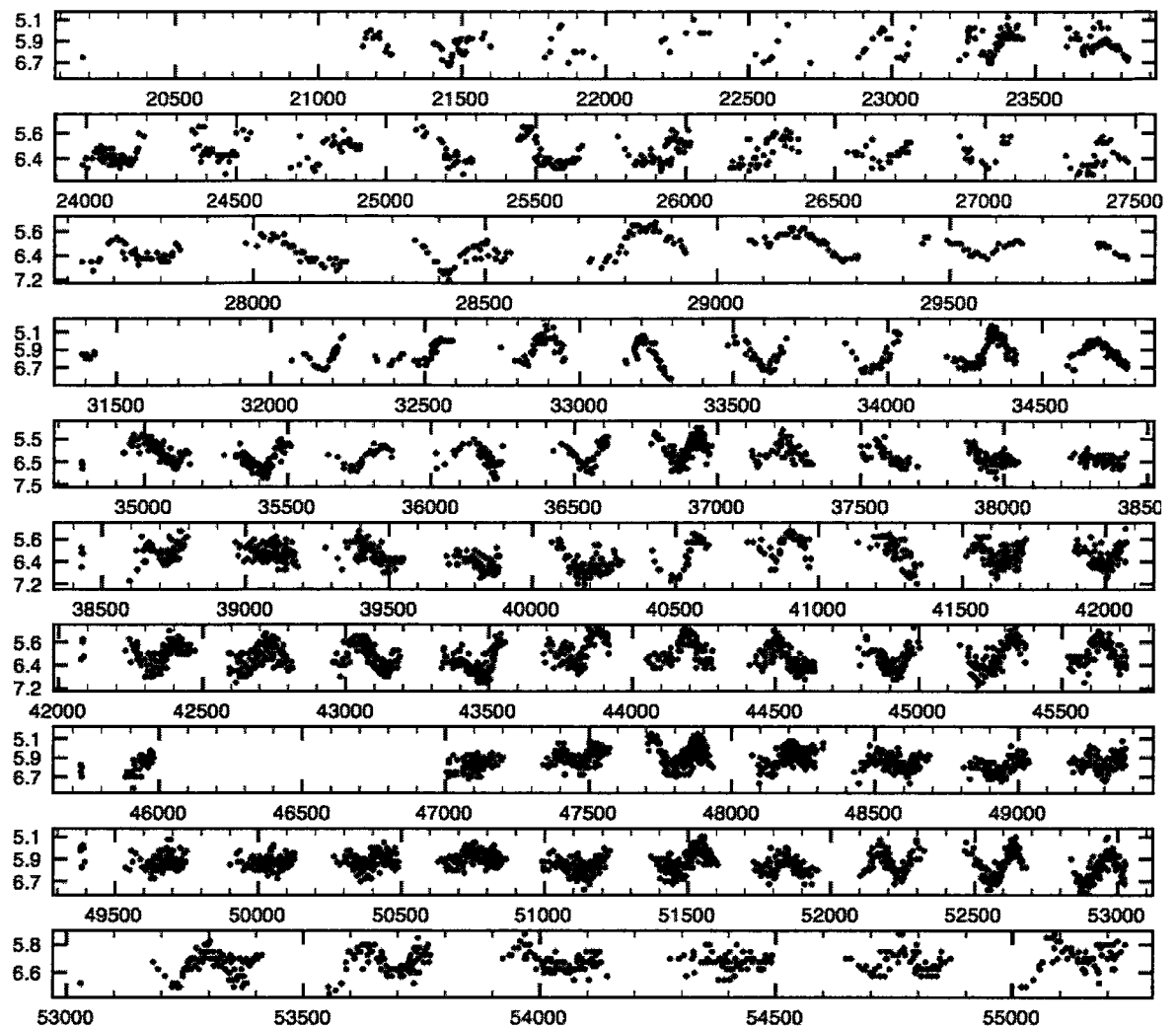


**Figure B.38:** T Cet visual (AAVSO) light curve - expanded view of figure B.37.

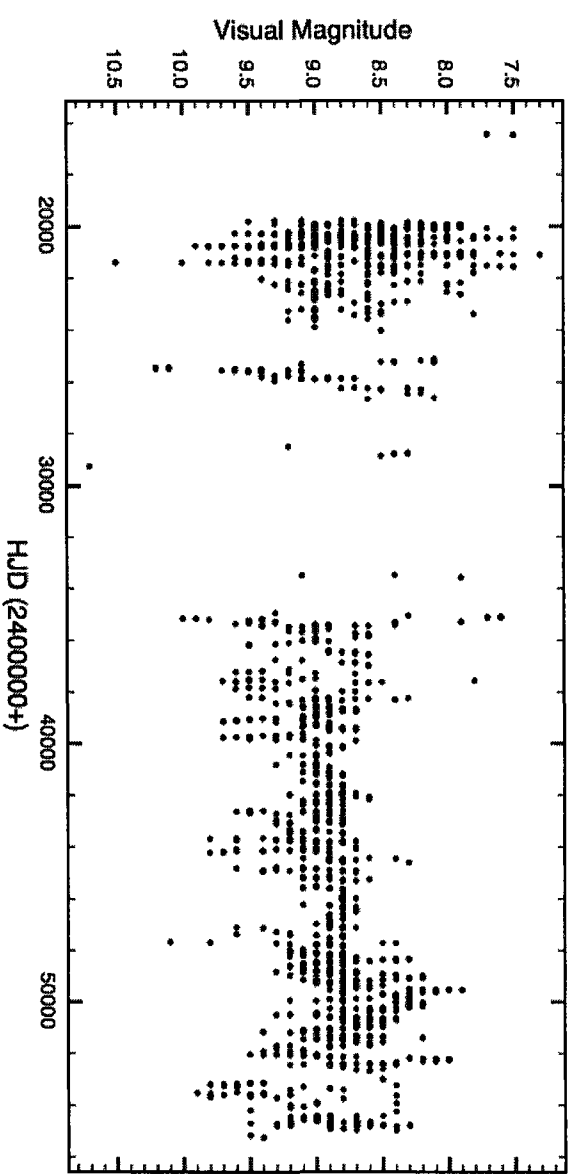
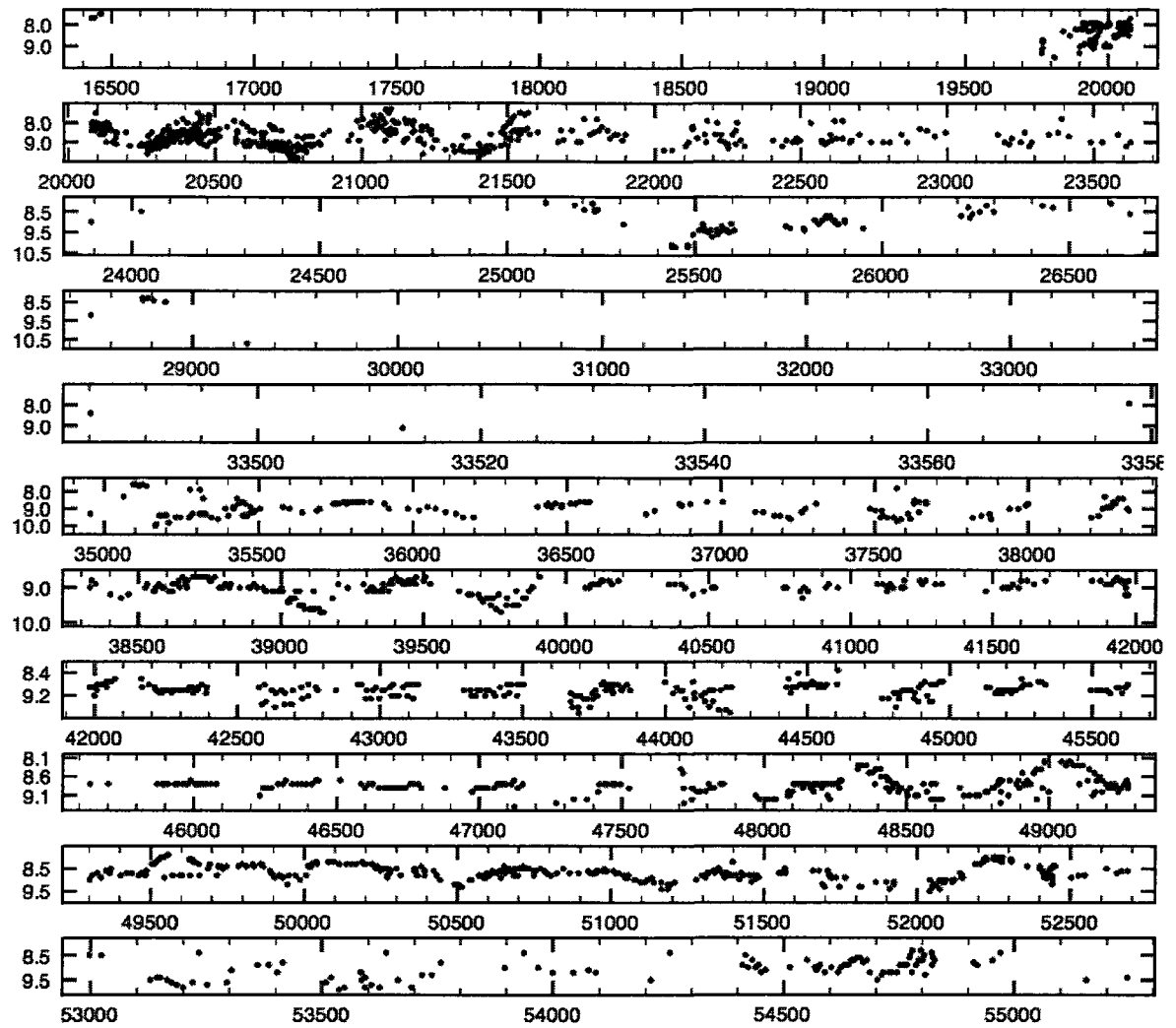


Figure B.39: RW Cygni visual (AAVSO) light curve.



**Figure B.40:** RW Cygni visual (AAVSO) light curve - expanded view of figure ??.

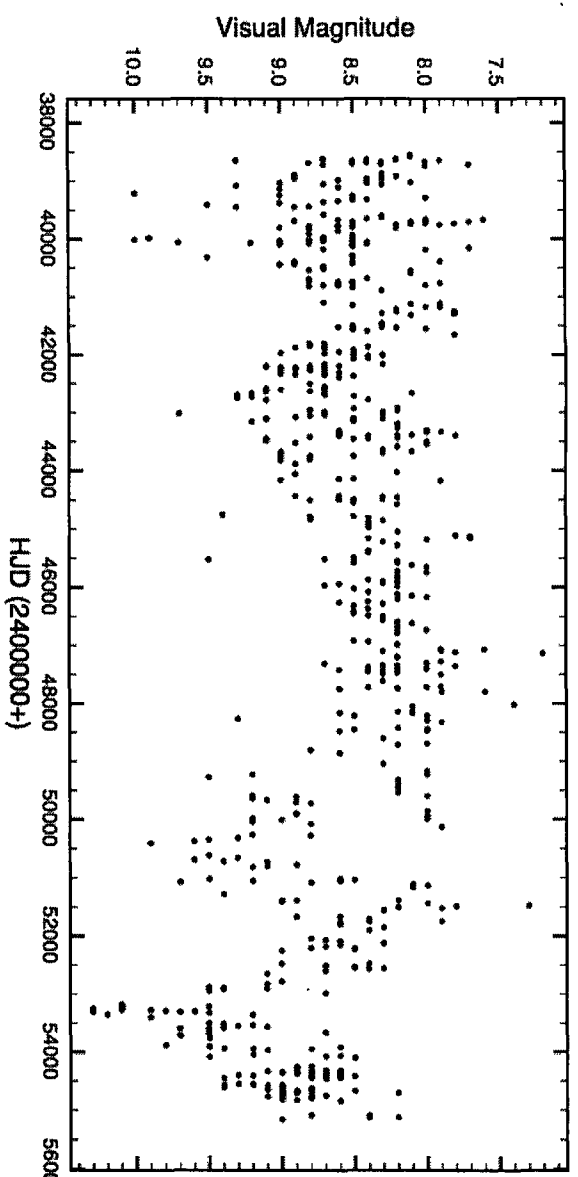


Figure B.41: AZ Cygni visual (AAVSO) light curve.

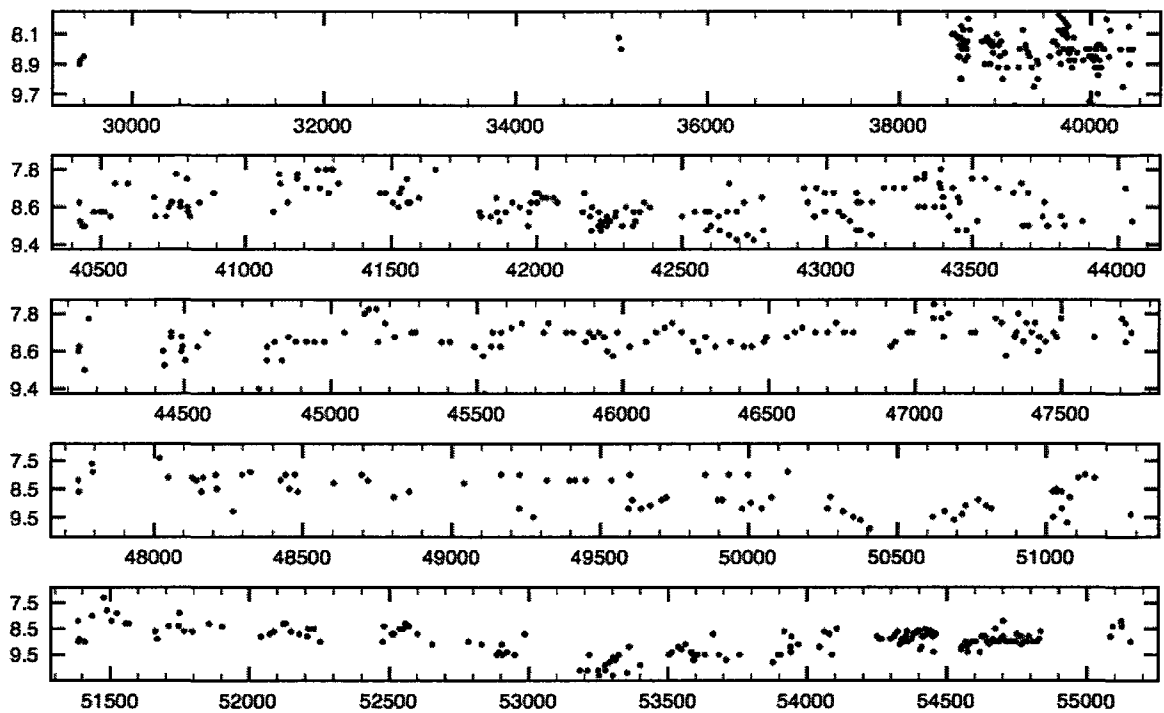


Figure B.42: AZ Cygni visual (AAVSO) light curve - expanded view of figure B.41.

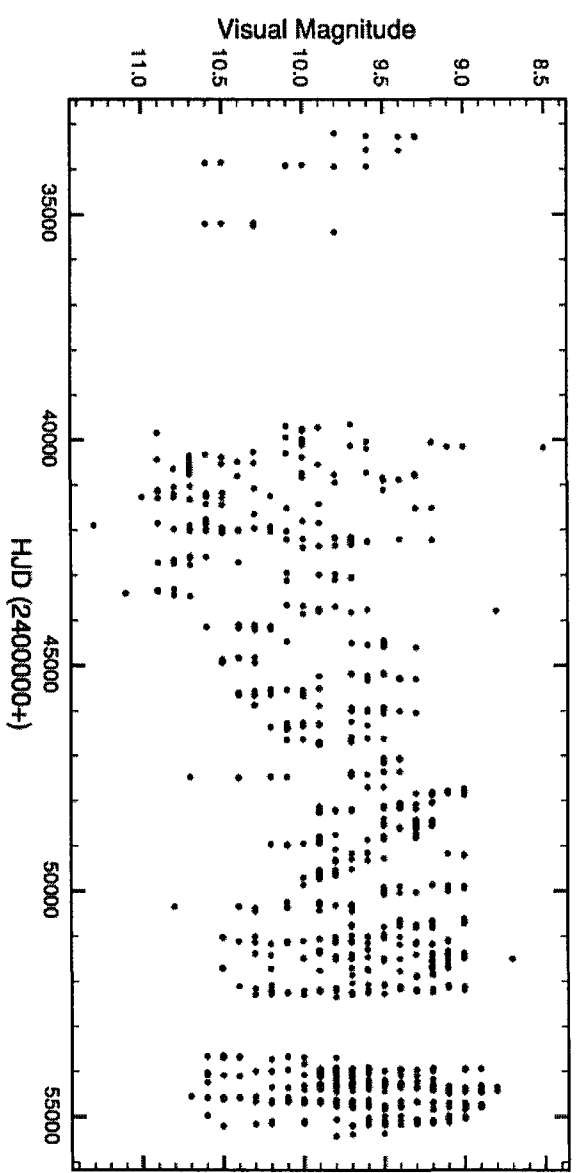
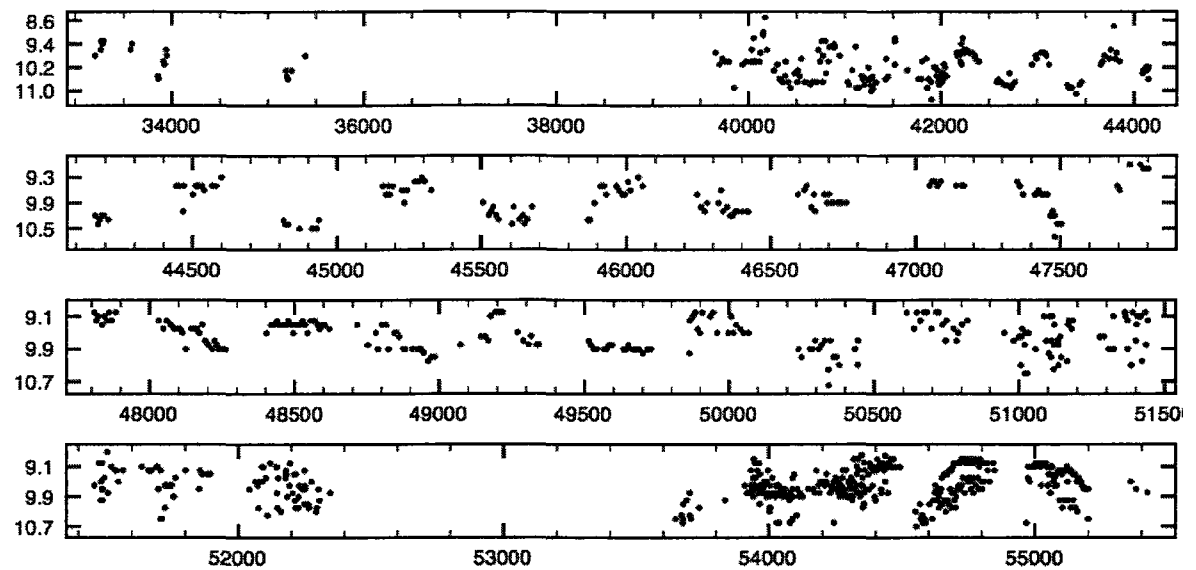
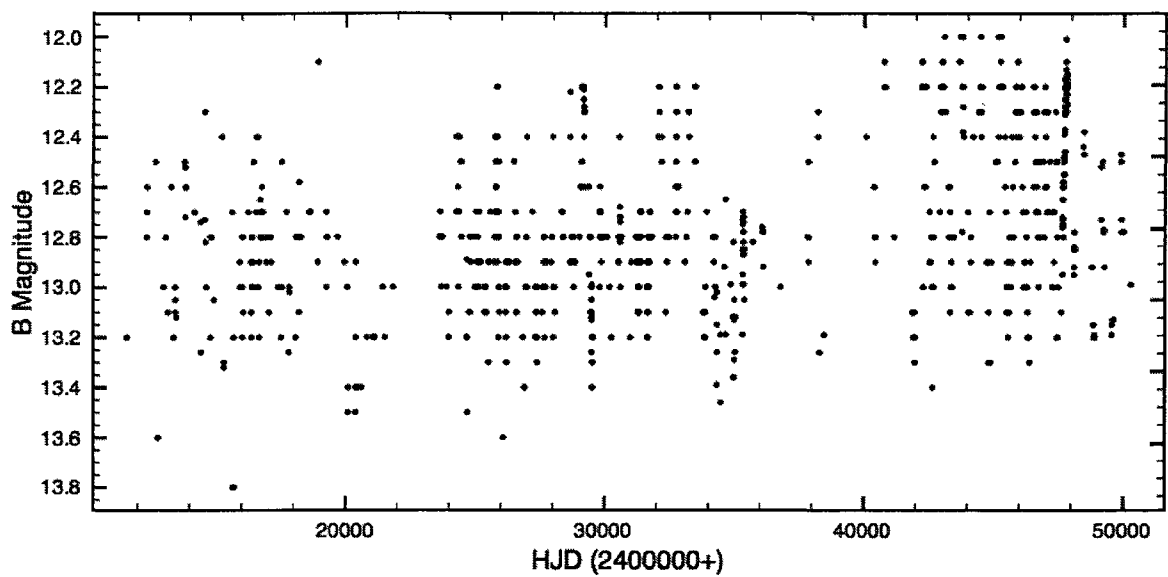


Figure B.43: BC Cyg visual (AAVSO) light curve.



**Figure B.44:** BC Cyg visual light curve - expanded view of figure B.43.



**Figure B.45:** BC Cygni photographic light curve.

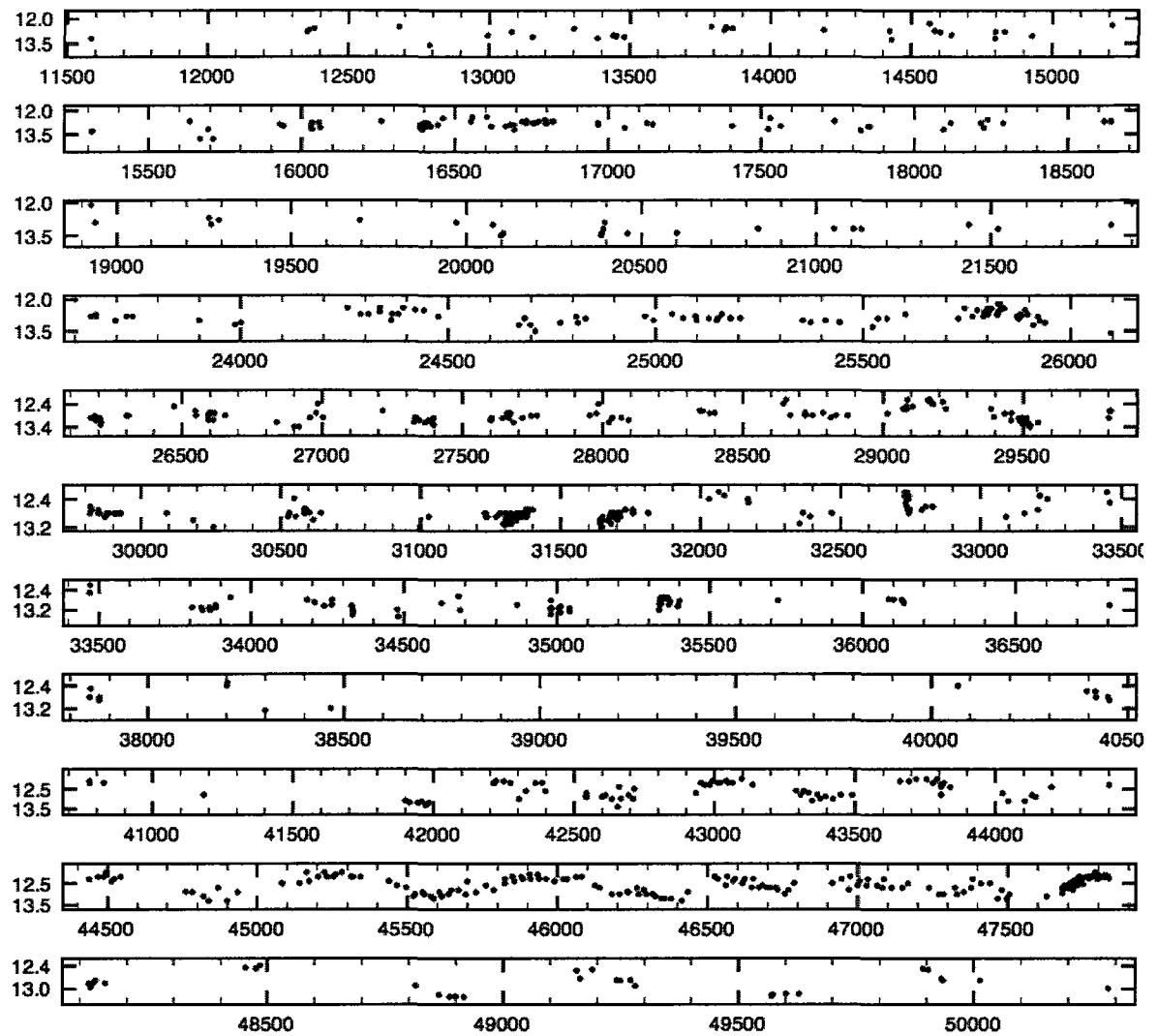


**Figure B.46:** BC Cygni photographic light curve - expanded view of figure B.45.

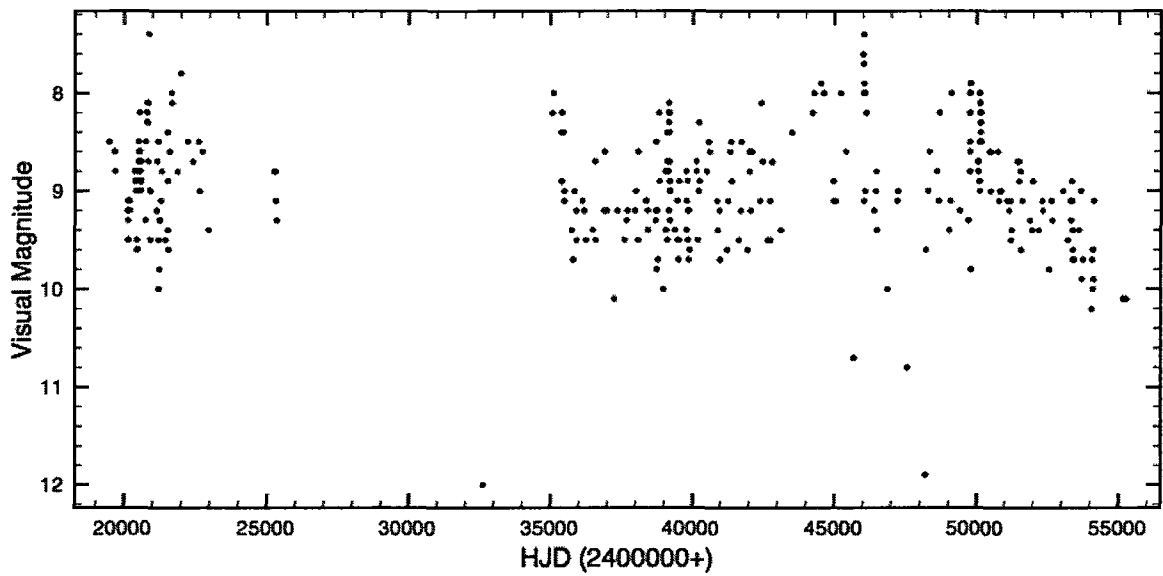


**Figure B.47:** V Eridanus visual (AAVSO) light curve.

S

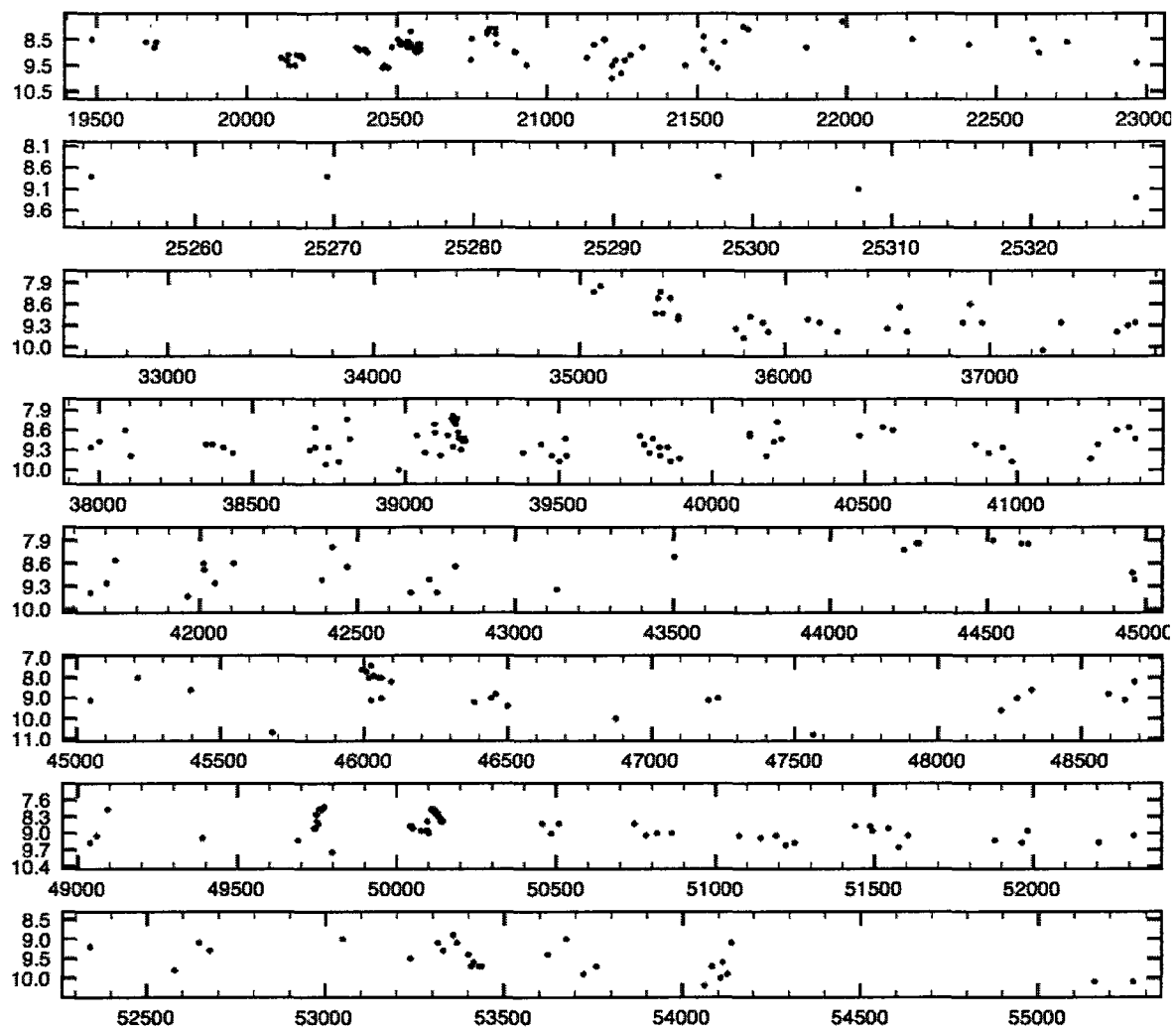


**Figure B.48:** V Eridanus visual (AAVSO) light curve - expanded view of figure ??.

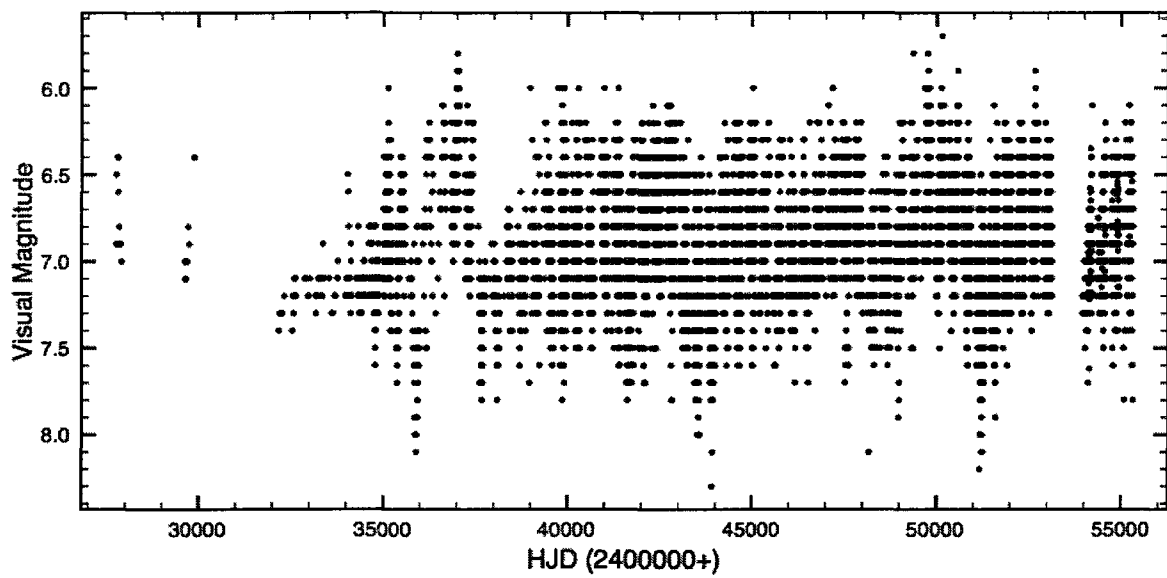


**Figure B.49:** TV Geminorum visual (AAVSO) light curve.

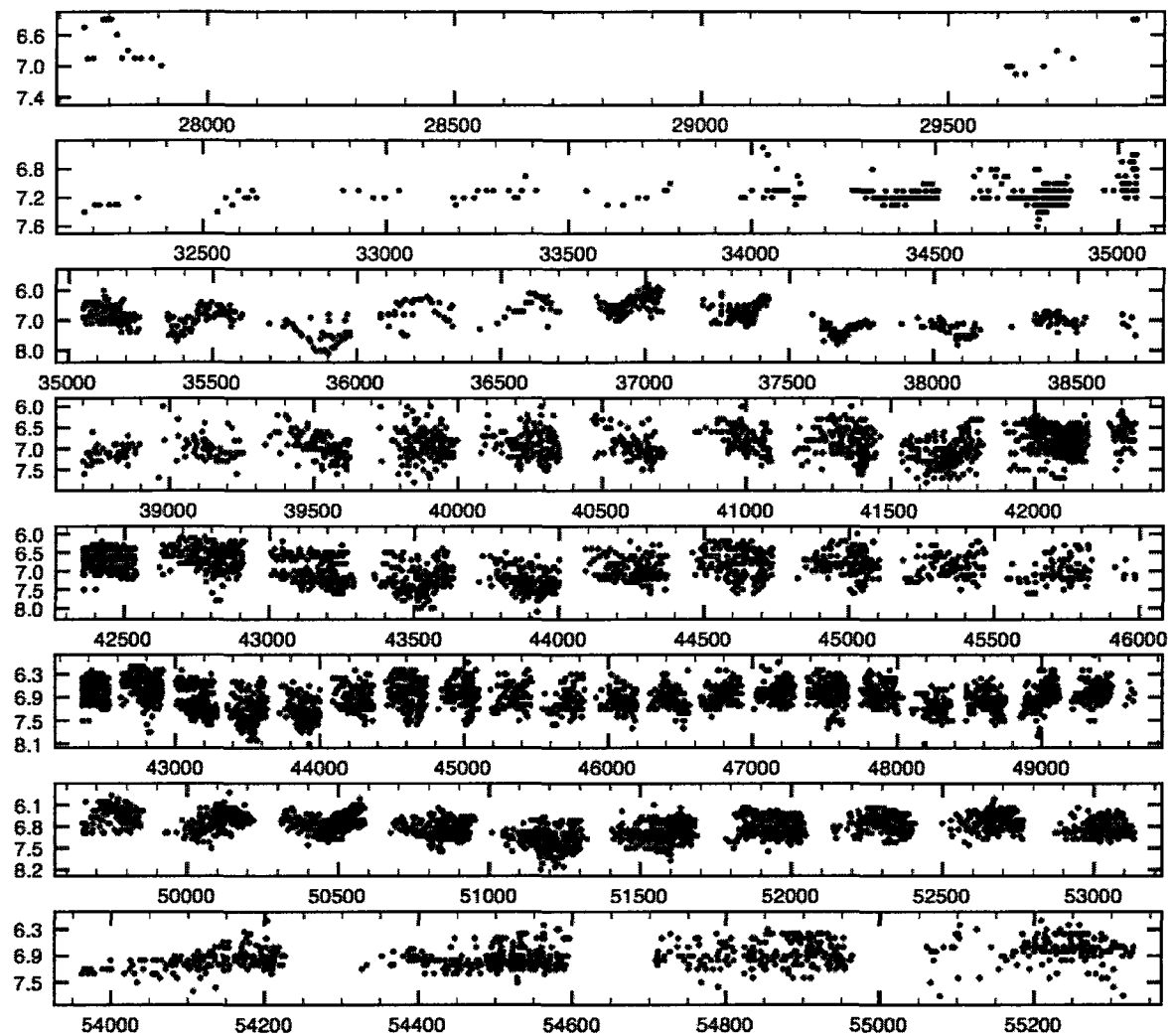


**Figure B.50:** TV Geminorum visual light curve - expanded view of figure B.49.

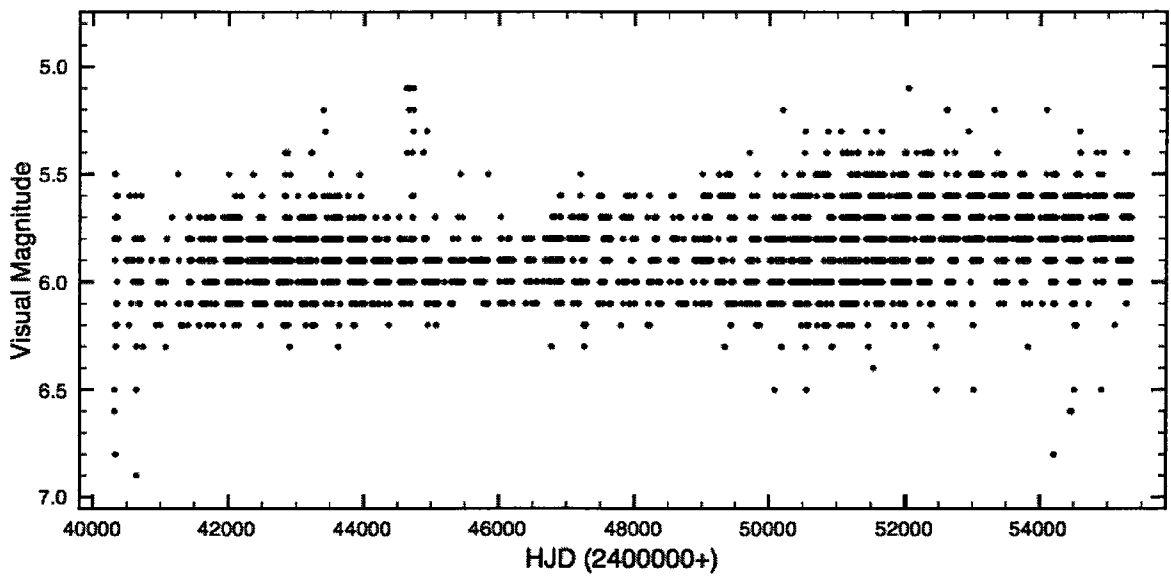


**Figure B.51:** IS Geminorum visual (AAVSO) light curve.

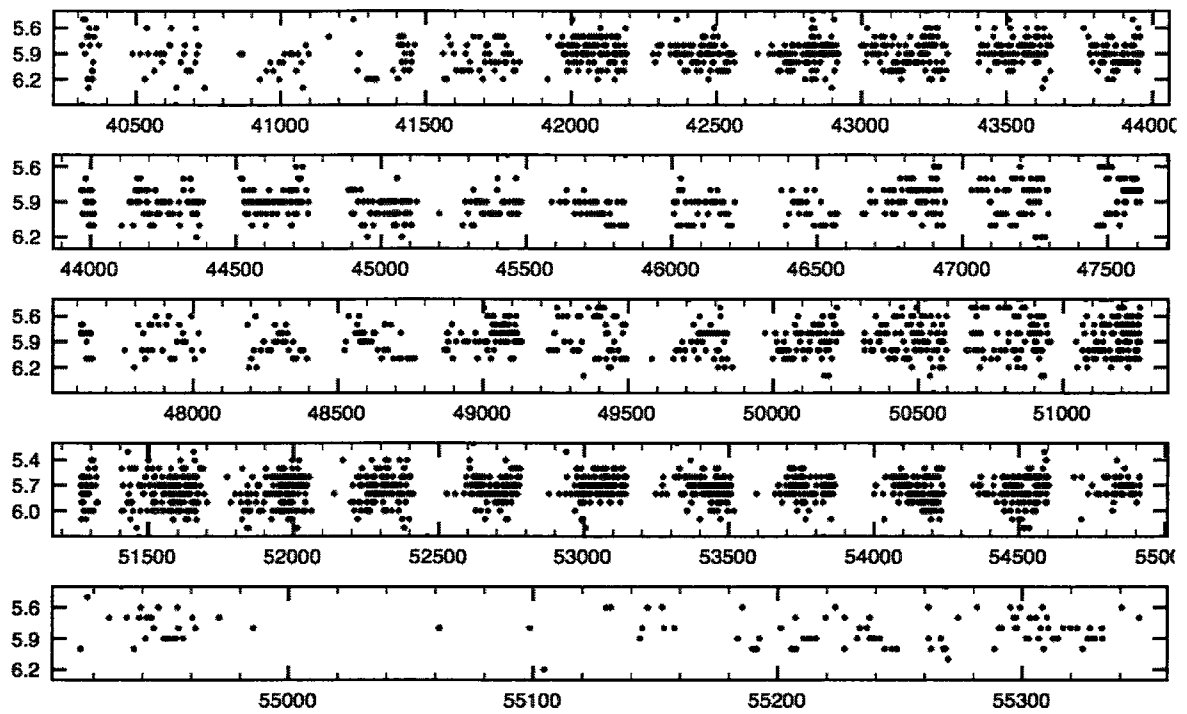
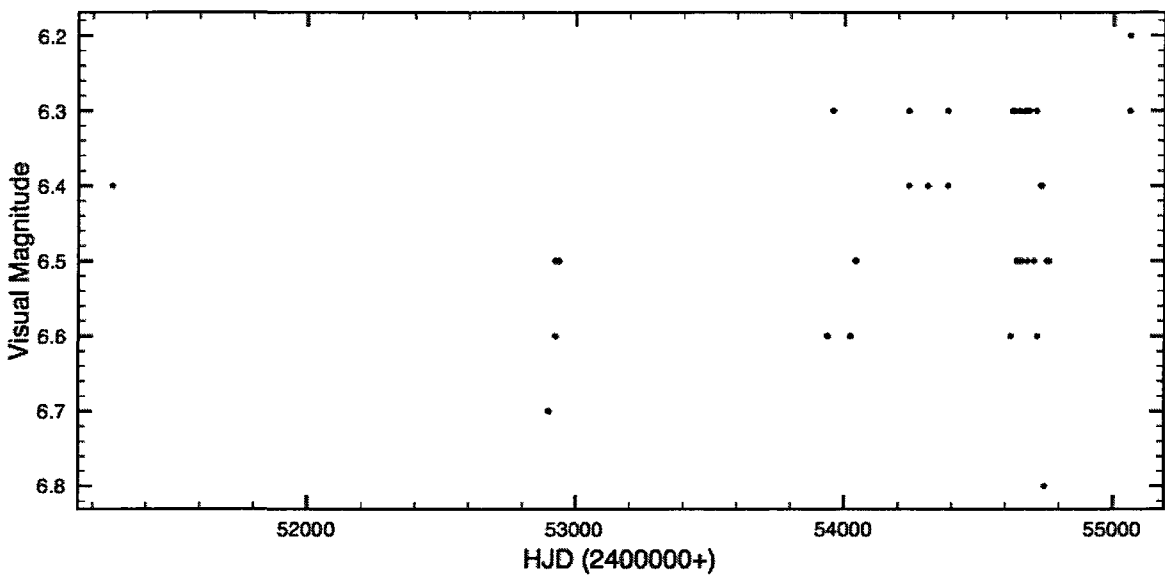


Figure B.52: IS Geminorum visual (AAVSO) light curve - expanded view of figure B.51.



**Figure B.53:** V959 Herculis visual (AAVSO) light curve.

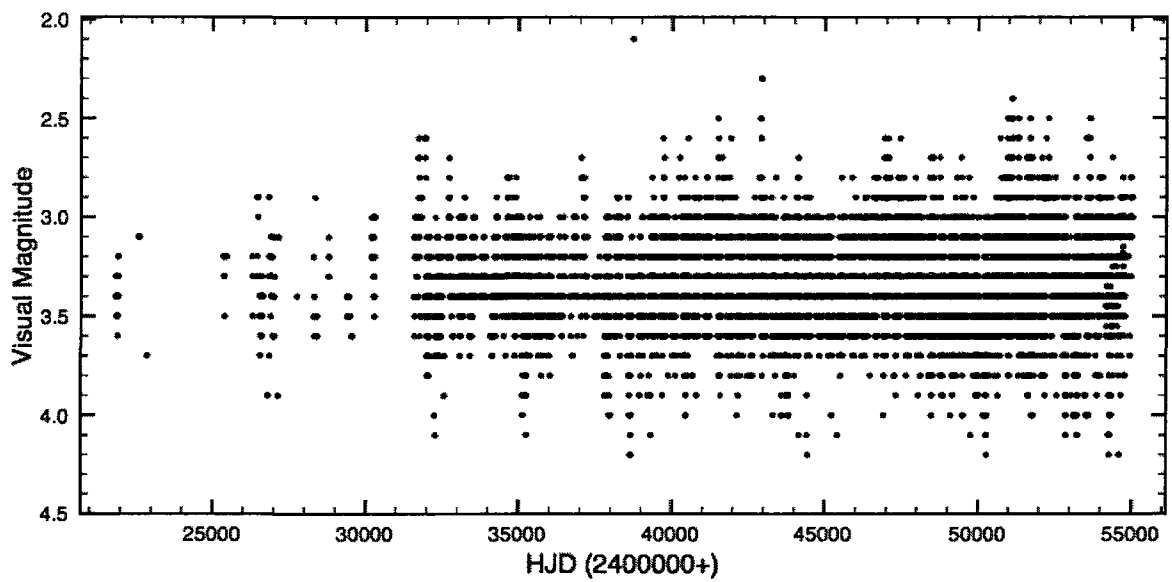
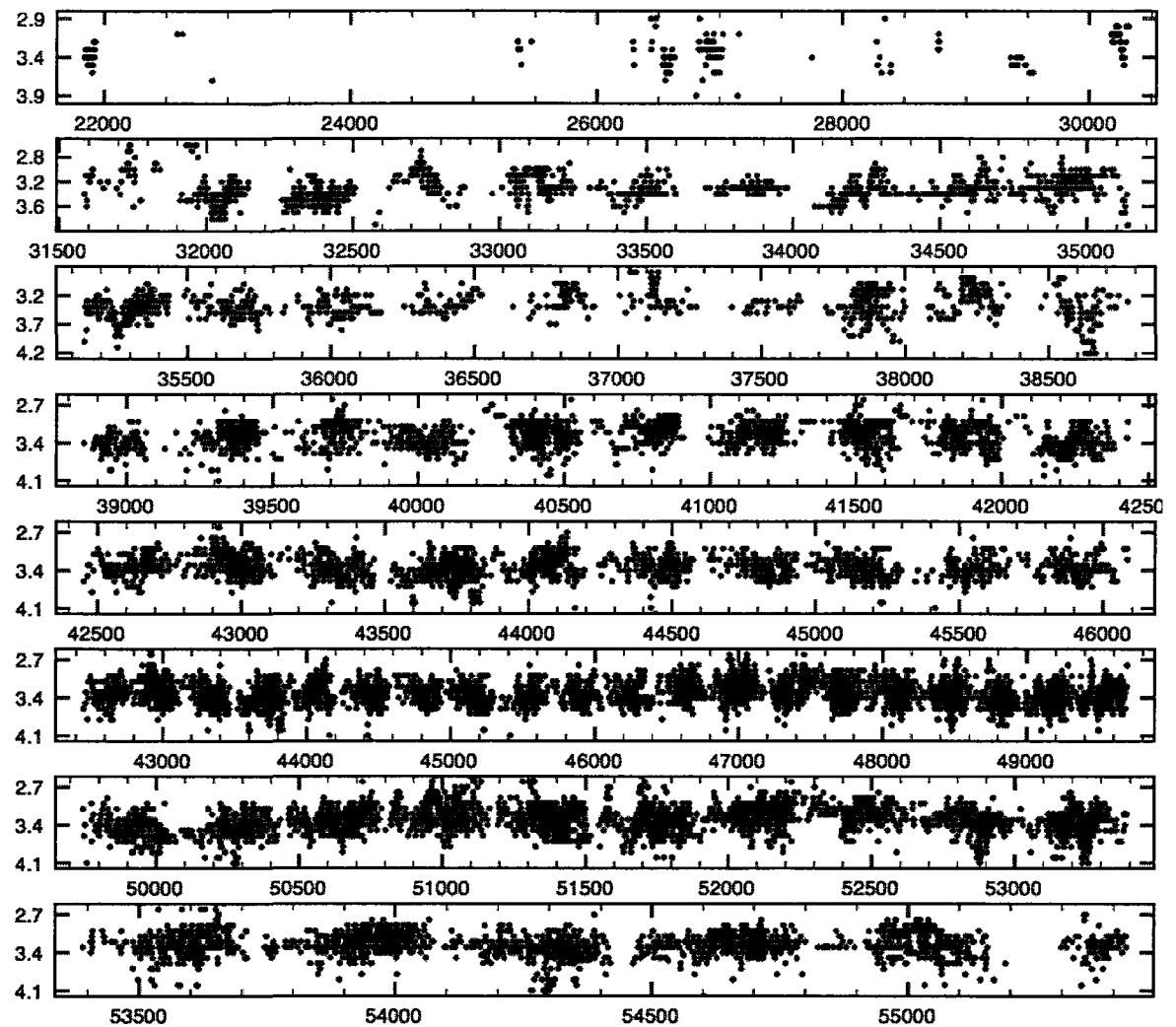
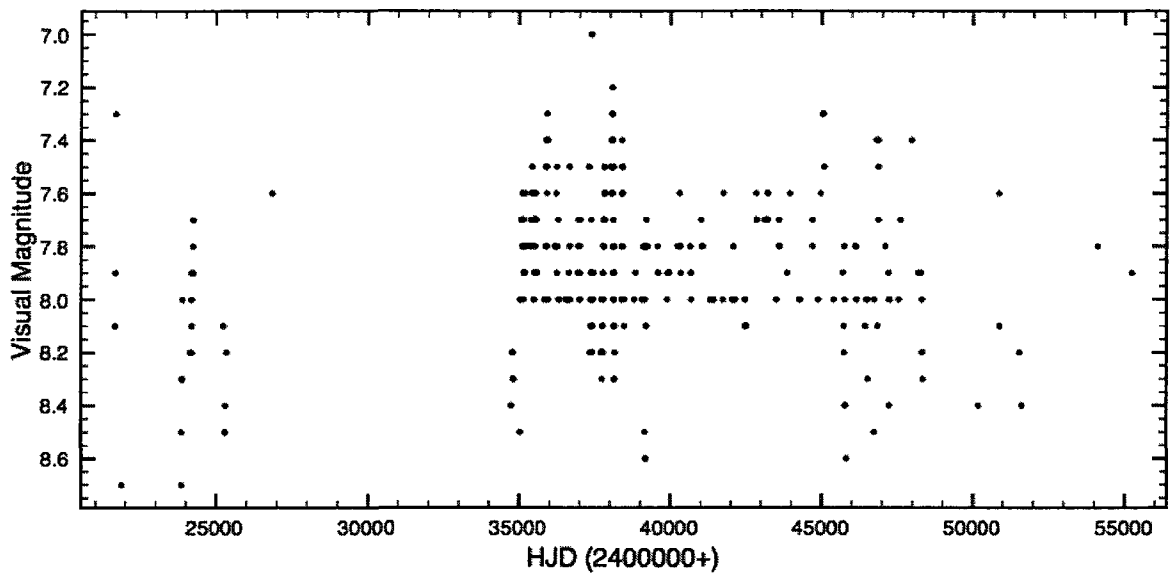


Figure B.54:  $\alpha$  Herculis visual (AAVSO) light curve.



**Figure B.55:**  $\alpha$  Herculis visual (AAVSO) light curve - expanded view of figure B.54.



**Figure B.56:** RV Hydrae visual (AAVSO) light curve.

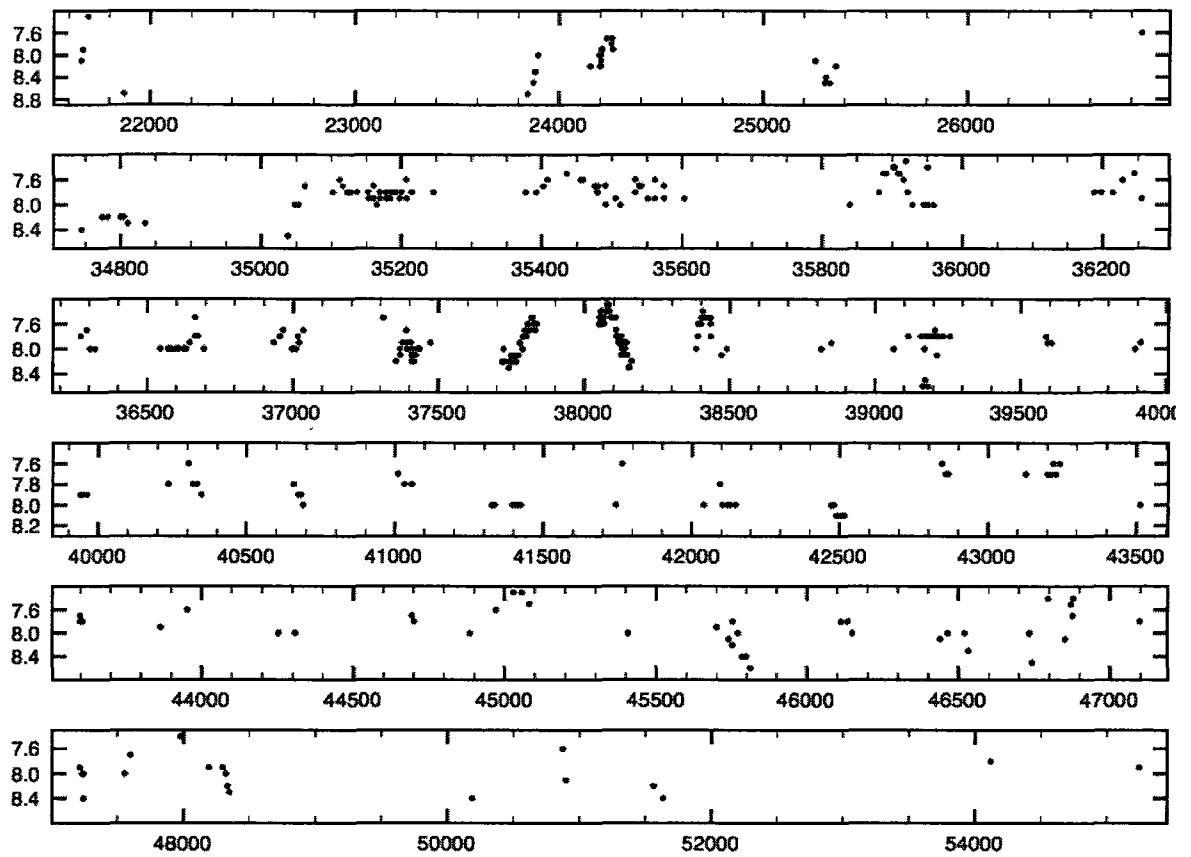


**Figure B.57:** RV Hydrae visual (AAVSO) light curve - expanded view of figure B.56.

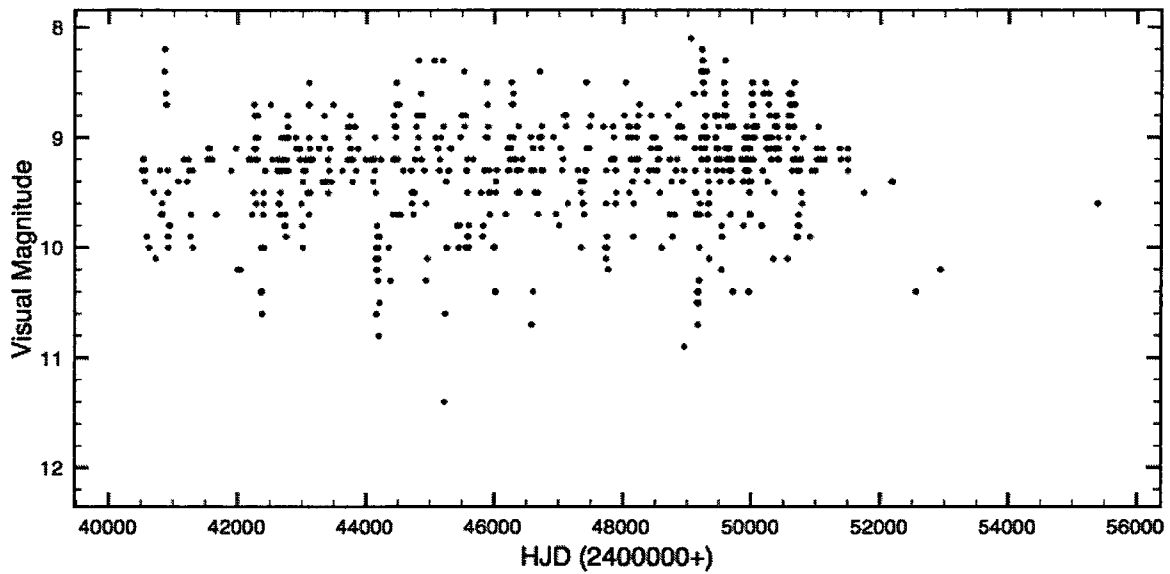


**Figure B.58:** W Indus visual (AAVSO) light curve.

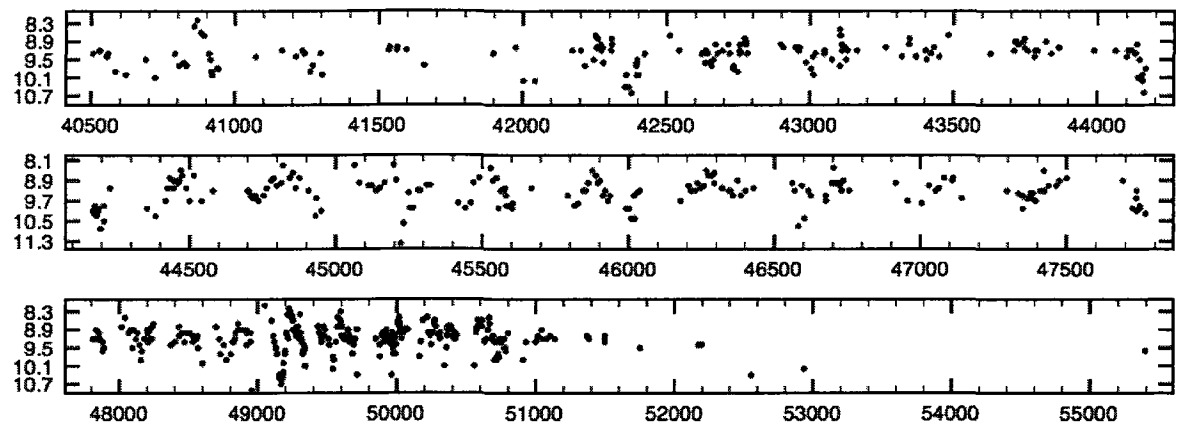


**Figure B.59:** W Indus visual (AAVSO) light curve - expanded view of figure B.58.

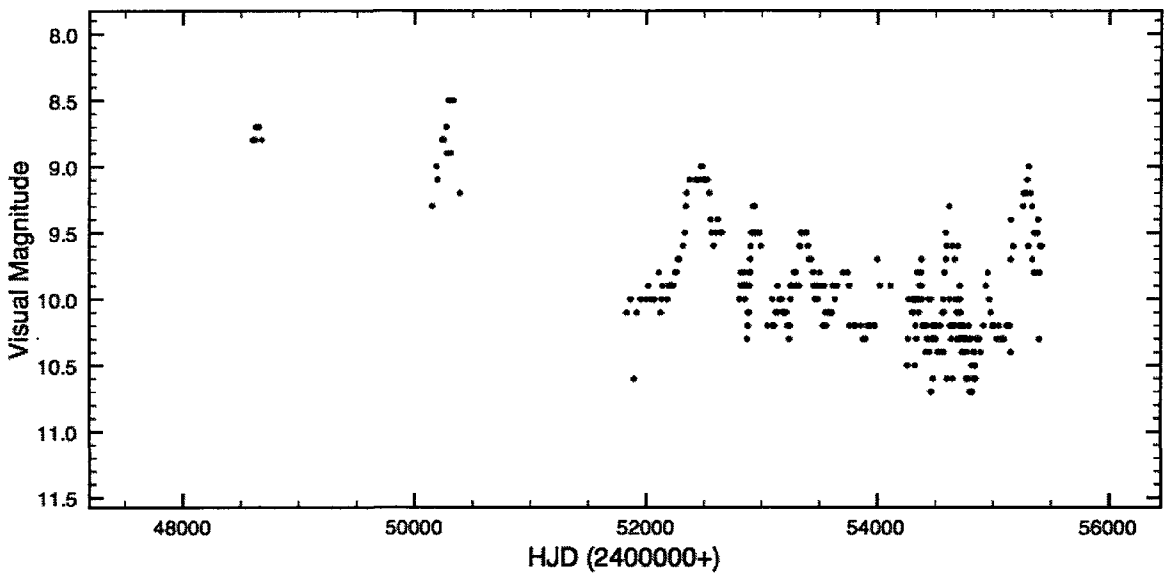


**Figure B.60:** U Lacertae visual (AAVSO) light curve.

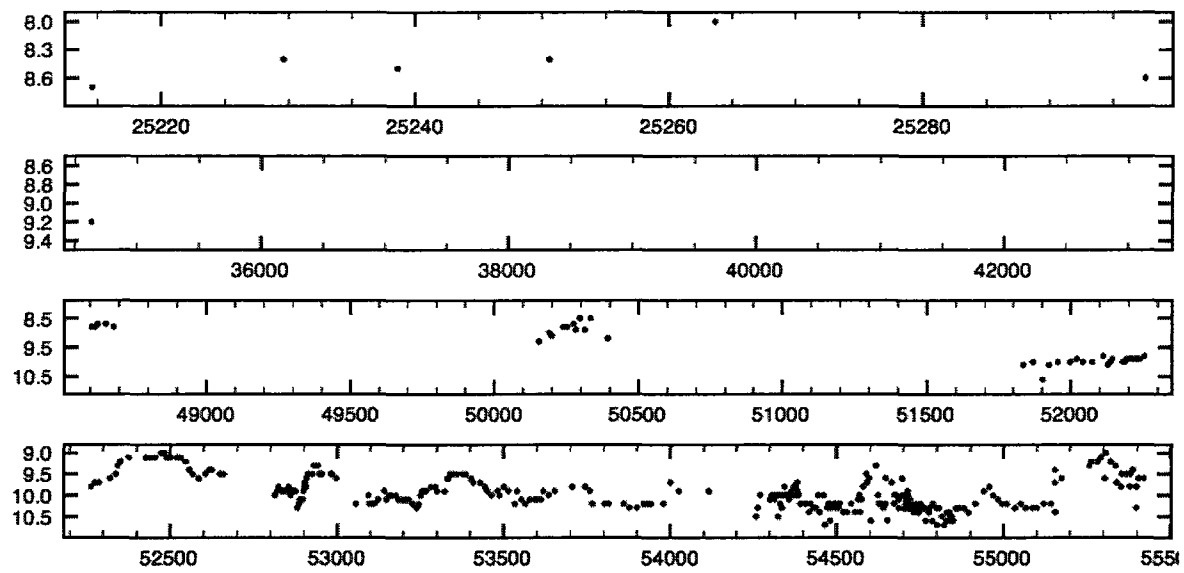


**Figure B.61:** U Lacertae visual (AAVSO) light curve - expanded view of figure B.60.

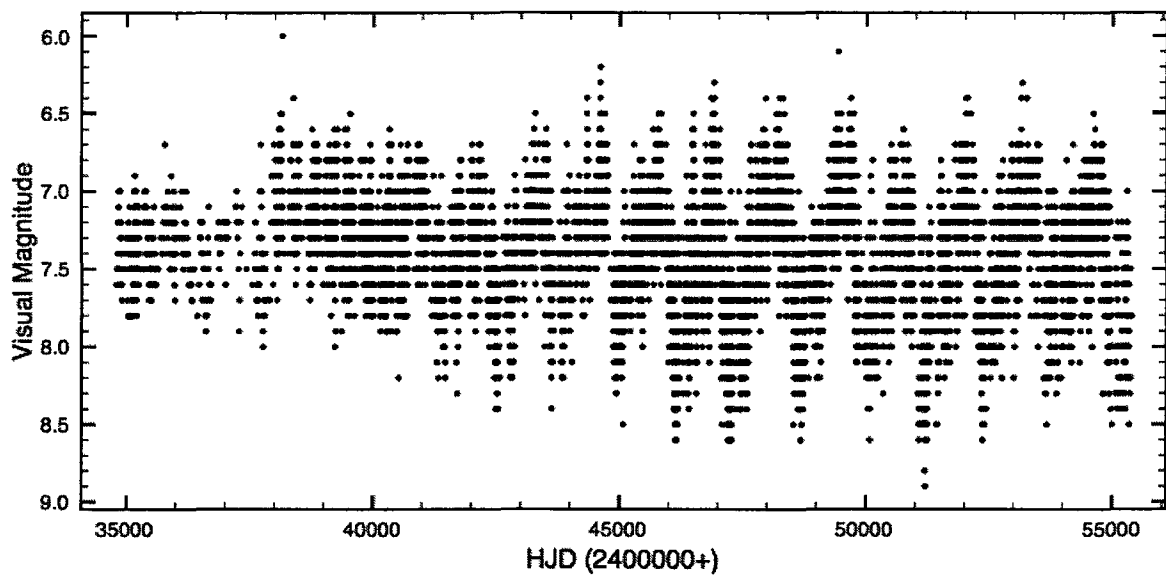
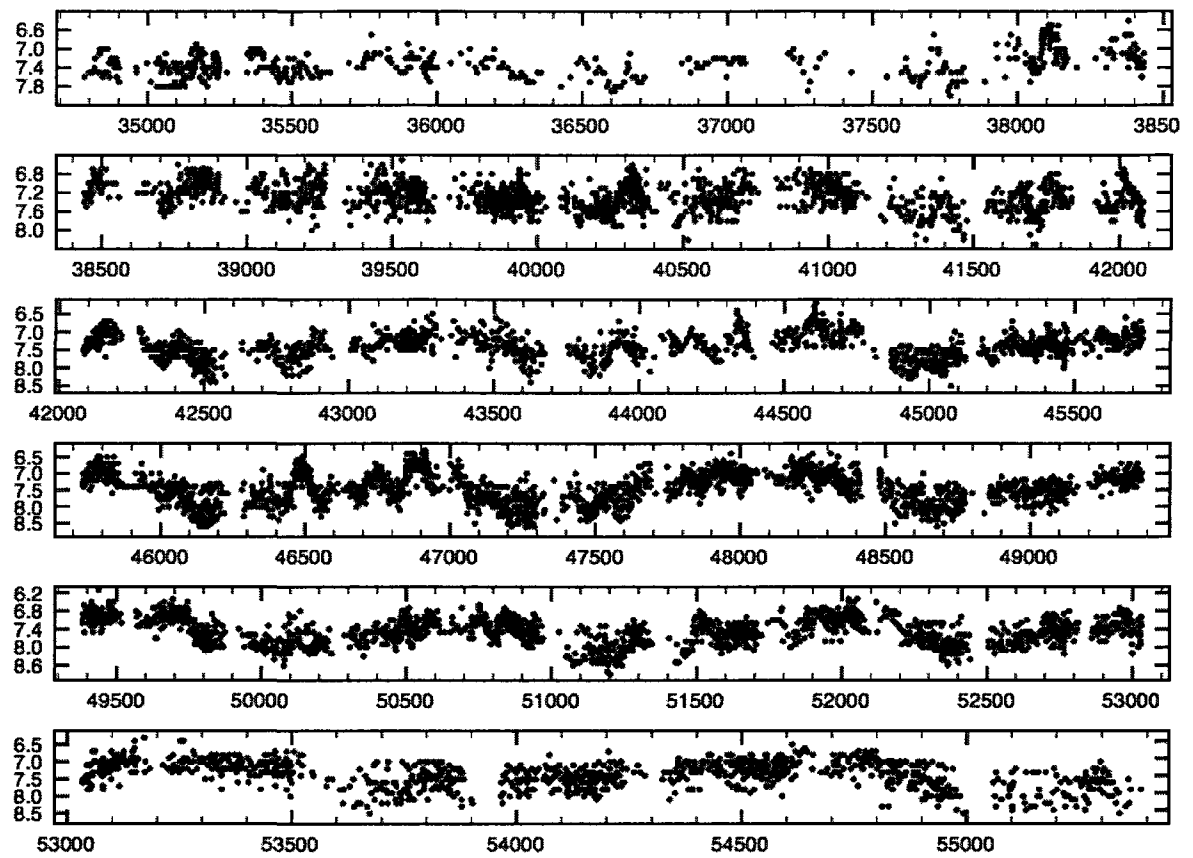
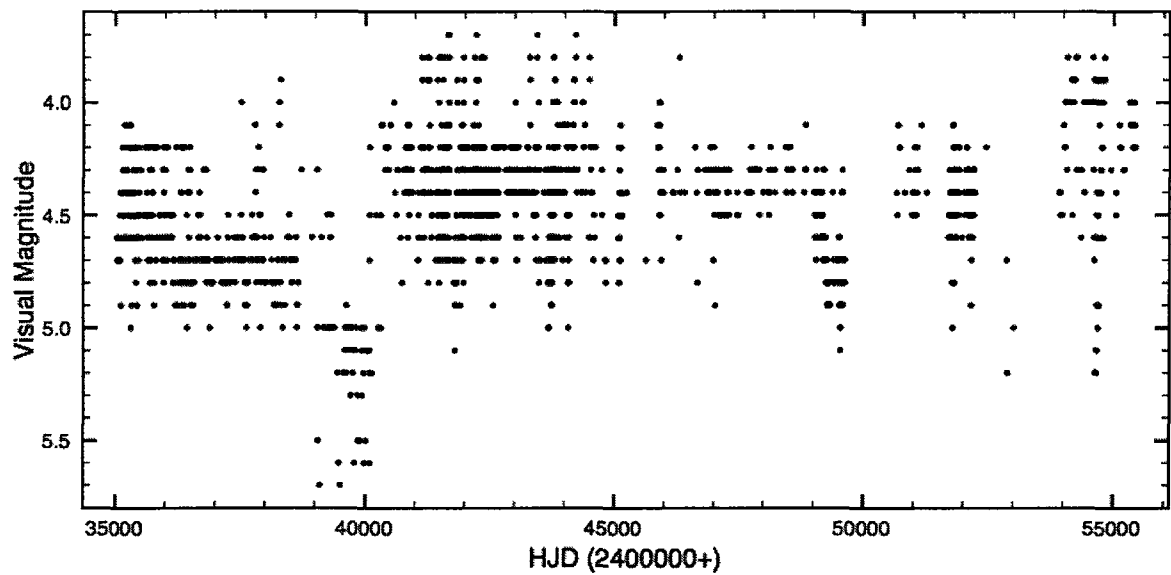


Figure B.62: Y Lyncis visual (AAVSO) light curve.



**Figure B.63:** Y Lyncis visual (AAVSO) light curve - expanded view of figure B.62.



**Figure B.64:**  $\delta^2$  Lyrae visual (AAVSO) light curve.

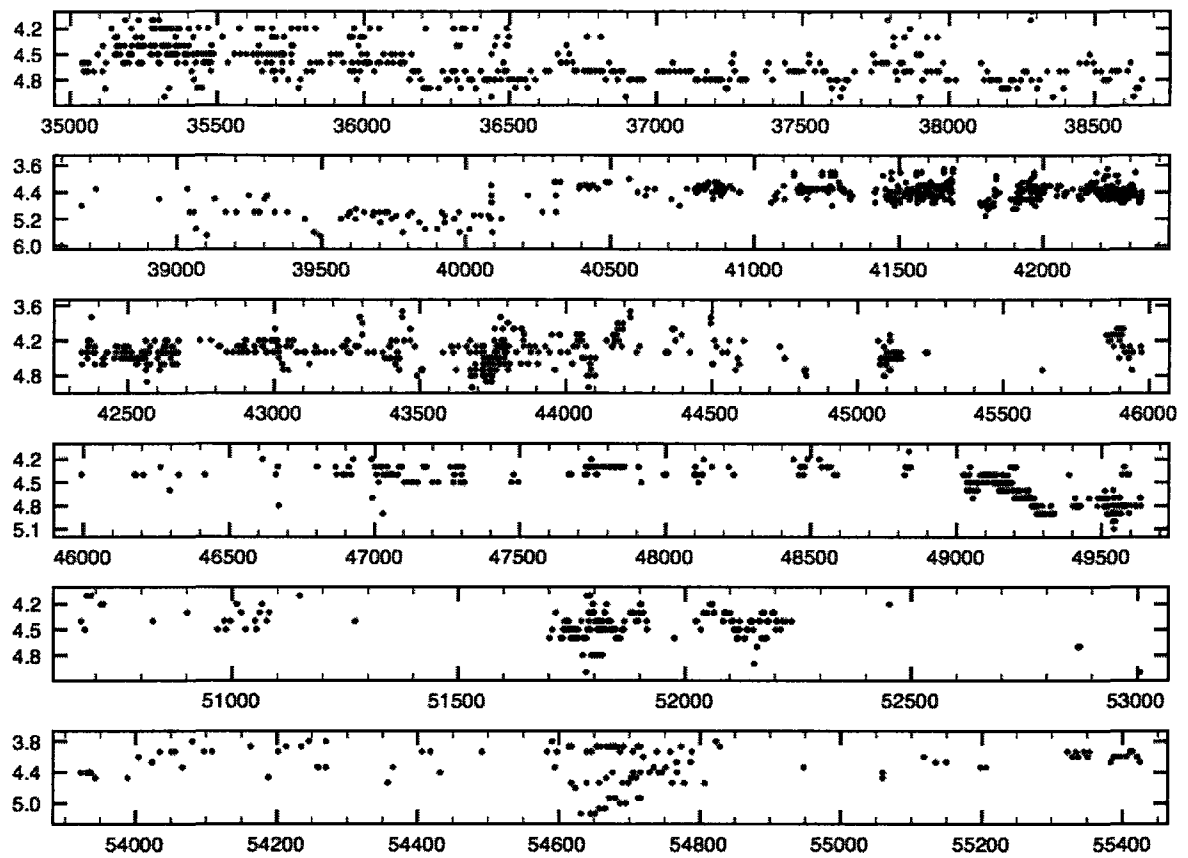


**Figure B.65:**  $\delta^2$  Lyrae visual (AAVSO) light curve - expanded view of figure B.64.

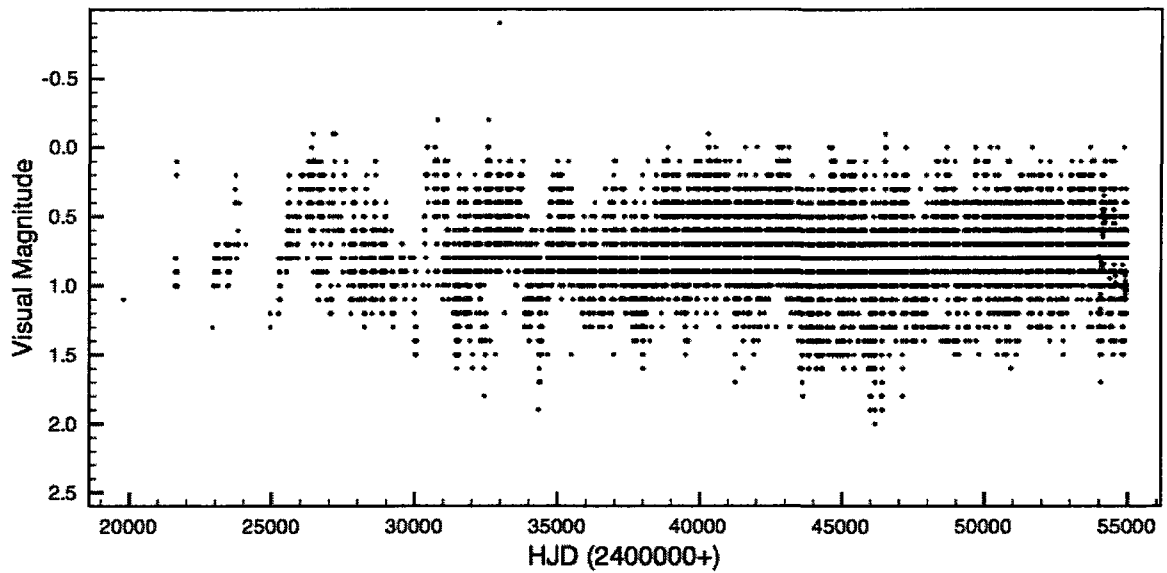


**Figure B.66:**  $\alpha$  Orionis visual (AAVSO) light curve.

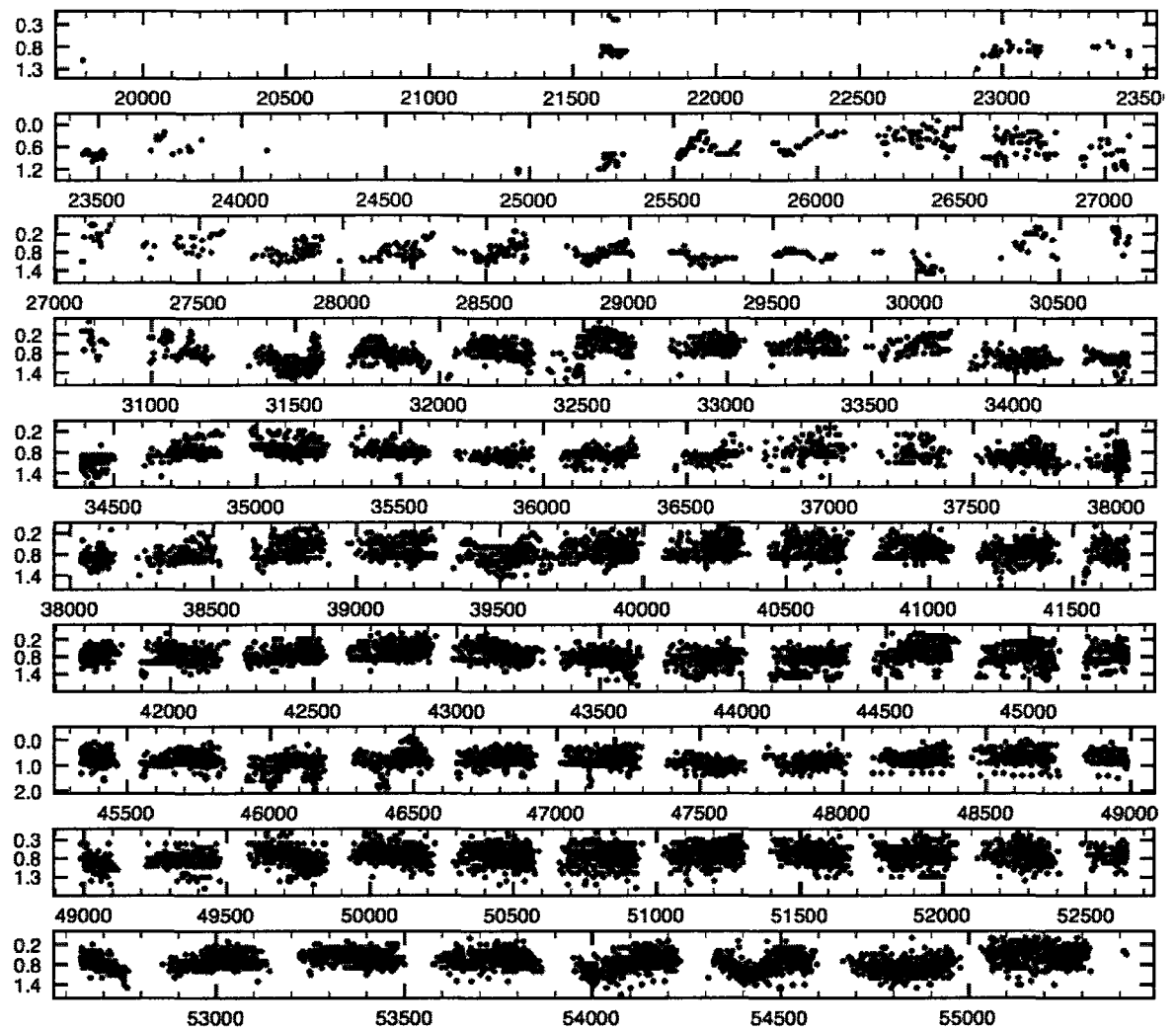


**Figure B.67:**  $\alpha$  Orionis visual (AAVSO) light curve - expanded view of figure B.66.

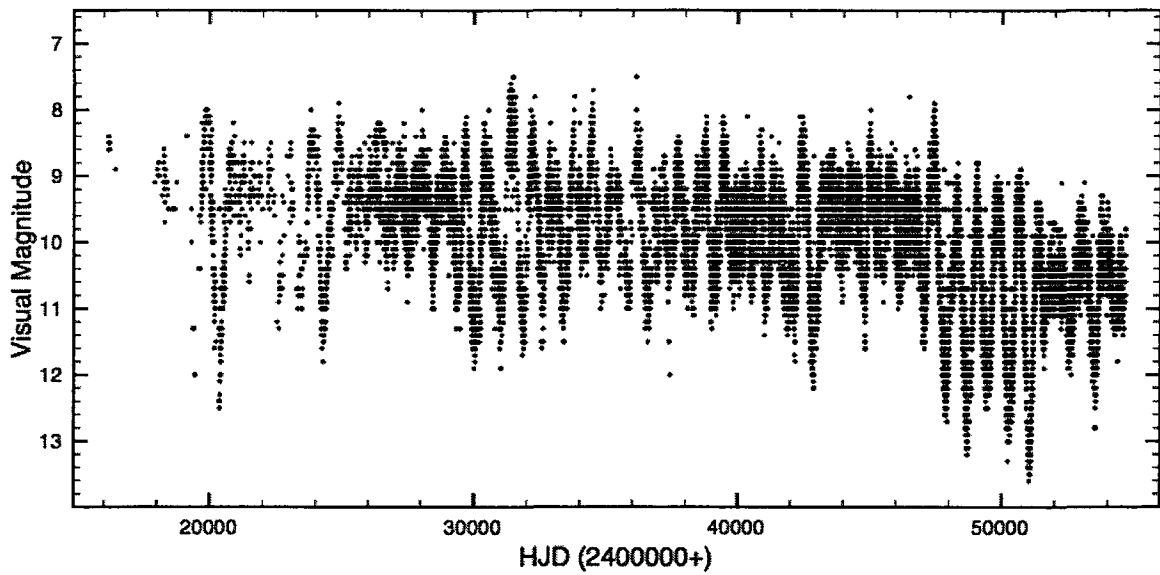


**Figure B.68:** S Persei visual (AAVSO) light curve.

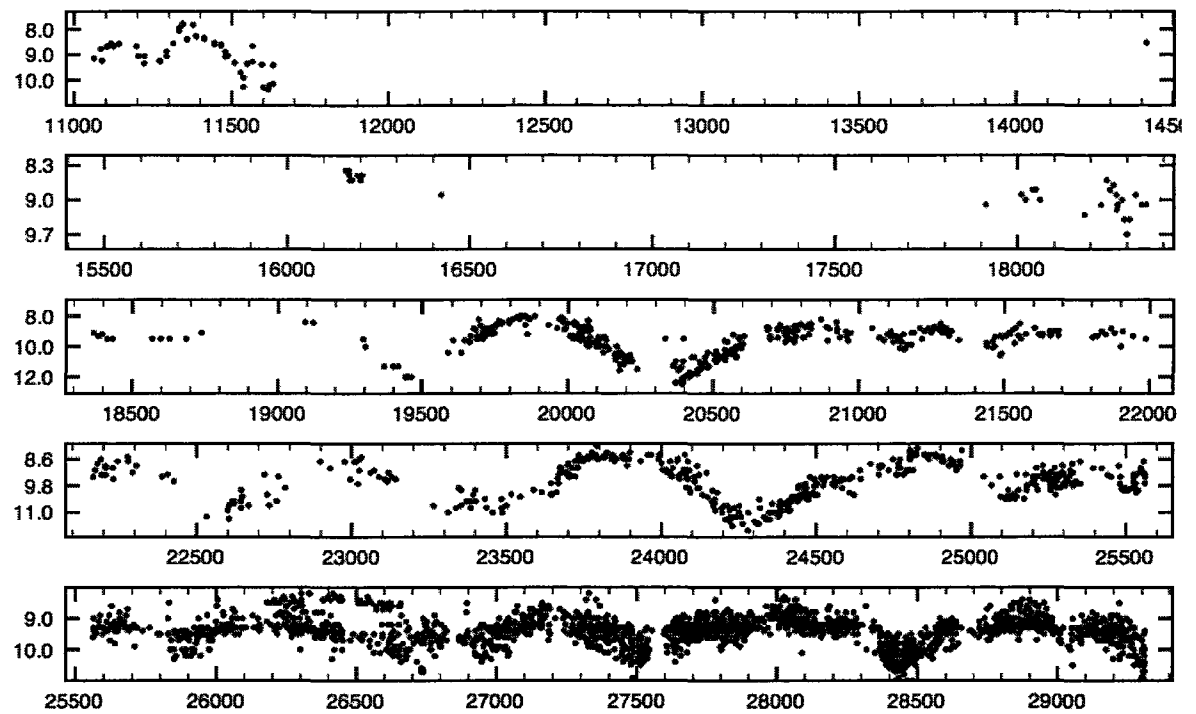


**Figure B.69:** S Persei visual (AAVSO) light curve - expanded view of figure B.68 (continued in next figure).

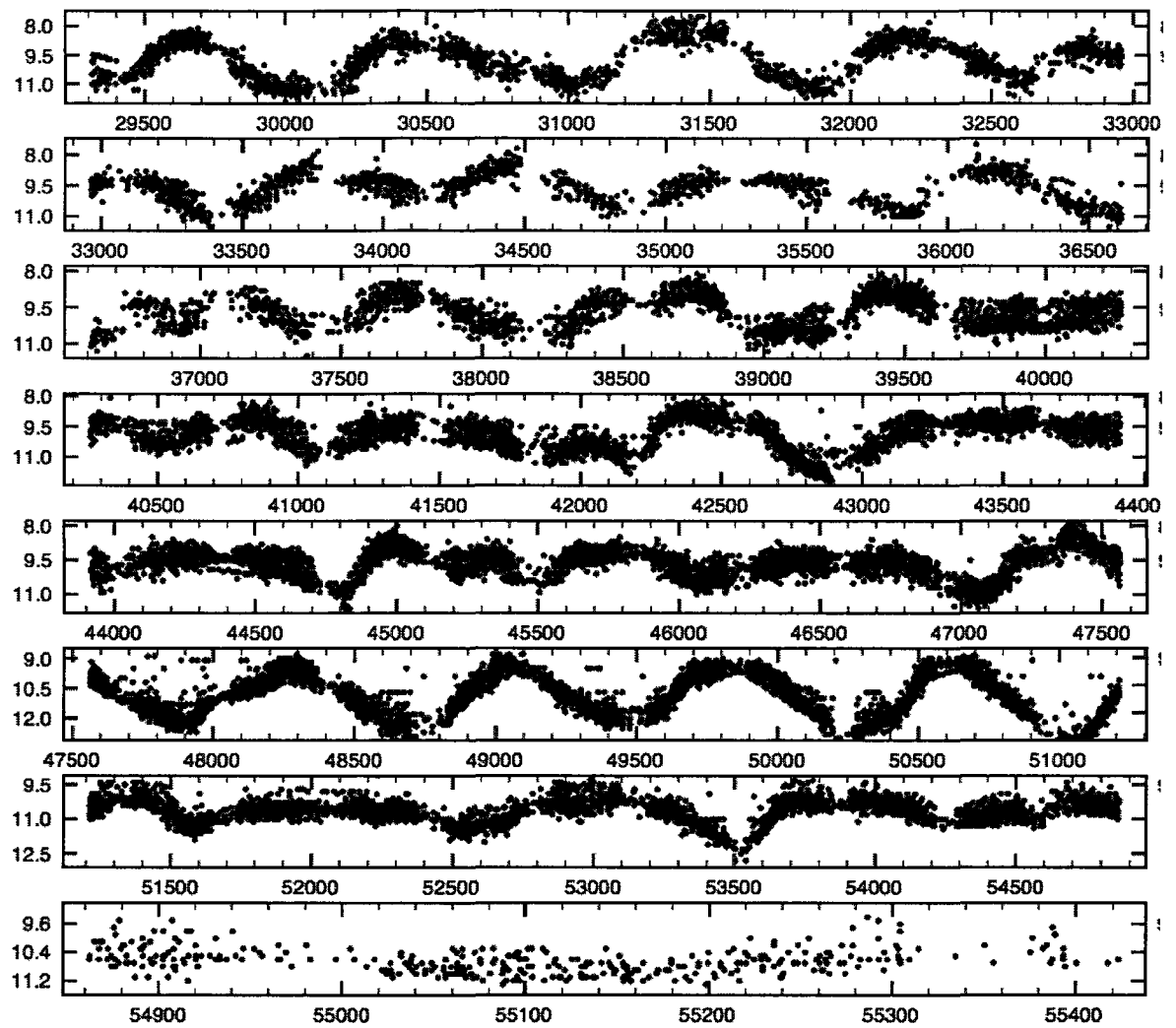


**Figure B.70:** S Persei expanded light curve (continued).

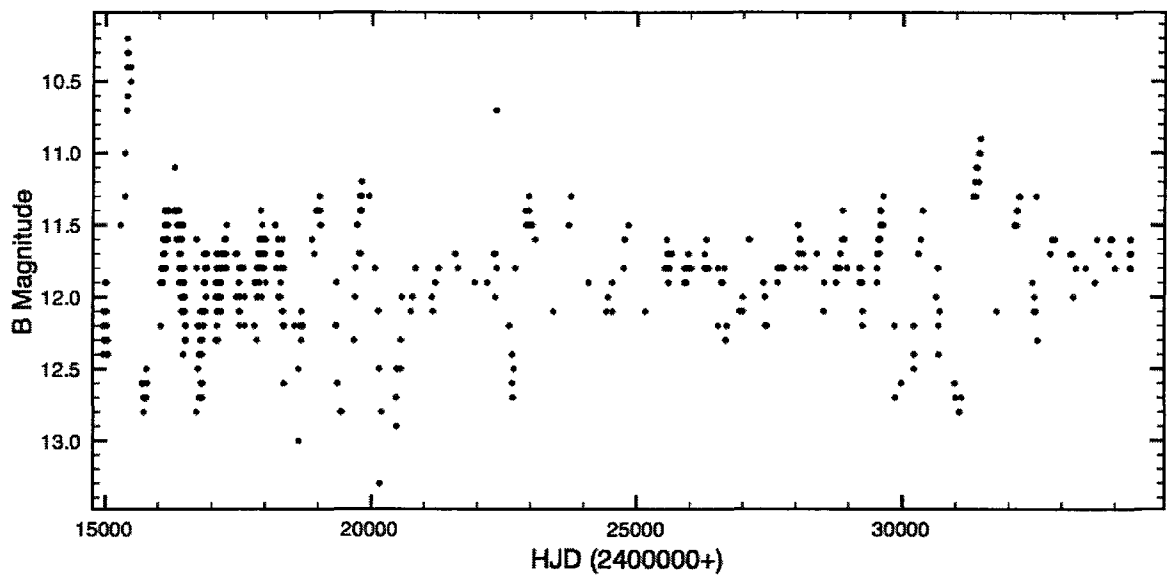


**Figure B.71:** S Persei photographic light curve.

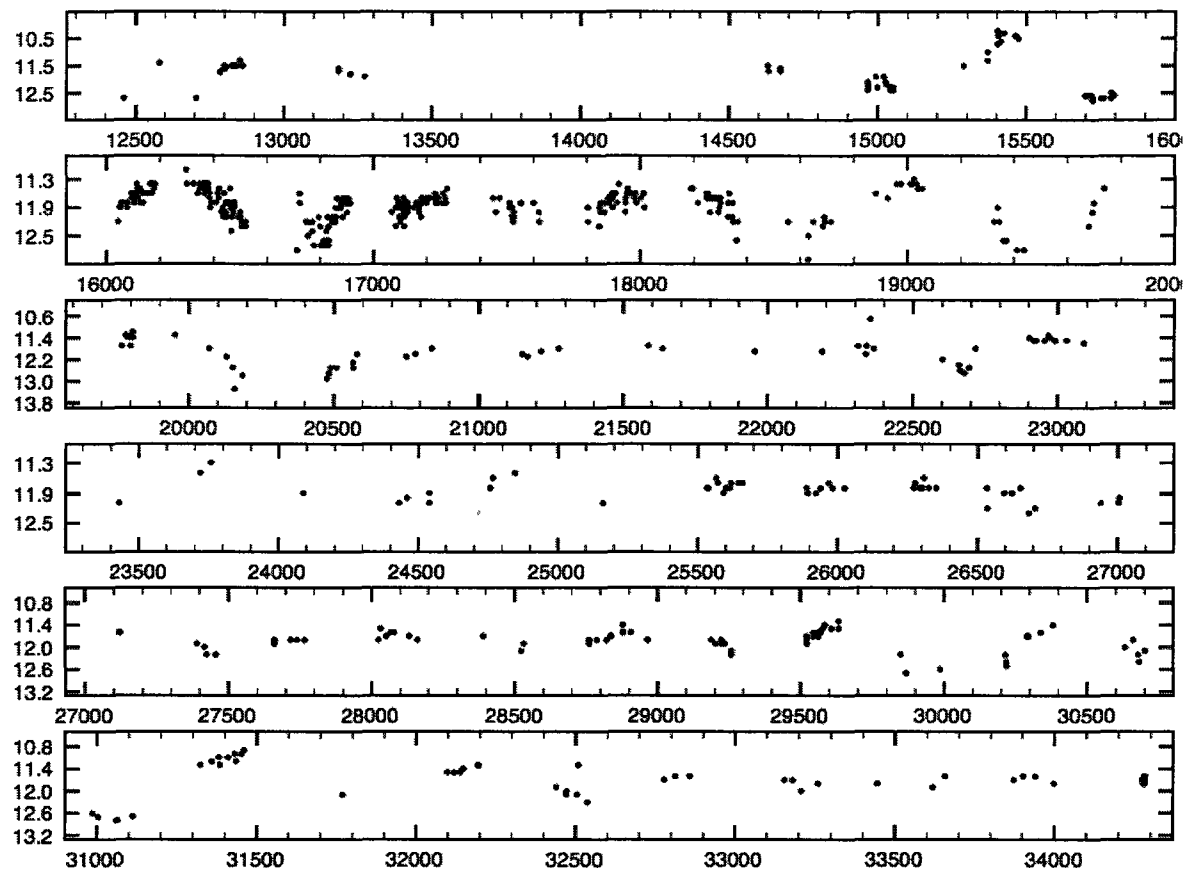


**Figure B.72:** S Persei photographic light curve - expanded view of figure B.71.

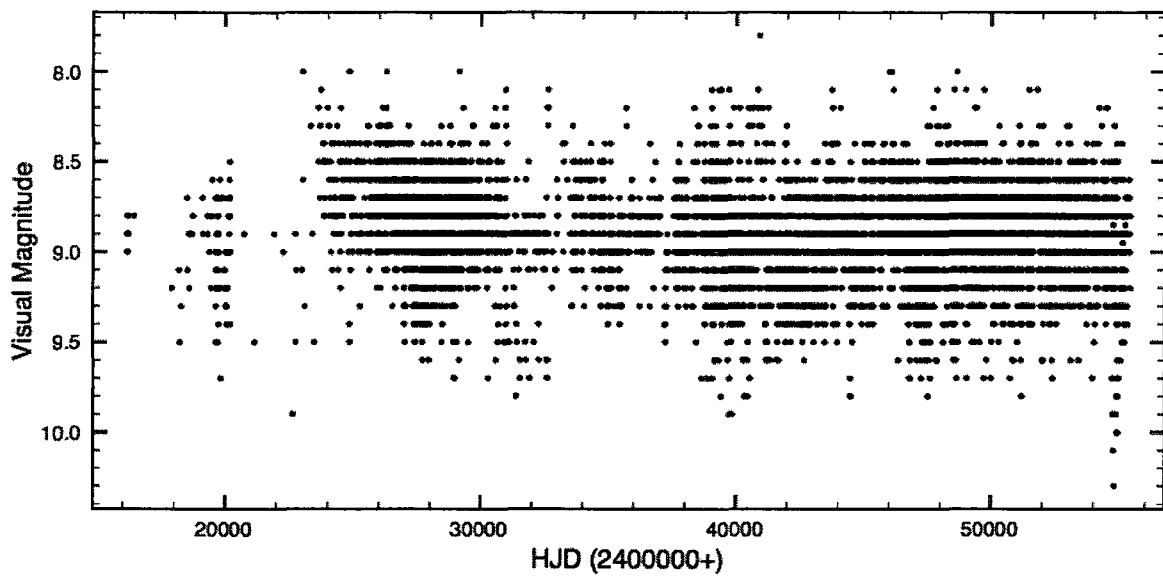


**Figure B.73:** T Persei visual (AAVSO) light curve.

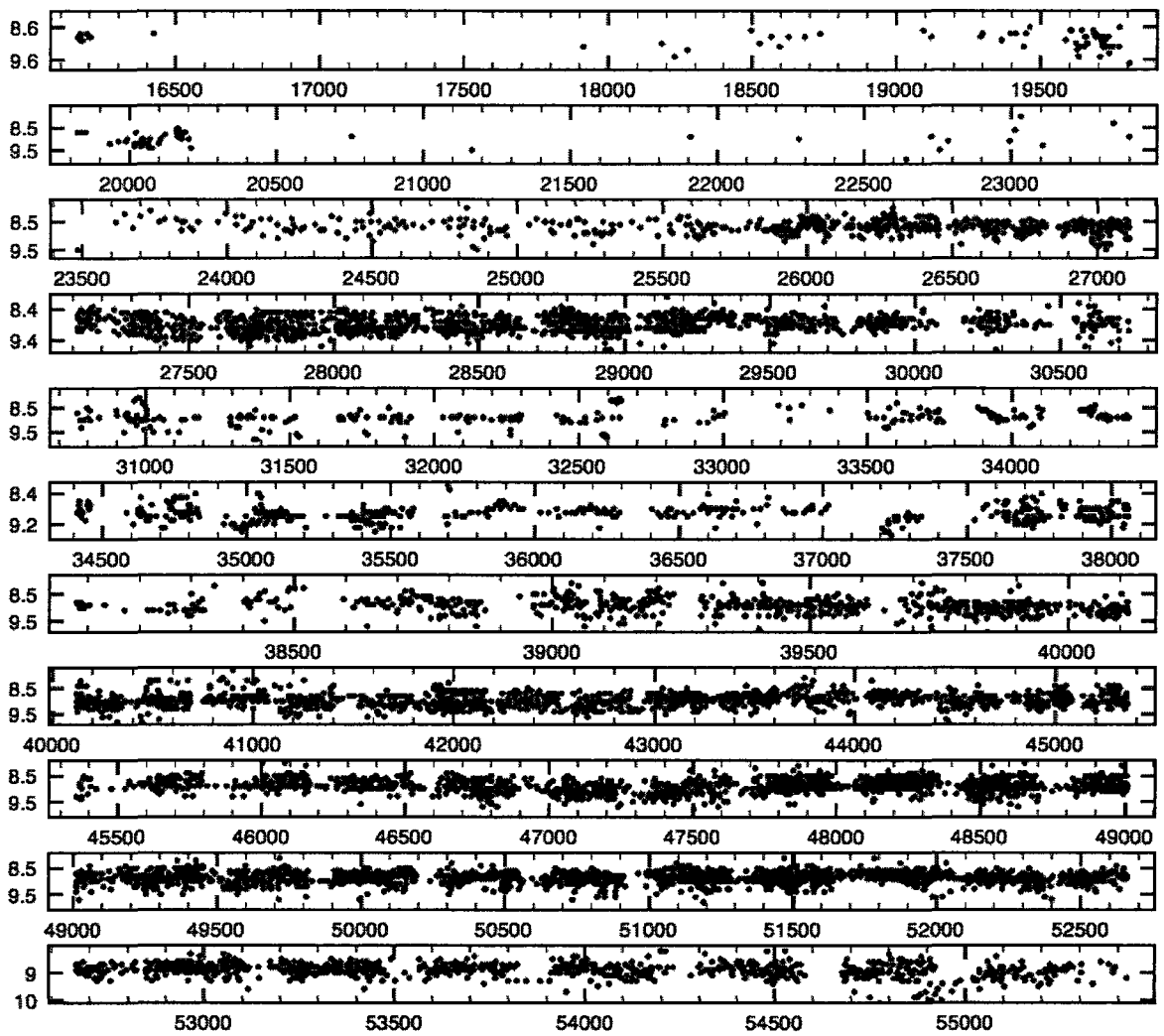


**Figure B.74:** T Persei visual (AAVSO) light curve - expanded view of figure B.73.

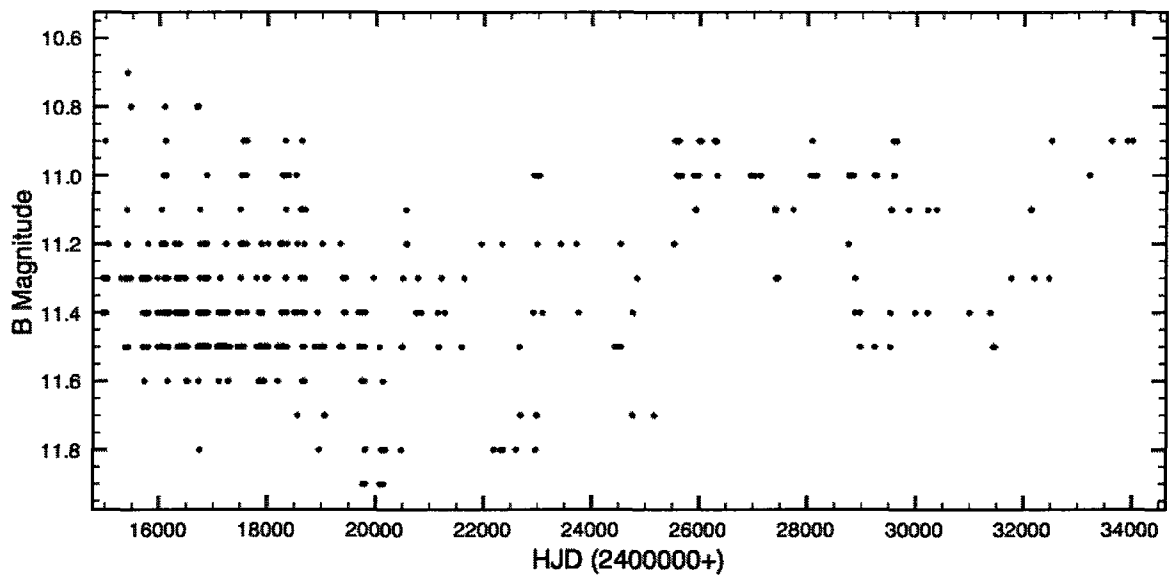


**Figure B.75:** T Persei photographic light curve.

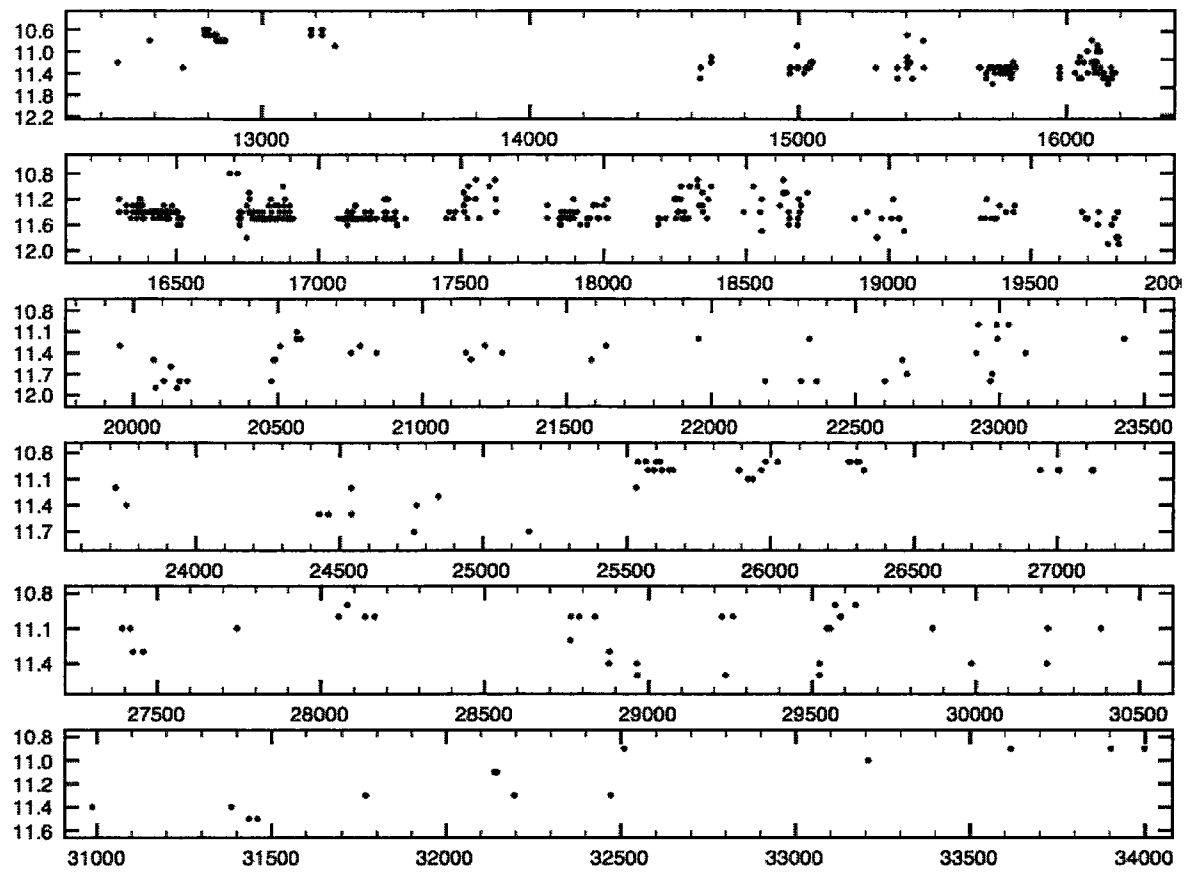


Figure B.76: T Persei photographic light curve - expanded view ??.

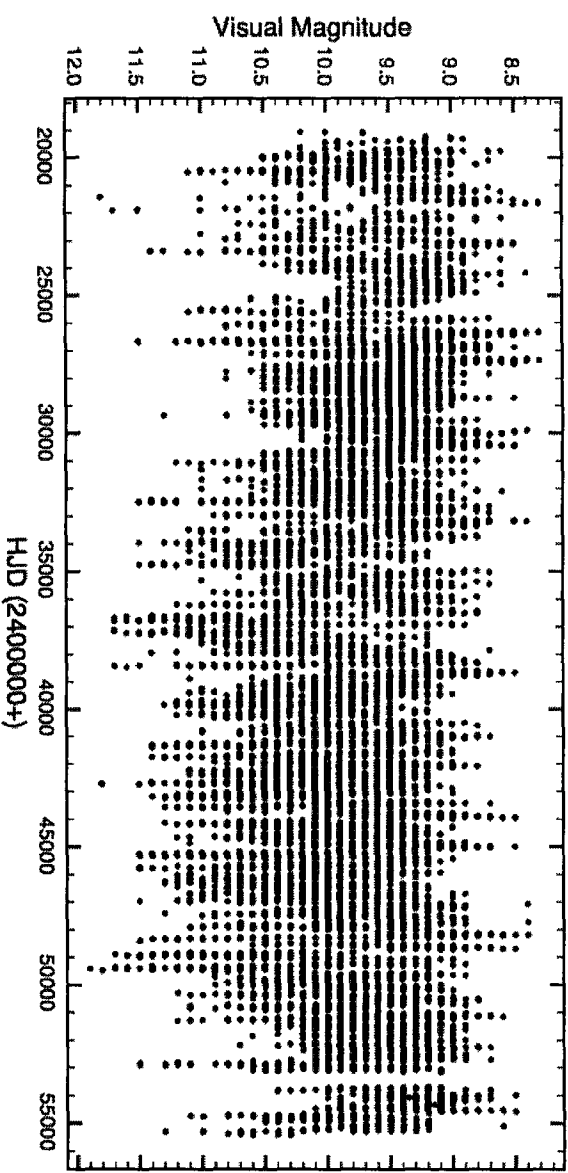
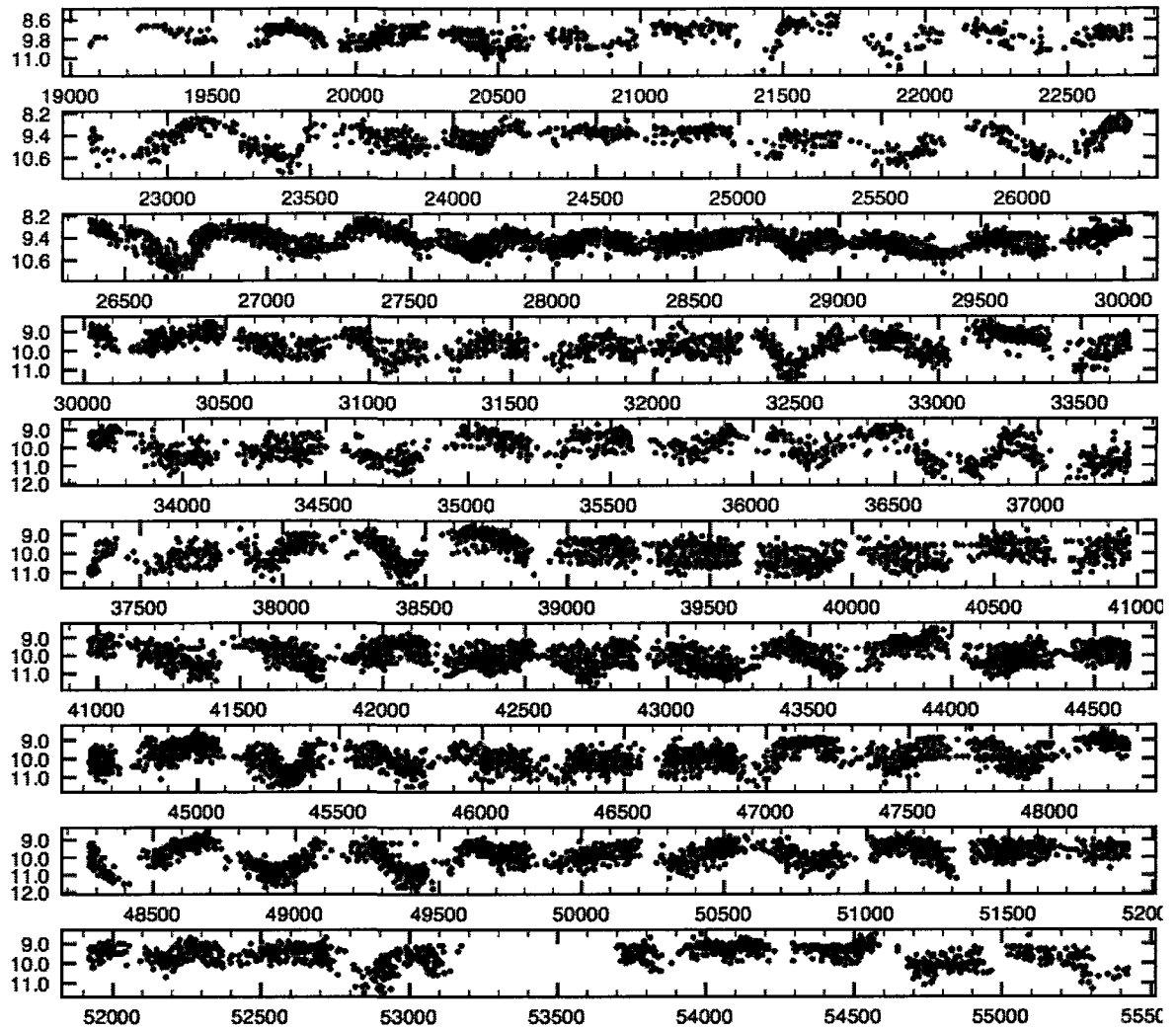
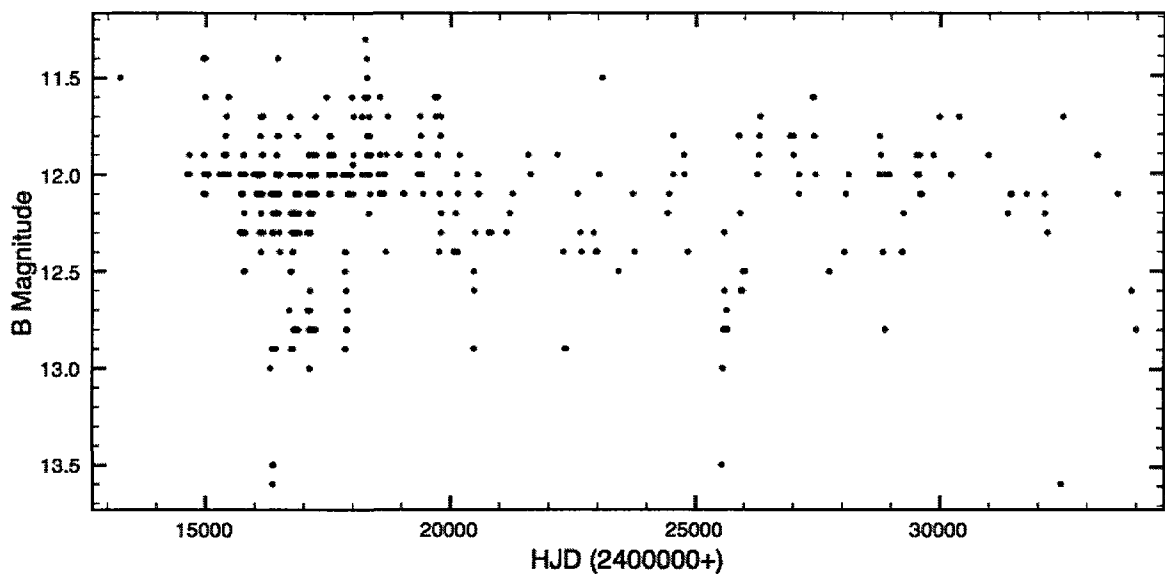


Figure B.77: W Persei visual (AAVSO) light curve.



**Figure B.78:** W Persei visual (AAVSO) light curve - expanded view of figure B.77.



**Figure B.79:** W Persei photographic light curve.

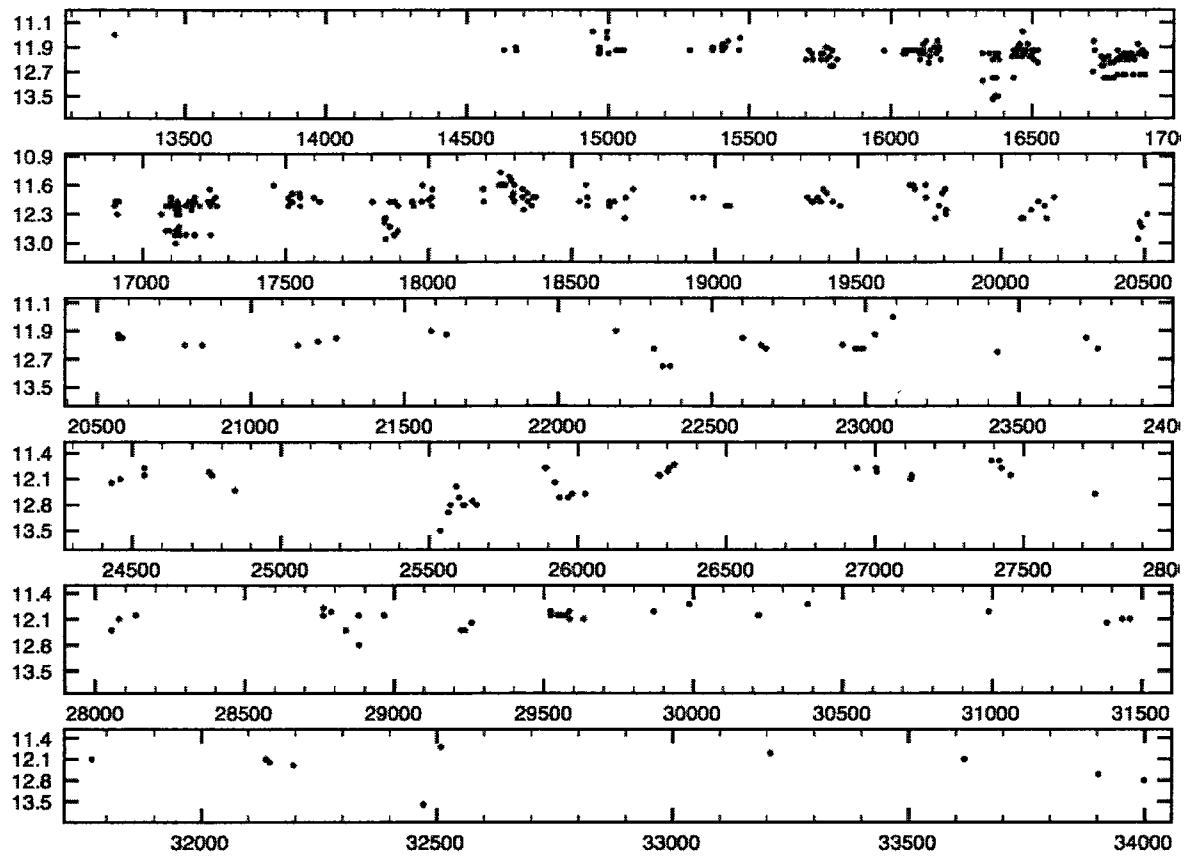


**Figure B.80:** W Persei photographic light curve - expanded view of figure B.79.

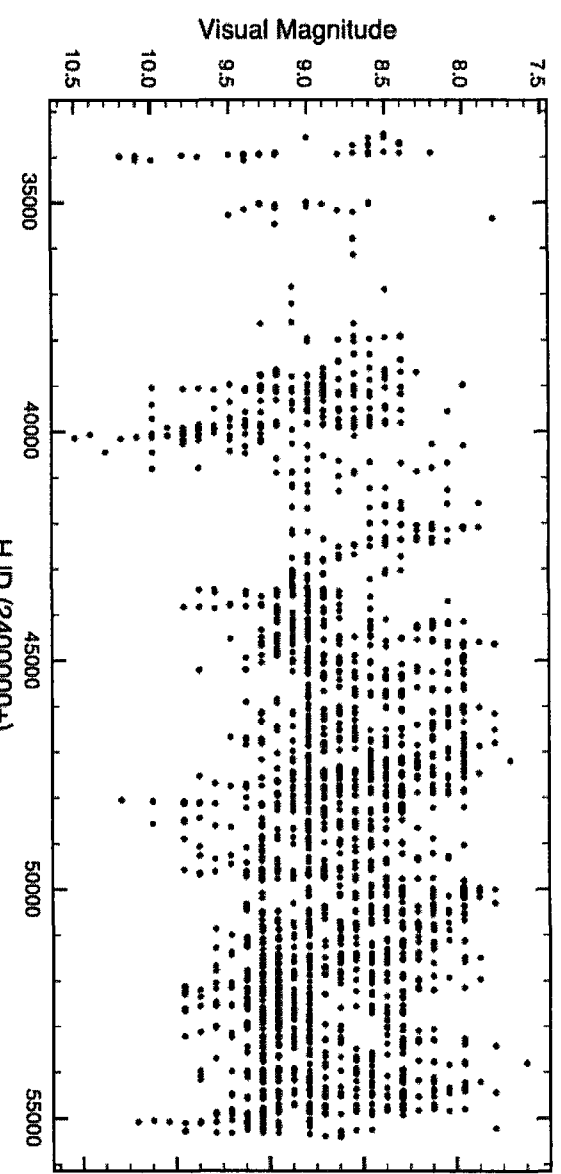
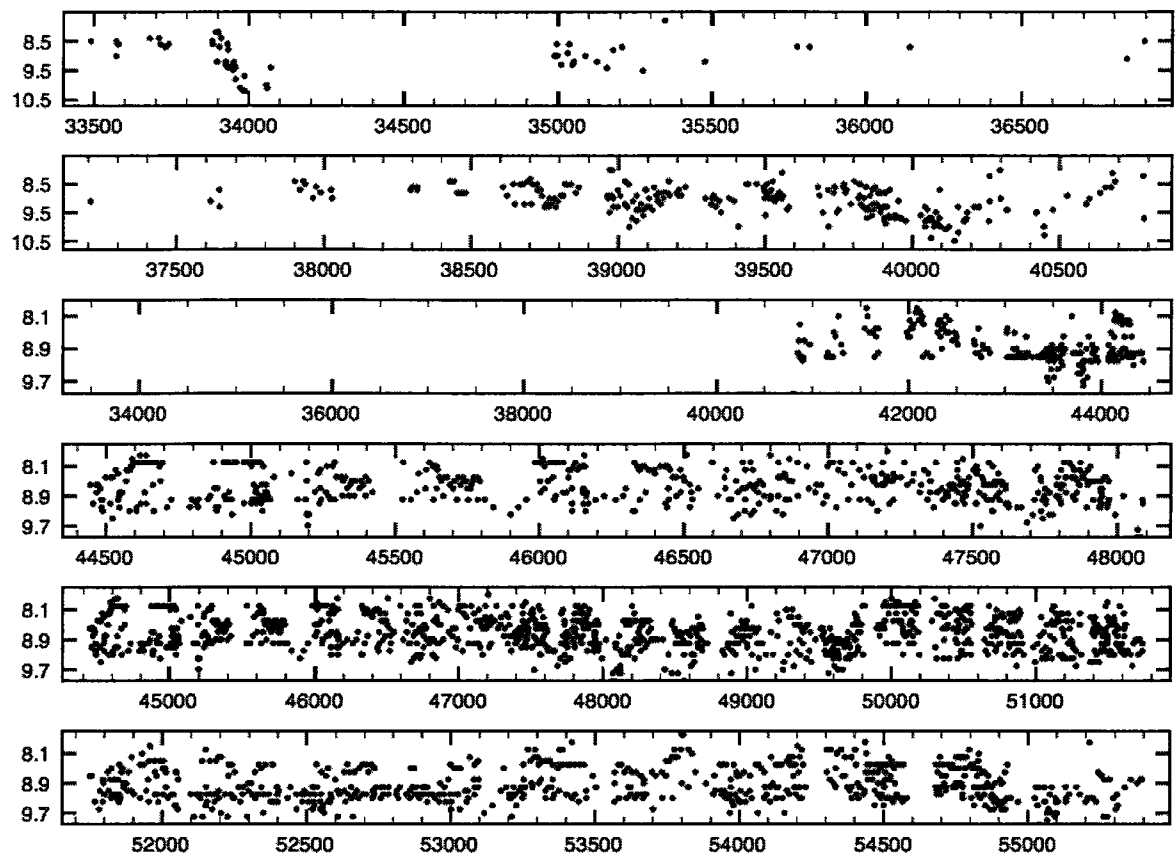
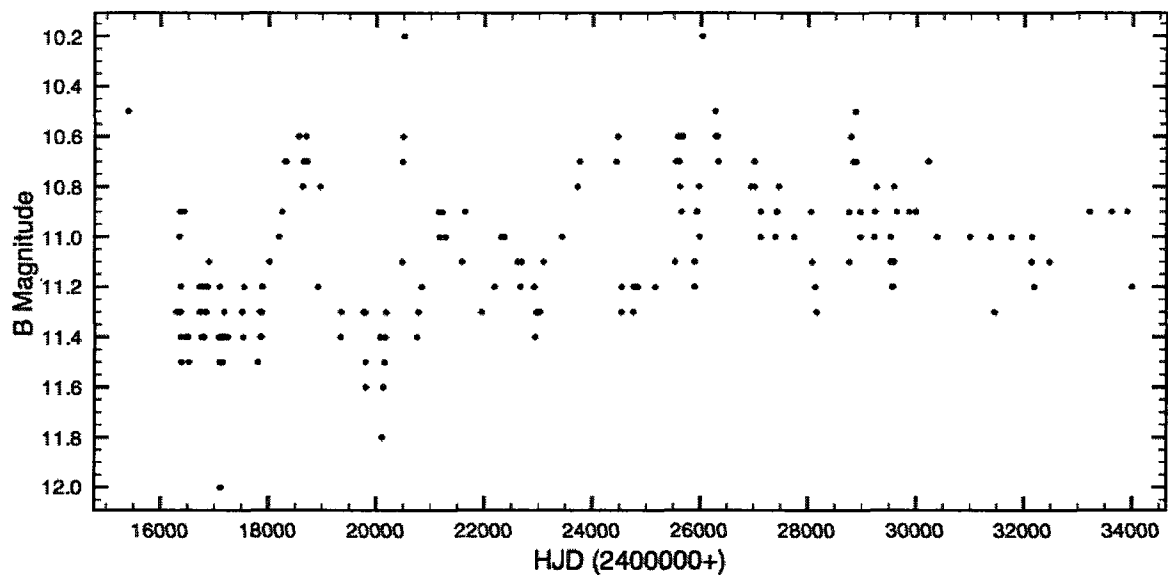


Figure B.81: RS Persei visual (AAVSO) light curve.



**Figure B.82:** RS Persei visual (AAVSO) light curve - expanded view of figure B.81.



**Figure B.83:** RS Persei photographic light curve.

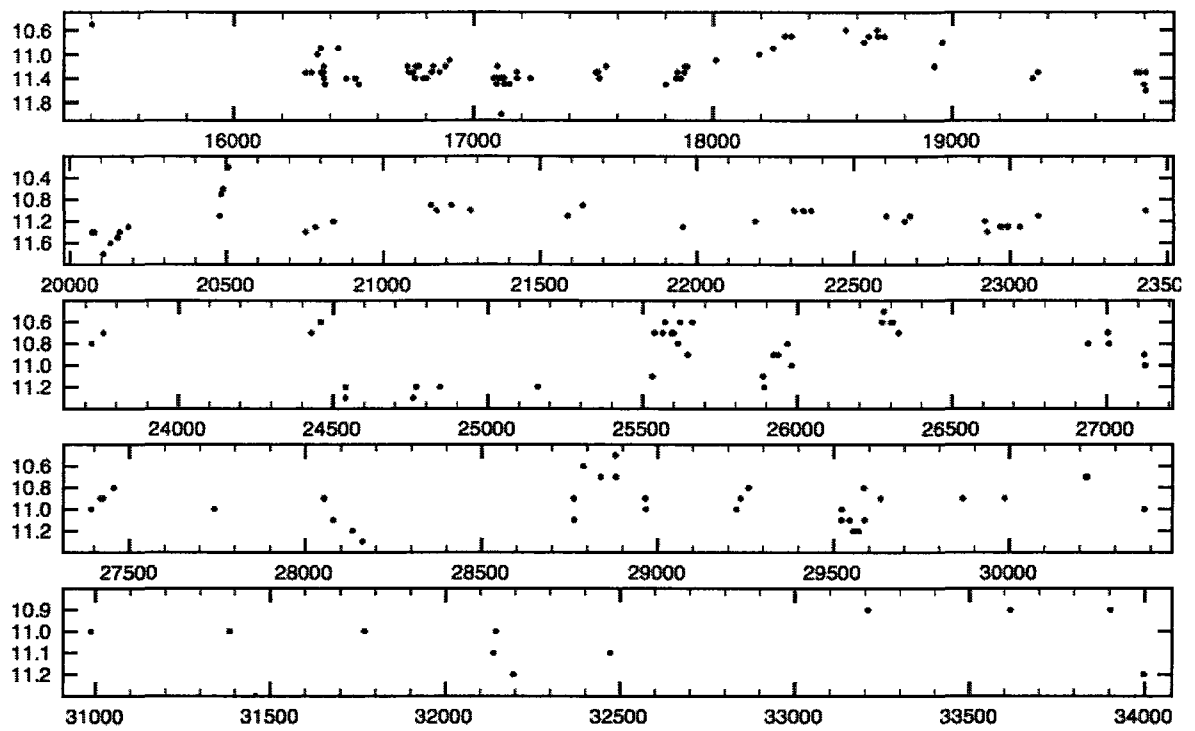


**Figure B.84:** RS Persei photographic light curve - expanded view of figure B.83.

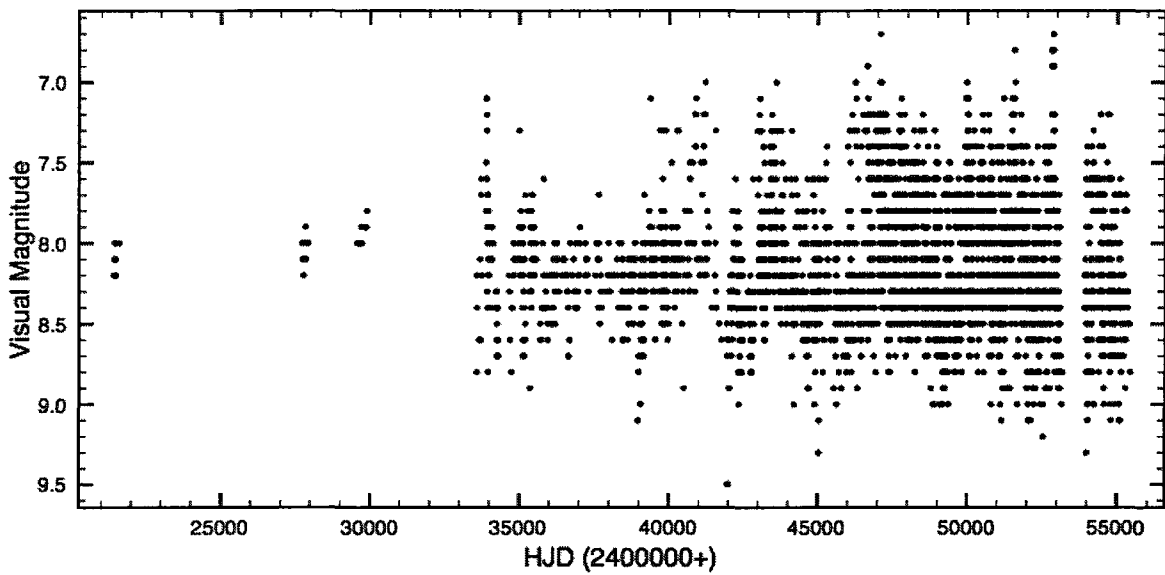


**Figure B.85:** SU Persei visual (AAVSO) light curve.

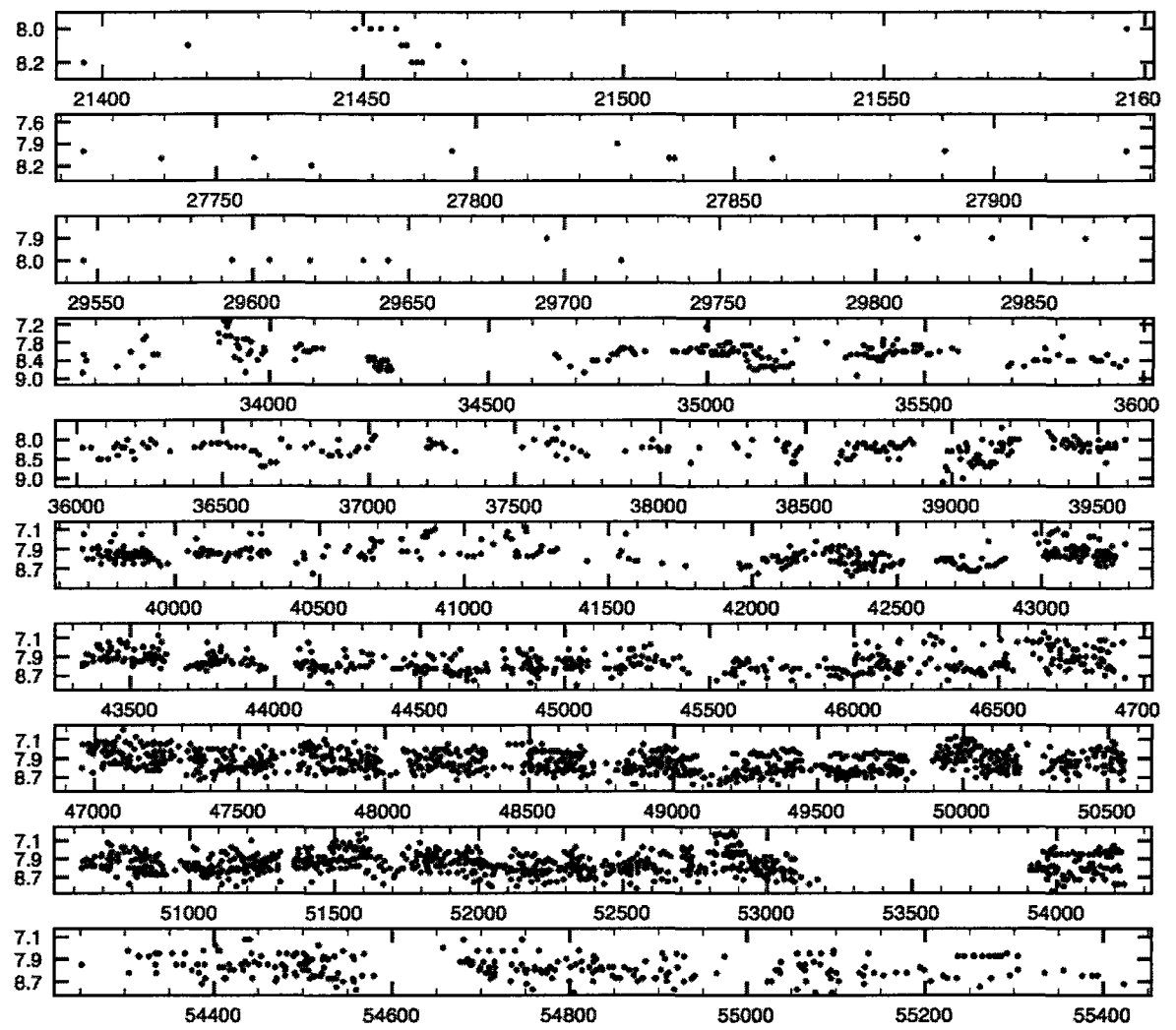


**Figure B.86:** SU Persei visual (AAVSO) light curve - expanded view of figure B.85.

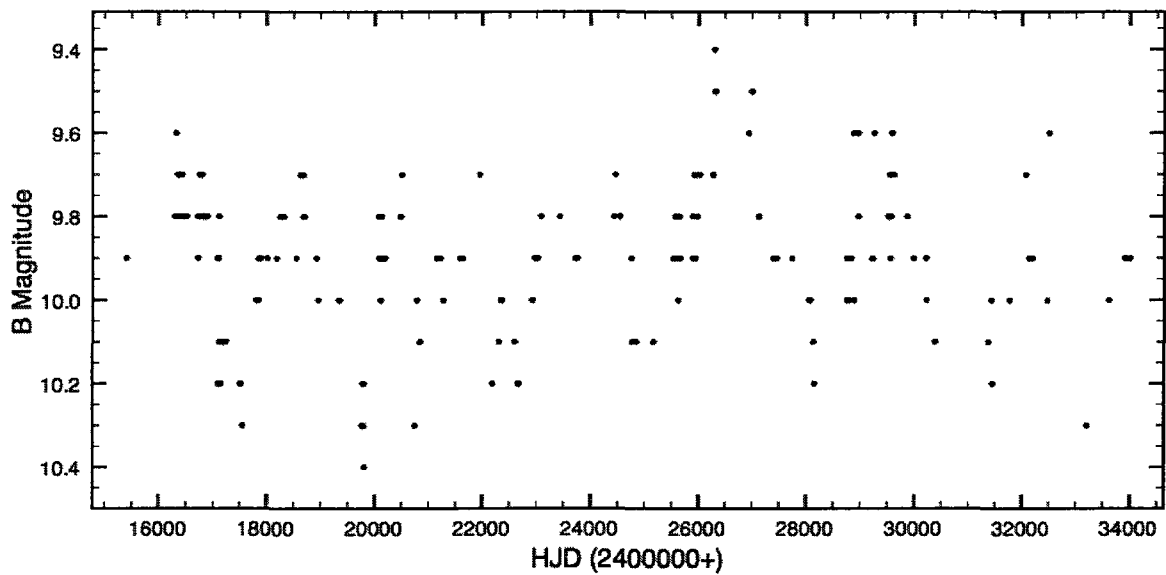


**Figure B.87:** SU Persei photographic light curve.

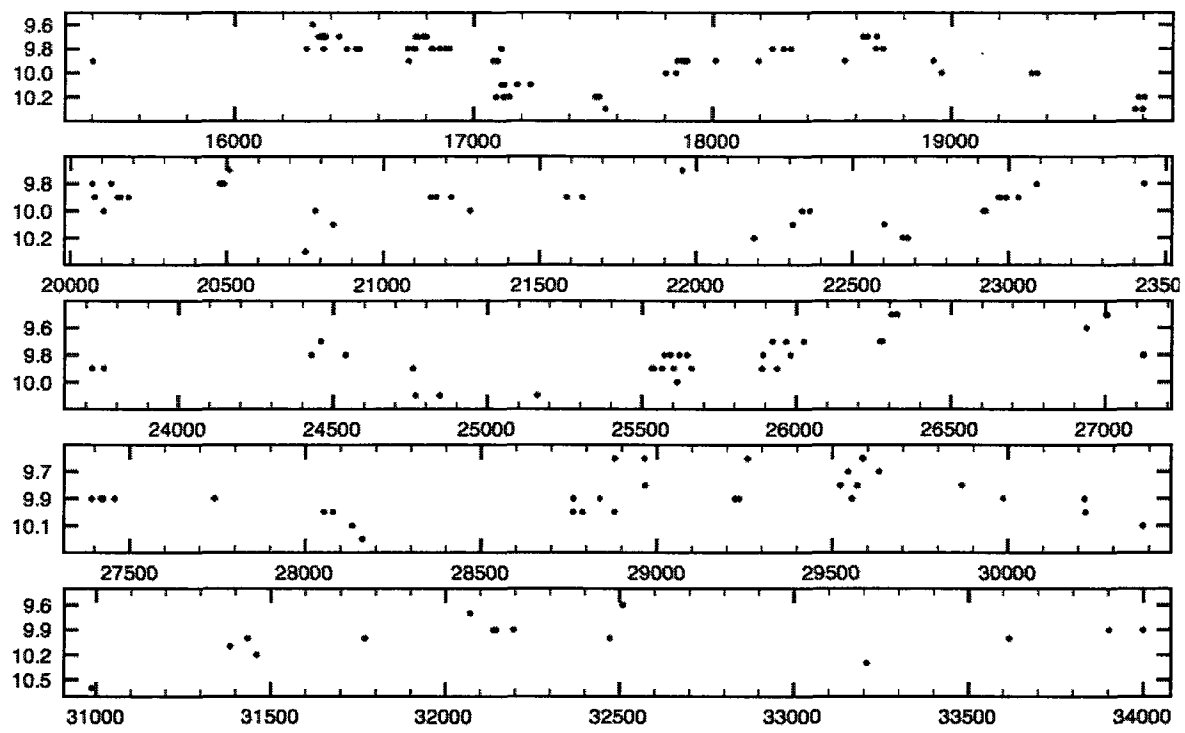


**Figure B.88:** SU Persei photographic light curve - expanded view of figure B.87.

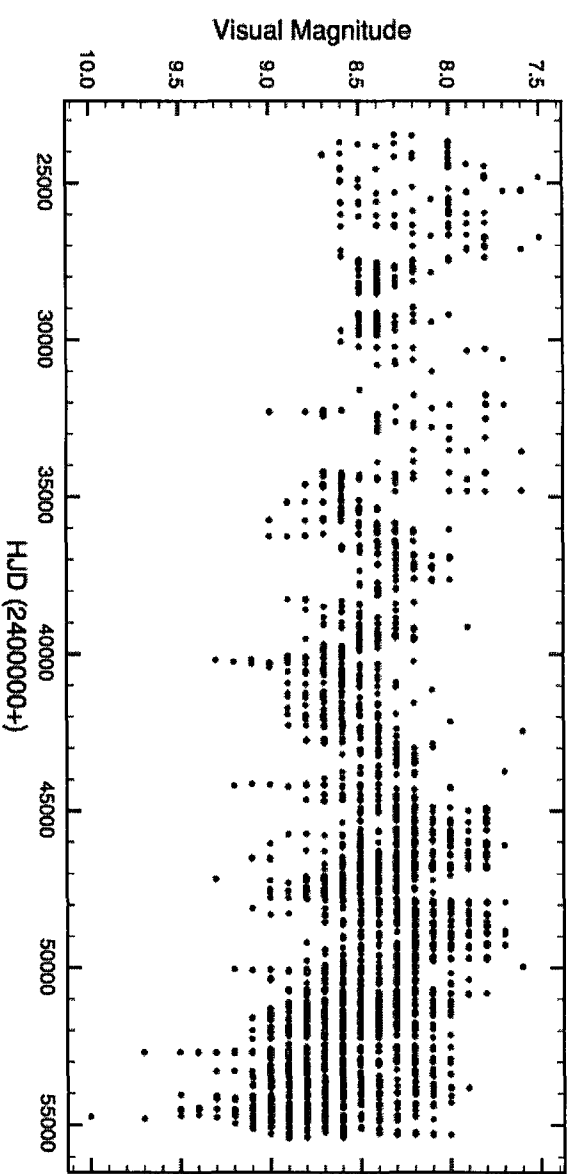
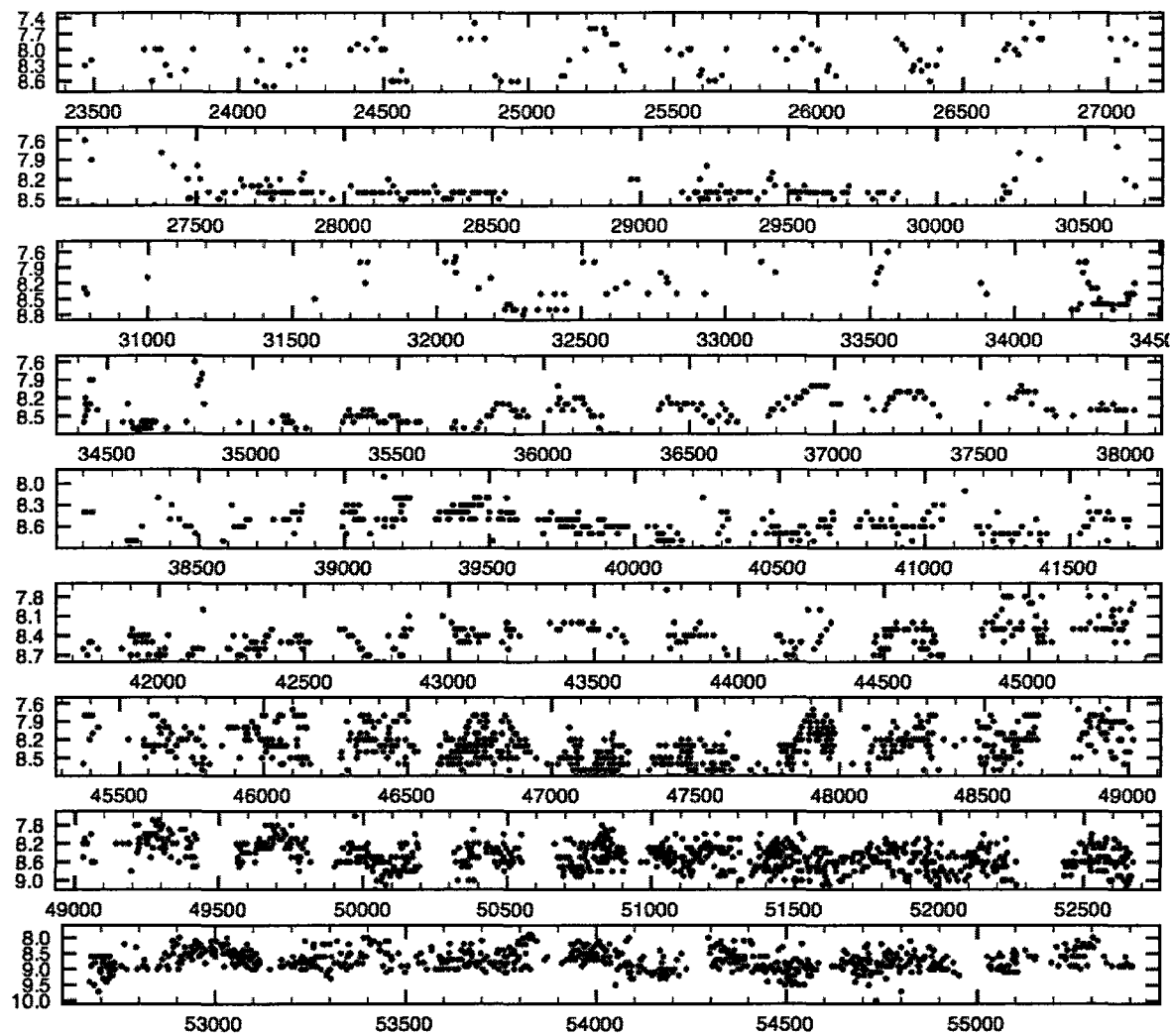
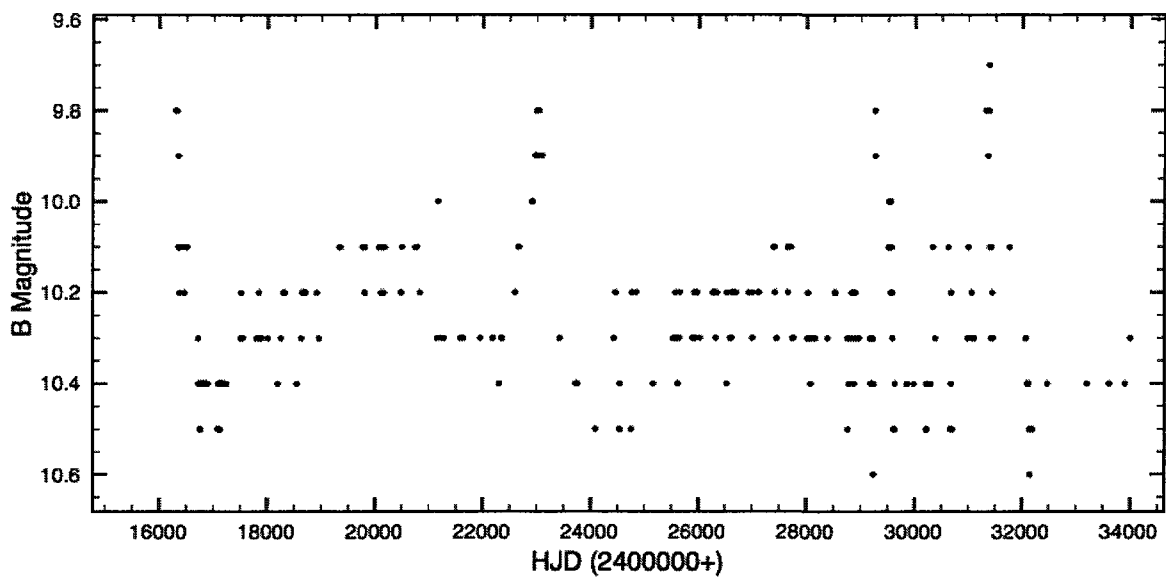


Figure B.89: XX Persei visual (AAVSO) light curve.



**Figure B.90:** XX Persei visual (AAVSO) light curve - expanded view of figure B.89.



**Figure B.91:** XX Persei photographic light curve.

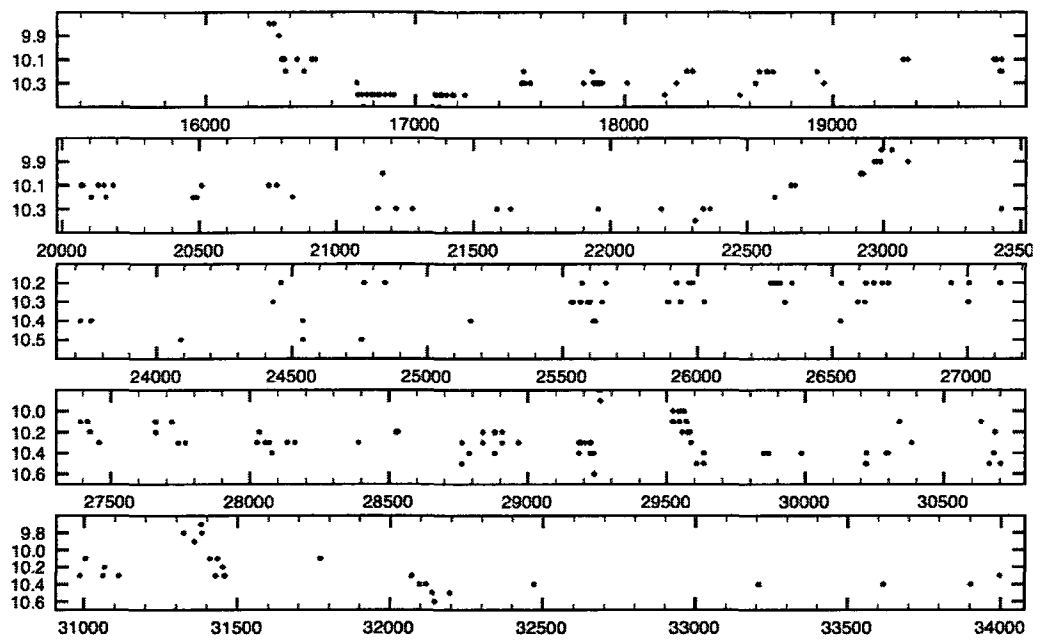


**Figure B.92:** XX Persei photographic light curve - expanded view of figure B.91.

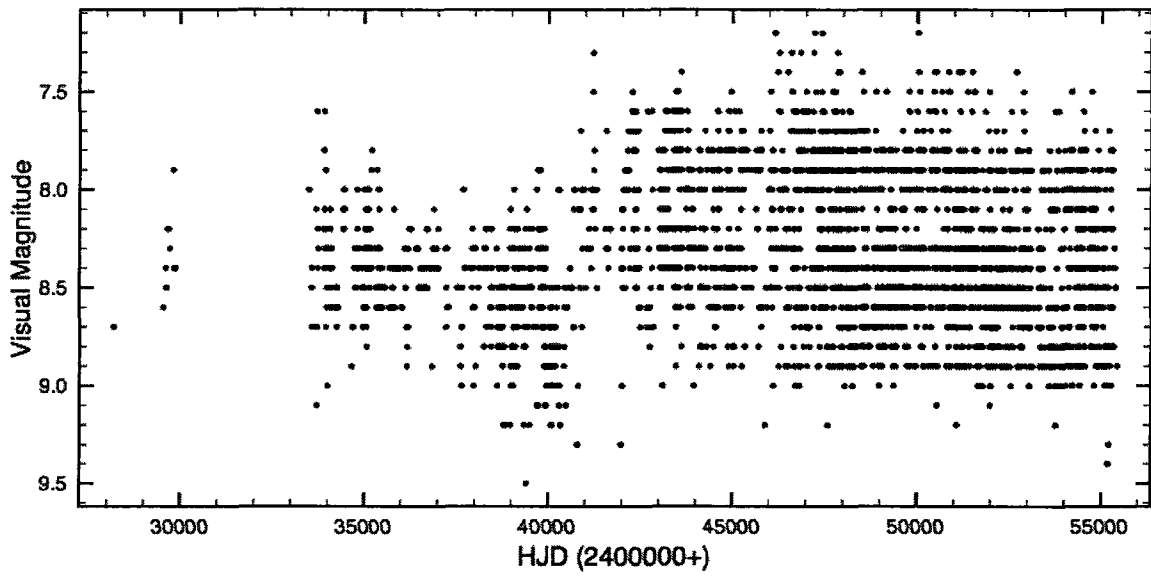


**Figure B.93:** AD Persei visual (AAVSO) light curve.

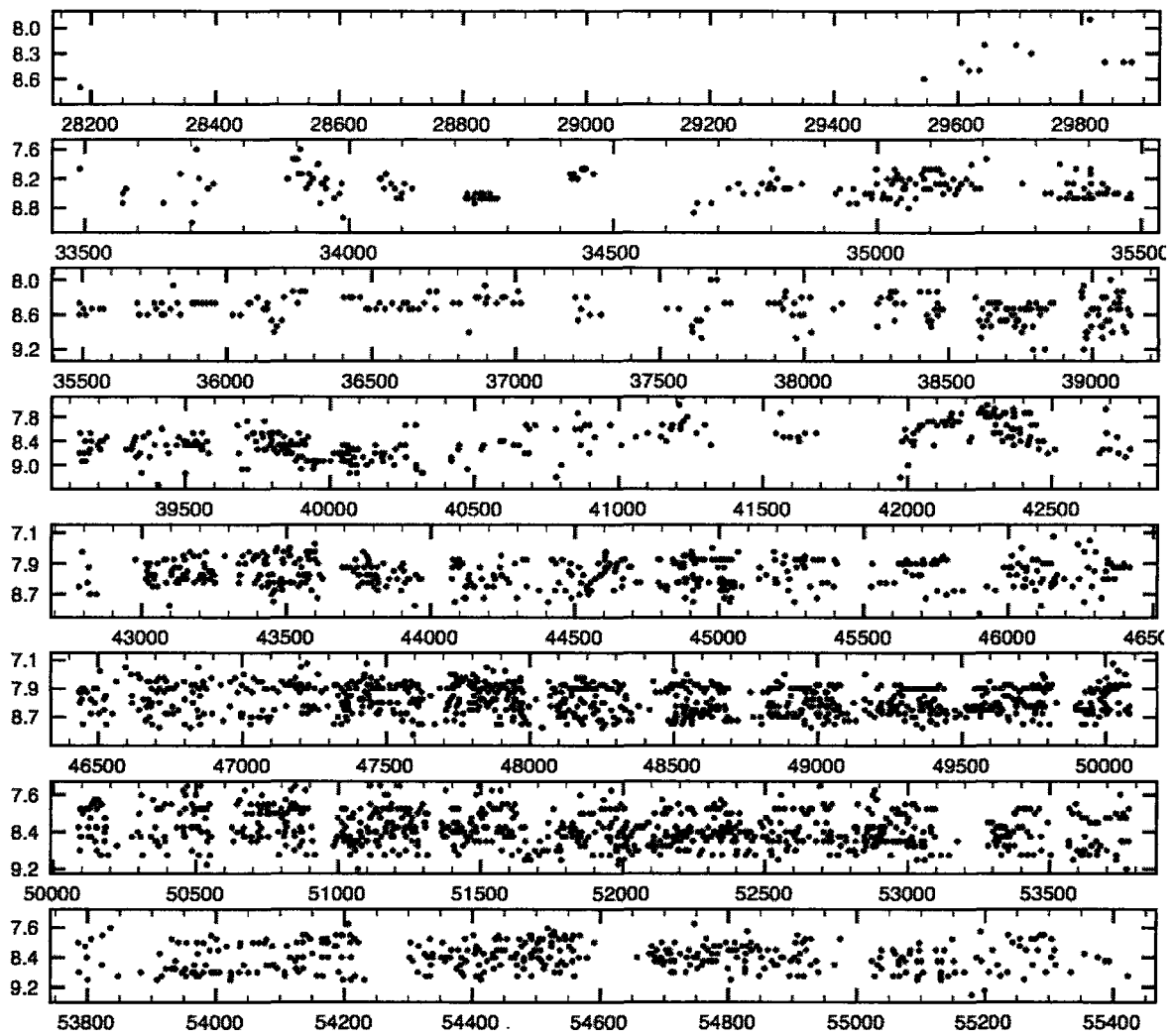


**Figure B.94:** AD Persei visual (AAVSO) light curve - expanded view of figure B.93.

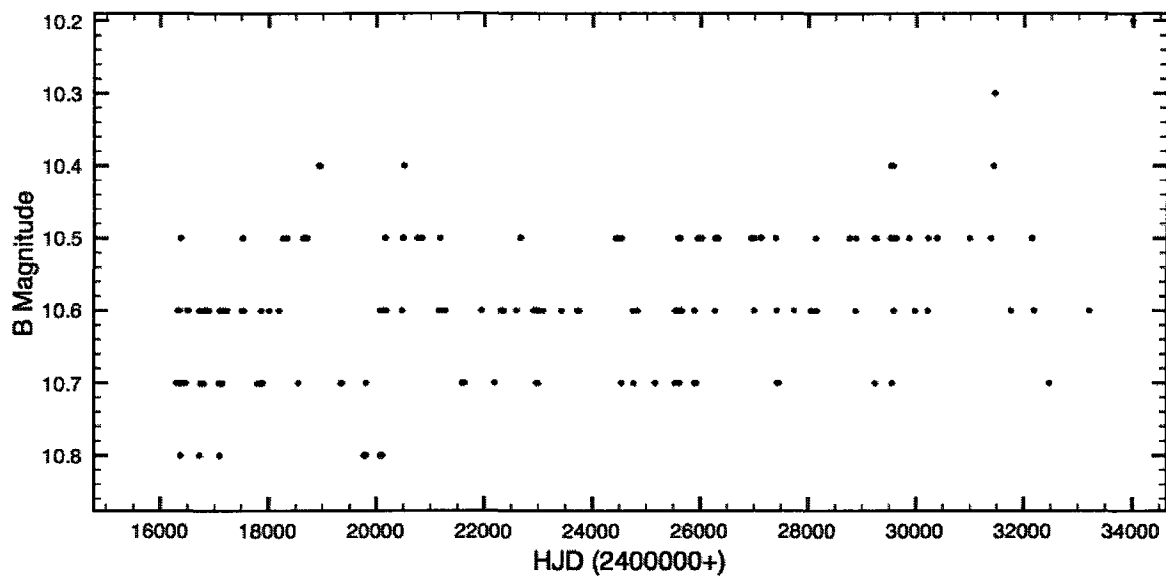


**Figure B.95:** AD Persei photographic light curve.

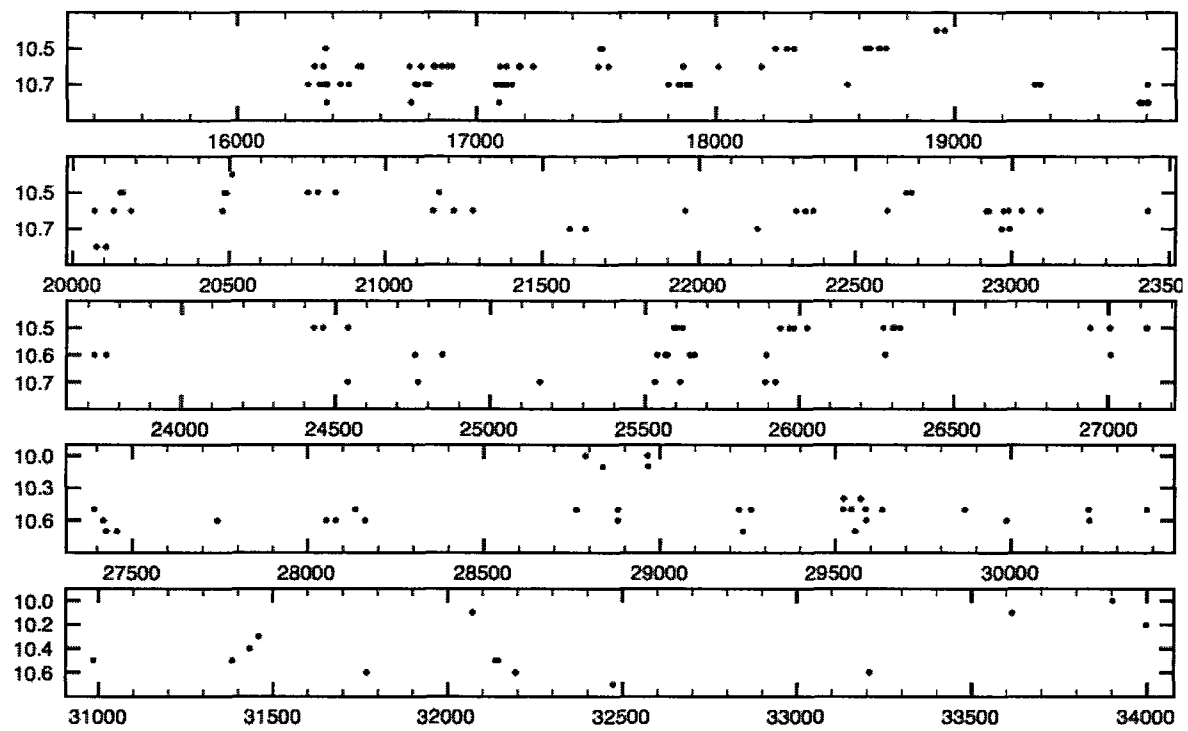


**Figure B.96:** AD Persei photographic light curve - expanded view of figure B.95.

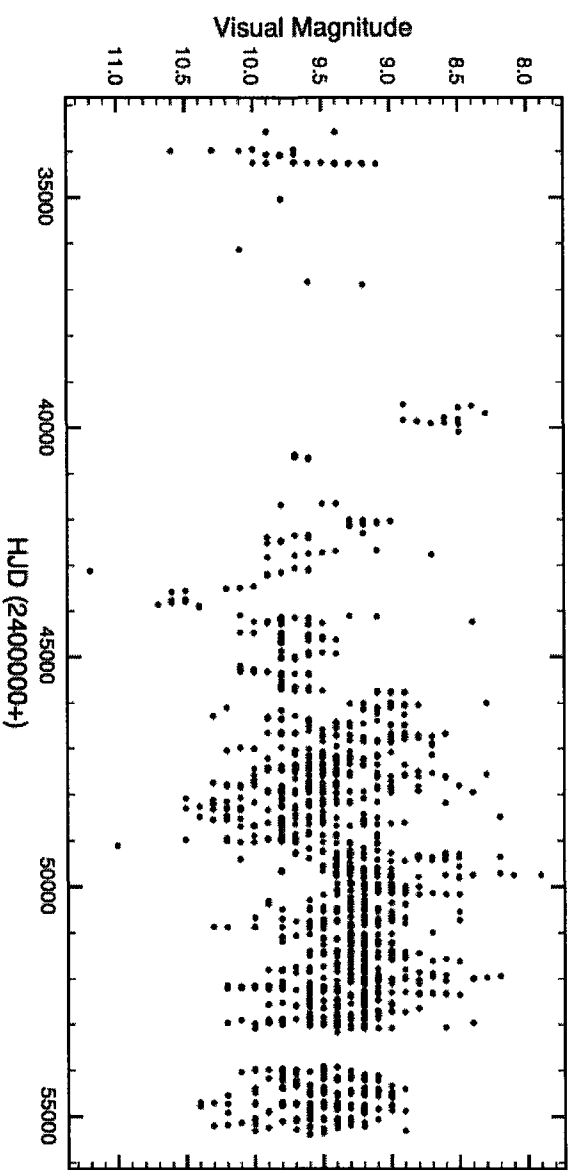


Figure B.97: BU Persei visual (AAVSO) light curve.

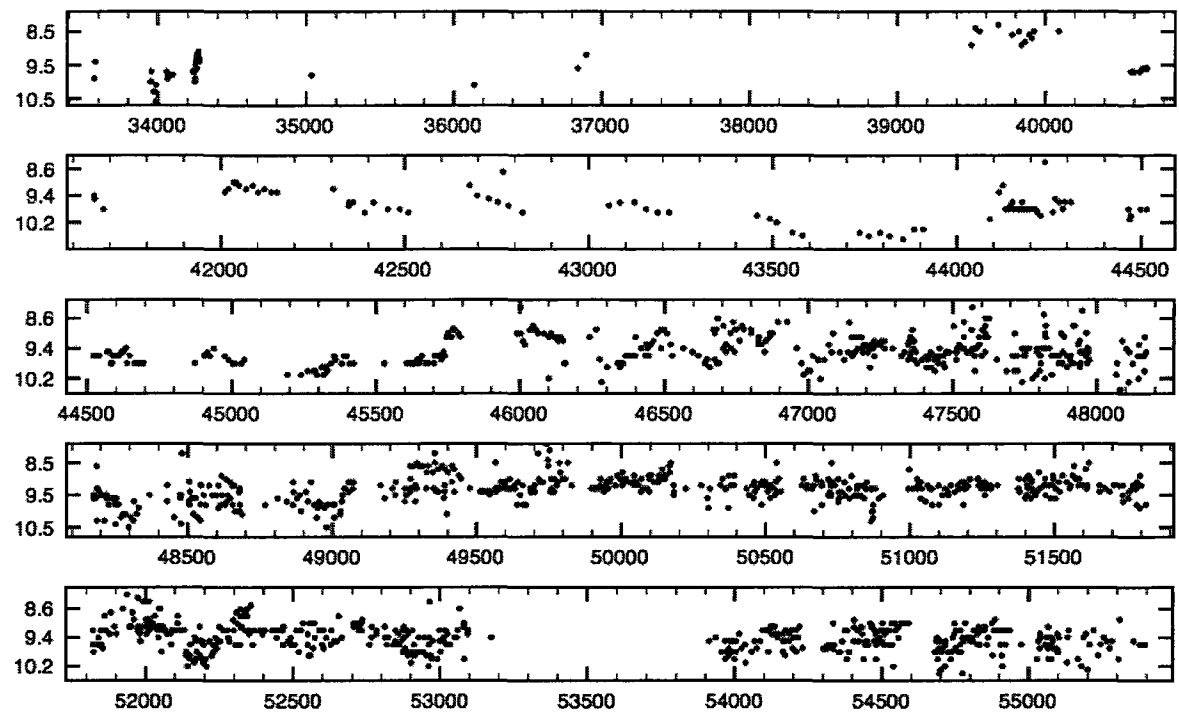
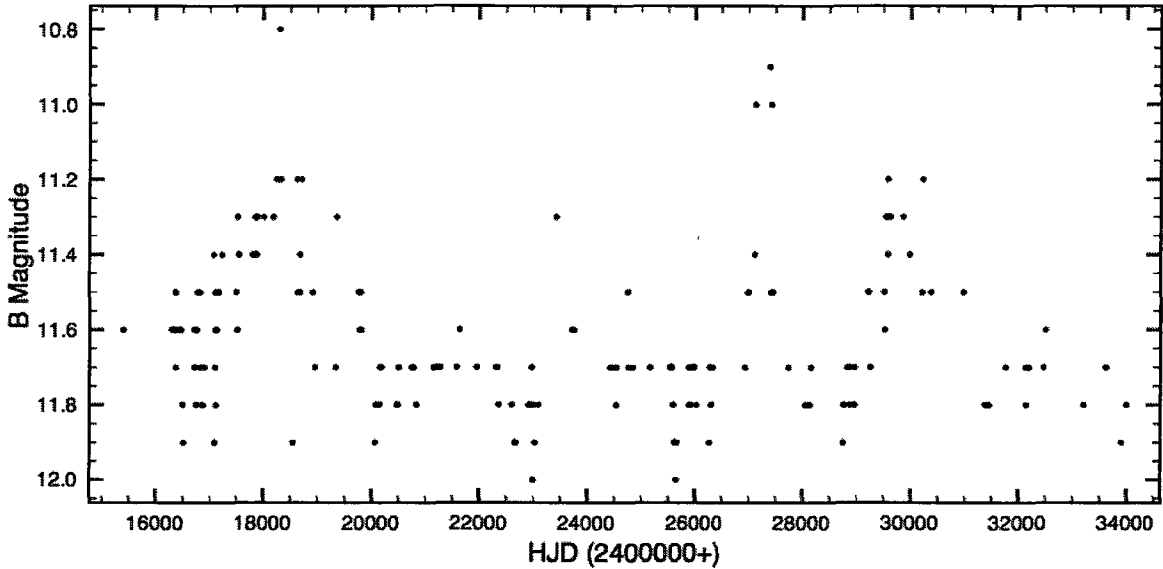
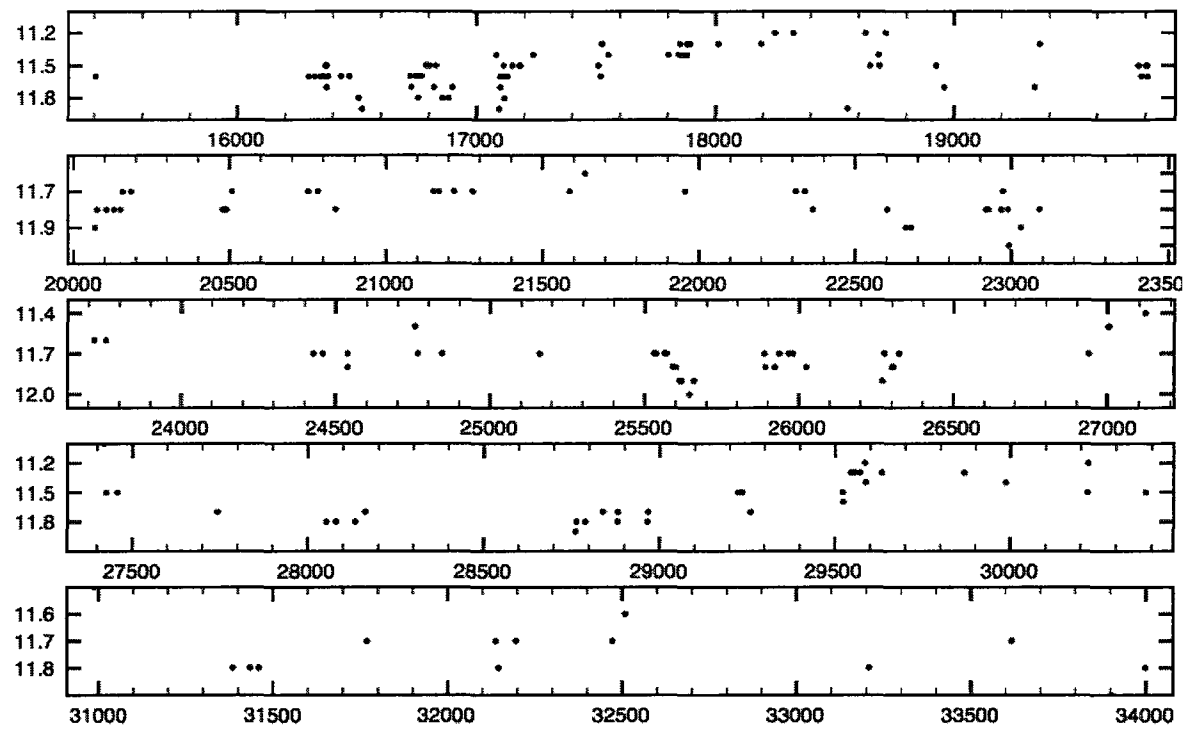


Figure B.98: BU Persei visual (AAVSO) light curve - expanded view of figure B.97.



**Figure B.99:** BU Persei photographic light curve.



**Figure B.100:** BU Persei photographic light curve - expanded view of figure B.99.

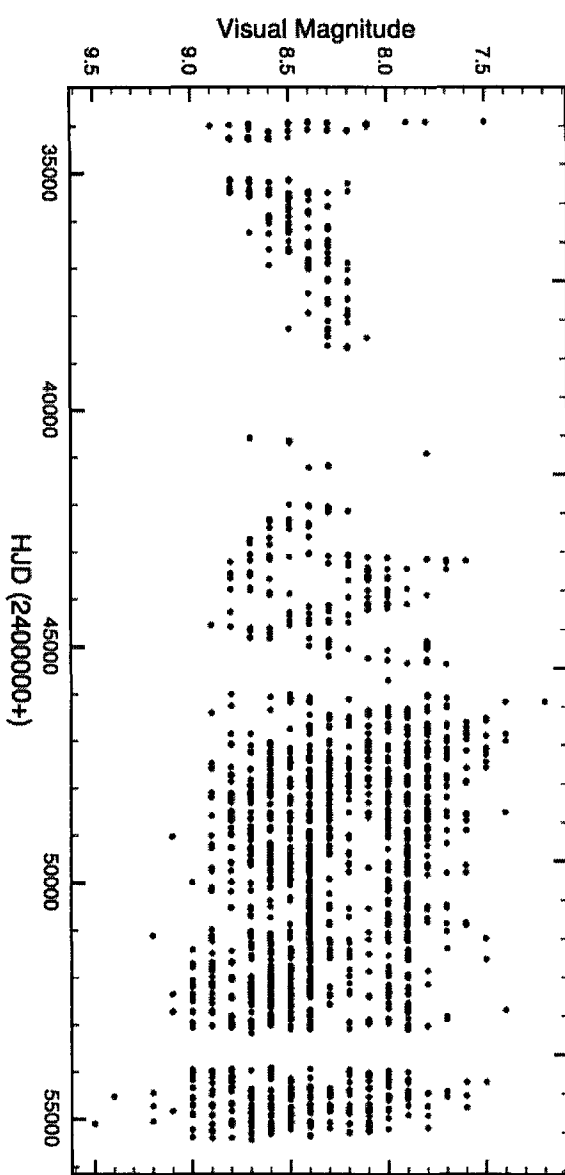
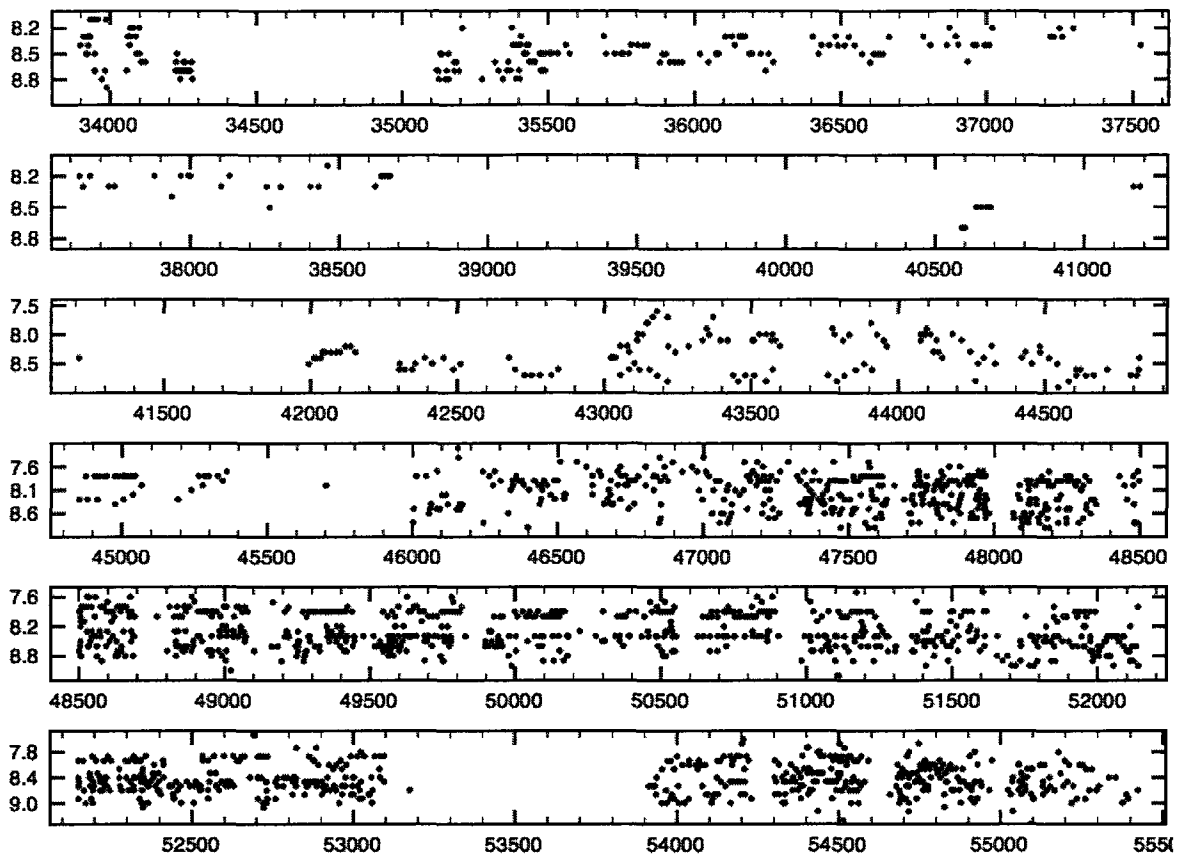
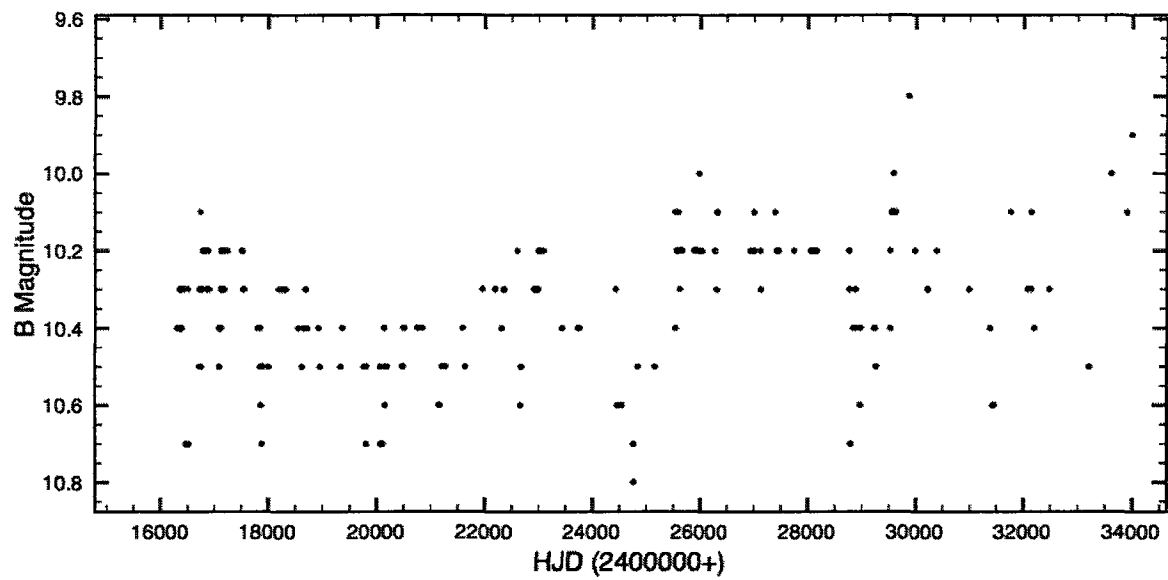


Figure B.101: FZ Persei visual (AAVSO) light curve.



**Figure B.102:** FZ Persei visual (AAVSO) light curve - expanded view of figure B.101.



**Figure B.103:** FZ Persei photographic light curve.

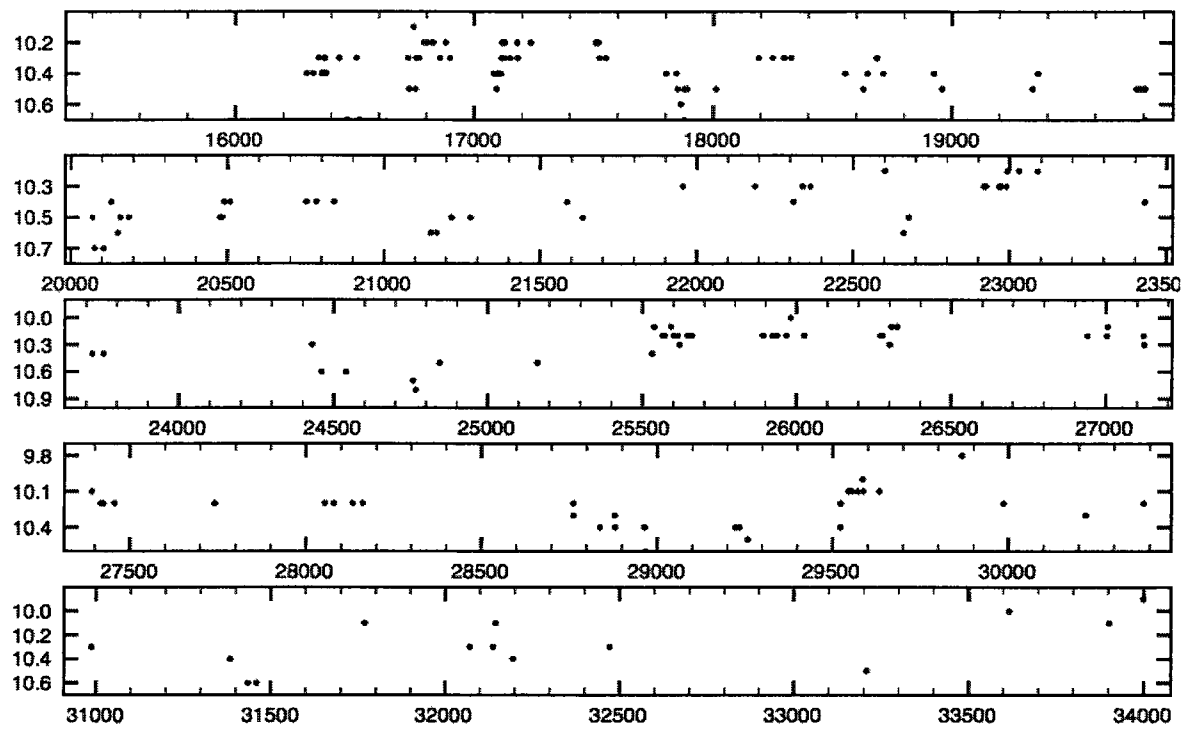


**Figure B.104:** FZ Persei photographic light curve - expanded view of figure B.103.

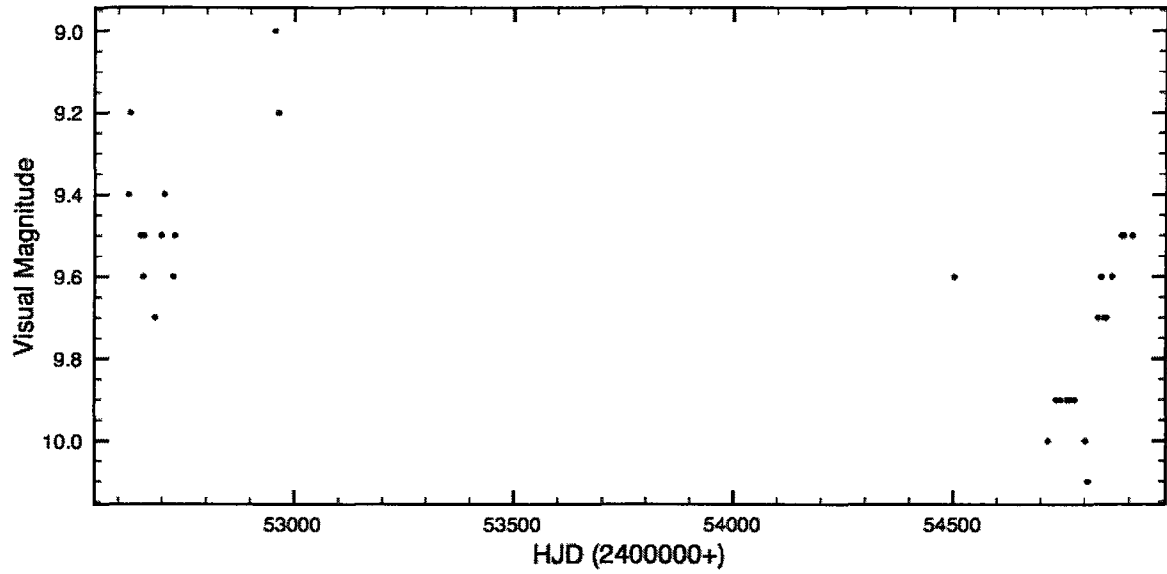


**Figure B.105:** V411 Persei visual (AAVSO) light curve.

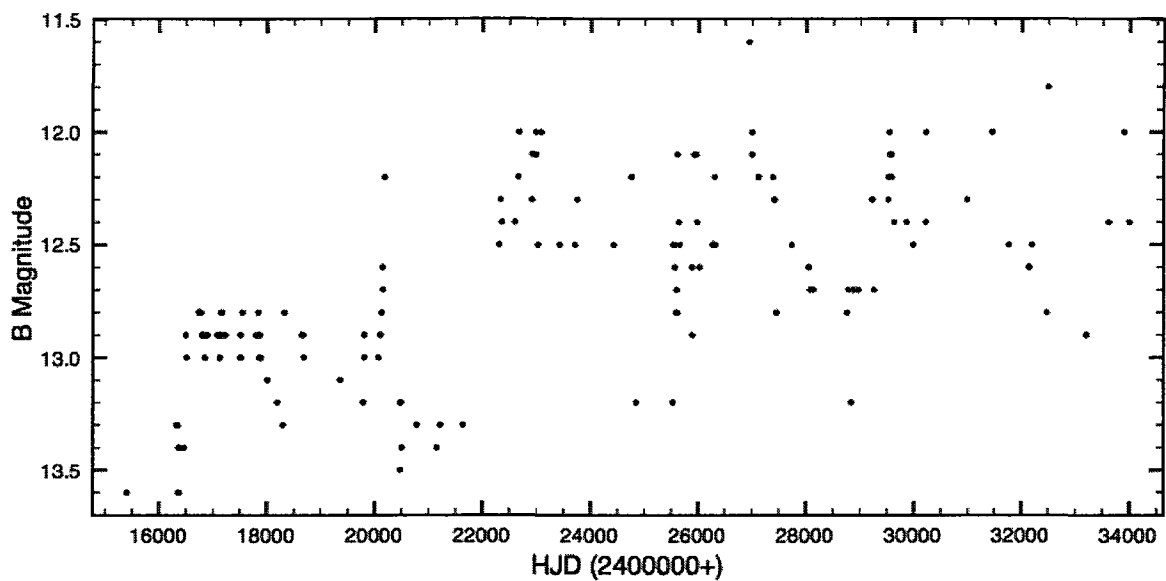


**Figure B.106:** V411 Persei photographic light curve.

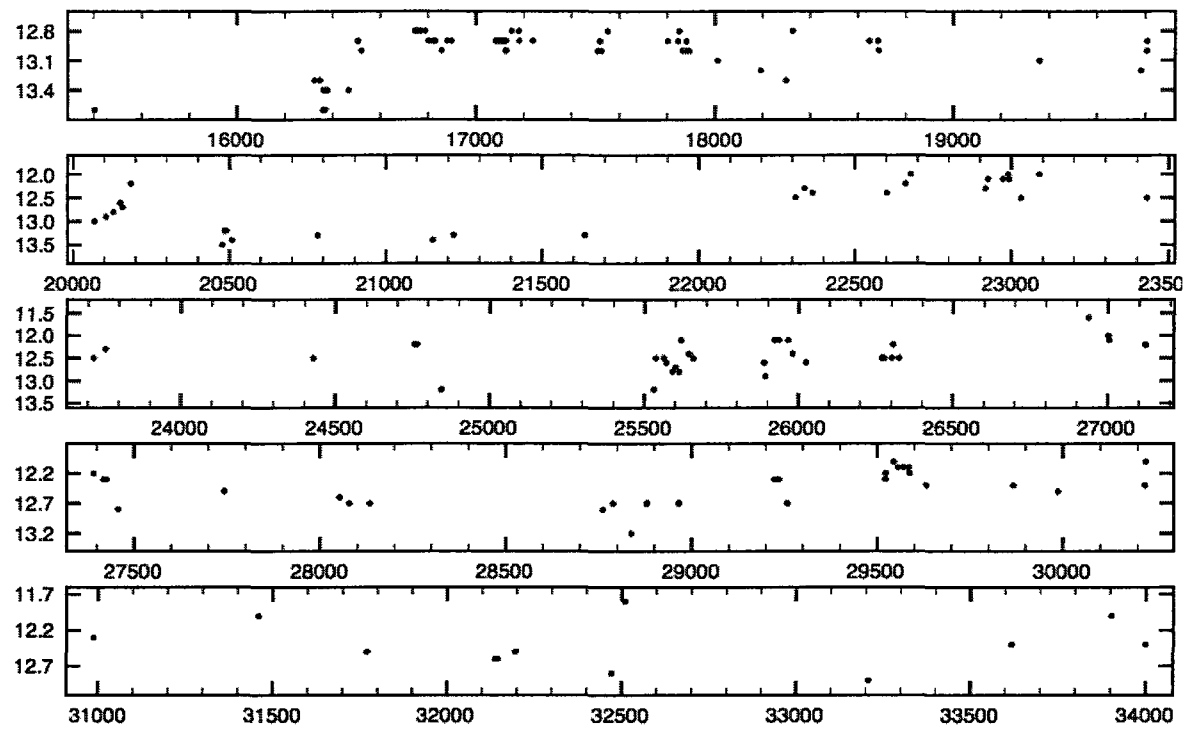


**Figure B.107:** V411 Persei photographic light curve - expanded view of figure B.106.

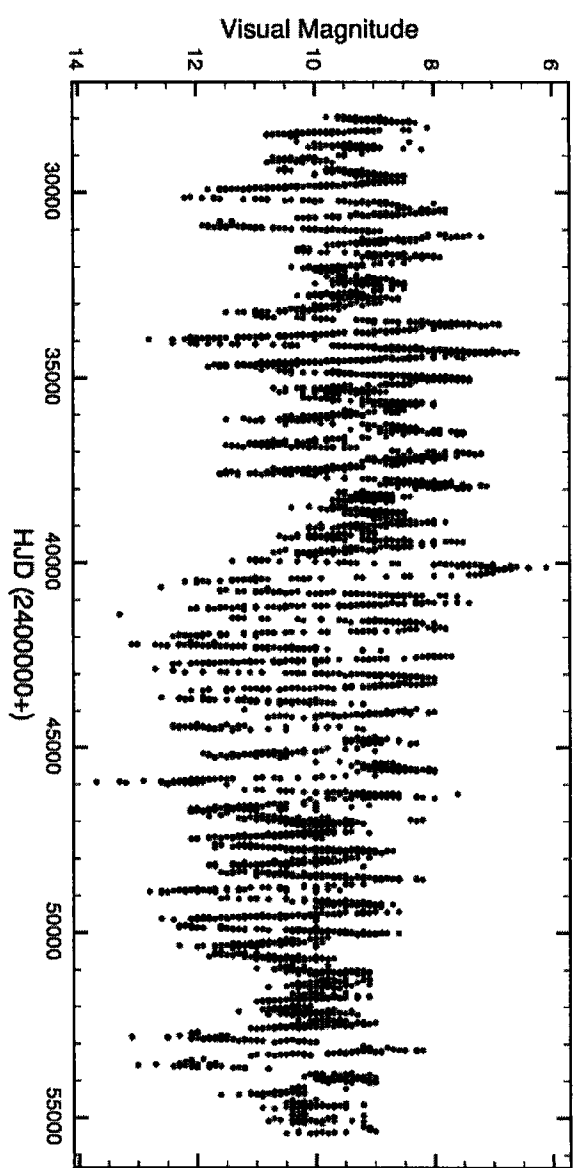
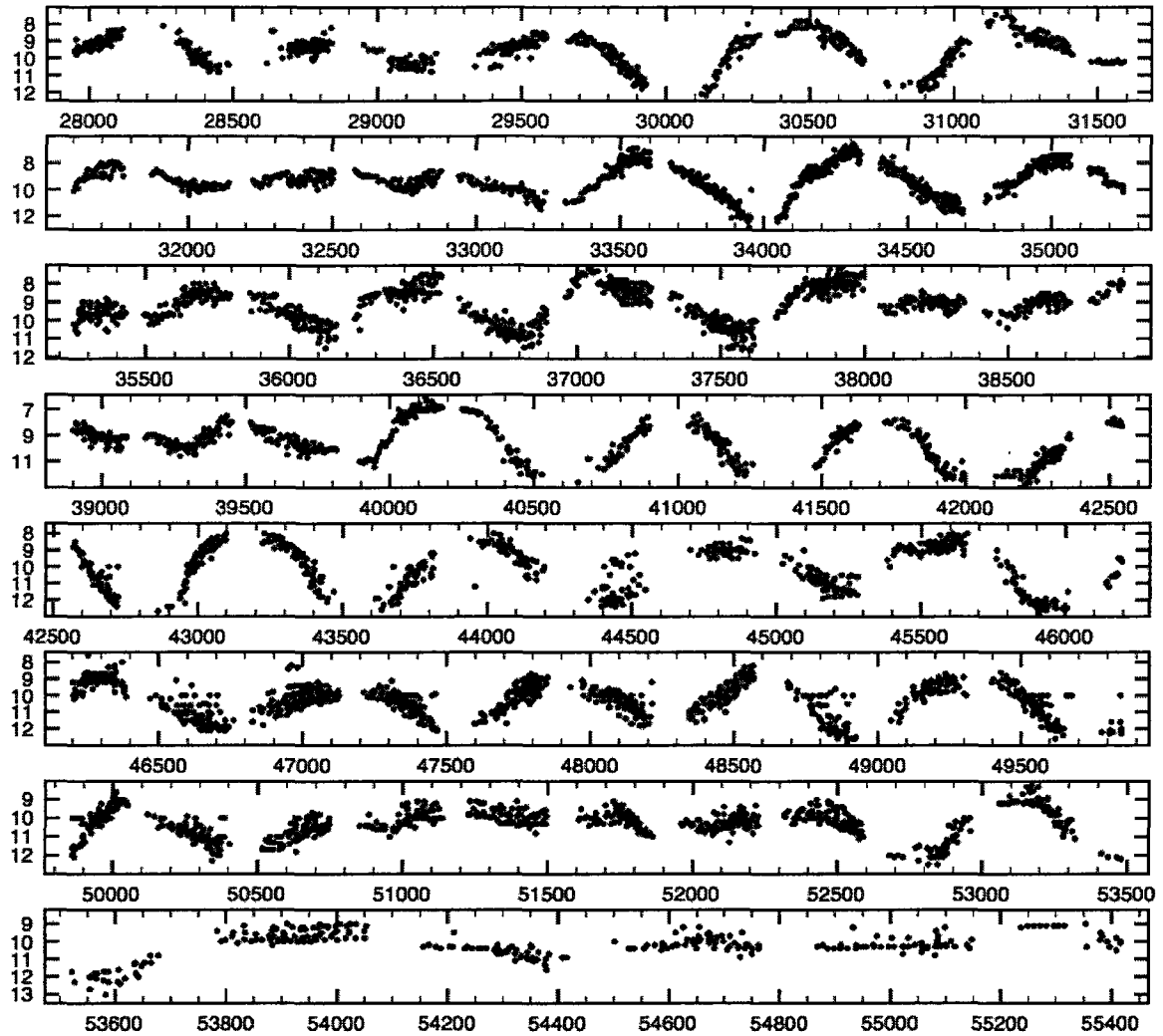


Figure B.108: VX Sagittarii visual (AAVSO) light curve.



**Figure B.109:** VX Sagittarii visual (AAVSO) light curve - expanded view of figure B.108.

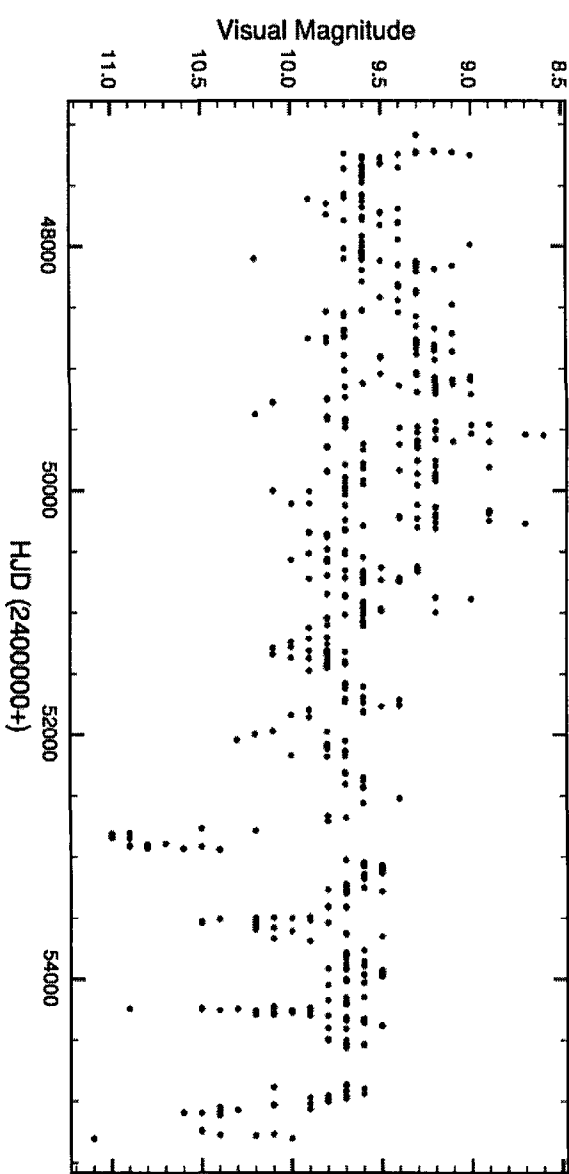
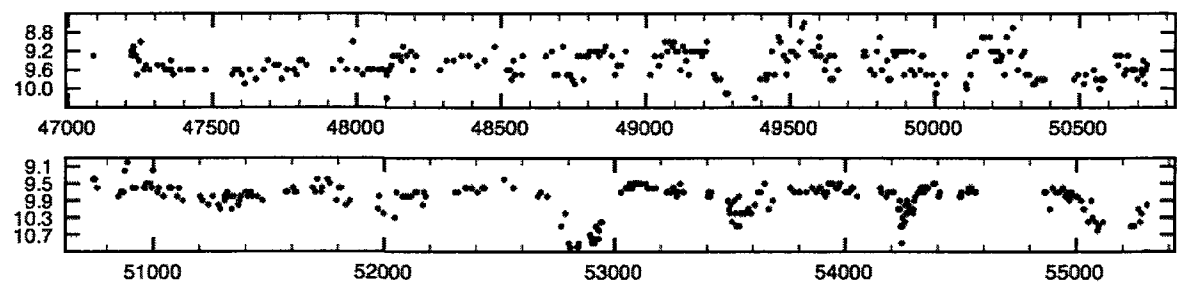


Figure B.110: KW Sagittarii visual (AAVSO) light curve.



**Figure B.111:** KW Sagittarii visual (AAVSO) light curve - expanded view of figure B.110.

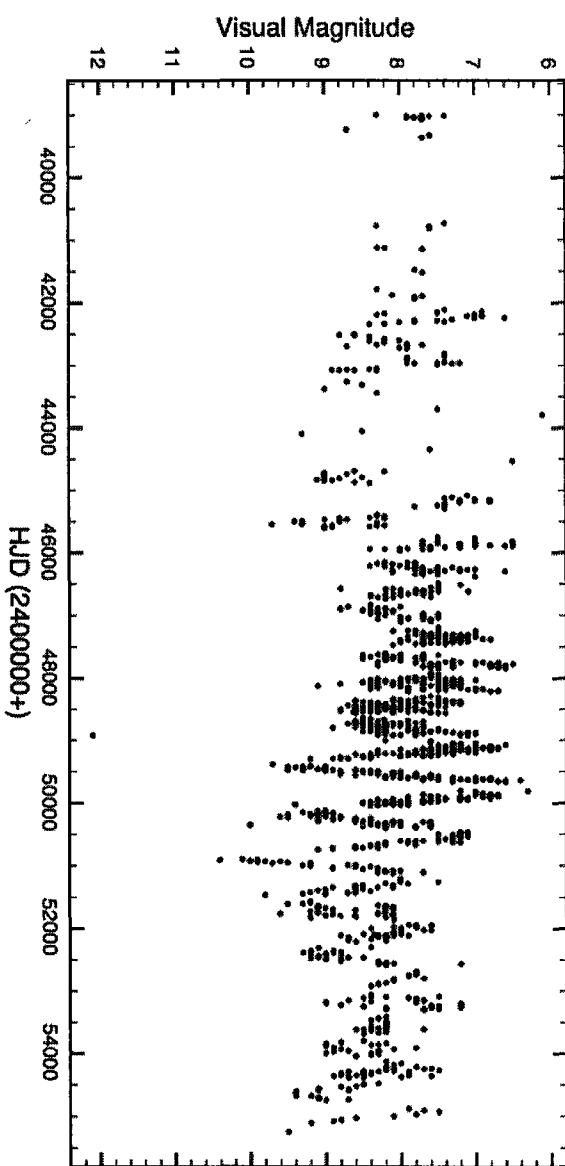
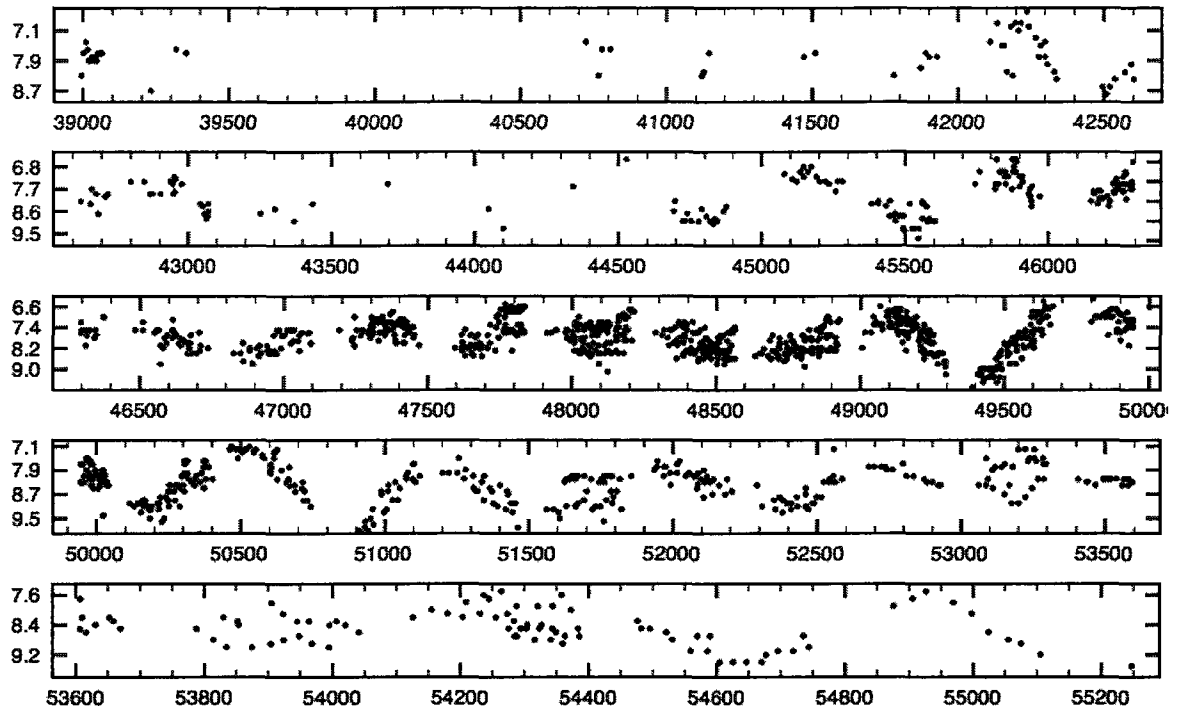


Figure B.112: AH Scorpii visual (AAVSO) light curve.



**Figure B.113:** AH Scorpii visual (AAVSO) light curve - expanded view of figure B.112.

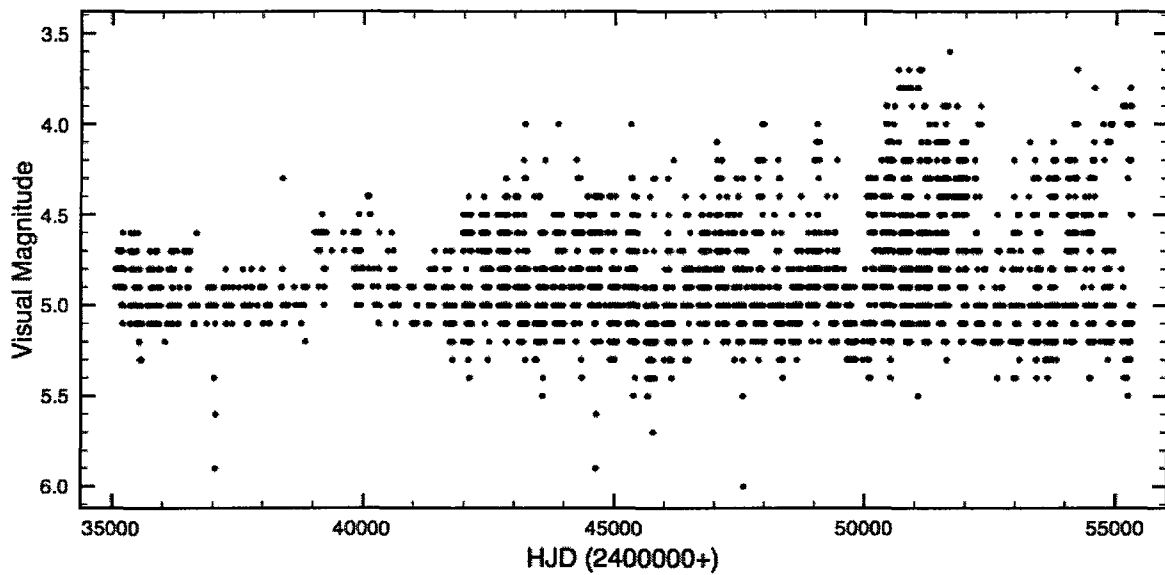
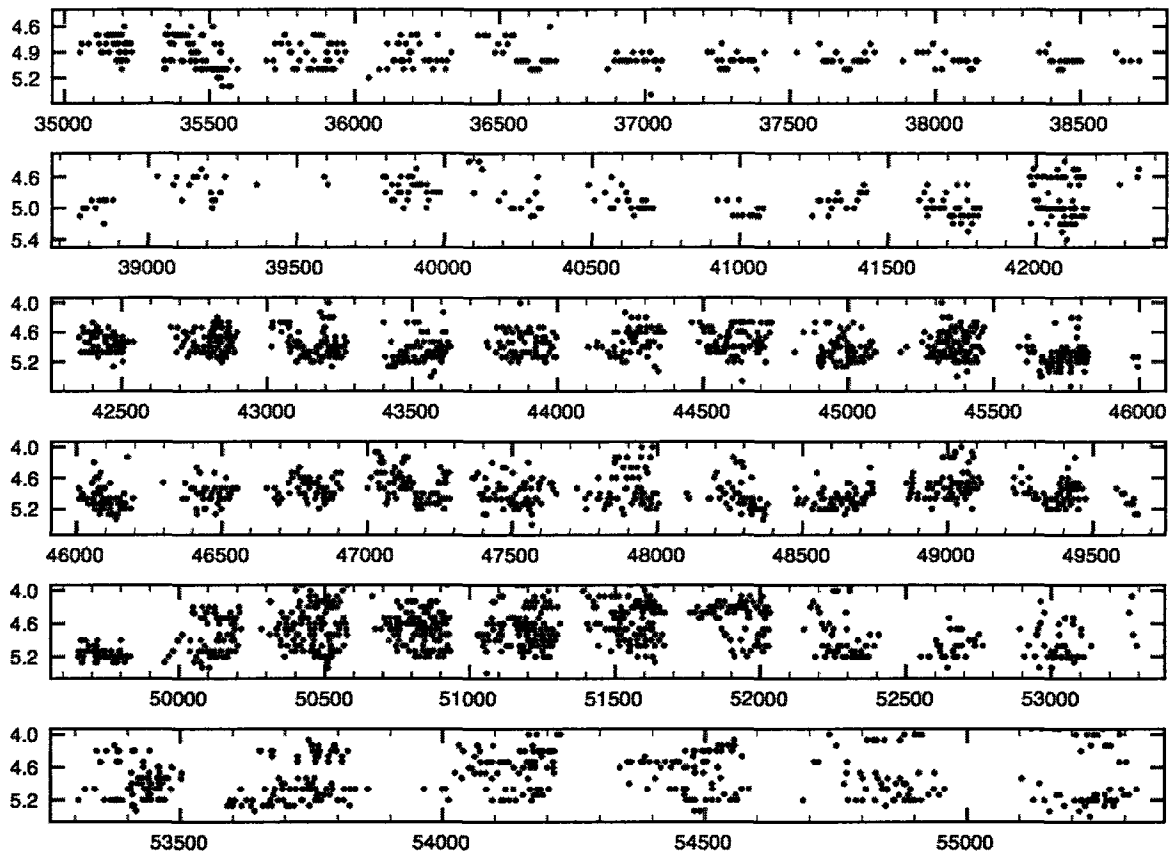


Figure B.114: CE Tauri visual (AAVSO) light curve.



**Figure B.115:** CE Tauri visual (AAVSO) light curve - expanded view of figure B.114.

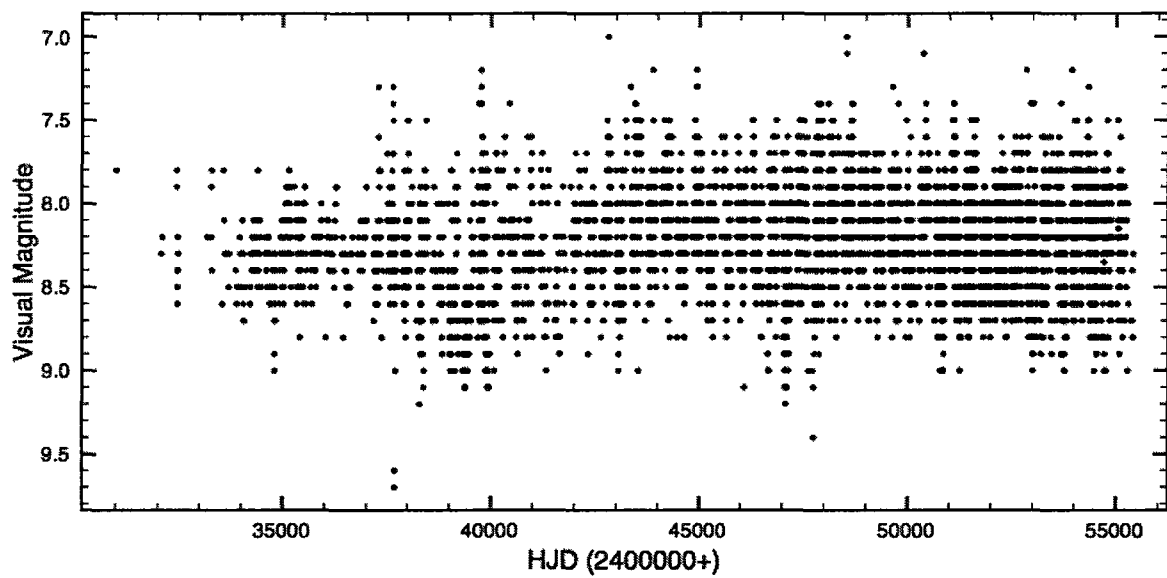


Figure B.116: W Triangulum visual (AAVSO) light curve.

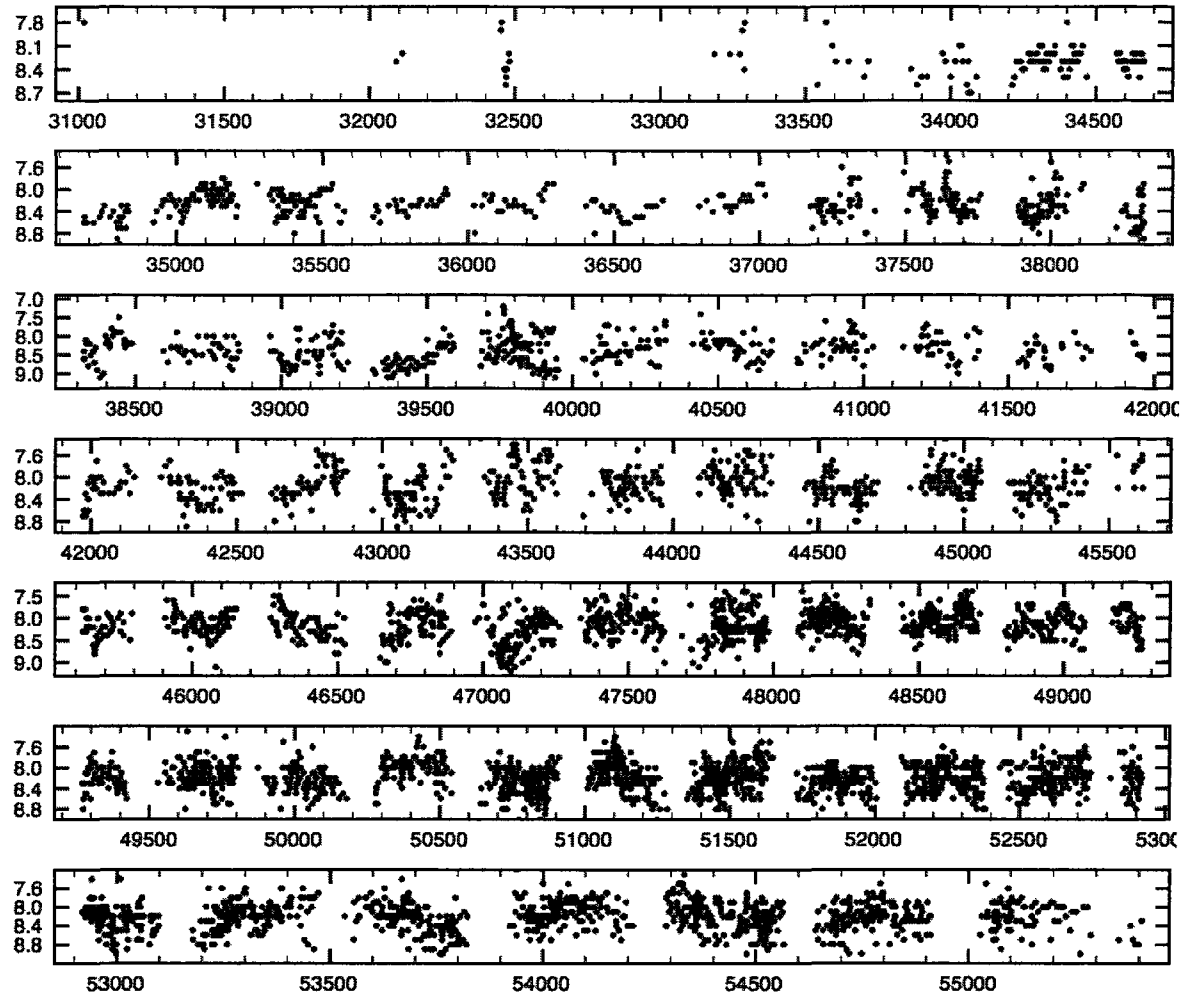
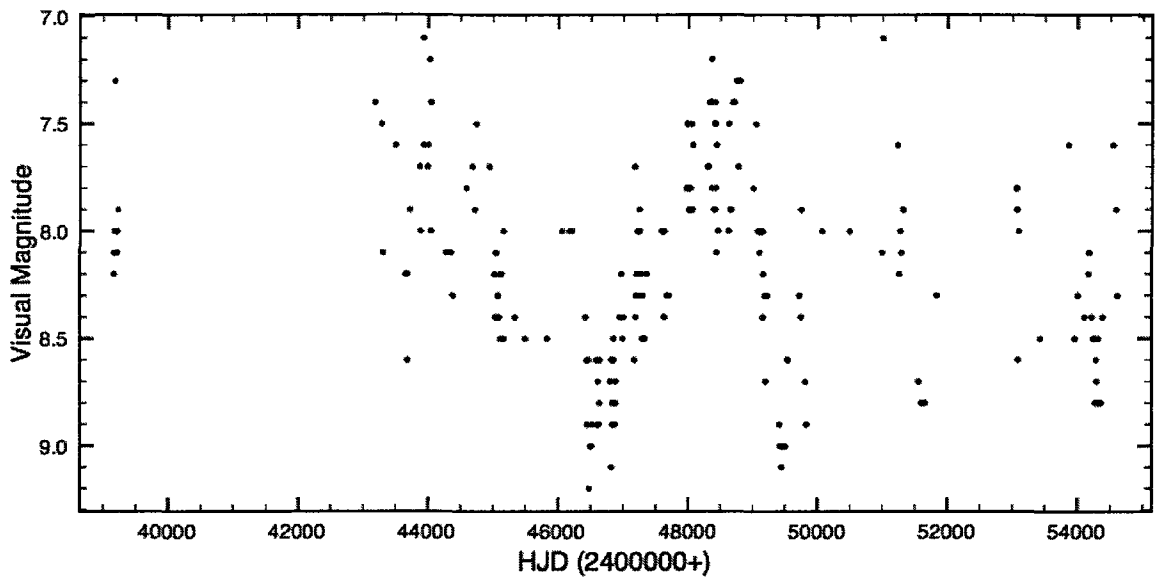


Figure B.117: W Triangulum visual (AAVSO) light curve - expanded view of figure B.116.



**Figure B.118:** CM Velorum visual (AAVSO) light curve.

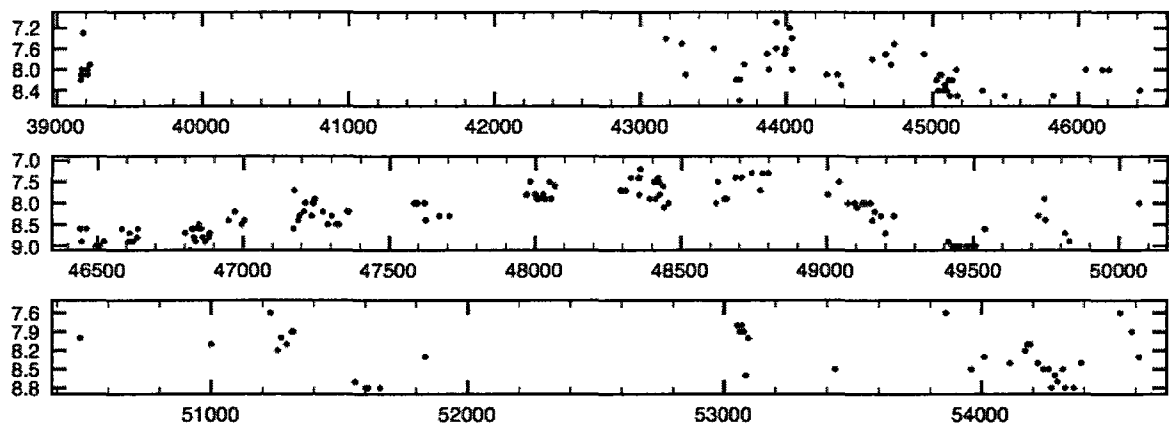
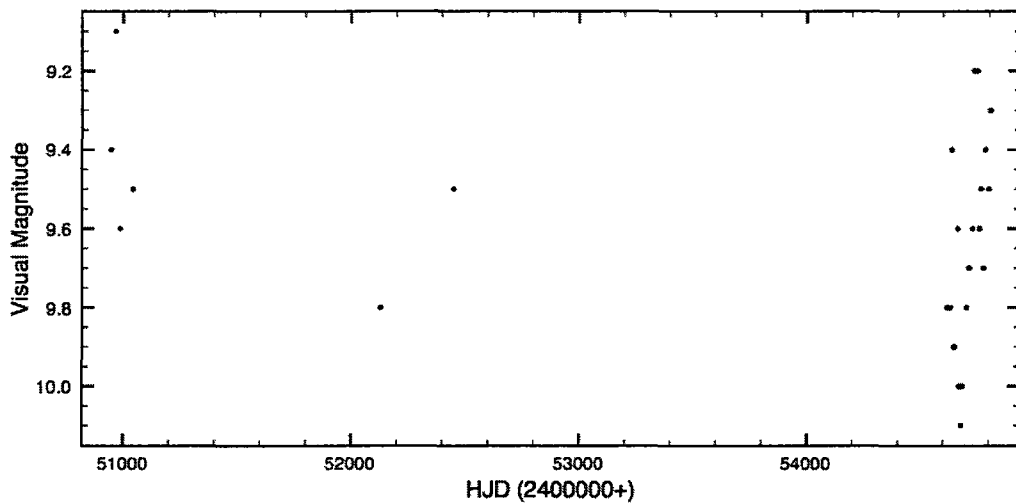


Figure B.119: CM Velorum visual (AAVSO) light curve - expanded view of figure B.118.



**Figure B.120:** FG Vulpeculae visual (AAVSO) light curve.

## **Appendix C**

### **Periodograms**

The following figures show periodograms for the AAVSO data for the 48 stars for which such data exist. Periodograms such as these were used to determine an rough period, then Fourier analysis was again performed over a smaller timescale near the period of interest in order to obtain a more precise value. The periodograms shown were made with the CLEANest routine, but in each case the ANOVA routine was also used as a check and gave nearly identical results.

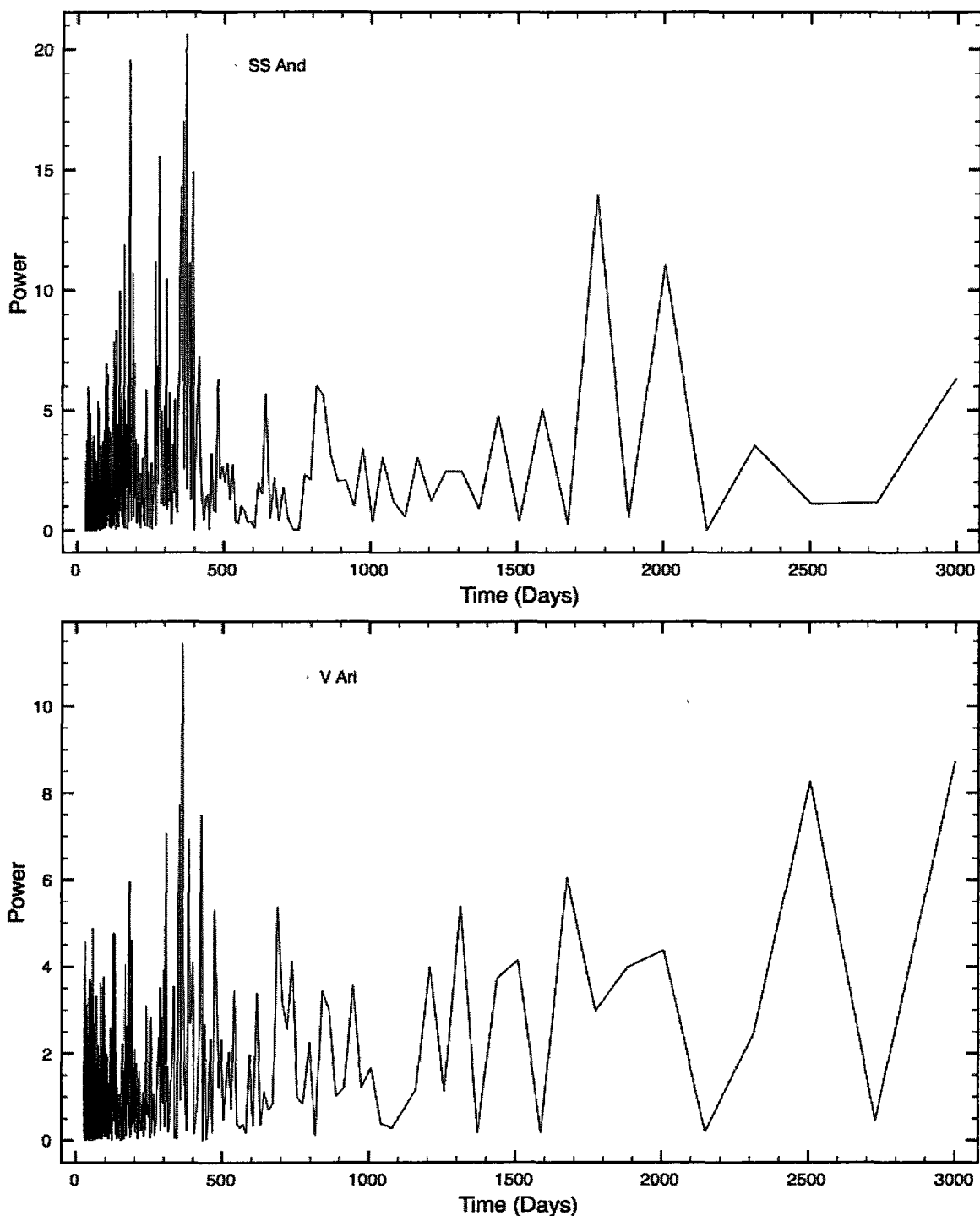


**Figure C.1:** Top: SS Andromedae, Bottom: V Arietis

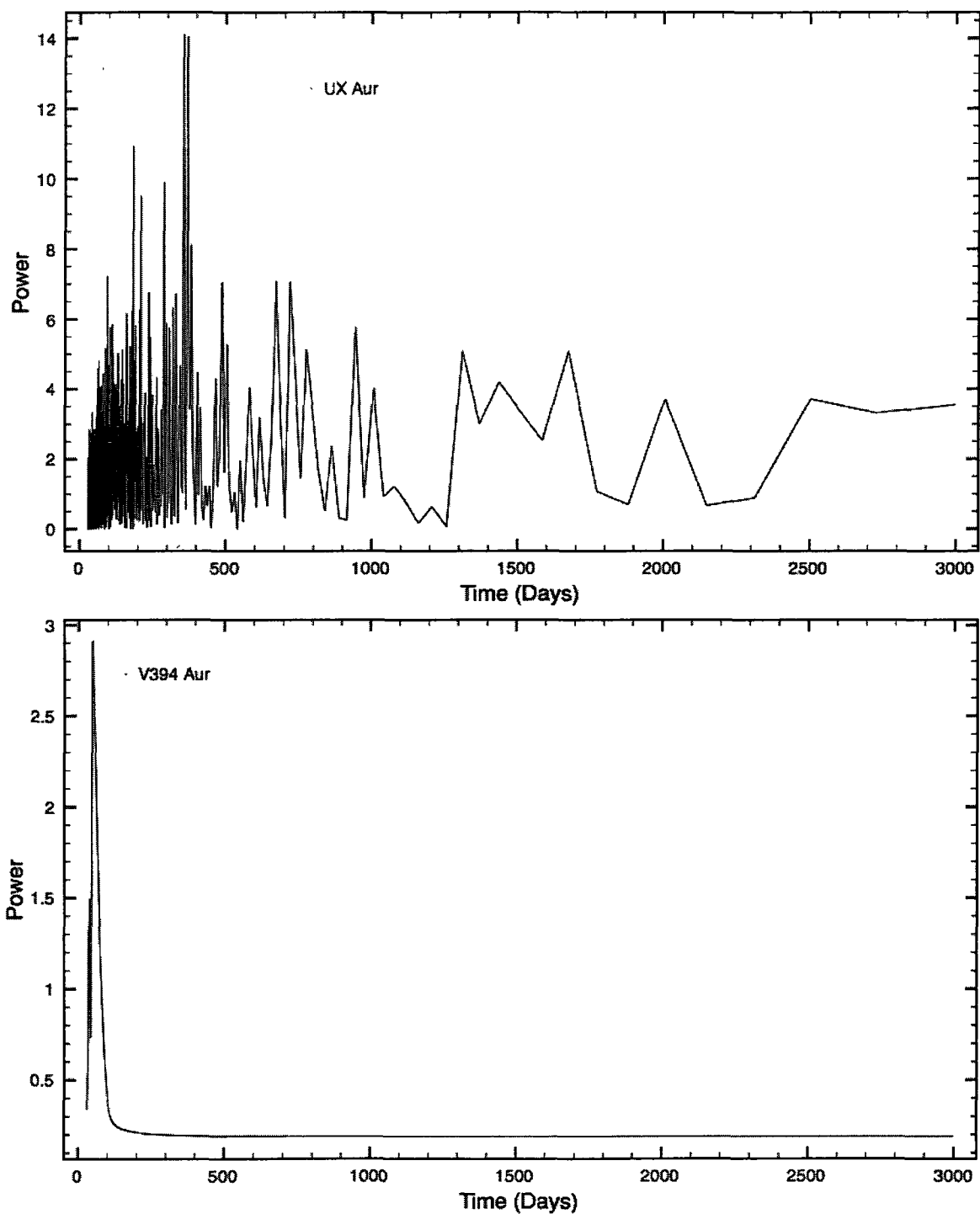


**Figure C.2:** Top: UX Aurigae, Bottom: V394 Aurigae

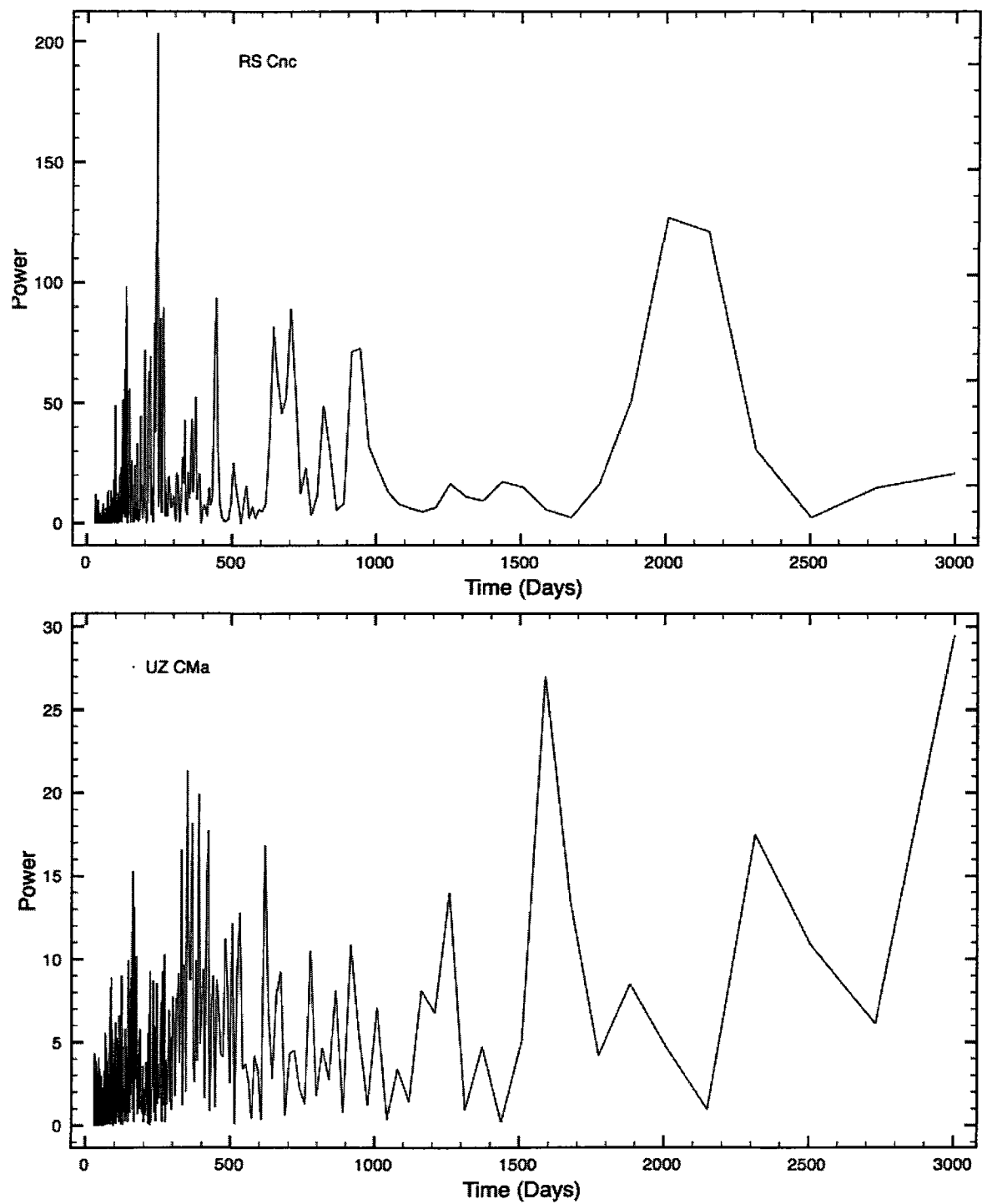


Figure C.3: Top: RS Cancri, Bottom: UZ Canis Majoris

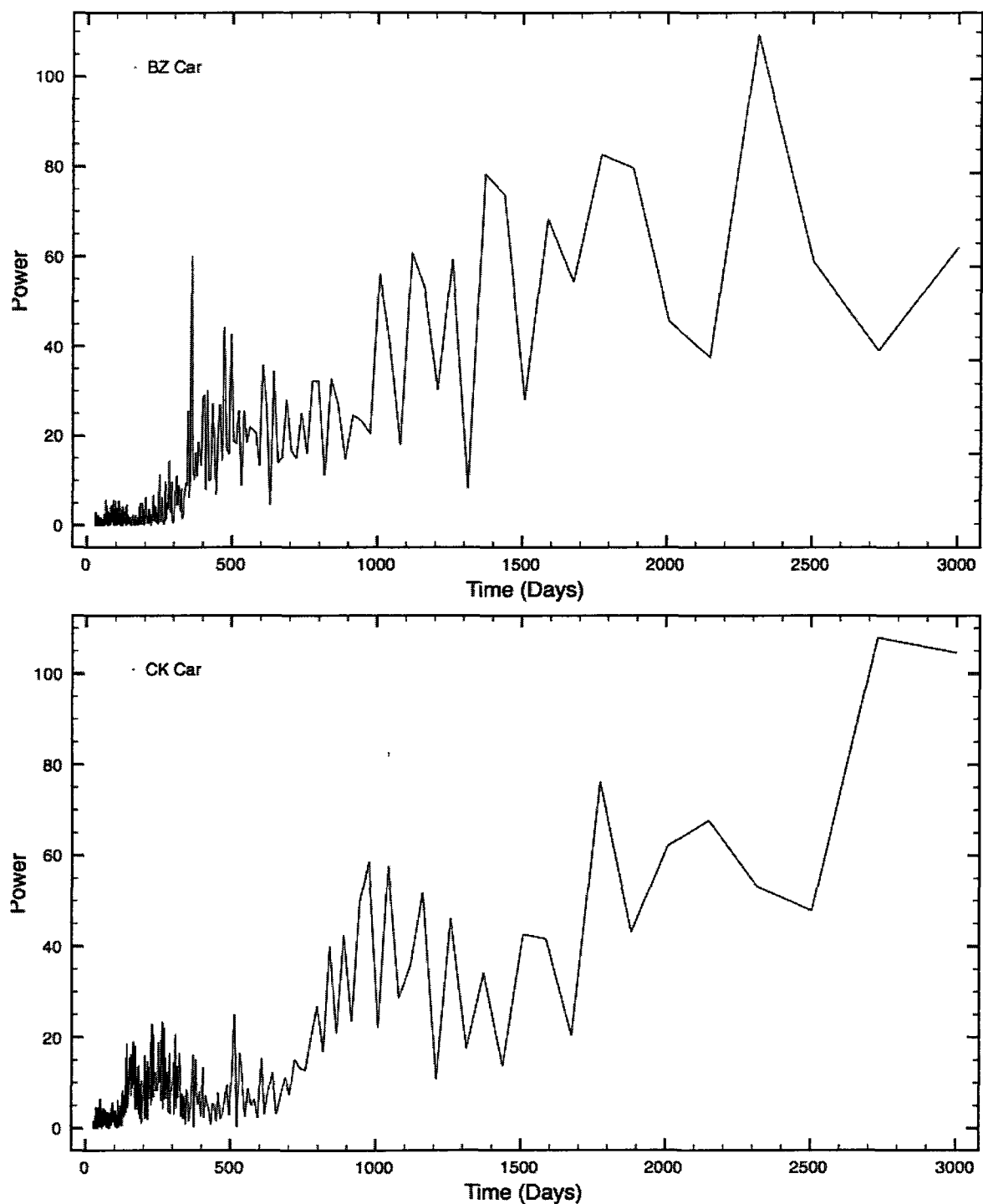
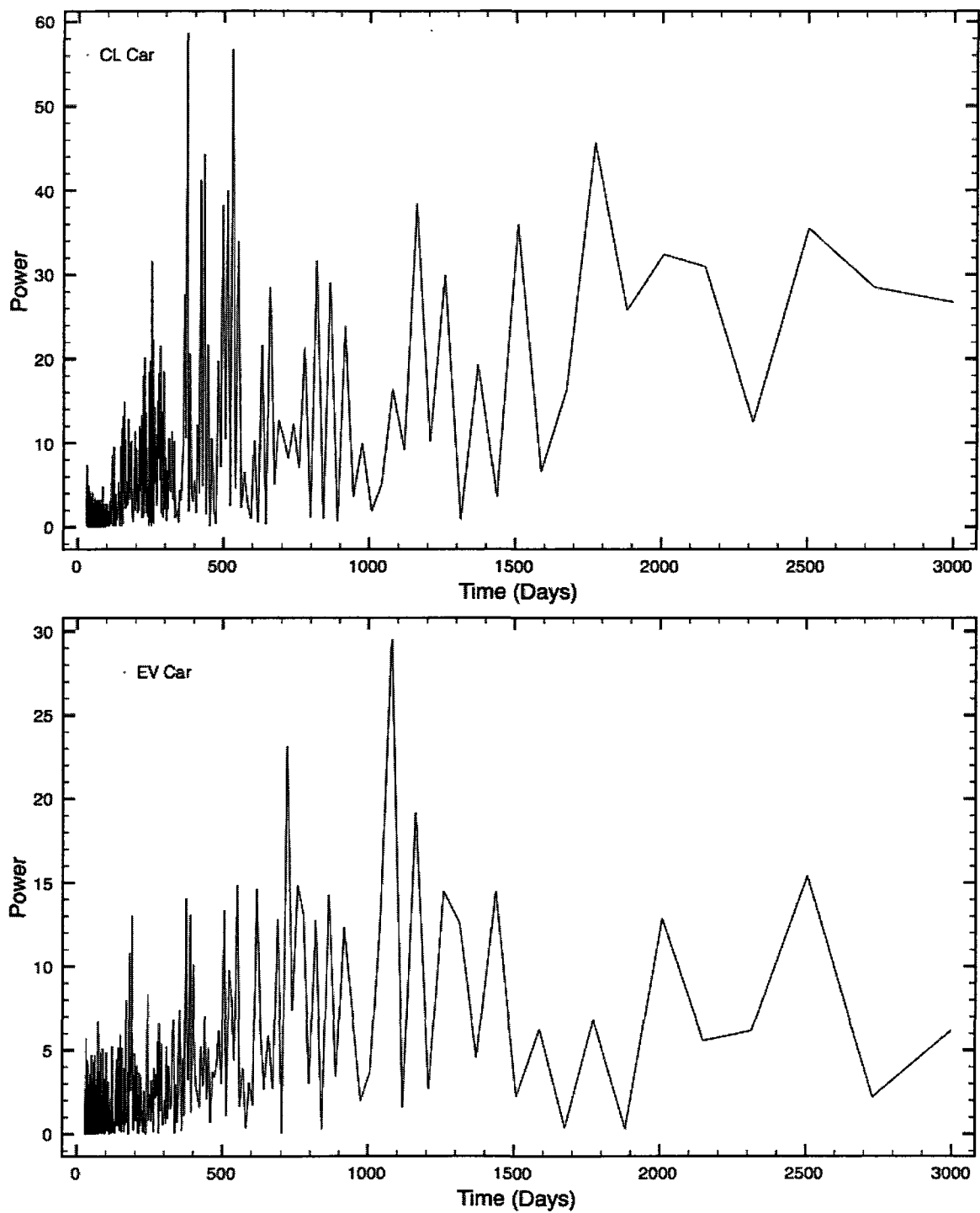
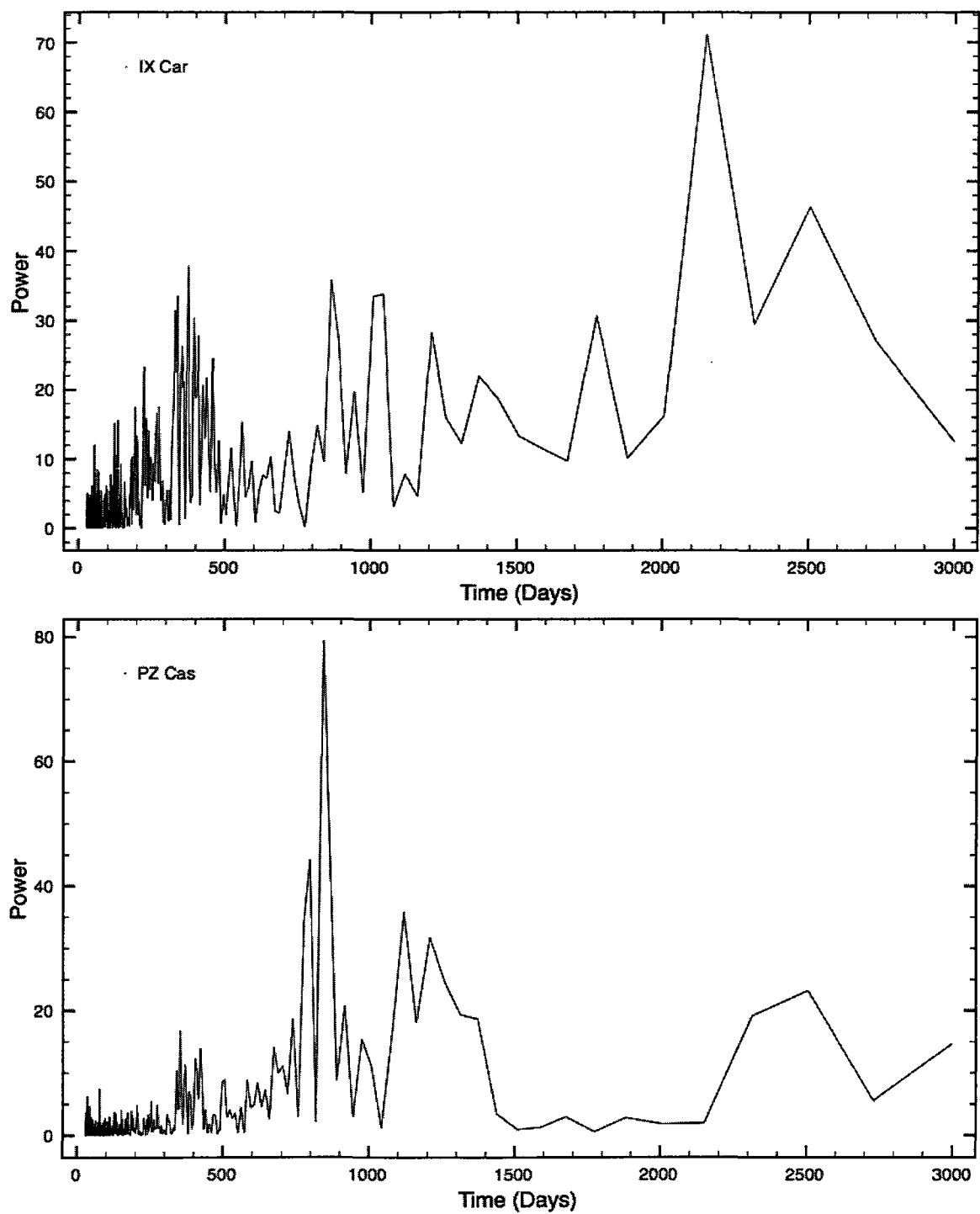


Figure C.4: Top: BZ Carinae, Bottom: CK Carinae



**Figure C.5:** Top: CL Carinae, Bottom: EV Carinae



**Figure C.6:** Top: IX Carinae, Bottom: PZ Casseopeiae

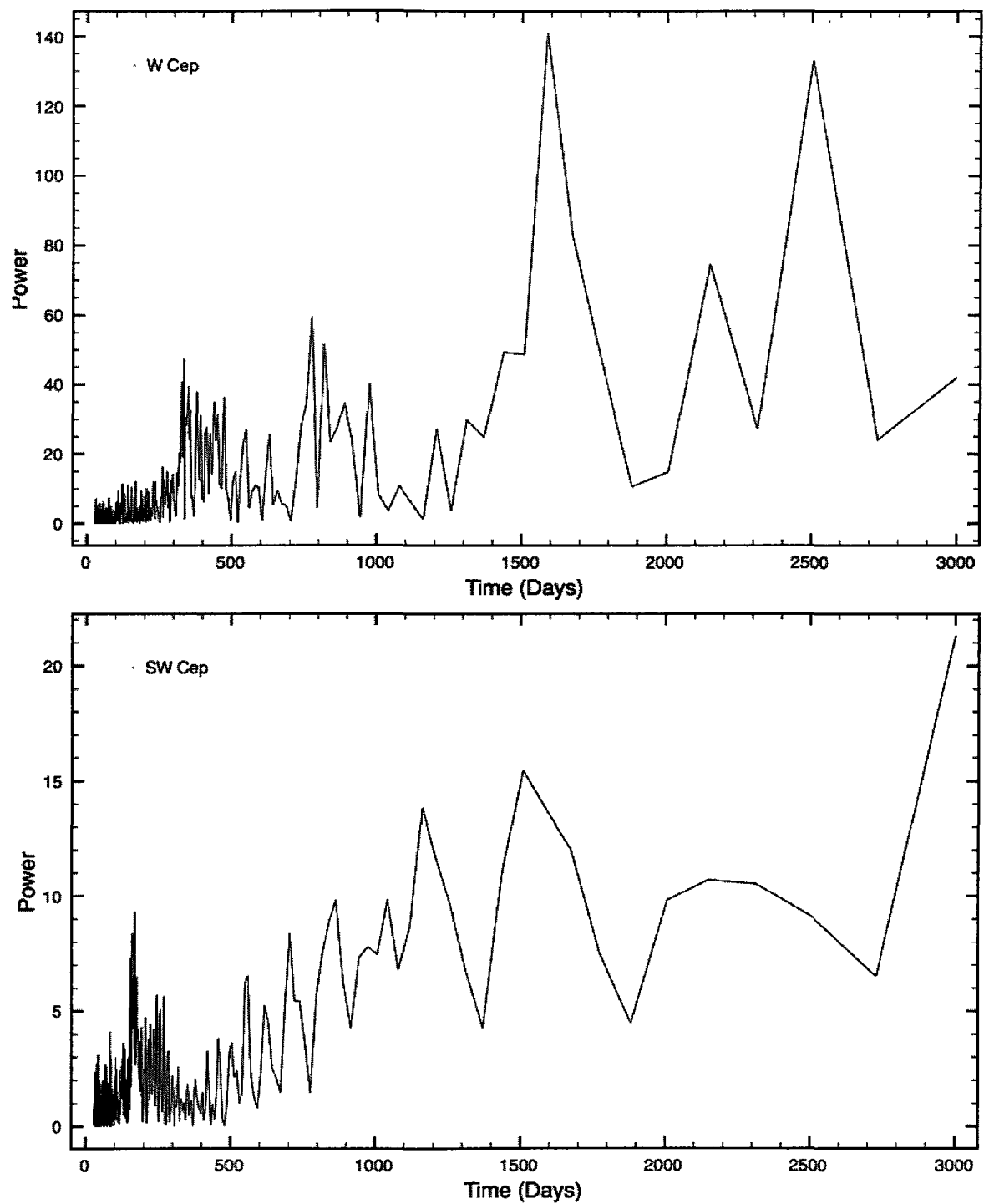


Figure C.7: Top: W Cephei, Bottom: SW Cephei

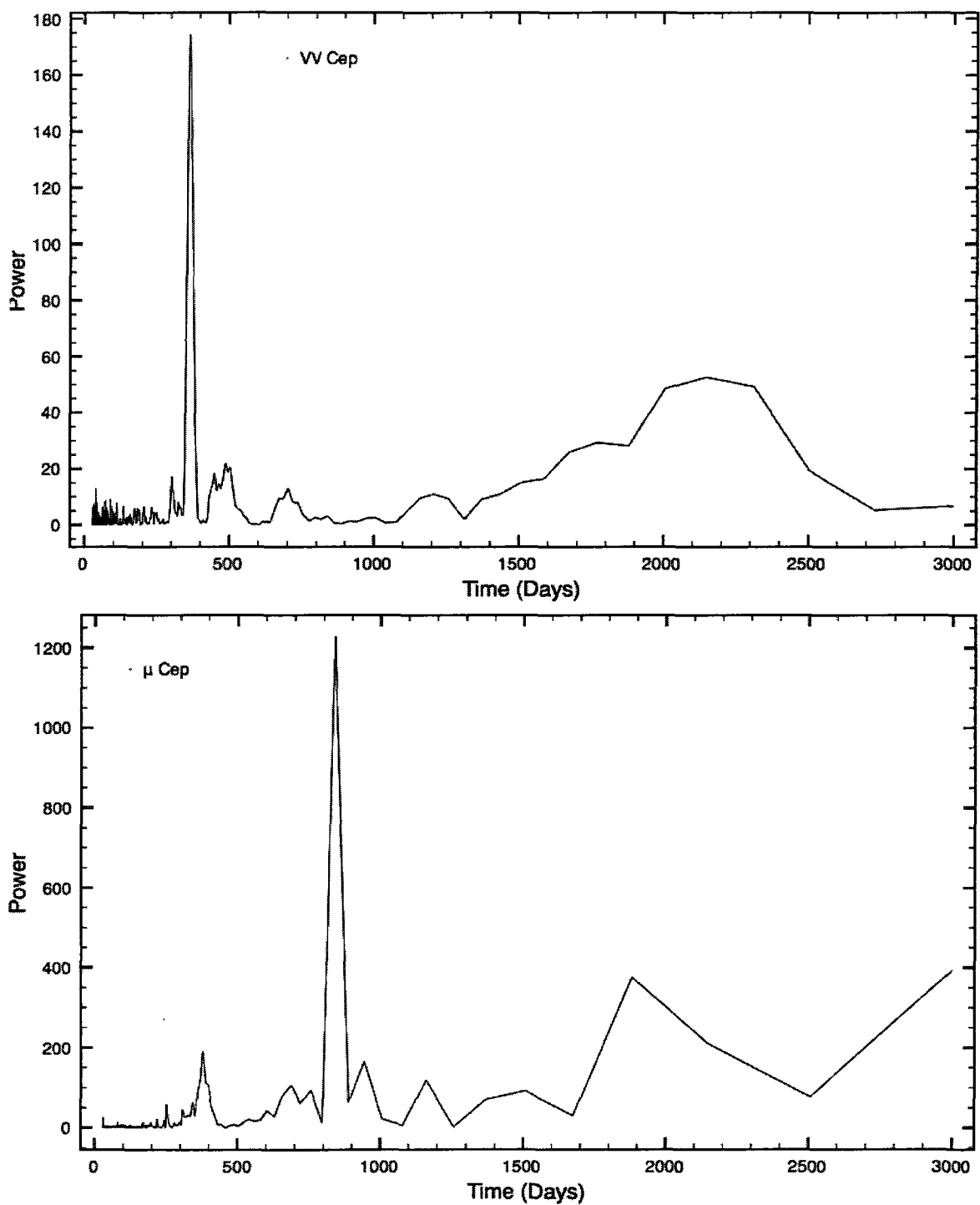
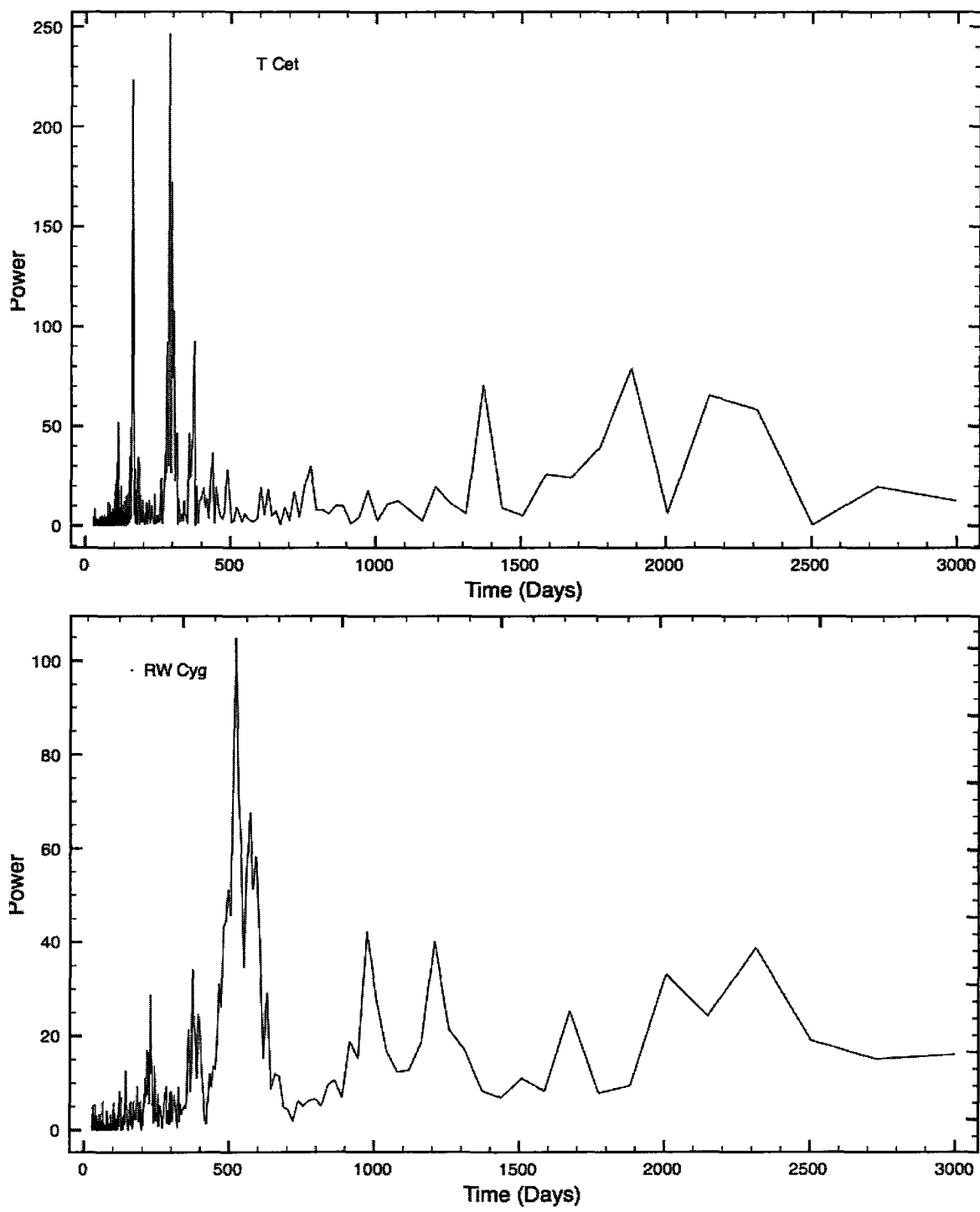
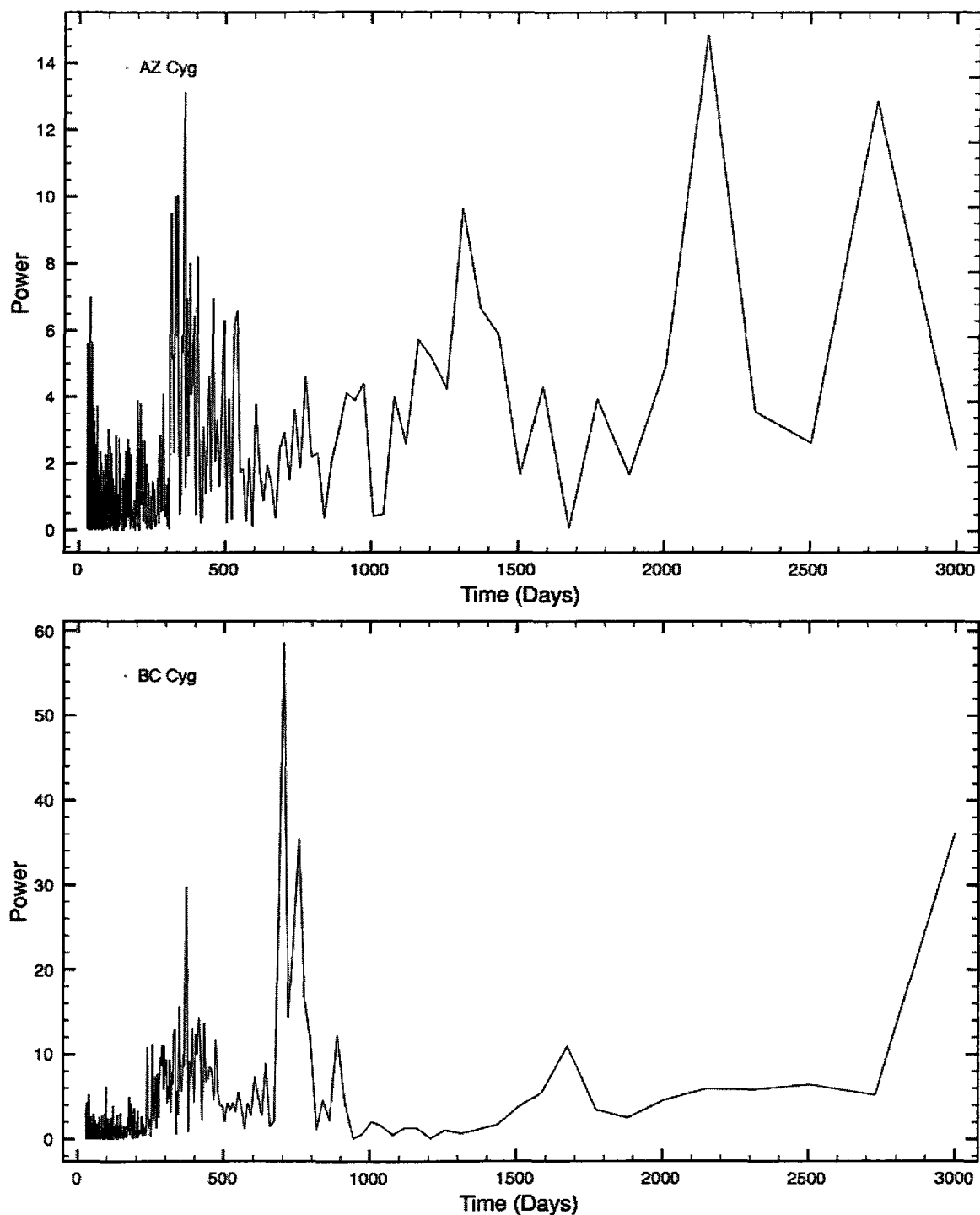


Figure C.8: Top: VV Cephei, Bottom:  $\mu$  Cephei



**Figure C.9:** Top: T Ceti, Bottom: RW Cygni



**Figure C.10:** Top: AZ Cygni, Bottom: BC Cygni

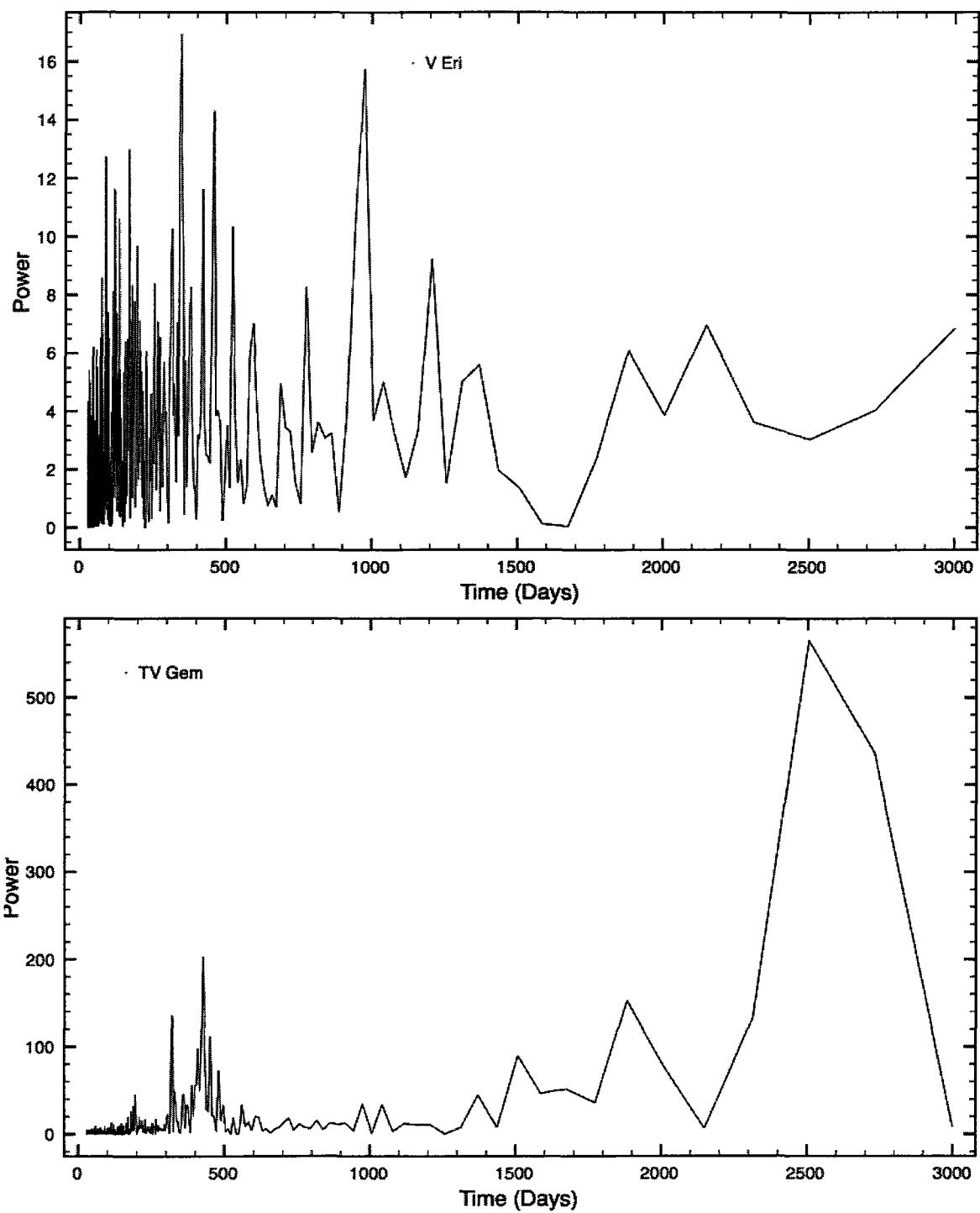


Figure C.11: Top: V Eridanus, Bottom: TV Geminorum

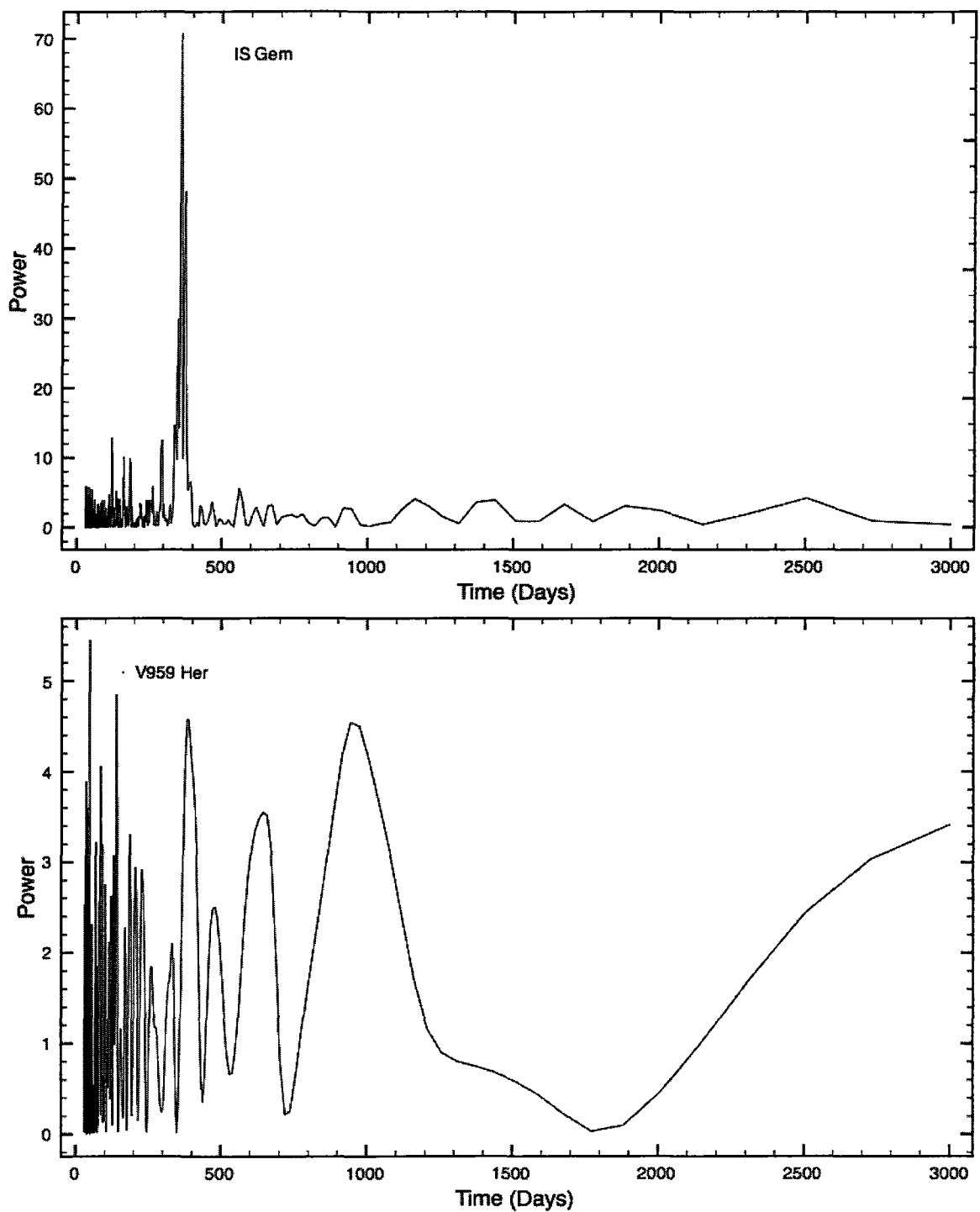
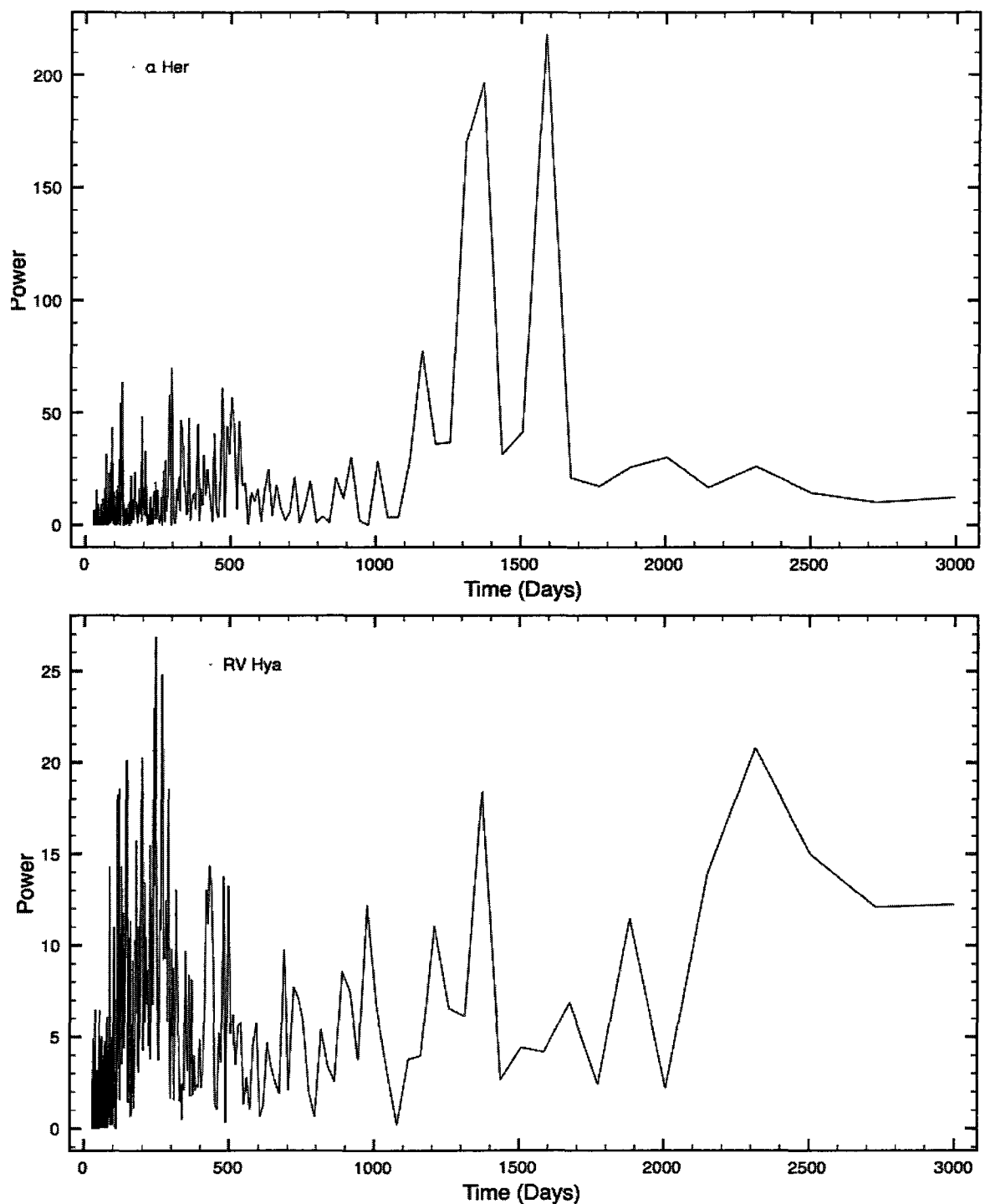


Figure C.12: Top: IS Geminorum, Bottom: V959 Herculis



**Figure C.13:** Top:  $\alpha$  Herculis, Bottom: RV Hydrae

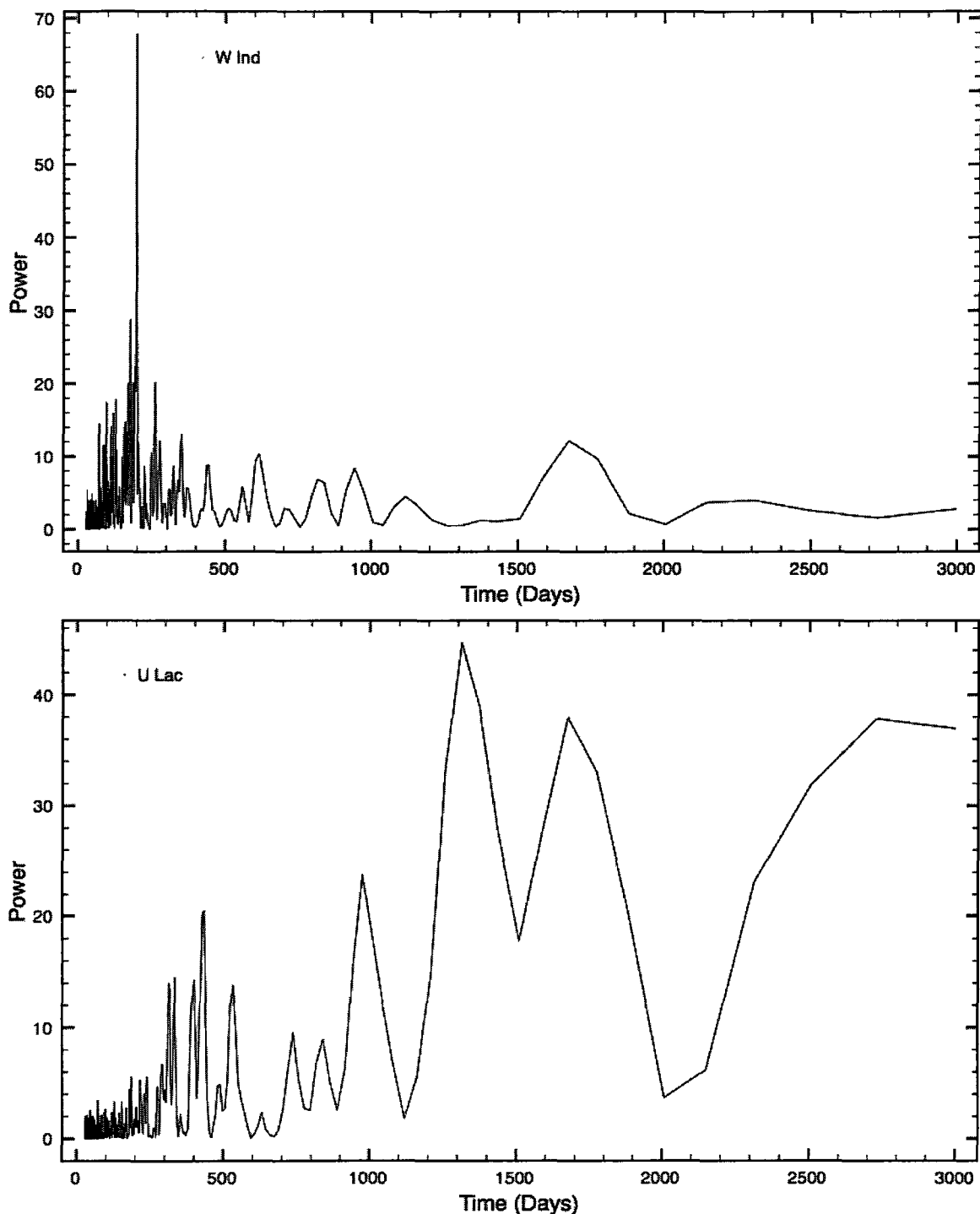
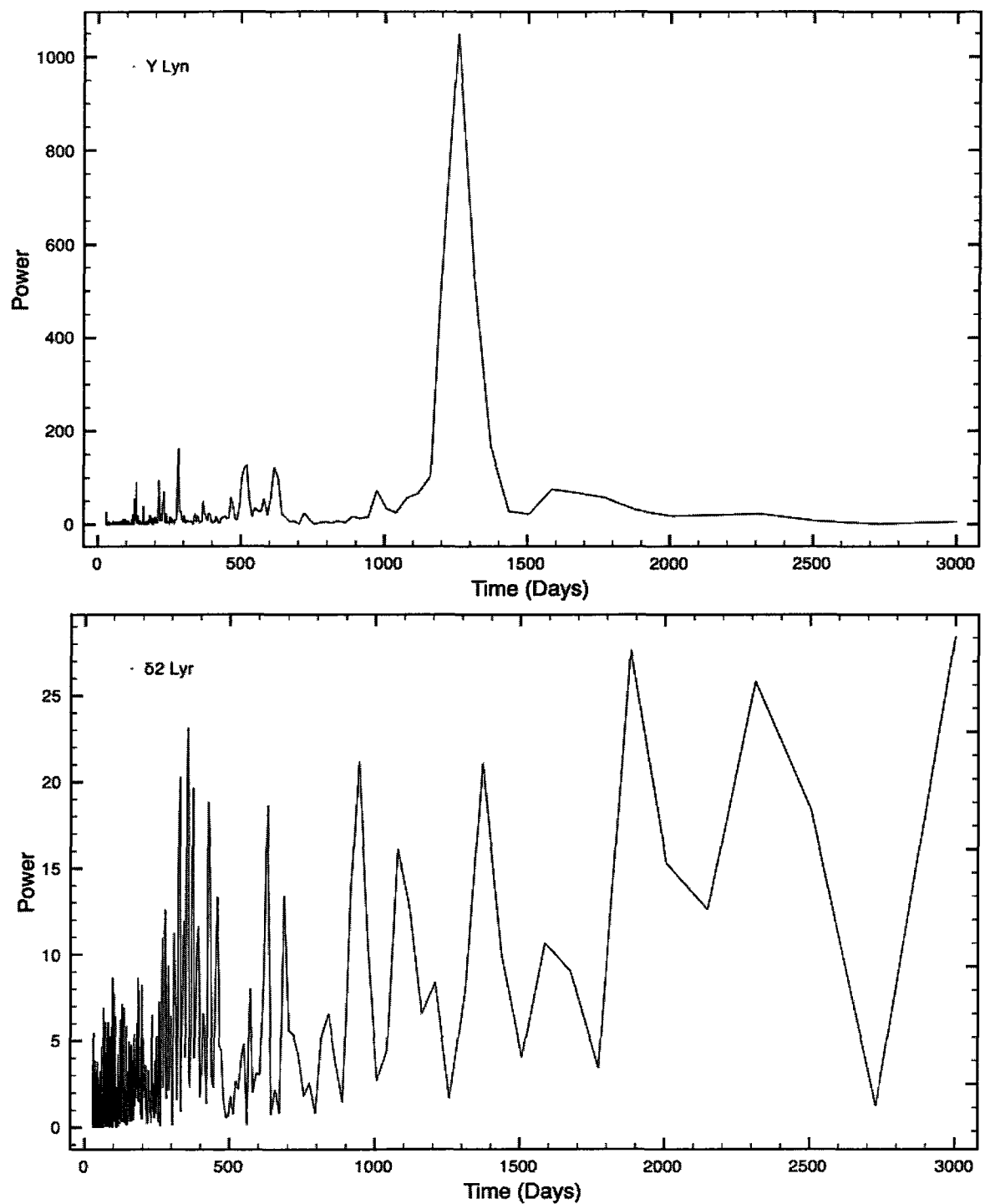
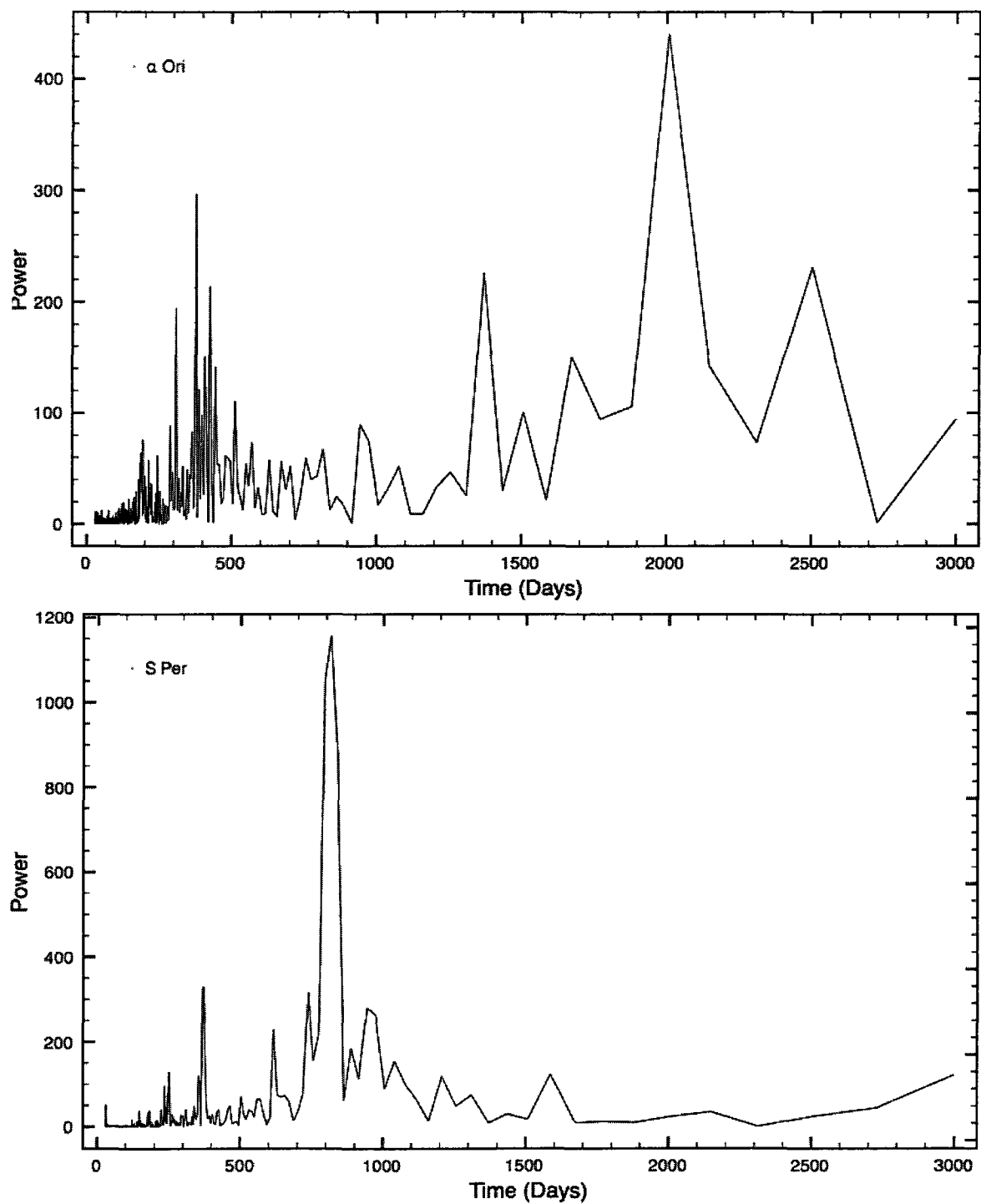


Figure C.14: Top: W Indus, Bottom: U Lacertae



**Figure C.15:** Top: Y Lyncis, Bottom: $\delta^2$  Lyrae



**Figure C.16:** Top:  $\alpha$  Orionis, Bottom: S Persei

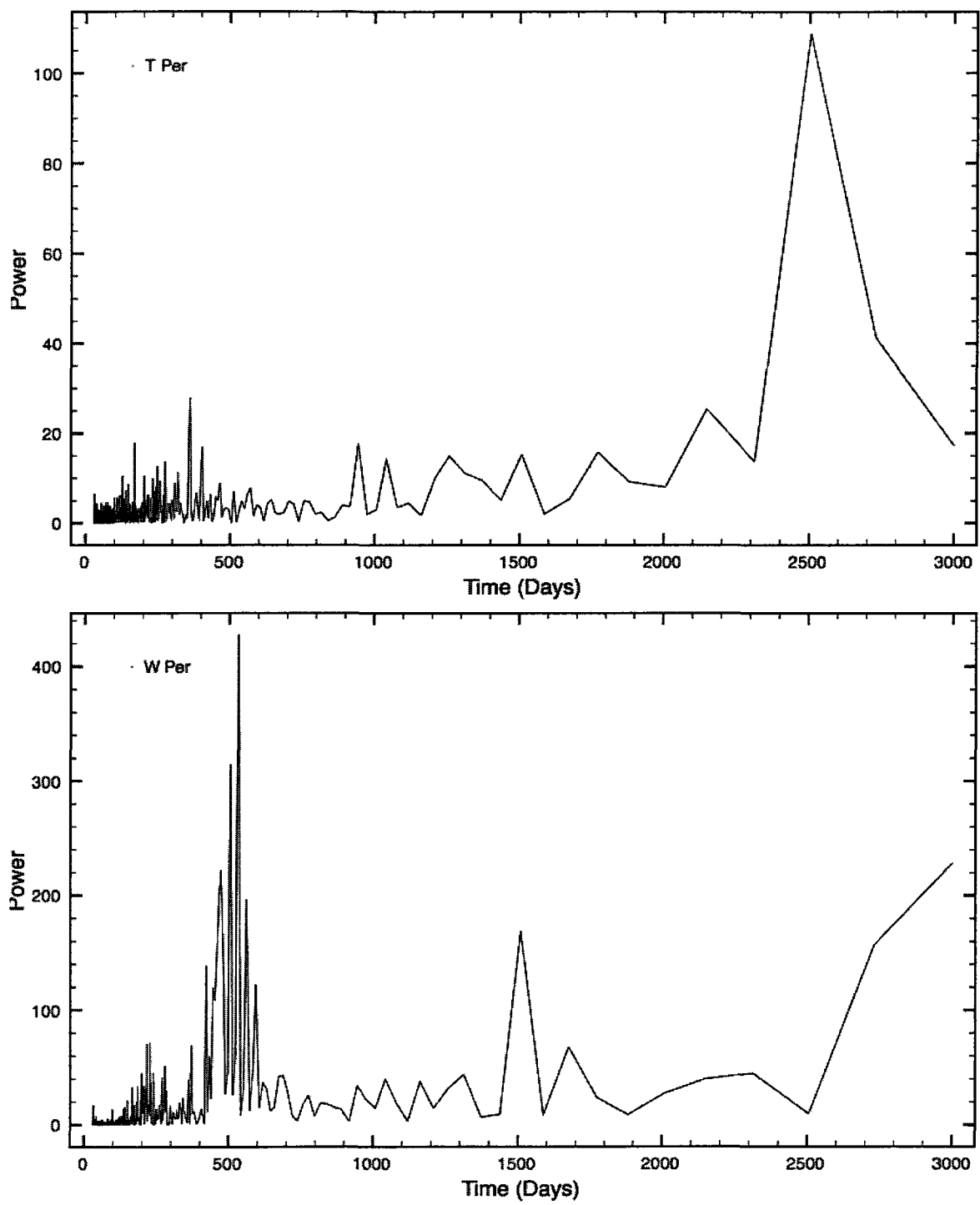
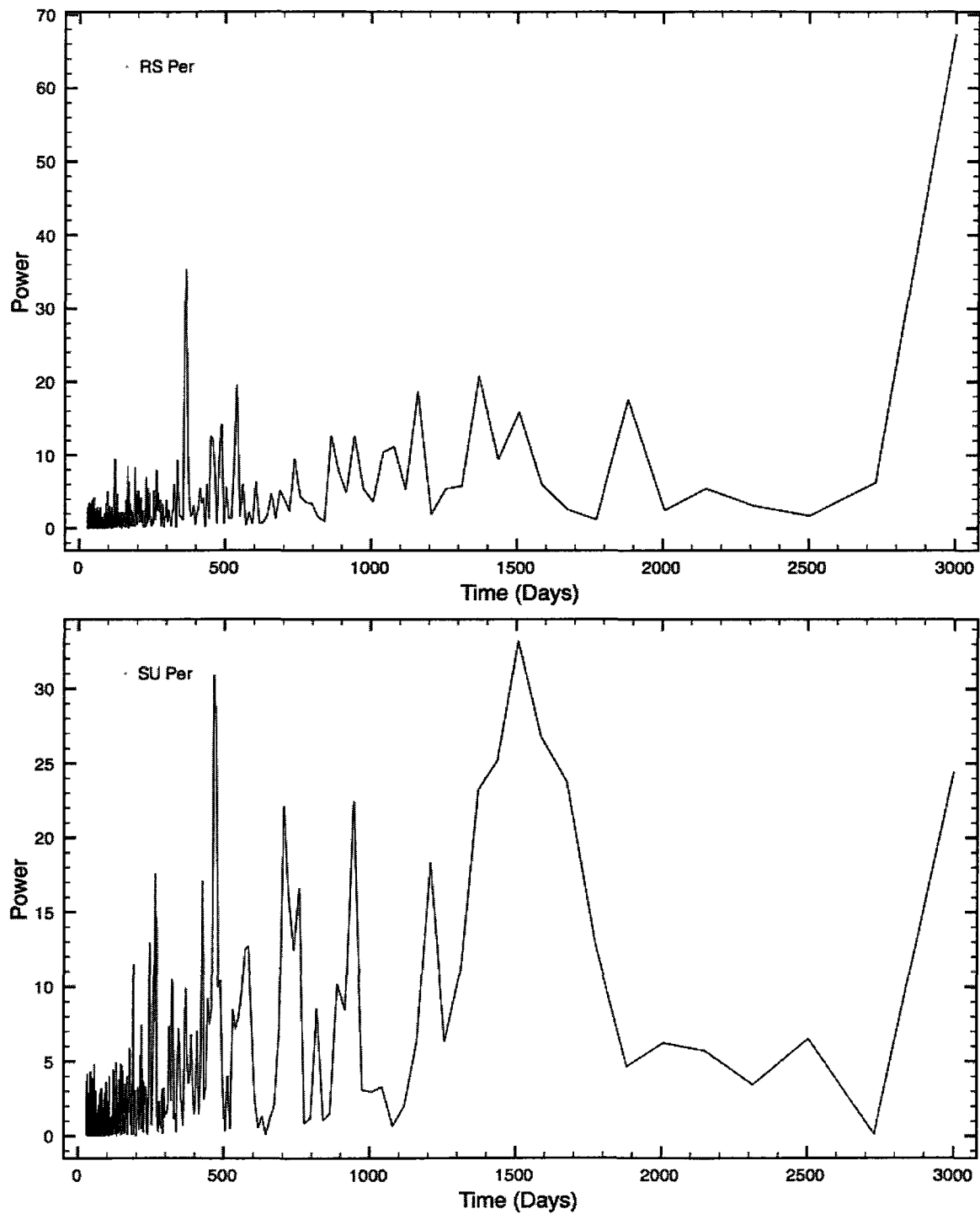


Figure C.17: Top: T Persei, Bottom: W Persei



**Figure C.18:** Top: RS Persei, Bottom: SU Persei

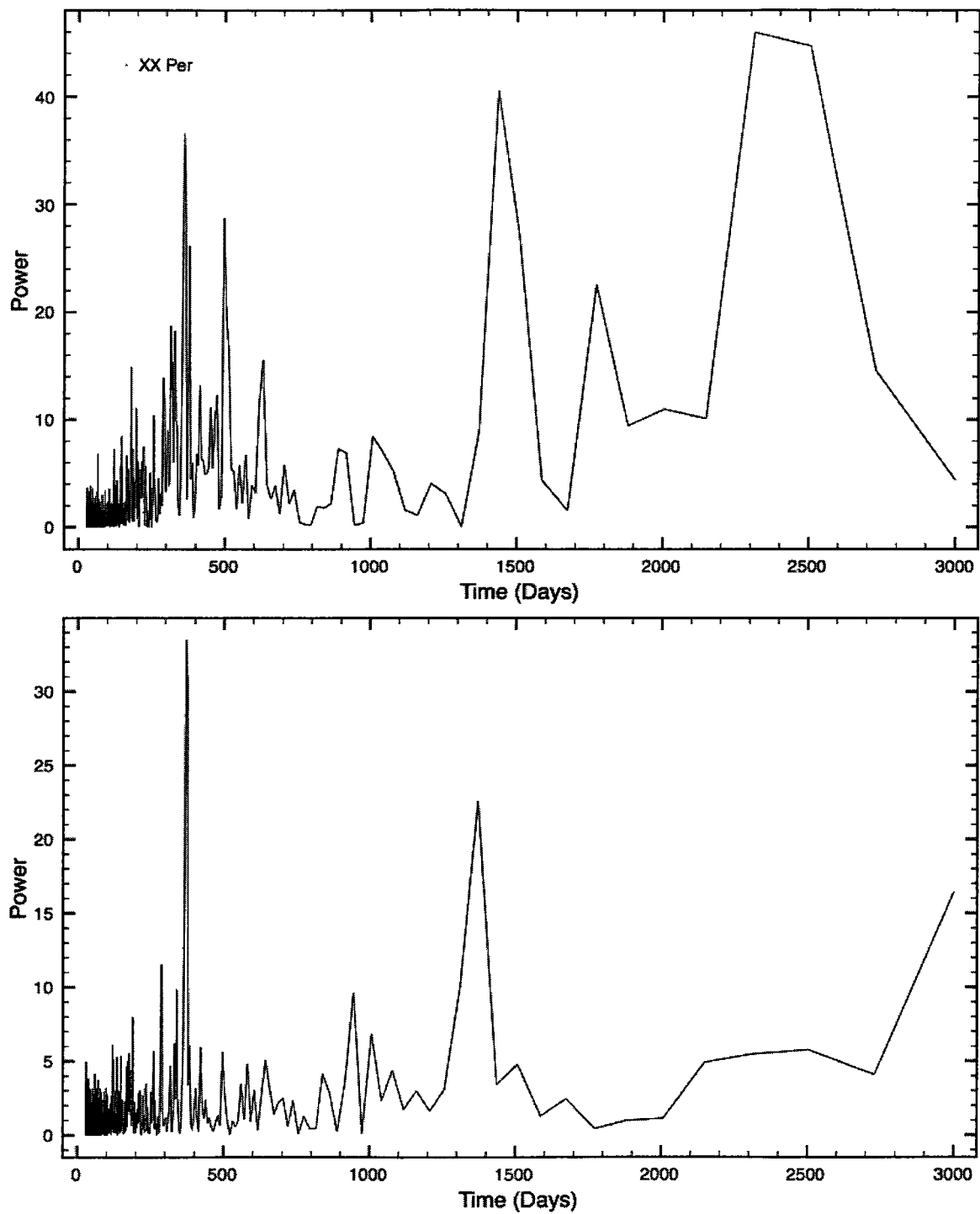


Figure C.19: Top: XX Persei, Bottom: AD Persei

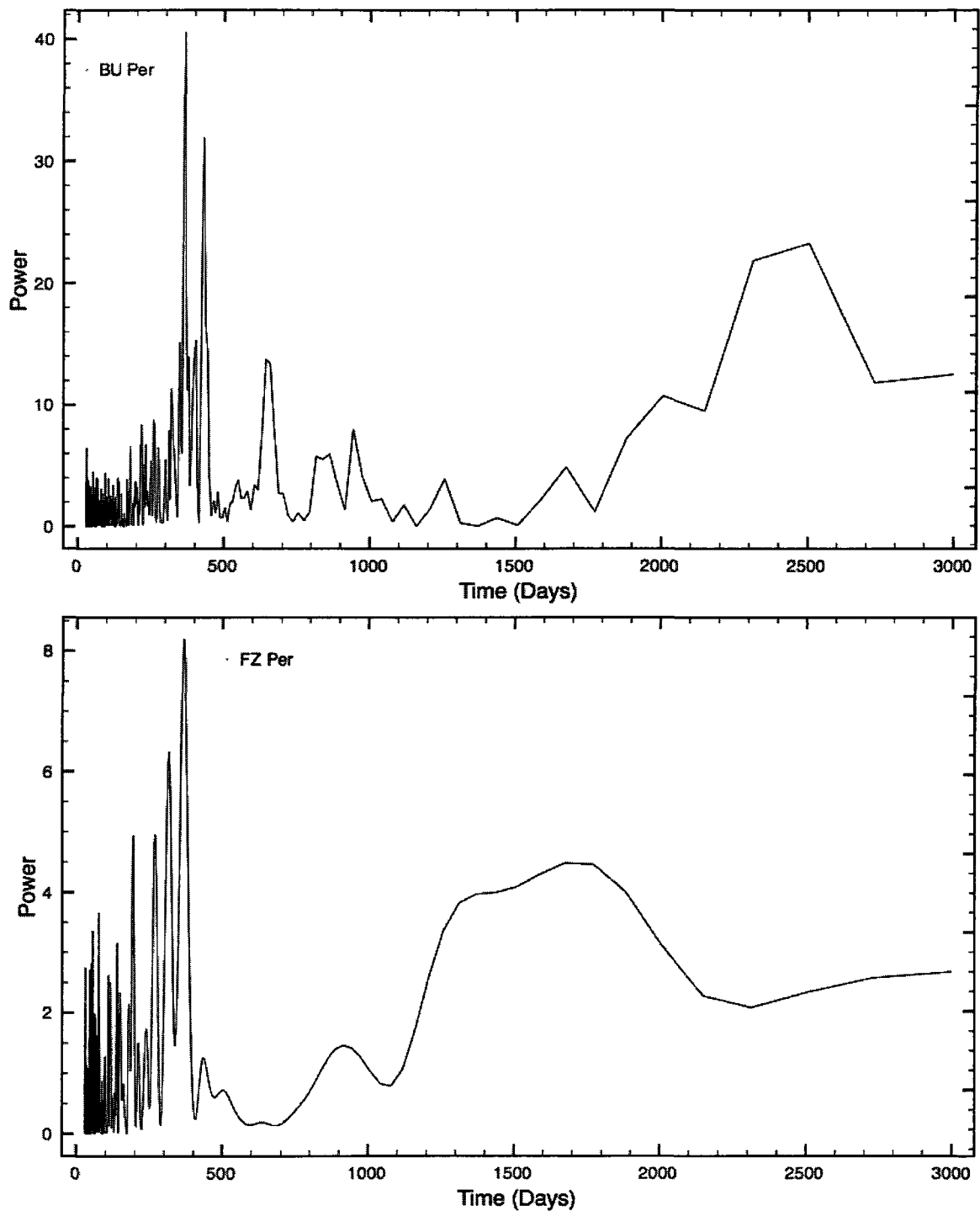
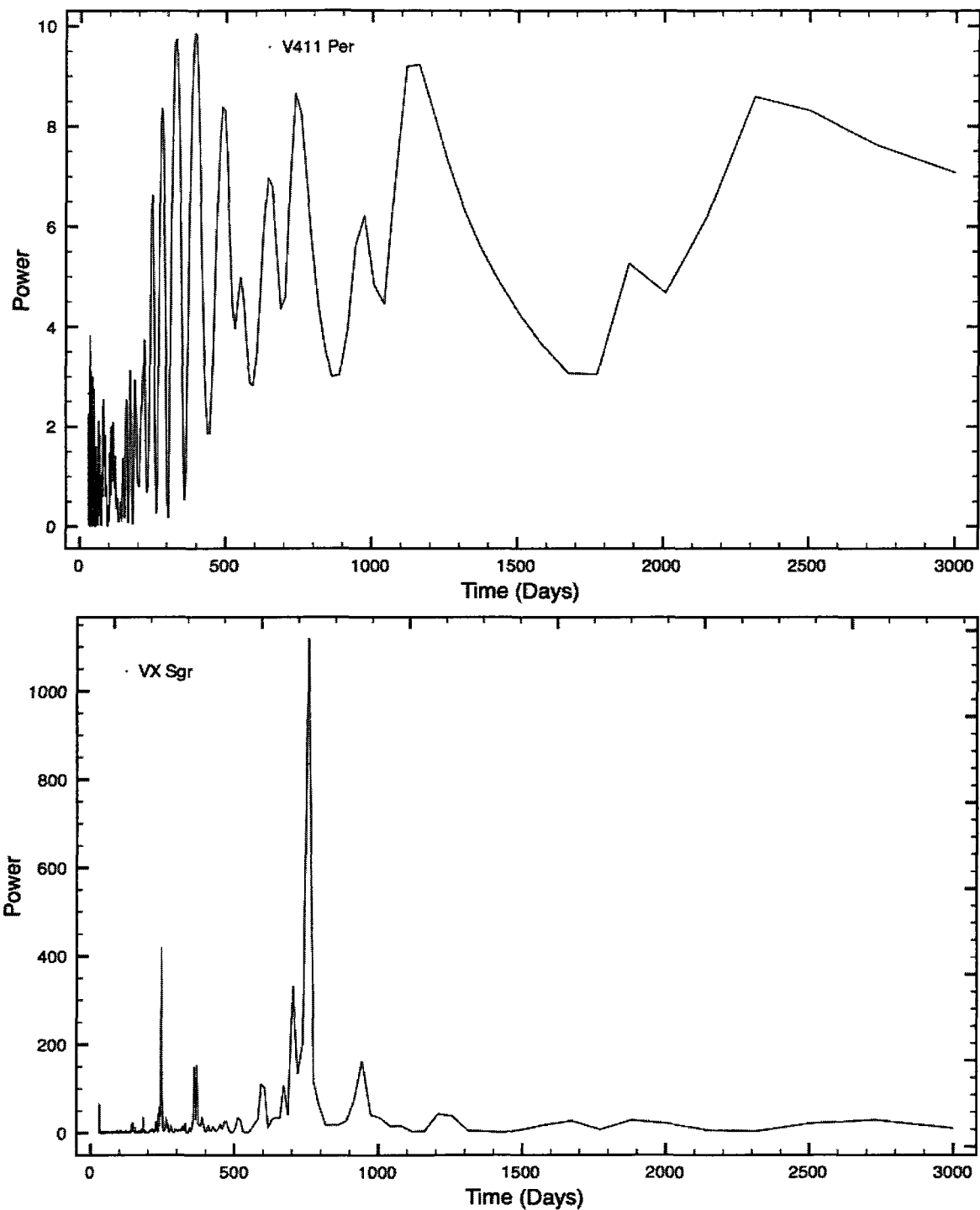


Figure C.20: Top: BU Persei, Bottom: FZ Persei



**Figure C.21:** Top: V411 Persei, Bottom: VX Sagittarii

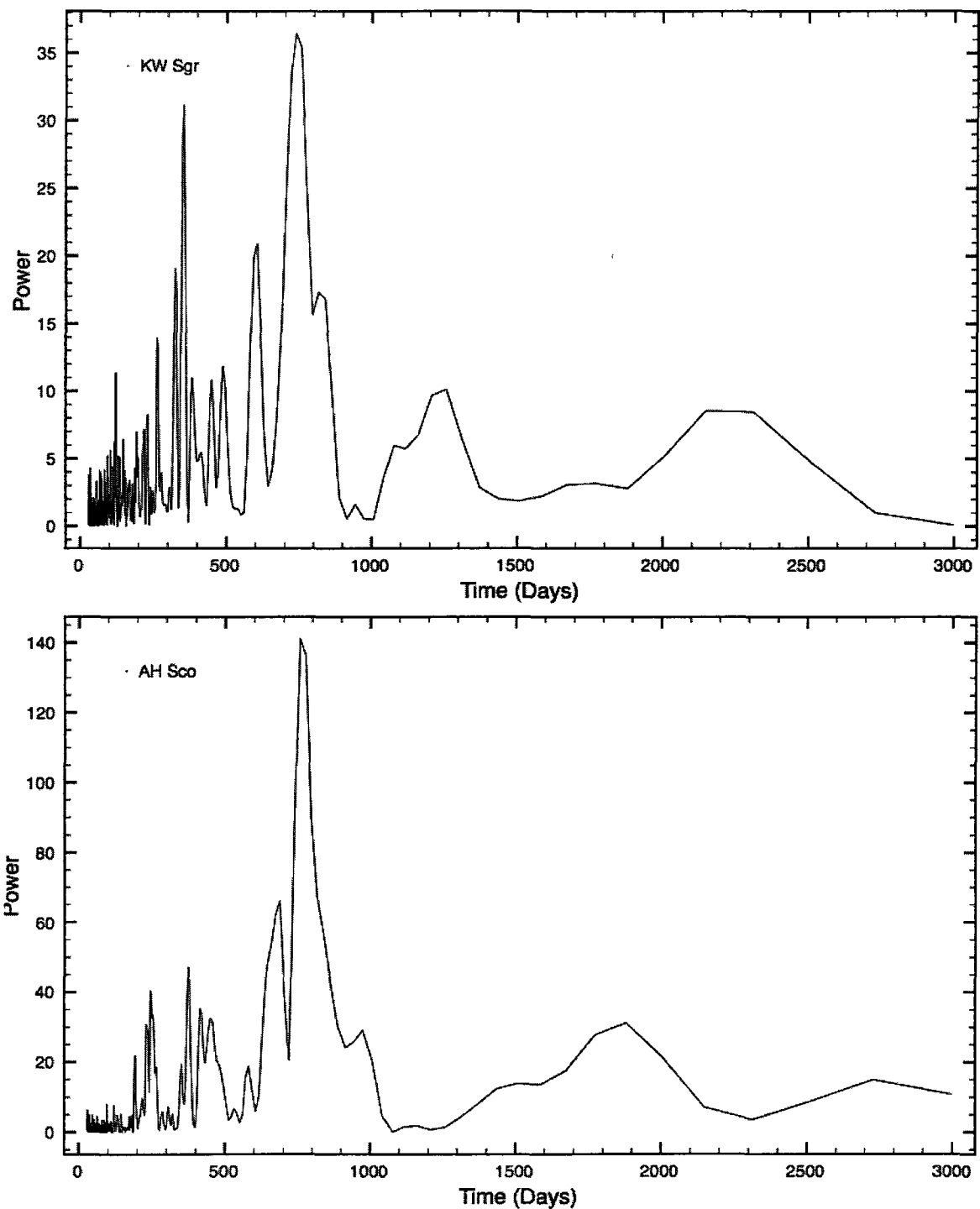
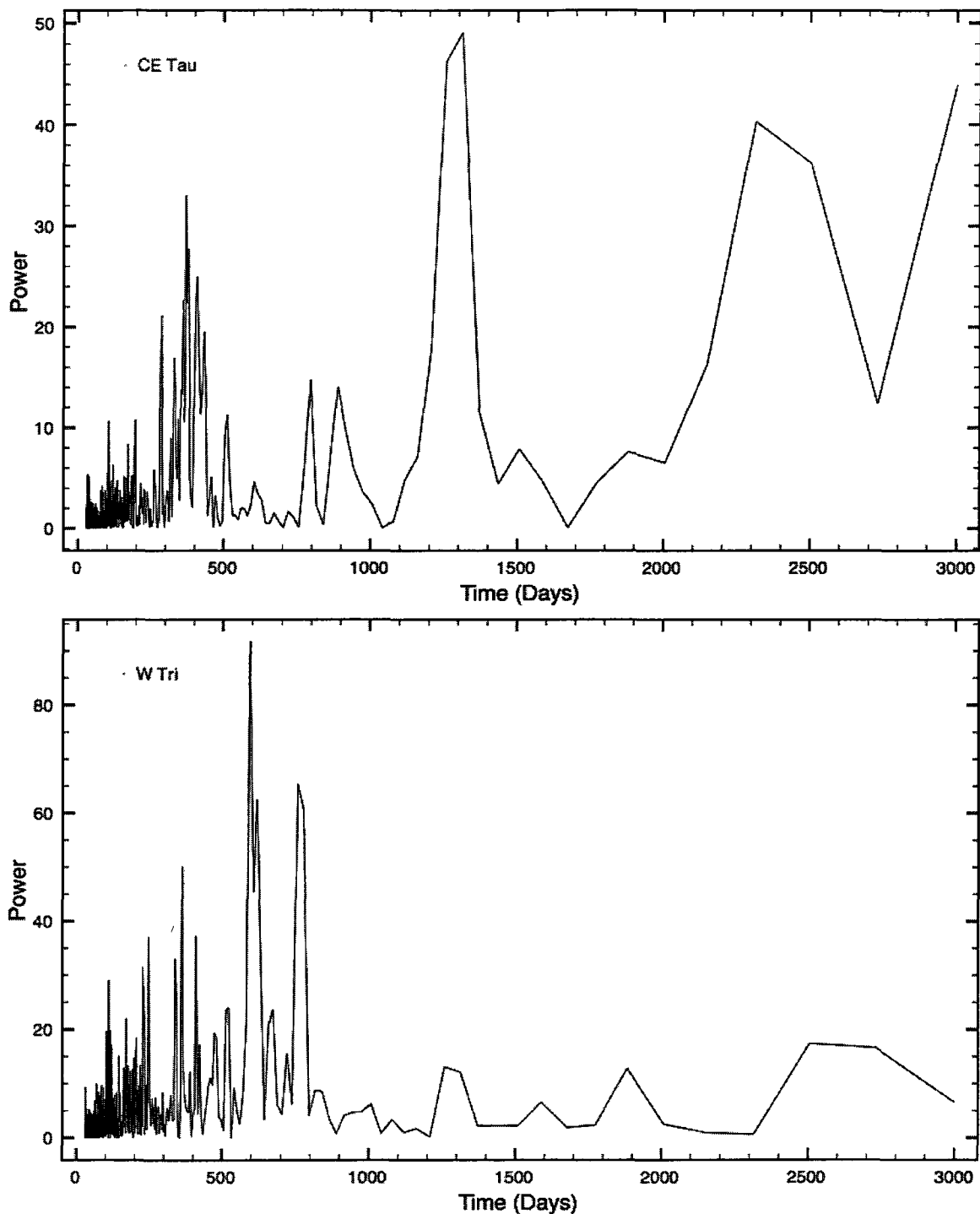
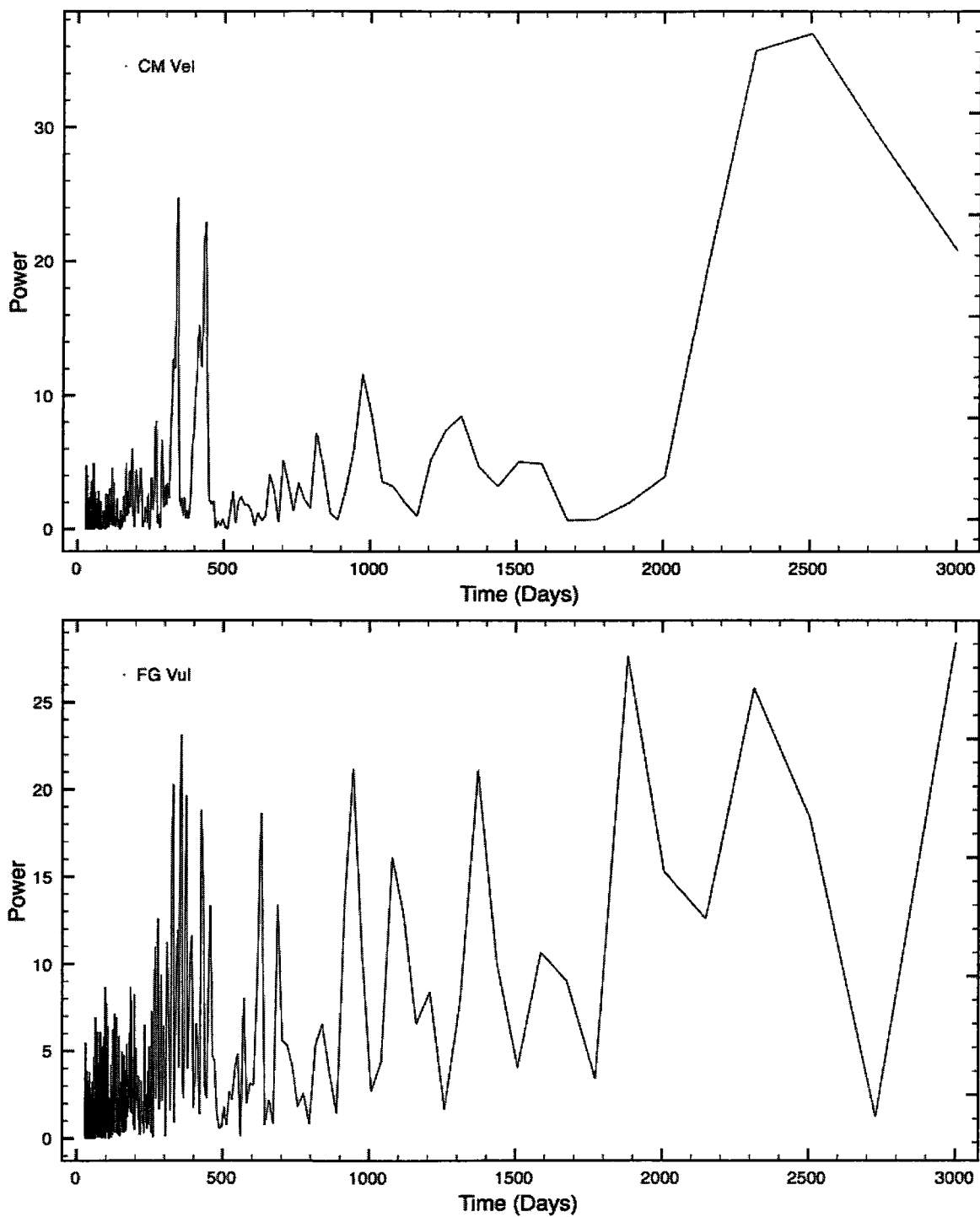


Figure C.22: Top: KW Sagittarii, Bottom: AH Scorpii



**Figure C.23:** Top: CE Tauri, Bottom: W Triangulum



**Figure C.24:** Top: CM Velorum, Bottom: FG Vulpeculae

## Appendix D

### Observing Logs

This appendix provides details for the new CCD spectra obtained at the DAO and the scanned photographic spectra from the DAO archives.

#### D.1 DAO CCD Spectra

The DAO CCD spectra were all obtained using the 1.8-m Plaskett telescope. The following tables contain information for each observing season (2005-2010). In each season, FeAr arc lamp spectra were used as comparison spectra, and an arc spectrum was taken before and after each object exposure to compensate for any spectrograph flexure effects. Each night 10-20 bias and flat frames were also obtained. Each spectrum was obtained at airmass < 2. The subsection for each season lists the CCD and grating used, the wavelength range, and the dispersion for the season. Detailed technical specifications for the CCD's can be found at <https://www.astrosci.ca/DAO/detectors.html> and for the gratings at <https://www.astrosci.ca/DAO/dao72.html>. All spectra are single-order. The table for each season gives the following information: Star (multiple observations for a given star are listed sequentially), date (HJD can be found in the table of information for each star in chapter 4), exposure time in seconds and signal-to-noise (calculated using IRAF's *SPLIT* package).

##### D.1.1 2005

Detector: SITe-2

Grating: 21(3/2) 1

Wavelength Range: 3550Å-6825Å

Dispersion: 2.0 Å/pixel

**Table D.1:** 2005 Observing Log

Star	Date	Exp (s)	S/N
PZ Cas	Oct 7/8	120	7.24
W Cep	Oct 7/8	60	8.53
VV Cep	Oct 10/11	5	7.87
MY Cep	Oct 7/8	1800	3.90
$\mu$ Cep	Oct 10/11	2	7.34
AZ Cyg	Oct 7/8	300	7.98
AZ Cyg	Oct 10/11	600	8.26
BC Cyg	Oct 7/8	600	8.09
BC Cyg	Oct 10/11	600	4.81
BC Cyg	Oct 10/11	900	4.78
U Lac	Oct 3/4	1200	6.94
S Per	Oct 3/4	500	7.70
T Per	Oct 3/4	250	9.51
W Per	Oct 3/4	200	6.39
RS Per	Oct 3/4	200	5.54
SU Per	Oct 3/4	100	5.43
XX Per	Oct 9/10	600	5.68
AD Per	Oct 3/4	200	8.86
FZ Per	Oct 3/4	60	7.70
V411 Per	Oct 3/4	250	6.33
W Tri	Oct 3/4	60	3.40

### D.1.2 2006

Detector: SITe-2

Grating: 2131 B

Wavelength Range: 3550Å-5240Å

Dispersion: 1.0 Å/pixel

**Table D.2:** 2006 Observing Log

Star	Date	Exp (s)	S/N
SS And	Oct 17/18	200	4.57
$\alpha$ Her	Oct 17/18	60	5.45
Y Lyn	Oct 19/20	120	2.48
BU Per	Oct 17/18	400	3.41

### D.1.3 2007

Detector: SITe-5

Grating: 2131 B

Wavelength Range: 3750-3240

Dispersion: 1.5 Å/pixel

**Table D.3:** 2007 Observing Log

Star	Date	Exp (s)	S/N
UX Aur	Oct 7/8	1200	3.80
PZ Cas	Oct 4/5	3600	5.65
PZ Cas	Oct 7/8	3600	5.67
W Cep	Oct 2/3	1800	11.47
VV Cep	Sep 28/29	120	10.83
SW Cep	Sep 28/29	1200	4.86
$\mu$ Cep	Sep 28/29	60	6.56
RW Cyg	Oct 7/8	1200	6.02
AZ Cyg	Oct 2/3	2400	6.16
BC Cyg	Sep 28/29	1800	5.72
BC Cyg	Oct 3/4	1800	5.46
BC Cyg	Oct 4/5	3600	5.55
U Lac	Sep 28/29	360	6.12
CE Tau	Oct 7/8	600	6.23
S Per	Oct 4/5	2400	5.31
T Per	Oct 4/5	3600	6.31
SU Per	Oct 4/5	3000	5.52
XX Per	Sep 28/29	1200	6.87
AD Per	Oct 7/8	1800	6.16
FZ Per	Oct 7/8	1000	6.30
V411 Per	Oct 7/8	1200	5.62

#### D.1.4 2008

Detector: SITe-5

Grating: 2131 B

Wavelength Range: 3750-5240

Dispersion: 1.5 Å/pixel

**Table D.4:** 2008 Observing Log

Star	Date	Exp (s)	S/N
W Cep	Oct 13/14	300	11.20
VV Cep	Oct 8/9	120	9.22
SW Cep	Oct 8/9	1800	5.33
$\mu$ Cep	Oct 8/9	60	5.57
RW Cyg	Oct 8/9	1800	3.57
AZ Cyg	Oct 8/9	1800	3.85
BC Cyg	Oct 8/9	1800	4.82
U Lac	Oct 14/15	1200	4.72
S Per	Oct 8/9	3600	4.20
T Per	Oct 8/9	1800	6.28
W Per	Oct 8/9	3600	4.21
SU Per	Oct 13/14	1800	4.62
RS Per	Oct 13/14	1300	4.72
AD Per	Oct 14/15	600	3.85
BU Per	Oct 14/15	1200	5.23
FZ Per	Oct 14/15	600	6.35
V411 Per	Oct 14/15	1800	5.01

### D.1.5 2009

Detector: SITe-5

Grating: 2131 B

Wavelength Range: 3750-5240

Dispersion: 1.5 Å/pixel

**Table D.5:** 2009 Observing Log

Star	Date	Exp (s)	S/N
RW Cyg	Sep 10/11	1800	5.18
AZ Cyg	Sep 15/16	1800	4.70
BC Cyg	Sep 10/11	3600	4.67
W Cep	Sep 10/11	1800	11.61
SW Cep	Sep 10/11	3600	5.07
$\mu$ Cep	Sep 10/11	60	6.10
$\alpha$ Her	Sep 10/11	10	3.67
$\alpha$ Her	Sep 10/11	10	3.67
U Lac	Sep 16/17	3600	5.56
S Per	Sep 11/12	5400	4.26
T Per	Sep 11/12	4200	6.05
W Per	Sep 14/15	2900	4.93
RS Per	Sep 15/16	1800	4.22
SU Per	Sep 15/16	1800	5.81
XX Per	Sep 16/17	900	6.15
AD Per	Sep 16/17	1200	5.37
FZ Per	Sep 16/17	1200	5.86
FG Vul	Sep 16/17	1800	3.48

### D.1.6 2010

Detector: SITe-5

Grating: 2131 B

Wavelength Range: 3750-5240

Dispersion: 1.5 Å/pixel

**Table D.6:** 2010 Observing Log

Star	Date	Exp (s)	S/N
SS And	Oct 18/19	1200	2.61
UX Aur	Oct 13/14	1200	3.19
PZ Cas	Oct 18/19	900	3.52
W Cep	Oct 18/19	300	7.44
SW Cep	Oct 18/19	1500	4.54
VV Cep	Oct 18/19	90	8.29
$\mu$ Cep	Oct 18/19	10	4.99
RW Cyg	Oct 12/13	600	3.70
AZ Cyg	Oct 18/19	600	4.21
BC Cyg	Oct 16/17	1200	3.81
TV Gem	Oct 19/20	240	6.26
U Lac	Oct 18/19	800	5.04
Y Lyn	Oct 13/14	400	2.85
S Per	Oct 13/14	600	3.83
T Per	Oct 12/13	600	5.06
W Per	Oct 13/14	800	4.79
RS Per	Oct 13/14	800	3.50
SU Per	Oct 12/13	600	4.15
AD Per	Oct 12/13	600	3.91
BU Per	Oct 12/13	800	4.65
FZ Per	Oct 12/13	600	5.54
XX Per	Oct 12/13	600	5.33
V411 Per	Oct 13/14	1600	4.41
CE Tau	Oct 13/14	60	5.14
W Tri	Oct 13/14	600	3.71
FG Vul	Oct 18/19	1200	3.05

## D.2 Scanned DAO Photographic Spectra

The scanned photographic spectra were taken from IIaO plates observed with the 1.2-m telescope in the 1960s and 1970s. Wavelength calibration was done using FeAr arc lamp spectra. The following table lists the spectra in chronological order and gives the star name, date (HJD can be found in individual star sections in chapter 4), exposure time in seconds, wavelength range, dispersion of the scanned spectrum, airmass, and signal-to-noise calculated using IRAF's *S PLOT* package.

**Table D.7:** Scanned DAO Photographic Spectra

Star	Date	Exp (s)	$\lambda$ Range (Å)	Dispersion (Å/pixel)	Airmass	S/N
$\alpha$ Her	Jun 16, 1966	300	3600-4925	0.01	1.39	10.19
$\alpha$ Her	Jun 16, 1966	300	3600-4925	0.01	1.32	4.76
$\alpha$ Ori	Apr 1, 1971	300	3700-4900	0.01	1.52	5.70
$\alpha$ Ori	Apr 1, 1971	300	3700-4900	0.01	1.56	7.36
$\alpha$ Her	Apr 5, 1971	300	3700-4874	0.01	1.28	6.61
$\alpha$ Her	Apr 12, 1971	300	3700-4874	0.01	1.21	5.19
$\alpha$ Ori	Jun 29, 1971	300	3700-4900	0.01	1.03	7.01
$\alpha$ Ori	Oct 8, 1971	300	3700-4868	0.01	1.35	5.99
$\alpha$ Ori	Feb 14, 1975	300	3700-4238	0.05	1.69	7.41
$\alpha$ Her	Apr 10, 1975	300	3700-4868	0.01	1.31	4.75
$\alpha$ Ori	Feb 10, 1976	300	3700-4876	0.01	1.39	5.66
RS Cnc	May 1, 1978	300	3700-5200	0.05	1.20	6.57
RS Cnc	May 1, 1978	300	3700-4876	0.01	1.20	4.93